

IAEA-TECDOC-1416

Advanced fuel pellet materials and designs for water cooled reactors

*Proceedings of a technical committee meeting
held in Brussels, 20–24 October 2003*



IAEA

International Atomic Energy Agency

October 2004

IAEA-TECDOC-1416

Advanced fuel pellet materials and designs for water cooled reactors

*Proceedings of a technical committee meeting
held in Brussels, 20–24 October 2003*



IAEA

International Atomic Energy Agency

October 2004

The originating Section of this publication in the IAEA was:

Nuclear Fuel Cycle and Materials Section
International Atomic Energy Agency
Wagramer Strasse 5
P.O. Box 100
A-1400 Vienna, Austria

ADVANCED FUEL PELLET MATERIALS AND DESIGNS FOR
WATER COOLED REACTORS

IAEA, VIENNA, 2004
IAEA-TECDOC-1416
ISBN 92-0-111404-4
ISSN 1011-4289

© IAEA, 2004

Printed by the IAEA in Austria
October 2004

FOREWORD

At the invitation of the Government of Belgium, and in response to a proposal of the IAEA Technical Working Group on Water Reactor Fuel Performance and Technology (TWGFPT), the IAEA convened a Technical Committee Meeting on Improved Fuel Improved Fuel Pellet Materials and Designs in Brussels, Belgium from 20 to 24 October 2003. The meeting was hosted by Belgatom.

This meeting was the second IAEA meeting on this subject. The first was held in 1996 in Tokyo, Japan. They are all part of a cooperative effort through the TWGFPT, with a series of three further meetings organized by CEA, France and co-sponsored by the IAEA and OECD/NEA. The first meeting was entitled Thermal Performance of High Burnup LWR Fuel and was held in 1998. The second meeting was entitled Fission Gas Behaviour in Water Reactor Fuels and took place in 2000, and the third meeting, Pellet-cladding Interaction, was held in March 2004. All four meetings supplemented each other.

In the seven years since the first meeting took place, the demands on fuel duties have increased, with higher burnup, longer fuel cycles and higher temperatures. This places additional demands on fuel performance to comply with safety requirements. Criteria relative to fuel components, i.e. pellets and fuel rod column, require limiting of fission gas release and pellet-cladding interaction (PCI). This means that fuel components should maintain the composite of rather contradictory properties from the beginning until the end of its in-pile operation. Fabrication and design tools are available to influence —and to some extent — to ensure desirable in-pile fuel properties. Discussion of these tools was one of the objectives of the meeting. The second objective was the analysis of fuel characteristics at high burnup and the third and last objective was the discussion of specific feature of MOX and uranium-gadolinia fuels.

Sixty specialists in the field of fuel fabrication technology attended the meeting from 18 countries. Twenty-five papers were presented in five sessions covering all relevant topics from the practices and modelling of fuel fabrication technology to its optimization.

The proceedings in this publication are accompanied by a CD-ROM, which has been organized in two parts. The first part contains a full set of the papers presented at the meeting. The second contains the full presentations reproduced from the original slides, and therefore more information is included than in part one.

The IAEA wishes to thank all the participants for their contributions to the meeting and to this publication, especially H. Druenne of Tractebel Energy Engineering and his staff for assisting with administrative matters and H. Bairiot of FEX who organized a technical visit to CEN-SCK in Mol, Belgium. J. Van Vyve, Chairman of Belgatom, chaired the meeting. The IAEA officer responsible for this publication was V. Onufriev of the Division of Nuclear Fuel Cycle and Waste Technology.

EDITORIAL NOTE

The papers in these proceedings are reproduced as submitted by the authors and have not undergone rigorous editorial review by the IAEA.

The views expressed do not necessarily reflect those of the IAEA, the governments of the nominating Member States or the nominating organizations.

The use of particular designations of countries or territories does not imply any judgement by the publisher, the IAEA, as to the legal status of such countries or territories, of their authorities and institutions or of the delimitation of their boundaries.

The mention of names of specific companies or products (whether or not indicated as registered) does not imply any intention to infringe proprietary rights, nor should it be construed as an endorsement or recommendation on the part of the IAEA.

The authors are responsible for having obtained the necessary permission for the IAEA to reproduce, translate or use material from sources already protected by copyrights.

CONTENTS

Summary.....	1
--------------	---

OPTIMIZATION OF FUEL FABRICATION TECHNOLOGY — PRACTICES AND MODELLING (Session 1)

Recent developments in design and manufacture of uranium dioxide fuel pellets for PHWRs in India.....	13
<i>R. N. Jayaraj, C. Ganguly</i>	
Finite element modelling of the pressing of nuclear oxide powders to predict the shape of LWR fuel pellets after die compaction and sintering.....	21
<i>G. Delette, Ph. Sornay, J. Blancher</i>	
Mixed oxides pellets obtention by the “Reverse Strike” co-precipitation method	31
<i>J.E. Menghini, D.E. Marchi, V.G. Trimarco, E.H. Orosco</i>	
Establishment of low density MOX pellet fabrication process.....	45
<i>K. Asakura, T. Ohtani</i>	
Development of technologies of nuclear ceramic grade fuel production.....	55
<i>S.A. Yashin, A.E. Gagarin, A.V. Manych</i>	
Evaluation of U-reclaimed fuel application in VVER reactors.....	69
<i>V.N. Proselkov, S.S. Aleshin, V.D. Sidorenko, P.D. Slaviagin A.V. Kuleshov, O.V. Milovanov, E.N. Mikheev, V.V. Novikov, Yu.V. Pimenov</i>	
Development of UO ₂ /MOX fuels of modified microstructure for improved performance	77
<i>U. Basak, S. Majumdar, H.S. Kamath</i>	
Investigation of thermal-physical and mechanical properties of uranium-gadolinium oxide fuel	85
<i>Yu.K. Bibilashvili, A.V. Kuleshov, O.V. Milovanov, E.N. Mikheev, V.V. Novikov, S.G. Popov, V.N. Proselkov, Yu.V. Pimenov, Yu.G. Godin</i>	
Westinghouse doped pellet technology.....	101
<i>J.-E. Lindbäck</i>	

UO₂, MOX AND UO₂-GD₂O₃ PELLETS WITH ADDITIVES (Session 2)

Densification behaviour of TiO ₂ doped UO ₂ pellet	113
<i>H.S. Yoo, S.J. Lee, J.I. Kim, J.G. Chung, K.T. Kim</i>	
Effect of sintering gas on the grain size of UO ₂ pellets derived from different powder routes	125
<i>Keon Sik Kim, Kun Woo Song, Jae Ho Yang, Youn Ho Jung</i>	
Sintered pellets obtained for advanced fuel manufacturing.....	133
<i>D. Ohai, M. Roth</i>	

Effect of additives on the sintering kinetics of the $\text{UO}_2\text{Gd}_2\text{O}_3$ system	147
<i>T.A.G. Restivo, A.E L.Cláudio, E.D. Silva, L. Pagano Jr.</i>	
Yibin Nuclear Fuel Element Plant's experience in manufacturing of large grain size pellet	155
<i>Deng Hua, Zhou Yongzhong, Yan Xuemin</i>	

FISSION GAS RELEASE FROM FUEL PELLETS UNDER HIGH BURNUP (Session 3)

Advanced PWR fuels for high burnup extension and PCI constraint elimination.....	163
<i>Ch. Delafoy, P. Blanpain, S. Lansart, Ph. Dehaudt, G. Chiarelli, R. Castelli</i>	
Synthesis of the results obtained on the advanced UO_2 microstructures irradiated in the tanox device.....	175
<i>S. Valin, L. Caillot, Ph. Dehaudt, Y. Guerin, A. Mocellin, C. Delafoy, A. Chotard</i>	
Fission gas release from high burnup UO_2 fuels under simulated out-of pile LOCA conditions	187
<i>Y. Pontillon, D. Parrat, M.P. Ferroud Plattet, S. Ravel, G. Ducros, C. Struzik, A. Harrer</i>	

EVOLUTION OF FUEL PELLET STRUCTURE AND THERMAL PROPERTIES AT HIGH BURNUP (Session 4)

The MICROMOX project: A study about the impact of alternative MOX fuel microstructures on FGR	207
<i>M. Lippens, P. Cook, P.H. Raison, R.J.M. Konings, K. Bakker, C. Hellwig</i>	
Oxide fuel — Microstructure and composition variation (OMIC)	213
<i>M. Verwerft, M. Wéber, S. Lemehov, V. Sobolev, Th. Aoust, V. Kuzminov, J. Somers, G. Toury, J. McGinley, C. Selfslags, A. Schubert, D. Haas, Ph. Vesco, P. Blanpain</i>	
On the characterization of plutonium distribution in MIMAS MOX by image analysis.....	221
<i>G. Oudinet, I. Munoz-Viallard, M.-J. Gotta, J.M. Becker, G. Chiarelli, R. Castelli</i>	
Modelling non-standard mixed oxide fuels with the mechanistic code MACROS: Neutronic and heterogeneity effects	235
<i>S.E. Lemehov, K. Govers, M. Verwerft</i>	

PELLET CLADDING INTERACTION (PCI) (Session 5)

Impact of fuel microstructure on PCI behaviour.....	259
<i>C. Nonon, S. Lansart, C. Struzik, D. Planq, S. Martin, G.M. Decroix, O. Rabouille, S. Beguin, B. Julien</i>	
A procedure for analyzing the mechanical behavior of LWR fuel rod.....	279
<i>Y.M. Kim, Y.S. Yang, C.B. Lee, Y.H. Jung</i>	

Development of low-strain resistant fuel for power reactor fuel rods	297
<i>Yu.K. Bibilashvili, F.G. Reshetnikov, V.V. Novikov, A.V. Medvedev, O.V. Milovanov, A.V. Kuleshov, E.N. Mikheev, V.I. Kuznetsov, V.B. Malygin, K.V. Naboichenko, A.N. Sokolov, V.I. Tokarev, Yu.V. Pimenov</i>	
Observation of a pellet-cladding bonding layer in high power fuel.....	307
<i>S. van den Berghe, A. Leenaers, B. Vos, L. Sannen, M. Verwerft</i>	
LIST OF PARTICIPANTS	315

SUMMARY

1. INTRODUCTION

The Technical Meeting on Improved Fuel Pellet Materials and Designs held in Brussels, Belgium in October 2003 focused on fabrication and design tools to influence, to some extent, and ensure desirable in-pile fuel properties. Emphasis was given to analysis of fuel characteristics at high burnup including thermal behaviour, fission gas retention and release, PCI (pellet-cladding interaction) and PCMI (pellet-cladding mechanical interaction). Specific features of large grain size UO₂, MOX and uranium-gadolinia fuels with and without additives were considered in detail.

This meeting is the second IAEA meeting in this area after the first meeting held in 1996 in Tokyo, Japan. Also, there is a co-operation, through the IAEA Technical Working Group on Water Reactor Fuel Performance and Technology, with a series of three seminars organized by CEA, France, and co-sponsored by the IAEA and OECD/NEA. The first seminar on Thermal Performance of High Burnup LWR Fuel was in 1998, the second one on Fission Gas Behaviour in Water Reactor Fuels in 2000 and the third seminar on Pellet-Cladding Interaction — in March 2004. Altogether these five meetings create a comprehensive picture of fuel pellet, fuel column and fuel rod behaviour at high burnup.

2. SESSION 1: OPTIMIZATION OF FUEL FABRICATION TECHNOLOGY — PRACTICES AND MODELLING

Eight papers were presented in this session which all were devoted to fuel fabrication technology. They mostly treated methods for optimizing fuel manufacturing processes, but gave also a good overview on nuclear fabrication needs and capabilities in different countries.

In India, for example, fuel is to be provided for 3 different reactor types, including BWRs, PHWRs and WWERs. According to that, an unusual big variety of fuel types and fabrication routes has been established. In the paper contributed by NFC (Nuclear Fuel Complex in Hyderabad), emphasis was given to the development of fuel for PHWR. A lot of efforts have been done to improve:

- pellet design;
- type of fuel pellet material;
- and the manufacturing processes.

The design adaptation comprises pellet density, shape and dimensions. Use of depleted uranium in MOX fuel (for higher burnup) brought new challenge for special loading patterns and for manufacturing. In the field of production, several new processes have been developed and successfully transferred into commercial manufacturing.

The Nuclear Fuels Group in Bhabha Atomic Research Centre, India contributed a paper on microstructure improvement for conventional and advanced U-Pu, Th-Pu and Th-U fuel. Advanced manufacturing processes like Low Temperature Sintering and the microsphere impregnation technique have been developed and realized for more economic fabrication. All modern methods for tailoring fuel for high burnup targets and improved performance have successfully been applied, including:

- High grain size by microdoping;
- Choice of special pore formers for optimized pore size and structure.

The adaptation of pellet microstructure for future demands was also the objective of the paper presented by Ulba Metallurgical Plant, in Kazakhstan. The use of additives for enhanced grain growth and pore former material with well-defined properties was investigated and realized in manufacturing. Special emphasis was put on revealing the mechanisms of pore and grain boundary interaction and their influence on final microstructure.

Some of the contributions gave specific aspects of single manufacturing processes. There is the development of a sophisticated way for co-precipitation of U-Pu and U-Gd, which has been performed in Argentina. A theoretical approach based on FEM calculation, for better understanding the mechanisms of compaction UO_2 powder during pressing has been presented by French participants; goal is to have a more economic pressing/grinding process mainly in MOX production.

A main objective in MOX fuel design for the FBR prototype Monju in Japan was to reduce fuel swelling in order to better control and minimize the pellet cladding mechanical interaction. A robust process for manufacturing fuel with low density has been developed by choosing new types of pore formers and by adapting powder transfer and granulation process.

Two papers were presented by Russian authors. In the first of them, a very comprehensive overview on the work done for introducing reprocessed uranium into the WWER fuel cycle was given. Neutron physical considerations for compensation the ^{236}U isotopes were necessary as well as new analytical methods and an adaptation on the manufacturing process. The positive irradiation experience collected up to now has been summarized. In the second paper, the measurement of all thermo-mechanical and thermo-physical properties of U-Gd fuel which are necessary as basis for fuel rod design have been presented.

Summarizing this session, one can say that the subjects reported here did cover a wide range of fuel types and, hence, a big variety of fabrication processes; all of them provide good examples of the specific use of application. Therefore, it is not possible to state that manufacturing processes are converging, but that is only for the technology itself. The targets for product development are similar everywhere, with improved fuel characteristics for high burnup required. In practice this means fission gas retention and lower PCI risks, and the manufacturing technology has to provide the means to realize these goals.

Recommendation for future work:

- To improve the fuel microstructure by continuing developments to increase grain size by fuel doping and control porosity with new types of pore formers.
- The main challenge with the doped fuel is the manufacturing technology, especially the dispersion of the dopant in the fuel and keeping it there during sintering is an important issue.

3. SESSION 2: UO_2 , MOX AND $\text{UO}_2\text{-GD}_2\text{O}_3$ PELLETS WITH ADDITIVES

Six papers were presented in this session, which dealt mainly with the technological advances attempted in doping of fuel pellets with the primary objective of obtaining larger grains. While most of the papers gave an account of the experimental studies on addition of various dopants in different fuel materials, some of them outlined the behaviour of such pellets at sintering process.

Westinghouse Atom, Sweden, in its paper, summarized a comprehensive study of various dopants that resulted in selection of Cr_2O_3 as candidate additive. This doping technology demonstrated the feasibility of obtaining pellets with high densities (typically 10.67 g/cm^3)

and larger grains (30–45 microns), which in turn yields higher uranium weight per fuel element and reduces the release of fission gas and volatile fission products. The paper also brought out the examinations performed to verify the irradiation behaviour of doped pellets, both out-of-pile and in-pile, that indicated superior performance even under power ramps. These pellets, with improved pellet corrosion resistance, indicated lower uranium leaching in case of in-core failure of fuel rod.

The study of densification behaviour of titania (TiO_2) doped UO_2 pellet was the main objective of the paper presented by KEPCO, Republic of Korea. The densification behaviour was investigated by annealing titania doped pellets, and also kaolin doped pellets for comparison, at 1700°C for 48 hours. The decrease in sintered density of titania doped pellets observed during resintering was attributed mainly to pore morphology (spherical shaped pores) that have more resistance to heat energy for moving and hence resulted in pellet swelling.

KAERI, South Korea brought out in its paper that when sintering is carried out in reducing atmosphere, there will be no difference in grain size of UO_2 pellets prepared from powders produced from three different routes – Ammonium Diuranate (ADU), Ammonium Uranyl Carbonate (AUC) and Dry Conversion (DC). However, in the slightly oxidising sintering atmosphere, the grain size increased considerably for the pellets made out of ADU- UO_2 powder while the pellets of AUC and DC origin showed no effect in the grain size. The presence of phosphorus in ADU- UO_2 powder as an impurity is believed to be the main driving factor for obtaining large grained (25 microns) structure, which the investigators proved by preferentially adding phosphorus to AUC- UO_2 powder, which also resulted in larger grained pellets when sintered in slightly oxidising atmosphere.

The Institute for Nuclear Research, Romania focussed on its programs of obtaining large grain sized UO_2 pellet by adding dopants like 1% Nb_2O_5 , Cr_2O_3 and TiO_2 . The paper also focused on sintering of $(\text{U,Th})\text{O}_2$ pellets produced by blending of UO_2 and ThO_2 powders. Characterisation of these pellets was established through sintered density, microstructure and technological parameters. Through mechanical testing of both the types of pellets, using radial compression technique, correlations were established between strength and dopant conditions and also the temperature. In the case of $(\text{U,Th})\text{O}_2$ pellets, the reduction in mechanical strength is observed when UO_2 concentration is increased.

The investigations carried out by Department of Nuclear Materials, Brazil to study the effect of additives on the sintering kinetics, confirmed the role of additives like $\text{Al}(\text{OH})_3$, SiO_2 , Nb_2O_5 and TiO_2 as sintering aids in improving sintered density of $\text{UO}_2 - 7 \text{ wt}\% \text{ Gd}_2\text{O}_3$ pellets. While the first three additives reduced the sintering barrier intensity and shifted it towards higher temperatures, TiO_2 totally suppressed the sintered barrier thus resulting in highest density. The characterisation of the above mechanisms through SID method indicated that the activation energy of TiO_2 doped pellets remained constant while it sharply increased for pellets with other additives. The kinetic parameter values for TiO_2 doped batch were observed to be systematically higher than those for the others, confirming that the TiO_2 addition promoted more effective sintering mechanism.

Yubin Nuclear Fuel Element Plant, China investigated the addition of U_3O_8 from grinding sludge to promote grain size as also the effect of other additives like Al_2O_3 and SiO_2 . The experiments conducted in several batches confirmed the role of U_3O_8 from grinding sludge as a useful grain size promoter when added in the range of about 5 wt%, which also incidentally reduced production cost and helps in utilising waste.

At the whole, the session was devoted to discuss various techniques developed for doping different fuel pellets like UO_2 , $(\text{U,Th})\text{O}_2$ and $\text{UO}_2\text{-Gd}_2\text{O}_3$ with Al_2O_3 , TiO_2 , SiO_2 , Cr_2O_3 , MgO , $\text{Al}(\text{OH})_3$ and Nb_2O_5 . The technology is being developed with the primary objective of enlarging grain size of the pellet to reduce Fission Gas Release (FGR) and PCMI and thus improve fuel performance up to high burn-ups. Depending upon the state of the UO_2 fuel development in each country, suitable R&D programmes have been initiated by respective States to implement the fuel pellet doping technology. The investigations carried out so far reveal the fabrication feasibility of fuel pellets with as larger grains as $48\ \mu\text{m}$ and with densities in the range of $\sim 96\%$ TD.

Issues to be understood/solved:

Though the technology of doping fuel pellets is showing promising results with respect to enhancing densities and enlarging grain size, the following points need to be addressed to, in order to take this technology from lab-scale to mass-scale fuel production shops:

- Develop an improved understanding of the mechanism of grain enlargement and density improvement due to the addition of dopants;
- Develop confidence in in-pile behaviour of doped fuel with respect to fission gas retention without swelling.

Recommendations for future work:

- Because some of the R&D programmes on doping of fuel pellets have already been shifted from laboratory to out-of-pile testing and to in-pile testing, it is expected to understand the mechanism of grain size enlargement due to doping and its effective contribution in reducing FGR. For this purpose, the programmes could be directed to carry out the following further works:
- Develop comprehensive modeling to predict quantitatively the retention of fission gases in large grains of different sizes obtained from various dopants;
- Develop data base for quantitative measurement of reduction in FGR from fuel with large grains and compare the FGR from normal fuel;
- Carry out similar studies for severe power ramp conditions to ensure the high performance of large grained doped pellets.

4. SESSION 3: FISSION GAS RELEASE FROM FUEL PELLETS UNDER HIGHBURNUP

(1) Advanced nuclear fuel development by Framatome-ANP, CEA and COGEMA is focusing on high burnup extension and greater plant maneuverability. Technically, this translates into the objectives of reducing fission gas release and improving the fuel viscoplasticity (PCI improvement). Both goals can be met by doping the UO_2 fuel with Cr_2O_3 . Cr_2O_3 doped fuels develop substantially larger grains ($>60\ \mu\text{m}$) with much higher creep rates ($> 10 \times$ at $T = 1500^\circ\text{C}$). Five irradiation cycles in a commercial reactor are completed and post-irradiation results after 2 cycles including transient tests under the most stringent PCI conditions (rod burnup $\cong 30\ \text{GWd/tM}$) have been performed.

The fuel rod behavior during base irradiation is identical to standard rod behavior regarding rod elongation and ridging, doped fuels showed slightly more overall clad deformation. The two available transient tests show substantially less fission gas release and improved resistance to PCI failure compared to standard UO_2 fuels (cause: no further primary ridging). Similar to UO_2 fuel development, the MOX development plans are aiming to achieve

discharge burnup of ~60 GWd/tM. Regarding fuel development, this will need a reduction of FGR. This is to be achieved through a modification of the MIMAS process itself with the development of more homogeneous Pu distribution and by the development of doped fuels. At the present stage, different fabrication routes and dopants are still being considered. In pile experimental research is already launched but no data are available yet.

(2) CEA, in collaboration with Framatome-ANP, showed the results of analytical laboratory and in-pile and post-irradiation test of an experimental matrix of fuel compositions that envelopes the industrial development of Cr₂O₃ doped fuel. The main objectives of these tests is to provide an analytical test basis for understanding the mechanisms leading to reduced fission gas release through dopants. The general tendencies of the effect of Cr₂O₃ doping are confirmed in a broader test matrix where also other dopants (Al₂O₃, SiO₂) were involved. Separate effect tests included an assessment of fabrication conditions (especially sintering atmosphere influence).

Detailed microscopic investigations of gas bubble distribution after isothermal anneal tests were used to address the mechanisms of release. Intragranular bubble nucleation and trapping sites (precipitation of excess Cr₂O₃ over solubility limit) are seen to be the key mechanism for reducing gas release rather than grain size as such. Even larger gas retention capacity can be obtained with improved intergranular retention by SiO₂ addition to Cr₂O₃. Additional analytic/modeling work would be needed to come to a complete understanding of the indulging mechanisms in the complex process of gas mobility.

Remarks on 1+2:

- Mechanisms of Cr₂O₃ in PCI and FGR reduction are demonstrated but not completely understood,
- Role of oxygen potential during sintering is not completely understood.

(3) CEA and EdF showed results of analytic tests on FGR out of 4 cycles standard UO₂ fuel in isothermal anneal experiments relevant to LOCA conditions (1000°C < T < 1600°C). The experimental tests included short-term low power re-irradiation in MTR conditions to replenish the matrix with short living isotopes (¹³³Xe). By making use of difference measurements, it becomes possible to distinguish the release of intergranular and intragranular gas. The experiment showed in an elegant way that in short-term anneals, only the intergranular gas fraction is released. With the modified version of the METEOR code, the complete mechanism of Fission Gas Release was calculated. Both the fraction of the intergranular gas that was released during an isothermal anneal and the pre-release gas distribution in intergranular locations could be modeled. On the basis of the faithful reproduction of release kinetics in these isothermal anneal experiment, it was concluded that the mechanisms for FGR in LOCA conditions are sufficiently understood. Some remarks were made about the fact that the present tests concerned axially unconstrained samples and that the calculation is essentially one dimensional. This situation is conservative with respect to real LOCA conditions where the fuel is constraint both radially and axially. It was repeated that the present tests concern analytic laboratory scale tests and that the calculations nor the experiment are geometrical representations for true LOCA conditions.

Remark on 1+2+3:

- Fuel developments for improved high burnup performance need industrial, analytic & safety research that go hand on hand. This session included input from all these aspects of fuel research.

Recommendations for future work:

- Further strengthening interactions industry – R&D – safety research;
- Underlying, fundamental research will be needed for more understanding of the mechanisms of Cr₂O₃ doping. This is important for predicting irradiation performance;
- The session demonstrated collaboration between fuel vendor, utility and research institutes. More initiatives like this are welcome;
- Separate effect tests (paper 2) focus on FGR mechanisms. Similar efforts of detailed research on viscoplastic behavior could be launched;
- Effect of grain size on High Burnup Structure development should be further investigated.

5. SESSION 4: EVOLUTION OF FUEL PELLET STRUCTURE AND THERMAL PROPERTIES AT HIGH BURNUP

The two first presentations of this session give good examples of international cooperation on R&D on nuclear fuel, through two European programmes: The MICROMOX programme and the OMICO programme. The first one is focused on the important issue constituted by the Fission Gas Release level at high burn-up, and the second one deals with in-pile behaviour of innovative mixed oxide (MOX) microstructures (U-Pu, but also Th-Pu) at low and intermediate burn-up. Both programmes associated fuel vendors and/or utilities, and research centers, through separate effect experiments in Material Test Reactor and in hot cell laboratory. Main advantages of this kind of common programme are:

- to elaborate several fuel microstructures, representative of current, improved fuels or innovative fuels, for power reactors, or fuels suited to be tested through separate effect experiments;
- to compare these microstructures in the same irradiation conditions and with the same measurement means;
- to develop on-line measurement techniques adapted to short samples, and to equip the samples with instrumentation;
- to implement an experimental protocol permitting to assess closely evolution of key parameters, e.g. central temperature of the fuel, internal pressure of the rod. Interest is to be able to point out unexpected evolution or cliff-edge effects, which could lead to an evolution of current safety criteria;
- to provide code developers with reliable input data, with the associated condition to reduce the uncertainties at a minimum value;
- to enhance cross-fertilization between teams involved in these common programmes, through definition of a unique experimental protocol, and use of in-pile or PIE measurement means at their best possibility;
- to improve codes development permitting :
 - to pre-calculate the experiment and to design the sample and the sample-holder;
 - to simulate the performed experiment with adjustment of data on physical models used by the codes;
- to implement out-of-pile or in-pile mock-ups to assess a specific parameter influencing the fuel behaviour during the real experiment (e.g. gamma heating).

These technical considerations show clearly all the interest to develop this kind of separate effects experiments and to implement them in an international frame. This permits also to share the costs. So with this approach, the number of integral tests in MTRs should be reduced at a minimum.

5.1. The Micromox Programme

The first paper describes the MICROMOX European Programme, started in October 2000 in the frame of the fifth Framework Programme. The main aim of this programme is to identify and to quantify the mechanisms, which could provoke an increase of Fission Gas Release (FGR) for MOX fuel at high burn-up, compare to the corresponding values normally observed with high burn-up UO₂. FGR is considered as an important safety issue, limiting the lifetime of the fuel in power reactor, both for normal and accidental conditions. Four different fuels are considered in this programme:

- Homogeneous MOX fuel with large grain size, that is expected to have a better gas retention capability;
- MOX fuel showing an uniform Pu distribution at microscopic level and a standard grain size;
- MOX fuel showing an inhomogeneous Pu distribution and a standard grain size, that probably has a lower gas retention capability;
- UO₂ fuel of standard characteristics, used as a reference.

These fuels are loaded in instrumented rodlets and are irradiated since October 2003 at moderate rating in the high Flux reactor (HFR) to achieve a burnup of 60 GWd/tm in 2 years. All along the irradiation, the central temperature and inner pressure evolution are recorded. The end of the irradiation consists in a temperature transient in which the fission gas release is followed as a function of fuel temperature. Post-irradiation examinations of fuels will be made, focusing on fission gas release and fuel microstructure. The behaviour of the irradiated fuels will be simulated by different codes dedicated to the in-reactor fuel thermal-mechanical performance.

Several mechanisms are probably involved in parallel in the release of gases:

- local neutronic spectrum;
- peripheral neutronic absorption;
- size of the UO₂ grains and of the Pu agglomerates;
- heterogeneity of the microstructure.

However the real effect of some of these is not clear and shall be better understood. For example, if additives have a positive effect on the grain size, the expected decrease of the FGR is not confirmed experimentally by some literature reports. Moreover modelisation of Fission Gas Release in heterogeneous microstructures, such as MOX fuel, appears as extremely complex, and needs a robust database to improve the models. For all these reasons, achievement of a separate effect experiment specifically devoted to FGR presents an undoubted interest. As the beginning of the irradiation phase is very recent, irradiation results are still not available.

5.2. The Omico programme

This presentation gives an overview of the objectives and status of the "Oxide Fuel — Microstructure and Composition Variation" (OMICO) project. It studies and models the influence of microstructure and matrix composition of MOX and (Th, Pu)O₂ pellets on fuel behaviour in Pressurised Water Reactor conditions. There are three fuel composition (UO₂, (U-Pu)O₂ and (Th,Pu)O₂ each with two microstructures (homogeneous and fine dispersed ceramic-in ceramic, which are prepared using the sol-gel method and the heterogeneous fuels are prepared by powder metallurgical routes.

The project is divided in six work packages, including detailed design of the experiments, fuel fabrication and instrumentation, irradiation experiments in BR-2, out-of-pile non-destructive post-irradiation tests and benchmarking of fuel performance code. The OMICO project started in October 2001. During the first two years of the program execution, the detailed design and fuel production were completed. The start of the irradiation is foreseen in March 2004. On the theoretical side, the first benchmarking exercise between three fuel performance codes (Transuranus, Copernic and Femaxi-V) was performed. The code calculations show good correspondence between all three codes regarding the UO₂ fuel rods, but more important discrepancies for both mixed oxide fuels (U,Pu)O₂ and (Th,Pu)O₂. However, the fuel performance calculations predict systematic higher temperatures for:

- (U,Pu)O₂ fuels as compared to UO₂ (despite of lower linear heat rates for MOX);
- MIMAS-type fuels as compared to sol-gel type fuels.

That is why, fuel modeling in general follows two main directions: development of models for individual fuel properties (such as thermal conductivity, heat generation profile, radial burnup distributions, isotope in-pile depletion/burning and build-up and development of integral tools. One of them is MACROS code.

In the course of the design optimisation process of experimental programs, calculations with different fuel performance codes showed limitations when confronted with off-standard fuels and/or irradiation conditions. The fourth paper in this session presented the development of the fuel performance code “Mechanistic Analysis Code for Reactor Oxide Systems” (MACROS), that addresses the recognised limitations of standard codes to cope with such non-standard fuels and/or irradiation conditions.

The MACROS code is based on multi-scale mechanistic approach. It was used for calculations fission gas release phenomenon for quasi-homogeneous and fine-dispersed uranium dioxide MOX fuels, irradiated in BWR conditions. It's known that neutronic effects determine non-uniform power generation and burnup distributions both in radial and axial directions. The MACROS code was designed with sufficient flexibility to account for either fast or thermal spectra. As neutronic subroutine is the most fundamental part of a fuel behaviour code MACROS, a special attention has been paid to description of the fuel isotopic composition (heavy nuclei, fission products and helium) and of the irradiation conditions (PWR, BWR, FR and ADS).

The last paper of this session is devoted to image analysis techniques for MIMAS MOX microstructure. A better understanding of MOX fuel in-pile behaviour requires a very detailed characterisation of the Pu distribution in the matrix before and after irradiation. Electron Microprobe Analysis (EPMA) can be used to determine elemental distributions with a spatial resolution of 1 μm. Quantitative EPMA investigations are generally performed along a straight line (linescan). This paper describes the development of X-ray microanalysis techniques to produce semi-quantitative “maps” of plutonium concentrations in order to characterise, in a short time, and with reasonable accuracy, large areas of fuel microstructure (1 mm²). An original segmentation technique is then proposed, based on statistics, in order to finely describe the MIMAS MOX fuel microstructure.

Concerning image analysis techniques, the use of the notion of domains with homogeneous properties appears to be a valuable approach to allow the comparison of different microstructures. The tools developed thanks to this approach can deliver characterizations of interest at the same time to qualify modifications to the fabrication processes, but also to feed

computer simulation processes. Finally, the phase of intermediate Pu concentration (called “coating phase” in the article) shows a great complexity. As it may contain a large portion of the plutonium introduced in the pellet, a better understanding of its structure (morphology, variations of the plutonium concentration...) would be appreciated.

Recommendations for future work:

- Technical considerations show clearly all the interest to develop this kind of separate effects experiments and to implement them in an international frame. This permits also to share the costs. So with this approach, the number of integral tests in MTRs should be optimized;
- The ability to characterize irradiated fuels with the same PIE techniques and tools as for fresh fuels is an interesting option that has to be further explored (more results on 2 cycles irradiated fuels, results on 3 and 4 cycles irradiated fuels);
- Heterogeneous microstructures need experimental tools adapted to multiphase systems and further development of mechanistic codes;
- There is a need for improving knowledge on helium behaviour in irradiated fuels and He out-of fuel release.

6. SESSION 5: PELLETT-CLADDING INTERACTION (PCI)

Fuel pellet cladding interaction (PCI) appears to be a complex phenomenon that may lead to cladding failure and subsequent release of fission products into the reactor coolant. Research efforts to understand better the PCI phenomenon and minimize it with design solutions are necessary. This session comprised four papers.

Impact of fuel microstructure on PCI behaviour has been investigated to understand and model the PCI rod behaviour. An experimental program with different kind of pellets and different rod burnups has been performed by CEA, EDF and FRAMATOME-ANP and experimental results revealed that the kinetics of the phenomena are different for each kind of pellet. It seems that there is an influence of the pellet cracking pattern on the stress induced in the cladding. Post-calculations of these experiments have also been performed by finite element modeling. Fuel creep enhancement and cracking pattern can both contribute to improve PCI behaviour.

A model for analyzing the mechanical behaviour of LWR fuel rod under the operational conditions that covers a contact analysis method during pellet cladding mechanical interaction has been developed by KAERI. This model has been validated by comparison with commercial codes at different LHGR and at different frictional coefficients.

Studies on the effects of various kinds of additives on the creep behaviour performed by VNIINM, MPhI, TSC TVEL and the Institute of Reactor Materials revealed that uranium dioxide fuel doped with Al-Si-Nb shows promising results of lowering the strain resistance due to intergranular precipitates of low shear resistant phases and formation of solid solution. Based on the stress and creep results from a number of in and out-of pile tests, it might be expected an enhancement of PCI resistance by the use of doped uranium dioxide pellets. Important that some experiences with extra large grain size pellets indicated that these pellets may be brittle and could produce some manufacturing problems. It seems that a maximum grain size around 50 μm may avoid these manufacturing problems, even though there are not enough data to assure it. An optimum grain size may allow to increase burnup without increasing stress level of the cladding.

SCK-CEN performed a detailed EPMA investigation on the bonding layers in high duty fuels. Various new sub-layers such as Zr-Cs-O and U-Cs-O were identified on high duty UO₂ fuels. Microstructural analysis results show the good bonding with amorphous and viscous layers between cladding and fuel. Separate effect tests performed to reproduce the interaction between cesium and Zircaloy confirmed the formation of the Cs-Zr-O interaction layers at low oxygen potentials.

Issues to be understood/solved:

- During the discussion, considerable attention was given in the topical meeting to the difficulties predicting PCI behaviour using calculations, due to irradiation effects. More data on fuels with lower concentration of dopants are needed to improve the understanding of the basic mechanism of the dopants in the pellet performance.

Recommendations for future work:

- Pellet and cladding behaviour modelling has to remain on a continuous effort, relying on both empirical correlation and first principles. Additionally, continuous efforts should be made related with the additives, considering manufacturability, creep behaviour and fission gas release behaviour.

7. FINAL REMARKS/CONCLUSIONS BY P. BLANPAIN AND M. LIPPENS, CHAIRMEN OF PANEL SESSION

- A large amount of data and information has been exchanged during the meeting. Abundant ideas and results were reported regarding use of dopant elements and impact on fuel properties;
- Relevant data about in-reactor performance are still missing, not allowing today convergence towards an optimum additive and associated fabrication technology;
- Last but not least, significant improvements in fuel fabrication technology were presented. Those improvements allow fabricating pellets with a higher productivity and better in-reactor performance.

OPTIMIZATION OF FUEL FABRICATION TECHNOLOGY
PRACTICES AND MODELLING

(Session 1)

Chairpersons

Yu. BIBILASHVILI
Russian Federation

W. DÖRR
Germany

RECENT DEVELOPMENTS IN DESIGN AND MANUFACTURE OF URANIUM DIOXIDE FUEL PELLETS FOR PHWRs IN INDIA

R.N. JAYARAJ, C.GANGULY
Nuclear Fuel Complex,
Department of Atomic Energy,
Hyderabad, India

Abstract

Nuclear Fuel Complex (NFC), an industrial unit of the Department of Atomic Energy, has been manufacturing over the past three decades, natural and enriched uranium oxide fuels for all the water-cooled nuclear power reactors in India. So far, more than 275,000 natural uranium oxide fuel bundles have been manufactured for the twelve operating Pressurised Heavy Water Reactors of 220MWe type (PHWR 220). Likewise, nearly 2,700 enriched uranium oxide fuel assemblies of the 6x6 type have been manufactured for the two operating Boiling Water Reactors of the 160MWe type (BWR 160). Over the years, several technological improvements were carried out in the UO_2 pellet production processes and in evolving fuel pellet designs for PHWRs. The PHWR fuel pellet design adopted earlier consisted of cylindrical shape with length by diameter ratio in the range of 1.2. The pellets had a flat surface on one end and a dish on the other. Through systematic analysis of various design parameters, in-reactor performance and production related factors, the design of fuel pellets were standardized by introducing edge chamfer and double dish on both ends for regular production. Similarly, innovative changes were brought-in in the pellet production lines, which include – production of UO_2 granules through roll-compactor instead of hydraulic presses; adoption of Admixed Solid Lubricant (ASL) route for granules over liquid die-wall lubricant followed earlier; use of high performance tooling for pellet compaction, etc. All these modifications have enhanced productivity & recovery and has improved the pellet integrity, which in turn led to better in-pile performance. Modifications have also been made in fuel element fabrication. Earlier, uranium oxide fuel pellets used to be loaded in graphite coated zircaloy 4 cladding tube and encapsulated. Next, zircaloy 4 bearing and spacer pad appendages were ‘resistance-welded’. In the modified route, the bearing and spacer appendages are first welded on the fuel cladding tube followed by graphite coating, pellet loading and encapsulation. Thus, the number of process steps after the fuel pellets are encapsulated are kept to the minimum thereby ensuring pellet integrity. The modified route also facilitates easy retrieval of UO_2 fuel pellets from defected fuel elements. The present paper highlights the improved fuel pellet design and manufacturing route for ensuring higher productivity & recovery and better in-pile performance.

1. INTRODUCTION

Nuclear Fuel Complex (NFC), Hyderabad is solely responsible for manufacturing of natural and enriched UO_2 fuel pellets and zirconium alloy clad fuel assemblies for all the operating power reactors and forthcoming PHWRs in the country. NFC has, in close coordination with Nuclear Power Corporation of India Ltd. (NPCIL), developed fuel pellets of different designs. The pellets are produced from nuclear grade UO_2 powder derived through ammonium diuranate (ADU) precipitate route following the standard “powder-pellet” techniques involving pre-compaction & granulation, cold pelletisation and high temperature ($1700^{\circ}C$) sintering followed by wet centreless grinding to produce high density pellets of uniform diameter. NFC has been self-reliant in upgrading the process technology and during the recent years, key developments have been accomplished in the production line that have resulted in significant improvement in equipment productivity, process-yield and in-reactor performance of the fuel. The major contribution has been derived from the following areas of developments:

- (i) Introduction of new pellet designs;
- (ii) Utilisation of different fuel pellet materials;
- (iii) Innovation in pellet production processes.

Through these developmental efforts, the plants are able to achieve a steady improvement in the process yield resulting in enhanced level of production of fuel bundles.

The following sections of the paper highlight various aspects of the above developments.

2. PELLETS DESIGNS FOR PHWRs

The fuel bundle for PHWRs is designed for maximum content of fissile material and minimum content of parasitic absorption material for operating at Linear Heat Ratings (LHR) of 57.5 kW/m and to a burnup of 15,000 MWD/TeU. As natural uranium is used as fuel, special emphasis is placed on neutron economy. Thus for increasing the natural uranium content in the fuel element and providing support to the collapsible clad, the pellet is designed for high density in the range of 95 – 98% of the theoretical density.

2.1. Pellet shape

For PHWR fuel element having collapsible clad, the pellet geometry influences the sheath stresses. A software package was developed by NPCIL for carrying out theoretical analysis to find out the deformation pattern of various pellet shapes and consequent sheath stresses/strains during fuel bundle operation in the reactor. The different pellet shapes checked are flat pellet with single dish, single dish with edge chamfer and double dish chamfered pellets. The pellet ridge heights and sheath stresses for various pellet shapes have been found out and compared. It was found that the double dish and chamfered pellet geometry gives the lowest stresses compared to any other designs.

The pellet land width and the dish radius influence the occurrence of maximum temperature on the land, which dictates the axial gap requirement within the fuel element. From the pellet fabrication point of view, the slight increase in land width was found essential for introducing the edge chamfer. This in turn required increase in axial gap in the element by reducing the stack length of uranium dioxide pellets. In the first stage, the pellet shape was changed from single dish flat type to chamfered type and fuel bundles manufactured with this pellet design were successfully irradiated in the power reactors. The chamfer is expected to reduce circumferential “bamboo ridge” formation of fuel elements during its operation in the reactor. However, chamfer has an effect on the land width and axial gap. As the maximum temperature is at the centre of the pellet, plastic region of UO_2 vary along the radius of the pellet. To allow the free expansion of UO_2 plastic region, dish radius of the pellet has been kept more than the radius of the plastic region. The dish radius edge is elastic and will have maximum temperature in land width. So, the linear expansion of the stack is controlled by the radius of the dish and hence the axial expansion at the dish edge dictates the axial clearance in the fuel element. Thus the final dimensions for the dish radius and the land width were finalised with the help of special softwares developed for this purpose which takes into account the LHR and diametrical clearance between the pellet and sheath inner diameter. The temperature profile of the fuel at the dish radius for 19-element fuel bundle for different LHRs and diametrical clearances are depicted in Fig.1. Based on the above analysis, 1 mm land width was finalized, which ensures the required axial clearance of 1.5 mm for 19-element fuel bundles.

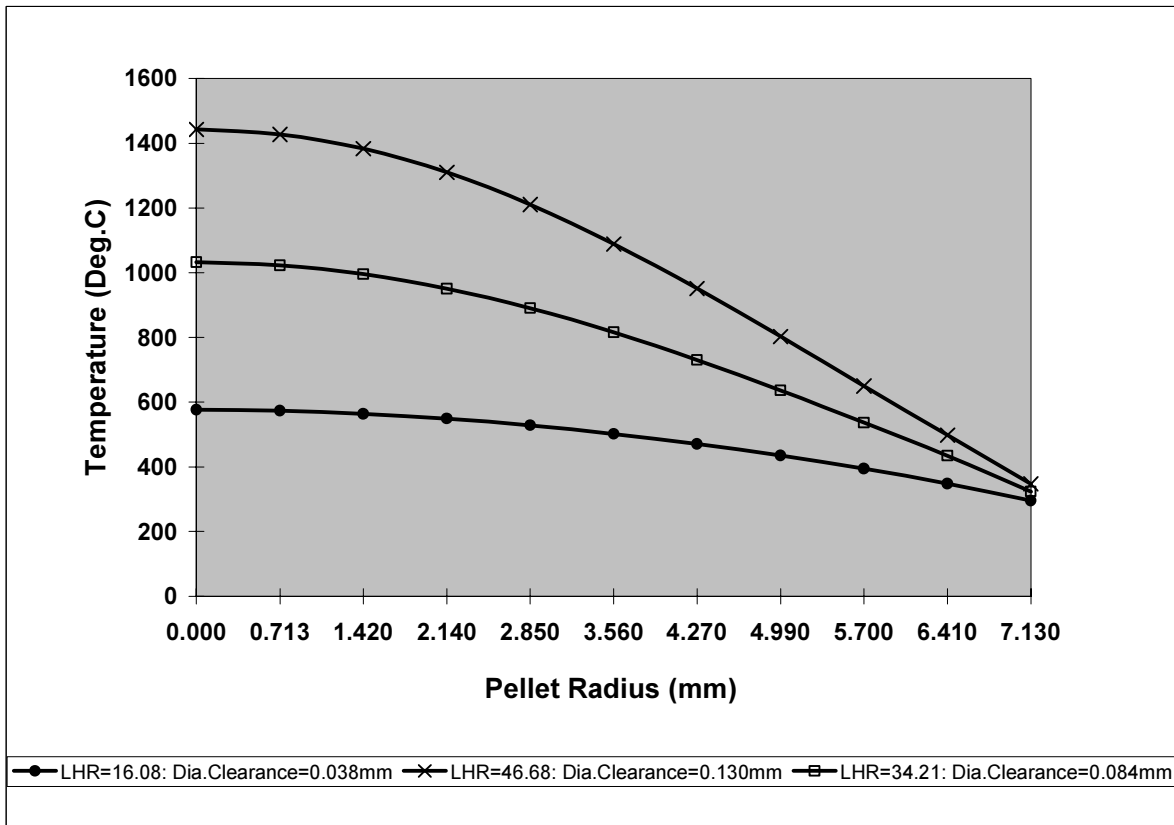


FIG. 1. Fuel Temperature along Pellet Radius for 19-Element Bundle.

In the second stage, based on the feedback of single dish chamfer type, the design of pellet was changed to double-dish chamfered shape, which is presently employed for regular production of fuel bundles for all the PHWRs in India. The salient features of different pellet shapes employed for Indian PHWRs is shown in Fig. 2. The introduction of the double-dish pellets has also reduced the necessity of handling each and every pellet on the shop floor for aligning the dishes in one direction before the pellet stack is loaded into the fuel tube.

2.2. Pellet Dimensions

For neutron economy, the wall thickness of zirconium alloy fuel sheath for PHWR fuel is kept to the minimum that lead to “collapsible” cladding. Hence, the pellets are centreless ground to ensure the diametrical clearance in the range of 0.05 – 0.13 mm. Higher length to diameter (L/D) ratio would result in density gradients within the pellet which can lead to hour glassing of pellets, higher ridge height in the sheath at inter-pellet locations. Hence, the pellet L/D ratio is maintained in the range of 1.0 to 1.1.

The pellets are dished at both the ends to provide allowance for thermal expansion of the hottest central region. It was estimated that the centre of the fuel pellet operating at \dot{q} of 40 W/cm will expand by 0.025 m/m of pellet length and hence a minimum dish depth of 0.25 mm has been provided.

A chamfer of about 10° with respect to flat surface of the pellet is provided at both the ends to reduce pellet-cladding interaction (PCI) in the reactor operation and also to reduce end chipping during pellet manufacturing.

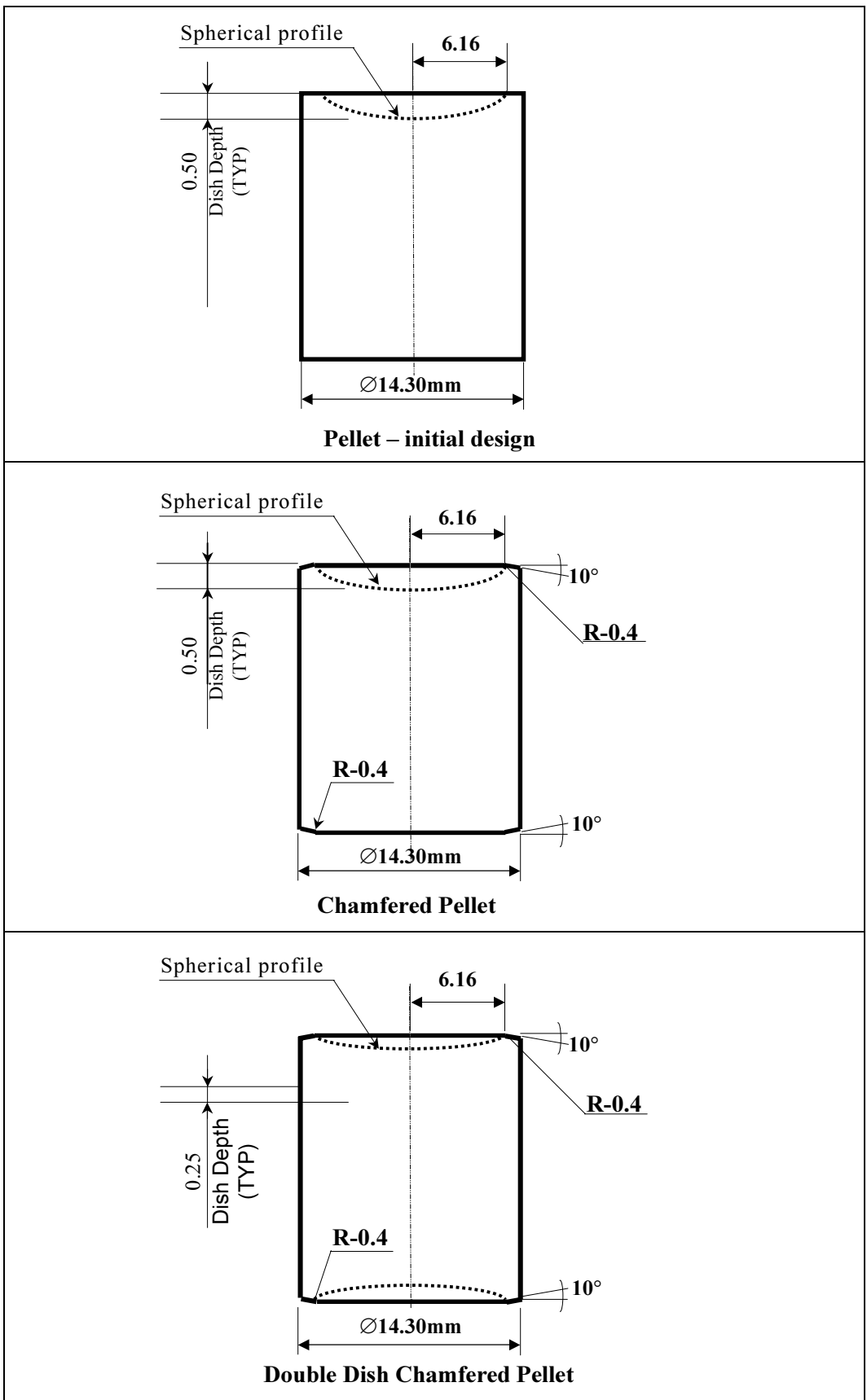


FIG. 2. Natural Uranium Oxide Pellet Designs for 19-Element Fuel Bundles.

2.3. Pellet Density

PHWR fuel bundle is designed for maximum content of fissile material. Accordingly, the density of the fuel pellets for PHWRs is maintained in the range of 10.45 g/cm³ to 10.75 g/cm³. The lower range of the density is specified keeping in view limited fissile content in natural uranium, possible in-reactor densification and consequent ridge formation by sheath collapse due to increased diametral gap.

3. NEW FUEL PELLETT MATERIALS FOR PHWRs

The average fuel burnup in PHWRs is about 6,700 MWD/TeU. In order to achieve higher burnups, it is envisaged to introduce new fuel cycles with Mixed Uranium Plutonium (MOX) pellets. Also a programme is initiated for utilisation of depleted uranium in the initial and equilibrium cores of PHWRs [1] for which special loading patterns of depleted uranium oxide bundles are evolved. In the recent years, some 1500 depleted UO₂ bundles were loaded in the initial core of Madras Atomic Power Station (MAPS-2). Similarly, some 2,200 depleted uranium oxide bundles are proposed to be loaded in the initial core of the forthcoming PHWR 540 unit at Tarapur.

3.1. Fabrication of depleted uranium oxide fuel

After reprocessing the spent PHWR fuel the depleted uranium material in the form of Ammonium diuranate (ADU) powder is received from Bhabha Atomic Research Centre (BARC). Unlike for the production of natural uranium oxide powder from Magnesium diuranate starting material, this DU material is not subjected to wet processing that involves dissolution, solvent extraction and precipitation but is taken directly for dry processing by subjecting it to air calcination followed by hydrogen reduction and stabilization. It was found that whenever the as received ADU contained larger and harder lumps of the material, it resulted in coarser depleted UO₂ powder, which after cold pelletisation, sintering and grinding showed pits in the unacceptable range. For such lots, the powder was subjected to re-oxidation and re-reduction to obtain the particle size of the DU powder in the acceptable range. The process flowsheet for the production of depleted uranium oxide powder is shown in Fig. 3.

The depleted uranium powder thus produced is converted into high density pellets by following conventional powder–pellet route involving precompaction, granulation, final compaction, high temperature sintering and centreless grinding. The DU pellets are then loaded into zirconium alloy clad tubes, which are encapsulated by following resistance welding techniques. These fuel elements are taken up for bearing and spacer pad weldings and 19 of such elements are assembled into specific configuration to manufacture fuel bundles for PHWR 220 units.

3.2. Fabrication of MOX fuel bundles

Utilisation of higher fissile content fuels like MOX in existing PHWRs required careful analysis due to limitation in the bundle power and channel power. NPCIL, after detailed reactor physics analysis, has evolved a loading pattern of MOX fuel bundle in PHWR 220 [1]. The design of the MOX 7 bundle consists of seven inner fuel elements containing mixed uranium plutonium oxide pellets with 0.4% plutonium and twelve outer fuel elements containing natural uranium oxide pellets.

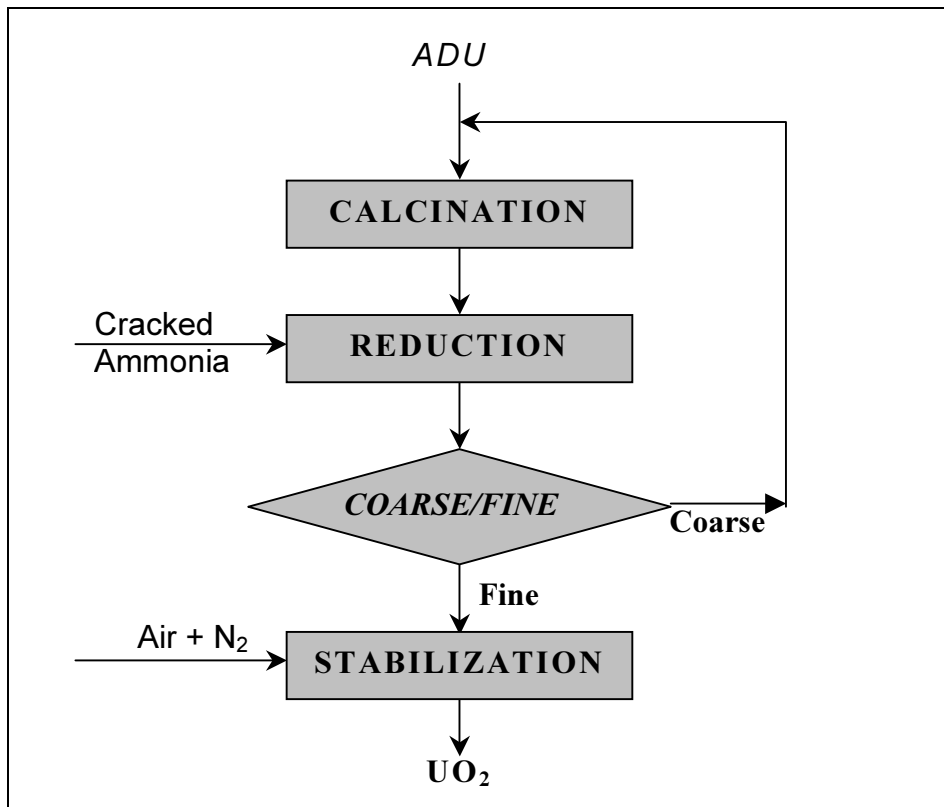


FIG. 3. Process Flow sheet for Production of Depleted Uranium Oxide Powder.

About 50 MOX fuel bundles have been manufactured by BARC in collaboration with NFC. The MOX fuel pellets were fabricated by co-milling the UO_2 powder and PuO_2 powder followed by pelletisation and high temperature sintering in hydrogen atmosphere. These pellets were used for fabricating seven inner fuel elements of the MOX fuel bundle.

4. IMPROVEMENTS IN PRODUCTION PROCESSES

4.1. Roll compaction & granulation

With increasing level of production targets, the lower productivity hydraulic pre-compaction presses were found to be a bottleneck in the production line. Plant took up the indigenous development of a Roll Pre-compactor with advanced designs. The general arrangement of the Press-components is shown in Fig. 4.

The following special features were incorporated in the press for pre-compacting UO_2 powder for production of uniform quality granules:

- Vertical arrangement of rolls;
- Screw conveyor for maintaining positive feed of powder to the rolls;
- Serrated rolls to produce powder flakes which yield granuals with better flowability;
- De-aeration of powder in the feed chamber to achieve better compaction;
- Adjustable roll gap with hydraulic system;
- Mechanization of powder handling through container.

The above advanced features of the press have resulted in development of a highly productive press. In addition, the roll press has helped in producing consistent quality granules, which in turn contributed to the production of superior quality pellets.

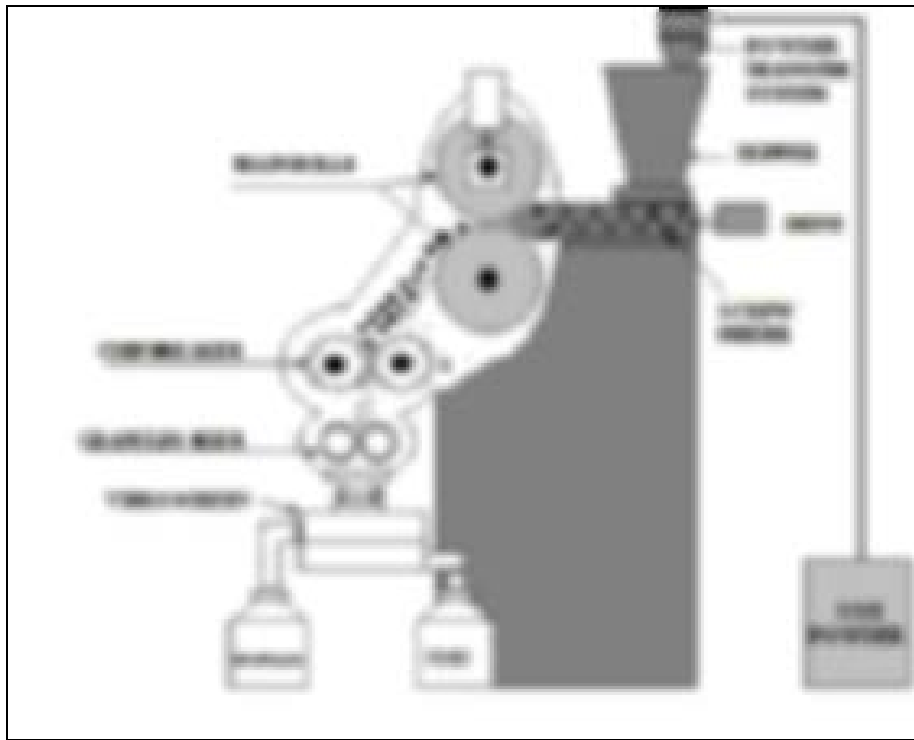


FIG. 4. Roll Compacting Press.

4.2. Development of admixed solid lubricant process route

Liquid die-wall lubricant for compaction of UO_2 pellets was found to be less effective in multi-die high productivity presses. The lubricant could not be pumped to all the dies uniformly even after continual developmental efforts resulting in either excess or inadequate lubrication of the dies. This led to increased amount of rejection of the pellets due to defects like chip and endcap.

Through systematic study, NFC has successfully developed and adopted Admixed Solid Lubricant route in place of liquid die-wall lubricant route. The admixing process was developed using ‘tumbling in-container’ to avoid powder handling in a separate blender. The process has been standardised with respect to method of lubricant addition in UO_2 granules, batch size, rotational speed of the cylindrical container and the blending time.

Initially, the admixed lubricant process was standardized using zinc-behenate/zinc-stearate lubricant. However, use of these metal containing lubricants led to many operational problems in sintering including boat stuck up mainly due to condensation of zinc in particulate form over the interior parts of the sintering furnace. Moreover, the zinc vapour is health hazardous. An alternative effective organic lubricant bearing no metal component that completely burns out only at 400°C was explored and adopted successfully by which the operational problems in sintering have been eliminated [2]. Additionally, use of this new admixed lubricant has resulted in increase of sintered density of UO_2 pellets, environment friendly emissions from the furnace.

4.3. Adoption of tungsten carbide press toolings

The compaction tool plays an important role for producing quality pellets. Tool material of lower Young’s modulus such as steel die undergoes greater extent of elastic deformation

during pressing. This leads to increased amount of residual stress on pellet on withdrawal of load resulting in initiation of defects in green pellet. Such dies also lack in adequate wear resistance leading to frequent tool replacements thus lowering the productivity of the press. High performance dies made of tungsten carbide were successfully developed indigenously and employed in place of steel dies. In the absence of wear in such dies, pellets of consistent quality with respect to physical integrity and diameter are being produced. However, steel punches were cryogenically treated for improving their performance. This development has helped in obtaining other important benefits like increase in tool life by 40 times thus reducing consumption of steel dies, reduce in tool change time, etc.

All the above developments together favoured a consistent higher level of pellet acceptance in the mass production of UO_2 fuel pellets compared to pellet acceptance before these developments were taken up.

5. CONCLUSION

Backed by three decades of nuclear fuel manufacturing experience, NFC has carried out several process improvements in the areas of UO_2 powder production, pelletisation and fuel bundle manufacturing for PHWRs. In coordination with Nuclear Power Corporation of India Ltd (NPCIL), several pellet designs were evolved and successfully taken up for mass scale production. In addition to natural UO_2 fuel bundles NFC has gained expertise in standardising manufacturing procedures for the production of fuel bundles with depleted uranium oxide material required for initial and equilibrium cores of PHWRs.

ACKNOWLEDGEMENTS

The authors are thankful to the Department of Atomic Energy, Government of India for permitting to prepare and present the paper at IAEA Technical Committee Meeting being held at Brussels, Belgium. Grateful thanks are also due to colleagues from NPCIL, especially Mr.S.A Bharadwaj and Mr P.N. Prasad who have provided valuable information with respect to pellet designs. The contributions made by Mr.G.V.S. Hemanth Rao and Mr.D. Pramanik in preparing the paper is highly acknowledged.

REFERENCES

- [1] GANGULY, C., "An overview of PHWR fuel in India", Candu Fuel (Proc. 8th Int. Conf. Honey Harbour, Ontario, Canada, 21–24 September, 2003), CNS, Toronto (in press).
- [2] PRAMANIK, D., et al., "Current Process Developments in Production of Natural UO_2 Green Pellets", (Proc. 8th Int. Conf. Honey Harbour, Ontario, Canada, 21–24 September, 2003), CNS, Toronto (in press).

FINITE ELEMENT MODELLING OF THE PRESSING OF NUCLEAR OXIDE POWDERS TO PREDICT THE SHAPE OF LWR FUEL PELLETS AFTER DIE COMPACTION AND SINTERING

G. DELETTE
CEA-Grenoble DRT/DTEN/SMP

Ph. SORNAY
CEA-Cadarache DEN/DEC/SPUA

J. BLANCHER
COGEMA

Abstract

Die pressing and sintering processes are extensively used in the fabrication of LWR UO₂ and MOX fuels. However, perfect cylindrical sintered pellets cannot be directly obtained by the current processes because slight heterogeneities of density are inevitably present in the green body as a result of frictional forces between powder and die. A cooperative program between COGEMA and CEA has been undertaken to improve the forming process in order to decrease diametrical scattering of sintered product. In this context, Finite Element Modeling (FEM) of the cold compaction stage has been used to simulate the die pressing stage of nuclear oxide powders and to predict the green density distributions. The shape of sintered pellet resulting from a non uniform shrinkage of the green compact can also be calculated by this numerical code developed by the CEA and called PreCAD[®]. The simulation shows that the axial repartition of frictional forces may be changed during die pressing by a modification of the sequence of punches displacement. Thus, it has been established that the pressing cycle may have an influence on the shape of sintered pellet through the axial repartition of green density. The code PreCAD[®] has consequently been used to optimize the sequence in which the tools move during pressing, in order to improve the cylindricity of pellets. Indeed, the displacement of press tools, i.e. die and upper punches, can be separately fitted on current presses. The main trends, confirmed through experiments, are finally discussed.

1. INTRODUCTION

The fabrication of LWR fuel elements includes a stage of pellet forming which is performed in two successive steps: die-pressing and sintering. Due to slight geometrical defects, a final grinding operation is currently performed on rough sintered pellet to accurately control the fuel diameter. Indeed, fuel element design implies small tolerance for the pellet diameter to obtain a calibrated gap between pellet and cladding into the fuel rod. For LWR designs, the pellet diameter must be within the range +/- 12 µm around nominal values (8–10 mm).

In order to reduce the impact of the final machining on the fabrication cost (particularly for MOX pellets), a cooperative program has been undertaken between the French nuclear agency (CEA) and the fuel element supplier COGEMA. This study aimed at improving industrial forming process to obtain a better control of the diameter of sintered pellets.

This paper presents an approach based on the use of numerical simulation of pellet forming which allows to search some gains by optimizing the die pressing cycles. Semi-empirical mechanical models have been implemented into a FEM code (CASTEM 2000) to develop a dedicated design tool named PreCAD[®] [1–2].

Specific powder characterizations have also been performed to supply the mechanical parameters of compaction model. Then, an experimental validation step of the code has been carried out.

After having described the development of the compaction modeling, the main results of the simulation, which show that the pressing cycle has an influence on the shape of cylindrical parts, are highlighted. This influence, confirmed through experiments, is finally discussed.

All the results presented here concern an UO_2 powder, however the study will be soon extended to MOX powders, which characterizations are under progress.

2. MECHANICAL MODELLING OF DIE-PRESSING

2.1. Main steps of pellet forming processes

At the beginning of the die pressing step, calibrated amounts of a given mixture of oxide powders, including lubricant and porogen, are poured into the closed die of a press and then compacted by the movement of an upper punch. The die filling density is about 20–30 % of the theoretical density (th.d) of the material though the green compact density reach 60–65 % th.d. Punches and die are designed by taking into account the shrinkage of the compact during sintering to obtain the specified shape for the pellet, which may include dishings and chamfered edges. The mechanical strength of green compact is enough to allow transportation of pellets to sintering furnaces. The sintering step, which includes a heating stage at about 1700°C under specific atmosphere leads to a consolidation of the compact which nearly reaches the theoretical density (95–98 % th.d).

2.2. Influence of frictional forces

During closed die pressing, the powder material is submitted to a quasi biaxial stress state where σ_z , the axial pressure, is transmitted by the punches and σ_r is the resulting radial constraint exerted by the cylindrical die (cf. figure 1). Significant frictional forces develop between the granular material and inner die surface and have to be taken into account. The equilibrium of axial forces on a given powder slice (width dz) situated at a distant z from lower punch can be written [3]:

$$\pi R^2 d\sigma_z = 2\pi R \tau_{rz} dz \quad (1)$$

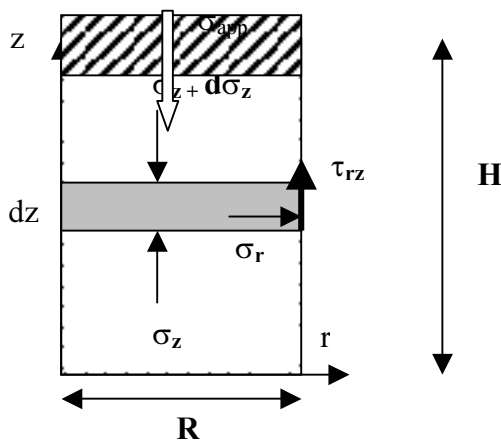


FIG. 1. Balance of forces acting on a powder slice during compaction (simple mode with upper punch movement).

Following assumptions are currently considered:

- the frictional force obeys to Coulomb's law : $|\tau_{rz}| = \mu\sigma_r$ (2)
- the radial stress is proportional to the axial component : $\sigma_r = \beta\sigma_z$ (3)

where μ is the friction coefficient and β is a powder dependant parameter (flow index).

In the simple case where the powder compaction results of the single downward displacement of the upper punch (single effect compaction), the direction of the frictional forces is the same along the interface so eq. (1) can be integrated as :

$$\sigma_z(z) = \sigma_{app} \exp\left[\frac{-2\mu\beta(H-z)}{R}\right] \quad (4)$$

where σ_{app} is the axial pressure applied by the upper punch.

This simple relation shows that due to friction forces, the compaction is non uniform along the powder column and the resulting stress and density gradients increase with the product $\mu\beta$ (called friction index).

For more complex cases corresponding to actual shaped pellets and press tools displacements, FEM has to be used to calculate stresses components.

2.3. Powder compaction model

The constitutive laws used to determine the powder density for a given stress state are based on a macroscopic elasto-plastic formulation (CAM-CLAY model [4]). In this approach, the density, ρ , is treated as an internal variable which allows to consider the effects of previous loadings. For a given density, the compacted powder obeys at low stresses to the Hooke's law when the current stress state belongs to the elastic domain sized by the value of density. The boundary of this domain in the space of stress tensor components is represented by the mathematical expression:

$$f(P,Q) = Q^2 + M^2(P - P_0)(P - P_1) = 0 \quad (5)$$

Where Q is the Von Mises stress and P the isostatic stress (first and second invariants of stress tensor).

With a such yield criterion, the summation of diagonal terms of the plastic strain tensor corresponds to the increment of powder density according to:

$$d\varepsilon_{ii}^p = \frac{d\rho}{\rho} \quad (6)$$

The elastic domain (which is elliptical in the P,Q plan) expands as the parameter P_1 rises according to the following consolidation law :

$$P_1 = \left[\frac{\rho}{\rho_0} \right]^k \quad (7)$$

where ρ_0 is the filling density and k a powder parameter.

An associated flow rule is used for calculating plastic strain when the yield condition $f(P,Q) = 0$ is fulfilled :

$$d\varepsilon_{ij}^p = d\lambda \cdot \frac{df}{d\sigma_{ij}} \quad (8)$$

The term $d\lambda$ ($d\lambda > 0$) is determined by the consistency condition ($df = 0$):

$$d\lambda = - \frac{\partial f / \partial Q \cdot dQ + \partial f / \partial P \cdot dP}{\rho \cdot \partial f / \partial \rho \cdot d\rho + \partial f / \partial P} \quad (9)$$

The system of equations (5) to (9) has to be solved numerically to determine the density increment $d\rho$.

This mechanical approach allows to take into account the impact of different stress states on the powder flow. For instance, Cold Isostatic Compaction (CIC) as well as die pressing processes can be treated by the same formalism. For die pressing, the effect of shear component, which can improve powder densification by grains gliding is well caught by this model.

Moreover, the elastic expansion of the compact (axial and radial springback) after ejection is calculated when appropriated elastic parameters are given (Young's modulus and Poisson's coefficient).

2.4. Calculation of pellet shrinkage after sintering

Finally, the dimensional changes induced by sintering are simply calculated with the hypothesis that the final pellet density is homogeneous. Indeed, the shrinkage of each part of the compact can be easily deduced from the difference between the local green density (previously calculated) and the sintered density by considering the mass balance.

3. IDENTIFICATION OF MODEL PARAMETERS

3.1. Methodology

Four material parameters (function of density) have to be experimentally determined:

- plastic flow parameters : $M(\rho)$ and $k(\rho)$
- elastic parameters : $E(\rho)$ and $\nu(\rho)$

A combination of the elastic parameters can be directly evaluated from the volume expansion corresponding to the springback of the green compact after ejection :

$$\bar{E}(\bar{\rho}_e) = \frac{3}{(1-2\nu)} \frac{\bar{P}}{\ln(\bar{\rho}_p / \bar{\rho}_e)} \quad (10) \quad \text{with} \quad \bar{P} = \frac{\bar{\sigma}_z + 2\bar{\sigma}_r}{3} \quad (11)$$

ρ_p is the mean compact density under loading at the end of die pressing (known by recording the punch displacement) and ρ_e the mean density after pellet removal determined by geometrical measurements.

The mean pressure P is evaluated by relation (11) from the experimental values of axial and radial stresses and is averaged all over the pellet volume.

Indeed, the instrumented press used allows to measure continuously the applied stress at the upper punch σ_{app} , the transmitted stress to the lower punch σ_{tr} ($\sigma_{app} > \sigma_{tr}$ due to friction) and also the radial forces σ_r exerted to the die [5]. Eq (4) is used to determine stresses value at different height.

A careful analysis of the evolution of the stresses σ_z and σ_r recorded during compact axial discharge gives an evaluation of Poisson's coefficient. Figure 2 compares the calculated and experimental paths that follows stress state in the (P,Q) plan during compact discharge. It is shown that the stress state evolution is closer to experimental data for $\nu = 0.1$ than for $\nu = 0.3$.

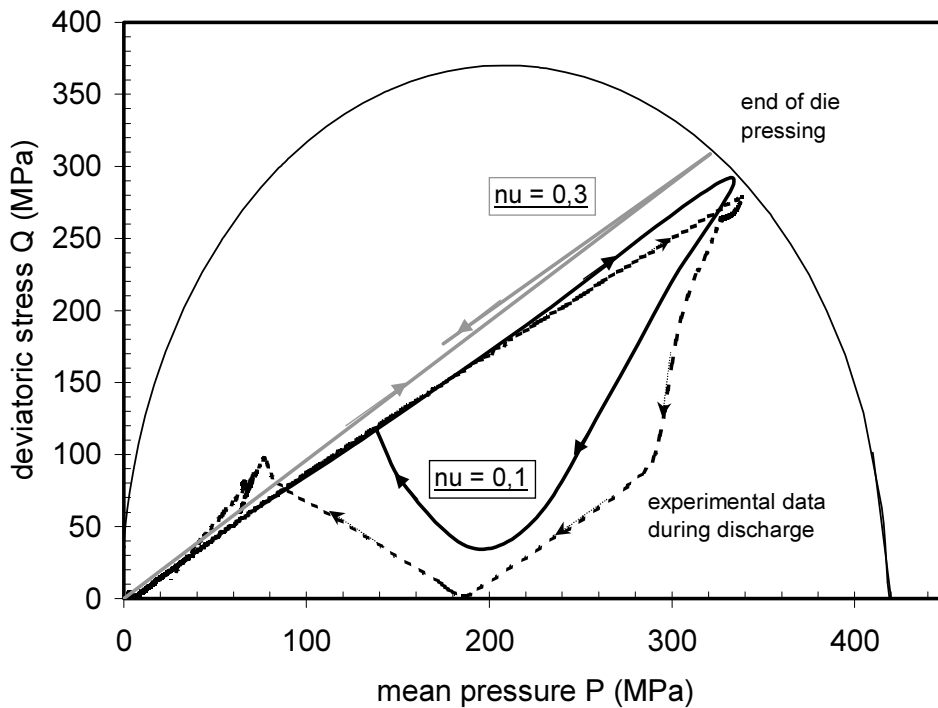


FIG. 2. paths of stress states in the (P,Q) plan during a die pressing of a UO_2 powder at 600 MPa (simple mode) and subsequent discharge. The elliptical curve represents the yield surface at the end of die pressing. The path corresponding to the springback and calculated with a Poisson's coefficient $\nu = 0,1$ is consistent with experimental data (dotted line).

The friction coefficient μ is then determined from the friction index deduced from single effect compaction tests where eq (4) can be transformed to :

$$\mu\beta = \frac{R}{2H} \ln \left(\frac{\sigma_{app}}{\sigma_{tr}} \right) \quad (12)$$

The parameter β (σ_r / σ_z) is known by dividing experimental values of σ_r by values of σ_z (rescaled at the height z_m where the measurement of σ_r is performed).

The flow parameters M and k are also determined from die pressing tests by considering two conditions:

- the current stress state always belongs to the yields surface i.e following relation is always true :

$$Q_m^2 + M^2(P_m - P_0)(P_m - P_1) = 0 \quad (13)$$

with $P_m = \sigma_z (1+2\beta)/3$ and $Q_m = \sigma_z (1-\beta)$ (14)

- the radial component of plastic strain can be neglected ($d\epsilon_r = 0$) so eqs (7) and (8) give after transformation :

$$\frac{2Q_m}{M^2[2P_m - P_0 - P_1]} = \frac{2}{3} \quad (15)$$

For low cohesive materials like nuclear ceramics, the traction resistance P_0 can be neglected and the resolution of Eqs. (13) and (15) gives a set of M and P_1 (or k) related to discrete values of density.

3.2. Model parameters for a UO₂ powder

Material characterization and parameters identification have been performed for a UO₂ powder (Mimas ADU dry route). The values of model parameters are given in table 1 for powder densities higher than 4 g/cm³. Indeed, it has been observed that macroscopic mechanical models give poor results for the first stage of densification where granules rearrangements take place (2–4 g/cm³). A rather good approximation is obtained by considering the powder with an uniform density of 4 g/cm³ (higher than filling density) at the beginning of the simulation (the height of the powder at the initial state is rescaled to assure mass conservation).

Table 1. Values of elasto-plastic parameters of the Cam-Clay model for a UO₂ powder.

Compact density g/cm³	Young's modulus ($\nu = 0,1$) MPa	Cam-Clay parameter M	Cam-Clay parameter P₁ MPa
4		1,77	35
4,5		1,77	50
5	4650	1,77	100
5,5	10450	1,77	180
6	15800	1,77	330
6,24	24750	1,77	420

4. CODE PERFORMANCES

4.1. Green compact characteristics

Several comparisons between simulation and experimental data have been carried out for this powder. FEM calculations have been performed by considering powder and tools (punches and die) geometries and mechanical behavior. The experimental value of friction coefficient

(0,15) is also introduced as an input data. Actual tools displacement recorded by the press instrumentation are specified as boundaries conditions for the compaction stage, so the resulting forces are calculated.

Figure 3 shows a good agreement between the axial evolution of green density for a single effect compaction (600 MPa) measured with a gamma densitometry technique and issued from FEM. It can be noticed that for this pellet with a ratio H/D of 1.5 the axial variation of green density is lower than 4 %. Despite this low value, the pellet has the shape of a truncated cone after sintering and the difference between the maximal and minimal radius reach 45 μm . Figures 4 and 5 present comparisons of calculated and measured values of green compact geometry (height and diameter) and forces acting on punches for different H/D (0,25–1,5) pellet ratios and green densities (5–6,5 g/cm^3).

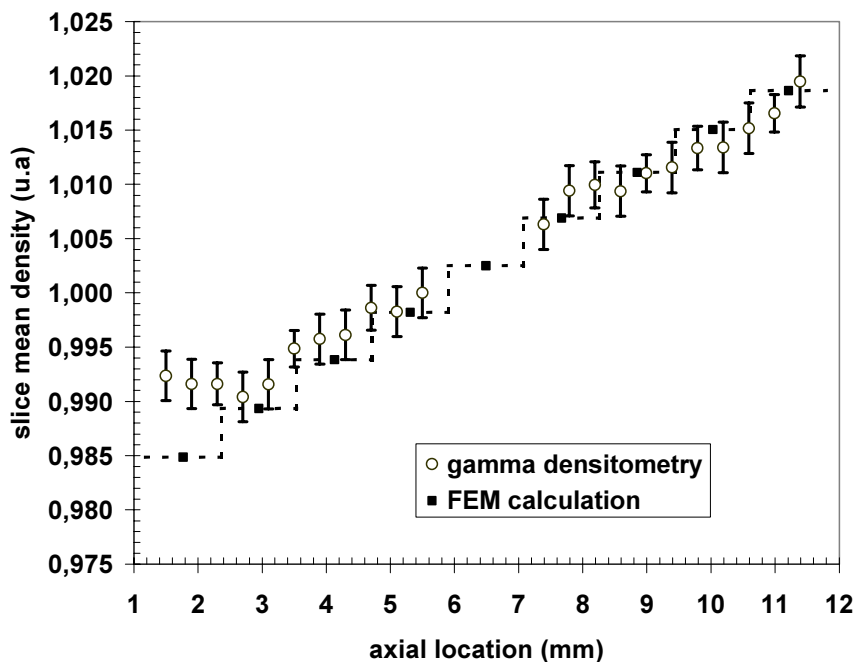


FIG. 3. Axial evolution of green density after compaction at 600 MPa (simple effect) of UO_2 powder. Each point correspond an averaged value of density over an axial slice (10 slices have been considered for FEM post-treatment).

4.2. Sintered pellets characteristics

Experimental and calculated values of sintered pellets dimensions are plotted on figure 6. Again, values are consistent within the range (0,25–1,5) of H/D ratios. Figure 7 depicts the values of the “Deviation from a Perfect Cylinder” (DPC), which is defined as the difference between the maximal and minimal pellet radius.

It can be noticed that the simulation reproduces the experimental sensitivity on H/D but tends to slightly overestimate the values of DPC.

This trend may be explained by the poor description of the pellet ejection, which is considered as purely elastic though inelastic strains (dilatancy) could occur during pellet extraction and could change the density distribution.

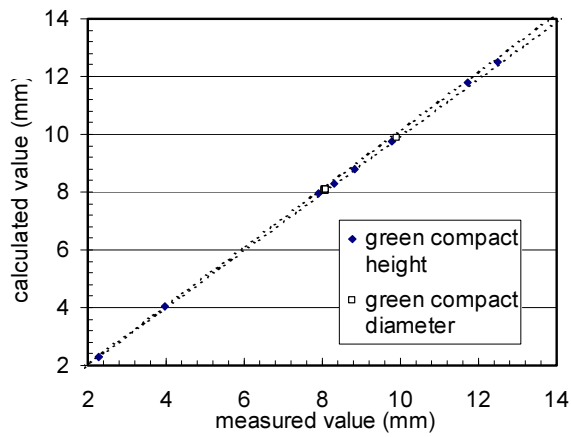


FIG. 4. calculated vs. experimental values of green compact dimensions after die pressing and ejection of a UO_2 powder, scattering is less than $\pm 1\%$.

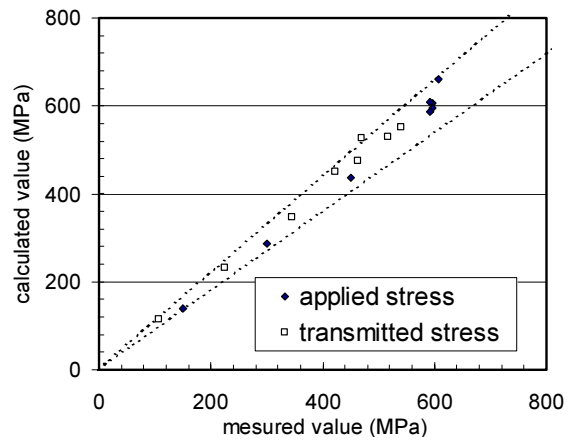


FIG. 5. calculated vs. experimental values of mean axial stress exerted on lower and upper punches at the end of a simple effect compaction of a UO_2 powder, scattering is less than $\pm 10\%$.

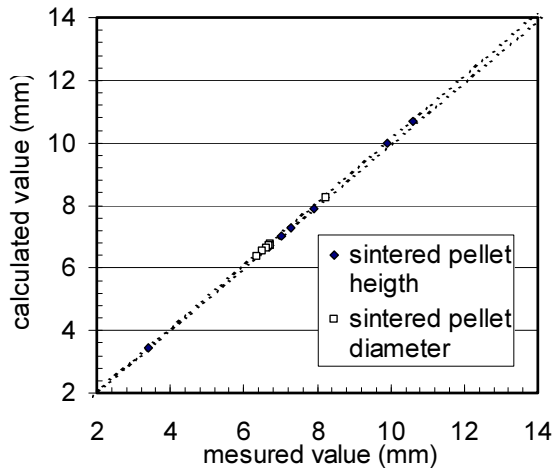


FIG. 6. calculated vs. experimental values of sintered pellet dimensions after forming of a UO_2 powder, scattering is less than $\pm 1\%$.

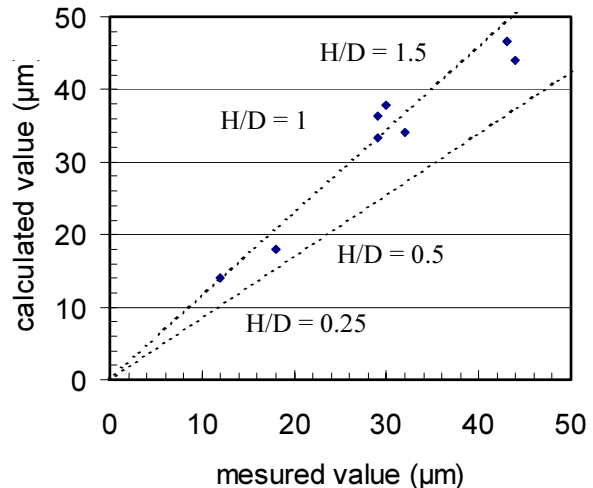


FIG. 7. calculated vs. experimental values of deviation from perfect cylinder ($R_{max}-R_{min}$) of sintered pellets, scattering is less than $\pm 15\%$.

5. ANALYSIS OF THE EFFECT OF TOOLS DISPLACEMENTS

Industrial presses used to form complex parts by powder metallurgy includes several tools (punches, cores and die) which can move separately in a specific sequence that prevent powder transfers from a part of high density to low density one during pressing.

Even for a simple shape like a fuel pellet, the displacement of upper punch that control the volume of powder is accompanied by a downward movement of the die which influences friction forces and density gradient as a consequence. Three main cases can be considered according to the ratio between the speed of the upper punch, V_p , and those of the die V_m (cf. figure 8). Simple effect modes lead to a monotonic decrease in density, the higher density

zone being in contact with the moving punch (relative to the die). Double effect mode ($V_m/V_p = 0,5$) produces a symmetrical density distribution, which gives a final “hourglass-like” shape after sintering.

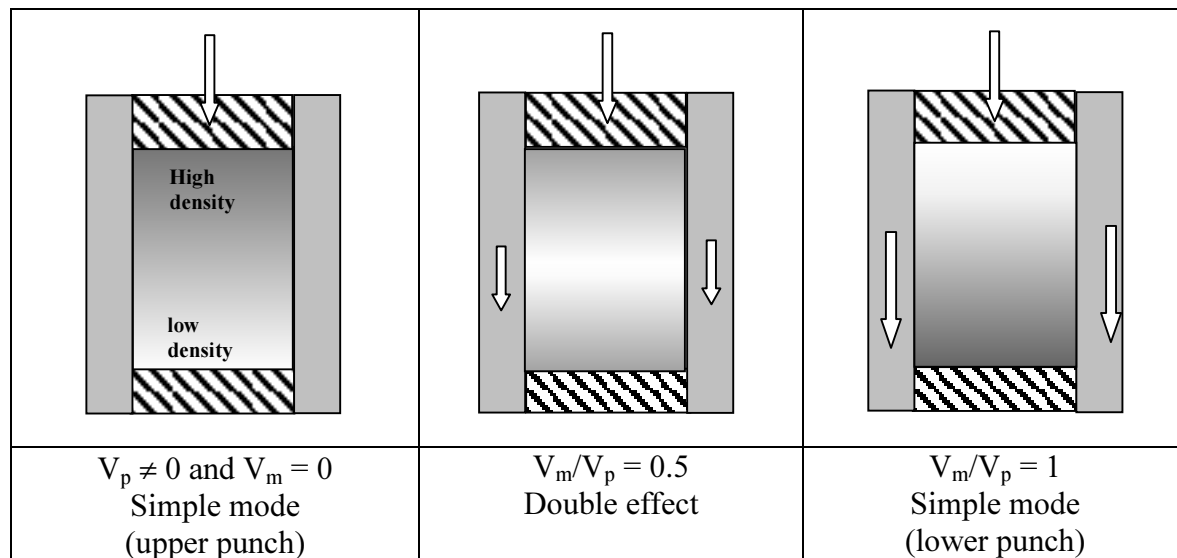


FIG. 8. powder density distribution according to die-pressing conditions for a cylindrical part.

However, the density gradients may differ from these ideal cases when the speeds ratio change during the pressing stage. We have considered the actual sequence where firstly both the upper punch and die move in a quasi double effect mode ($V_m/V_p \sim 0,5$) and then, at a given moment, the die stops and the upper punch moves downward till the end of pressing.

Simulation shows that the time when the die stops is a key parameter. An optimized value of this time has been numerically determined and then experimentally tested. Comparisons of two pellet diametrical profiles obtained after sintering are reported on the figure 9, one concerns a reference pressing cycle, the second is related to an optimized cycle. In the first case, the volume of material removed by grinding to obtain a perfect cylinder reaches 0.92% of the pellet volume (0.75% calculated) while it is lowered to 0.29% (0.23 calculated) after optimization. In these calculations, the diameter of the cylinder is defined as the minimal value obtained on the sintered pellet and it has to be noticed on figure 9 that this value also depends on the cycle.

Moreover two limiting cases have been reported on figure 9: an experimental profile obtained when the die stops early in the cycle (quasi simple mode) and a profile obtained when the die moves till the end of the cycle and goes on after the upper punch has stopped. In the latest case, a complete inversion of the profile is observed as a result of a stresses redistribution (at constant volume) due to friction between powder and the moving die. It is thus shown that the variation of pellet shapes may be sharply correlated with the variation of a simple press parameter.

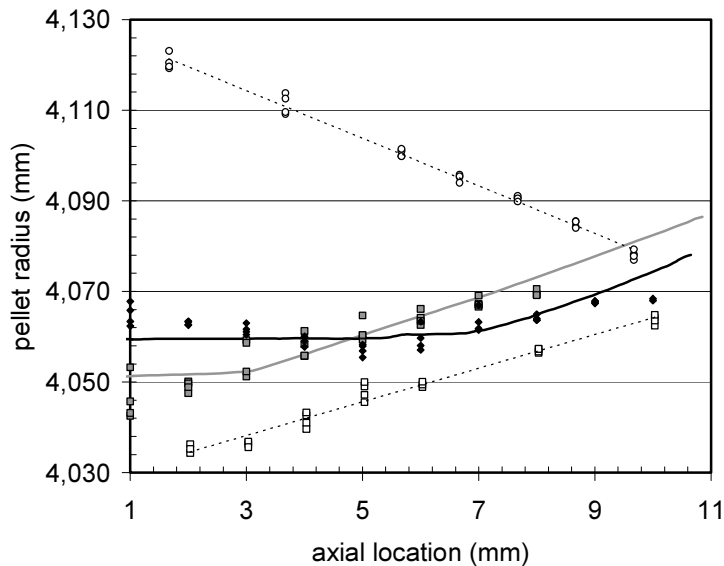


FIG. 9. Pellet diametrical profiles obtained after different pressing cycles : reference cycle (gray) and optimized cycle (black), symbols denote measured values, continuous lines represent the calculated profiles. Open marks combined with dotted lines correspond to 2 cases: a case where die stops early (squares) and a case where die stops after the punch has stopped (circles)

6. CONCLUSION

FEM simulations and experimental results clearly show that the diametrical profile of fuel pellet depends on the die-pressing conditions as a consequence of frictional forces between die and powder. Since friction depends on relative movements, the pressing cycle parameters (speeds ratio and changes) may be adapted to minimize the density gradient and to lower the geometrical defects of the sintered pellet. In this study, the volume of material that has to be removed to obtain a perfect cylinder has been reduced by a factor 3, just by fitting a single press parameter.

FEM simulation of shaping process constitutes an interesting tool to perform one or even multi-parameter optimizations (a specific algorithm has been implemented in the PreCAD[®] software). This code may be also used for design purposes (tools, cycles...) or to perform sensitivity analysis (powder properties, friction coefficient...). Experimental characterization of powders remains necessary to supply model parameters. On-going programs aimed at extending the database to actual MOX powders are performed in the CEA facilities (Cadarache). Further calculations will be also carried out to determine optimized cycle conditions adapted to this material.

REFERENCES

- [1] BACCINO R., MORET F. Numerical modeling of powder metallurgy processes, *Materials and Design*, 21, 359–364 (2000).
- [2] DELLIS C. et al.: PRECAD, a Computer Assisted Design and Modelling Tool for Powder Precision Moulding, HIP'96 Proceeding, Proceedings of the International Conference on Hot Isostatic Pressing, 20–22 May 96, Andover, Massachusetts. Pages 75–78.
- [3] PAVIER E., PhD thesis, Institut National Polytechnique de Grenoble, France. (1998).
- [4] PAVIER E et al., Analysis of die compaction of tungsten carbide and cobalt powder mixtures, *Powder Metallurgy*, vol. 42, n°4, 345–352 (1999).
- [5] FOURCADE, J. Thesis, Université de Montpellier 2 (2002).

MIXED OXIDES PELLETS OBTENTION BY THE “REVERSE STRIKE” CO-PRECIPITATION METHOD

J.E. MENGHINI, D.E. MARCHI
V.G. TRIMARCO, E.H. OROSCO
Comisión Nacional de Energía Atómica,
Centro Atómico Constituyentes,
Buenos Aires, Argentina

Abstract

In order to obtain mixed oxides of uranium/plutonium and uranium/gadolinium, the “reverse strike” co-precipitation method was studied. The objective was to verify that it is possible to obtain sintered pellets with the required physicochemical characteristics, furthermore a good micro homogeneity and, in the case of plutonium, an easy scrap recycling by dissolution with nitric acid without the fluorhydric acid adding. This method consists in the co-precipitation of ammonium diuranate (ADU) and plutonium hydroxide, $\text{Pu}(\text{OH})_4$, or ADU and gadolinium hydroxide, $\text{Gd}(\text{OH})_3$, from its nitric mixed solutions using gaseous ammonia and keeping the pH and temperature controlled. The tests with uranium and plutonium were carried out inside glove boxes using a mixed solution of this element where the $\text{Pu}/(\text{U}+\text{Pu})$ ratio is 20% (w/w). The tests with U and Gd were carried out using solutions with different $\text{Gd}/(\text{U}+\text{Gd})$ ratios between 0 % and 8% (w/w). The different steps of these processes in order to obtain the fuel pellets and the characterization of intermediate products are shown. The results show that this method assures a mixed-homogeneous precipitate obtaining. Regarding the ADU- $\text{Gd}(\text{OH})_3$, the existence of a mixed phase was verified. In sintered pellets a single phase of solid solution was observed. In the case of plutonium, its solubility in nitric acid without FH (fluorhydric acid) was rapidly reached. Sintered pellets showed high density and an inhomogeneous pore distribution, probably, due to problems during the pressing because of the low powder density. The low content of actinides in the filtrate was verified; therefore a previous treatment of it before its discarding is unnecessary. The method is appropriate for the obtention of mixed-oxide pellets having high densities and a good micro- homogeneity. It also assures the formation of a solid solution in the ceramic structure.

1. INTRODUCTION

Several methods have been studied in the world in order to obtain mixed oxides containing uranium for the fabrication of fuel pellets used in power reactors. We are especially interested in those fuels that use plutonium because of the recycling of this element proceeding from the burned fuels and from the scrap of fabrication, and also those containing gadolinium as a burnable poison.

The aim is to obtain a final product within the required specifications, having a good micro homogeneity and features that allow to improving its behavior inside the reactor. In the case of the uranium-plutonium, furthermore, the simple operability of the method and the easy treatment of generated wastes, are considered. For this, it is very important also, a fast and simple dissolution of the fabrication scraps.

One of the evaluated methods in our laboratory, alongside the direct denitration using microwaves, is the “**reverse strike**” co precipitation method .In this method, contrary to the direct precipitation one (where the chemical species are precipitated from the acid solution by means of the addition of ammonia gas or ammonium hydroxide with a gradual increase of pH of the medium), the reactive and the solution containing the actinides are added simultaneously inside the reactor using a controlled temperature, agitation, and pH previously

fixed which remains constant during all the process. Thus, the two species, uranium-plutonium or uranium-gadolinium, precipitate at the same time and in a quantitative way.

By means of the “reverse strike” co precipitation method, it is possible to obtain a precipitate, and consequently, a mixed oxide powder for the pellets fabrication with a high homogeneity grade regarding the dispersion of one element to the other, all this due to the simultaneous formation of precipitated species, as well as a good sinterability behavior.

In the present work, the method and the experiments carried out with U-Pu and U-Gd solutions are described, and the obtained results are shown.

2. METHOD DESCRIPTION AND EQUIPMENT

The process consists, basically, in the simultaneous adding of the gaseous ammonia (or ammonium hydroxide solution) and the acid solution containing the actinides, keeping the pH, temperature and agitation, constant along all the process.

The precipitant agent used in our case was the ammonia gas and not the ammonium hydroxide because it is very important for us to reduce the liquid wastes as much as possible when the work is carried out inside glove boxes during the fabrication of mixed fuel using uranium – plutonium. Figure 1. shows the different steps of the process.

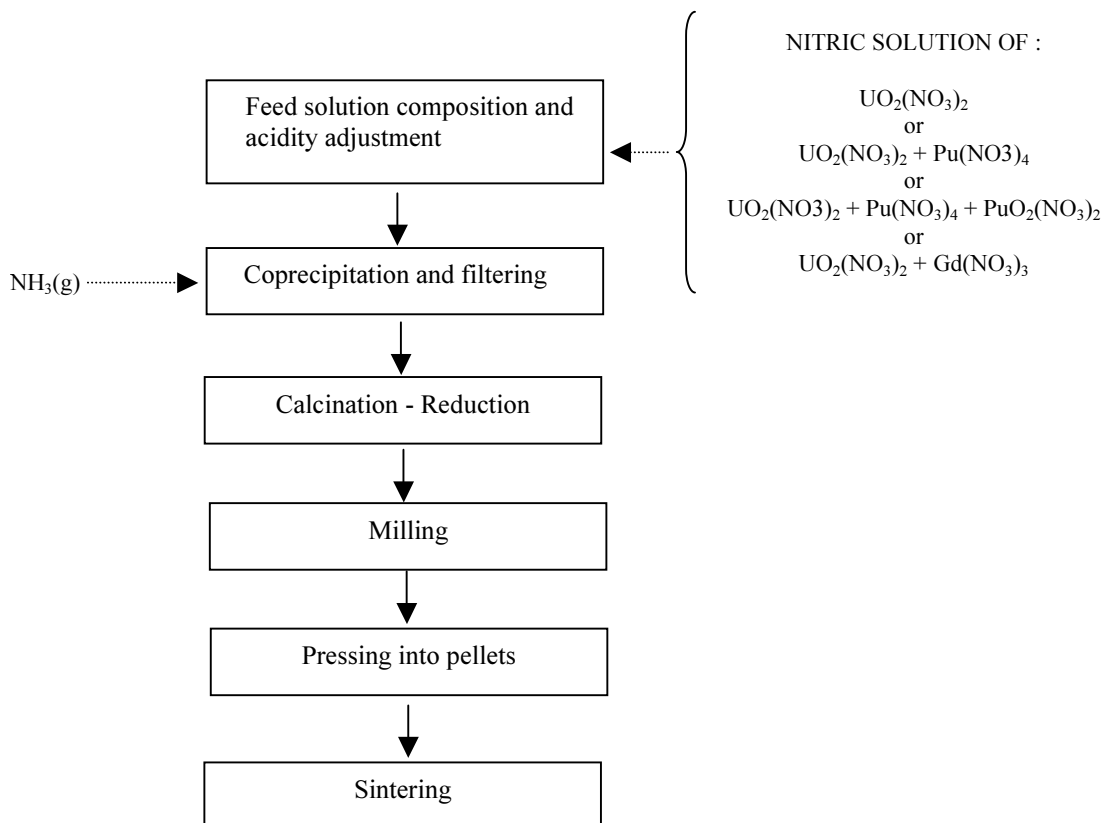


Fig. 1. A generalized flow sheet for conversion of mixed solutions of uranium into sintered pellets.

The simplified chemical reactions involved in each step are shown in Table I.

Table I.

Adjustment of oxidation state (for Pu ⁺⁴ precipitation only)		
$\text{PuO}_2^{+2} + \text{H}_2\text{O}_2 + 2 \text{H}^+$	\rightarrow	$\text{Pu}^{+4} + 2\text{H}_2\text{O} + \text{O}_2 \uparrow$ (1)
Precipitation reactions		
$\text{NH}_3 + \text{H}_2\text{O}$	\rightarrow	$\text{NH}_4^+ + \text{OH}^-$ (2)
$\text{H}^+ + \text{OH}^-$	\rightarrow	H_2O (acid neutralization) (3)
$2 \text{UO}_2^{+2} + 6 \text{OH}^-$	\rightarrow	$\text{U}_2\text{O}_7^{=} + 3\text{H}_2\text{O}$ (4)
$\text{U}_2\text{O}_7^{=} + 2 \text{NH}_4^+$	\rightarrow	$\text{U}_2\text{O}_7(\text{NH}_4)_2 \downarrow$ Ammonium diuranate (ADU) (5)
$\text{Pu}^{+4} + 4 \text{OH}^-$	\rightarrow	$\text{Pu}(\text{OH})_4 \downarrow$ Plutonium hydroxide (6)
$2 \text{PuO}_2^{+2} + 6 \text{OH}^-$	\rightarrow	$\text{Pu}_2\text{O}_7(\text{NH}_4)_2 \downarrow$ Ammonium diplutotate (ADPu) (7)
$\text{Gd}^{+3} + 3 \text{OH}^-$	\rightarrow	$\text{Gd}(\text{OH})_3 \downarrow$ Gadolinium hydroxide (8)
Thermal Decomposition		
$\text{U}_2\text{O}_7(\text{NH}_4)_2$	$\xrightarrow{400^\circ \text{C}}$	$2\text{UO}_3 + 2\text{NH}_3 + \text{H}_2\text{O}$ (9)
3UO_3	$\xrightarrow{400^\circ \text{C to } 650^\circ \text{C}}$	$\text{U}_3\text{O}_8 + \frac{1}{2} \text{O}_2$ (10)
$\text{Pu}(\text{OH})_4$	$\xrightarrow{400^\circ \text{C to } 650^\circ \text{C}}$	$\text{PuO}_2 + 2 \text{H}_2\text{O}$ (11)
$2 \text{Gd}(\text{OH})_3$	$\xrightarrow{400^\circ \text{C to } 650^\circ \text{C}}$	$\text{Gd}_2\text{O}_3 + 3 \text{H}_2\text{O}$ (12)
Reduction		
$\text{U}_3\text{O}_8 + 2 \text{H}_2$	$\xrightarrow{650^\circ \text{C}}$	$3 \text{UO}_2 + 2 \text{H}_2\text{O}$ (13)
Sintering		
UO_{2+x} (green pellet) + x H ₂	$\xrightarrow{\sim 1700^\circ \text{C}}$	$\text{UO}_{2,00}$ (sintered pellet) + x H ₂ O (14)

2.1. Precipitation reactor

The precipitation reactor consists of a double-wall Pyrex glass tube through which water at constant temperature circulates; thus, the selected work temperature of the solution in the inner container remains constant along all the process. Furthermore, the reactor has a vertical stirrer with a propeller powered by an electrical motor. A glass electrode connected to a pH-meter allows to testing the solution pH constantly. A peristaltic pump with a constant flow

pumps the solution into the reactor. The ammonia gas supply is controlled using a manual flow regulation valve.

Both, the ammonia and the acid solution of actinides enter simultaneously through a lid on the top of the reactor. The end of either dosage pipe is placed very close to the stirrer propeller.

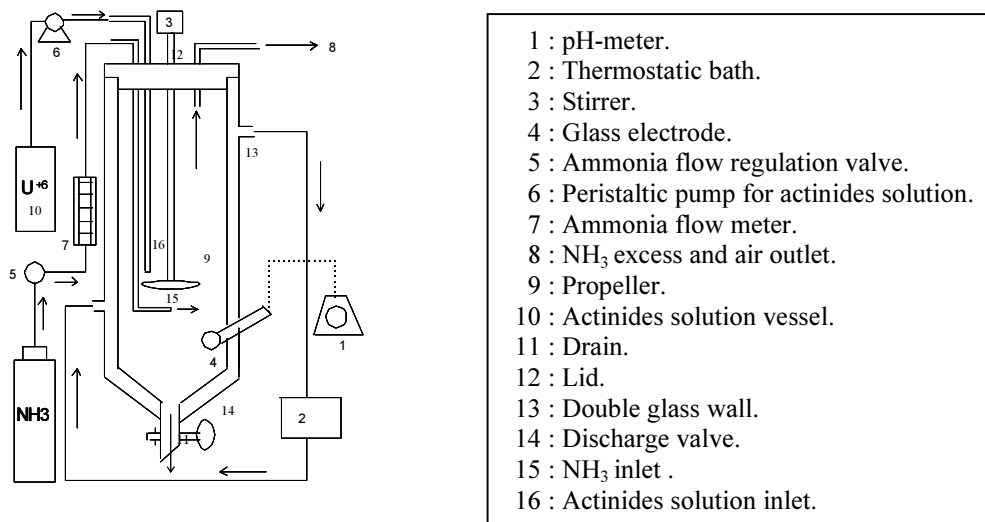


FIG. 2. Schematic drawing of the precipitation reactor.

3. EXPERIMENTAL

3.1. Assays with uranium only

The co precipitation method adjustment and the powder thermal treatments were carried out in a first step, with uranium only and outside glove boxes.

3.1.1. Actinides solution preparation

For the first assays and the determination of work parameters three uranyl-nitrate solutions with different uranium concentration in 1M free nitric acidity were prepared. This acid concentration assures the non-polymerization of Pu⁺⁴ when the assay is carried out with solutions containing plutonium, and is low enough to avoid a high spending of ammonia due to the acid neutralization with formation of a high quantity of ammonium nitrate salt. The selected actinide concentration was 300 g/l in order to increase the yield in each precipitation batch without affecting the powder quality.

3.1.2. Precipitation pH selection

From experiments carried out in other countries and from the subsequent bibliography, we concluded that the best precipitation pH is between 4 and 6 [1]. This pH range assured a simultaneous and quantitative precipitation of both elements and avoided the selective precipitation of one of them as it could occur in the direct method with variable pH. Besides, the precipitate obtained under those conditions presented an easy filtration process.

3.1.3. Precipitant agent selection

The selected precipitation agent was the gaseous ammonia according to the reasons explained in Section 2.

3.1.4. Precipitation temperature choice

Previously, three constant working temperatures were tested to heat the actinide solution: 20°C, 40°C and 60°C. The ADU (ammonium diuranate) precipitate, formed at 60°C and proceeding from a solution with 300 g/l of uranium, was easily filterable with an average particle size of ~12 microns. On the other hand, the precipitate formed at 40°C showed smaller particle sizes (~6 microns) and a longer filtration time, and the 20°C one was gelatinous and very difficult to filtrate. That is why the selected temperature was 60°C.

3.1.5. Precipitation

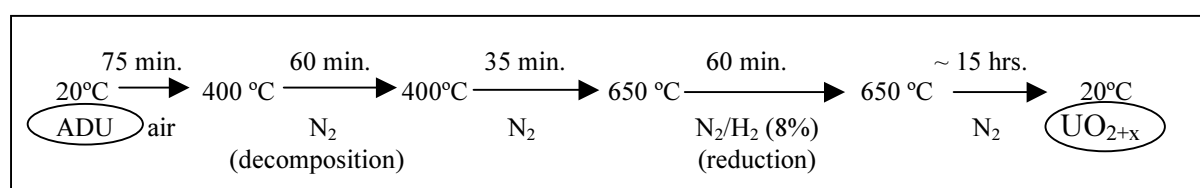
Every experiment was performed using 1000 ml of actinide solution that were pumped into the reactor at a rate of ~ 17 ml/min. The ammonia gas flowing was manually controlled using a regulation valve in order to maintain the pH shown in the pH-meter within the range 4 – 6.

3.1.6. Filtration

The slurry of yellow ADU precipitate remained in the reactor one more hour at the same temperature, pH and agitation speed to allow the particles to grow. Afterwards, the reactor was drained and the mother water was separated by filtration using a vacuum pump and a Büchner funnel provided with the adequate filter paper. The retained precipitate is then washed with a diluted ammonium hydroxide solution, and later, dried 24 hrs in an oven at 120°C in air. The analysis of the mother water showed an uranium content lower than 3 ppm, which means, a quantitative precipitation.

3.1.7. Decomposition-reduction. Thermal treatment.

In a horizontal electric furnace, the ADU precipitate was heated according to a controlled heating program. In the following diagram, the times to reach each temperature and the corresponding atmosphere are shown.



Where N₂ means nitrogen atmosphere, and N₂/H₂ (8%) means mixed atmosphere of nitrogen-hydrogen (8% hydrogen).

UO_{2+x} indicates that the oxide composition is not stoichiometric (O/U ratio greater than 2.00).

3.1.8. Milling

A portion of the UO_{2+x} powder obtained from the thermal treatment was milled in a cylindrical horizontal mill provided with stainless steel balls during 4 hours. This process was necessary to increase the bulk density of the powder, which facilitates the press die loading, and increases subsequently, the density of “green” pellets and sintered pellets.

The processes described below were carried out on both kinds of powders: milled and non - milled ones.

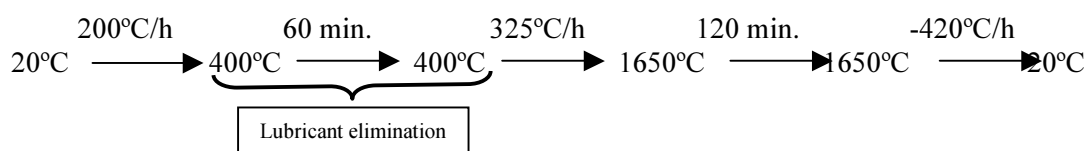
3.1.9. Pressing

Several pressures were assayed using an automatic press. Two methods of lubrication were tested: internal lubrication, by adding zinc diestearate into the powder (~0.4%) and mixing homogeneously, and external lubrication, applying vegetal oil on the die wall.

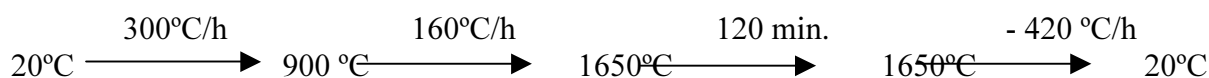
3.1.10. Sintering

Two thermal cycles in argon–hydrogen (8%) atmosphere, were studied depending on the used lubrication method. The mentioned cycles are as is indicated:

Cycle 1 (used to eliminate the internal lubricant):



Cycle 2 (without an elimination “plateau”, for pellets pressed with external lubrication):



3.1.11. Characterization of the obtained products

The following table shows the product features:

Table II

Measured parameter	Non-milled powders	4-hour milled powders
Specific surface area (m ² /g)	3.32	4.09
O/U ratio	2.06	2.08
Average particle diameter (microns)	8.93	3.10
Tap density (g/cc)	2.61	3.33

In table III, the average densities of 10 pellets are shown, depending on the way of conditioning and pressing pressure.

As we can see in Table III, the pellets proceeding from milled powders, pressed using external lubrication and sintered according the cycle 2 (Section 3.1.10.) showed sintered densities equal or higher than 95% T.D. (theoretical density) being this one the lowest density admitted for the pellets required to be used in power reactors such as Atucha or Embalse (Candu fuel) existing in Argentina at present time (year 2003).

Table III

▼	NON-MILLED POWDER						4-HOUR MILLED POWDER					
	Internal Lubrication			External Lubrication			Internal Lubrication			External Lubrication		
Pressing Pressure	500 MPa*	600 MPa	500 MPa		600 MPa		500 MPa	600 MPa	500 MPa		600 MPa	
Green density (g/cc)	5.94	6.09	6.54		6.71		6.56	6.21	6.53		6.74	
Cycle used	1	1	1	2	1	2	1	1	1	2	1	2
Sintering density (g/cc)	10.0	10.2	9.9	10.3	10.0	10.3	10.3	10.3	10.4	10.6	10.4	10.6
%T.D. (Theoretical density)	91.2	93.1	90.3	94.0	91.2	94.0	94.0	94.0	94.9	96.7	94.9	96.7

* : MPa = mega-pascal pressure unit = 10^{-2} Ton/cm².

3.2. Glove box assays using a mixed uranium-plutonium (IV) solution

With the results and knowledge acquired with uranium, the “reverse strike” co precipitation technique was carried out inside glove boxes with a mixed solution of uranium-plutonium. The plutonium was stabilized as Pu (IV) using hydrogen peroxide (H₂O₂) as it is shown in the reaction (1) in Table I.

Due to the smaller working place inside the glove box, the precipitation reactor used was smaller than the one used outside with uranium only, and the volume of the mixed solution was 500 ml only.

The solution characteristics and work conditions are summarized as follows:

Feeding solution	Work conditions and results
Volume.....500 ml	Temperature.....60°C
Acid concentration.....0.9 M (nitric acid)	pH.....4 – 6
Uranium concentration.....228.10 g/l	Used solution volume....474 ml
Plutonium concentration.....57.05 g/l	Precipitant reactive NH ₃ (g)
U+Pu concentration.....285.15 g/l	Liquid wastes volume....1000 ml
	Filtration time~ 10 min.

The resultant mother water was analyzed and no presence of U or Pu was detected, then, the precipitation was entirely quantitative.

3.2.1. Thermal treatments

The obtained mixed precipitate was calcined under the conditions detailed in Section 3.1.7. The result was a pyrophoric mixed oxide. That is why the calcination – reduction cycle had to be modified in order to reduce the specific surface area of the powder and, therefore, avoid its re oxidation in air at laboratory temperature. Three thermal cycles (A, B and C) were studied. In one of them the reduction temperature was increased and in all of them the reduction “plateau” time was also increased.

Table IV shows the characteristics of the powders obtained under those conditions.

Table IV

►	Reduction temperature (°C)	Reduction step duration (hours)	N ₂ atmosphere application (hours)	N ₂ /H ₂ atmosphere application (hours)	TAP density (g/cc)	Specific surface area (m ² /g)
Cycle A	650	3	2 (initials)	1 (the last one)	1.36	9.83
Cycle B	650	3	0	3	1.42	8.31
Cycle C	700	3	0	3	1.46	5.74

As we can see, cycle C is the treatment that gave the lowest specific surface area and the highest tap density. These two features are the most convenient to the next treatments of powders.

3.2.2. Pressing

Due to the low tap density of the powders, it was necessary to select pressures lower than the ones used in the experience with uranium in order to obtain pellets with the required dimensions. The extremely low density of the powders obtained with cycle A, made its pressing very difficult, so, the results were not repetitive. In all cases, external lubrication with vegetal oil was used. The next table shows some pressures applied and the resulting “green” densities obtained, depending on the cycle used.

Table V

Pressing pressure (MPa)	Cycle B	Cycle C
	(Green density –g/cc-)	(Green density –g/cc-)
110	4.73	---
112	4.47	4.78
115	---	4.77
120	---	4.83
140	5.12	---
160	---	4.87
170	4.80	---

3.2.3. Sintering

The sintering of pellets was carried out using the Cycle 2 (Section 3.1.10.) because this one gave the best results in the assays with uranium only. The sintered pellet density was measured by weighing each one, first, in air, and after that, in water (Archimedes’ principle). Some results are shown in table VI, where the pressing pressure applied and the thermal cycle used, are indicated (T.D. = 11.06 g/cc for 20% of Pu).

Table VI

Pressing pressure (MPa)	Cycle B (Sintering density –g/cc-)	Cycle C (Sintering density –g/cc-)
110	10.61	---
112	10.67	10.61
115	---	10.60
120	---	10.65
140	10.68	---
160	---	10.56
170	10.65	---

3.2.4. Pellet solubility

A solubility assay was done using one of the sintered pellets. The pellet was attacked with 7 M nitric acid in a reflux bath during 6 hours without fluorhydric acid (FH) adding. At the end of three hours, the pellet was entirely dissolved. Nevertheless, after 6 hours, the solution was cooled and filtered through the finest pore filter paper. The filtered solution and the content on the paper were analyzed, and the following result was found:

$$\text{Solubility \%} = \frac{\text{Mass of Pu found in solution}}{\text{(Mass of Pu found in solution + mass of Pu found on the paper)}} \times 100 = 99.7 \%$$

It is interesting to compare this result to the solubility of pellets proceeding from mechanical blending of $\text{UO}_2 + \text{PuO}_2$ powders (with a Pu content of 0.55% w/w in the pellet) used in a previous fabrication for irradiation assays [2]. In this case the results obtained for the solubility in the same conditions and furthermore with FH adding, were only ~ 97 % .

3.2.5. Ceramographic characterization

Some pellets were cut, polished and attacked using conventional ceramographic techniques to study their microstructures. The porosity distribution observed in these pellets was inhomogeneous but not in the case of the grain size distribution, which turned out to be homogeneous, with an average grain size of 11 microns. Individual PuO_2 particles were not observed in the alpha-auto radiographies.

3.3. Glove box assays with mixed solution of uranium and ($\text{Pu}^{+4} + \text{PuO}_2^{+2}$)

In this experiment with mixed solution of U and Pu, the plutonium was not conditioned to be only as Pu^{+4} using hydrogen peroxide, as it was in the previous one. Thus, both species, Pu^{+4} and PuO_2^{+2} were present (~60% and ~40% respectively), as well as the UO_2^{+2} , all of them proceeding from the attack with nitric acid of scraps resultant from previous fabrications. The aim was to study the final quality of the products and their features. Almost all the other work conditions and processes were preserved. The dried precipitate obtained under these conditions, was divided into two portions (A and B). Portion A was calcined using the cycle C described in Section 3.2.1. taking into account the reasons already mentioned for the assay with Pu^{+4} . Portion B was calcined with the same cycle, but using a temperature of 800°C during the reduction step in order to decrease the specific surface area even more.

Table VII shows the obtained results.

Table VII

	TAP density (g/cc)	Specific surface area (m ² /g)
Portion A (700 °C)	2.62	6.70
Portion B (800 °C)	2.68	3.60

Both powders showed a homogeneous appearance and a very stable behavior regarding the oxidation when the samples were exposed to the air.

3.3.1. Pressing

The higher tap density of these powders allowed to apply a pressure greater than the ones already used in powders of Pu⁺⁴ (250 MPa).

3.3.2. Sintering

The green pellets were sintered using Cycle 2 (Section 3.1.10.). The results are shown in the next table.

Table VIII

Reduction temperature (°C)	Green density (g/cc)	Sintering density (g/cc)	% Theoretical density
700 (Portion A)	5.38	9.84	88.9
800 (Portion B)	5.67	9.83	88.9

The T.D. of sintered pellets were much lower than the ones observed in the assays with Pu⁺⁴. The ceramographic analysis showed a greater amount and volume of pores that agrees with the observed T.D. decrease in the pellets. The assay of solubility with nitric acid without FH adding showed a similar result to the one of previous step with Pu⁺⁴ (greater than 99.7%).

3.4. Co precipitation assays with mixed uranium-gadolinium nitric solutions outside glove boxes

The “reverse strike” co precipitation method was also used to obtain mixed oxides of U-Gd for pellets fabrication. The supposed and simplified chemical reactions involved in different steps of the process were already mentioned in Table I. The precipitation reactor, the calcination furnace and the mill, are the same as those used in the experiments with uranium only.

3.4.1. Preparation of the uranium-gadolinium solution

Five solutions of 1000 ml each containing 0, 2, 4, 6 and 8% of gadolinium regarding the total present metal, were prepared. The total metal content (U+Gd) in each solution was ~300 g per liter. As always, the medium was 1 M nitric acid.

3.4.2. Precipitation pH selection

The selected working pH was 9, which proceeded from previous experiments carried out in order to obtain a quantitative and simultaneous precipitation for both elements. The other process parameters were the same as those that were used with uranium. The following table summarizes the characteristics of the obtained precipitate for each Gd concentration.

Table IX

% of Gd (U + Gd = 100% w/w)	Average particle diameter (Microns)	Specific surface area (m ² /g)
0	0,37	8,8
2	1,00	12,2
4	2,60	10,8
6	11.5	9.4
8	12,5	8,8

All the precipitates were analyzed by X-ray diffractometry. The diffractograms showed peaks that had no correspondence with those observed for ADU, Gd(OH)₃ or another known compound of U or Gd that could be formed under these physicochemical conditions. For this reason, the existence of a new mixed phase is presumed (see Fig. 3):

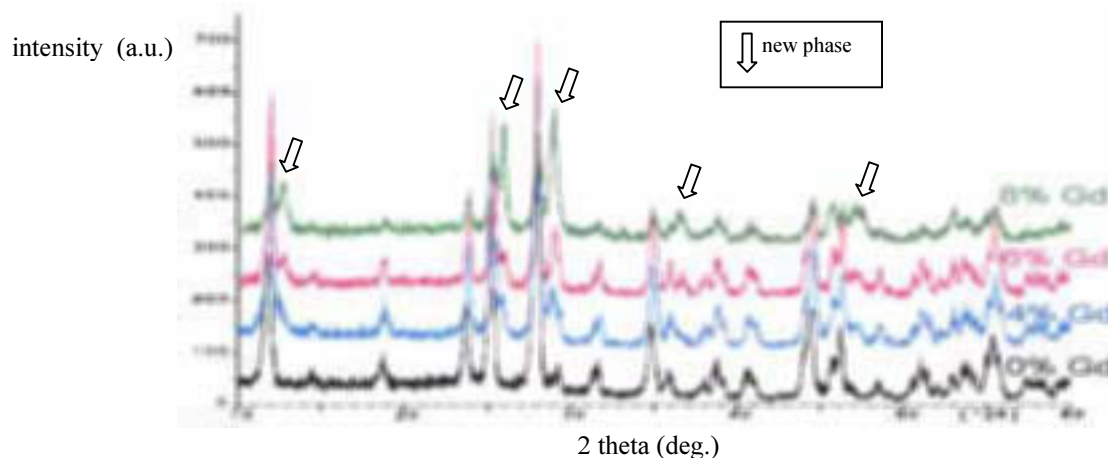
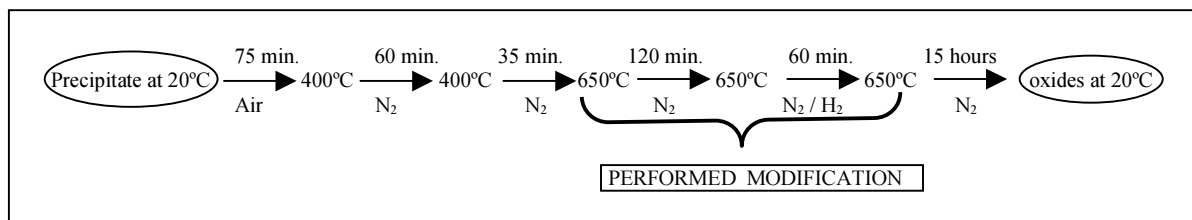


FIG.3. Diffractograms of obtained precipitates with different gadolinium content.

3.4.3. Thermal treatment of the precipitates

Previous calcination assays of the 0% Gd powder (uranium only, precipitated at pH 9) with the cycle mentioned in Section 3.1.7. showed that the resulting powder had a specific surface area about 5 m²/g . Considering that the same powder obtained at pH 4-6 had a specific surface area of 4.09 m²/g, some modifications of that cycle were performed in order to decrease that parameter and consequently to get a greater stability in air. All the obtained precipitates of U-Gd were calcined under the cycle shown below.



3.4.4. Milling, pressing and sintering

The powders thus obtained, were milled during four hours in a stainless-steel ball mill in order to increase their bulk densities. The results obtained after the milling are shown in the next table. Data of milled UO_2 powder precipitated at pH 4-6 are also given in order to compare.

Table X

% Gd (metal)	Average diameter (microns)	Specific surface area (m ² /g)	Oxygen / metal Ratio	TAP density (g/cc)
0	0,21	3,75	2,07	2,66
2	0,10	8,00	2,09	2,54
4	0,55	10,10	2,19	2,39
6	0,38	11,80	2,16	2,45
8	0,80	11,02	2,24	2,26
Milled UO_2 (pH 4-6 precipitation)	3,10	4,09	2,08	3,33

Several pressing pressures were studied, resulting the 240 MPa the selected one because it gave the highest “green” density in each case. Afterwards, the green pellets were sintered according to Cycle 2 (Section 3.1.10.). The final obtained features can be summarized in the following table.

Table XI

Tested oxide	Green density ⁽¹⁾ (g/cc)	Sintering density ⁽²⁾ (g/cc)	Theoretical density (T.D.) * (g/cc)	% T.D.
0% Gd	5,72	10,55	10,96	96,37
2% Gd	5,46	10,51	10,89	96,70
4% Gd	5,37	10,52	10,82	97,46
6% Gd	5,28	10,49	10,74	97,51
8% Gd	5,16	10,49	10,67	98,35

(1) : Average 10 pellets measured in each case.

(2) : Average 2 pellets measured in each case.

(*) : The theoretical density for each gadolinium content, can be calculated upon the data issued by Fukushima [3].

The analysis by X-ray diffraction of both mixed powders of U–Gd oxides and their corresponding sintered pellets, showed the existence of a single phase that crystallized in the face centered cubic system, f.c.c., whose lattice parameters changed according to the Gd concentration [4]. These parameters were smaller than the ones observed in the UO_2 lattice (5.471 Angström). This lattice shrinking was due, apparently, to the gadolinium incorporation into the UO_2 lattice [3,5]. The qualitative analysis carried out by EDS (Energy Dispersive Spectroscopy) and WDS (Wavelength Dispersive Spectroscopy) techniques on sintered pellets, showed a homogeneous distribution of gadolinium inside the uranium matrix.

4. RESULTS AND DISCUSSION

The “reverse strike” co precipitation method allows us to obtain UO_2 powders suitable for fabrication into pellets whose densities are the especificated for the reactors operating in our country at the present time. Nevertheless, in the obtention of mixed oxides the presence of a second element produced modifications on the physical characteristics of the obtained powders. For this reason, modifications on the intermediate steps of the process (calcination,

reduction, pressing) were necessary to improve the final quality of the obtained products. The presence of gadolinium, for example, forced us to use a higher pH in order to obtain a quantitative precipitation of this element and the uranium, but unfortunately, this pH led to the obtention of powders with higher specific surface areas and smaller particle sizes (see tables II and X). On the other hand, from comparison between tables II and IV, it is verified that the presence of plutonium in the feeding solution modified considerably some of the powder physical features, increasing its specific surface area and decreasing its tap density, even when the precipitation pH used is the same in both assays.

Modifications on the mixed powders characteristics are observed depending on the oxidation state of Pu in the feeding solution. This topic presumes that different species precipitated. The presence of Pu (VI) leads to the obtention of (U,Pu)O₂ powders with higher tap density (compare tables IV and VII) and lower sintering density (compare tables VI and VIII).

The analysis of U-Gd powders using X-ray diffraction, EDS and WDS described in 3.4.4, showed the existence of a mixed phase in the precipitate and the formation of a solid solution in the sintered pellets.

Although those analysis could not be performed on powders and U-Pu pellets due to operative difficulties, the same behavior can be presumed on the basis of the good solubility of the sintered pellets in nitric acid without fluorhydric acid adding (see Section 3.2.4.) and of the results of their ceramographic analysis (see Section 3.2.5.).

5. CONCLUSIONS

The “reverse strike” co precipitation method was applied to the UO₂, (U,Pu)O₂ and (U,Gd)O₂ obtention and the following advantages were found:

- The precipitation under the selected conditions in this work was quantitative thus, the liquid wastes treatment results to be easy due to the low amount of remaining actinides in solution. It is possible to obtain pellets with the adequate density by the adjustment of the working parameters appropriately according to the products to be obtained (mixed oxides of U and Pu or U and Gd).
- This method assures the total formation of a new single phase in the obtained pellets, attaining a high-grade micro homogeneity and making easy the treatment of the mixed U-Pu scraps.
- The relative simplicity of the method and its feasibility to be applied inside glove box environment was verified.

REFERENCES

- [1] KINCAID, C.B., ZIMMER, J.J., WADEKAMPER, D.C., TAYLOR, I.N., AITKEN, E.A., “Coprecal: co-conversion of Pu, U mixed nitrate to mixed oxide”, Transactions of the American Society, USA (1979) v. 33 p. 470-471.
- [2] ADELFRANG P., et al., “Fabrication and control of mixed oxide fuel rods (U,Pu)O₂ for irradiation in the HFR-Petten reactor”, 14th Scientific Meeting of the AATN (Asociación Argentina de Tecnología Nuclear), Córdoba, Argentina (1986), AATN (in Spanish).

- [3] FUKUSHIMA, S., OHMICH, T., MAEDA, A. and WATANABE, H., "The Effect of Gadolinium Content on the Thermal Conductivity of Near- Stoichiometric (U,Gd)O₂ Solid Solutions", J. Nucl. Mater. (1982) Vol. 105, p. 201.
- [4] LEYVA, A.G., VEGA, D., TRIMARCO, V.G., MARCHI, D.E., "Homogeneity characterization of sintered (U,Gd)O₂ pellets by X-ray diffraction", J. Nucl. Mater (2002) v. 303 p. 29-33.
- [5] HO, S. M., RADFORD, K.C., "Structural chemistry of solid solutions in the UO₂-Gd₂O₃ system", Nuclear Fuels, June 1986, v. 73, p. 350-360.

ESTABLISHMENT OF LOW DENSITY MOX PELLET FABRICATION PROCESS

K. ASAKURA, T. OHTANI
Plutonium Fuel Center, Tokai Works,
Japan Nuclear Cycle Development Institute,
Ibaraki, Japan

Abstract

One of the important subjects to be considered in fuel design phase is to reduce Pellet Cladding Mechanical Interaction, PCMI, which might be caused by swelling of MOX pellet at higher burn up stage. Reduction of smear density of MOX fuel is the practical resolution to improve PCMI resistance. In general, two methods such as low density pellet by using organic additive (hereinafter referred to as "pore former") and annular pellet can be utilized so as to decrease smear density of MOX fuel. Before the launch of the operation of Plutonium Fuel Production Facility, PFPP, which was designed and constructed with the purpose to fabricate MOX fuel for the proto-type Fast Breeder Reactor, FBR, "MONJU", a laboratory scale examination had conducted to determine the process to decrease pellet smear density adopted for PFPP. This examination had concluded provisional scheme of fabrication process for low density MOX pellet by using paraffin type additive as pore former. In 1989, JNC started low density MOX pellet fabrication for MONJU initial load fuel. At the beginning of pellet fabrication, densities of sintered pellets widely spread over because pore former was deformed by decay heat of plutonium, and it distributed heterogeneously in the matrix of sintered pellet. In order to resolve these problems, JNC examined alternative pore former with higher heat resistance than paraffin type, and selected cellulose type. At the same time, JNC introduced new designed powder transfer container to decline temperature of MOX powder. In connection with these improvements, granulation method was modified to distribute pore former uniformly in the blended MOX powder. Through these modification and improvements, low density MOX pellet fabrication process at PFPP had been established and about 5.4 millions of low density MOX pellets had been fabricated by the end of 1996.

1. INTRODUCTION

The core of MONJU reactor consists of two regions such as inner core and outer core, and numbers of fuel assembly composing each region are 108 and 90 respectively. Each fuel assembly is composed of 169 fuel pins containing MOX pellets with about 20 wt.% of plutonium for inner core fuel and about 30 wt.% of plutonium for outer core one. The nominal geometrical density of MOX pellet for "MONJU" is established at 85.0% of the theoretical density taking consideration into PCMI resistance of MOX pellet at higher burn up stage. Typical fuel specifications for MONJU MOX pellet are shown in Table I.

2. PELLET FABRICATION PROCESS

2.1. Characteristics of low density MOX pellet fabrication

In the ordinary MOX fuel fabrication process, feed PuO_2 and UO_2 powder are blended together with recycled MOX powder to meet fuel specification, pressed into the pellets and sintered at high temperature around 1700 degrees centigrade. Normally, the sintered density of this pellet reaches to around 95 % of theoretical density and this value is close to density specification of MOX pellet for other reactors. Because MONJU adopts low density MOX pellet to decrease smear density of fuel, it is necessary to decline the density of MOX pellet by approximately 10% relative lower than ordinary sintered density. The addition of pore

former is, therefore, necessary during powder treatment steps. This pore former is required to be decomposed and removed from the matrix of MOX pellet completely with other organic additives such as binder and lubricant during de-waxing step prior to sintering, which results in the formulation of closed pores within MOX pellet to meet the specification of density. The original process flow for low density MOX pellet fabrication in PFPF is shown in Figure I. In this flow, the paraffine type additive was assumed to be used as pore former and mixed into blended MOX powder with lubricant after granulation.

Table I. Typical specifications for MONJU MOX pellet

Item	Nominal Value of Specification
Equivalent Fissile Content	0.153 (For inner core fuel)
(For initial load fuel)	0.224 (For outer core fuel)
Uranium Enrichment	0.2 wt%
Impurities (typical)	C: 300 ppm N: 200 ppm Volatiles: 180 $\mu\ell/g$ MOX (including moisture)
O/M Ratio	1.97
Pellet Density	85.0
Dimensions of Pellet	Diameter: 5.40 mm Height: 8 mm (referenced value)

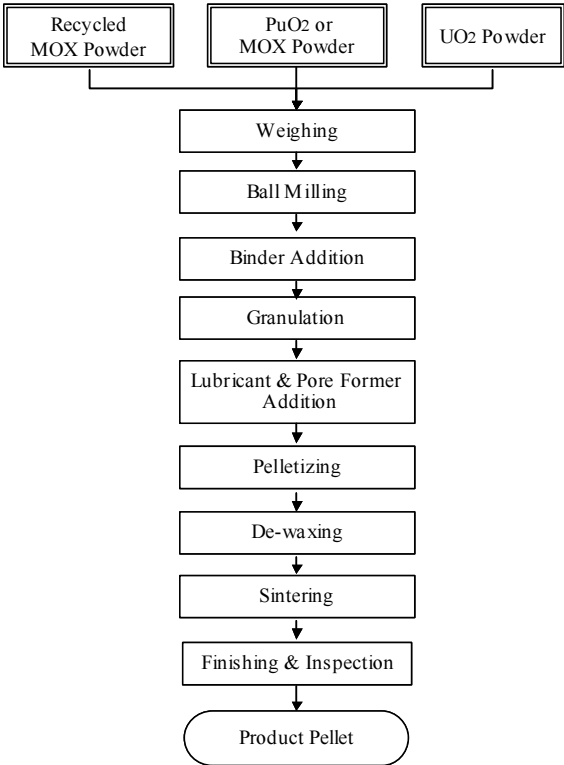


FIG. 1. The original process flow for low density MOX pellet fabrication in PFPF.

2.2. Decay heat by plutonium and its influence on organic additives

In the PFPF, a size of production lot for MONJU fuel fabrication is about 36 kilograms of MOX with about 20 and 30 wt.% of plutonium contents. After operation of each process step, these 36 kilograms of MOX powder are divided into two portions and each of them is accommodated into the powder transfer container. At the design stage of PFPF, the power transfer container was also designed to accommodate about 18 kilograms of MOX powder (about 3.2 ~ 4.7 kgPu) and was made of aluminum taking decay heat by plutonium into account. The heat generation rate from plutonium accommodated in this container was about 10 watts/kg of plutonium as shown in Ref. [1]. This heat generation rate was not significant, however the thermal conductivity of MOX powder is quite low, so the actual temperature of MOX powder at the center part of container raised up to about 180 degrees centigrade, while the surface temperature of container didn't raise significantly thanks to the radiation fins attached to the outer surface of container. An approximate expression for the thermal conductivity of MOX powder was calculated by using measured temperature of MOX powder in the container as shown in Figure 2. On the basis of this expression, the thermal conductivity of MOX powder at 100 degrees centigrade is estimated at about 0.12 watts/(m°C) for 3 g/cm³ of powder density. The temperature distribution of MOX powder within this container is calculated by using this thermal conductivity of MOX powder and measured temperatures at center and surface of container as shown in Figure 3. This temperature distribution of MOX powder within the container gave an affect on the organic additives such as Zinc-Stearates and pore former blended into the MOX powder, especially large affect to them in the portion close to the center of container. The temperature of MOX powder in this portion reached to about 180 degrees centigrade as shown in Figure 3, and this temperature was beyond the melting point of these organic additives as shown in Table II.

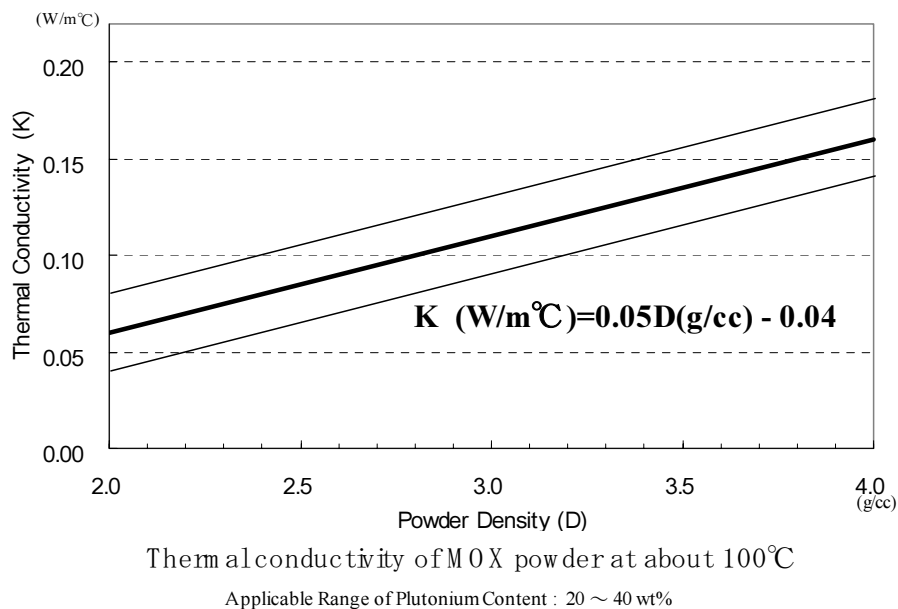


FIG. 2. Approximate expression of thermal conductivity of MOX powder.

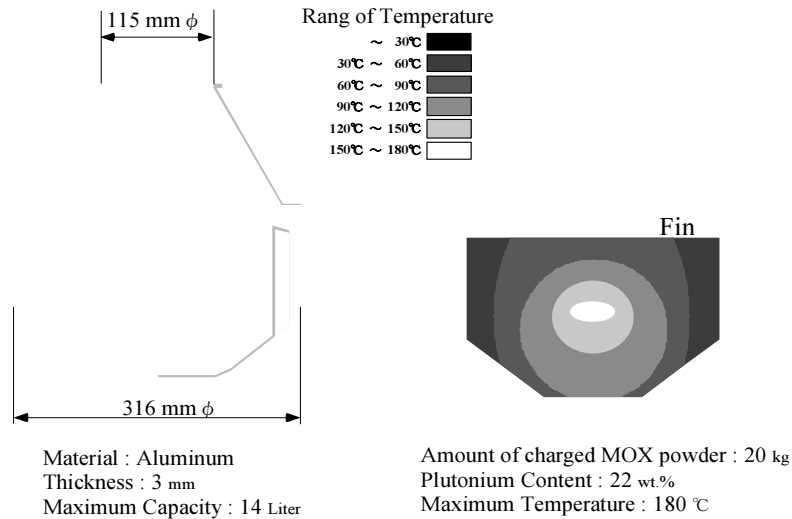


FIG. 3. Configuration of powder transfer container and temperature distribution of MOX powder within container.

Table II. Melting point of organic additives

Organic Additives	Melting Point (degrees centigrade)
Zinc-Stearates (Binder, Lubricant)	140
Paraffin Type Pore Former	85 ~ 87

Because of this temperature distribution, a certain parts of the organic additives were destructed by decay heat. This destruction of organic additives created poor quality of closed pore and wide distribution of pellet densities, which resulted in lower yield than expected production level.

2.3. Improvements and stabilization for powder treatment process

Improvements and stabilization for powder process should be required for resolving the situations described in former sections. For this purpose, the investigations with small scale testing conducted focusing on the following points:

- (1) For the alternative pore former; selection and utilization of a heat stable material being stable at least up to 200 degrees centigrade with optimized particle size;
- (2) For the powder transfer container; introduction of new designed one that could decline the temperature of accommodating MOX powder under 80 degree centigrade;
- (3) For the blending procedure of pore former with MOX powder; development of new procedure to improve the quality of closed pore distribution in the sintered pellet;
- (4) For the sintering operation; adjustment on the selected pore former.

3. TESTING FOR PROCESS IMPROVEMNTS

3.1. Selection of pore former with higher melting point

In order to find out alternative pore former with higher melting point, JNC selected several materials focusing on its chemical creation by thermal decomposition. After small scale testing for candidate pore formers to check density distribution of sintered pellets, quality of closed pore distribution in the pellet matrix and retained impurities in the sintered pellet, the crystal cellulose type pore former was selected as alternative one. The result of small scale testing concerning the closed pore distribution in the pellet matrix is shown in Figure IV.

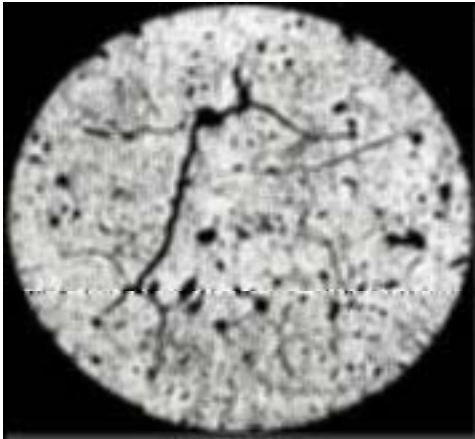


Photo-1. Ceramography of MOX pellet
with Paraffine type pore former
Pore Former Content: 1.5 wt.%
Pore Former Particle Size: 150~250 μ m

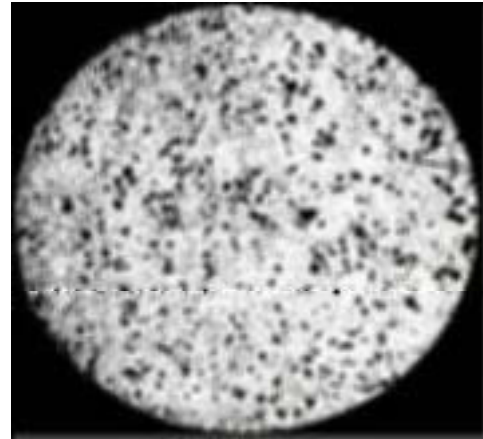


Photo-2. Ceramography of MOX pellet
with Cellulose type pore former
Pore Former Content: 1.2 wt.%
Pore Former Particle Size: 100~150 μ m

FIG. 4. Closed pore distribution in the matrix of MOX pellet.

For the purpose of optimizing the particle size of pore former, a parametric survey for optimum size of pore former were carried out as shown in Figure 5. On the basis of this result, the pore former with the particle size from 100 μ m to 150 μ m was selected for MONJU fuel fabrication. The properties of crystal cellulose type pore former are also shown in Table III.

Table III. Properties of crystal cellulose type pore former

Molecular formula	$C_6H_{10}O_5$
Decomposition temperature	350 ~ 400 degrees centigrade
Average particle size	~ 40 μ m
Bulk density	~ 0.3 g/cm ³

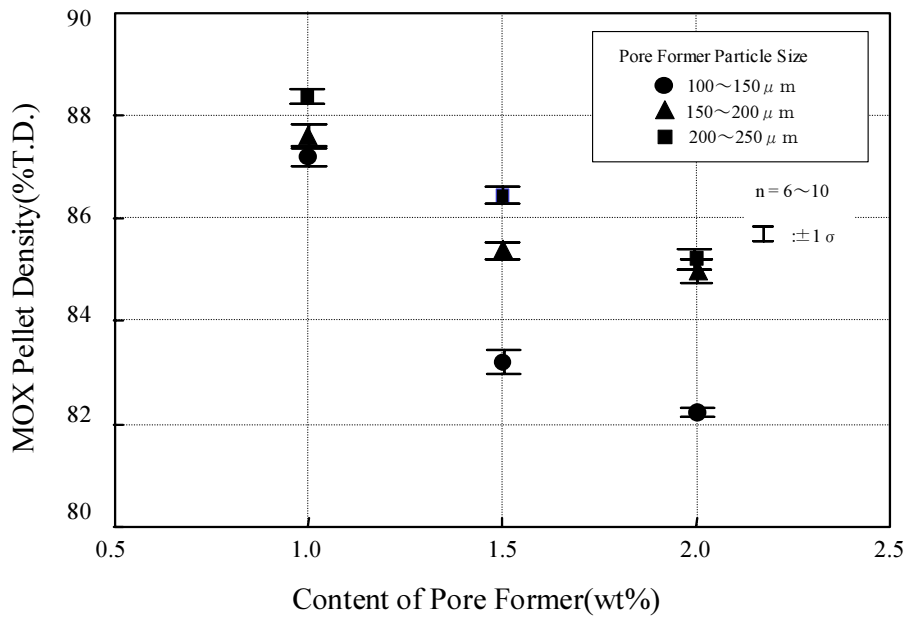


FIG. 5. Relationship between pore former content and density of sintered MOX pellet.

3.2. Introduction of new designed powder transfer container

As described in the section 2.2, the temperature of MOX powder accommodated in the powder transfer container increased up to 180 degrees centigrade at the center by decay heat of plutonium. Because of this decay heat, O/M ratio of MOX powder was drifted from around 2.0 to 2.3 by oxidation during powder treatment. This increased O/M ratio gave a certain influences on the sintering property of MOX powder. In general, increased O/M ratio enhances the sintering behavior of MOX powder. Consequently, it was understood that closed pores in the pellet matrix with higher O/M portion were easily formed at relatively low temperature in early stage of sintering. Therefore, some created gas was trapped in these closed pores during sintering and it also resulted in wide distribution of pellet densities. (See Ref.[1]) In order to decrease the temperature of MOX powder accommodated in the transfer container, new designed one was introduced. The temperature of MOX powder in this container could be decreased to 80 degrees centigrade at the center by the introduction of center pole with surface fines as shown in Figure 6.

3.3. Change on blending procedure in connection with granulation

As shown in Table III, the density of pore former is about one a tenth of MOX powder. Because of this large difference of powder density between MOX powder and pore former, timing to add pore former into blended MOX powder has a significant importance to make a homogeneous distribution of pore former in the MOX powder. At the beginning stage of low density MOX pellet fabrication, the pore former was blended with the MOX powder after granulation. Because the grain size of granulated MOX powder was distributed from 250 μm to 900 μm, the pore former was only distributed around granulated MOX powder after it was blended with granulated MOX powder. Furthermore, this pore former was easily separated from granulated MOX powder during powder treatment until pressing, and it resulted in the wide distribution of sintered pellets densities.

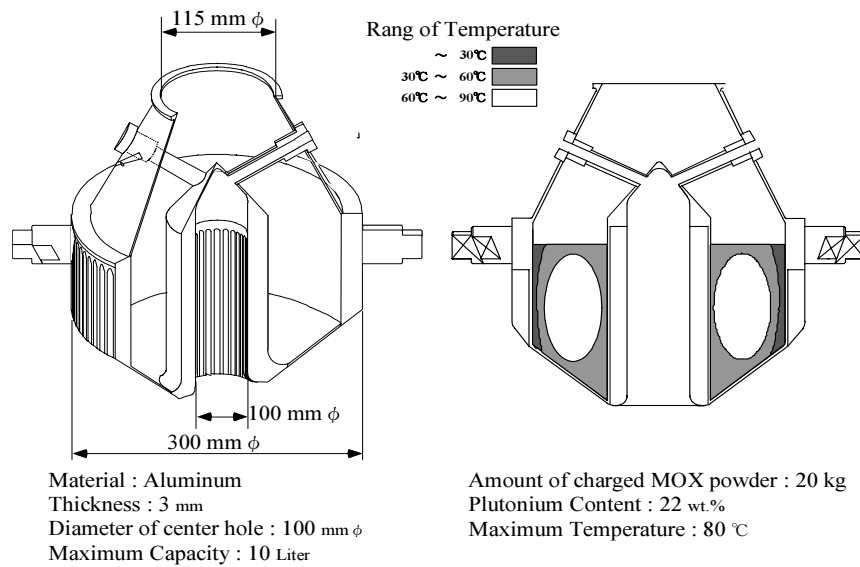


Figure 6. Configuration of new powder transfer container and temperature distribution of MOX powder within container.

In order to improve the distribution of pore former in the sintered pellet, the timing to blend pore former with MOX powder was changed from “after granulation” to “before granulation”. Because of this improvement, each pore former was covered by fine MOX powders milled by ball mill and could be maintained in the granulated MOX powder by roll press operation in a granulator. It resulted in the improved distribution of pore former in the granulated MOX powder and also in the sintered MOX pellet as shown in photo-2 of Figure 7.

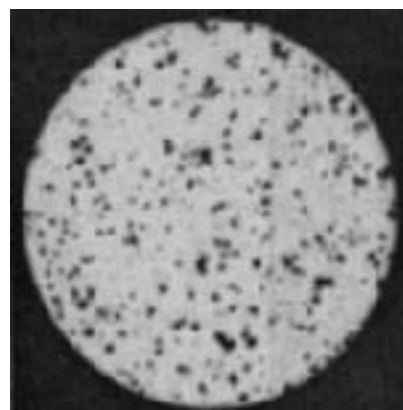
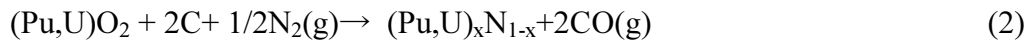
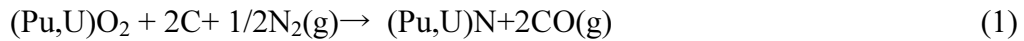


Photo-1. Ceramography of MOX pellet adding pore former after Granulation
 Photo-2. Ceramography of MOX pellet adding pore former before Granulation
 Pore Former Content: 2 wt%
 Pore Former Particle Size: 100 ~ 150 μ m

FIG. 7. Improved pore former distribution in the matrix of sintered MOX pellet.

3.4. Improvements on sintering operation

At the beginning of pellet fabrication, nitrogen contents retained in the sintered MOX pellet raised up to a several thousands ppm over the specified value of 200 ppm. It was estimated that this nitrogen came from sintering atmospheric gas, 95vol.%N₂-5vol.%H₂ mixture gas, and nitrogen was remained in the pellet matrix as plutonium and/or uranium nitride during sintering by following reactions.



On the basis of this estimation, a small scale testing was also carried out to confirm if 95vol.%Ar - 5vol.%H₂ mixture gas was effective to reduce the nitrogen contents in the sintered MOX pellet. According to this testing result, the sintering atmospheric gas was changed from 95vol.%N₂ - 5vol.%H₂ mixture gas to 95vol.%Ar - 5vol.%H₂ mixture gas in parallel with change of pore former as described in Ref. [2]. Therefore, it was also certified that selected pore former was effective to decline the density of MOX pellet under this new sintering atmospheric gas. After this improvement, a certain amount of carbon contents over specification limit was still observed. A reason of this high carbon content in sintered MOX pellet was considered that decomposed organic additives, especially CO, could not be completely removed during de-waxing step. Therefore, an additional keeping point at around 1200 degree centigrade was introduced in the temperature profile of sintering operation to promote the elimination of additives from the matrix of MOX pellet.

3.5. Full scale testing

On the basis of the improvements described in former sections, a full scale testing conducted to check out an adoptability of new process flow for actual fabrication process in PFPF. In this full scale testing, operational conditions of granulator and sintering furnace were adjusted as described in below.

1. Granulator:

In order to increase an ability of granulated MOX powder maintaining pore former in it, the distance and pressure of two roles composing a role press of granulator were optimized.

2. Sintering furnaces:

It was become clear that trapped gas such as CO in the closed pore of pellet matrix obstructed shrinking of MOX pellet during sintering and it resulted in wide distribution of pellet densities. Furthermore, this phenomenon was only observed in the MOX pellet for outer core fuel with about 30wt% of plutonium content. In order to remove this trapped gas from the matrix of MOX pellet and sinter MOX pellet completely, vacuum off gas operation and re-sintering were added to the original process flow.

Through this full scale testing, the low density MOX pellet fabrication process in PFPF on a large scale had been established as shown in Figure 8.

3.6. Performance of Improved Process

The low density MOX pellet fabrication was restarted in 1991 based on the established process flow shown in Figure XIII, and it resulted in completion of 205 fuel assemblies, 198

fuel assemblies for core fuel and 7 fuel assemblies for irradiation test fuels, for the MONJU initial load fuel in 1993. Followed by initial load fuel fabrication, the MOX pellet fabrication for the first reload fuel was started in October 1994 and fabrication of 80 fuel assemblies, 43 fuel assemblies for inner core and 37 fuel assemblies for our core, was completed successfully in March 1996. The amounts of MOX pellets fabricated for each core are shown in Figure 9.

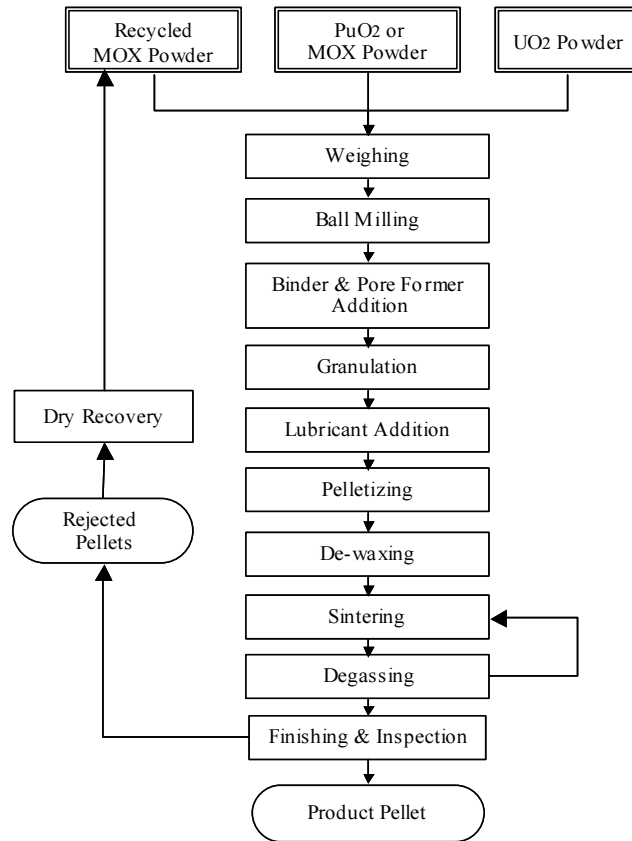


FIG. 8. Established process flow for low density MOX pellet fabrication in PFPF.

Although the averaged yield of product MOX pellets was quite lower level during low density MOX pellet fabrication with paraffine type pore former, it was drastically raised up after improvements on process. Furthermore, it still had continued during the first reload fuel fabrication for MONJU and it reached to almost production level.

4. FUTURE DIRECTION

Through the fuel fabrication for the MONJU initial and first reload fuel, the low density MOX pellet fabrication process could be established as almost same level of high density MOX pellet fabrication. It is one of the missions given for JNC to develop and demonstrate the FBR and its related technologies for future commercial use of plutonium. Under this mission, JNC has carried out development of MOX fuel and fuel fabrication technology to reduce fuel cost. For reducing MOX fuel cost, it is effective to introduce MOX pellet with larger diameter because the number of MOX pellets and fuel pins composing a fuel assembly could be decreased. In order to achieve same generating power per fuel assembly by decreased number of fuel pins, it is required to increase linear power for each fuel. However, linear power for

fuel pin consisted of low density MOX pellets is limited compared to high density one because of low thermal conductivity of low density MOX pellet. Therefore, adoption of annular pellet with larger diameter is effective to realize high linear powder fuel pin for high burn up FBR fuel. Under this recognition, JNC has already started the development of annular pellet fabrication technology prepared for MONJU high burn up fuel. Now development of pressing machine with die-wall lubricating mechanism by dry method is underway for annular pellet fabrication.

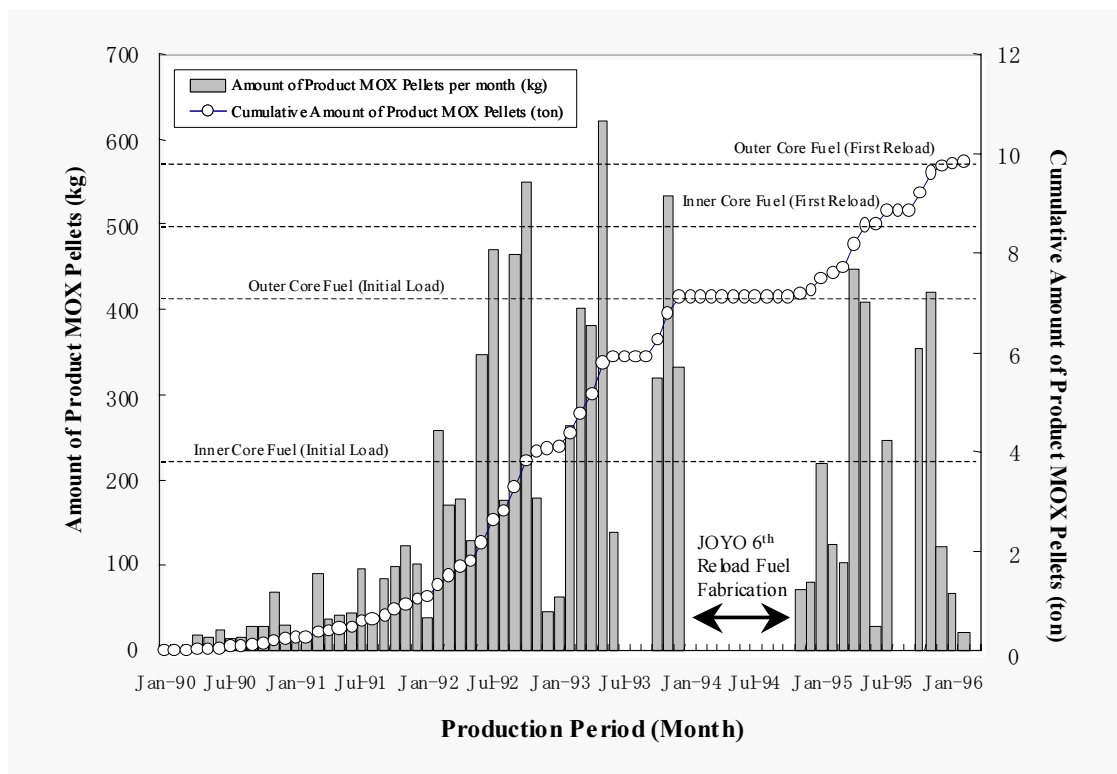


FIG. 9. Amounts of MOX pellets fabricated in MONJU fuel fabrication.

5. CONCLUSION

1. Through the MOX fuel fabrication for the MONJU initial load fuel and first reloaded fuel, the low density MOX pellet fabrication process in PFPF had been established;
2. Annular pellet fabrication technology has been developed for MONJU higher burn up fuel.

REFERENCES

- [1] AOKI, Y., KASHIMURA, M., YAMAGUCHI, T., "Development of Fabrication Technology of Low Density Pellet for FBR", Future Nuclear Systems (Proc Int. Conf. Yokohama, 1997), JNS, Tokyo (1998).
- [2] ASAKURA, K., AONO, S., YAMAGUCHI, T., DEGUCHI, M., "Current Developments of Fuel Fabrication Technologies at the Plutonium Fuel Production Facility, PFPF", MOX Fuel Cycle Technologies for Long Term Deployment (Proc. Int. Symp. Vienna, 1999), IAEA, Vienna (2000) 118.

DEVELOPMENT OF TECHNOLOGIES OF NUCLEAR CERAMIC GRADE FUEL PRODUCTION

S.A. YASHIN, A.E. GAGARIN, A.V. MANYCH
Joint Stock Company “Ulba Metallurgical Plant”
Republic of Kazakhstan

Abstract

JSC “Ulba Metallurgical Plant” has developed and implemented unique technologies of fuel pellets production that allow:

- Regulating the average grain size and grain distribution by sizes within wide ranges by using methods of pellet alloying: from bimodal structure with the grain size of 1–3 μm of fine grain phase and 10–30 μm of coarse grain phase to homogeneous mono-modal structure with the average grain size about 20–50 μm . The summary boron equivalent of alloyed pellets not exceed 1.0 $\mu\text{g/gU}$;
- Regulating pore distribution by sizes (while the homogeneous pore structure is maintained) by adding special pore-forming agents: from mono-modal distribution with average pore sizes around 1.5–3.5 μm to bimodal distribution with average size of small pores around 1–3 μm and average size of large pores around 10–50 μm .

The principles of microstructure control are based on laws and mechanisms of microstructure evolution at all stages of sintering. For example, the interaction between regular pores and grain boundary is an important element in initiation of grain and pellet density increase. The control over pore mobility allows improving plasticity of pellets through increasing the amount of pores on grain boundaries and creating the conditions for plastic deformation

1. INTRODUCTION

JSC “Ulba Metallurgical Plant” (“UMP”) produces different types of uranium products for more than forty years. Today, these products include fuel pellets for nuclear reactors from uranium dioxide and uranium dioxide with burnable poisons such as erbium and gadolinium oxides. Besides, “UMP” produces uranium dioxide ceramic powders with high level of nuclear purity and powders from natural uranium.

Fuel pellets production technology at JSC “UMP” is based on conventional methods of powder metallurgy – uranium dioxide powder preparation, preliminary compaction and homogenization of its properties, preparation of moulding powder with addition of binding and lubricating substances, formation of green pellets in hydraulic and mechanical automatic presses, sintering of green pellets in hydrogen atmosphere, cylindrical grinding of sintered pellets. The high level of stability and maturity of technological processes allow producing pellets that meet high quality requirements of our customers.

At the same time, in 2000-2003 JSC “UMP” conducted a range of works focused on improving fuel pellets characteristics, that influence the operating efficiency of fuel assembly during fuel irradiation under high level of burning-out and in reactor capacity maneuvering mode. First of all, these are such characteristics of pellets as uniformity and homogeneity of microstructure, level of open porosity, pore distribution according to size, grain size, thermal stability, and plasticity of pellets.

Improvement of microstructure, morphology of which is responsible for all essential properties of pellets, was achieved by step-by-step analysis of physicochemical contents of events at each stage of technological process of uranium dioxide powder and pellets production, by searching for interconnections between those events, and finally, by defining the basic “levers” for the control of microstructure.

2. OPTIMIZATION OF PELLET PORE STRUCTURE

As a result of research it was determined that the degree of pore structure homogeneity depends to a great extent on stress-strain fluctuations during mechanical treatment of uranium dioxide powders, that leads to different shrinkage rate of individual microscopic volumes during sintering, and therefore, to heterogeneous pore structure. Taking this into account, the purposeful optimization of technological process allowed producing pellets with pore structure with high level of uniformity and homogeneity (Fig. 1). The maximum level of open porosity do not exceed 0.3% (Fig. 2). Besides, such microstructure optimization allowed reducing the range of density values (Fig. 3).

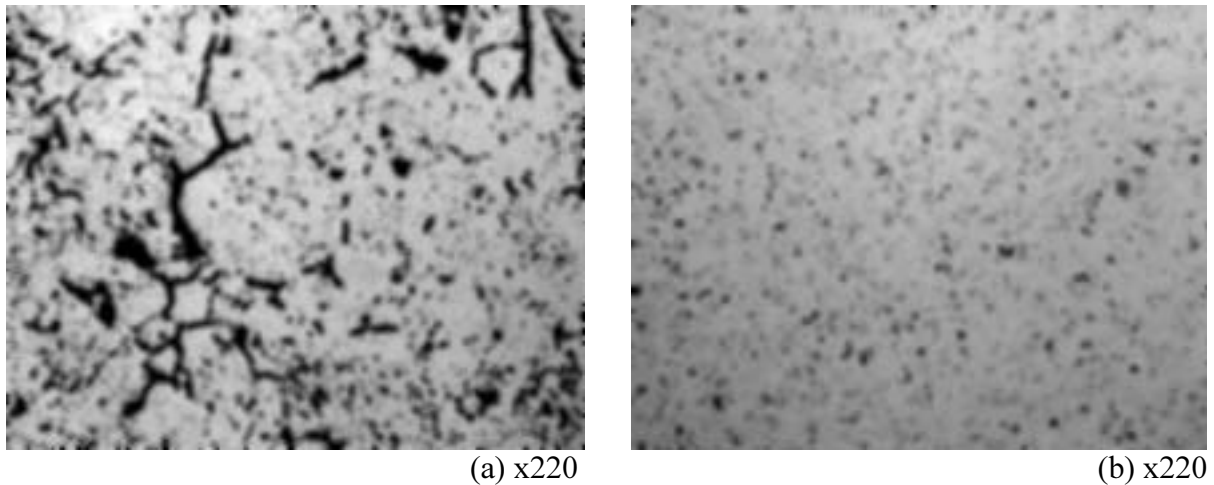


*FIG. 1. Pore structure of a sintered pellet UO_2 :
a – non-optimal pore structure;
b – optimal pore structure.*

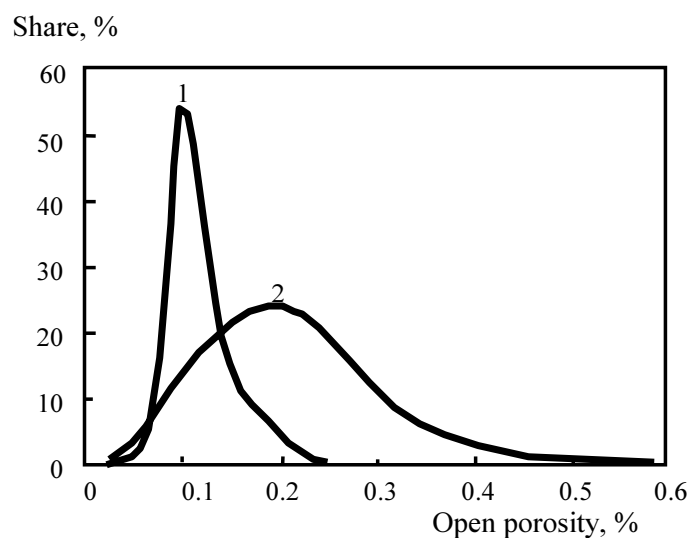


*FIG. 2. Distribution of open porosity values. Statistics by pellet lots:
1 – optimized pellets;
2 – usual pellets.*

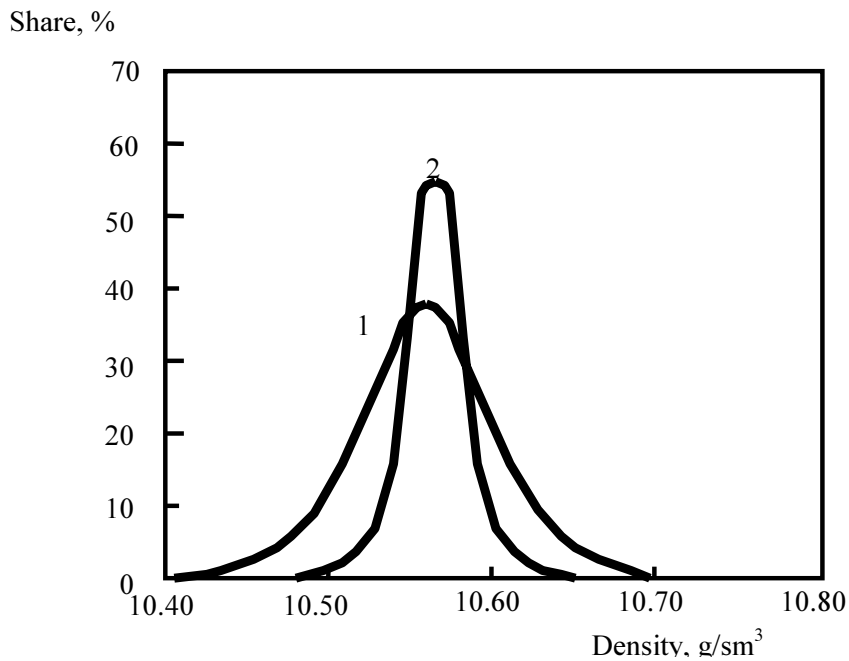


FIG. 3. Pellet density values distribution. Statistics by pellet lots:
 1 – usual pellets;
 2 – optimized pellets.

JSC “UMP” has developed the technology that allows regulate pore structure and density of the pellets using special pore agents burning out at the first stage of sintering. The use of pore-forming agents does not change chemical composition of pellets. Regulation of initial size of pore agents allows regulating pore distribution by sizes (while the homogeneous pore structure is maintained): from monomodal distribution with average pore sizes around 1.5÷3.5 μm to bimodal distribution with average size of small pores around 1÷3 μm and average size of large pores around 10÷50 μm (Fig. 4). Regulation of the amount of pore agent allows regulating pellet density to desired value while the optimal thermal stability of pellets during additional test roasting is maintained (Fig. 5).

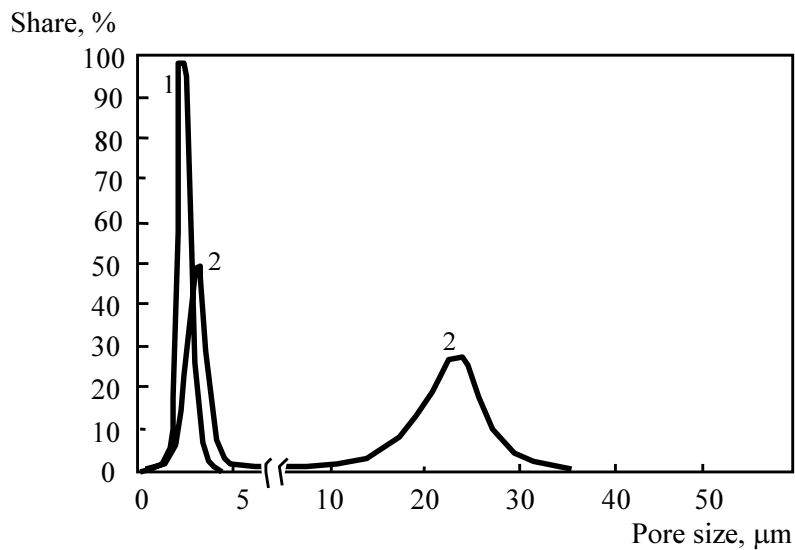
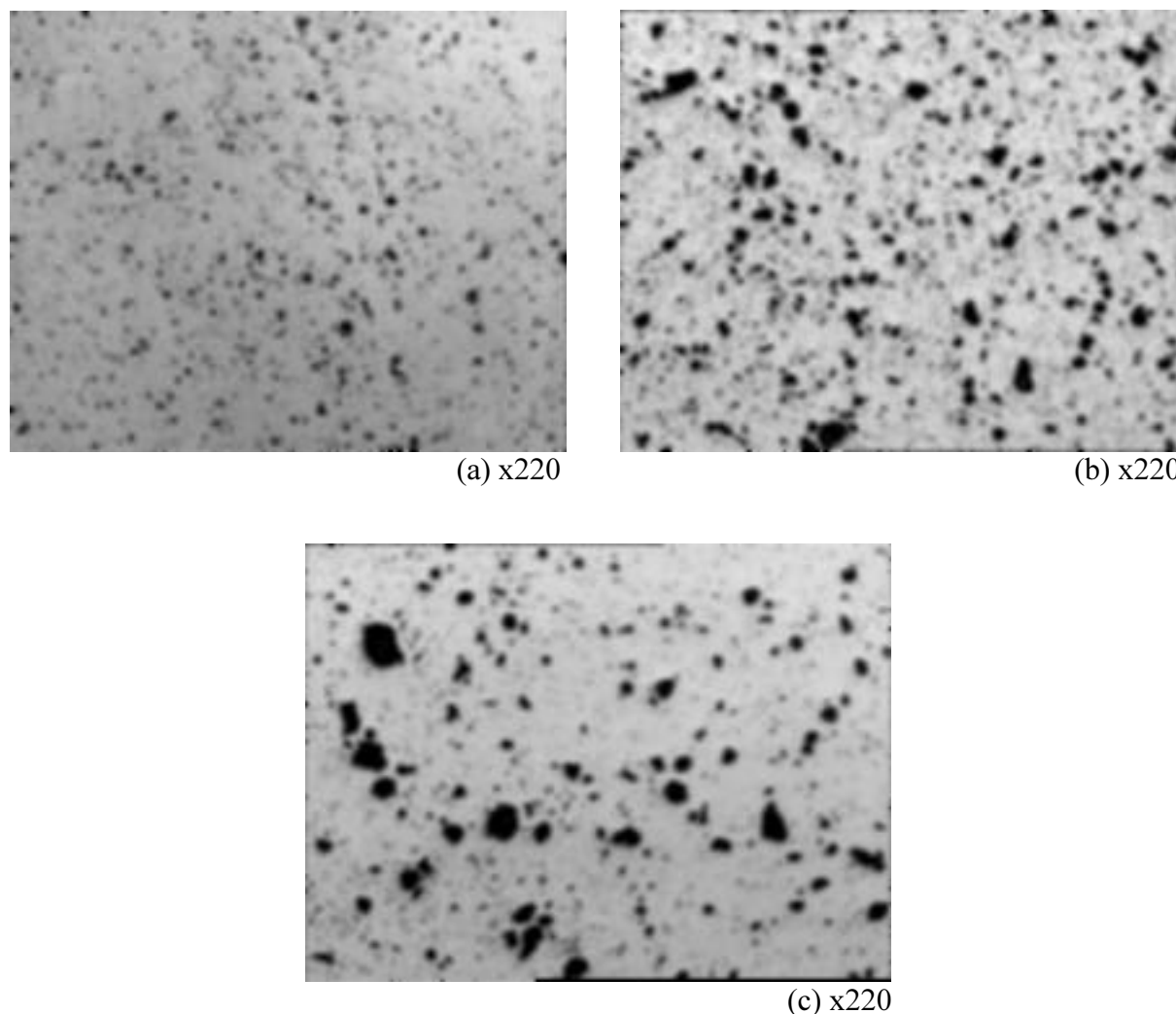


FIG. 4. Pore distribution in sintered pellets by size:
 1 – monomodal pore distribution;
 2 – bimodal pore distribution.

It is necessary to mention that achievement and maintenance of high quality and, more important, stability of properties of initial powders play an important role in optimization of fuel pellets characteristics. Technology of ceramic uranium dioxide powders production at JSC “UMP” is based on hydrolysis extraction procedure and processing of obtained solution of uranyl nitrate by precipitation of ammonium polyuranate to uranium dioxide (ADU process). While this procedure is quite traditional, there are always continuous improvement of the technological process, re-equipment of production facilities, and use of new highly effective equipment.



*FIG. 5. Pore microstructure of a sintered pellet UO_2 with addition of pore agent:
a – 0.1 wt %, b – 0.5 wt %, c – 1.0 wt % of pore agent.*

The use of statistical methods and analysis for controlling the technological process of powders and pellets production based on electronic database allows using the obtained information for the technological process regulation using control cards, repeatability indexes and analytical tables. Analysis for the period of 2002–2003 allows talking about stability of the technological process of powders and pellets manufacturing for a set of controllable parameters.

3. GRAIN SIZE INCREASE AND IMPROVEMENT OF PLASTIC PROPERTIES OF PELLETS

The problem of increase of average grain size and improvement of pellets' plasticity are the most interesting and complicated problems from the scientific and technological points of view. Solution of these problems is connected to the need to study and apply the laws and mechanisms of microstructure evolution at all stages of sintering.

Mechanisms of admixtures' impact on activation of ceramic fuel pellets' grain size growth during sintering are well known today [1,2]. Kinetics of these mechanisms lies either in modification of grains that facilitates boundary interaction or in increase of defectiveness of UO_2 crystal lattice during solid solution generation that accelerates diffusion processes. At the same time, these mechanisms do not cover the problem of interaction between regular and technological pores. However, this interaction plays an important role in pellet microstructure formation at the final sintering stage and also is an important element in initiation of grain increase, increase of pellet density and improvement of plastic properties.

So, closed isolated pores, forming of which corresponds to the completion of the first stage of sintering process, are located in the deepest energetic sinks – on grain boundaries. Depending on linear dimensions of elements of local “pore-grain boundary” systems, the results of their interaction during initialization of boundary migration (grain growth) can be as the follows [3]:

- Pores stay attached to grain boundary and prevent their migration, which is similar to dispersal inclusions of the second phase when boundary separation is pointless because of increase in boundaries extension. Completion of such type of interaction corresponds to complete dissolution of pore through surface diffusion on grain boundaries;
- Pores stay attached to grain boundaries and migrate with them with the rate equal to the rate of boundary motion and, therefore, do not prevent grain growth;
- Pores get detached from boundaries and get captured inside the grain. It occurs when the speed of boundary motion exceeds the maximum possible speed of pore motion. Get captured inside the grain, pores do not experience its volume reduction and, therefore, do not impact the shrinkage of the pellet.

The final result of the analysis can be presented as a diagram showing the interaction between pores and grain boundaries (Fig. 6), where two limiting conditions determine the boundaries of separation area (R - radius of grain's curvature, M_b - mobility of the grain's boundary, $D_s\delta_s$ - surface diffusion parameter, a_0 - pore radius, Ω -atomic volume)

Application of this diagram for the evaluation of interaction between pores and grain boundaries during sintering of “pure” UO_2 (given the constant amount of admixtures) gives results that correspond to the effects observed in practice.

Analysis of the problem of ensuring the fuel pellets (from UO_2) size within the range of 20–30 μm and more, which is necessary for intra-granulate retention of gaseous products of fission, allowed examine and distinguish particular interaction between pores and grain boundaries that is caused by presence in UO_2 powder of alloy admixtures, particularly, double addition of aluminum oxide (Al_2O_3) and silicon oxide (SiO_2). Combined use of these additions as a different aluminum silicates (separate use of these admixtures do not have a significant impact on grain growth) changes the nature of interaction between pores and grain boundaries significantly that is indicated by the research of kinetics of sample roasting and ceramography.

As can be seen from Figure 6, the process of UO_2 samples shrinkage stops at the grain size of $12\div 14\ \mu\text{m}$ that corresponds with locations of the pores with minimal critical size on the grain boundaries. Further isothermal sample roasting and related collective crystallization cause reduction of pore's volume and further grain growth.

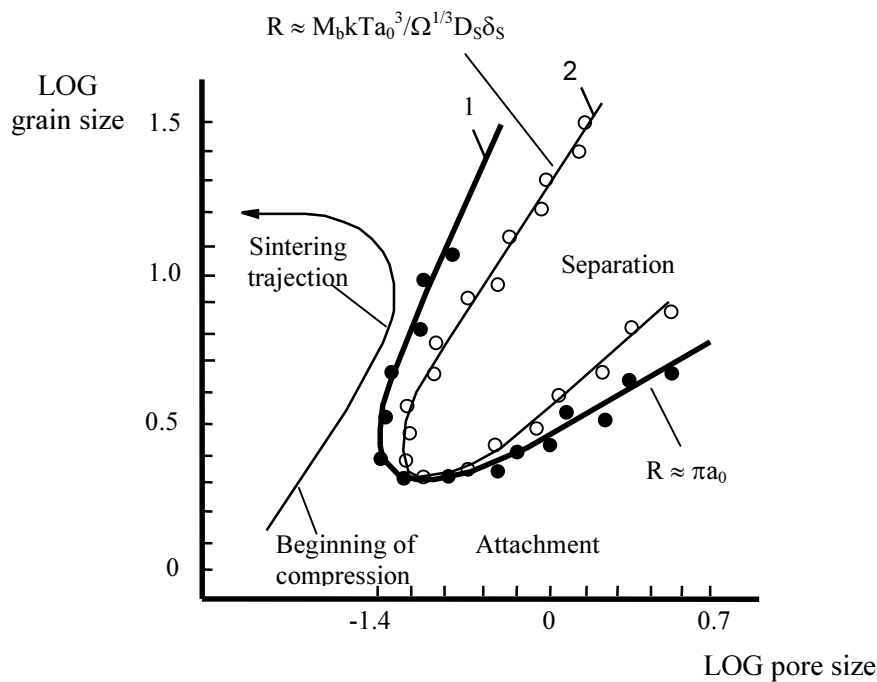


FIG. 6. Diagram of interaction between pores and grain boundaries:

- 1 – «theoretical» curvature of diagram for “pure” UO_2 ;
 - – experimental data for “pure” UO_2 ;
- 2 – ○ – experimental curvature of diagram in the case of UO_2 alloying with aluminum silicate admixture in the amount of 0.005 %.

Thus, amount and size of pores that are close to constant at the final stage of sintering and, therefore, density of sintered products, which is a result of unified nature of the material and stable production technology, ensure traditional and almost always constant average value of pellets' grain size (given the constant amount of admixtures). Besides, inhibitory influence of pores on the speed of grain boundary motion is the reason why grain structure during the sintering almost never achieves the full degree of recrystallization. Therefore, the traditional average size of a fuel pellet's grain form UO_2 is about $10\div 15\ \mu\text{m}$.

Undoubtedly, limited amount of admixtures as to powder, as to fuel pellets, which ensures the nuclear grade of the fuel, directly influences the nature of interaction between pores and grain boundary. Including into UO_2 powder aluminum silicate admixture up to 0.010 wt % of Al and Si to U content do not change the nature of sample shrinkage (compressed pellets) but causes the grain growth up to $25\div 30\ \mu\text{m}$ (Fig. 7).

Evaluation of grain growth and size of pores attached and detached from grain boundaries allowed plotting an experimental curve - diagram of interaction between pores and grain boundaries in the process of sintering in the case of alloying UO_2 with aluminum silicate admixture (Fig. 6). Nature of such dependence does not explain the pore motion only due to surface diffusion. Taking into account the fact that Al_2O_3 has high gas pressure under the UO_2 sintering temperature of about 1700°C , it was assumed that in this case the basic mechanism that causes the pore motion is a mechanism of “evaporation-condensation”. In this case, the

nature of interaction between pores and grain boundaries can change significantly both in the area of attachment and in the area of detachment of pores from grain boundaries.

According to this model curvature or curvature gradient of leading surface of moving pore causes substance redistribution through surface diffusion from leading surface to support surface of the pore (Fig. 8). Surface diffusion and “evaporation-condensation” have to redistribute Al_2O_3 over the migrating pore surface constantly. The difference between Al_2O_3 concentration on the leading and support surfaces results in Al_2O_3 flow (during vapor phase) to the leading surface that causes reverse stream of uranium containing components of the vapor. To achieve permanent process of substance circulation inside the pore, evaporation has to be balanced and constant excess of Al_2O_3 on the supporting surface has to be supported by its surface diffusion from leading surface of the pore to support surface. Movement of uranium atoms in the mechanism of evaporation-condensation, which is initiated by presence of Al_2O_3 , supplements pore motion by the surface diffusion and, therefore, causes increase in the speed of pore motion (and also widens the range of pores able to move with the grain boundaries) making it comparable with the speed of grain boundary motion.

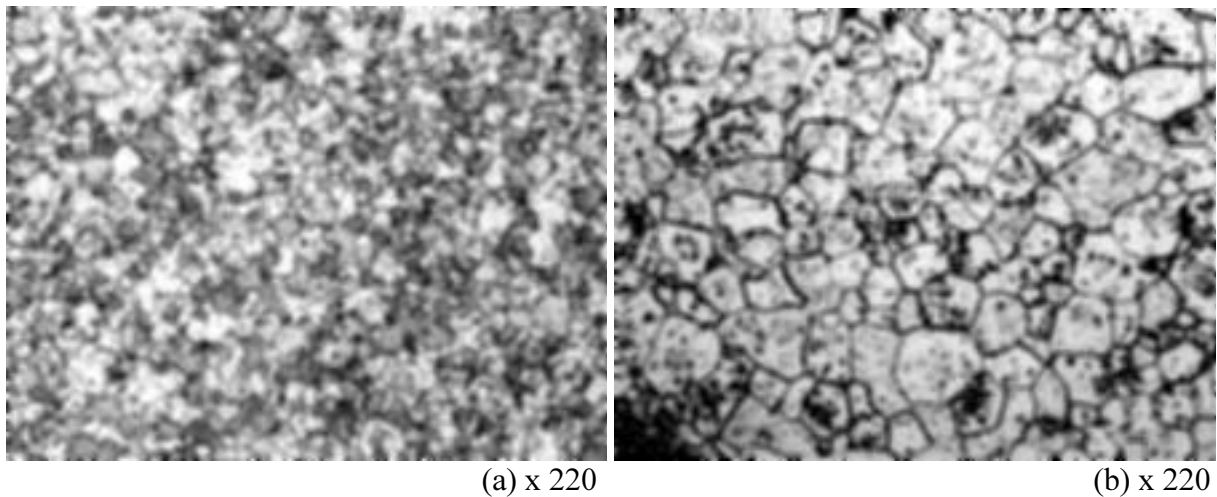


FIG. 7. Microstructure of UO_2 sintered pellet:
a – microstructure of “pure” UO_2 ;
b – microstructure of UO_2 alloyed with aluminum silicate admixture.

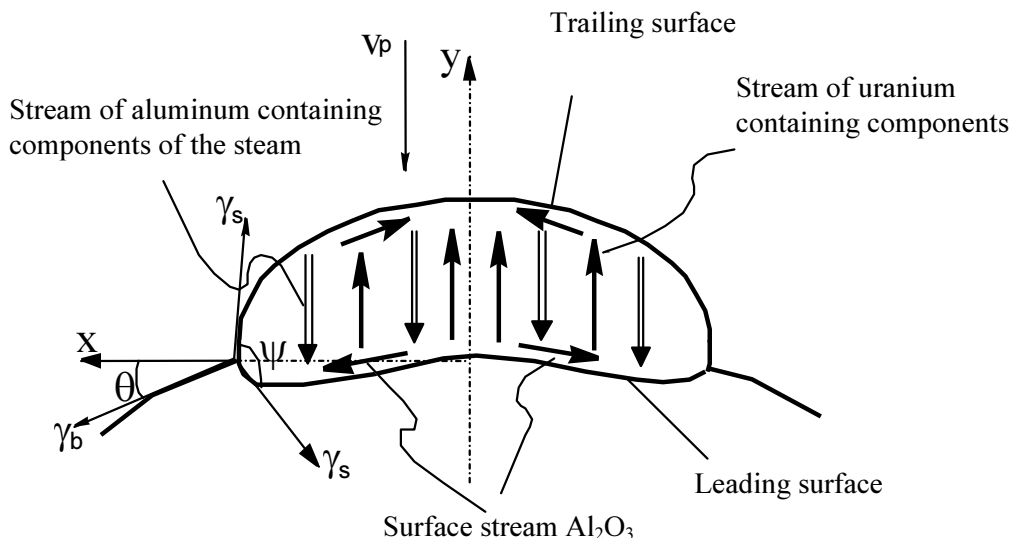
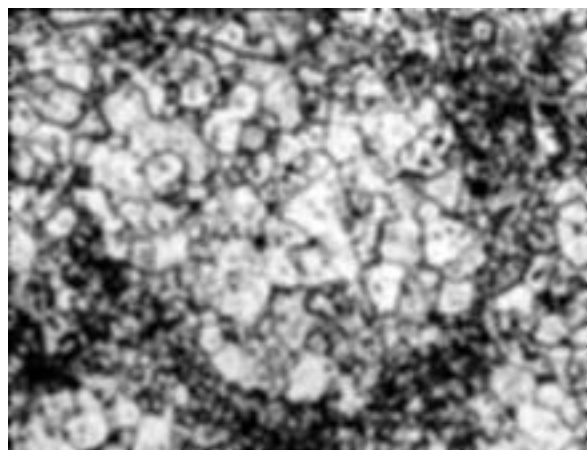


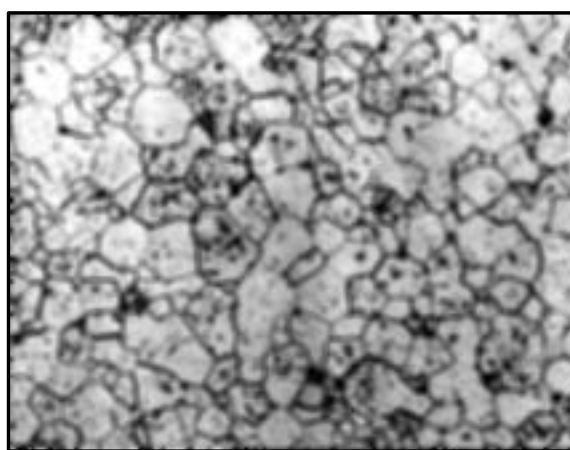
FIG. 8. Pore motion by “evaporation-condensation” mechanism.

According to the described model, the role of SiO_2 in addition comes to the role of acceleration of the migration of grain boundaries at the first stage of grain growth due to formation of liquid silicon phase on the grain boundaries. This ensures the necessary “initial” grain size required for involvement of higher amount of pores into the motion by mechanism of evaporation-condensation. Almost any admixture that accelerates the grain size growth (such as oxides of ferrum, niobium, titanium, etc) can be used as admixtures. In any case, using this addition with Al_2O_3 , the resulting grain size will be higher than using addition separately (higher size of $100\ \mu\text{m}$ can be achieved with the total admixture content less than $0.020\ \text{wt}\%$).

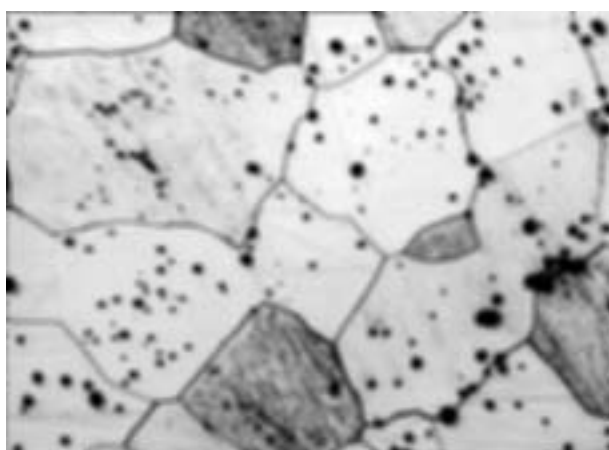
The results of studies of UO_2 microstructure evolution during the sintering with alloy admixtures allow achieving required density values, average grain size and grain distribution by size (varying the amount of admixture). Specialists of JSC “UMP” developed the unique methods of using admixtures while providing uniform distribution inside pellets. The obtained results gave the opportunity to modernize the existing technologies, develop and implement a new unique technology of pellet production that allows regulate grain size and grain distribution by size within the wide range: from bimodal structure with the grain size of $1\div 3\ \mu\text{m}$ of fine-grained phase and $10\div 30\ \mu\text{m}$ of coarse-grained phase to homogeneous monomodal structure with the average grain size about $20\div 50\ \mu\text{m}$. Summary boron equivalent of alloyed pellets does not exceed $1.0\ \mu\text{g/gU}$ (Fig. 9,10).



(a) x220



(b) x220



(c) x220

*FIG. 9. Grain microstructure of fuel pellets:
a – pellet with bimodal structure;
b – pellet with monomodal ($G \sim 23\ \mu\text{m}$);
c – pellet with monomodal ($G \sim 90\ \mu\text{m}$).*

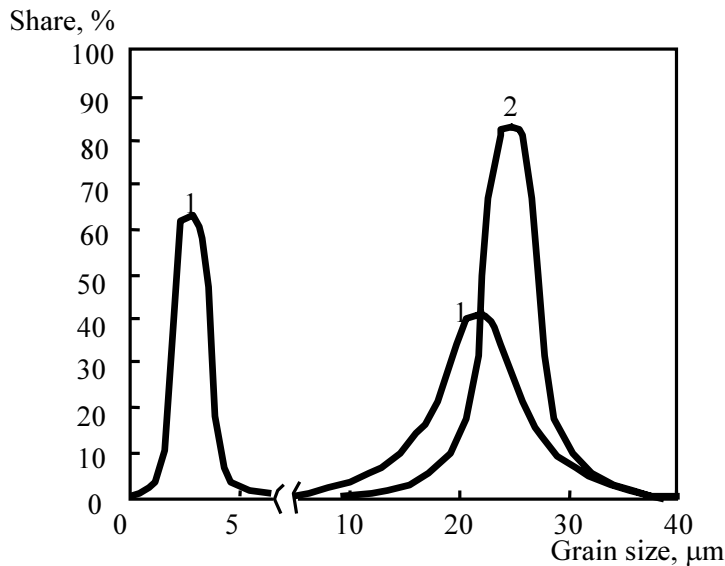


FIG. 10. Grain size distribution in sintered pellet:
 1 – pellet with bimodal structure;
 2 – pellet with monomodal structure.

The most problematic issue is to achieve the grain size about 20÷30 μm in pellets with burnable poisons (oxides of erbium and gadolinium). While trying to solve this problem, for example, for the pellets of uranium-gadolinium fuel, researcher comes across the necessity to neutralize conservative influence of solid solution (U,Gd)O₂ that is formed during the process of pellet sintering. Adding small quantity of alloy admixtures, which do not affect nuclear purity of the fuel, do not activate grain growth. It occurs because in the process of solid substitutional solution forming according to the following pattern: $2\text{Gd}^{3+} \rightarrow 2\text{U}^{4+} - \text{O}^{2-}$ it is necessary to have an excess of anion vacancy in oxygen sublattice. As a result of it, the process of (U,Gd)O₂ formation is most likely at the final sintering stage, or at the temperature not more than 1600⁰C. At this stage the compensation mechanism of excessive positive charge is caused by vacancy flow to the front edge of forming solid solution. In some cases of deficit of oxygen atoms at sublattice at the final stage of sintering, formation of solid solution (U,Gd)O₂, to some extent, causes the formation of complex: gadolinium atom – vacancy. At the low oxygen partial pressure this leads to the deficit of punctual effects of additions that result in lower speed of all processes controlled by diffusion. As our investigations showed, one of the solutions of this problem is a highly accurate control of atmosphere humidity in the sintering furnace. Another solution that is implemented in our technology is achieving maximum delocalization of solid solution (U,Gd)O₂ in fuel pellet by adding gadolinium atoms into compressed powder UO₂ as different gadolinium solutions. In this case, the maximum homogeneous distribution of gadolinium in the pellet is achieved and problem of grain growth is solved (Fig. 11).

In addition, we have developed the method of the average grain size increase other than adding alloying admixtures. This method consists in the use of highly active UO₂ powders with specific area value within the range of 6÷8 m²/g. To prevent uncontrolled oxidation of such powders it is necessary to include the stage of its surface passivation that is carried out in nitrogen –aerial mixture with controlled oxygen content. Further, there is no significant powder oxidation during the mechanical treatment of passivated powders. High compression rate of pellets produced from such powders at the initial stage of sintering causes the early beginning of the collective recrystallization process and by the end of sintering the average grain size is up to 25÷30 μm.

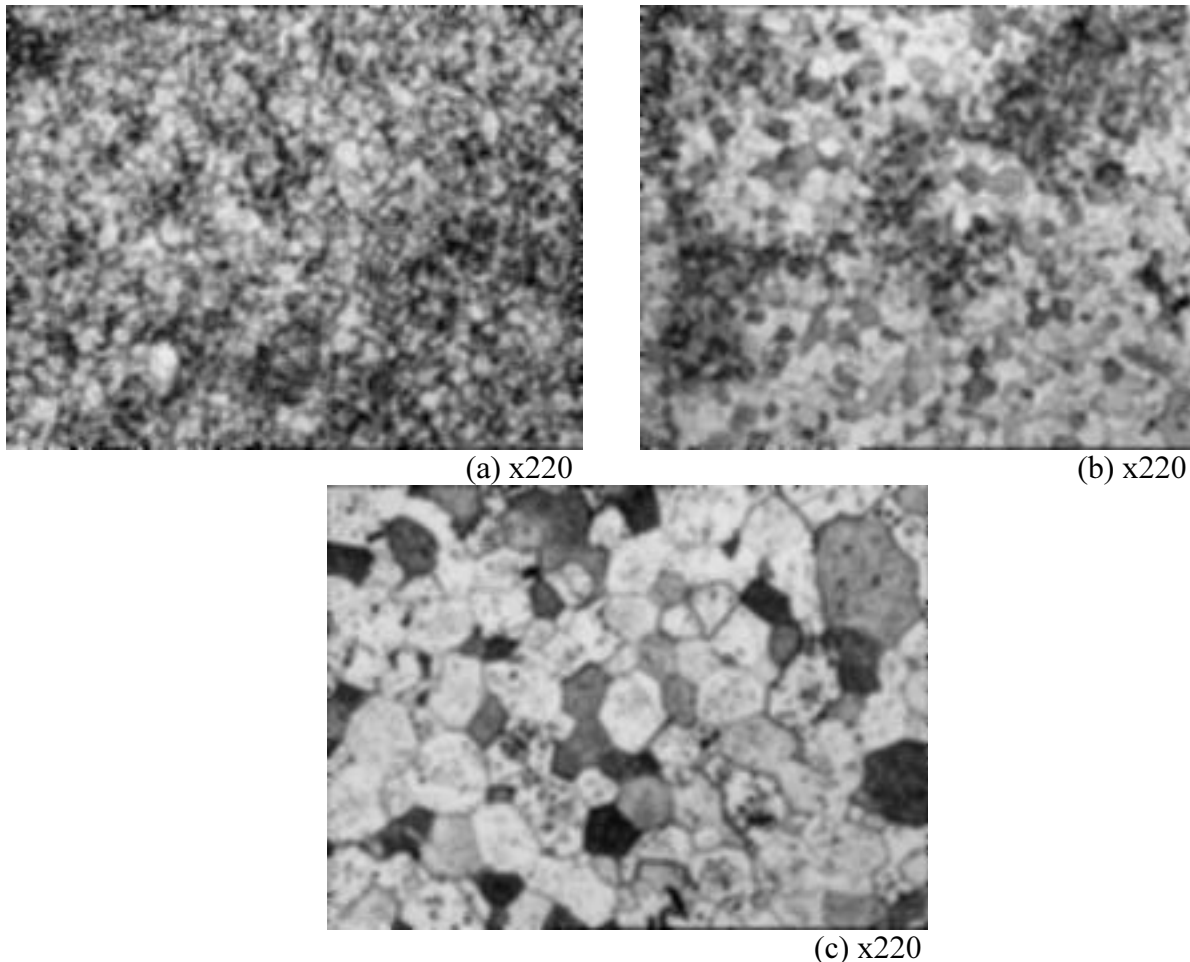


FIG. 11. Microstructure of the pellet of uranium-gadolinium fuel:

- a – microstructure of non-optimized pellet of uranium-gadolinium fuel (average grain size 11 μm);*
- b – microstructure of the pellet alloyed with aluminum silicate admixture in the amount of 0.010 wt % (average grain size 14 μm);*
- c – microstructure of the pellet optimized by adding gadolinium and alloying with aluminum silicate admixture in the amount of 0.010 wt % (average grain size 30 μm).*

JSC “UMP” carried out a wide range of works to optimize plastic properties of pellets. It is known that the technology of production of such fuel is also based on pellets alloying. Analysis of plastic properties of pellets with bimodal grain structure showed that such microstructure has some advantages over monomodal structure. While trying to achieve the grain size of about 30 μm, the plastic properties of the pellet are reduced significantly. This necessitates additional alloying that can affect nuclear grade of fuel. In the case of pellets with bimodal grain structure plastic properties remain at the same level while the concentration of alloy admixtures is low and the grain size is quite large. This can be seen from Figure 12 (rate of plastic deformation under constant load), that shows the creep rate in the function of inverse temperature for fuel pellets modified by different quantity of admixtures.

Regulation of pore mobility using aluminum-containing admixtures (as it was shown in the description of mechanism of grain growth activation) also allows improving plastic properties of pellets through increasing the amount of pores on grain boundaries and creating the conditions for plastic deformation. If the admixture (for example, aluminum silicate) concentration is high (within the range of 0.025÷1.00 wt %) then the high pellet creep rate is

caused by activation of grain-boundary sliding because of formation of easily-melted eutectic on the grain boundaries. Otherwise, if the admixture concentration is within the range 0.002÷0.010 wt %, then the increased creep rate can be explained by the increased quantity of pores on grain boundaries.

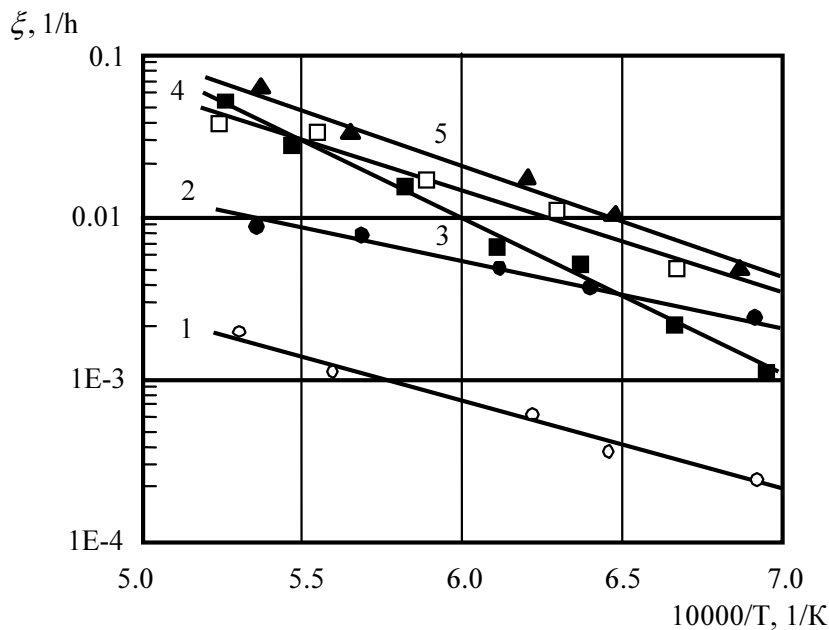
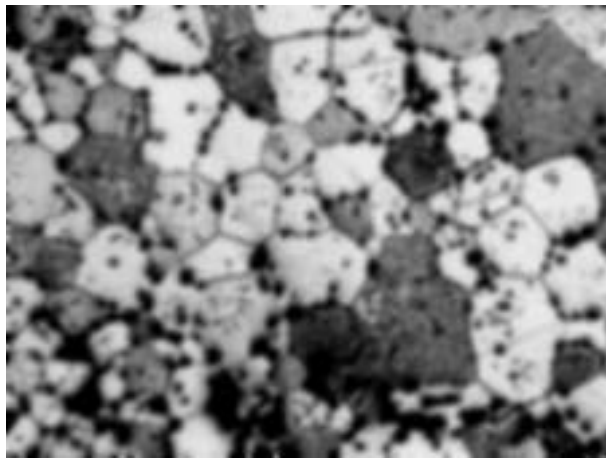


FIG. 12. Correlation of fuel pellets creep rate in the function of inverse temperature under the strain of 30 MPa:

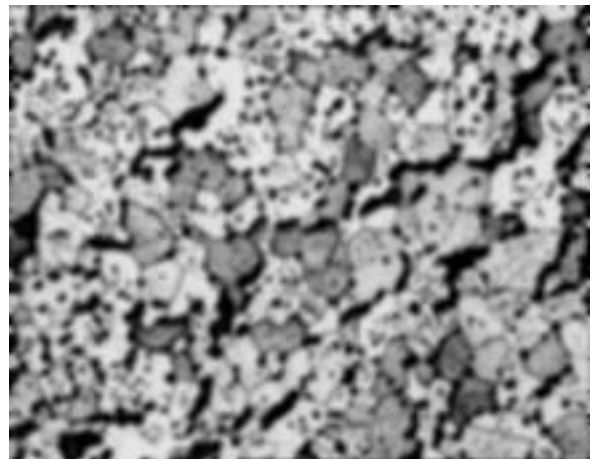
- 1 – fuel pellet from “pure” UO_2 (average grain size $13 \mu m$);
- 2 – fuel pellet from UO_2 alloyed with aluminum silicate admixture (admixture concentration 0.0050 wt %, average grain size $25 \mu m$);
- 3 – fuel pellet from UO_2 with bimodal microstructure alloyed with aluminum silicate admixture (admixture concentration 0.0030 wt %, average grain size $20 \mu m$);
- 4 – fuel pellet from UO_2 alloyed with aluminum silicate admixture (admixture concentration 0.010 wt %, average grain size $30 \mu m$);
- 5 – fuel pellet from UO_2 alloyed with aluminum silicate admixture (admixture concentration 0.025 wt %, average grain size $30 \mu m$).

As our investigations showed, in order to keep the UO_2 nuclear grade of ceramic fuel (the summary boron equivalent is not more than $1.0 \mu g/gU$) and to increase its plastic properties at operating temperatures of active zone of reactor, it is sufficient to add alloy aluminum-silicate admixture in the amount not exceeding 0.010 wt %. Evaluation of creep rate of such pellets showed that it is significantly higher than that of pellets without alloy admixtures (Fig. 12). Further increase of admixture concentration up to 0.5 wt % increases the fuel creep rate, while increase of concentration from 0.5 wt % and higher do not have significant impact on creep rate.

Analysis of fuel pellet microstructure alloyed with aluminum silicate admixtures within the concentration of 0.0020÷0.10 wt % showed the expected pore accumulation on grain boundaries (Fig. 13). However, when the concentration of admixture is higher than 0.025 wt % these pores can be subjected to coalescence and decrease the pellet density. During mechanical load under high pellet temperature with optimal concentration of alloy admixture and, therefore, with controlled amount of pores on the grain boundaries, exertion around such pores increases, that activates dislocational creeping mechanisms that require such exertion.



(a) x560



(b) x220

*FIG. 13. Microstructure of UO₂ fuel pellet alloyed with aluminum silicate admixture:
a – with admixture concentration of 0.010 wt.%;
b – with admixture concentration of 0.025 wt.%.*

During mechanical load under high pellet temperature with optimal concentration of alloy admixture and, therefore, with controlled amount of pores on the grain boundaries, exertion around such pores increases, that activates dislocational creeping mechanisms that require such exertion.

Implementation of plastic fuel production technology does not create any difficulties because it was based on highly adjusted methods of alloying for pellets' grain size enlargement.

CONCLUSIONS:

1. Optimized microstructure of fuel pellets produced at JSC "UMP" ensures the level of open porosity not higher than 0.3% while preserving the high level of pore structure uniformity.
2. Use of special pore forming agents allows regulating pellets density and pore distribution by size: from monomodal distribution with average pore sizes about 1.5÷3.5 μm to bimodal distribution with average pore size of small pores about 1÷3 μm and the average size of large pores about 10÷50 μm .
3. Technology of fuel pellets microalloying allows regulating the average grain size and grain distribution by sizes within wide ranges: from bimodal structure with the grain size of 1÷3 μm of fine grain phase and 10÷30 μm of coarse grain phase to homogeneous monomodal structure with the average grain size about 20÷50 μm . At the summary boron equivalent of alloyed pellets not exceed 1.0 $\mu\text{g/gU}$, the alternative method of grain size increase up to 25÷30 μm is the use of highly active UO₂ powders in the production of pellets.
4. Implemented principles of regulation of pore-grain boundary interaction at the final stage of sintering using alloying admixtures allow improving plastic properties of pellets significantly.
5. JSC "UMP" invites to cooperation and is ready to produce pellets of high quality that meet any specification of customer.

REFERENCES

- [1] RADFORD K.C., POPE J.M., *Journal of Nuclear Materials*, v.116 (1983) 305-308.
- [2] DEHAUDT P., CHOTARD A., Concerto: French R&D of advanced fuels from lab to NPPs, *Nuclear Worldscan*, v.11-12 (1997) 65.
- [3] HSUEH C.H., EVANS A.G., COBLE R.I., Microstructure development during final/intermediate stage sintering. Pore/grain boundary separation. *Acta metal*, v.30 (1982) 1269-1279.

EVALUATION OF U-RECLAIMED FUEL APPLICATION IN VVER REACTORS

V.N. PROSELKOV, S.S. ALESHIN
V.D. SIDORENKO, P.D. SLAVIAGIN
Russian Research Centre “Kurchatov Institute”,
Institute of Nuclear Reactors

A.V. KULESHOV, O.V. MILOVANOV

E.N. MIKHEEV, V.V. NOVIKOV
A.A. Bochvar ARSRIIM

YU. V. PIMENOV
JSC “TVEL”

Moscow, Russian Federation

Abstract

At present the task is set to show in principle the possibility of implementing the U-reclaimed fuel into the VVER fuel cycle. The analysis of possible U-reclaimed fuel application in the VVER reactors was carried out. The requirements to the initial isotope compositions of experimental batches of fuel pellets of 4.0% effective enrichment were developed, the compensation factor is calculated, the requirements to the check of isotope composition are developed, the technology of RF manufacturing fuel pellets from the U-reclaimed fuel (RF) is determined. It is shown that the main neutronic characteristics meet the restrictions adopted in the VVER-440 and VVER-1000. The radiation influence on the population and environment in the transition to the uranium-reclaimed fuel is practically the same as during the use of normal oxide fuel.

1. INTRODUCTION

Development of nuclear power suggests returning the spent FA uranium into the NPP fuel cycle. This process is being realized, to one or other extent, in many countries. We can say that this problem has also been solved, in part, in Russia – since the 80s the RBMK-1000 reactors are loaded jointly with the U-235 enriched FA and FA manufactured from the U-reclaimed fuel (RF). The RF feature is that, in addition to the traditional U-235 and U-238 isotopes, it also contains U-236, U-234 and U-232. Uranium-236 adds insignificant neutron absorption to the fuel, and radioactively disintegrating U-232 gives thallium-208 emitting hard γ -rays and thorium-228 giving off the α -radiation.

Today the possibility of implementing the reclaimed uranium to the fuel cycles of VVER-440 and VVER-1000 reactors is shown in principle, and the technology of manufacturing the fuel pellets for these reactors, effectively enriched to $\sim 4.0\%$, was developed.

By the present time the requirements to the initial isotope compositions of experimental batches of 4.0% effectively enriched fuel pellets have been developed, the compensation factor has been calculated, requirements to checking the isotope composition has been worked out, and the technology of RF pellets manufacturing has been determined.

2. TECHNOLOGY OF MANUFACTURING U-RECLAIMED FUEL FOR VVER REACTORS

The experimental batches of U-reclaimed fuel for the VVER-440 and VVER-1000 reactors were produced in the following way.

First the uranyl-nitrate fusion cake with 2.4–2.5% U-235 content was fabricated by mixing the reclaimed uranium from the VVER-440 spent (U-235 content - 0.8–1.2%) and medium-enriched reclaimed uranium (U-235 content - 14 - 17%).

Then, using the hydrolysis-extraction method, the initial uranium dioxide powder with 4.0% U-235 enrichment was produced from the uranyl-nitrate fusion cake (U-235 content – 2.4–2.5%) and reclaimed uranium monoxide-oxide U-235 content 14–17%). The actual enrichment of this powder was 4.139%, with the U-236 content amounting to 0.463%, i.e. 0.3 taking into account the compensation factor. The hydrolysis-extraction method (ADU-process) for manufacturing this powder involves the following technological operations:

- separate dissolving of the uranyl-nitrate fusion cake and reclaimed uranium monoxide-oxide in nitric acid;
- check of U-235 content in the solutions;
- mixing the two solutions in a ratio ensuring production of the solution with the actual U-235 content - 4.139%;
- extraction and reextraction of the produced solution for removing impurities;
- treatment with aqueous ammonium solution for precipitation of ammonium polyuranate;
- filtration of precipitate, drying and calcination;
- reduction of uranium monoxide-oxide in hydrogen;
- check for corresponding to the following normative indices: fraction of total mass of uranium isotope mixture; conventional fractions of total mass of U-235, U-236, U-234 and U-232 isotopes; oxygen ratio (O/ U); total specific surface; fraction of total moisture mass; total boron equivalent (TBE). The reclaimed uranium dioxide powder produced met the normative requirements and was used for manufacturing the fuel pellets.

The fuel pellets of experimental U-reclaimed fuel batch were fabricated by the normal technology of manufacturing the fuel pellets for the VVER-reactors [1]:

- consolidation of the initial uranium dioxide powder;
- mixing the consolidated powder with the binder in the mixer-granulator;
- sieving of the granulate produced through the vibrosieve;
- cold compaction using “Courttoy” press;
- drying of the pressed pellets in the low-temperature furnace in the nitrogen environment;
- high-temperature sintering of pellets in the BTU furnace in the hydrogen environment;
- grinding of pellets on the centerless grinding machine with cooling liquid;
- preliminary drying of pressed pellets in air in the oscillating conveyer and final drying in the low-temperature furnace in the nitrogen environment;
- quality control of the experimental batch of pellets.

The QC results showed that the U-reclaimed fuel pellets of experimental batch fully met the requirements stated in the normative-technical documents. The QC results are listed in Table 1.

Table 1. The results of quality control of U-reclaimed fuel pellets

Quality index, unit of measurement	Actual value of quality index
Fraction of total mass of uranium isotopes, mass %	≥87.9
Calculated fraction of total mass of ²³⁵ U, % to uranium	4.139
Fraction of total mass of ²³⁶ U, % to uranium	0.30 – 1.00
Fraction of total mass of ²³² U, % to uranium	< 1.7*10 ⁻⁷
Fraction of total mass of plutonium, % to uranium	Not normalized
Density, g/cm ³	10.41 – 10.69
Mass of 1000 mm long pellet stack, g	444.2 – 449.1
After-caking (ΔD/D), %	0,1 – 0,3
Volume fraction of open voids, %	< 1
Average conventional grain size, μm	10.2 – 12.8
Total boron equivalent, %	< 0.0018

The investigations showed that the radiation-hygienic situation during the production of experimental batches of RF fuel pellet does not differ from that during the production of fuel pellets by the normal technology except for the areas of raw material accommodation and storage of finished products in boats and containers.

In addition, it should be noted that manufacturing of U-reclaimed fuel can be accomplished by another process flowsheet involving the following technological operations; dissolution of reclaimed uranium monoxide-dioxide, reprocessing into uranium hexafluoride, enrichment up to the desired U-235 level, manufacturing of uranium dioxide powder from uranium hexafluoride using the gas-flame) torch technology, fabrication of fuel pellets from uranium dioxide powder by the normal technology for the VVER reactors.

3. NEUTRONIC CHARACTERISTIC OF U-RECLAIMED FUEL

Unlike the normal fuel which contains the natural isotopes, the reclaimed fuel (RF) has the isotopes U-236, U-234 and U-232. The influence of U-232 on the neutronic characteristics is negligibly small because of its low content in the reclaimed uranium. This isotope essentially affects the radiation characteristics. The influence of U-236 manifests itself in an additional neutron absorption, i.e. it deteriorates the neutronic characteristics of the fuel (shortening of the fuel cycle duration). In order to keep the neutronic characteristics of RF fuel similar to the normal fuel, the effect of U-236 should be compensated by increasing the initial U-235 concentration.

The compensation factor is meant as:

$$K_{236} = (C_{U235}^{RF} - C_{U235}^{norm}) / C_{U236}^{RF} .$$

where C_{U235}^{RF} – is the ^{235}U concentration in the RF fuel.

C_{U235}^{norm} – is the ^{235}U in the normal fuel,

C_{U236}^{RF} – is the ^{236}U concentration in the RF.

The compensation factor is determined from the requirement that the time of work interval between the reloadings, when the normal fuel is replaced by the reclaimed fuel, should be kept. For the determination of U-236 compensation factor a series of neutronic calculations of burnup of the fuel with the fixed initial concentration of U-236 and different initial concentration of U-235 were carried out. The calculation results made it possible to determine the initial concentration of U-235 in the RF at which the multiplication factor average over the fuel cycle is the same as that for the normal fuel. In the calculations the actual operation of the VVER-type reactor was taken into account. The calculations of the U-236 compensation factor for the RF fuel for the VVER-440 reactors with the initial enrichment 2.4% and 3.6% were performed for changes in the U-236 concentrations in the RF fuel ranged from 0.3% to 1.5%. The similar calculations were made for the RF fuel with the initial enrichment 4.4%, intended for the VVER-1000 reactors. The analysis of the calculated values of the U-236 compensation factor allows to make a conclusion that for the experimental batch of RF fuel for the VVER-440 and VVER-1000 reactors the U-236 compensation factor of 0.30 ± 0.05 may be recommended. Actually it means that for each kilogram of U-236 in the RF fuel the content of U-235 should be increased by (300 ± 50) gram comparing with its content in the normal fuel of the same enrichment.

The preliminary technical requirements to the check of the nuclide composition are given in Table 2.

Table 2. Preliminary technical requirements to the regular check of the nuclide composition in the batches of fresh U-reclaimed fuel for the VVER.

Isotope	Fraction of total mass,	Absolute measurement error ^{*)} , %
U-238	95.5-96.3	0.11
U-236	0.5-0.7	0.04
U-235	2.4-4.6	0.02
U-234	0.02-0.05	0.004

^{*)} – at the confidence level 0.95

4. NEUTRONIC CHARACTERISTICS OF VVER-440 AND VVER-1000 CORES

VVER-440

The calculation of neutronic characteristics of the 21st fuel loading of the Kola NPP-1 with six FA with 2.4% U-235 enrichment, fabricated from the reclaimed uranium showed that:

The FA peaking factor is

$$K_q=1.28 < K_q^{add}=1.35.$$

The fuel element peaking factor is

$$K_r=1.45 < K_r^{add} 1.48.$$

The maximum linear heat generation rate is

$$Q_l=314 < Q_l^{add}=325 \text{ W/cm.}$$

In the beginning of the fuel cycle, with all the CPS control rods withdrawn, the critical boric acid concentration and the inlet coolant temperature 260°C:

The coolant temperature coefficient of reactivity is

$$d\rho/dT_{H_2O}=-3.5\cdot 10^{-5} \text{ 1/ }^\circ\text{C} < 0.$$

The coolant density coefficient of reactivity is

$$d\rho/dG=4.71\cdot 10^{-5} \text{ g/cm}^3 > 0.$$

The scram system efficiency with allowance for possible sticking of one most efficient CPS control rod is

$$\Delta\rho = 7.3\% > \Delta\rho^{add}=6.3\%.$$

the reactor subcriticality in cold condition, with all the CPS control rod with drawn and the shutdown boric acid concentration 12 g/kg

$$|\Delta\rho| = 6.1\% > |\Delta\rho^{add}| = 2\%.$$

Basing on the analysis of the neutronic calculation results it was concluded that the twenty first fuel loading of the Kola NPP-1 with the first experimental batch of six FA with 2.4% U-235 enrichment, fabricated from the reclaimed uranium fully satisfy the design requirements.

In the RRC KI the project of implementation of the advanced fuel cycle for the Kola NPP-2 with FA make up 3.82% was worked out. In the frame of this project the first transition fuel loading (25-th) will be furnished with the make up containing the experimental batch of 12 profiled FA with equivalent U-235 enrichment 3.82% with the fuel rods made of the reclaimed uranium. The FA profiling: 24 normal 3.6% enriched fuel rods (periphery row), 18 normal 3.3% enriched fuel rods (corner fuel rods) and 84 fuel rods based on the U-reclaimed fuel with equivalent enrichment 4.0%. The RF isotope composition with allowance for U-236 compensation (the compensation factor is 0.3) is: U-234-0.043 mass %, U-235 – 4.139 mass %, U-236 – 0.463 mass %. U-238 – 95.355 mass %. The maximum fuel calculation burnup of these FA in unloading is 41.2 MWday/kg. Basing on the analysis of calculation results of the main neutronic characteristics of loadings with the experimental batch of FA with reclaimed fuel and those with the normal fuel it may be concluded that they are practically identical and that the experimental operation of FA with the reclaimed fuel in the VVER-440 reactor is feasible.

VVER-1000

The 15th fuel loading of the Kola NPP-2 contains 12 FA with the reclaimed uranium with U-235 enrichment equivalent to 4.00%. The calculation of multiplying properties of FA with the normal fuel (the fuel rods U-235 enriched to 4.0%) and the FA with uranium-reclaimed fuel

(the rods U-235 enriched to 4.139%, which corresponds to U-235 enrichment to 4.0% for the normal fuel at the compensation factor 0.3), revealed that they are close. The results of neutronic calculations show that the main neutronic characteristics of the 15-th fuel loading meet the restrictions adopted in the VVER-1000 (V-320) reactor design.

5. EXPERIENCE OF OPERATION

In Russia the reclaimed uranium is successfully used in the fuel for the RBMK reactors. The experience of RF operation in the VVER-440 reactors has not been wide yet, and in the VVER-1000 reactors this fuel has not been used at all so far.

To check the possibility of the use of U-reclaimed fuel at the Kola NPP six FA were fabricated for the experimental operation. The fuel composition was the following: U-235–2.4%. U-236–0.45%. The compensation for U-236 was not carried out. The FA with reclaimed uranium were installed into the Kola NPP-1 reactor the 21st fuel loading.

The uranium-reclaimed fuel assemblies and the FA with the fresh 2.4% enriched normal fuel were set into the symmetric (30° symmetry) cells. The analysis of experimental operation results revealed that the neutronic and thermal-physical properties of U-reclaimed fuel assemblies used in the Kola NPP practically fully correspond to those for the normal uranium fuel assemblies. For example, the deviation in the peaking factor in the U-reclaimed FA differs from those in the normal FA symmetric to them not more than by 0.04. The spread in the thermocouple indications for the U-reclaimed FA is $\sim 2\%$ and coincides with this characteristic for the normal fuel assemblies. The axial power distribution in the U-reclaimed FA has the same character as that in the normal fuel assemblies. In the process of experimental operation of six U-reclaimed fuel assemblies during the 21st and 22nd fuel cycles at the Kola NPP1 fuel burnup in them reached 19.81 MWday/kg. During the 21st and 22nd fuel cycles at the Kola Unit1 the coolant activity was normally monitored. No excess over the admissible level was recorded. The fuel failure detection during refuelings did not either revealed any deviations from the permissible value. The final conclusion is the following: the fuel assemblies containing reclaimed uranium with the U-236 concentration of about 0.5% are identical to the normal FA in their physical properties.

6. RADIATION SAFETY

As a result of nuclear transformations during irradiation in the reactor the isotope composition of uranium in the discharged fuel differs qualitatively from that of the starting fuel: the former contains isotopes U-232 ($T_{1/2}=72$ years) and U-236 ($T_{1/2}=3.4 \cdot 10^6$ years) which are absent in the starting fuel manufactured from the natural raw material. Uranium-232 determines to the significant degree the radiation situation in all the phases of fuel cycle. In the process of its radioactive decay thallium-208 emitting hard γ -radiation is produced. The U-232 concentration in the reclaimed uranium depends on many factors of which the most important is the time of spent FA storage before reprocessing. For the evaluation of the radiation characteristics the calculations of the isotope composition of reclaimed uranium were made. Table 3 lists the calculation isotope compositions of reclaimed fuel for the VVER-440 and VVER-1000 fuel (enrichment $\sim 4.0\%$, compensation factor – 0.3). The data are given for two variants of storage: three years (variant A) and seven years (variant B).

Table 3. Isotope composition of U-reclaimed fuel of effective U-235 enrichment ~4.0% with the compensation factor for U-236 equal to 0.3

Isotope	Concentration, mass %	
	Variant A	Variant B
U-232	$1.38 \cdot 10^{-7}$	$1.68 \cdot 10^{-7}$
U-234	0.043	0.043
U-235	4.139	4.139
U-236	0.463	0.463
U-238	95.355	95.355

It follows from Table 3 that the maximum calculation U-232 concentration in uranium for the experimental fuel batch is about $1.7 \cdot 10^{-7}$ mass %. However the U-232 concentration in the reclaimed uranium depends on many factors, which cannot be currently accounted for in the calculations with a sufficient accuracy. Therefore for carrying out evaluations of the radiation characteristics and factors of dose realization in fuel manufacturing the value $2 \cdot 10^{-7}$ mass % is recommended.

The calculation evaluation of fission product (FP) accumulation in the fuel and at the air-tight fuel rod claddings walls, evaluation of FP release and evaluation of the radiation situation at the NPP with the VVER-440 and VVER-1000 reactors with failed normal fuel rods and those with the U-reclaimed fuel. The mechanisms of fission product release from the uranium dioxide for the normal irradiation conditions in the VVER reactors do not depend on the isotope composition of uranium. Therefore at the same rate of FP production in the fuel the same velocity of FP release should be expected both for the fuel from natural uranium dioxide and for that produced from the reclaimed uranium dioxide.

The analysis of calculation data on FP accumulation in the fuel and at the air-tight fuel rod cladding walls for the VVER-440 and VVER-1000, with the fissile U-235 isotope uniformly distributed in the fuel pellet, reveals that the calculation results for the normal fuel do not practically differ from the calculation data for the RF. This means that the radiation consequences of design and beyond-design accidents do not increase in the transition from the normal to the uranium-reclaimed fuel. In mechanical mixing the uranium powders (low- and medium-enriched uranium) non-uniform distribution of uranium-235 is possible (grains with the increased U-235 content). In this case the higher fission product release because of increased local fission density should be expected. However, further experiments are needed for supporting this supposition.

The calculation the limiting activity of main dose-producing radiologically hazardous FP in the coolant of operating VVER-440 reactors (V-213 design) and VVER-1000 (V-320 design) was performed for the conditions with 0.02% fuel rods with “gas-untightness” defects and 0.02% fuel rods with the direct contact of fuel with the coolant in the core. For the VVER-44-reactors the calculation was carried out for the 28 kV medium rating fuel rods with 28 kV power, 3.82% U-235 enriched RT fuel and 30 MWday/kg average fuel burnup over the core. For the VVER-1000 reactors the similar calculations were made for the superposition of two groups of fuel rods: one of medium rating fuel rods with 53.7 kV power, the other of highest rating fuel rods with 75.4 kV power. It is adopted that the U-235 enrichment of fuel is 4.4% and the average fuel burnup over the core is 30 MWday/kg. The analysis of the calculation

results of the limiting activity of main dose-producing radiologically hazardous FP in the coolant of both the VVER-440 and VVER-1000 reactors shows that the calculation results for the normal fuel do not practically differ from the calculation data for the RF. This means that the radiation influence of NPP on the population and environment does not practically change in the transition to the uranium-reclaimed fuel

The comparison of the calculation data and the data on the admissible total activity of iodine isotopes and admissible activity of iodine-131 in the coolant of operating VVER-440, in accordance with [2.3], and VVER-1000, in accordance with [2.4] shows that in application of the reclaimed uranium the above limits are not violated.

7. CONCLUSION

The analysis of the results presented above shows that:

- Main neutronic characteristics meet the restrictions adopted in the designs of VVER-440 reactor (V-230 design) and VVER-1000 (V-320 design);
- Radiation effect on the population and environment in the transition to the reclaimed uranium fuel is practically the same as in the use of normal oxide fuel.

REFERENCES

- [1] RESHETNIKOV F.G., BIBILASHVILI YU.K., GOLOVIN I.S. et al. "Development, production and operation of fuel elements for power reactors". Book 1, Moscow, Energoatomizdat. 1995.
- [2] MIGLO V.N., LUZANOVA L.M., SLAVYAGIN P.D. "Fuel failure detection system for VVER-440 and VVER-1000 reactors. State and prospects". Paper presented at the Bulgarian Russian Seminar on fuel for the VVER-440 and VVER-1000 reactors. October 2-6, 2000, Bulgaria, Bulgarian AEC, Sofia (in press).
- [3] "Instruction on fuel failure detection of fuel rods of the VVER-440 reactors (V-230 and 213 designs) during operation and after shutdown of the apparatus" 62444-03-DIK for the VVER-440 reactors (V-213 design), ROSENERGOATOM.
- [4] "Instruction of fuel failure detection of fuel rods of VVER-1000 reactors during operation and after shutdown of the apparatus" 0401.00.00.000 DNK for the VVER-1000 reactors (V-320 design), ROSENERGOATOM.

DEVELOPMENT OF UO_2 / MOX FUELS OF MODIFIED MICROSTRUCTURE FOR IMPROVED PERFORMANCE

U. BASAK, S. MAJUMDAR, H.S. KAMATH
Nuclear Fuels Group,
Bhabha Atomic Research Centre, Mumbai, India

Abstract

The performances of conventional and advanced $(\text{UPu})\text{O}_2$, $(\text{ThPu})\text{O}_2$ and $(\text{ThU})\text{O}_2$ fuels in PHWRs / LWRs could be significantly improved and burn-up could be extended by proper control of the microstructure of these fuels. Stable density pellets which are resistant to in-reactor densification, large grain sized pellets, which release less fission gas and pellets with high plasticity & creep rate are some of the examples of advanced fuels developed at BARC. Apart from 2-3 fold increase in the burn-up range, the R&D programme in oxide fuels also aims at: (i) modifications in microstructural characteristics leading to improved thermal conductivity and better performances of the conventional and advanced UO_2 / MOX fuels and (ii) developing advanced fuel fabrication methods such as sol-gel microsphere pelletisation process combined with low temperature oxidative sintering (SGMP-LTS) for UO_2 & MOX fuels and impregnation techniques for ThO_2 - UO_2 fuels. These fuel fabrication methods are not only amenable to automation and remotisation, but also minimize fuel fabrication costs, radiotoxic aerosols and process losses.

1. INTRODUCTION

Fuel cycle economy, proliferation resistance and reduced volume generation of environmentally compatible radioactive waste are some of the driving forces for the development of new generation nuclear fuels which can be operated at high thermal rates for high burn-ups, extending the fuel life time period in the reactor. Maximum fuel utilization combined with cost effective fuel fabrication methods significantly improves fuel cycle economy. UO_2 , $(\text{UPu})\text{O}_2$, $(\text{ThPu})\text{O}_2$ and $(\text{ThU}^{233})\text{O}_2$ are considered as advanced high burn – up fuels for water cooled reactors on the basis of well established fuel fabrication technology and good irradiation performances. Thoria based fuels are also proliferation resistant and generate waste with lower minor actinides leading to disposal without any further processing. These fuels, not only have the potential for good performances at high burn – up but also would like to play an important role in controlling the plutonium inventories in water cooled reactors.

Increase in burn – up improves the fuel cycle economy by (i) maximizing fuel utilization (ii) reducing the fuel re-load requirement leading to less fuel pellets fabrication (iii) reducing the frequency of reprocessing leading to less waste volume generation. However, fission gas release (FGR), pellet - clad interaction (PCI), corrosion of clad etc. are some of the factors which affect and limit the performance of the fuel at high burn – up. The greater reliability of fuels during extended burn – up is to be ensured by modifying either the fuel pin design or the fuel pellet microstructure. Fuel pellet & pin design modifications mainly focus on efficient heat removal from pellets so that the fuel remains cool even operating at high thermal rates at high burn – up. This leads to reduced fission gas release and less swelling as these are temperature dependent phenomena. Alternatively, oxide fuel pellets with modified microstructure consisting of large grain size with better grain boundary conditions and controlled porosity have the following effects on performances:

- (i) reduce fission gas release & swelling during irradiation and temperature ramp by increasing the fission gas atom diffusion distance from the interior of grains to the grain boundaries.
- (ii) increase resistance to in – pile densification.
- (iii) minimize pellet – clad interaction by increasing creep rate.
- (iv) improve thermal conductivity by decreasing phonon – defects interactions at the grain boundaries.

2. LARGE GRAIN PELLETS

Addition of small quantities of metal oxides like TiO_2 , Nb_2O_5 , MgO etc. as dopants to UO_2 / $(\text{UPuO})_2$ matrix material brings about the microstructural changes in the fuel pellets in terms of large grains and pore morphology desirable for improved performances at high burn – up [1]. These additives or dopants, within their solubility limits, form solid solution with matrix oxide material and produce defect structure which enhances diffusion controlled processes namely densification, grain growth, creep etc. Among the additives, TiO_2 predominantly promotes grain boundary diffusion leading to grain growth. In Bhabha Atomic Research Centre (BARC), UO_2 and $(\text{UPu})\text{O}_2$ fuel pellets with large grain size in the range of 40 – 50 micron have been fabricated by both conventional powder pellet route and sol gel microsphere pelletisation (SGMP) process using very small quantity of TiO_2 (0.05 wt%) as dopants[2-3]. Thermal conductivity of such pellets has been found to be 10 – 15% higher than that of standard fuel pellet. Other additives such as silicates namely Al – Si – O, Ti – Si – O, Nb – Si – O etc. are also found to be effective in increasing the grain size of the fuel pellets [4]. These additives do not dissolve in the matrix, but provide short circuit diffusion path for grain boundary diffusion leading to grain growth. Table I shows the characteristics of sintered UO_2 pellets with silicate additives.

3. CONTROLLED POROSITY PELLETS

Amount of pores and its distribution in the fuel pellets play a vital role in determining its in – pile performances such as in – pile densification and swelling. The ideal pores should be spherical & closed in nature and in the size range of 2–5 microns. Pores less than 2 microns disintegrate into vacancies during irradiation and diffusion of these excess vacancies over the equilibrium concentration leads to in – pile densification. Controlled porosity UO_2 and $(\text{UPu})\text{O}_2$ fuel pellets have been fabricated in BARC by addition of special volatile pore formers namely methyle cellulose (MC) or polyvinyle alcohol (PVA).

4. FUEL FABRICATION TECHNOLOGY

Advanced fuel fabrication techniques based on sol – gel microsphere pelletisation, low temperature sintering and impregnation method developed at BARC for the fabrication of UO_2 , $(\text{UPu})\text{O}_2$ and $(\text{ThU})\text{O}_2$ fuel pellets have the following unique features over the conventional fuel fabrication process :

avoids handling and generation of fine powders leading to significant reduction in radioactive aerosols and radioactive dust hazards.

amenable to automation and remotisation leading to substantial minimization of personnel exposure to radiation.

Table I: Characteristics of sintered UO₂ pellets with silicate additivesSintering temperature: 1923K, Sintering atmosphere : N₂ – 8 % H₂

Composition	Sintered Density		Porosity		Average grain size (micron)
	g/cm ³	%T.D.	Closed (%)	Open (%)	
UO ₂	10.44	95.28	4.71	0.01	15
UO ₂ + 0.1% Al-Si-O	10.45	95.35	4.64	0.01	35
UO ₂ + 0.1% Ti-Si-O	10.41	94.95	5.04	0.01	88
UO ₂ + 0.1%Nb-Si-O	10.67	97.39	2.60	0.01	40

- # avoids number of process steps leading to significant reduction in fuel fabrication costs.
- # ensures excellent micro homogeneity and desirable pore structure.
- # restricts highly gamma active U²³³ handling area to a bare minimum for fabrication of thoria based fuels.

4.1 Sol gel microsphere pelletisation (SGMP)

The SGMP process uses sol – gel derived calcined, dust – free, free – flowable and easily crushable microspheres as feed materials for pellet pressing and subsequent sintering. In BARC, a process flow sheet has been developed for the fabrication of high density UO₂ and (U_{0.97}Pu_{0.03})O₂ pellets [5]. The hydrated gel – microspheres were prepared at Fuel Chemistry Division , BARC by ammonia internal gelation process using hexa methylene tetra amine (HMTA) as ammonia generator and hot silicon oil as gelation bath [6]. A few batch was doped with 0.05%TiO₂ for the fabrication of large grain pellets. Addition of TiO₂ was done by dispersion of fine powders in the broth prior to gelation. Gel microspheres were subjected to calcination followed by reductive treatment at 1048K and stabilization at room temperature. The calcined microspheres were directly cold – pelletised at ~ 300 MPa to green density ~ 50% T.D. in a double action hydraulic press using 1% stearic acid in acetone for die wall lubrication. Pellets were sintered at 1923K for four hours in N₂ – 8% H₂ atmosphere to achieve sintered densities ≥ 96% T.D.

4.2. Low temperature oxidative sintering

High density was also achieved at lower sintering temperature of 1473K in CO₂ atmosphere for one hour followed by N₂ – 8%H₂ for stoichiometry adjustment [2]. Densification during low temperature oxidative sintering is due to enhanced diffusivity of uranium cation (D^u) at the rate of x² in UO_{2+x} (x ≤ 0.25). Table II. shows the characteristics of UO₂ and (U_{0.97}Pu_{0.03}) pellets sintered under different conditions . Two 19 pin fuel bundles containing high density UO₂ pellets prepared by sol gel microsphere pelletisation process combined with low temperature oxidative sintering (SGMP – LTS) have been successfully irradiated to a burn –

up of more than 10,000 MWD/T in pressurized heavy water reactor at Madras Atomic Power Stations, Kalpakkam [5].

4.3. Impregnation Process

The impregnation process being developed in BARC, is particularly suitable for the fabrication of (ThU²³³) O₂ fuel pellets which requires a heavily shielded facility as U²³³ always contains some amount of U²³² which has high energy gamma emitting daughter products [7]. The major advantage of this process is that a large part of the fabrication processes including the handling of fine thoria powders for low density pellet fabrication and that of thorium nitrate solution for the preparation of gel microspheres could be carried out in an unshielded facility. The remaining process steps including the impregnation of pellets or microspheres with U²³³ bearing nitrate solution could be carried out in the shielded facility.

In pellet impregnation process, partially sintered thoria pellets fabricated by conventional powder metallurgical process were used for impregnation with uranyl nitrate solution under vacuum. The impregnated pellets were dried and finally sintered to high density at 1923K in N₂ – H₂ atmosphere. The amount of uranium impregnated into partially sintered pellets depended mainly on the initial porosities and the molarity of the solution. However under similar conditions, the uranium content increased with the use of annular pellets.

In microsphere impregnation technique, dried thoria gel microspheres prepared by ammonia internal gelation process at Fuel Chemistry Division, BARC [8] were impregnated with uranyl nitrate solution. Impregnated microspheres were dried, calcined and reduced at 973K to obtain free flowable porous microspheres. Irregular shaped pores obtained within the microspheres due to dissociation of uranyl nitrate made the microspheres easily crushable.

Table II: Characteristics of undoped and doped pellets

(a) low temperature oxidative (1473K , 1h , CO₂ followed by N₂ – 8%H₂)(b) high temperature reductive (1923K , 4h , N₂ – 8%H₂)

Material	Green density g/cm ³ (%T.D.)	Sintering conditions		Sintered density (geometrical g/cm ³ (%T.D))	Bulk density g/cm ³ (%T.D)	Pore volume	
						Closed (%)	Open (%)
UO ₂ pellet	5.43 (49.54)	Low temp.oxidative	temp.	10.68 (97.49)	10.83 (99.86)	1.14	nil
				High reductive	10.70 (97.65)		
(U _{0.97} Pu _{0.03}) pellet	5.48 (49.95)	Low temp.oxidative	temp.	10.57 (96.39)	10.83 (98.72)	1.28	nil
				High temp.reductive	10.48 (95.54)		
TiO ₂ doped UO ₂ pellet	5.47 (49.91)	High reductive	temp.	10.53 (96.12)	10.78 (98.38)	1.29	0.33

These microspheres were cold – pelletised at 300 MPa to green pellets of density ~ 60% T.D. Pellets were sintered at 1923K in reductive atmosphere for four hours. The process flow sheet is shown in Fig.2. The characteristics of calcined ThO₂ – UO₂ microspheres used as feed materials and the pellets made from these microspheres are shown in Table III. Higher density could have been achieved with MgO doped ThO₂ microspheres.

Lattice parameters (Table IV) calculated from the high angle X-ray diffraction patterns of sintered pellets confirmed the formation of solid solution between ThO₂ and UO₂. The compositions of solid solutions were also found out from Vegard' s law (Table IV). Depending on the molarity of uranyl nitrate solution, a wide range of uranium loading is possible in this technique. Electron probe micro-analysis results show the non-uniform distribution of uranium and thorium in the pellets made from micro spheres impregnated with 3.0 M uranyl nitrate solution. This may be due to poor penetration of highly viscous higher molarity uranyl nitrate solution to the fine pores of thoria micro spheres. However, U and Th distribution were substantially improved in case of lower molarity solutions as shown.

Table III: Characteristics of thoria – urania microspheres and pellets

Molarity of uranyl nitrate soln.	0.5 M	1.0 M	3.0M
Apparent density of calcined microspheres	1.37 g / cm ³	1.31 g / cm ³	1.57 g / cm ³
Tap density of calcined microspheres	1.44 g / cm ³	1.40 g / cm ³	1.70 g / cm ³
Green density of pellet compacted at 300 MPa	6.02 g / cm ³ (59.54%T.D)	5.98 g / cm ³ (58.89%T.D)	5.81 g / cm ³ (56.73%T.D)
Sintered density	8.97 g / cm ³	9.05 g / cm ³	9.09 g / cm ³
Sint. Temp: 1923K	(88.72%T.D)	(89.34%T.D)	(88.77%T.D)
Uranium homogeneity in sintered pellet (by EPMA)	uniform	Uniform	non - uniform
Phase analysis of sintered pellet (by XRD)	Single phase	Single phase	Single phase

Table IV: lattice parameters and solid solution compositions of (ThU)O₂ pellets.

Sl.No.	Material	Lattice Parameter (nm)	Solid solution. Composition
1	Pellets made from microspheres impregnated with 0.5 M uranyl nitrate solution	0.5585	(Th _{0.881} U _{0.119})O ₂
2	Pellets made from microspheres impregnated with 1.0 M uranyl nitrate solution	0.5583	(Th _{0.865} U _{0.135})O ₂
3	Pellets made from microspheres impregnated with 3.0 M uranyl nitrate solution	0.5568	(Th _{0.744} U _{0.256})O ₂

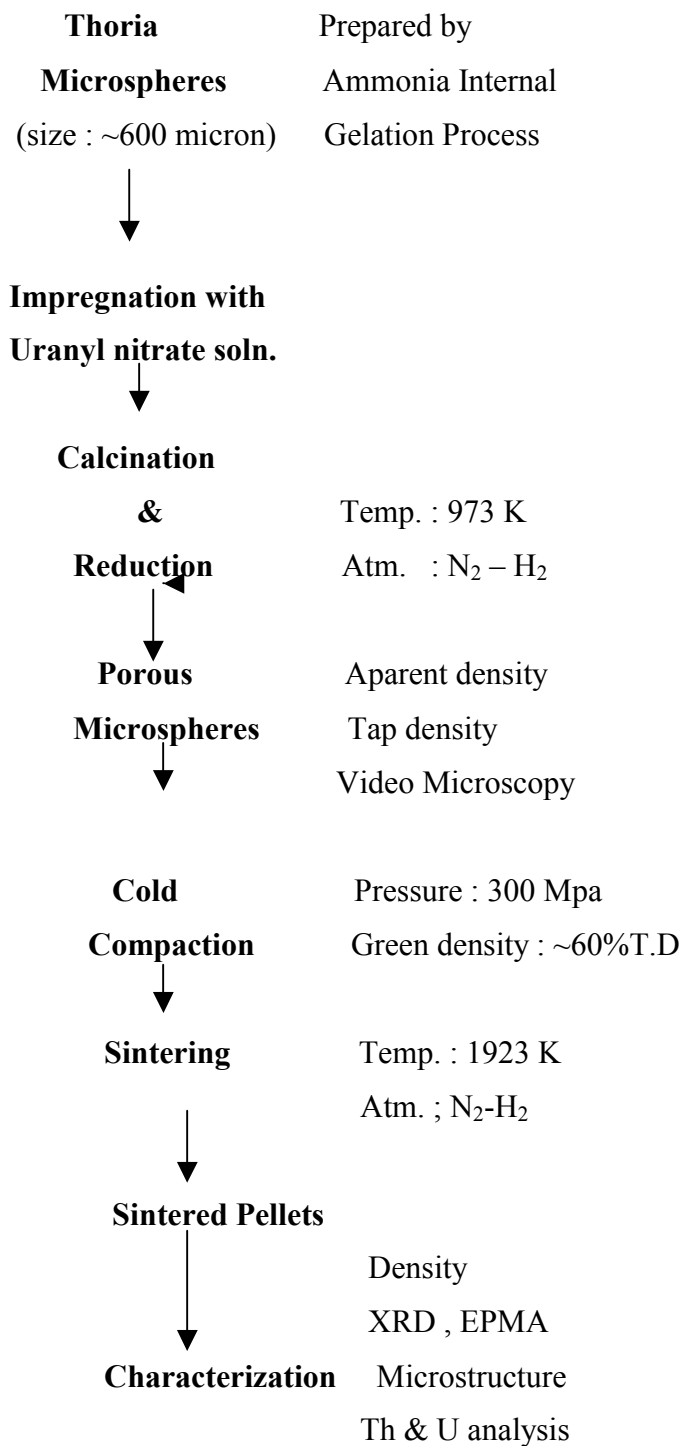


FIG. 1. Flowsheet for the fabrication of thoria – urania fuel pellets by microsphere impregnation technique

5. CONCLUSIONS

1. The feasibility of SGMP-LTS route for the fabrication of UO₂ and (UPuO₂) pellets has been demonstrated. Two fuel bundles containing UO₂ pellets prepared by SGMP – LTS route have already been irradiated in pressurized heavy water reactor.

2. TiO₂ dopant and silicate additives were found to increase the grain size of oxide fuel pellets sintered in reducing atmosphere. Large grain pellets have also found to be higher thermal conductivity by 10–15%.
3. Fuel pins containing low temperature sintered (UPu) O₂ pellets and pellets with modified microstructure (large grain & controlled porosity) have been test irradiated in research reactor at BARC.
4. Impregnation technique appears to be more suitable for the fabrication of highly gamma active U²³³ bearing mixed oxide fuel pellets. The most attractive feature of this technique is that the major part of fabrication processes can be carried out in an unshielded facility. Handling of fine powders are not involved in the shielded facility.

REFERENCES

- [1] RADFORD, K.C., POPE, J.M., UO₂ pellet microstructure modification through impurity addition, J. Nucl. Mat. 116 (1983) 305.
- [2] GANGULY, C., BASAK, U., Fabrication of high density UO₂ fuel pellets involving sol-gel microsphere pelletisation and low temperature sintering, J.Nucl.Mat.178 (1991)179.
- [3] GANGULY, C., BASAK, U., SOOD, D. D., VAIDYA, V.N., ROY, P. R., “Sol-gel microsphere pelletisation of UO₂ and UO₂ - PuO₂ pellets of PHWR fuel specification using internal gelation process”, CANDU Fuel (Proc. 2nd Int. Conf. 1989), CNS, Toronto (1990) 108.
- [4] ALTEKAR, R.M.,BASAK, U.,PANDEY, V.D.,SHEIKH,I.H.,RAMCHANDRAN,R., MAJUMDAR,S.,Microstructural modifications of UO₂ fuel pellets through silicate additives,Trans.PMAI.27 (2001) 92.
- [5] GANGULY, C., BASAK, U., SOOD, D.D., VAIDYA, V.N., BALARAMAMOORTHY, K., “SGMP – LTS process for fabrication of high density UO₂ and (UPu)O₂ fuel pellets”, CANDU Fuel (Proc. 3rd Int. Conf. 1992), CNS, Toronto (1993).
- [6] VAIDYA, V.N., MUKHERJEE, S.K., JOSHI, J.K., KAMATH, R.V., SOOD,D.D., A study of chemical parameters of the internal gelation based sol-gel process for uranium dioxide, J. Nucl. Mat. 148 (1987) 324.
- [7] BASAK, U., MISHRA, S., NAIR,M.R., RAMACHANDRAN, R., MAJUMDAR, S., KAMATH, H.S., “Process development for the fabrication of thorium and thorium based nuclear fuel, Characterization and Quality Control in Nuclear Fuel Fabrication (Proc. Int. Conf. Hyderabad, 2002), NFC, Hyderabad (in press).
- [8] KUMAR, N., SHARMA, R.K., GANATRA, V.R., MUKHERJEE, S.K., VAIDYA, V.N., SOOD, D .D., Studies on the preparation of thorium and thorium –uranium microspheres using and internal gelation process, Nucl. Techn. 96 (1991) 169.

INVESTIGATION OF THERMAL-PHYSICAL AND MECHANICAL PROPERTIES OF URANIUM-GADOLINIUM OXIDE FUEL

YU.K. BIBILASHVILI, A.V. KULESHOV
O.V. MILOVANOV, E.N. MIKHEEV, V.V. NOVIKOV

A.A. Bochvar ARSRIIM

S.G. POPOV, V.N. PROSELKOV
Russian Research Centre “Kurchatov Institute”,
Institute of Nuclear Reactors

YU.V. PIMENOV
JSC “TVEL”

YU. G. GODIN
MEPhI
Moscow, Russia Federation

Abstract

The work is devoted to investigation of thermal-physical (coefficient of linear thermal expansion, thermal conductivity coefficient) and mechanical (brittle-ductile transition temperature, Young's modulus, thermal creep) properties of uranium-gadolinium oxide fuel.

1. INTRODUCTION

For compensation for the initial excess reactivity, power flattening over the core volume and maintaining the temperature coefficient of reactivity at the specified level in the VVER, PWR and BWR reactors, the burnable absorbers (BA) are used. In the PWR reactors the BA made of ^{10}B in the form of tetraboron carbide (B_4C) is conventionally used. As B_4C is chemically incompatible with uranium dioxide it was found necessary to provide some fuel rods in the fuel assembly (FA) with the burnable absorber (BAR). The use of BAR as an independent structural element has the following disadvantages: the BAR takes some useful space in the FA thus increasing the linear heat generation rate of fuel rods; neutron-absorbing structural material of BAR claddings is introduced into the FA; necessity of storing and transportation of irradiated BAR. This made the FA designers to search for other ways of BA introducing into the FA. One of these solutions was to deposit a thin layer of zirconium diboride on the fuel pellet surface. However the use of gadolinium distributed in the form of oxide in the uranium dioxide fuel matrix, has found a wider application. Gadolinium possesses rare properties due to a high neutron absorption cross section (essentially higher than that of ^{10}B) and the rate of burnup close, in the case of optimal composition, to the rate fuel burnup of ^{235}U . In addition, in irradiation of gadolinium gives no daughter products with a high neutron capture cross section, and gadolinium oxide interacting with uranium dioxide forms solid solutions with concentration up to ≈ 30 wt % Gd_2O_3 at the temperature 1873K [3]. The technology of uranium-gadolinium fuel does not, in principle, differ from production of fuel pellets from uranium dioxide [11,12]. Although the uranium-gadolinium oxide fuel has been used for a long time (in the BWR – since the 70s) its physical-chemical properties has not been sufficiently studied. For example, the data on its thermal-physical properties (thermal expansion, thermal conductivity) are available, though not completely, in the open literature,

while there are almost no data on the mechanical properties of uranium-gadolinium oxide fuel. This work is devoted, in part, to elimination of this deficit.

2. MAIN CHARACTERISTICS OF SPECIMENS

In the investigations the specimens in the form of actual fuel pellets were used. The uranium-gadolinium oxide fuel pellet with 5,6,8 and 10 wt % of Gd₂O₃ were produced from moulding powder prepared by mechanical mixing the uranium and gadolinium oxide powders. The specimens had been sintered in the hydrogen environment at 1720°C for 3 hours.

The X-ray phase analysis of the fuel pellets was performed on the DRON-3 diffractometer. The diffraction pattern showed that all samples were only single-phase with fluorite structure.

At large angles the diffraction peaks were clearly split into K_{α1} and K_{α2} components, which evidences the full solubility of gadolinium oxide in the uranium dioxide.

The oxygen ratio of the pellets, measured by the EMF-method in the solid-electrolyte galvanic cell was within the range 2.001-2.003 (O/M units).

3. LINEAR THERMAL EXPANSION

For the measurements of linear thermal expansion the differential dilatometer with inductive displacement sensor was used. The dilatometer sensitivity is as high as 5.5µm.

The specimens had the form of bush ~ 7.5 mm in diameter and 22-25 mm in height. The heating of specimens was performed at a rate of ~ 10K/min in the environment of purified helium. The temperature was measured by the platinum-platinum-rhodium thermocouple installed close to the specimen.

The experimental data on the relative linear thermal expansion ($\Delta L(T)/L_{293}$) of the examined specimens of uranium-gadolinium oxide fuel and uranium dioxide in the range 375-1755K are shown in Fig.1. In the same figure the dependence ($\Delta L(T)/L_{293}$)=f(T) obtained in Ref. [10] for specimens of uranium-gadolinium fuel with the mass content of Gd₂O₃ 10 wt % is also given. The experimental data of the two works are in good agreement.

The analytical dependence of linear thermal expansion of uranium-gadolinium oxide fuel within the range 293-1775K is described by the expression:

$$(\Delta L(T)/L_{293}) = A + BT + CT^2, \quad (1)$$

where: $\Delta L(T)=L(T)-L_{293}$ is the elongation of specimen at the temperature T (m); L_{293} is the specimen length at room temperature (m); T is the temperature (K); A,B,C are the constants obtained by the least-squares method and having values listed in Table 1.

Table 1. Constants A,B and C in equation (1)

Content of gadolinium oxide, mass %	A, · 10 ⁻³	B, · 10 ⁻⁶	C, · 10 ⁻⁹
0	-2.237	7.164	2.097
6.0	-2.128	7.242	2.049
8.0	-2.137	7.218	2.048
10.0	-2.072	7.167	2.163

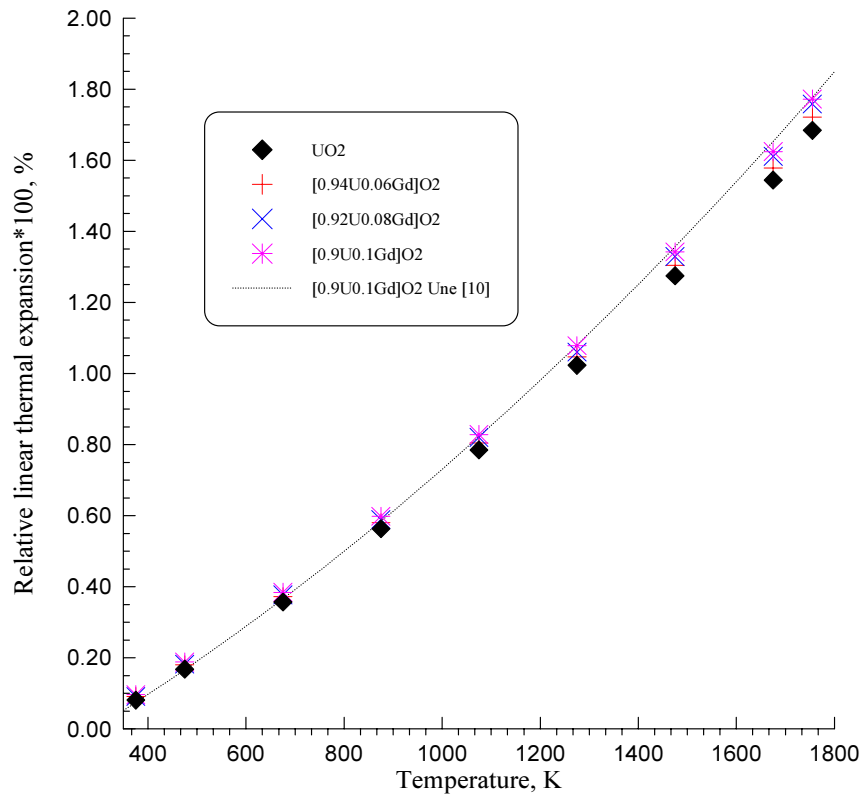


FIG.1. Temperature dependence of relative linear thermal expansion of uranium-gadolinium fuel and UO_2

The investigations performed showed that with the increase in the gadolinium oxide content the thermal expansion of uranium-gadolinium oxide fuel specimens somewhat rises as compared with the unalloyed uranium dioxide.

The true linear thermal expansion coefficient was found, following its determination, from the relation:

$$\alpha = (1/L_{293}) * (dL(T)/dT) = d(\Delta L(T)/L_{293})/dT = B + 2CT, \quad (2)$$

The temperature dependence of the true linear thermal expansion coefficient of pellets made of uranium dioxide and of uranium-gadolinium oxide fuel is shown in Fig.2.

Thus, the increase in the content of gadolinium oxide in the fuel does not noticeably affect the true coefficient of thermal expansion of fuel pellets.

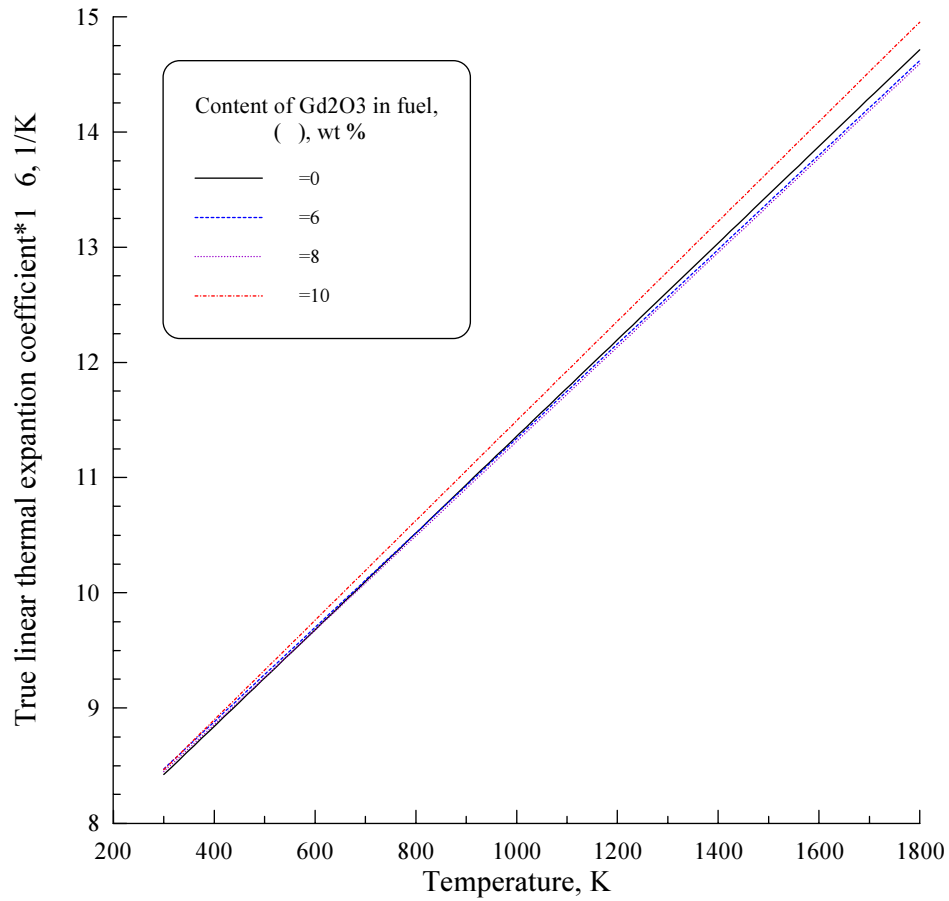


FIG.2. Temperature dependence of the true linear thermal expansion coefficient ($\alpha \cdot 10^6, K^{-1}$) of fuel pellets made of uranium dioxide and of uranium-gadolinium oxide fuel.

4. THERMAL CONDUCTIVITY OF FUEL PELLETS

The thermal conductivity (λ) was found by the formula:

$$\lambda(T) = a \cdot C_p \cdot \rho_T \cdot (1 + 3 \cdot \Delta L(T)/L_{293})^{-1} \quad (3)$$

where: a – is the thermal diffusivity, (m^2/c); C_p – is the specific thermal capacity, ($J/(kg \cdot K)$); ρ_T – is the theoretical density of specimen at room temperature, (kg/m^3); $\Delta L(T)/L_{293}$ – is the relative linear thermal expansion.

The thermal diffusivity was measured by the Parker's pulse method [1]. The essence of the pulse method consists in measuring the time interval during which the thermal energy pulse passes through a thin specimen. Provided that the pulse duration is short comparing with the time of its passage through the specimen and the heat losses are negligible, the thermal diffusivity of the specimen material can be found from the relation:

$$a = 1.37 \cdot l^2 / (\pi \cdot \tau_{1/2}) \quad (4)$$

where: l is the specimen thickness, (m); $\tau_{1/2}$ is the time required for the temperature on the rear surface of specimen to reach the half of the maximum value, (s).

The specimens had the form of thin discs ~10 mm in diameter and ~0.8-0.9 mm in thickness. The heat pulse incident to the flat surface of the disc was produced by means of laser radiation.

The thermal capacity of specimens at temperatures from 575 K to 1775 K was calculated using the Kopp-Neumann rule [2]:

$$C_p = X \cdot C_p(\text{Gd}_2\text{O}_3) + (1-X) \cdot C_p(\text{UO}_2) \quad (5)$$

where: X – is the mole fraction of Gd_2O_3 ; $C_p(\text{Gd}_2\text{O}_3)$, $C_p(\text{UO}_2)$ are and the thermal capacity of gadolinium and uranium oxides taken from [14,15], respectively; C_p – is the thermal capacity of solid solution $(\text{U}_{1-X}\text{Gd}_X)\text{O}_2$.

The theoretical density ρ_T of $(\text{U}_{1-X}\text{Gd}_X)\text{O}_2$ specimens at room temperature was found from expression [3]:

$$\rho_T = 10.96 - 3.3W, \text{ (g/cm}^3\text{)} \quad (6)$$

where W is the Gd_2O_3 content in the fuel, weight fraction

The experimental data on the thermal diffusivity and thermal conductivity of uranium-gadolinium fuel with the Gd_2O_3 content 6.0; 8.0; 10.0 wt % is shown in Figs. 3 – 4. All the data are normalized relative to the density equal to 95% of the theoretical one using the modified Maxwell-Eiken relation:

$$\lambda_{0.95} = \lambda_M \cdot 0.95 / (1 + 0.05 \cdot k) \cdot (1 + k \cdot P) / (1 - P) \quad (7)$$

where: λ_M is the measured value of the thermal conductivity coefficient; $\lambda_{0.95}$ – is the value corresponding to the density 95 % of the theoretical one P is the porosity; $k = 0.5$.

It follows from Fig.4 that the thermal conductivity of uranium-gadolinium fuel is lower than that of uranium dioxide, and it decreases as the gadolinium oxide concentration rises.

The data obtained reasonably agree with the published results [4] within the measurement error (15 %).

The results of experimental investigations obey well to the following dependence:

$$\lambda = 1 / (A + BT) \quad (8)$$

where the constant A corresponds to the interaction of phonons with the crystal defects (vacancies, clusters, dislocations, crystallite boundaries, specimen surface, alien inclusions) and the constant B – to the phonon-phonon interaction. Using the temperature dependences λ of uranium-gadolinium fuel pellets, shown in Fig.4, the values of constants A and B were calculated and are listed in Table 2.

Table 2. Values of constants A and B in equation (10) for the thermal conductivity coefficients of (U,Gd)O₂

Composition of specimens	A, $\times 10^{-2}$, (mK)/W	B, $\times 10^{-4}$ m/W
U _{0.913} Gd _{0.087} O ₂ (6.0 wt % Gd ₂ O ₃)	17.1 \pm 0.19	1.80 \pm 0.02
U _{0.885} Gd _{0.115} O ₂ (8.0 wt % Gd ₂ O ₃)	21.4 \pm 0.22	1.69 \pm 0.02
U _{0.858} Gd _{0.142} O ₂ (10.0 wt %Gd ₂ O ₃)	25.9 \pm 0.22	1.50 \pm 0.02

It is seen that the increased concentration of gadolinium oxide in the uranium dioxide results in the rise in the constant A, i.e. an additional thermal resistance is created because of interaction of phonons with the lattice defects. Even more significant contribution to the increase in the thermal resistance comes from the stress in the uranium dioxide lattice, arising when the U⁴⁺ ions are replaced by the Gd³⁺ ions. The B value then decreases and, as a result, the temperature dependence of the thermal conductivity coefficient of uranium-gadolinium fuel decreases of about the stoichiometric composition.

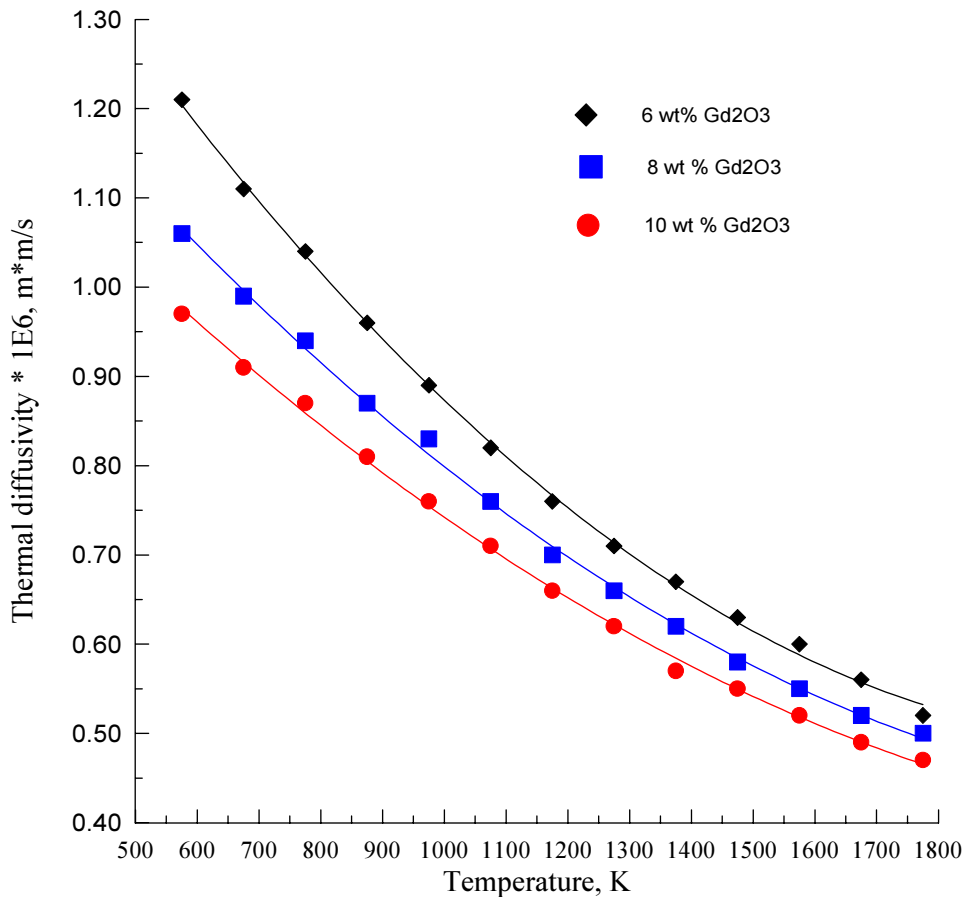


FIG. 3 Temperature dependence of the thermal diffusivity an of the uranium-gadolinium fuel with the Gd₂O₃ content 6.0 wt %, 8.0 wt % and 10.0 wt %.

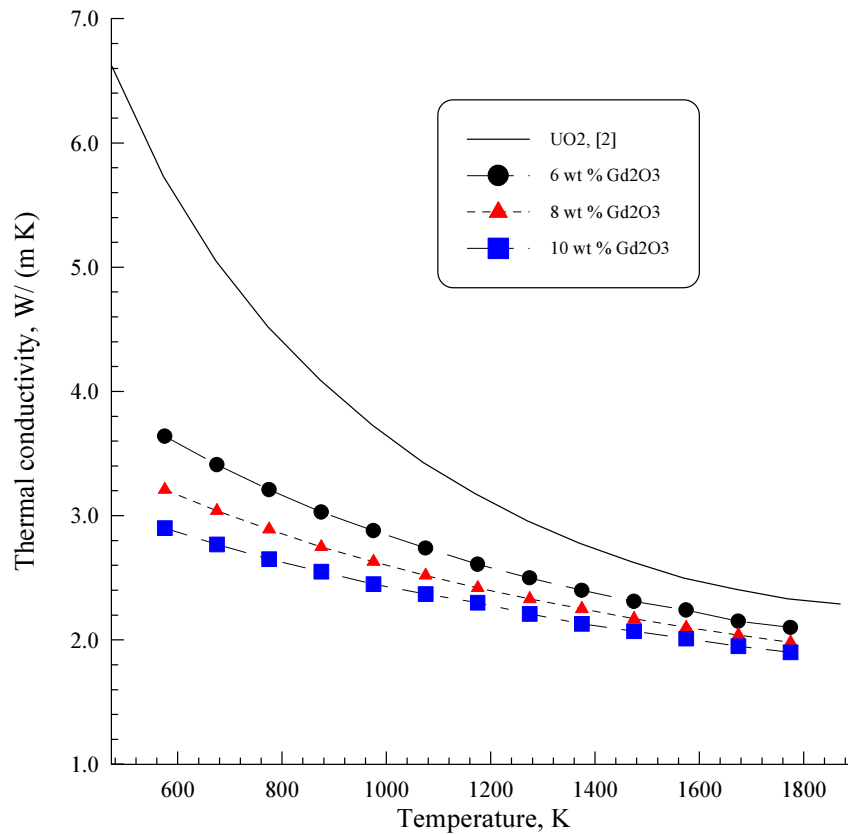


FIG. 4. Temperature dependence of the thermal conductivity of uranium-gadolinium fuel and uranium dioxide.

5. MECHANICAL PROPERTIES OF URANIUM-GADOLINIUM FUEL PELLETS

5.1. Temperature of brittle-ductile transition

For the determination of the temperature of brittle-ductile transition (T_{bd}) using the method described in [6] the temperature dependences of fuel pellet strength (σ_B) are plotted. Usually the temperature range studied is from room temperature to 1873 K. On the curve $\sigma_B = F(T)$ the temperature corresponding to the transition from the elastic to plastic deformation is found. For the determination of T_{bd} by this method several dozens of pellets (not fewer than three pellets at each point) must be carried to destruction. This method requires much labour and time expenditures. In order to increase the accuracy and rate of measurements of T_{bd} as well as to reduce essentially the quantity of tested specimens a new method for the determination of the brittle-ductile transition temperature was used. Its essence consists in the determination of specimen deformation (ϵ) at fixed stress values (σ) and time under loading (τ) within the temperature range 1073 K–1773K. Using the measured values of ϵ and at $\sigma = \text{const.}$ and $\tau = \text{const.}$ the dependence of $\lg \epsilon$ on the reverse temperature ($1/T$) is built, the inflection point which corresponds to the brittle-ductile transition is found. By means of this method the tests of specimens made of UO_2 and 90 wt% $\text{UO}_2 + 10$ wt% Gd_2O_3 were carried out at $\sigma = 30$ MPa and $\tau = 45$ min. The experimental results obtained were used for building dependences $\lg \epsilon$ vs $1/T$ (Fig. 5). It is seen that adding of 10 wt% of Gd_2O_3 (or 14.2 mol. %) to the uranium dioxide increases the brittle-ductile transition temperature by ~ 200 K.

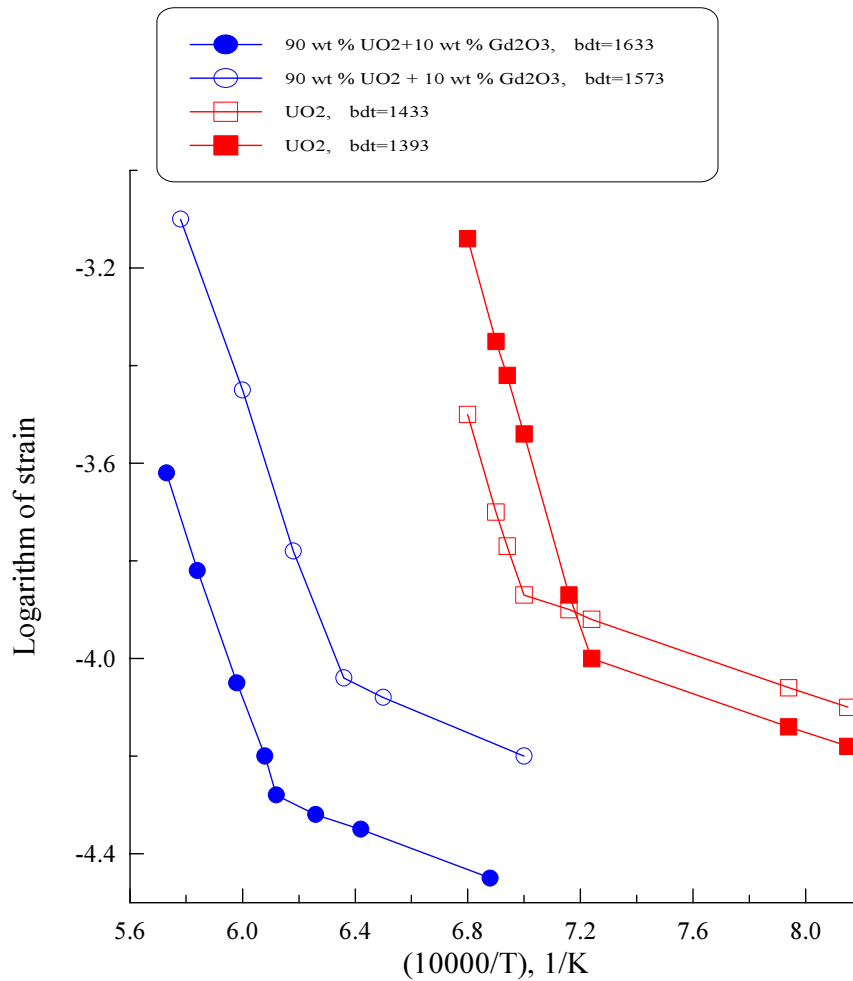


FIG. 5. Dependence of deformation logarithm on the reverse temperature at $\sigma=30$ MPa and $\tau=45$ min.

5.2. Modulus of elasticity of uranium-gadolinium oxide fuel pellets

The modulus of normal elasticity (Young's modulus) of UO_2 and $0.9\text{UO}_2+0.1\text{Gd}_2\text{O}_3$ fuel pellets was determined by the "stress-deformation" diagrams obtained in the compression tests in the temperature range 1573–1673 K. The specimen was heated up to 1723 K, then a compressing load was applied to it for eliminating gaps between the specimen ends and punches. After that the temperature was reduced to 1673 K loading corresponding to 40 MPa was applied and the specimen deformation was registration. Using the measured values of σ and ε , the Young's modulus (E) was calculated by Hook's law:

$$E=\sigma/\varepsilon \quad (9)$$

where: σ is the stress, MPa; ε is the relative deformation.

The values obtained for the UO_2 and 90 wt % UO_2+10 wt% Gd_2O_3 specimens are listed in Fig. 6. It is seen that in alloying the uranium dioxide by the gadolinium dioxide the Young's modulus increases, i.e. the specimens become more "rigid".

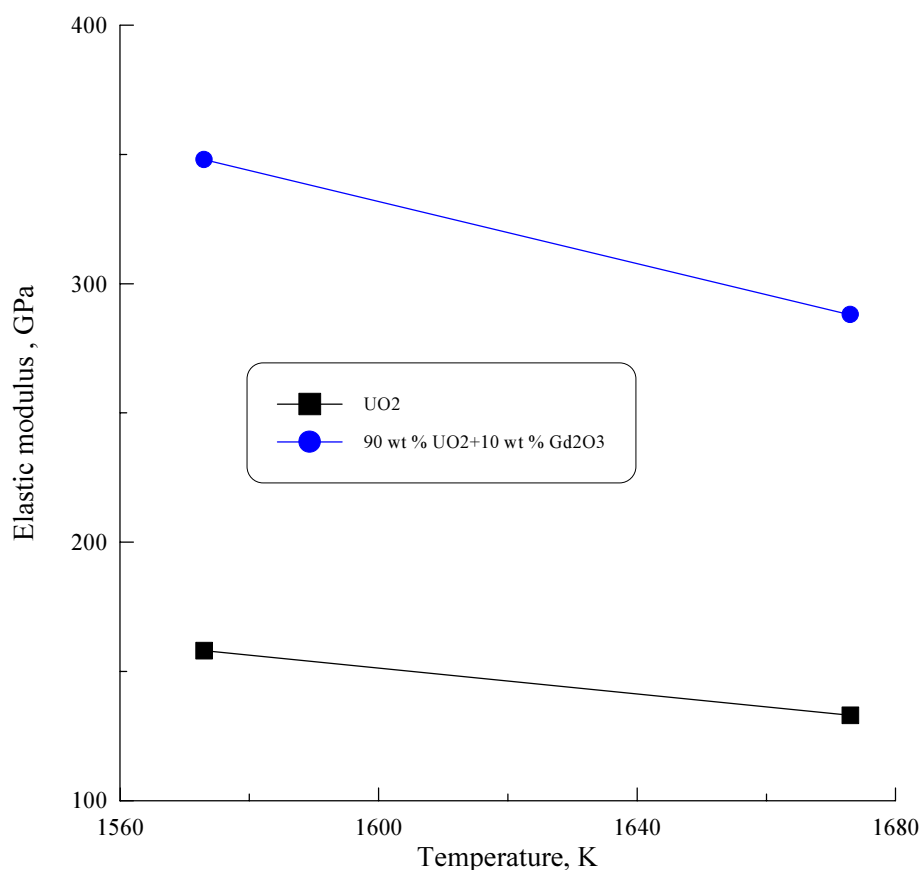


FIG. 6. Temperature dependence of Young's modulus of UO_2 and 90 wt% UO_2 +10 wt% Gd_2O_3 fuel pellets

5.3. Investigation of thermal creep of uranium-gadolinium fuel

For the creep investigation of uranium-gadolinium oxide fuel containing 5.14 mass % of Gd_2O_3 , fuel pellets with the outer diameter $\sim 5,7$ mm, central channel diameter ~ 1.4 mm, and 9–11 mm in height were used. The fuel pellet density was 10.45–10.50 g/cm^3 .

The creep tests of compressed specimens were performed on the “Kapriz-M” type installation with pneumatic loading system. The temperature in the central hole of specimen was measured by the thermocouple. The temperature range was 1150°C–1450°C (below this temperature the thermal creep was not recorded), the test environment was pure helium. The stress in the test of each specimen was increased stepwise up to 60 MPa at a constant temperature.

The creep curves obtained basing on the test results have the ordinary “classical” form with distinguished process phases. The typical creep curves for different temperatures are shown in Figs 7–10, where the values and times of actions of stepwise increased stresses are given. The maximum specimen deformation was about 5%.

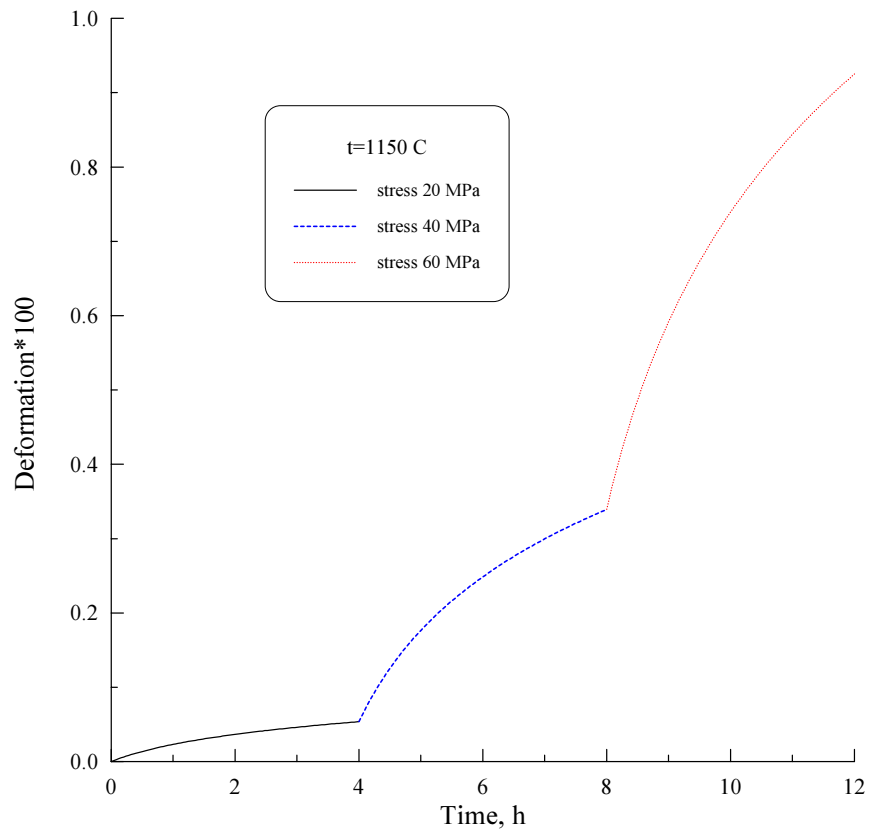


FIG. 7. Creep of uranium dioxide with addition of 5.14 wt% of Gd_2O_3 at 1150°C.

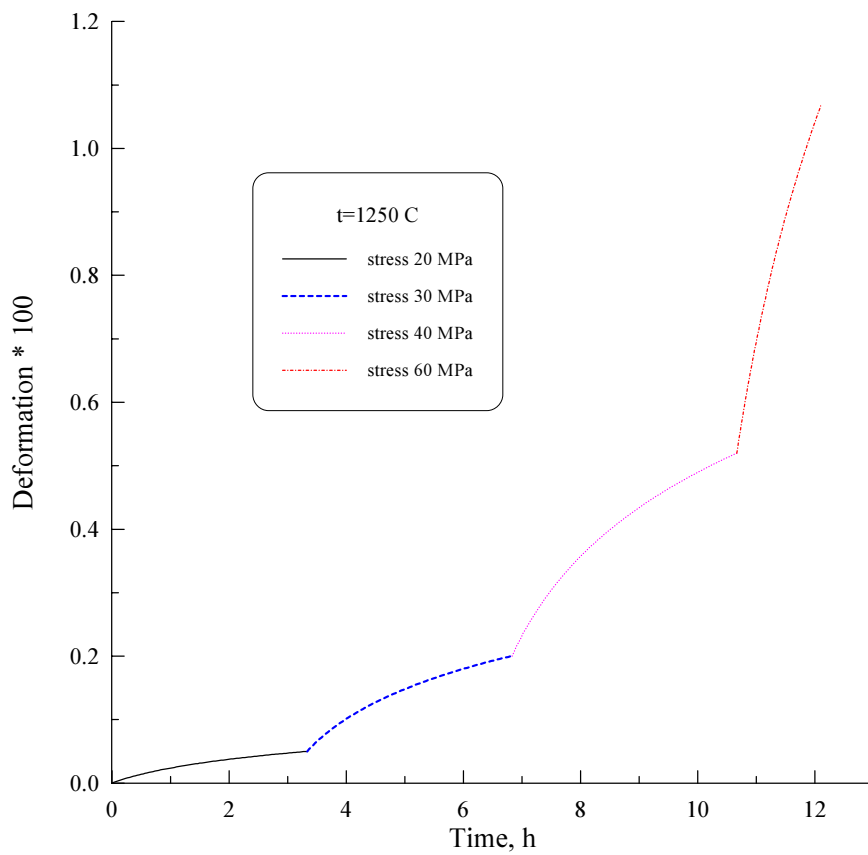


FIG. 8. Creep of uranium dioxide with addition of 5.14 wt% of Gd_2O_3 at 1250°C.

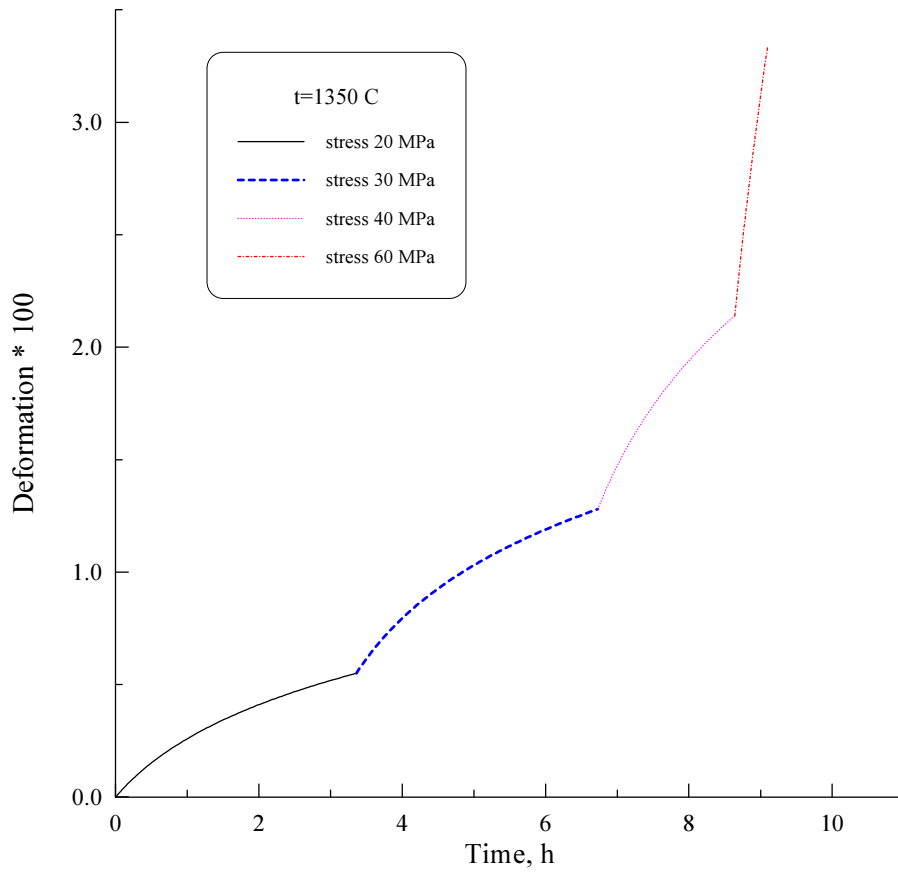


FIG. 9. Creep of uranium dioxide with addition of 5.14 wt% of Gd_2O_3 at 1350°C.

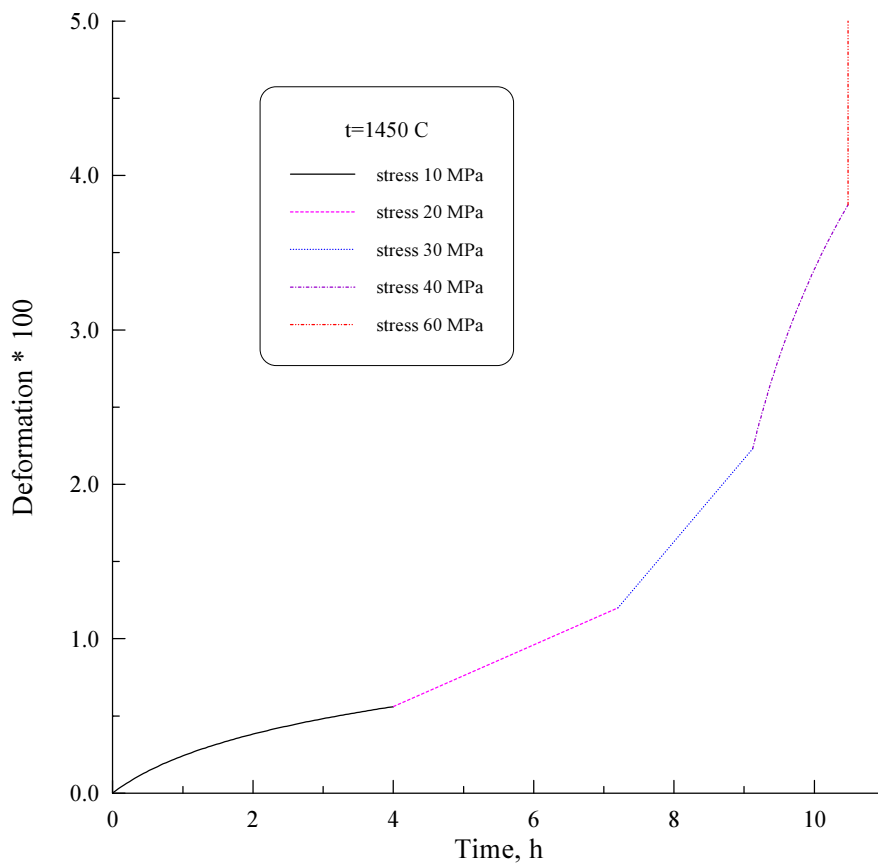


FIG. 10. Creep of uranium dioxide with addition of 5.14 wt% of Gd_2O_3 at 1450°C.

The dependences of minimum creep rates on the stress and temperature were determined by the deformation curves for different test regimes. The minimum creep rates determined by the curves lie in the range $3 \cdot 10^{-5}$ – $8 \cdot 10^{-2} \text{h}^{-1}$. These dependences are close to the linear ones practically within the whole tests range in the chosen semi-logarithmic coordinates (Fig. 11). The essential dependence of minimum creep rate on stress should be pointed out. For example, at the temperature 1450°C the values of minimum creep rates at the stress 10 MPa and 40 MPa differ by an order of magnitude. It has been established, in particular, that the values of minimum creep rates at the temperatures 1150°C and 1250°C and the stress 30 MPa are close, while at the stress 20 MPa the creep rate corresponding to a higher temperature is nearly twice lower

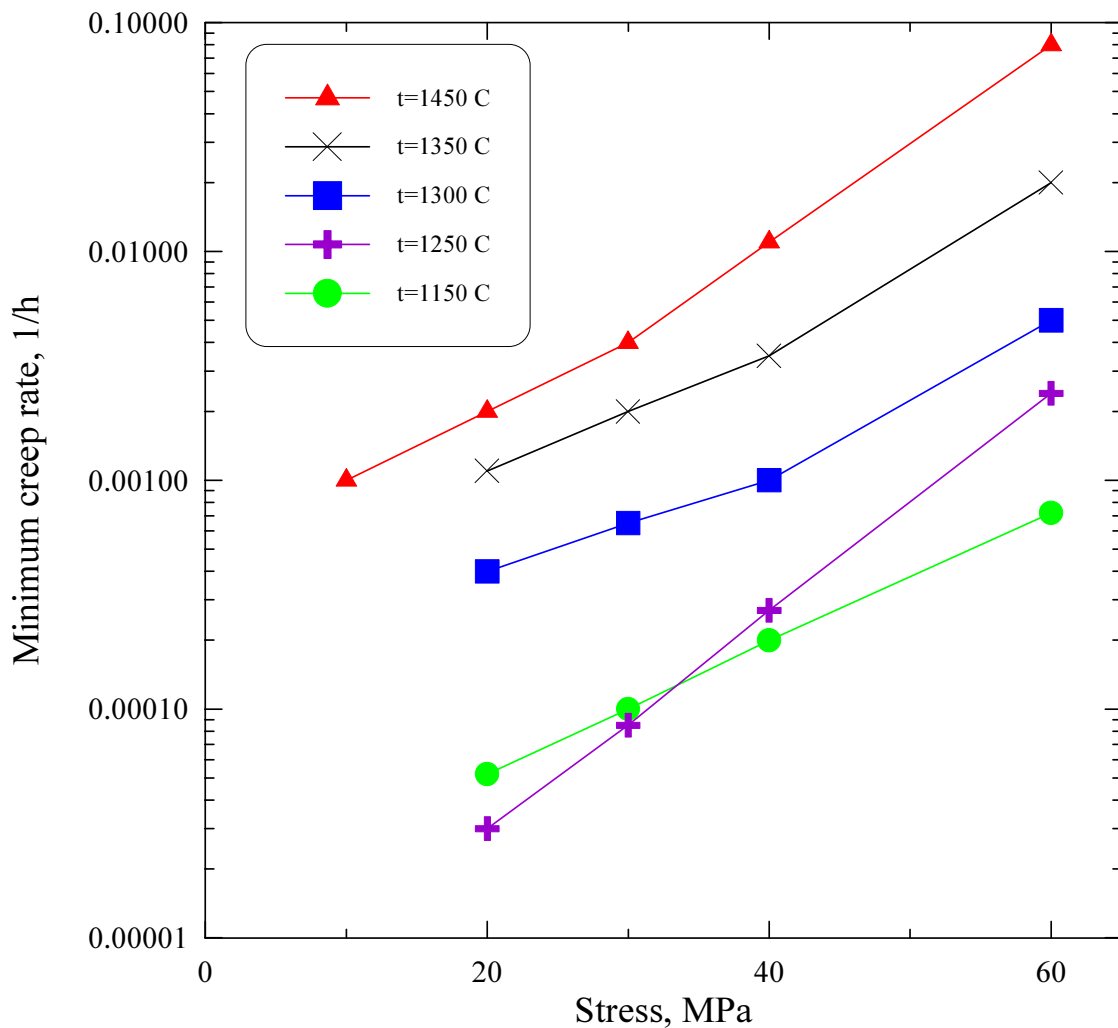


FIG. 11. Dependence of the minimum creep rate of uranium dioxide with addition of 5.14 wt % of Gd_2O_3 on the test stress at different temperatures.

The dependence of the minimum creep rate on the reverse temperature for different stresses is presented in Fig. 12. In the above-mentioned coordinates this dependence is close to the linear one at high stresses, however at temperatures of about 1250 C the local deviation from the local dependence toward lower rates (“gap”) and the higher the lower is the test stress. As a result of this behavior of the dependencies, for example, for stresses 20 MPa the minimum creep rate at 1150 C. is almost twice as high as at the temperature 1250 C.

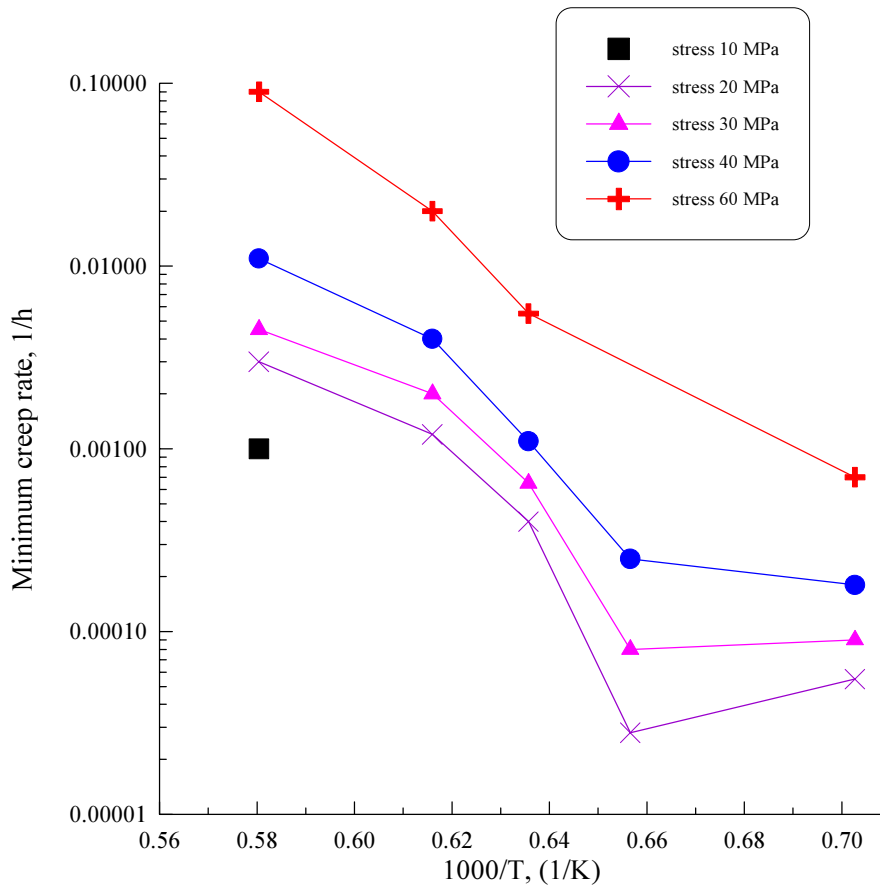


FIG. 12. Dependence of the minimum creep rate of uranium dioxide with addition of 5.14 wt% of Gd_2O_3 on the test temperature at different stresses.

In Table 3 show the results of comparative creep tests for specimens of UO_2 and $(U_{1-x}Gd_x)O_2$, where the weight fraction of Gd_2O_3 in the fuel is 0.06, 0.08, 0.1.

Table 3. Creep rate of UO_2 and $(U_{1-x}Gd_x)O_2$

Content of Gd_2O_3 wt %	$d\epsilon/dt \cdot 10^5, h^{-1}$									
	T, K	1473			1573			1673		
	σ , MPa	20	30	40	20	30	40	20	30	40
0		38.5	72.0	128.0	65.1	223.0	730.0	140.0	601.0	1850.
6.0		6.0	9.5	14.8	36.1	59.4	82.3	91.0	152.1	273.2
8.0		5.5	8.2	12.7	20.3	37.2	48.1	89.3	138.6	265.1
10.0		3.3	6.4	11.1	18.0	24.6	32.5	86.2	115.0	231.0

The experimentally found dependencies of creep rates on the stress at the temperature 1473, 1573 and 1673 K are reasonably well described by the relation of the form:

$$d\epsilon(\sigma)/dt = A_1 \cdot \exp(\alpha \cdot \sigma), \text{ (at } T = \text{const)} \quad (12)$$

where:

$d\epsilon/dt$ - is the creep rate, (h^{-1}); σ - is the stress, (MPa); A_1 - is the constant, (h^{-1}); α - is the constant, (MPa^{-1}).

In Table 4 the values of constants A_I and α in formula (12), obtained by the least squares method are listed.

Table 4. Values of constants A_I and α

Content of Gd ₂ O ₃ Mass %	Temperature, K					
	1473		1573		1673	
	A_I, h^{-1}	α, MPa^{-1}	A_I, h^{-1}	α, MPa^{-1}	A_I, h^{-1}	α, MPa^{-1}
0	$1.20 \cdot 10^{-4}$	0.060	$5.80 \cdot 10^{-5}$	0.120	$1.06 \cdot 10^{-4}$	0.130
6.0	$2.52 \cdot 10^{-5}$	0.044	$1.58 \cdot 10^{-4}$	0.041	$3.03 \cdot 10^{-4}$	0.055
8.0	$2.38 \cdot 10^{-5}$	0.042	$8.57 \cdot 10^{-5}$	0.043	$3.01 \cdot 10^{-4}$	0.054
10.0	$9.80 \cdot 10^{-6}$	0.061	$1.00 \cdot 10^{-4}$	0.030	$3.20 \cdot 10^{-4}$	0.049

It is seen from the data of Table 4 that no clear regularity in the change of constants A_I and α with the increase in the temperature and Gd₂O₃ content in the oxide fuel has been established. The spread in the values of A_I and α seems to be due to existence of microcracks in the actual fuel pellets.

The addition of gadolinium oxide to uranium dioxide reduces the rate of (U_{1-x}Gd_x)O₂ fuel pellet creep comparing with the UO₂ pellets. The replacement of uranium ions by Gd³⁺ ions whose size is larger by 5% than that of U⁴⁺ ions and by 20 % larger than U⁵⁺ significantly affect the diffusion processes in the (U_{1-x}Gd_x)O₂ solid solution. It is supposed [9] that the uranium ions with high valence together with Gd³⁺ ions form local complexes, which prevent the diffusion of uranium ions.

6. CONCLUSION

1. The thermal-physical properties of uranium-gadolinium oxide fuel were studied.

1.1. In the studied region of compositions within the temperature range 293K-1755K the increase in the gadolinium oxide content in the fuel does not noticeably affect the coefficient of thermal expansion of fuel pellets.

1.2. The addition of gadolinium oxide to the uranium dioxide reduces the thermal conductivity of fuel pellets, the effect of gadolinium oxide concentration decreasing as the temperature increases. The decrease in the thermal conductivity of uranium-gadolinium oxide fuel pellets is accounted for by increasing interaction of phonons with the polycrystal defects, whose concentration increases significantly with the rise in the gadolinium oxide content, and the stresses in the uranium dioxide lattice arising when the U⁴⁺ ions are replaced by the Gd³⁺ ions.

2. The mechanical properties of pellets made of the uranium-gadolinium oxide fuel were studied.

2.1. The application of the new method of determining the brittle-ductile transition temperature allowed the T_{bd} of the specimens made of uranium dioxide and uranium-gadolinium dioxide fuel to be determined with a high accuracy. It has been established that for the uranium dioxide pellets T_{bd} is $1413K \pm 20K$, which reasonably agrees with the data

available in the literature. The addition of 10.0 mass % of Gd_2O_3 to the uranium dioxide increases T_{bdt} to $1603K \pm 30K$.

2.2. Alloying the uranium dioxide with 10.0 mass % of gadolinium oxide results in the growth of Young's modulus by two times, which seems to make a contribution to appearance of microcracks in the uranium-gadolinium oxide fuel pellets under the action of thermal gradients.

2.3. The thermal creep of uranium-gadolinium oxide fuel at temperatures $1150^{\circ}C$ - $1450^{\circ}C$ and stresses 10MPa-60 MPa was investigated. The creep curves were obtained, dependences of minimum creep rates on the temperature and stress were found.

REFERENCES

- [1] PARKER, W.J., BUTTER, C.P., ABBAT, J.L., JENKINS, R.J., *J. Applied Physics*, (1961) **31** N4, 1679.
- [2] LUCUTA, P.G., et al., "Thermal conductivity of SIMFUEL", *J. Nucl. Mater.*, (1992) **188** 198.
- [3] WADO, L. et al. "Behaviour of UO_2 - Gd_2O_3 fuel", Nuclear Fuel Performance (Proc. Int. Conf, London, UK, 1973) BNES, London (1973) 631-633.
- [4] FUKUSHIMA, S., et al., "The effect of gadolinium content on the thermal conductivity of near-stoichiometric (U,Gd) O_2 solid solutions", *J. Nucl. Mater.*, (1982) **105** 201.
- [5] *Gmelin Handbook of Inorganic Chemistry*, Springer-Verlag, Berlin - Heindelberg - New-York, v.5, p.317, (1986).
- [6] CANON R.J., ROBERTS J.T.A., BEALS, R.J., *J. Amer. Ceram. Soc.*, **54** (1971) 105.
- [7] MILOSERDIN, YU.V., NABOICHENKO, K.V., GOLOVIN, I.S. et al. *Atomnaya energiya* (1977), v.35. N6, p. 371 (in Russian).
- [8] HAGLUND J., HUNTER D., *J. Amer. Ceram. Soc.*, (1973), v.56, 327.
- [9] HO S., RADFORD K., *Nucl. Technol.*, (1985) **73** N3, 350.
- [10] UNE K., *J. Nucl. Sci. Tech.*, (1986), v.23, N11, 1020.
- [11] MILOVANOV, O.V., PROSELKOV, V.N. et al. Preprint IAE-5744/4, (1994) (in Russian).
- [12] Development, production and operation of fuel rods for power reactors. In two books, Book 1/Ed.F.G. Reshetnikov M., Energoatomizdat, 1995, p.320.
- [13] KITTEL, Ch., *Introduction to solid state physics*. M., Nauka, 1978, p.235.
- [14] PANKRATZ, L.B., KING, E.G., KELLEY, K.K., US Bur. Mines, Rep. Inv. No 6033, 1962.
- [15] FINK, J.K., "Thermophysical properties of uranium dioxide", *J. Nucl. Mater.*, **279** (2000) 1.

WESTINGHOUSE DOPED PELLETT TECHNOLOGY

J.-E. LINDBÄCK

Westinghouse Atom AB,
Västerås, Sweden

Abstract

Different types of doped pellets have been presented lately to improve fuel irradiation performance. Westinghouse Atom has developed pellets with additives resulting in high densities (typically $10,67 \text{ g/cm}^3$) and larger grains (typically $30\text{--}45 \text{ }\mu\text{m}$). Examinations have been performed to verify their irradiation behaviour. The performance of the doped pellets is verified by irradiation in power and research reactors. Power ramp testing to $57,5 \text{ kW/m}$ terminal power has been successful. This new pellet generation allows increased uranium weight in the fuel assemblies, improves the pellet corrosion resistance and is expected to reduce fission gas release.

1. INTRODUCTION

Articles about UO_2 fuel pellets containing additives have been published frequently lately. A few examples are [1-3]. This could reflect a wide interest to significantly improve pellet properties, which would be a natural step to further optimise integral fuel performance since fuel pellet fabrication related fuel defects have become unusual through optimised pellet production processes and efficient quality assurance.

Doped fuel has been the subject of several projects within the BNFL-Westinghouse group over the last three decades. A project in the 1980's at Westinghouse Atom (the Swedish branch of Westinghouse Electric) with Nb_2O_5 addition resulted in large grain fuel pellets and fuel with good PCI resistance. However, considerable fuel swelling and too high neutron absorption terminated the development. Development of a new pellet generation started in 1998. A pre-runner project to attain higher density with process changes had been successful, but further increased density was wanted and thought possible only by the use of additives. A comprehensive study with candidate additives such as Al_2O_3 , TiO_2 , SiO_2 , MgO , Cr_2O_3 , Nb_2O_5 was conducted. The study resulted in the selection of Cr_2O_3 as such and in combination with other additives.

Characteristic for the doped fuel pellets is higher density and larger grains than normal. Several benefits are achieved. Through higher density, typically around $10,67 \text{ g/cm}^3$, an increase of the uranium weight per fuel element is possible. This is important when end-of-life burnups increase and fuel assembly maximum U-235 enrichment approaches the manufacturing license limit. Reduced fission gas release is anticipated through larger grains. The margin to fuel rod PCI failure is maintained or improved through a changed cracking pattern, augmented pellet creep or plasticity combined with reduced release of volatile fission products. Testing also indicates that lower uranium leaching in case of a rod failure in-core could be possible through improved pellet corrosion resistance.

2. THE EFFECT OF ADDITIVES

Two main mechanisms can be evocated that may explain how shrinkage and grain growth of pellets is stimulated [4, 5].

The first mechanism assumes that the additives enter the UO_2 lattice substitutionally as cations with higher valence. The diffusion rate in the UO_2 lattice (fluorite structure) is limited by cation (U^{4+}) diffusion. The higher valence (≥ 4) cations enhance uranium diffusion. With smaller valence (< 4), the diffusion of uranium is decreased. Enhanced boundary diffusion improves sintering, but for increased shrinkage volume diffusion has to be improved.

Another type of mechanism, liquid-phase sintering, takes place on a structural level during the densification step of the sintering process. The powder particles are coated with a layer of melted metal oxides. The liquid between the particles acts as a lubricant and as transport medium through solution-precipitation. This is however less likely to be the mechanism since additive concentrations are too small.

3. ANUFACTURING

Pellets are manufactured using powder produced with the ammonium-uranyl carbonate (AUC) conversion process. The powder is free flowing and pellets are produced without granulation or internal lubricant. Doping agents are added to the powder via a pre-blend in order to ensure a good homogeneity. The pre-blend is a mix of around 5% of the final UO_2 powder lot and the doping agents. This is mechanically blended to the rest of the powder.

Green pellets are produced using a 16-position uni-axial rotary press. The die walls are lubricated with oil. Pressures ranging from 400 to 600 MPa lead to a green density of at least 50% of the theoretical density. Sintering is performed in a continuous production furnace in an H_2 atmosphere with small additions of CO_2 and maximum temperature around 1700°C . The temperature history and CO_2 concentration have been varied in order to find the optimum sintering parameters.

4. TESTING OUT OF PILE

4.1. Production quality check data

The usual production inspection is performed on the doped pellets with special attention to the accuracy of the characteristic properties such as grain size and density. The density of the pellets are determined using the immersion (or Archimedes) method. Density is typically $10,67 \text{ g/cm}^3$ although higher can be obtained.

Pellet grain size is measured on samples that are cut in the axial direction, ground, polished and etched. The grain size is determined by the cross intercept method on three different parts of the pellet cross section. Grain sizes (3-D) are typically 30–45 μm .

Grains have a hexagonal geometry, which is typical of well-developed structures. The distribution has been kept unchanged. No displacement of the peak can be noted. The porosity is reduced simply by a scaling factor.

Doped pellets ($10,67 \text{ g/cm}^3$) are found more stable than standard ($10,52 \text{ g/cm}^3$) and high-density ($10,60 \text{ g/cm}^3$) pellets from thermal stability testing.

4.2. Oxidation tests

Samples have been tested in order to quantify the improvement of the pellet resistance against corrosion. Two methods have been used. One is the thermo-balance and the other is autoclave testing.

4.2.1. Thermo-balance

The thermo-balance allows testing in highly oxidising controlled atmosphere with simultaneous weight gain measurement. The pellet is placed inside a glass tube on a platinum support, as seen in the sketch of the equipment in Fig 1.

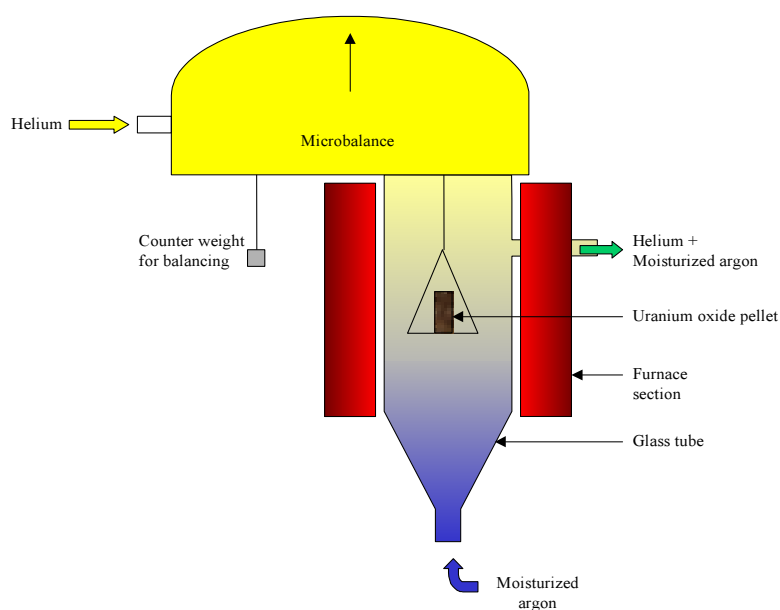


FIG. 1. Thermo-balance equipment schematic.

In the experiment the temperature was raised to 400°C at 10°C/min. After the temperature had increased and stabilised the atmosphere was changed from argon (used during heating period) to moisturised argon. The argon flow was 100 ml/min. The temperature was maintained for 20 hours and then cooled down to room temperature at 10°C/min. The weight change of the sample was monitored throughout the experiment.

Samples are prepared before testing by grinding to a smaller diameter of around 8 mm to fit the equipment. The weight, length, diameter and surface roughness is carefully controlled.

After the experiment samples were mounted in epoxy resin, and subsequently ground, polished and etched for light optical microscopy. Particular attention was dedicated to the identification of secondary phases, inclusions, and oxidised layers covering the sample as well as measurement of the depth of penetration.

Curves obtained from the microbalance measurements are analysed, corrected and interpreted in order to have a classification of the pellet susceptibility to oxidation. The graph in Fig 2 shows the rate of oxidation of the doped pellets compared to pure UO₂ pellets.

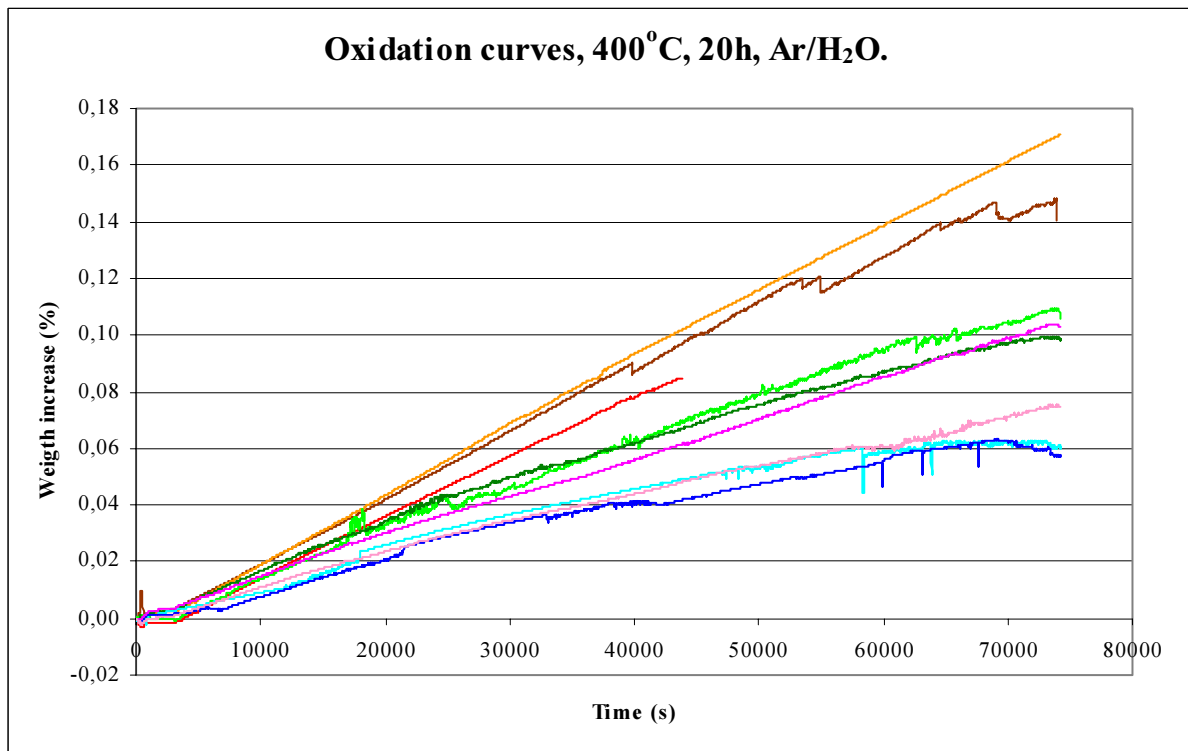


FIG. 2. Oxidation curves obtained from the thermo-balance. Pure UO_2 (top 3 curves) and UO_2 with additives.

It can be seen that the additives reduced the weight gain in the range 30 to 50%. Over the all range of temperature 20-1500 °C the oxidation potential of oxygen is lower (in absolute value) for the couple Cr/Cr₂O₃ than for UO₂. This means Cr will tend to oxidise quicker than UO₂. The oxidation of UO₂ is delayed; the oxidation front progression rate within the grain is reduced. The second explanation takes into account that the oxidation occurs via the grain boundaries. Due to the fact that the grain size of the doped pellets has been increased, the ratio $V_{\text{grain boundaries}} / (V_{\text{grains}} + V_{\text{grain boundaries}})$ decreases. The oxidation attack is therefore more difficult. The second mechanism is believed to be predominant.

It was noted that the UO₂ pellets exhibited a large amount of powder on their surface at the end of the experiment. This powder, assumed to be U₃O₈, was not present on the surface of the doped pellets.

4.2.2. Autoclave

The purpose of the autoclave experiment was to simulate the corrosive environment after primary and secondary fuel rod cladding failures. Two experiments, one in steam and one in water were performed.

The pellets were first exposed to a flow of steam ($\leq 0,5$ kg/h) at a temperature of 350°C under 60 bar pressure. Oxygen was added to the water at room temperature to a nominal concentration of 35 ppm O₂. Hydrogen gas content was measured with a gas chromatograph connected to the exit of the autoclave. After an exposure of 6 days, the pellets were weighed and photographed.

Some of the samples underwent a subsequent experiment to simulate a secondary fuel failure. The pellets were now exposed to a flow of water (≥ 20 kg/h) at a temperature of 288°C and a pressure around 80 bar. In order to obtain a water chemistry representative for in-core conditions, hydrogen peroxide (H_2O_2) was added to the water up to a nominal content of 600 ppb. Afterwards the pellets were again weighed and photographed.

Pictures of a UO_2 and a doped pellet are presented in Fig 3.

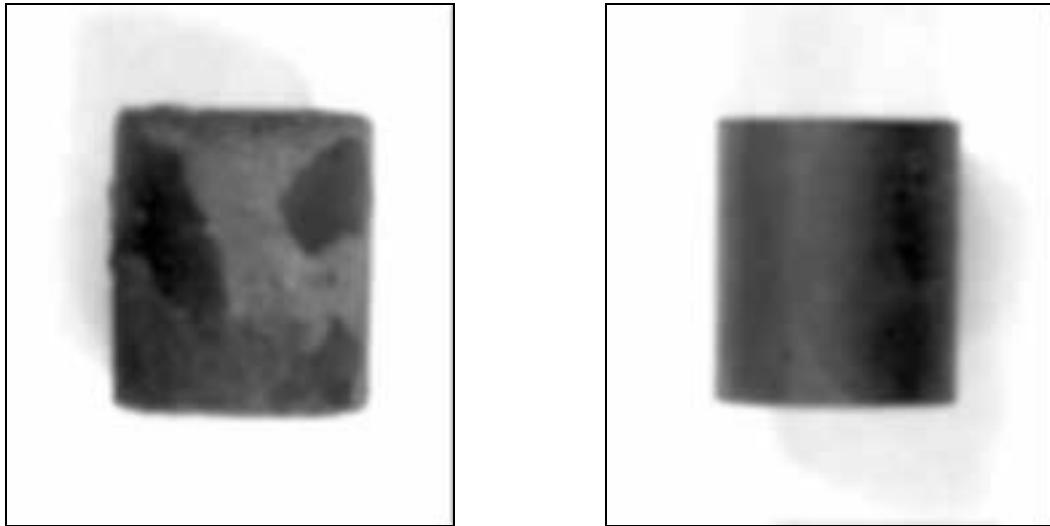


FIG. 3. Samples after autoclave tests. Pure UO_2 (left) and doped pellet (right).

The two pellets have been tested at the same time during a test to define experimental parameters. It can be seen that a crust has been formed on the surface of the UO_2 pellet and lots of particles have fallen apart. The doped pellet appearance, on the contrary, is almost unchanged. The oxidising atmosphere had no effect on its structure. The result confirms the conclusion from the thermo-balance experiment.

4.3. Creep test

A pellet creep test was performed in order to quantify the plasticity and creep properties of the doped pellets. The goal was to have an idea about PCI/PCMI behaviour.

Special equipment was built to allow high temperature creep testing. A sketch of the equipment is given in Fig 4.

Tests were conducted at 1000°C during approximately 20 hours. A controlled atmosphere (a mix of argon and 2,5% H_2) was used in order to prevent oxidation and stoichiometry changes of the samples. An external load of 25 MPa was applied and maintained constant with a tensile testing machine. The deformation of the samples was recorded using an extensometer connected to a computer.

Comparison of creep rate under compression is possible between a standard production UO_2 pellet and the doped pellet. Doped pellets were anticipated to have increased deformation, but no significant creep rate difference was found between UO_2 and doped pellets. It is possible that there exists a difference but that the temperature was too low to reveal it.

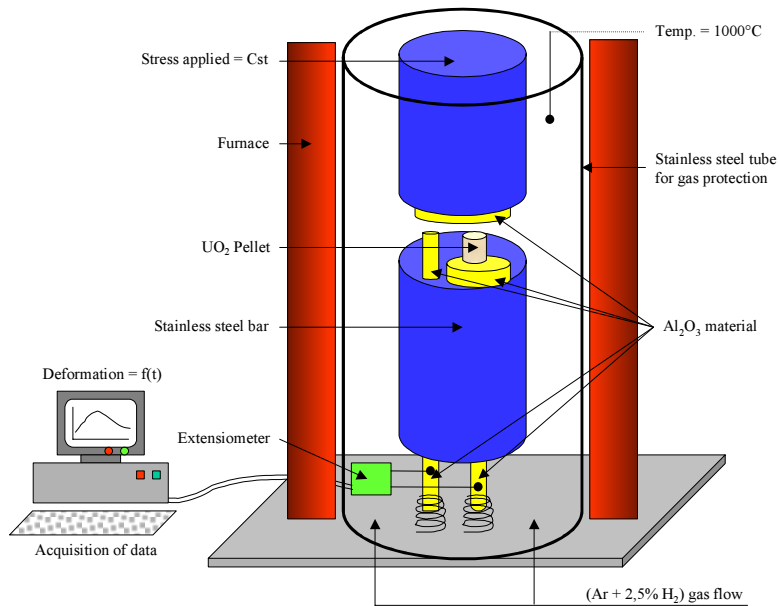


FIG. 4. Picture of creep test apparatus.

4.4. Thermal shock

An important step that takes place in the beginning of the irradiation in reactor is the fracture of the pellet and relocation of the fragments inside the cladding. Thermal shock analysis is a possibility to partially reproduce phenomena that happen in reactor.

Both UO_2 and doped pellets underwent this thermal shock at $\Delta T = 200^\circ C$, $400^\circ C$, $600^\circ C$. Heating up to $400^\circ C$ was performed in air. For $600^\circ C$, heating was performed under controlled atmosphere to avoid deep oxidation of the pellets. The quenching was made in distilled water at room temperature. The time to quench the pellets was quick enough to avoid any intermediate cooling phase. An example of crack patterns after thermal shock testing is seen in Fig 5.

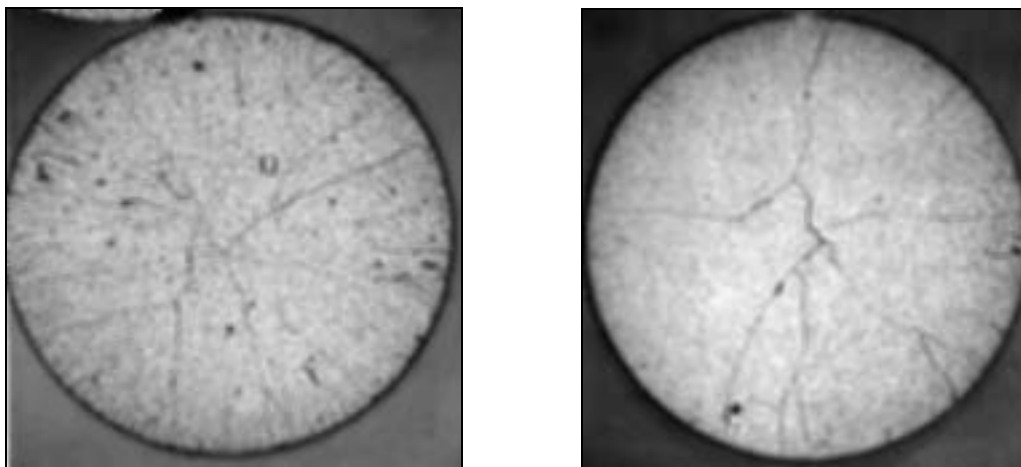


FIG. 5. Results from thermal shock test with $\Delta T 600^\circ C$. Pure UO_2 to the left, doped pellet to the right.

4.5. Thermal conductivity

The thermal conductivity λ depends on the thermal diffusivity α , the density ρ and heat capacity C_p through the following relation.

$$\lambda = \alpha \cdot \rho \cdot C_p$$

Thermal diffusivity measurements have been performed with the laser flash technique. Samples were prepared from UO_2 and doped pellets sliced into 2 to 3 mm thick discs. The discs are placed in a furnace and the topside radiated with an energy pulse by a laser. The energy pulse is absorbed by the surface and the heat conducted through the sample. Detecting radiation with a photovoltaic infrared detector monitors the temperature on the rear of the sample. The thermal diffusivity can then be calculated by the formula.

$$\alpha = \frac{K \cdot L^2}{t_{1/2}}$$

K is a constant, L is the thickness of the specimen and $t_{1/2}$ is the time for the back face to reach half of its maximum temperature.

The thermal diffusivity was measured for temperatures ranging from room temperature to 1400°C . The thickness of the sample was corrected for thermal expansion using pure UO_2 thermal expansion data, even though the thermal expansion was very small. A maximum correction of about 2,5% was made for thermal diffusivity values at 1400°C .

The data presented in Fig 6 demonstrate that no significant thermal diffusivity difference can be observed between UO_2 pellets and doped pellets. The difference between the pellets is smaller than the estimated measurement accuracy of $\pm 5\%$.

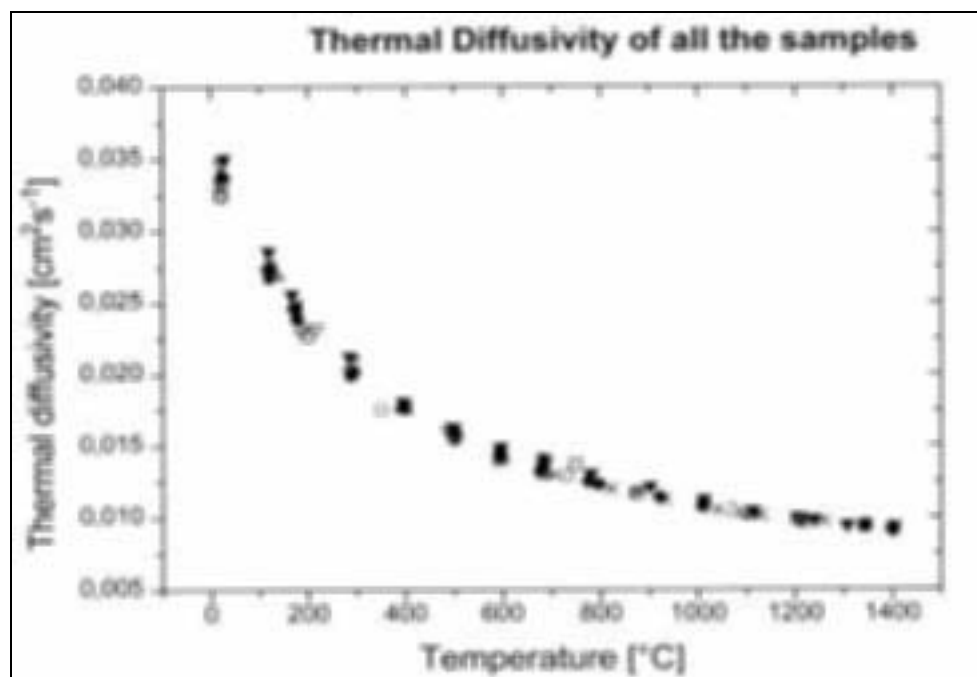


FIG. 6. Thermal diffusivity of pure UO_2 (X,+) and doped pellets(+, ▼, ●).

The heat capacity measures the quantity of heat required to raise the temperature of the sample through one degree. The heat capacity was measured in comparison to a reference material. The doped samples and the reference were placed in two separate furnaces and the heat input was monitored during all the experiment. Measurements were performed between room temperature and 1000°C, under argon atmosphere. The results are not final yet, but no major difference is expected.

In conclusion, thermal conductivity seems to be similar for doped and pure UO₂ pellets.

4.6. SEM examination

Extensive observations of the pellets using scanning electron microscopy (SEM) technology enables us to determine any special feature of the pellet structure compared to pure UO₂ pellets. Also precipitates or local high concentrations of doping elements can be revealed. Focus is on the characterisation of the grain boundaries (presence of precipitates) and the porosity distribution (inter-grain and at the grain boundaries) in the doped pellets.

Extensive examinations have been performed using a scanning electron microscope. Particular attention was dedicated to identifying precipitates or secondary phases at grain boundaries or within grains. Back scattered electron cartography and mapping for chemical analysis was used.

No precipitation has been visible at the grain boundaries, neither using the back-scattered electron mode or even the mapping procedure. The inside surface of the pores was of particular interest due to their smooth shape. This is again an indication of a well-developed structure, which means a stable structure.

5. TESTING IN-PILE

In addition to the out-of-pile testing fuel is irradiated. Lead fuel assemblies containing fuel rods with pellets manufactured with additives are currently being irradiated in power and research reactors. Fuel rods base irradiated in a power reactor (BWR) have been transported to a nuclear test facility for post irradiation examination and further irradiation and testing.

Some of these rods have been subject to power ramp testing. The ramp test allows comparison of PCI performance of fuel rods containing additive pellets with reference objects. Two rods irradiated to approximately 30 MWd/kgU rod average burnup were ramp tested with terminal power levels of 57,5 kW/m without signs of failure. See one example of ramp irradiation power history in Fig 7.

PCI is thought to improve through a changed cracking pattern, increased pellet creep or plasticity, reduced release of volatile fission products or a combination of these. The rods are undergoing PIE that will give us more detailed knowledge of the fuel performance behaviour.

Fission gas release is anticipated to improve through the larger grain size. This should be the case unless possible counter effects such as increased diffusion rate or smaller solubility at grain boundaries of gaseous fission products level this effect. This will be evaluated in irradiation tests. One test is planned within the OECD Halden Project. Doped pellets from Westinghouse are included and the irradiation will begin in 2004. Another test is includes fuel rods base irradiated in a power reactor that will continue irradiation in a research reactor.

REFERENCES

- [1] BOURGEOIS, L., et al., Factors governing microstructure development of Cr₂O₃-doped UO₂ during sintering, *Journal of Nuclear Materials* **297** (2001) 313–326
- [2] FUJINO, T., et al., Post-irradiation examination of high burnup Mg doped UO₂ in comparison with undoped UO₂, Mg-Nb doped UO₂ and Ti doped UO₂, *Journal of Nuclear Materials* **297** (2001) 176–205
- [3] KASHIBE, S., UNE, K., Effect of additives (Cr₂O₃, Al₂O₃, SiO₂, MgO) on diffusional release of ¹³³Xe from UO₂ fuels, *Journal of Nuclear Materials* **254** (1998) 234–242
- [4] KINGERY, W.D., BOWEN, H.K., UHLMANN, D.R., *Introduction to Ceramics*, John Wiley & Sons, New York (1975)
- [5] RICHERSON, D.W., *Modern Ceramic Engineering*, Marcel Dekker, Inc., New York (1992)

UO₂, MOX AND UO₂-GD₂O₃ PELLETS WITH ADDITIVES

(Session 2)

Chairpersons

R.N. JAYARAJ

India

K. ASAKURA

Japan

DENSIFICATION BEHAVIOR OF TiO₂ DOPED UO₂ PELLET

H.S. YOO, S.J. LEE, J.I. KIM, J.G. CHUNG, K.T. KIM
KEPCO Nuclear Fuel Co. Ltd,
Daejon, Republic of Korea

Abstract

Microstructural change of UO₂ pellet due to titania(TiO₂) addition has been examined. The test samples were fabricated with the addition of titania in the range of 0.06 to 0.2wt% in pure H₂ atmosphere at 1740°C for 4hrs. For the purpose of comparing, kaolin (Al₂Si₅O₅(OH)₄) doped UO₂ pellets were prepared at the same conditions. In order to investigate the densification behavior, the sintered pellets were annealed at 1700°C for 48 hrs. The average grain size increased with the addition of TiO₂ and it grew up to 48 μm when 0.2 wt% TiO₂ was added while sintered density decreased. On the contrary, grain size of UO₂ pellets in which the same amount of Al₂Si₅O₅(OH)₄ was added was only 20 μm. Grain boundaries of TiO₂ and Al₂Si₅O₅(OH)₄ doped pellets showed low dihedral angle which proves the formation of liquid phase during sintering. Different from undoped pellet, TiO₂ doped pellet had pores with spherical shape. In general, spherical shape is the most stable morphology so that pores with such shape have more resistance to heat energy for moving and being removed. Densities of the TiO₂ doped pellets were decreased by 0.08 ~ 0.15% T.D. after annealing for 48 hrs, which means that pellet swelling occurred. Swelling of the TiO₂ doped pellet can be explained by the above mentioned pore morphology. Large grains partly contribute to swelling but the spherical pore shape is believed to play a dominant role. It can be confirmed by the result that Al₂Si₅O₅(OH)₄ doped UO₂ pellet which had a large grain and oblong pore shape was densified rather than swelled after annealing for 48 hrs.

1. INTRODUCTION

In-pile densification of UO₂ pellet during irradiation has been a major concern to those who design nuclear fuel and operate nuclear power plant since it affects fuel rod integrity.

W.Chubb[1] had reported in 1974 that densification was controlled by the microstructure of the fuel, particularly its pore size distribution and average pore size. He had concluded that sintering conditions determining the microstructure of pellet were the main factor that could control in-pile densification.

In-pile densification has been believed to occur by the fission induced resolution of pores. The resolution of pores produces a dispersion of excess vacancies in the fuel and the migration of some of these excess vacancies to external surface results in local increase in density and corresponding dimensional changes. Therefore, it is important to control the microstructure of UO₂ pellet, especially, pores, to maintain the integrity of fuel rod during operation.

As mentioned earlier, microstructure of UO₂ pellet strongly depends on sintering conditions. However, sintering variables such as temperature and time are directly related to the productivity so that other methods by which optimum microstructure of UO₂ pellet can be obtained without altering sintering conditions are highly recommended.

The most promising way is to add dopant to UO₂. Up to now, massive studies on the effect of additives such as Nb₂O₅, MgO, TiO₂ and Al-compounds have been carried out [2-5]. Most of

the studies have been concentrated on coarsening grain size of pellet since fission gas release is a prime concern to the researchers. It has been known that TiO₂ is the most effective additive to increase grain size. However, there is a little information about the densification behavior of TiO₂ doped UO₂ pellet.

In general, resintering test is performed to predict the densification behavior of UO₂ pellet during irradiation. It has been verified that microstructural changes in pellet due to resintering in the lab is coincident with those in the reactor at the early stage of operation [6]. This work has been undertaken to study the densification behavior of TiO₂ doped UO₂ pellet. To do this, various amounts of TiO₂ in the range of 0.06 to 0.2 wt% was added in the fabrication of UO₂ pellet and sintered pellets were annealed up to 48 hrs. For comparison, Al₂Si₅O₅(OH)₄ doped UO₂ pellets that were known to have the same mechanism for increasing grain size as TiO₂ doped pellet were fabricated and annealed.

2. EXPERIMENTAL PROCEDURES

2.1. Manufacturing of mixed powder

UO₂ powders produced by Dry Conversion process were used in this experiment. The impurities and characteristics of undoped UO₂ powder are shown in Table I. In order to simulate the commercial UO₂ pellet, U₃O₈, AZB as a pore former and ACROWAX as a lubricant were added as much as 12, 0.3 and 0.2wt%, respectively.

Table I. Characteristics of UO₂ powder

Properties		Value	
O/U ratio		2.046	
Particle Size		<400μm 100%	
Specific Surface Area (m ² /g)		2.34	
Apparent Density (g/cm ³)		1.1	
Moisture Content (ppm)		1200	
Impurity	Value (ppm)	Impurity	Value (ppm)
Al	0.8	Cr	1.3
B	0.2	Cu	<10
Bi	0.3	Fe	<20
Ca	<5	In	0.8
Cd	0.06	Mg	2.3
C	32	Mn	0.2
Cl	2	Mo	0.3
F	7	Ni	1.0
N	25	Pb	<5
Co	<5	Si	<20

Mixing was carried out for 1.5 hrs in “Turbula Mixer”. The mixed powders including U_3O_8 , pore former and lubricant were used as standard powders. When the standard powder was mixed with TiO_2 and $Al_2Si_5O_5(OH)_4$ powders, two-step mixing was performed to enhance the homogeneity.

The standard powder was mixed with additives with the ratio of 9 to 1 for 1.5 hrs in the first mixing, and in the second mixing step, the mixture was diluted with additional standard powder to get a final composition and then mixed again for 1.5 hrs. In the mixed powder, the contents of TiO_2 and $Al_2Si_5O_5(OH)_4$ were in the range of 0.06 to 0.2% by weight.

2.2. Pelletizing

The prepared powders were pressed to have green densities of $5.95 \pm 0.05 \text{ g/cm}^3$. The green pellets were sintered in a tube furnace at 1740°C for 4 hrs. These sintering conditions were the same as those of commercial plant. The furnace was heated at the rate of $5^\circ\text{C}/\text{min}$ and held at 700°C for 1 h to burn the lubricant out. Pure H_2 gas was blown to keep the interior of the furnace in a reduced atmosphere. The flowing rate of H_2 gas was 20 ml/min.

2.3. Annealing

After sintering, all the sintered pellets were annealed at 1700°C up to 48 hrs. Annealing process was performed at the same condition as the sintering process except temperature and time.

2.4. Measuring properties

Sintered density and open porosity were measured using immersion method. In all cases the densities were reported as a percentage of the theoretical density of UO_2 (10.96 g/cm^3). Pellets were sectioned longitudinally and polished to observe microstructure. For measuring grain size, thermal etching was performed at 1250°C for 1.5 hrs. Grain size was determined by a linear intercept method.

3. RESULTS AND DISCUSSION

The UO_2 pellets containing TiO_2 or $Al_2Si_5O_5(OH)_4$ showed lower density than the standard pellet as shown in Figure 1. The density tended to slightly decrease with additive content and the effect of $Al_2Si_5O_5(OH)_4$ was greater than that of TiO_2 at the same amount.

Both of these additives had an influence on reducing open porosity of UO_2 pellet (Figure 2). A large amount of open porosity was decreased by doping additives but there was no significant difference in the amount of open porosity with additive content and types.

The grain size increased with the addition of additive as shown in Figure 3. Apparently, substantial increases in grain size can be obtained with the addition of additives. TiO_2 was more effective to increase grain than $Al_2Si_5O_5(OH)_4$. The grain was coarsened up to $48 \mu\text{m}$ when 0.2 wt % TiO_2 was added while $Al_2Si_5O_5(OH)_4$ doped pellet increases its grain only to $20 \mu\text{m}$ at the same amount.

It is widely known that liquid sintering is the main cause of grain growth of TiO_2 and Al-Si compound doped pellets. From the grain morphology it appears that a liquid phase was

present during sintering(Figure 4). It is correspondent with the phase diagram of Ti-O-U in which the eutectic phase begins to appear at the temperature of 1645°C.

The formation of eutectic phase in Al-Si-U-O system commences at the similar temperature as that of Ti-O-U system. As all the test specimens were sintered at 1740°C, temperature is high enough to form liquid phase in both UO₂ pellets including TiO₂ and Al₂Si₅O₅(OH)₄. It is evident that uranium ions can increase their mobility in the liquid phase.

The enhanced diffusion rate of uranium ion accelerates sintering process resulting in the coarsening of grain. In the case of TiO₂, charge compensation upon the addition of Ti²⁺ to UO₂ matrix can occur by creating the uranium vacancies. Since diffusion of uranium ions is the rate controlling step in the process of UO₂ sintering, sinterability of the matrix can be increased by forming these uranium vacancies. The difference of grain size between TiO₂ and Al₂Si₅O₅(OH)₄ doped UO₂ pellet shown in Figure 3. can be explained by the increased uranium vacancies.

The enhanced uranium ion diffusion rate also affects the pore morphology in the matrix as shown in Figure 5. The standard UO₂ pellet has pores with irregular shape while pores of pellet doped with TiO₂ are round. The pore size of Al₂Si₅O₅(OH)₄ doped pellet are larger than those of the standard pellet and had a slightly round shape, but the degree of roundness is not completed.

Pores change their shape in order to reduce free energy. The free energy of a substance is determined by the ratio of surface area to volume and spherical shape is the most stable morphology since its ratio is lower than any other shapes. Therefore, a shape of pore would be transformed to round one if there is a sufficient driving force. The addition of TiO₂ may give enough driving force for changing of pore from irregular to round shape ascribing to the enhanced diffusion rate resulting from the formation of liquid phase and uranium vacancies. On the contrary, UO₂ pellet containing Al₂Si₅O₅(OH)₄ has oblong shaped pores and their size is small compared with those of TiO₂ doped UO₂ pellet.

Figure 6 shows the effect of additives on the pore size distribution of pellet. The pore size shown in Figure 6 represents the average values of certain range, i.e., >1, 2~5, 5~10, and <10 μm. The addition of TiO₂ and Al₂Si₅O₅(OH)₄ reduce the amount of small pores with diameter under 1 μm and increase large pores with diameter over 10 μm. Both additives show a similar trend but the fraction of pore over 10 μm is greater in TiO₂ doped pellet. It is thought that these large and spherical shaped pores led to swelling rather than densification after annealing for 48 hrs. while the standard pellet and Al₂Si₅O₅(OH)₄ doped UO₂ pellet were densified(Figure 7).

Densification process that is a typical phenomenon for pellet with pore if sufficient thermal energy is provided occurs by elimination of pores. Accordingly, the amount of open porosity as well as the size and morphology of pore existing in the matrix are major factors in determining the degree of densification. Grain size of pellet is also important because it affects the diffusion rate of pore.

In comparison with small pore with irregular shape, large pore with spherical one is difficult to move and hard to dissolve out. Instead of being removed, they tend to grow by consuming neighboring small pores. This is confirmed by Figure 8 that shows the difference of pore size distribution of 0.2% TiO₂ doped UO₂ pellet before and after annealing for 48 hrs. It can be clearly seen that pores having the size greater than 10 μm are definitely increased by annealing while the amount of pore with diameter less than 10 μm is decreased. The additive

content seems no profound effect on density change after annealing in case of TiO_2 is added. On the other hand, there was an inverse linear relationship between additive content and density change in the UO_2 pellet containing $\text{Al}_2\text{Si}_5\text{O}_5(\text{OH})_4$.

4. CONCLUSIONS

The microstructural changes of TiO_2 and $\text{Al}_2\text{Si}_5\text{O}_5(\text{OH})_4$ doped UO_2 pellets have been examined. These two additives are known to increase grain size of pellet by forming liquid phase. The typical features of liquid phase sintering can be found in both test specimens.

The sintered density and open porosity decrease by the addition of additive. TiO_2 is more effective for grain growth than $\text{Al}_2\text{Si}_5\text{O}_5(\text{OH})_4$ and the largest grain size was $48\ \mu\text{m}$ when 0.2 wt% TiO_2 was added. These two additives also change the morphology of pore from irregular to spherical shapes.

The amount of pores with diameter greater than $10\ \mu\text{m}$ increases while that of small pores less than $1\ \mu\text{m}$ is significantly reduced by the additive. Pore size and morphology are somewhat different between TiO_2 and $\text{Al}_2\text{Si}_5\text{O}_5(\text{OH})_4$ doped UO_2 pellets and the difference of temperature at which liquid phase begin to emerge is believed to be the main reason of difference in pore size and morphology.

TiO_2 doped UO_2 pellets have a sufficient mobility for grain growth and round pore because its liquid phase begins to appear at the temperature below 100°C from sintering temperature. The density decrease shown in TiO_2 doped UO_2 pellet after annealing for 48 hrs is attributed to these microstructural characteristics.

It can be found that fraction of pores with diameter over $10\ \mu\text{m}$ increase while that of small pores decreases. There was no tangible difference in density change depending on the amount of additives.

REFERENCES

- [1] W. CHUBB AND A.C. HOTT, "The influence of fuel microstructure on in-pile densification," *Nucl. Technol.*, **26**, 486–495 (1975).
- [2] H. ASSMANN, W. DOERR, G. GRADEL AND M. PEECHS, "Doping UO_2 with Niobia-beneficial or not," *J. Nucl. Mater.*, **98**, 216–218 (1981).
- [3] P.T. SAWBRIDGE, C. BAKER AND R.M. CORNELL, "The irradiation performance of Magnesia-doped UO_2 fuel," *J. Nucl. Mater.*, **95**, 119–128 (1980)
- [4] J.B. AINSCOUGH, F. RIGBY AND S.C. OSBORN, "The effect of titania on grain growth and densification on sintered UO_2 ," *J. Nucl. Mater.*, **52**, 191–202 (1974).
- [5] K.W. LAY, "Grain growth in $\text{UO}_2\text{-Al}_2\text{O}_3$ in the presence of a liquid phase," *J. Am. Ceram. Soc.*, **51**, 373–376 (1968).
- [6] G. MAIER, H. ASSMANN, "Resinter testing in relation to in-pile densification," *J. Nucl. Mater.*, **153**, 213–220 (1988).

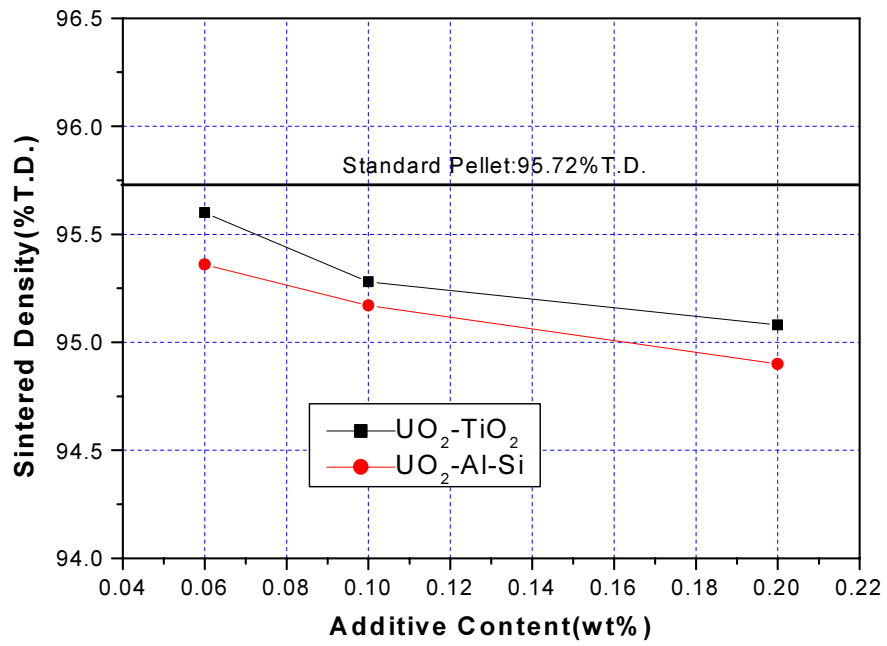


FIG. 1. Variation of sintered density due to additives.

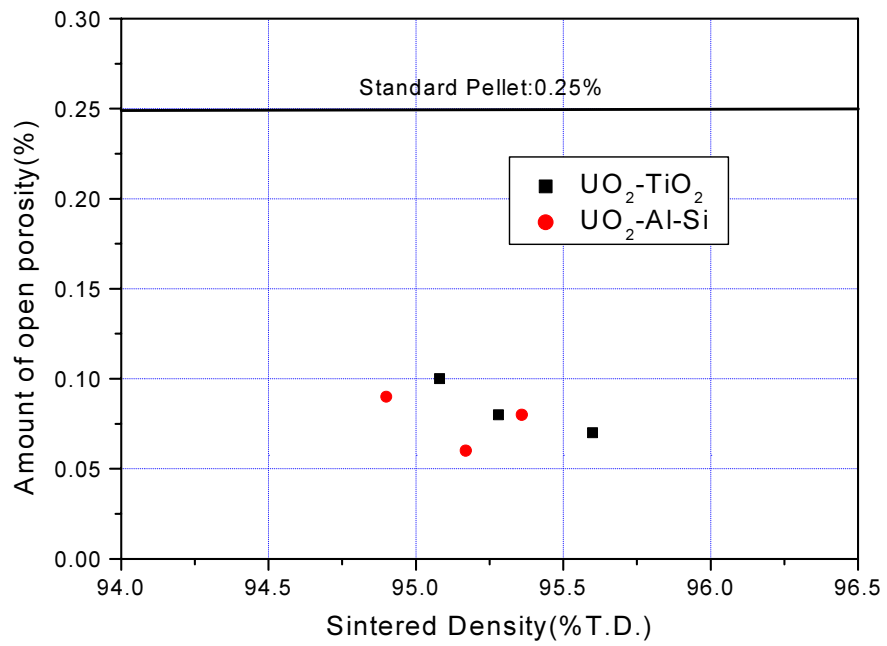


FIG. 2. Variation of open porosity due to additives.

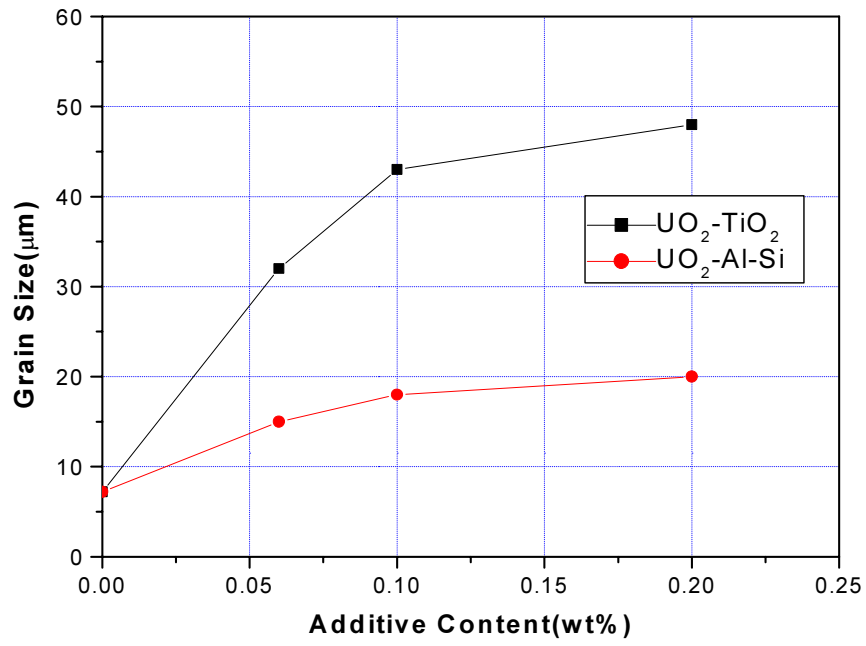
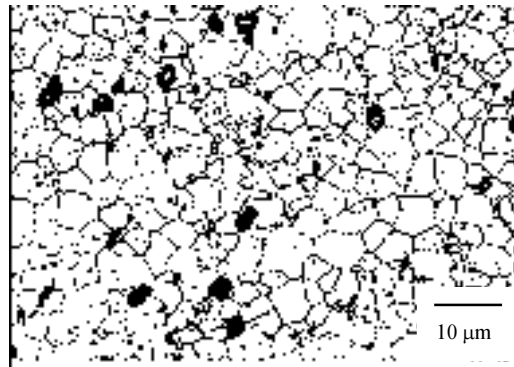
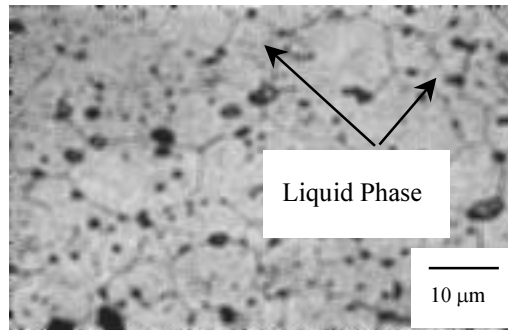


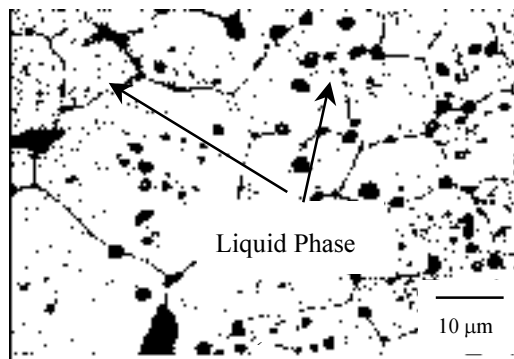
FIG. 3. Variation of grain size due to additives.



(a)



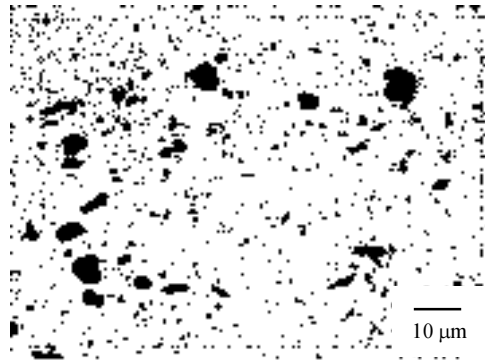
(b)



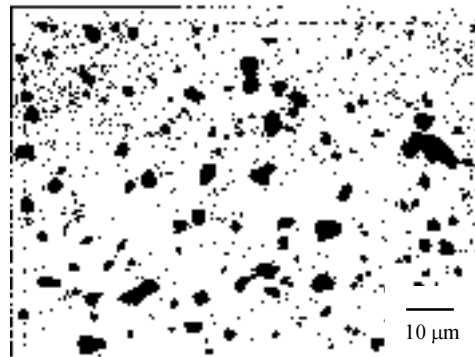
(c)

FIG. 4. Metallography showing grain growth due to additives.

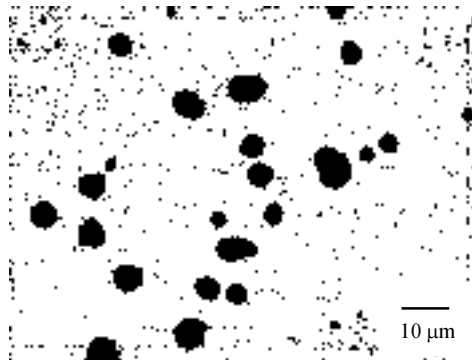
(a) Standard pellet (b) $Al_2Si_2O_5(OH)_4$ (c) TiO_2



(a)



(b)



(c)

FIG. 5. Variation of pore morphology due to additives.

(a) Standard pellet (b) $Al_2Si_2O_5(OH)_4$ (c) TiO_2

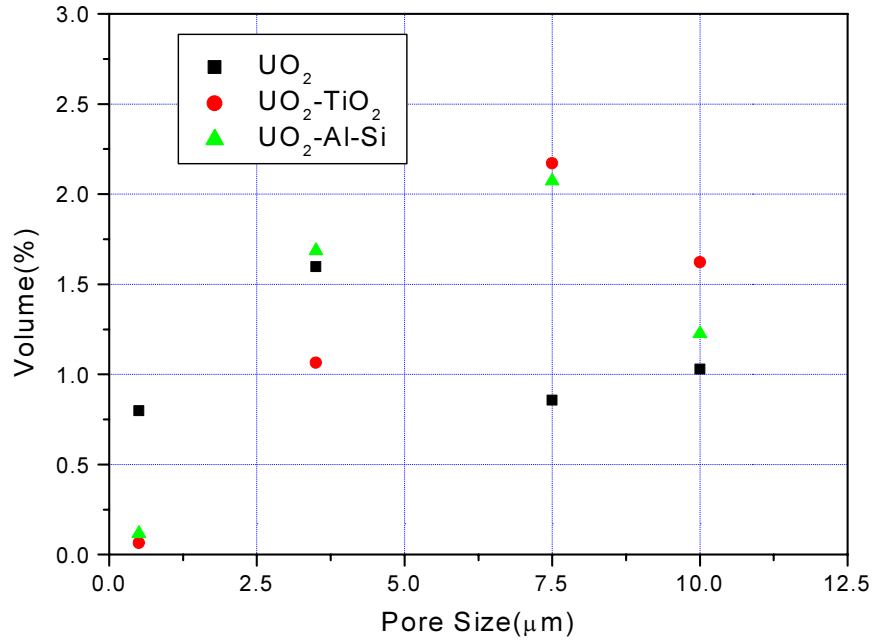


FIG. 6. Variation of pore size distribution.

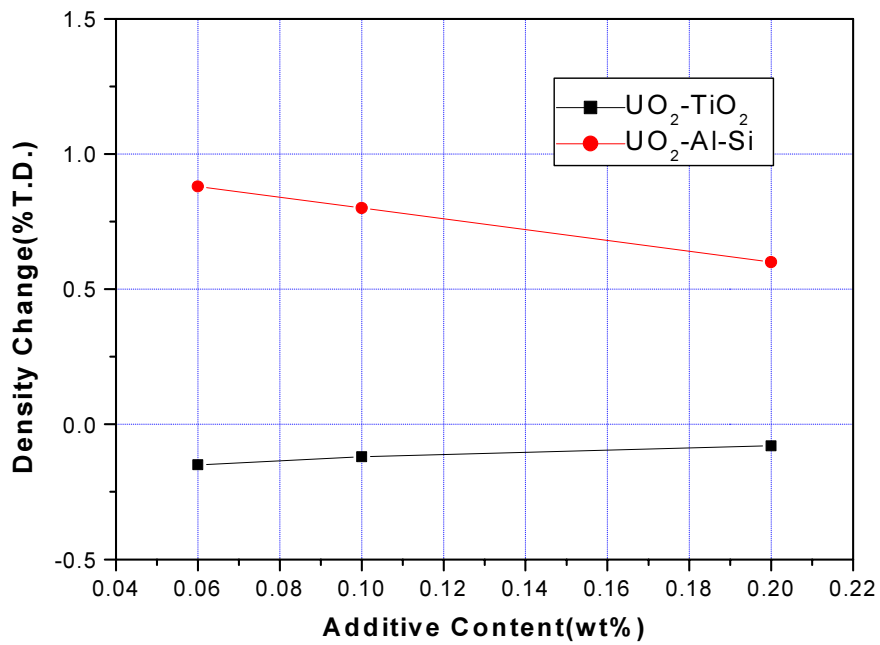


FIG. 7. Density change of pellet after being annealed for 48 hrs.

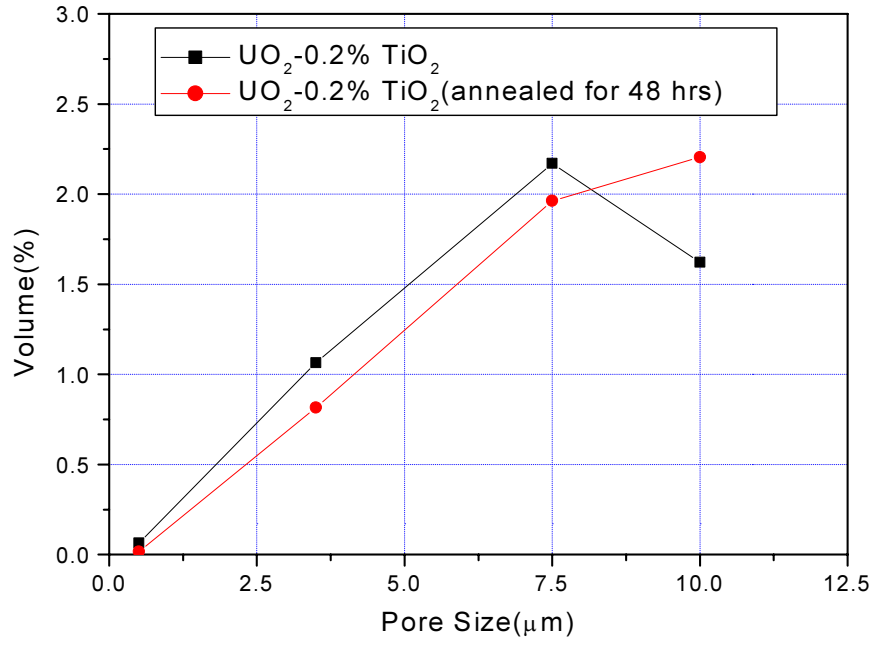


FIG. 8. Pore size distribution of TiO₂ doped UO₂ pellet.

EFFECT OF SINTERING GAS ON THE GRAIN SIZE OF UO₂ PELLETS DERIVED FROM DIFFERENT POWDER ROUTES*

Keon Sik Kim, Kun Woo Song**, Jae Ho Yang, Youn Ho Jung
Advanced LWR Fuel Development,
Korea Atomic Energy Research Institute,
Daejeon, Republic of Korea

Abstract

UO₂ pellets were sintered at 1600-1700°C using three different UO₂ powders - the ADU, AUC and DC routes. The oxygen partial pressure of sintering gas was controlled using the method of adding CO₂ gas to H₂ gas, and the CO₂-to-H₂ ratio ranged from 0.1 to 0.4. The grain size of UO₂ pellets is nearly independent of the CO₂-to-H₂ ratio when the AUC- or DC-UO₂ powder is used, but it is increased up to 25 μm for the ADU-UO₂ powder if the CO₂-to-H₂ ratio is higher than 0.25. Impurity analysis of the three UO₂ powders reveals that phosphorus is high in the ADU-UO₂ powder but not in the other powders. Phosphorus was added to the AUC-UO₂ powder, and then UO₂ pellets were sintered in the mixed gas of CO₂ and H₂ (CO₂/H₂=0.25). It has been found that the grain size of about 25 μm is achieved with a phosphorus content as small as 30 ppm. So a large-grained UO₂ pellet can be produced if the P-doped UO₂ powder is sintered in the slightly reducing gas.

1. INTRODUCTION

Uranium dioxide (UO₂) fuel pellets which are widely used in light water reactors are manufactured by a conventional powder processing method [1]; UO₂ powder is pressed into green pellets and then sintered at 1700-1780°C in hydrogen-containing gas. The UO₂ pellet properties — density, pore structure, and grain size — greatly influence the in-reactor performance of the UO₂ pellet. Especially, the amount of fission gas released during irradiation decreases as the grain size of UO₂ pellets increases [2], and thus large-grained UO₂ pellets are desirable at high burnup.

The fabrication of large-grained UO₂ pellets has been investigated extensively, so that many fabrication methods have been developed. The most prevailing method is simply to add sintering agents to UO₂ powder. Many sintering agents are known such as niobia[3,4], titania[5], chromia[6], and magnesia[7]. It is also known that the grain size of UO₂ pellets can be increased, without sintering agents, by using the UO₂ powder with a high sintering activity [8]. Wood and Perkins [9] have reported that the addition of UO₂ seeds to UO₂ powder enhances grain growth, and Song et al. [10] have found that the addition of U₃O₈ seeds to UO₂ powder increases the grain size.

In addition, it has been reported that the grain size of UO₂ pellets can be increased by a high oxygen partial pressure in the sintering gas [11]. This technique is based on the fact that an oxidizing gas provides excess oxygen for UO₂ and the uranium diffusion is accelerated in this hyperstoichiometric state. According to Assmann et al [11], the UO₂ pellet that was sintered at 1300°C in CO₂ gas using the UO₂ powder derived from the AUC (Ammonium Uranyl Carbonate) route, has a bimodal grain structure; a mixture of large grains and small grains. The bimodal grain structure is not formed when the UO₂ powder derived from the ADU (Ammonium Diuranate) or DC (Dry Conversion) route is used [12]. However, the grain size of UO₂ pellets is, generally, not different from each other between the powder routes when each UO₂ powder is sintered in a reducing gas. These results suggest that UO₂ powder properties, which are dependent on the powder routes, might affect the grain size of UO₂ pellets if UO₂ powder is sintered in non-reducing gas.

The sintering gas can be classified into three types depending on its oxygen partial pressure; reducing, slightly reducing, and oxidizing. UO₂ pellets are usually fabricated in a reducing gas, which is a

* This work has been carried out under the nuclear R&D program supported by the Ministry of Science and Technology in Korea.

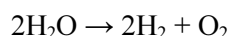
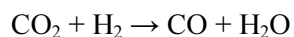
** corresponding author, e-mail: kwsong@kaeri.re.kr telephone: +82-42-868-2579 fax: +82-42-861-7340

hydrogen gas containing additionally H₂O or CO₂ gas up to about 3 vol%. But a slightly reducing gas is a gas mixture made by adding the larger amount of H₂O or CO₂ to H₂. The sintering of UO₂ pellets under this slightly reducing gas has not been much investigated. This paper deals with the sintering of UO₂ pellets in a slightly reducing gas and especially describes the effect of powder routes on the grain size.

2. EXPERIMENTAL PROCEDURES

The UO₂ powders used in this work were produced through three different powder routes; AUC, DC and ADU. The former two powders were made by KNFC (Kepco Nuclear Fuel Co.), and the last powder was purchased from Canada. The UO₂ powders were characterized in impurity, O/U ratio, apparent density, BET surface area, and shape. Zinc stearate, a lubricant, was added to the three UO₂ powders. The UO₂ powder from the ADU or DC route was granulated before pressing into green pellets, but the UO₂ powder from the AUC route was directly pressed into green pellets because it is has a good flow ability. The pressing pressures were fixed to be 310 MPa.

The green pellets were heated up to 1600°C or 1700°C and then held for 2h, followed by cooling. The sintering gases were mixtures of H₂ and CO₂ gases, and the ratios of CO₂ to H₂ gas were controlled to be 0.1, 0.15, 0.25, and 0.4, respectively. In parallel, the green pellets were sintered in pure hydrogen gas. The ratio of CO₂ to H₂ gas was fixed throughout the whole sintering (heating, holding and cooling) period. The oxygen partial pressure of the mixed H₂ and CO₂ gas is determined by the thermodynamic equilibrium of the following reactions:



The oxygen partial pressure was calculated with the aid of the SOLGASMIX program [13]. Figure 1 shows the relation between oxygen partial pressure and temperature for the mixed CO₂ and H₂ gases. The oxygen partial pressure tends to increase with the ratio of CO₂ to H₂.

The density of sintered pellets was measured by the water immersion method (Archimedes method). The internal structure of sintered pellets was examined by microscopy, and the grain size was

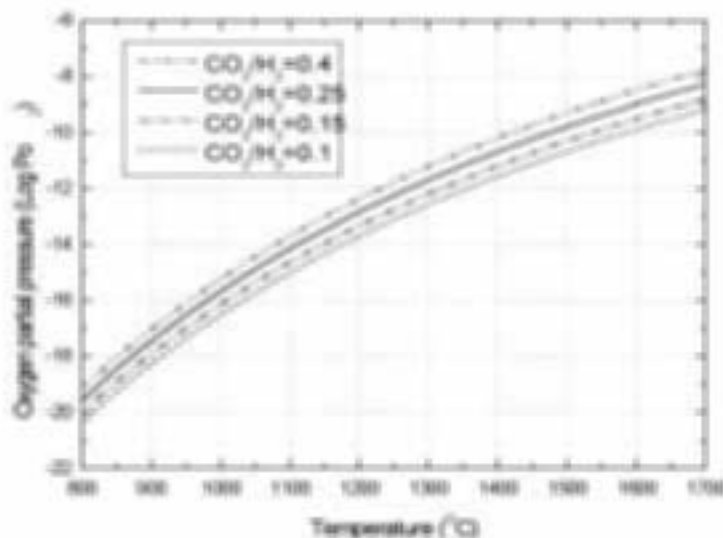


FIG. 1. Oxygen partial pressures as a function of temperature for various sintering gases.

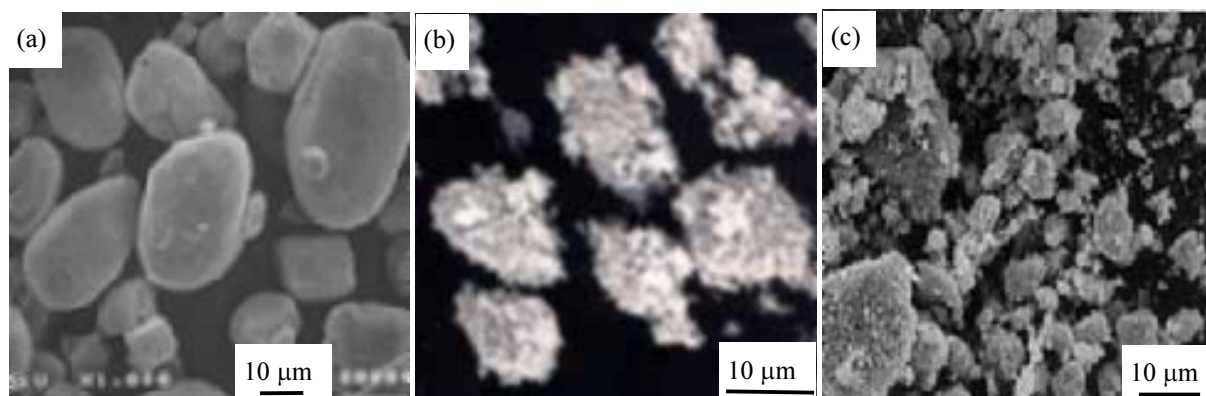


FIG. 2. SEM micrographs showing powder morphology. (a)AUC route, (b)DC route, (c)ADU route.

measured by the linear intercept method. In addition to the pellet fabrication, the shrinkage of green pellets during sintering was analyzed by dilatometry.

3. RESULTS AND DISCUSSION

The SEM micrographs are shown in Fig. 2 for the three kinds of UO_2 powders. The UO_2 powder derived from the AUC process is characterized as a round shape with no agglomeration. But the UO_2 powder derived from the ADU or DC process is softly agglomerated, so the size appears larger than the real size. The physical properties of the three UO_2 powders are listed in Table I. The oxygen to uranium ratio and BET surface area are different depending on the powder routes. The impurity content is shown for the three UO_2 powders in Table II. Impurities are also a little dependent on the powder routes. However, the physical properties and impurities satisfy with the technical specification, in spite of the slight differences in properties between the powder routes.

Table I. Properties of the three UO_2 powders

Properties	DC	AUC	ADU
O/U ratio	2.03	2.10	2.15
Moisture Content (ppm)	750	1540	1030
Specific Surface Area($m^2/g-UO_2$)	2.29	5.45	2.30
particle size (μm)	4.8	15	2.5
U content (wt%)	87.896	87.446	87.235

Table II. Impurity in the three types of UO_2 powders

Impurity	DC	AUC	ADU
Al	1.2		1.3
C	15	71	33
Cl	3	4	
F	12	68	8
N	24	6	
V	0.21		5.2
P	-	-	22
Na	-	-	7
K	-	-	12

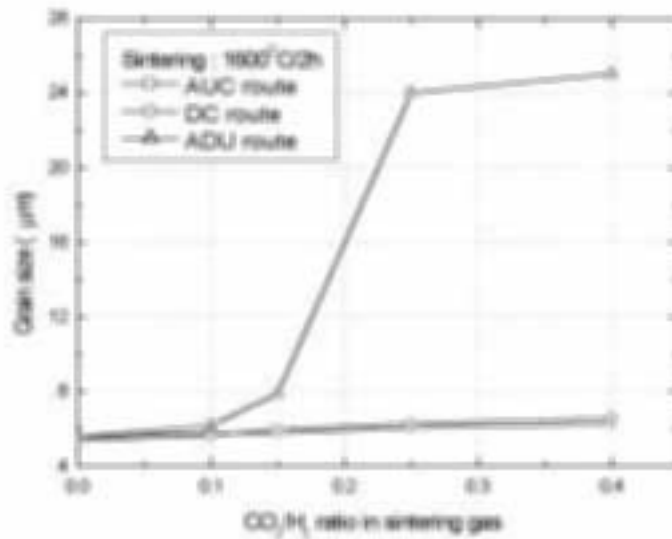


FIG. 3. Dependence of grain size on the CO₂/H₂ ratio for the UO₂ pellets sintered at 1600°C using different powders.

Figure 3 shows the relation between grain size and CO₂-to-H₂ ratio when the three UO₂ powders are sintered for 2 h at 1600°C. Fig. 4 shows the same relation for the 1700°C sintering. The dependency of grain size on the CO₂-to-H₂ ratio seems to be very similar between 1600 and 1700°C. The grain size of UO₂ pellets remains nearly constant over the whole range of gas ratios for both the AUC- and DC-UO₂ powders, but it rises greatly for the ADU-UO₂ powder when the CO₂-to-H₂ ratio is increased from 0.15 to 0.25. The grain size can be increased up to 25 µm at 1600°C and 30 µm at 1700°C. A large grain results from fast grain growth during sintering and thereby means that the uranium diffusion was fast in the sintering of only the UO₂ powder from the ADU. This increase in uranium diffusion might not be associated with the initial O/U ratio of powder since the three powders are sintered in the same gas atmosphere.

Figure 5 shows the microstructure of UO₂ pellets sintered at 1600°C for the CO₂-to-H₂ ratio of 0.25. Figures 5(a), Fig. 5(b), and Fig. 5(c) stand for the AUC route, the DC route and the ADU route, respectively. The UO₂ pellet derived from the ADU route seems to be distinct from the other pellets in

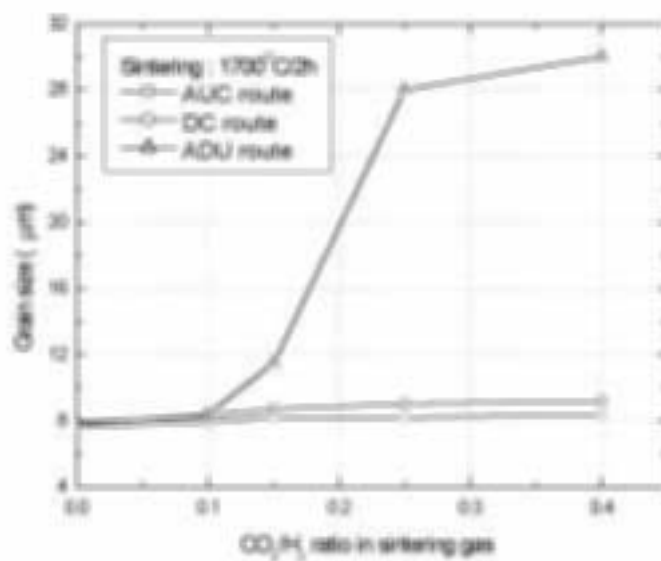


FIG. 4. Dependence of grain size on the CO₂/H₂ ratio for the UO₂ pellets sintered at 1700°C using different powders.

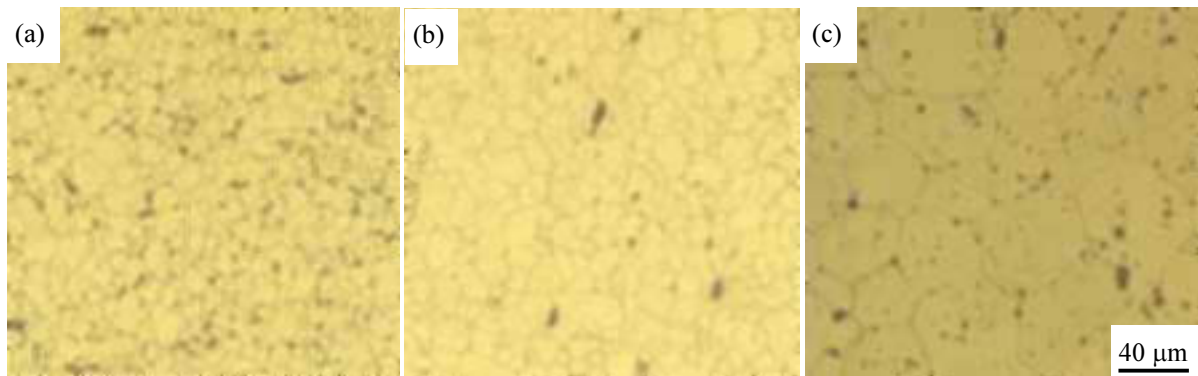


FIG. 5. Microstructures of UO_2 pellets sintered at $1700^\circ C$ in a slightly oxidizing gas $CO_2/H_2=0.25$) using various UO_2 powders. (a)AUC route, (b)DC route, (c)ADU route

both grain size and pore shape: The grain size is much larger and pore shape is more spherical in Fig. 5(c) than in Figs. 5(a) and 5(b). These differences in the microstructure support that uranium diffusion is faster in the sintering of UO_2 powder derived from the ADU route.

Fig. 6 shows the effect of sintering gases on the microstructure of UO_2 pellets that are sintered at $1600^\circ C$ for 2 h using the ADU- UO_2 powder. We can easily see that as the CO_2 -to- H_2 ratio increases the fine pores disappear and thus the number of pores decreases. In addition, the grain size is dramatically increased by the change in the gas ratio from 0.15 to 0.25.

The above results strongly suggest that a favorable condition for the large-grained UO_2 pellet is to sinter ADU- UO_2 powder in the sintering gases in which the CO_2 -to- H_2 ratio is higher than 0.25. In

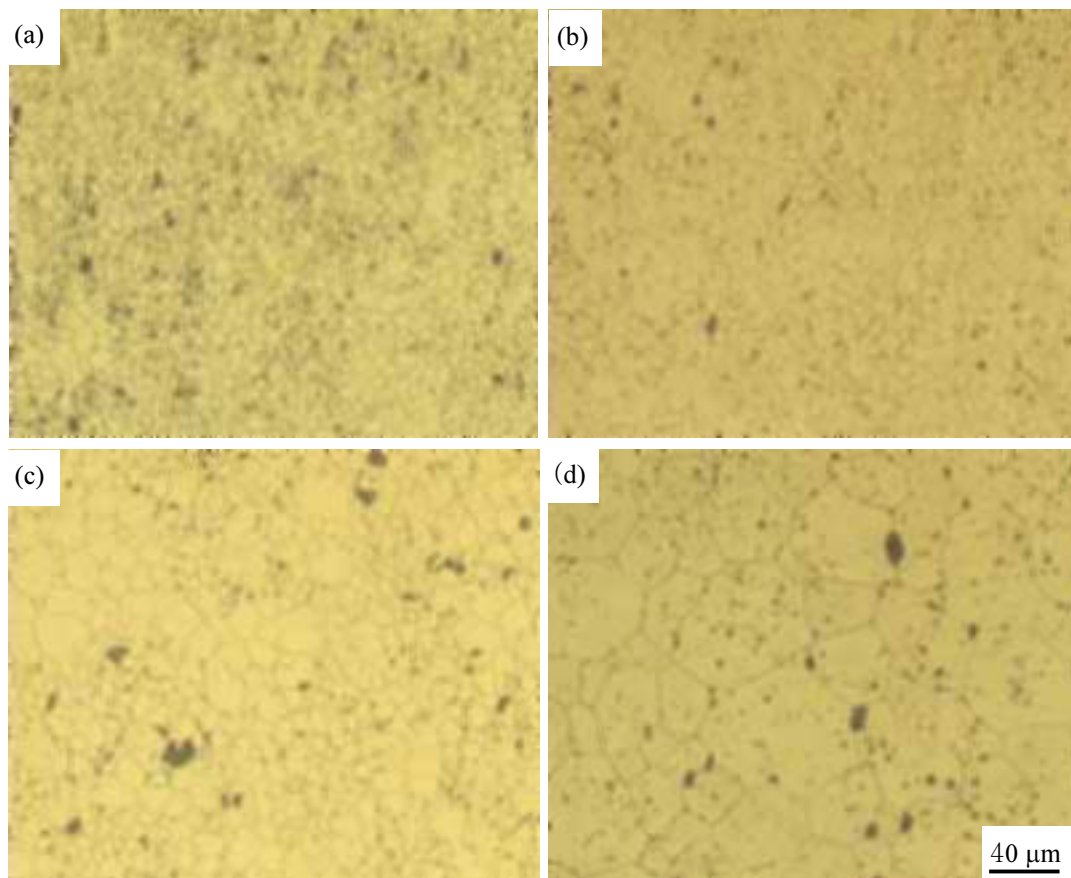


FIG. 6. Microstructures of UO_2 pellets sintered at $1600^\circ C$ in various gases using the ADU- UO_2 powder. (a) pure H_2 gas, (b) $CO_2/H_2 = 0.1$, (c) $CO_2/H_2 = 0.15$, (d) $CO_2/H_2 = 0.25$

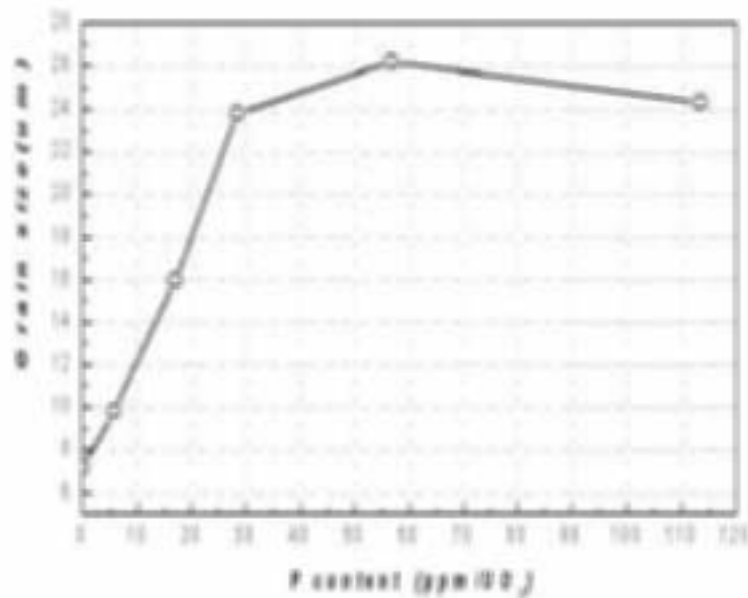


FIG. 7. Relation between grain size and P content for the P-doped UO_2 pellets sintered at $1700^\circ C$ in a slightly oxidizing gas ($CO_2/H_2=0.25$) using the AUC- UO_2 powder.

In addition, the higher oxygen potential might increase the uranium diffusion in the sintering of ADU- UO_2 powder but not in the sintering of AUC- UO_2 or DC- UO_2 powder. This peculiar effect of the oxygen potential might be associated with the difference in impurity between the powder routes. Table II indicates that there are some impurity differences, and the ADU- UO_2 powder has some phosphorus content but the other powders not. Thus, we pay attention to the phosphorus content.

We added phosphorus oxide (P_2O_5) to the AUC- UO_2 powder and then fabricated UO_2 pellets in the

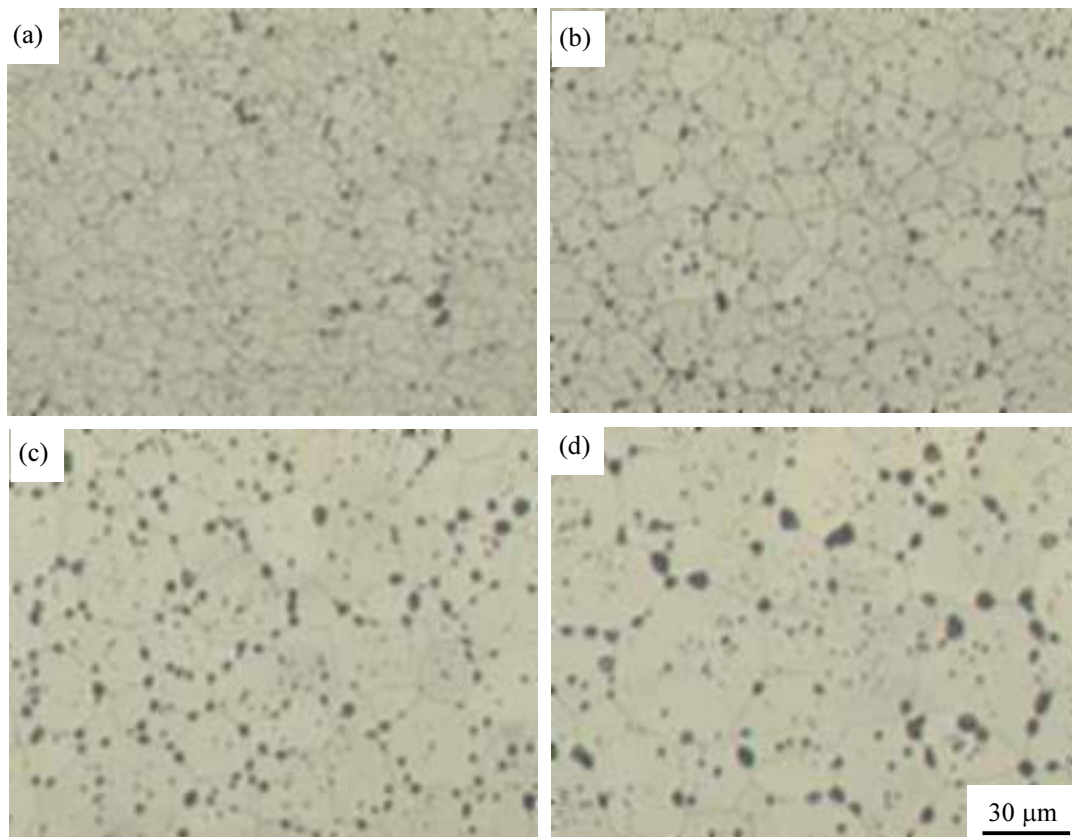


FIG. 8. Microstructures of P-doped UO_2 pellets sintered at $1700^\circ C$ in a slightly oxidizing gas ($CO_2/H_2 = 0.25$) using the AUC- UO_2 powder. (a)no doping, (b)6 ppm, (c)17ppm, (d)28 ppm

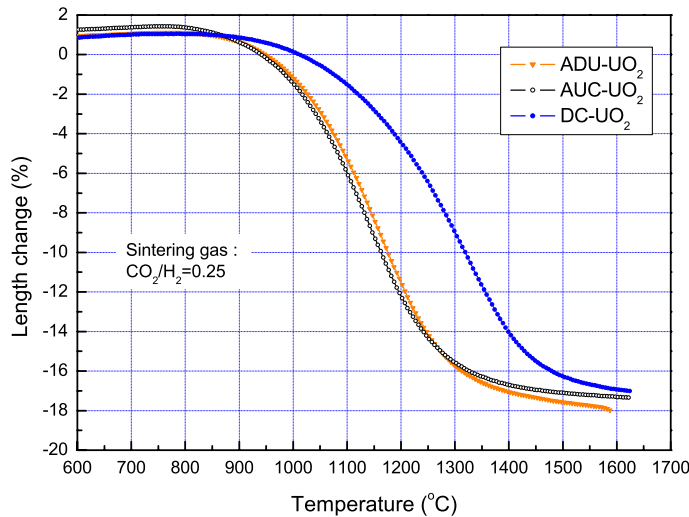


FIG. 9. Relation between shrinkage and temperature for the three UO_2 powders.

same way. We found that the grain size of UO_2 pellet was greatly increased even by the impurity-level of phosphorous. This effect was found in slightly reducing gas but not in hydrogen gas. Fig. 7 shows the relationship between grain size and P content for the UO_2 pellets which were sintered at $1700\text{ }^\circ\text{C}$ in the gas mixture of CO_2 and H_2 (CO_2/H_2 ratio=0.25). The grain size increases greatly and linearly with the P content in the range of about 30 ppm of phosphorus, and then the grain size remains almost invariant with P content up to about 110 ppm. The maximum grain size is between 24 and 26 μm .

The microstructure of P-doped UO_2 pellets is shown in Fig. 8. We can see that the grain size increases as the P content increases. In addition, it has been found that pore size increases and the number of pores decreases.

The shrinkage (densification) of green pellets on heating was analyzed by dilatometry, and the results are shown in Fig. 9. In the mixed gas of CO_2 and H_2 (CO_2 -to- H_2 ratio = 0.25), the final densification is more or less similar for the three UO_2 powders, but the ADU- and AUC- UO_2 powder start to shrink at lower temperature and achieve more shrinkage at temperatures up to about $1400\text{ }^\circ\text{C}$ than the DC- UO_2 powder. We also have found that the shrinkage curves are very similar for the AUC- UO_2 powder with and without phosphorus, suggesting that phosphorus negligibly affects the shrinkage during the heating stage of the whole sintering cycle.

4. CONCLUSION

The UO_2 powders derived from different powder routes - AUC, ADU, and DC - have different physical and chemical properties. The differences in powder properties do not lead to a difference in the grain size of UO_2 pellets when the three UO_2 powders are sintered at $1600\text{--}1700\text{ }^\circ\text{C}$ in a reducing gas. In the mixed gas of CO_2 and H_2 the grain size of UO_2 pellets is not affected much for the AUC- UO_2 and DC- UO_2 powders by the CO_2 -to- H_2 ratio, but the grain size is exceptionally increased up to 25 μm for the ADU- UO_2 powder when the CO_2 -to- H_2 ratio is higher than 0.25. It is found that phosphorus is present as an impurity in the ADU- UO_2 powder but not in the other powders.

Phosphorus-doped UO_2 pellets are sintered in the mixed gas of CO_2 and H_2 ($CO_2/H_2=0.25$) using the AUC- UO_2 powder. The grain size increases linearly up to about 25 μm with the P content in the range of about 30 ppm and then remains nearly constant with any further P content. The effect of phosphorus on the grain size is negligible in hydrogen sintering. Therefore, a large-grained UO_2 pellet can be produced by a sintering technique that involves both P-doped UO_2 powder and a slightly reducing gas.

REFERENCES

- [1] H. ASSMANN and H. BAIRIOT, "Process and Product Control of Oxide Powder and Pellets for Reactor Fuel Application", in Guidebook on Quality Control of Water Reactor Fuel, Tech. Report Series No. 221, IAEA, Vienna (1983) 149-180.
- [2] J.A. TURNBULL, J. Nucl. Mater., "The effect of grain size on the swelling and gas release properties of UO_2 during irradiation", **50** (1974) 62.
- [3] Y. HARADA, J. Nucl. Mater., "Sintering behaviour of niobia-doped large grain UO_2 pellet", **238** (1997) 237.
- [4] K.W. SONG, K.S. KIM, K.W. KANG, *et al.*, J. Korean Nucl. Soc. **31** (1999) 335.
- [5] J.B. AINSCOUGH, F. RIGBY, S.C. OSBORN, J. Nucl. Mat., "The effect of titania on grain growth and densification of sintered UO_2 ", **52** (1974) 191.
- [6] L. BOURGEOIS, PH. DEHAUDT, C. LEMAIGNAM, *et al.*, "Factors governing microstructure development of Cr_2O_3 -doped UO_2 during sintering", J. Nucl. Mater. **297** (2001) 313.
- [7] B.E. INGLEBY, K. HAND, in: Fission-Product Behavior in Ceramic Oxide Fuel, Advances in Ceramics vol. 17, I.J. Hastings (eds), Amer. Ceramic Soc., 1986, p. 57.
- [8] Y. HARADA and S. DOI, J. Nucl. Sci. Technol., **35** (1998) 411.
- [9] G.A. WOOD and C.P. PERKINS, "Grain size distribution in seeded large grain size UO_2 ", Advances in Pellet Technology for Improved Performance at High Burnup, IAEA-TECDOC-1036, IAEA, Vienna, (1998) 49.
- [10] K.W. SONG, K.S. KIM, K.W. KANG, and Y.H. JUNG, "Grain size control of UO_2 pellets by adding heat-treated U_3O_8 particles to UO_2 powder", J. Nucl. Mater. **317** (2003) 204.
- [11] H. ASSMANN, W. DOERR, M. PEEHS, "Control of UO_2 microstructure by oxidative sintering", J. Nucl. Mater., **140** (1986) 1.
- [12] K.W. SONG, D.S. SOHN, W.K. CHOO, "Effects of sintering processes on the duplex grain structure of UO_2 ", J. Nucl. Mater., **200** (1993) 41.
- [13] Outokump Research, HSC Chemistry for Windows, 1994.

SINTERED PELLETS OBTAINING FOR ADVANCED FUEL MANUFACTURING

D. OHAI, M. ROTH
Institute for Nuclear Research,
Pitesti, Romania

Abstract:

The paper presents the Romanian experience in the UO_2 sintered pellets manufacturing for large grain size. The experimental results obtained in (U,Th) O_2 sintered pellets manufacturing are presented, also. Two experimental programs has been performed at the Institute for Nuclear Research from Pitesti-Romania having the objectives to obtain UO_2 sintered pellets with large grain size and (U,Th) O_2 sintered pellets also. The large grain size UO_2 sintered pellets were obtained by dopants addition (up to 1% Nb_2O_5 , Cr_2O_3 and TiO_2) in UO_2 sinterable powder. The (U,Th) O_2 sintered pellets were obtained from blending of UO_2 and ThO_2 sinterable powders. All the sintered pellets were characterized by sintered density and microstructure establishing the correlations between technological parameters and sintered pellets characteristics. Both types of sintered pellets (UO_2 and (U,Th) O_2) were mechanical tested using the radial compression method. The correlations between strength and dopant nature, dopant concentration and temperature were established. Also the correlation between strength and uranium concentration was put into the evidence. The macro- and microscopical aspects of fractured pellets are presented.

1. INTRODUCTION

A main concern all over the world is to increase the fuel burn up for reducing nuclear electricity costs and the high active level waste (spent fuel) amount. Very good results were obtained in the clarification of the factors affecting the burn-up increase and the theoretical and practical (experimental results) solutions proposed to diminish adverse effects.

Table 1 presents few factors affecting the burn-up increase and the solutions.

Table 1. Factors affecting burn up increase

Factor	Solutions
increase of internal temperature	reducing of elements diameter [1] pellets with central hall [2] duplex pellets [3] graphite discs between pellets [4], [5]
increase of internal pressure	large grain size pellets [6], [7], [8] controlled closed porosity
pellet-cladding mechanical interaction (PCMI)	pellet length/diameter < 1 [9] pellet geometry modifying [10]
stress corrosion cracking	Zircaloy-4 sheath covered with pure Zr [11]
oxidation and hydriding of the Zircaloy-4 sheath	new microstructure for Zircaloy-4 [12] new Zr alloys (ZIRLO-Nb1%, Sn1% and Fe 0.1%) [13]

A way to increase the fuel burn-up is to diminish the internal pressure of the elements by adequate UO_2 fuel pellet structure (large grains or controlled closed porosity). In the large grain size UO_2 pellets, fission gas release rate decreases and the internal pressure of elements increases slowly. Similarly, in the UO_2 sintered pellet with controlled closed porosity the fission gas accommodation is better and the elements internal pressure increases slowly.

A way to increase the pellets grain size without increasing sintering temperature and time is the addition of small quantities ($< 1\%$ wt M/U) of sintering additives (aliovalent metal or rare earth oxide).

By the addition of certain dopant in the UO_2 powder (TiO_2 , Nb_2O_5 , Cr_2O_3 , CaO , V_2O_5 .) the grain size, porosity and the mean free diffusion path are increased, whereas the grain boundary area is reduced [14], [15], [16].

For the production of niobia doped UO_2 fuel the “direct pelletizing process” which has been developed in relation with the AUC powder technology can be applied without any change beside the admixture of niobia to the UO_2 powder.

In a master mix UO_2 and Nb_2O_5 powders are added and homogenized. The blended powder is directly pressed without the addition of a lubricant. The green pellets are sintered in the sintering furnace. Under the same sintering conditions, the density of the pellets can be adjusted by U_3O_8 addition, UO_2 - Nb_2O_5 pellets with densities between 9.9 – 10.75 g/cm^3 and grain size between 2 – $50 \mu\text{m}$ being obtained [17].

Other methods to obtain uranium dioxide pellets with large grain sizes are the followings:

- heating sintered pellet of uranium dioxide at temperatures higher than 1700°C in hydrogen stream containing silicate vapours, resulted from the aluminium silicate decomposition. The grain size values can be increased to more than $50\mu\text{m}$ [18];
- production of sintered uranium dioxide pellets by the addition of sintering agent (10 – $55\text{wt}\%$ MgO and 90 – $45\text{wt}\%$ SiO_2) or precursor thereof in the composition ranging from 0.1 – $0.8\text{wt}\%$ of a sinterable mixture. The resulting mixture is turned into a compact. The sintering process is performed at a temperature where the sintering agent forms a liquid phase to produce a sintered product. The precursor is thermally decomposed below the sintering temperature [19];
- obtaining of sintered UO_2 nuclear fuel pellets, with the average grain size ranging from about 30 to $80\mu\text{m}$ by addition of magnesium aluminosilicate in uranium dioxide powder. The pores volume is ranging between 2 and 10% [20];
- addition of Cr_2O_3 or Al_2O_3 and a of small quantities of SiO_2 into the uranium dioxide powder.

2. EXPERIMENTAL WORKS

2.1. UO_2 sintered pellets with large grain size manufacturing

In the UO_2 non-free flowing powders, manufactured by ADU (P1) and IDR (P2) routes, Nb_2O_5 , Cr_2O_3 and TiO_2 were added, the content of metals being 0.05 – 1% wt M/U. The blends were homogenized in a Y-con master mix. The blended powders were compacted by bilateral pressing at 270MPa . The green pellets were directly sintered in a hydrogen atmosphere (4 hours at 1700°C) in a standard sintering furnace. Supplementary, green pellets doped with Nb_2O_5 were sintered at 1600°C , the rest of parameters being identical.

The green pellets density was determined geometrically. The sintered pellets density was determined by immersion method. The sintered pellets were cut on an axial plan, polished, chemical attacked to distinguish the grain boundaries. The grain size was determined by linear interception Heyn method.

For mechanical testing, 4 lots (10 pellets/lot) of UO_2 sintered pellets with large grain size were manufactured, the Nb_2O_5 concentration in UO_2 powder being in the range 0% up to 0.4%. The UO_2 powder was mixed with Nb_2O_5 , the blend was pre-pressed and resulted compacts grained. The granules mixed with 0.3% Zn stearate were pressed and the green pellets sintered in H_2 atmosphere at 1750°C , 4h.

2.2. (U, Th) O_2 sintered pellets manufacturing

A ThO_2 powder, manufactured by precipitation of Thorium nitrate with oxalic acid, was pre-pressed at 400 MPa. The compacts were granulated and sorted in two graininess: $<150\ \mu\text{m}$ and $150\text{--}250\ \mu\text{m}$. The granules mixed with 0.3% Zn stearate were pressed at 300–500 MPa. The green pellets were pre-sintered at 1200°C and 1300°C , 1h, in H_2 atmosphere, with a dewaxing step at 400°C , 1h. All pre-sintered compacts were impregnated, in a vacuum chamber (10^{-3} torr) with a sub-stoichiometric uranyl nitrate solution (800gU/l), dried, calcined and sintered at 1750°C , 4h, under H_2 atmosphere.

The green and pre-sintered pellets were characterized by density, the sintered pellets by density and uranium content.

For mechanical testing of (U, Th) O_2 sintered pellets, 6 lots (10 pellets/lot) were manufactured with uranium content from 0% to 70%. ThO_2 and UO_2 powders were mixed, the blend was pre-pressed and the resulted compacts grained. The granules mixed with 0.3% Zn stearate were pressed and the green pellets sintered in H_2 atmosphere at 1750°C for 4h.

2.3. Diametral compression testing method

The testing method consists of the diametral compression of a disk specimen (Figure 1) under a biaxial state of stress. The stress is compressive in the direction of the loading axis (y) and tensile in the transverse direction (x). The size of the compressive stress depends on the angle over which the load is distributed, while the tensile stress is maximum always in the centre of the specimen and conducts to the specimen rupture. Reference [20] presents the distribution and the values of the stresses in a disk specimen, tested under a compressive load, the maximum tensile stress (σ_{HC}) being of the following type [21]:

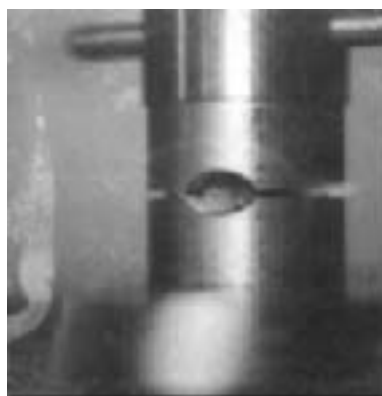


FIG. 1. Testing Device.

$$\sigma_{HC} = \left[1 - 1.15 \left(\frac{b}{D} \right)^2 + 0.22 \left(\frac{b}{D} \right)^3 \right] \sigma_p \quad (1)$$

where: σ_p - the uniform stress along the loading axis ($\sigma_p = 2 \cdot F/\pi \cdot D \cdot H$)
 F - the contact force
 H - specimen height
 D - specimen diameter (=2R)
 b - contact width (=2b')

The dependence between the $\frac{b'}{R}$ ratio $\left(= \frac{1}{2} \left(\frac{b}{D} \right) \right)$ and diametral compressive strength was also reported in reference [21]. If the ratio $\frac{b'}{R}$ is greater than 0.27, the σ_{HC} values are independent from shearing stress near the contact surface. This imposes a ratio greater than 1.2 between the specimen radius (R) and the compression anvil radius (r).

3. RESULTS AND DISCUSSIONS

3.1. UO₂ sintered pellets with large grain size manufacturing

3.1.1. Green pellet characteristics

The powders used in this project were manufactured by two different routes: P1-ADU and P2-IDR. Some characteristics of powders are presented in Table 2.

Table 2. Powders characteristics

Lot	Agglomerates distribution (%)							Bulk density g/cm ³	Pores volume cm ³ /g
	>2	2-0.9	0.9-0.63	0.63-0.315	0.315-0.1	0.1-0.04	<0.04		
Dimension (mm)									
P1	0.2	2	4	11.5	14	16	52.3	1.03	0.13
P2	0	0.1	1	23	42.8	20.8	12.3	1.79	0.066

The green pellets obtained from doped UO₂ powders by bilateral pressing were characterized by geometrical density. For each powder type and dopant concentration, ten pellets were manufactured.

The mean value of green density for each dopant concentration is presented in Table 3.

The green density is strongly dependent on powder type. The difference between green pellets density manufactured from P1 powder (ADU route) and P2 powder (IDR route) is about 0.8 g/cm³.

The Nb₂O₅ addition in the powders does not modify very much the green density but a little tendency to decrease with dopant percentage increasing exists. Cr₂O₃ addition has an influence appreciatively the same like Nb₂O₅, maybe a little more for P1 powder. TiO₂ addition has a pregnant influence on green pellets density comparatively to Nb₂O₅ addition.

Table 3. Green density of doped UO₂ pellets

Dopant concentration	Green density [g/cm ³]					
	P1-Nb	P2-Nb	P1-Cr	P2-Cr	P1-Ti	P2-Ti
0	5.10	5.72	5.10	5.72	5.10	5.72
0.05	5.02	5.73	-	-	-	-
0.1	-	-	4.96	5.69	4.94	5.73
0.15	5.01	5.70	-	-	-	-
0.3	4.90	5.67	4.95	5.71	4.93	5.72
0.5	4.93	5.65	4.94	5.71	4.89	5.68
1	4.93	5.62	4.98	5.64	4.80	5.60

The dopants concentration increasing from zero up to 1% induces green pellets density decrease, especially for P1 powder.

The behaviour of doped powders to pressing is dependent on dopant and powders microstructural and physical properties. The powders, obtained by different routes, have different microstructural and physical properties and different aptitude for pressing. Similarly, the obtaining methods for dopants manufacturing are different.

3.1.2. Sintered pellets density

The variation in density of Nb₂O₅ - doped UO₂ pellets as a function of Nb content is presented in Figure 2

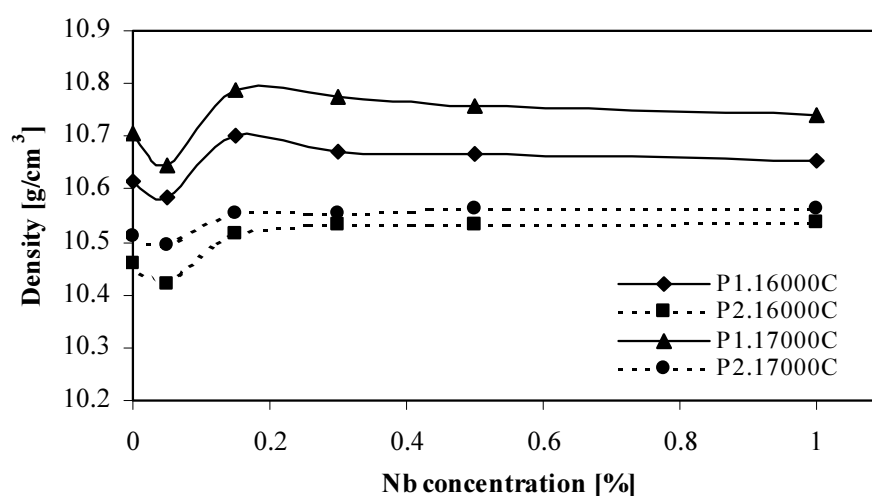


FIG. 2. Sintered pellets density versus Nb concentration.

A very small concentration of Nb₂O₅ (0-0.1%Nb/U) leads to a minimum value of the UO₂ pellet density. The density of UO₂ pellets increases with the increase of the Nb content for low concentrations (0.1 ÷ 0.2% Nb/U). At concentrations higher than 0.2%Nb/U, the density values are different, depending on the manufacturing routes: the increase of the Nb concentration diminishes slowly the density (P₁ -ADU route) or remains constant (P₂ - IDR route).

The sintering temperature has an impact on UO₂ sintered pellets density. The decrease of sintering temperature can observe the diminishing of sintered pellets density. However, the influence of dopant concentration is similar.

The importance of powders quality can be observed following Figure 2. Nevertheless, the pellets green density from P2 powder is better than the pellets green density from P1 powder. The sintered pellets densities from P1 powder are better than sintered pellets density from P2 powder.

The influence of Cr_2O_3 dopant on sinterability of both powders is shown in Figure 3. The behaviour of doped powders is different. Increasing of Cr_2O_3 content in P1 type powder determines a continuous decrease of UO_2 sintered pellets density. Little quantities of Cr_2O_3 dopant ($< 0.3\%$) in P2 powder type determine the increasing of UO_2 sintered pellets density. After that, increasing of Cr_2O_3 quantities determines a very slow decrease of sintered pellets density.

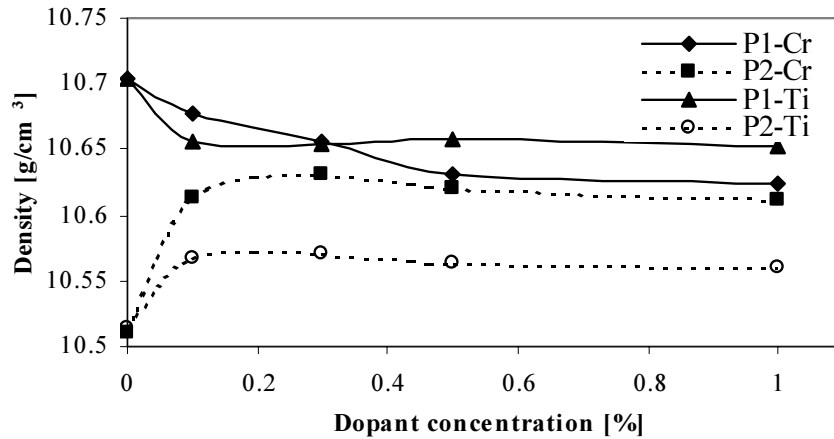


FIG. 3. Density versus Cr and Ti concentration.

The presence of TiO_2 dopant in both powders has the same impact on UO_2 sintered pellets density like Cr_2O_3 , Figure 3. Hereby, TiO_2 content up to 0.1% in P1 powder type determine a visible decrease of UO_2 sintered pellets density. After that the decreasing of sintered density with the increase of TiO_2 content is almost indistinguishable. Concentrations of TiO_2 up to 0.1% in P2 powder type determine a visible increasing of UO_2 sintered pellets density. The TiO_2 content increasing determines a very slowly decrease of UO_2 sintered pellets density.

3.1.3. Dopant influence on the grain size of UO_2 sintered pellets

The influence of Nb_2O_5 dopant on the UO_2 sintered pellets grain size is presented in Figure 4.

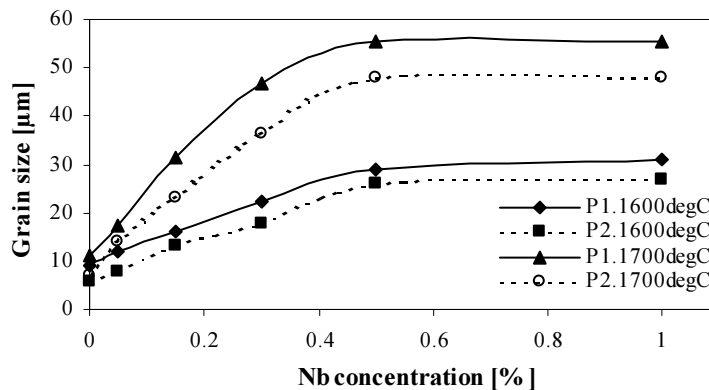


FIG. 4. Grain size function of Nb concentration.

The dopant addition determines a significant grain growth. The increasing of Nb₂O₅ content (up to 0.5%) determines the increasing of grain size up to 56 μm for P1 powder type and up to 48 μm for P2 powder type sintered at 1700 °C. In the same conditions, but sintered at 1600°C, the grain size is 31 μm and 27 μm for P1 and P2 powder type, respectively.

The temperature influence on the grain size growth in the presence of Nb₂O₅ dopant is significant. For P1 powder type doped with 0.5% Nb₂O₅, the difference between grain sizes sintered at 1700 °C and 1600°C is 25 μm.

The increasing of Nb₂O₅ content more than 0.5% does not produce important grain size modifications.

The influence of Cr₂O₃ and TiO₂ dopants is presented in Figure 5.

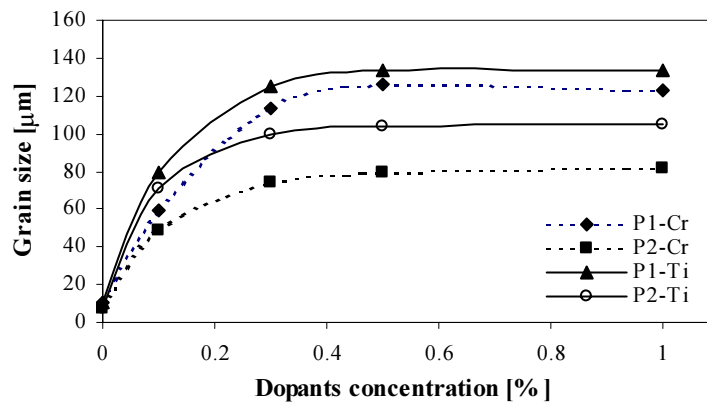


FIG. 5. Grain size versus Cr and Ti concentration

The increasing of Cr₂O₃ content up to 0.5% induces a grain size growth up to 126 μm for P1 powder type and up to 80 μm for P2 powder type. Grain size growth, when Cr₂O₃ content increases up to 1%, is undistinguishable. The increasing of TiO₂ content up to 0.5% induces a grain size growth up to 133 μm for P1 powder type and up to 104 μm for P2 powder type. When TiO₂ content increase over 0.5% no eloquent growth appears.

3.1.4. Diametral compression tests of UO₂ large grain size sintered pellets

A fractographical examination was performed on mechanical tested sintered pellets. The fracture takes place on the slip plane, oriented at 45° from the loading axis, its character being intergranular, transgranular or mixed, function of the testing temperature. The transgranular fracture observed at low temperature (≤400°C) point out the intense cohesion between the grains (Figure 6). If the temperature increase, the intergranular fracture is dominant Figure 7 and only this type of rupture takes place at high temperature (≥850°C), Figure 8.

Taking into account the “F” and the contact width “b”, the compressive strength to fracture σ_{HC} was calculated in accordance with relation (1) for each type of tested specimen and at different temperature. The results are presented in Figure 9.

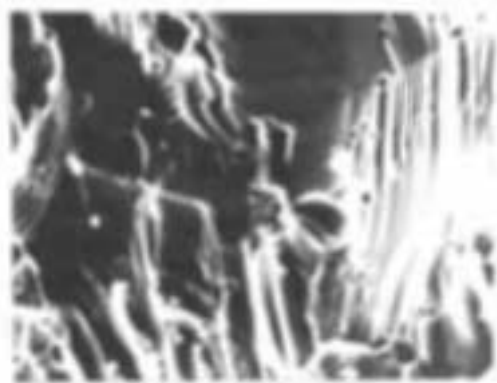


FIG. 6. SEM Analysis. UO₂+0.25%wtNb/U pellet tested at room temperature ($\times 2000$).

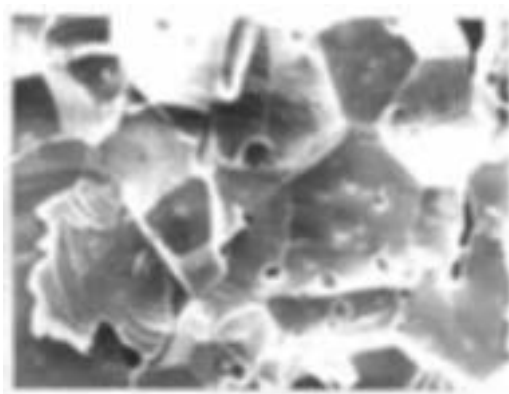


FIG. 7. SEM Analysis. UO₂+0.25%wtNb/U pellet tested at 700°C ($\times 1000$).

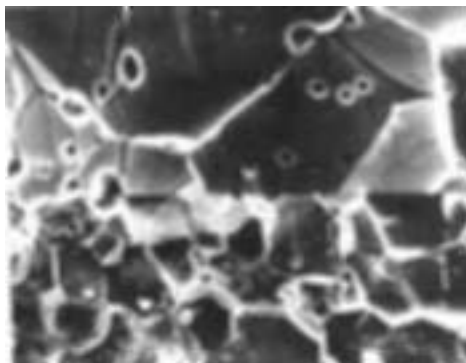


FIG. 8. SEM Analysis. UO₂+0.25%wtNb/U pellet tested at 950°C ($\times 2000/\times 600$).

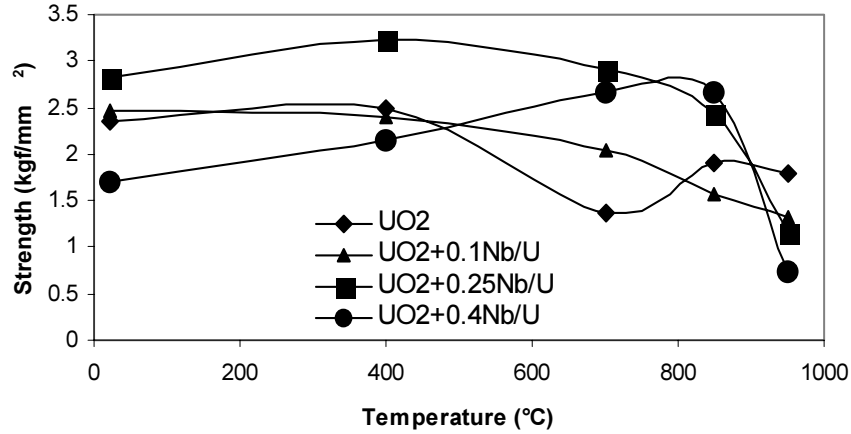


FIG. 9. The diametral compressive strength as function of temperature, for UO_2 pellets having different dopant concentrations.

The results of mechanical tests are in accordance with SEM analysis. The effect of the Nb additive is to strengthen the material, if the Nb content increases (Figure 9). The slope of the $\sigma_{HC} = f(T)$ dependence is negative for 0,1% wt Nb/U and attains positive values for 0,4% Nb/U, at temperatures between 400 and 800°C. We suggest that the transgranular fracture at low temperature is due to the solid solution, formed at the grain boundaries during the sintering phenomenon, effect emphasised in [22]. At temperatures greater than 850°C, the σ_{HC} values are strongly diminished. The strengthening effect is reduced, the influence of the Nb on the mechanical strength disappears completely at 950°C. At this temperature the diametral compressive strength can be correlated by means of a classical relation, useful for the ceramic material:

$$\sigma_{HC} = C(d)^\alpha \quad (2)$$

where σ_{HC} -the compressive diametral strength;
 d -the grain size;
 C, α -material constants;

At 950°C the obtained constants are: $C = 6,57$ and $\alpha = -0,52$

The fitness between the experimental and theoretical data predicted by relation (2) is good in the experimental errors limit, as presented in Figure 10.

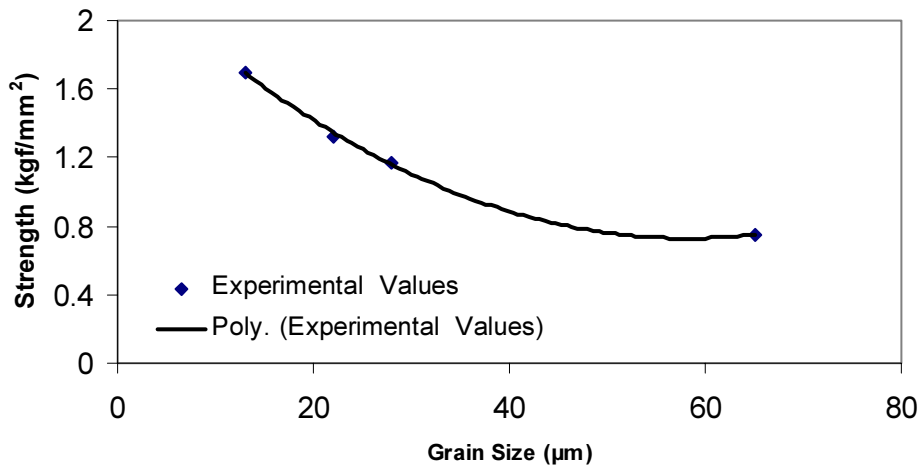


FIG. 10. Diametral compressive strength “ σ_{HC} ” as function of grain size parameter “ d ”, for UO_2 pellet doped with Nb, tested at 950°C.

A relation as that mentioned above is proposed in reference [23]. In addition, it includes the contribution of the porosity to the mechanical strength. In the present tests, the addition of the niobium dopant leads only to grain size variation, for a given concentration, but with the same porosity. The contribution of the porosity is included in the “C” constant (relation 2).

3.2. (U, Th) O₂ sintered pellets manufacturing

3.2.1. (U, Th) O₂ sintered pellets manufacturing by impregnation

Result of sintered pellets manufacturing by impregnation are presented in Table 4. The mean values are presented for 10 pellets/lot.

Table 4. Manufacturing conditions and characteristics of ThO₂-UO₂ pellets

Lot No	Graininess [μm]	Pressing pressure [MPa]	Green density [g/cm ³]	Pre-sint. temp. [°C]	Pre-sint. density [g/cm ³]	U content [%]	Sintered density [g/cm ³]
1	150-250	300	6.14	1200	8.24	1.90	9.34
2	150-250	300	6.14	1300	8.53	1.51	9.35
3	150-250	400	6.22	1200	8.37	1.76	9.37
4	150-250	400	6.22	1300	8.65	1.33	9.40
5	150-250	500	6.36	1200	8.38	-	-
6	150-250	500	6.36	1300	8.67	1.34	9.48
7	<150	300	6.11	1200	8.24	1.94	9.33
8	<150	300	6.11	1300	8.54	1.38	9.34
9	<150	400	6.19	1200	8.38	1.74	9.38
10	<150	400	6.19	1300	8.65	1.28	9.41
11	<150	500	6.32	1200	8.37	-	-
12	<150	500	6.32	1300	8.72	1.22	9.48

The density of ThO₂ green pellets increases with the increasing of pressing pressure. The influence of graininess is small.

The pre-sintered density of ThO₂ compacts is dependent on ThO₂ green pellets density (pressing pressure of ThO₂ green pellets) and pre-sintering temperature. It increases with the increasing of ThO₂ green pellets density (pressing pressure of ThO₂ green pellets) and pre-sintering temperature.

Uranium content in ThO₂-UO₂ pellets decreases with the increasing of the pre-sintered density of ThO₂ compacts, ThO₂ green pellets density or pressing pressure of ThO₂ green pellets and pre-sintering temperature.

The density of ThO₂-UO₂ sintered pellets increase with the increasing of the pre-sintered density of ThO₂ compacts, ThO₂ green pellets density or pressing pressure of ThO₂ green pellets and pre-sintering temperature. The dependency of the of ThO₂-UO₂ sintered pellets density on Uranium content

3.2.2. Diametral compression of ThO₂-UO₂ sintered pellets

Weibull's statistical theory of brittle fracture is a well established procedure for relating the variability observed in the mechanical tests under different state of stresses due to the effect,

size and stress distribution. As a consequence the Weibull theory was applied to the statistical corrections on the diametrical compressive strength σ_{HC} . The σ_{HC} parameter was correlated with the fracture probability P using the relation:

$$P(\sigma) = 1 - \exp(-k\sigma^m) \quad (3)$$

where m and k are factors including the dimension of the specimen and the effect of stress distribution.

A mean value respecting the Weibull distribution is the following, [24] :

$$\sigma^* = \frac{\Gamma\left(1 + \frac{1}{m}\right)}{k^{1/m}} \quad (4)$$

where Γ is the Euler function.

The fracture probabilities have been calculated using the relation:

$$P_i = (i - 0.3)/(n + 0.4) \quad (5)$$

where i is the order of a tested specimen from the total n number.

The experimental values, processed using the Weibull procedure σ^*_{HC} , as function of the oxide composition are presented in Table 5.

Table 5. Statistical mean values for different (ThU)O₂ pellets, [25]

Type of sintered pellets	% Theoretical Density (DT)	σ^*_{HC} (kgf/mm ²)
ThO ₂	96.4	6.04
ThO ₂ – 5%UO ₂	97.3	6.34
ThO ₂ – 13%UO ₂	96	5.68
ThO ₂ – 20%UO ₂	93	5.51
ThO ₂ – 50%UO ₂	97	5.36
ThO ₂ – 75%UO ₂	97.3	4.88

Taking into account that all the pellets were obtained in identical conditions, the dependence of the diametral strength as function of the composition was studied.

A linear correlation was proposed as following:

$$\frac{\sigma_{HC}}{\rho} = (a + b \cdot c) \cdot (1 - f \cdot c) \quad (6)$$

where ρ is the density (g/cm³), c the UO₂ concentration (%), f is a factor as function of the dimension and pores distribution.

The fitness between the experimental and the theoretical data predicted by relation (6) is good in the experimental errors range, Figure 11.

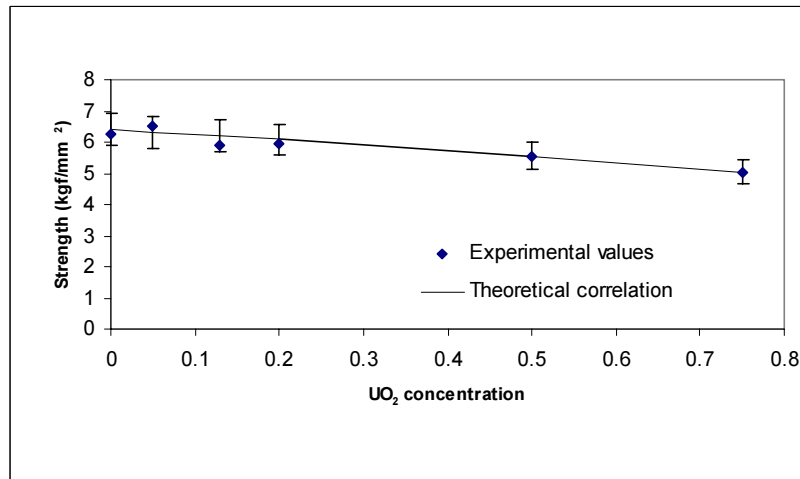


FIG. 11. Diametral Compressive Strength versus Mixed Oxide Concentration.

The decrease of the mechanical strength once the concentration of the uranium increased in the mixed (ThU)O₂ pellets, can be explained in accordance with the microstructural analysis. At low concentrations the pores number was reduced, theirs shape being spherical. If the UO₂ concentration increased, the shape and the size of these inhomogenities have been changed, Figures 12 and 13.

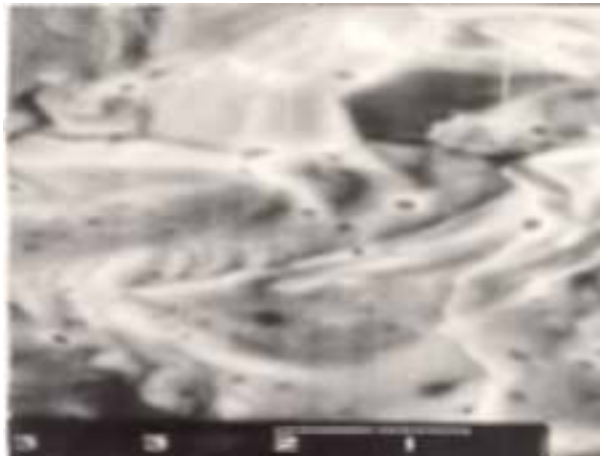


FIG. 12. Microstructural aspect, (Th+0.2U)O₂ pellet ($\times 3000$).

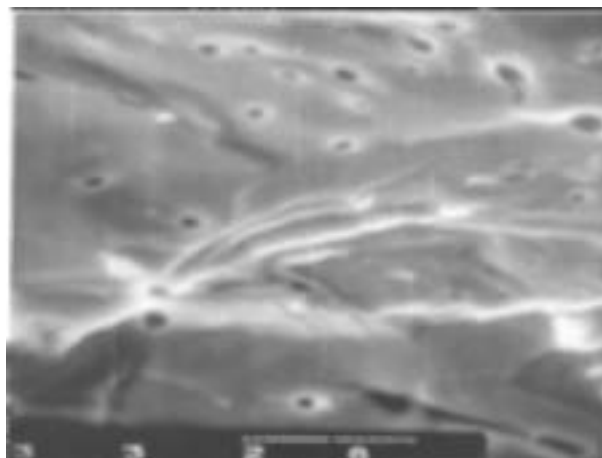


FIG. 13. Microstructural aspect, (Th+0.5U)O₂ pellet ($\times 3000$).

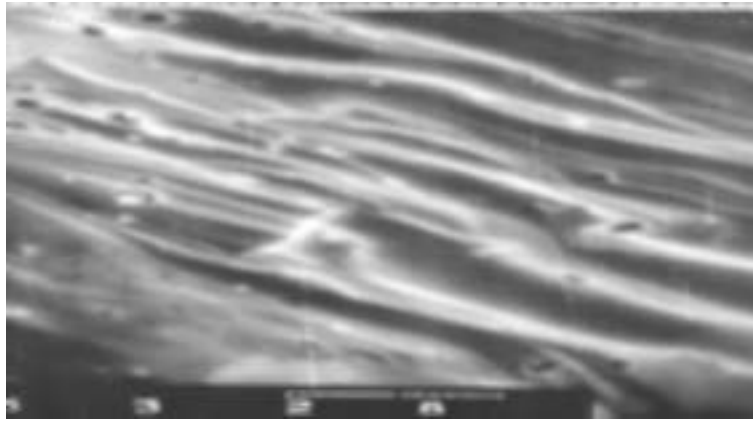


FIG. 14. Transgranular type of fracture.

The fracture take place on the slip planes oriented al 45° from the loading axis, the transgranular character being dominant, Figure 6. This is the specific type of fracture of nuclear sintered oxide pellets at room temperature.

4. CONCLUSIONS

The experimental program for UO_2 sintered pellets with large grain size was performed to establish the correlation between the nature of dopant and the technological conditions. As consequence of the experimental results, we established and verified different technology variants. It is clearly that equal quantity of different dopants has different effects on grain size increasing. The beneficial effect increase in the following order: Nb_2O_5 , Cr_2O_3 and TiO_2 . The modification of physical properties and behavior under irradiation of doped UO_2 matrix, and the impact on the fission product chemistry are arguments for dopant choice.

However the beneficial effect is not the better, the Nb_2O_5 dopant can be a solution because Nb appears like fission product at the burn of fuel.

From the mechanical point of view, both types of pellets were characterized using the diametral compression testing method. This method is adequate taking into account that the stress distribution during the test simulates the main mechanical state of stress of the fuel elements pellets during the reactor operation.

The mechanical results outline the influence of the Nb addition on the UO_2 strength. The effect of Nb is to strengthen the material in the 0.1–0.25 Nb/U range at temperature lower than 900°C .

As regarding the mechanical behavior of the mixed fuel (Th, U) O_2 , the strength is reduced if the UO_2 concentration increased, following a polynomial dependence.

REFERENCES

- [1] H. GROSS, R. MANZEL, "LWR fuel rods extended burn up: design and experimental basis", Improved Utilization of Water Reactor Fuel with Special Emphasis on Extended Burnup and Pu - Recycling (Proc. IAEA Tech. Com. Meet Mol, Belgium, 1984), IAEA, Vienna, IWGFPT/20 (1984) 134.
- [2] T.J CARTER, The effects of UO_2 pellet shape on strains induced in collapsible Zy cladding, Rapport AECL 5978 (1977).
- [3] J.D. PALMER, K.W. HESKETH, P.A. JACSON, Water Reactor Fuel Element performance Computer Modeling, Applied Science, UK (1983) 221.

- [4] W.B. LEWIS, Large scale nuclear energy from the Th fuel cycle, Raport AECL 3980 (1971).
- [5] MACDONALD, R.J. HASTINGS, Graphite disk UO_2 fuel element designed for extended burn up at high power, Nucl. Tech., 71 (1985) 430.
- [6] S. DOI, S. ABETA, Y. HAVADA, "Improvement of fuel pellet for high burnup", Fuel Performance at High Burnup for Water Reactors (Proc. IAEA Tech. Com. Meet Studsvik, Sweden, 1990), IAEA, Vienna (1991) IWGFPT/36 119.
- [7] I. HARADA, S. DOI, S. ABETA, K. YAMATA, "Behavior of large grain UO_2 pellet by new ADU powder" Water Reactor Fuel Element Modeling at High Burnup and its Experimental Support (Proc. IAEA Tech. Com. Meet. Windermere, UK, 1994), IAEA-TECDOC-957, Vienna (1997) 429.
- [8] J.A. TURNBULL, The effect of grain size on the swelling and gas release properties of UO_2 during irradiation, J. Nucl. Mater. **50** (1974) 62.
- [9] T.J. CARTER, Experimental investigation of various pellet geometries to reduce strains in zirconium alloy cladding, Nucl. Technology **45** (1977) 166.
- [10] E. ROLSTAD, K.D. KNUDSEN, Studies of fuel-clad mechanical investigation at the resulting interaction failure mechanism, Technology, **13** (1972) 168.
- [11] S. ROSENBAUM, T.C. ROWLAND, Large-scale demonstration of Zy - barrier fuel, Improvements in Water Reactor Fuel Technology and Utilization (Proc. IAEA Symp. Stockholm 1986) IAEA, Vienna (1997) 117.
- [12] F.GARZAROLLI, R. HOLZER, Waterside corrosion performance of light water power reactor fuel, Nucl. Energy, **31** (1992) 65.
- [13] G.R. KILP et al., "Corrosion experience with Zircaloy and ZIRLOTM in operating PWRs," LWR Fuel Performance (Proc. ANS/ENS Topical Meeting Avignon, France 1991), ENS, vol.2, p. 730.
- [14] K.C. RADFORD, J.M. POPE, UO_2 Fuel pellet microstructure modification through impurity additions - J. Nucl. Mat, **116** (1983), 305–313.
- [15] M. El. SAYED, R. LORENZELLI, Kinetics of initial stage of sintering of UO_2 and UO_2 with Nb_2O_5 addition, J. Nucl. Mat, **87** (1979), 90–96.
- [16] K.W. SONG, S.H. KIM, S.H. NA, Y.W. LEE, M.S. YANG, Effects of Nb_2O_5 addition on grain growth and densification in UO_2 pellets under reducing and/or oxidizing atmospheres - J. Nucl. Mat, **209** (1994), pp.280–285.
- [17] H. ASSMANN et.al., Doping UO_2 with niobia - beneficial or not? - J. Nucl. Mat. **98**, 1981, 216.
- [18] I. TANABE, M. OGUMA, H. Masuda, JP patent document 3-287096/A/, JP patent document 2-78.
- [19] K.W. LAY et. al, US patent document 4, 869, 868/A/.
- [20] H. AWAJI, S. Sato, Diametral Compressive Testing Method, J. of Eng. Mat. and Tech. **101** (1979), pp 139–147.
- [21] V. PITIGOI et. al, Institute for Nuclear Research, Internal Report, No. 822/1981.
- [22] P.T. SAWBRIDGE et. al, "The creep of UO_2 fuel doped with Nb_2O_5 " of Nucl. Mat. **97** (1981), pp 300.
- [23] G. ENGELHARDT et. al., Internal Report KFK 729, Kernforschungszentrum Karlsruhe, Febr. 1968.
- [24] P.M. BRAIDEN – An introduction to Weibull Statistics, AERE Harwell, Oxfordshire, 1975.
- [25] M. ROTH et.al. – Institute for Nuclear Research, Internal Report No. 1495/1984.

EFFECT OF ADDITIVES ON THE SINTERING KINETICS OF THE $\text{UO}_2\text{-Gd}_2\text{O}_3$ SYSTEM*

T.A.G. RESTIVO, A.E.L. CLÁUDIO, E.D. SILVA, L. PAGANO JR.
Department of Nuclear Materials,
CTMSP – Aramar,
Iperó, Brazil

Abstract

The sintering process of $\text{UO}_2\text{-7wt\%Gd}_2\text{O}_3$ with additives was investigated using conventional dilatometry coupled with mass spectrometry TG-MS and stepwise isothermal dilatometry-SID at H_2 atmosphere. Four batches of doped pellets were prepared with Al(OH)_3 , SiO_2 , Nb_2O_5 and TiO_2 at 0.5wt% as sintering additives. Their sintering kinetics were compared to those obtained from co-precipitated and mechanically blended $\text{UO}_2\text{-7wt\%Gd}_2\text{O}_3$ powders with no additive, and from pure UO_2 . Conventional dilatometry revealed a sintering barrier that delayed densification for the batches with Al(OH)_3 , SiO_2 , Nb_2O_5 , likewise found for the blended powder. These additives have reduced the barrier intensity and shifted it towards higher temperatures, improving the final pellet density. The TiO_2 added compacts have shown an early densification and no sintering barrier, likewise the co-precipitated powder, and reached the highest final density among the samples with additives. The SID method showed a sharp increase for the activation energy of the Al(OH)_3 , SiO_2 and Nb_2O_5 added compacts in the 1100-1200°C range, whereas it remained constant for the TiO_2 added pellets. The Al(OH)_3 added compacts showed the lowest activation energy among all compositions. The kinetic parameter n varied over a wide range and reached very low values, indicating that the sintering mechanism is very complex in all cases. However, the n values for TiO_2 added compacts were systematically higher than those for the others, suggesting that the TiO_2 addition promoted a more effective sintering mechanism.

1. INTRODUCTION

It is known that some additives can improve microstructure and density of $\text{UO}_2\text{-Gd}_2\text{O}_3$ pellets [1]. Despite their low concentration, they play a major role in the sintering kinetics, and to understand it is of technological importance. The amount of additive used is usually very small, typically a few hundreds parts per million, due to the maximum content of impurities allowed by most specifications. Because of their low content, it is difficult to determine how they influence the sintering mechanism. In this work, large amounts of additives (0.5wt%) were used as a first approach to overcome this difficulty, trying to enhance their effect, likewise done before for UO_2 [2]. This amount will be steadily reduced in further work, aiming to reach amounts in compliance with burnable poison specifications.

2. EXPERIMENTAL

2.1. Sample preparation

A nuclear grade UO_2 (ex-AUC) powder was used to prepare all samples. Its main characteristics were: BET $5.8\text{m}^2/\text{g}$, average particle size $7.4\mu\text{m}$ (Sedigraph) and O/U ratio 2.12. The Gd_2O_3 raw powder was of commercial grade, 99.8% pure, BET $4.6\text{m}^2/\text{g}$, average particle size $3.3\mu\text{m}$ (Sedigraph), and its main contaminants were Ca 64ppm, Al 57ppm, Mo 52ppm, Nb 35ppm and Ti 19ppm. Both UO_2 and Gd_2O_3 powders were dried in an oven and

*Work performed as part of the IAEA TC Project BRA4052.

handled in a glove box under inert gas. All additive powders were P.A. grade supplied by Aldrich and were mechanically blended to the $\text{UO}_2\text{-Gd}_2\text{O}_3$ powder. Five batches of mechanically blended powders were prepared in a turbula mixer, 32rpm for 60min. A sixth batch was prepared from co-precipitated $\text{UO}_2\text{-7wt}\%\text{Gd}_2\text{O}_3$ powder, obtained by dissolving the UO_2 and Gd_2O_3 raw powders in 1N nitric acid and adding ammonium hydroxide. The ADU powder thus obtained was calcined in air at 900°C for 3h, reduced in H_2 in a fixed bed at 600°C and passivated in mixture of N_2 and air. The resulting powder had BET $6.1\text{m}^2/\text{g}$ and an average particle size of $4.9\mu\text{m}$ (laser diffraction, Cilas). The seventh batch was pure UO_2 , as follows:

1. $\text{UO}_2\text{-7wt}\%\text{Gd}_2\text{O}_3$ plus 0.5wt% $\text{Al}(\text{OH})_3$
2. $\text{UO}_2\text{-7wt}\%\text{Gd}_2\text{O}_3$ plus 0.5wt% SiO_2
3. $\text{UO}_2\text{-7wt}\%\text{Gd}_2\text{O}_3$ plus 0.5wt% Nb_2O_5
4. $\text{UO}_2\text{-7wt}\%\text{Gd}_2\text{O}_3$ plus 0.5wt% TiO_2
5. $\text{UO}_2\text{-7wt}\%\text{Gd}_2\text{O}_3$ with no additive
6. co-precipitated $\text{UO}_2\text{-7wt}\%\text{Gd}_2\text{O}_3$ with no additive
7. pure UO_2 with no additive

From these batches, green pellets were obtained from a 350 - 400MPa pressing process in a floating table press. Green densities were in the range 50-51%TD.

2.2. Dilatometry and SID tests

All samples were sintered under a 99.999% H_2 atmosphere, 200mL/min, in a vertical TMA-dilatometer (Setaram Setsys 24) with a load of 1g, where both set of experiments, conventional dilatometry and SID, were performed. The former set was carried out with $10^\circ\text{C}/\text{min}$ heating rate and isotherm at 1700°C for 3h with a Balzers mass spectrometer coupled to the gas outlet. The mass spectrometer chamber and its connection to the dilatometer were heated to 200°C , hence trace amounts of water vapor coming off the sample could be detected.

Developed by Sørensen in the eighties [3], the SID method has shown good results in connecting kinetic data, such as activation energy and the kinetic parameter n , with the mass transfer mechanisms. The method requires that the temperature remains constant, i.e. isothermal sintering, while the shrinkage rate is within a given narrow range. The data acquired at each isotherm provides information about the sintering mechanism for that particular heating cycle. The kinetic parameter n can be interpreted as the order of the densification process, an analogy with the concept order of equation borrowed from the chemistry kinetics theory. It may provide information about the reaction mechanism.

The forced SID mode [4] was employed in this work, with the isotherms fixed to 50°C intervals and the shrinkage rate released to vary. It was observed that the shrinkage rate for all batches was always smaller than $7\mu\text{m}/\text{min}$ during densification and an average heating rate of $3.35^\circ\text{C}/\text{min}$ was observed in the 850°C - 1700°C range. The basic SID equation relating the shrinkage to time is:

$$y = \Delta L/L_0 = [K(T).t]^n \quad (1)$$

where

- y is relative linear shrinkage (dimensionless),
 L sample length at a given time (m),

- L_o sample initial length (m),
- $K(T)$ is the specific rate constant depending on the temperature (s^{-1}),
- T is the temperature (K),
- t is the time on the isotherm (s),
- n is the kinetic parameter (dimensionless),

Equation (1) may be taken in the differential form, as:

$$\text{Ln}(dy/dt) = \text{Ln}[n \cdot K(T)] - (1/n - 1) \text{Ln}y \quad (2)$$

At each isothermal step, the plot $\text{Ln}(dy/dt)$ versus $\text{Ln}y$ gives the n values from the slope, whereas the $K(T)$ values can be calculated from the intercept. The last parameter obeys an Arrhenius type equation, hence, one can calculate the activation energy Q from the plot $\text{Ln}[K(T)] \times 1/T$.

Replacing in the Equation (1) the relative linear shrinkage $\Delta L/L_o$ by the relative volumetric shrinkage and combining it with Equation (2), a normalized equation can be developed [5]:

$$dY/dt = nK(T)Y(1-Y)[(1-Y)/Y]^{1/n} \quad (3)$$

where $Y/(1-Y) = (V_o - V_t)/(V_t - V_f) = (L_o^3 - L_t^3)/(L_o^3 - L_f^3)$,

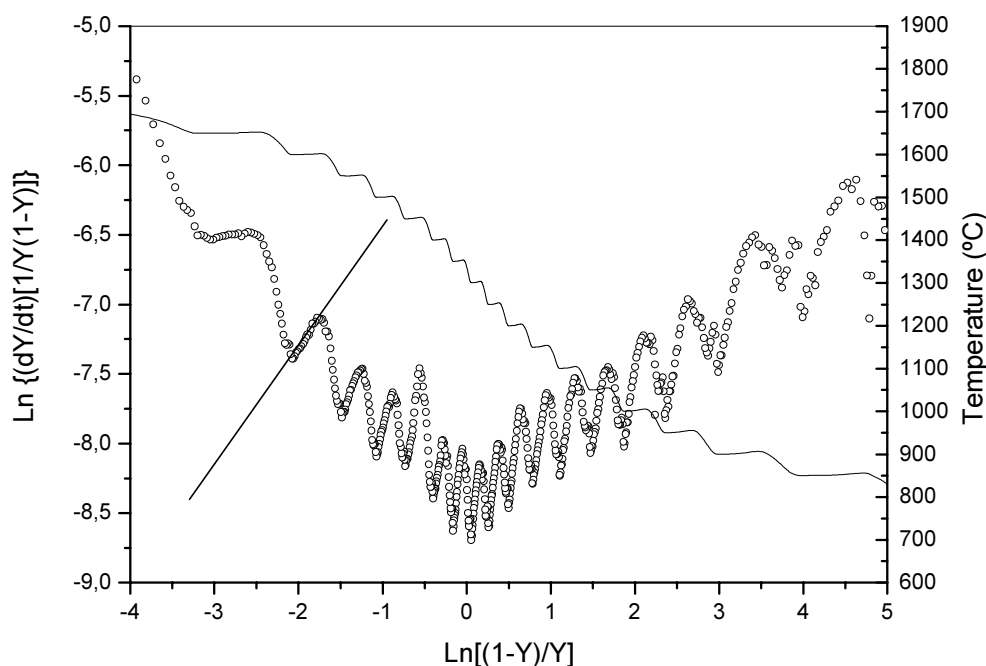


FIG. 1. Typical SID plot showing the isothermal steps.

The basic assumption is that the sintering process is isotropic (the subscripts o , t and f stand for the dimension values at the beginning, at a time t and at the end of the sintering). The isotropic behavior is specially valid when a vertical TMA/dilatometer is used, because the load over the pellet can be set as low as 1g. The plot $\text{Ln}\{(dY/dt)[1/Y(1-Y)]\}$ versus $\text{Ln}[(1-Y)/Y]$ yields a straight line from which K and n can be calculated [5, 6]. A typical SID plot is shown in Figure 1, as well as the temperature profile.

3. RESULTS

Figure 2 shows the densification curves obtained from the conventional dilatometry with a mass spectrometer coupled. The water release for all compositions took place around 500°C and no difference was observed in the release patterns. Relative densification (% shrinkage) and densification rate (% shrinkage/min) curves are plotted against the temperature profile. The curves for pure UO₂ (no Gd added), UO₂-7wt%Gd₂O₃ with no additive and co-precipitated UO₂-7wt%Gd₂O₃ with no additive are shown in the same figure curve for the sake of comparison.

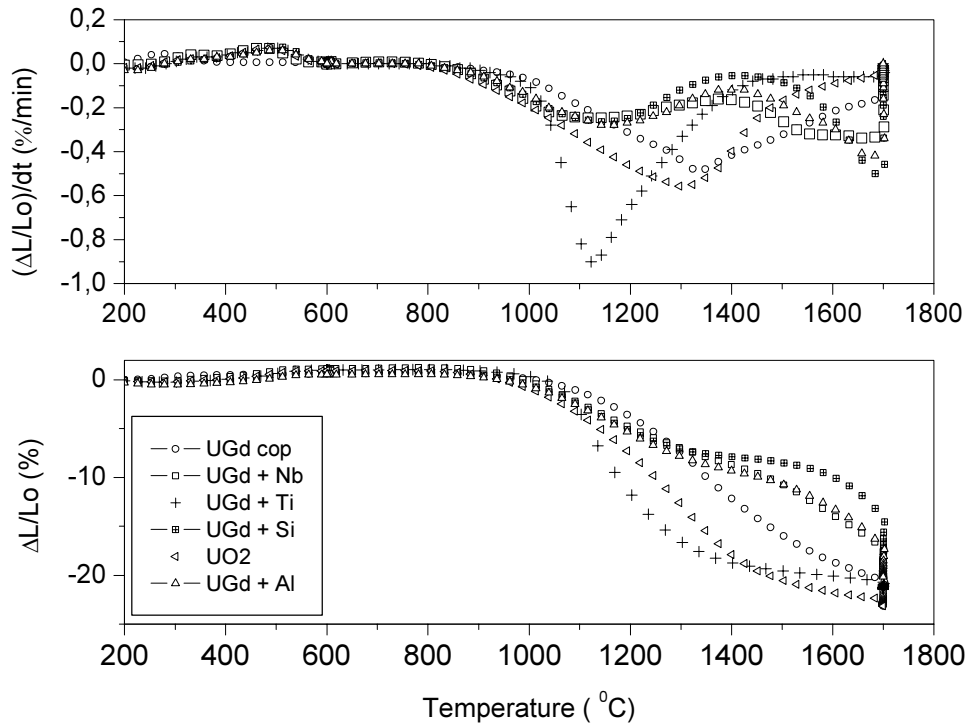


FIG. 2. Densification and densification rate dilatometry curves.

Table 1 summarizes the final sintered densities obtained for all compositions.

Table 1 Sintered densities after isothermal step at 1700°C for 3h under H₂

Batch	Nb ₂ O ₅	SiO ₂	Al(OH) ₃	TiO ₂	[UGd]O ₂	Co-precipitated
Density (%)	90.0	90.9	93.2	94.9	83.0	95.6

The constant $K(T)$ and the kinetic parameter n at each isothermal step can be obtained from the intercept values and the slope, respectively, of the SID plot. Thus, an Arrhenius plot can be built for each composition and the activation energies determined. Figures 3 and 4 show the Arrhenius plot for the batches with TiO₂ and Nb₂O₅, respectively. Other plots are not shown, but their results are summarized in Table 2. A sharp increase in the activation energy

was observed for all compositions, except for the TiO₂ batch (and the UO₂ batch has not been tested). This increase was observed in the 1100°C-1200°C range. Thus, Q₁ refers to the activation energy in the range 850°C - 1100°C, and Q₂ refers to the range 1200°C – 1450°C. The kinetic parameter is shown in Figure 5.

Table 2 Activation energies obtained from the SID plot

Batch	SiO ₂	Al(OH) ₃	Nb ₂ O ₅	TiO ₂	UGd	Co-precipitated
Q ₁ ^a (kJ/mol)	376	207	325	355	240	221
Q ₂ ^b (kJ/mol)	445	305	476	355	357	659

^a Activation energy calculated for the low temperature range.

^b Activation energy calculated for the high temperature range.

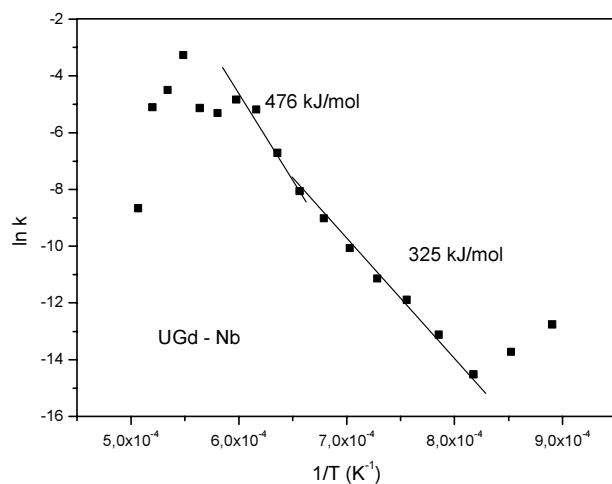


FIG. 3. Arrhenius plot for SID data of the TiO₂ batch.

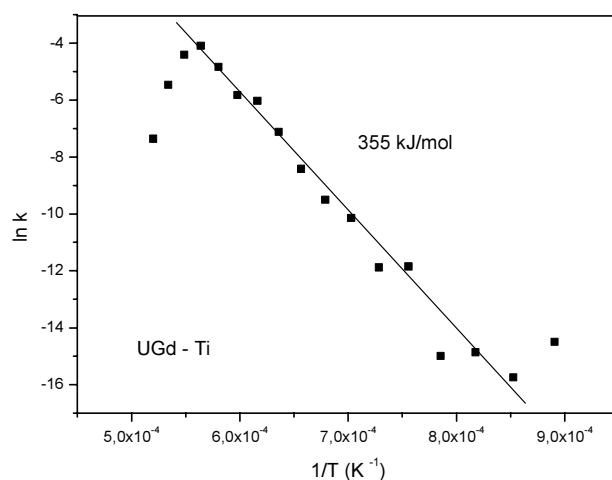


FIG. 4. Arrhenius plot for SID data of the Nb₂O₅ batch.

4. DISCUSSION

The dilatometry curves (Figure 2) have showed that the shrinkage rate slowed down for the batches with $\text{Al}(\text{OH})_3$, SiO_2 and Nb_2O_5 in the $1100^\circ\text{C} - 1300^\circ\text{C}$ range, and increased again at higher temperatures. In this work, such shrinkage hindrance with a later increase will be referred as a sintering barrier. This sintering behavior was similar to that observed for the mechanically blended $\text{UO}_2\text{-Gd}_2\text{O}_3$ with no additive, as reported before [7, 8], but these additives have reduced the barrier intensity and shifted it towards higher temperatures. The final densities have been improved, compared to the mechanically blended batch (Table 1), but they were still smaller than that for the co-precipitated batch. Nb_2O_5 additive has lead to the smallest sintered density, as expected. It has been used for UO_2 to control grain size, not for to increase density, and the sintering atmosphere used in this work was very reducing [9].

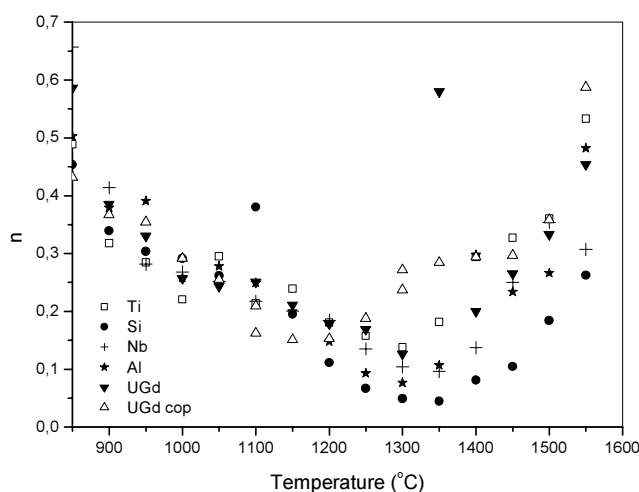


FIG. 5. The kinetic parameter n at each isothermal step.

The batch with TiO_2 has shown no sintering barrier, similarly to the co-precipitated $\text{UO}_2\text{-Gd}_2\text{O}_3$ and pure UO_2 batches. It has also shown a sharp increase in the shrinkage rate in the $1100^\circ\text{C} - 1300^\circ\text{C}$ range and a steady reduction from this point on. Despite this early densification, the final density was the highest of all compositions with additives. It is known that TiO_2 at 1wt% promotes liquid phase sintering in UO_2 [10] and this mechanism may also play a role in the $\text{UO}_2\text{-Gd}_2\text{O}_3$ system.

No trace amounts of volatile metals or oxides have been detected by the mass spectrometer, whose chamber and connection to the dilatometer is heated only to 200°C . Hence, volatile oxides coming off the samples, if there were any, certainly solidified in the dilatometer outlet before detection. The water vapor, generated by the reaction of the oxygen excess in the samples with the sintering atmosphere, was detected at the same temperature range for all batches, suggesting that the additives have not retained the oxygen excess up to higher temperatures.

The SID method trends to departure from experimental results in the final sintering stages. For the $\text{UO}_2\text{-Gd}_2\text{O}_3$ system, the data were scattered above 1450°C and no information from SID plots was used beyond this point. The SID tests revealed that the activation energies for the batches with $\text{Al}(\text{OH})_3$, SiO_2 and Nb_2O_5 have sharply increased in the $1100^\circ\text{C} - 1200^\circ\text{C}$ range, similarly to the mechanically blended and co-precipitated batches [8]. Unlike the others, the

TiO₂ batch has shown a single value for the activation energy from 850°C to 1450°C, suggesting that a single mechanism is controlling the process in the entire temperature range. It was also observed that the Al(OH)₃ batch activation energy was the smallest among all batches with additives, despite the its sharp increase in the 1100°C – 1200°C range.

The kinetic parameter, also obtained from the SID plots, indicates how complex the mass transfer mechanism is, for a given system [11]. For all batches (except for UO₂, that was not tested), it dropped steadily to very low values and lifted back. The values for the TiO₂ batch were systematically higher than those for the other batches with additives, suggesting that its sintering mechanism is somewhat more effective than that for the others. The TiO₂ batch values were also higher than those found for the mechanically blended batch (with no additive), and lower than those for the co-precipitated batch. This suggested that the TiO₂ additive promotes a sintering behavior intermediate the co-precipitated and dry blended batches.

5. CONCLUSIONS

The addition of Al(OH)₃, SiO₂, Nb₂O₅ and TiO₂ at 0.5wt% as sintering aids has improved the sintered density. The first three additives have reduced the sintering barrier intensity and shifted it towards higher temperatures. The TiO₂ has suppressed it completely and lead to the highest final density. The activation energies for the Al(OH)₃, SiO₂ and Nb₂O₅ batches were found to sharply increase in the 1100°C – 1200°C range, likewise reported for pure [U,Gd]O₂. For the TiO₂ batch, it was found a single value for the activation energy, suggesting that there is a single controlling mechanism for the entire temperature range. The kinetic parameter drifted to very low values, but the values for the TiO₂ batch were systematically higher, suggesting a more effective sintering mechanism.

REFERENCES

- [1] INTERNATIONAL ATOMIC ENERGY AGENCY, Characteristics and Use of Urania-Gadolinia Fuels, IAEA TECDOC-844, Vienna (1995).
- [2] MATSUDA, T., Y. YUSA, S. KOBAYASHI, M. TOBA, “Characteristics of fuel pellet with additive of Al and Si, Advances in Fuel Pellet Technology for Improved Performance at High Burnup, IAEA TECDOC-1036, Vienna (1998) 9.
- [3] SØRENSEN, O.T., *Thermochim Acta* **50** (1981) 163.
- [4] SØRENSEN, O.T., *J. Thermal Analysis* **38** (1992) 213.
- [5] WANG, H., LIU, X., CHEN, F., MENG, G., SØRENSEN, O.T., *J. Am. Ceram. Soc.*, **81** 3 (1998) 781.
- [6] TRÜMMLER, F., THOMMA, W., *Metal Reviews*, 12 review **115** (1967) 69.
- [7] MANZEL, R., DÖRR, O., *Am. Ceram. Soc. Bulletin* **59** 6 (1980) 601.
- [8] RESTIVO, T.A., PAGANO Jr, L., Sintering Studies on the UO₂.Gd₂O₃ Sistem Using the SID-method, Conference on Characterization and Quality Control of Nuclear Fuels, Hyderabad, India, 10–12 December (2002), (in press).
- [9] MARSH G., G.A. WOOD, C.P. PERKINS, “Niobia-doped UO₂ fuel manufacturing experiwnce at British Nucleae Fuels Ltd”, Advances in Fuel Pellet Technology for Improved Performance at High Burnup (Proc. IAEA Tech. Mtg Tokyo, 28 October–1 November 1996) IAEA TECDOC-1036, Vienna (1998) 19.
- [10] KINGERY, W.D., BOWEN, H.K., UHLMANN D.R., *Introduction to Ceramics*, 2nd edition, Wiley-Interscience Publication, (1975) 286.
- [11] MENG, G., O.T. SØRENSEN, Riso National Laboratory, Report I-455, Denmark (1989).

YIBIN NUCLEAR FUEL ELEMENT PLANT'S EXPERIENCE IN MANUFACTURING OF LARGE GRAIN SIZE PELLETT

DENG HUA, ZHOU YONGZHONG, YAN XUEMIN
Yibin Nuclear Fuel Element Plant,
Yibin, Sichuan, China

Abstract

Yibin Nuclear Fuel Element Plant (YFP) began to make large grain pellet for gaining experience since 1999. Two ways to promote grain growth were studied. One is to add U_3O_8 from grinding sludge, the other is to add other additives. In this paper, the production data with addition of U_3O_8 from grinding sludge are reviewed. It is proved by experience that addition of U_3O_8 from grinding sludge is a useful way to promote grain size. The affect of addition of Al_2O_3 and SiO_2 powder on the grain size of UO_2 pellets was studied in detail. It is confirmed that doping with a small amount of Al_2O_3 and SiO_2 powders can promote grain growth during sintering process and the properties of UO_2 pellets satisfied the technical specification completely. And other additives we also studied, such as Cr_2O_3 .

1. INTRODUCTION

In order to reduce LWR nuclear cycle cost, the nuclear power station of China, such as JVC discharge burnup The increase in fuel rod internal pressure due to high fission gas release (FGR) and the increase in pellet cladding interaction (PCI) by gas bubble swelling are key problems affecting fuel reliability at high burnup. FGR and bubble swelling can be reduced by using the large grain pellets.

As statement in abstract, two ways were used to get gain large grain pellets. One is to add U_3O_8 from grinding sludge; the other is to add additives. Two additives— Al_2O_3 and SiO_2 were used in the research on understanding the effect of additives on the fabrication conditions and properties of the pellet. The effect of grinding sludge was studied too. The representative studies are stated in detail below.

2. STUDY ON Al/Si DOPING PELLETT

The work was mainly carried out in laboratory and small scale production scale investigation also was done.

2.1. Raw materials

UO_2 powder from ADU process powder was used in this study. We took about 2kg UO_2 powder from a representative homogeneous batch. Table 1 shows the main characteristics of the UO_2 powder. The main characteristics of U_3O_8 powder is shown in Table 2. The main characteristics of Al_2O_3 and SiO_2 powder are shown in Table 3.

The main works of the experiment are:

- (a) Effect of different amount of Al_2O_3 and SiO_2 on pellet;
- (b) Effect of different proportion of Al_2O_3 and SiO_2 on pellet;
- (c) Effect of U_3O_8 of different type (from pellet with Al_2O_3 or without) on pellet.

Table 1 Main characteristics of UO₂ power

Properties		Value from test
O/U		2.10
Specific surface area (m ² /g)		4.2
Bulk density (g/cm ³)		1.62
Tap density (g/cm ³)		2.53
Impurity content (μg/gUO ₂)	aluminum	<10
	silicon	<20

Table 2 Main characteristics of U₃O₈ power

Properties		Value from test
O/U		2.65
Specific surface area (m ² /g)		0.50
Bulk density (g/cm ³)		1.76
Tap density (g/cm ³)		2.62
Impurity content (μg/gUO ₂)	aluminum	13
	silicon	<20

Table 3 Main characteristics of Al₂O₃ and SiO₂ power

Properties	Parameter type	
	Al ₂ O ₃	SiO ₂
Molecular weight	101.96	60.08
Mass fraction of chloride(%)	0.01	0.005
Mass fraction of ferrum (%)	0.01	0.005
Mass fraction of sulphate(%)	0.05	0.005
Mass fraction of heavy metal (%)	0.005	0.005

2.2. Process of experiment

The schematic diagram of experiment process is shown in Figure 1.

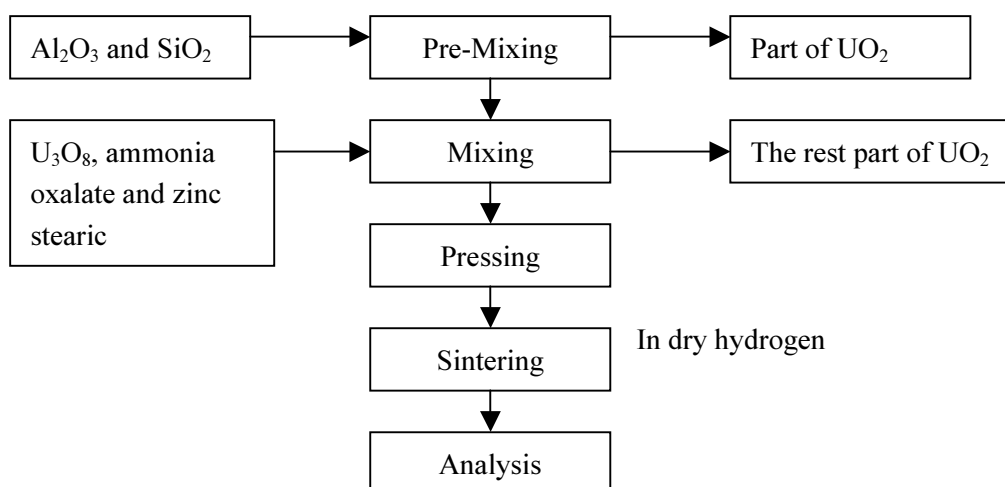


FIG. 1 Schematic diagram of experiment process.

2.3. Result and discussion

2.3.1. Effect of different amount of Al_2O_3 and SiO_2 of on pellet

Same proportion of Al_2O_3 and SiO_2 are added before mixing. The density of green pellet is around 5.80 g/cm^3 . Chart 4 shows that with increasing of the amount of Al_2O_3 and SiO_2 , the grain size increases too, and the increasing rate is not linear with the adding content. Adding very small amount of Al_2O_3 and SiO_2 (20ppm to 40ppm) doesn't bring big effect on the pellet grain size. Adding small amount of Al_2O_3 and SiO_2 (50ppm to 100ppm) can markedly promote the grain size growth. An excess amount of Al_2O_3 and SiO_2 can not promote further grain growth but reduce pellet density.

Table 4 Effect of different amount of Al_2O_3 and SiO_2 of on pellet

Sample number	content of each additive (ppm)	Density after sintering (g/cm^3)	Grain size of pellet (μm)
1	0	10.387	8.0
2	20	10.403	10.8
3	30	10.412	10.7
4	40	10.398	10.4
5	50	10.452	17.0
6	60	10.469	20.4
7	80	10.481	25.8
8	100	10.481	25.9
9	200	10.483	26.2
10	1000	10.419	28.2
11	5000	10.021	31.7

2.3.2. Effect of different proportion of Al_2O_3 and SiO_2 on pellet

Chart 5 shows that with the constant total amount of additives (100ppm), adding only one additive (SiO_2), there is no obvious difference of grain size between the pellets without additive. With the increasing of the content of Al_2O_3 , the grain size of pellet increases. Grain size of the pellet adding only Al_2O_3 is the largest one among all.

2.3.3. Effect of U_3O_8 of different type (from pellet with Al_2O_3 or without) on pellet

In this study, two kinds of U_3O_8 were used. One was oxidized from pellet without addition of Al_2O_3 ; the other was oxidized from the pellet with addition of Al_2O_3 . Both two kinds of U_3O_8 were produced in the same condition. It is shown in Table 6 that as the amount of Al in U_3O_8 is very small, so the grain size difference is very little.

3. STUDY ON GRINDING SLUDGE

Grinding sludge is produced while grinding the pellet. From 1994 to 1999, we had produced more than 400 tons pellets. As a result, a lot of grinding sludge has been stored for further dealing with. The conventional means is wet route reclaiming. But it is not economical, and at the same time brings a lot of trash and liquid waste that hard to deal with. Therefore it's necessary to find a useful way to deal with the grinding sludgy which is used now.

Table 5 Effect of different proportion of Al₂O₃ and SiO₂ on pellet

Sample number	Al ₂ O ₃ :SiO ₂ (ppm)	Content of both additives (ppm)	Density after sintering (g/cm ³)	Grain size of pellet (μm)
12	0:10	100	10.391	9.6
13	2:8	100	10.458	11.5
14	4:6	100	10.468	17.7
15	6:4	100	10.481	17.5
16	8:2	100	10.480	19.3
17	10:0	100	10.483	21.6

Table 6 Effect of U₃O₈ of different type on pellet

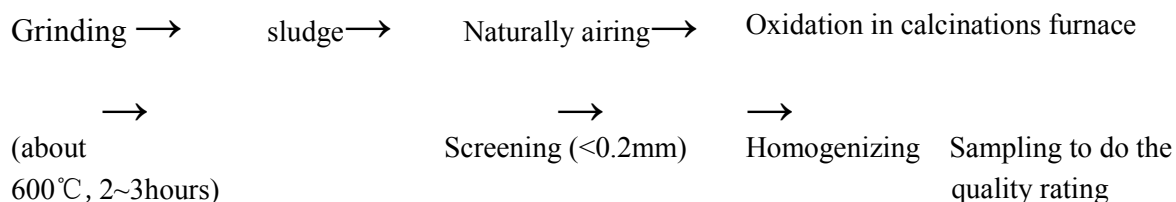
Sample number	Type of U ₃ O ₈	Content of U ₃ O ₈ (%wt)	Density after sintering (g/cm ³)	Grain size of pellet (μm)
18	Without Al	10	10.412	9.9
19	With Al	5	10.390	10.7
20	With Al	10	10.388	10.0
21	With Al	15	10.392	10.2
22	With Al	20	10.318	9.1

The original purpose that we made research on the grinding sludge was to find a way to solve the problem of storage and to reduce production cost. But after the first several experiments, by chance, we found that it is a new way to promote pellet grain size.

The process for deal with the grinding sludge is divided into two steps:

- (1) Oxidize the grinding sludge to U₃O₈;
- (2) Use the U₃O₈ powder as an additive.

3.1. Oxidize the grinding sludge into U₃O₈



The U₃O₈ oxidized from grinding sludge is smaller in granularity than that oxidized from waste pellet. The representative characteristics of two kinds of U₃O₈ powder are given in Table 7. The decrease density coefficient of U₃O₈ from grinding sludge is 0.04%T.D/0.1% wt, which is a statistics from experiments and production.

Table 7 Contrast of two kinds of U₃O₈ powder

U ₃ O ₈ oxidized from grinding sludge		U ₃ O ₈ oxidized from pellet	
Properties	Value	Properties	Value
O/U	2.66	O/U	2.65
Specific surface area (m ² /g)	1.48	Specific surface area (m ² /g)	0.50
Bulk density (g/cm ³)	1.10	Bulk density (g/cm ³)	1.76
Tap density (g/cm ³)	2.00	Tap density (g/cm ³)	2.62

3.2. Use the U₃O₈ powder from grinding sludge as an additive to manufacture pellets

After tested to be qualified to the technical specification, the U₃O₈ from grinding sludge can be used as additive in the UO₂ pellet manufacturing. It is mainly used to promote the pellet grain size.

The U₃O₈ from grinding sludge is added in the blending stage as well as other additives by weight of less than 10%wt. It was investigated that adding small amount of U₃O₈ from grinding sludge didn't affect the final grain size of pellet well. Now in the pelletization of YFP, 5%wt is usually used.

In 2000, we used the U₃O₈ from grinding sludge as an additive to produce UO₂ pellets for the first time. The data of pellet grain size are shown in Figure 2. As a contrast, the data of pellet grain size without addition U₃O₈ from grinding sludge are also shown in Figure 3. The two figures show great difference of the two kinds of pellets.

Although it is concluded that U₃O₈ from grinding sludge is a useful grain size promoter, the theory why U₃O₈ from grinding sludge can promote grain size growth is still under researching. We can only guess it is by reason of the characteristics of the U₃O₈. And of course other reasons may be found in the further researching.

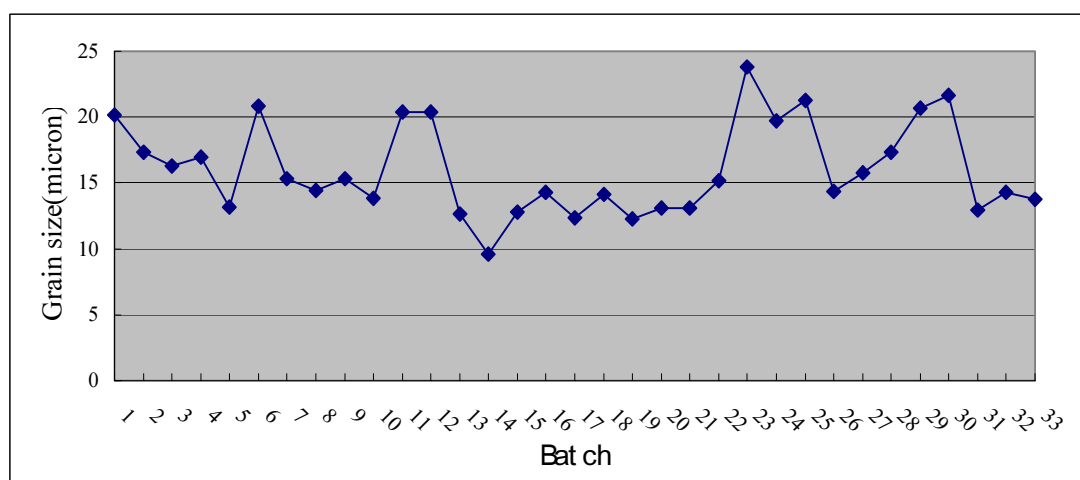


FIG. 2 Pellets manufactured with adding of U₃O₈ from grinding sludge.

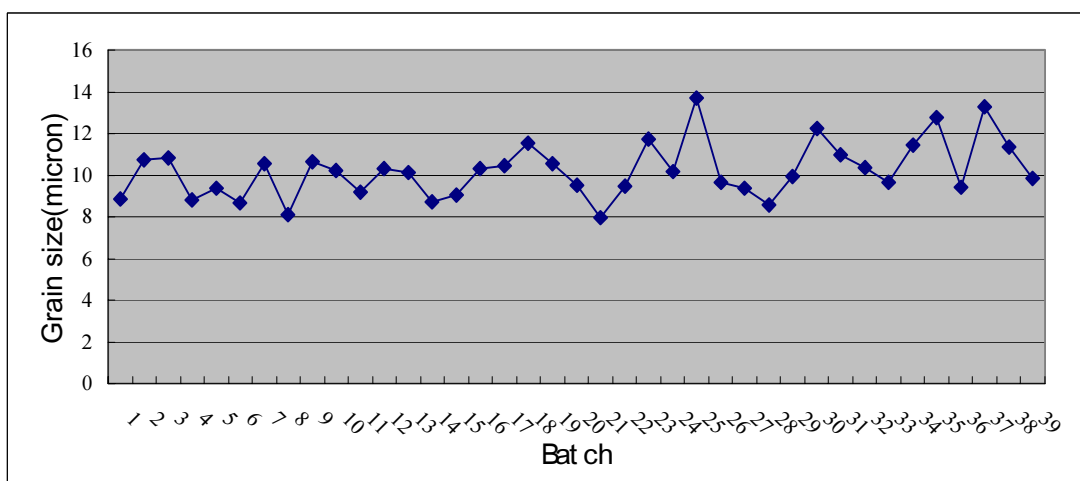


FIG. 3 Pellets manufactured without addition of U_3O_8 from grinding sludge.

4. CONCLUSION

(1) Adopting Al_2O_3 and SiO_2 is a useful way to promote pellet grain size. The pellet gained with addition of 50ppm Al_2O_3 and 50ppm SiO_2 has an optimal result considering the grain size and other properties such as density.

(2) Study on applying grinding sludge to pelletization helps to find a way to reduce production cost and utilize waste. Most important, the grinding sludge can be used as a grain size promoter.

REFERENCES

- [1] CAI WENSHI, SU BAOHUA, "UO₂ ceramic fuel pellet manufacturing", Internal Report, Yubin Nuclear Fuel Element Plant, China 1987 (in Chinese).
- [2] T. MATSUDA, Y. YUASA, S. KOBAYASHI, M. TOBA, "Characteristics of fuel pellet with additive of Al and Si", Advances in Fuel Pellet Technology for Improved Performance at High Burnup (Proc. IAEA Techn. Com. Mtg Tokyo, 1996), IAEA, Vienna, TECDOC-1036 (1998) 9-18.

FISSION GAS RELEASE FROM FUEL PELLETS UNDER HIGH BURNUP

(Session 3)

Chairpersons

J.-E. LINDBÄCK

Sweden

M. VERWERFT

Belgium

ADVANCED PWR FUELS FOR HIGH BURNUP EXTENSION AND PCI CONSTRAINT ELIMINATION

Ch. DELAFOY¹, P. BLANPAIN¹, S. LANSIART²,
Ph. DEHAUDT³, G. CHIARELLI⁴, R. CASTELLI⁴

¹Framatome ANP Nuclear Fuel, Lyon

²Commissariat à l'Energie Atomique, Cadarache

³Commissariat à l'Energie Atomique, Saclay

⁴Cogema Recycling Business Unit, Bagnols-sur-Cèze

France

Abstract

The concern of the nuclear industry to improve economics while keeping satisfactory safety margins, leads to a general trend for extending the discharge burn-up of UO₂ and MOX fuels, with the use of high duty fuel management schemes. Depending on specific market needs, additional operational flexibility and manoeuvrability are also required to adapt reactor load to the grid demand at any time. Such requests translate into fuel products requirements as follows:

- Reduction of Fission Gas Release (FGR) under normal and accident conditions;
- Elimination of Pellet-Clad Interaction (PCI) constraints.

The FRAMATOME ANP's development of advanced UO₂ and MOX fuels, involving COGEMA and CEA laboratories is carried out based on feedback acquisition data regarding the behaviour of both products under irradiation and power ramp tests. As observed with MOX fuel, reduction of PCI consequences can be achieved by an enhancement of the fuel viscoplastic deformation under power transient situations. For FGR, the fuel microstructure characterised by its grain size and level of homogeneity has a direct influence on the phenomena.

- The addition of chromium oxide as a doping compound changes the microstructure of UO₂ by enlarging the grain size. The experimental results obtained show that this advanced doped fuel can endure very large power ramp conditions without failure in relation to an enhancement in the fuel creep rate and an increase in pellet cracking at the periphery. Furthermore, this fuel has a better fission gas retention capability up to high burn-ups compared to standard UO₂ fuel. For MOX fuel, the improvement of the MIMAS microstructure stems from the reduction of the PuO₂-rich particle size to decrease FGR.

Lead fuel rods with advanced UO₂ and MOX pellets are now under irradiation with M5™ cladding to acquire, up to high burn-up, all data required to demonstrate the ability of these fuels to satisfy customer needs for the future and to establish behaviour laws needed for their licensing.

1. INTRODUCTION

In order to improve the competitiveness of nuclear energy as a viable economic source of electrical power, constant enhancements in fuel performances are desired, while maintaining or improving safety margins. The major issues identified by utilities are [1]:

- Burn-up extension up to 70 GWd/t;
- Nuclear power plant operating flexibility and manoeuvrability with associated objectives of licensing higher duty fuel management schemes while keeping improvement of operating margins;
- Fuel reliability and integration of the back end of the fuel cycle.

In this context, the R&D conducted in France on PWR UO₂ and MOX fuels is performed on the basis of feedback acquisition data regarding the behaviour of both products under irradiation and power ramp tests. The development of UO₂ and MOX fuels directed to the investigation of innovative solutions to satisfy customer requests and expectations is mainly focussed on:

- ***Fission gas release at high burn-up.*** The feedback experience on irradiated fuels shows that fission gas release accelerates with burn-up most notably above 40 GWd/t. This evolution is mainly related to an increase in fuel temperature due to a decrease of the fuel thermal conductivity and to fuel microstructural changes. Rod puncture data indicated a somewhat higher fractional fission gas release for MOX fuel than for UO₂ fuel. That behaviour, for the most part, is due to the higher linear heat rates of the MOX rods at high burn-ups, but also to the specific MOX fuel material properties [2].

Higher fission gas retention within the fuels matrix, leads to lower end-of-life internal pressures in the fuel rods. These operational margins are required to raise fuel assembly burn-up limits up to 70 GWd/t. Thus higher fission gas retention in the fuel matrix will contribute to an improvement in the fuel behaviour under accident conditions for high burn-up safety criteria relating to LOCA and RIA. Finally, lower internal pressures in the fuel rods give improved conditions for the back end of the fuel cycle, notably to ensure the integrity of irradiated assemblies during handling and long-term interim storage.

- ***Pellet-clad interaction improvement.*** Fuel under irradiation should be able to withstand normal operating transients (load follow), as well as class 2 incident transients without failure due to pellet-clad interaction (PCI). To operate satisfactorily and to maintain appropriate safety margins, it has been necessary to introduce restraints that limit total flexibility in the reactors operation through the authorised parameters used for the core monitoring of French NPPs. Relaxing these restraints by improving the fuel behaviour would give an appropriate solution to PCI limitations and therefore comply with the objectives of greater manoeuvrability to adapt NPP to the grid demand at any time. It has been proved by ramp tests that MOX fuel behaves particularly well from the pellet-cladding interaction concern, and therefore from the power plant manoeuvrability standpoint [3]. This behaviour is attributed to a higher MOX pellet creep rate compared to the UO₂ pellet during power transients [4].

This paper gives an overview of the results acquired in the developments made on advanced PWR UO₂ and MOX fuels for high burn-up extension and PCI elimination constraints.

2. ADVANCED UO₂ FUEL DEVELOPMENT PROGRAM

2.1. Cr₂O₃-doped pellet characteristics

The fission gas release rate from fuel is at first mainly controlled by the Xe and Kr diffusion through the pellet grain. Therefore, enlarging the grain size of the UO₂ pellet could reduce the FGR because of the longer diffusion distance to the grain boundary, provided the diffusion rate coefficients are not enhanced. Changing the UO₂ pellet microstructure is also a concept known for modifying fuel plasticity [5].

To modify the microstructure of UO₂ by means of a viable industrial scale process, the addition of crystal growth accelerators was considered. Doping UO₂ with soluble metallic oxides, specially doping compounds of the corundum type has been widely studied [6]. In particular, it was demonstrated that chromium oxide (Cr₂O₃) can be partially dissolved in the UO₂ matrix under appropriate sintering conditions, leading to an increase in the diffusion coefficients that control the sintering mechanisms such as densification and grain growth. Figure 1 illustrates the microstructural change that can be achieved with the addition of a small amount of Cr₂O₃ to UO₂ after sintering in a slightly wet hydrogen atmosphere. Such an

atmosphere maintains the correct valence for the chromium ion and avoids its reduction to the metallic state. Compared to a grain size of 8 μm for standard UO_2 fuel, a value around 60 μm is reached for the Cr_2O_3 doped fuel pellet.

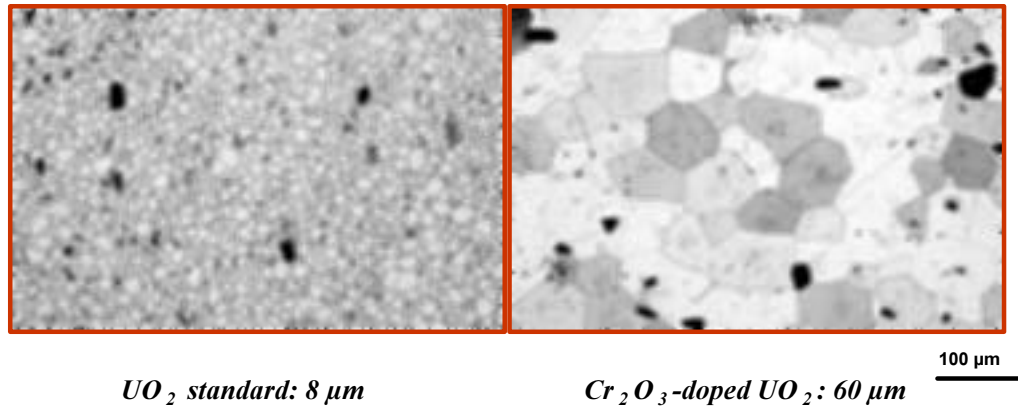


FIG. 1. Advanced UO_2 fuel microstructure.

To verify the improvement made to the viscoplastic properties, the advanced UO_2 fuels were thoroughly tested for creep and constant strain-rate. The tests were made by compression on a screw-type machine equipped with a suitably adapted furnace and under a controlled atmosphere to maintain the stoichiometry of the pellet samples during the tests [7]. All the mechanical tests performed on large grain UO_2 doped with Cr_2O_3 showed that doping improves the plasticity of the fuel while maintaining a good cohesion of the pellets.

Contrary to the inverse relationship generally observed between material creep properties and large grain microstructures, the impact of the crystal growth activator on the reorganisation of the lattice has a particularly beneficial effect on the fuel creep rate. With the addition of Cr_2O_3 , the deformation of UO_2 is rate-controlled by dislocations movements involving sliding and climb mechanisms with an activation energy close to the self-diffusion rate of uranium in UO_2 . As shown on Figure 2, the addition of Cr_2O_3 significantly increases the rate of deformation of UO_2 from the early stages after the loading. The improvement, measured in a large stress range (30 to 70 MPa), is all the more important than temperatures are elevated.

From constant strain-rate tests it was demonstrated that the addition of Cr_2O_3 provides a lower-stress resistance capability on the fuel, as illustrated in Figure 3. Standard UO_2 fuel is characterised by a stress peak, which generally appears when the initial density of mobile dislocations is not sufficient to allow deformation according to the imposed strain rate [8]. This behaviour can indicate that the dislocations are blocked by grain boundaries in undoped UO_2 so that a certain amount of stress is required to initiate the deformation [7]. For Cr_2O_3 doped fuel, the matrix is hardened by the formation of a $(\text{U-Cr})\text{O}_x$ type solid solution and of micrometer or nanometer scale inclusions formed by a small fraction of Cr_2O_3 that remain undissolved after sintering and precipitate during cooling. However, this hardening effect is largely compensated by the increase of the grain size, which promotes the dislocation movements in the fuel matrix [9]. Thus, the addition of Cr_2O_3 in UO_2 removes the peak and reduces the stress required to initiate the deformation.

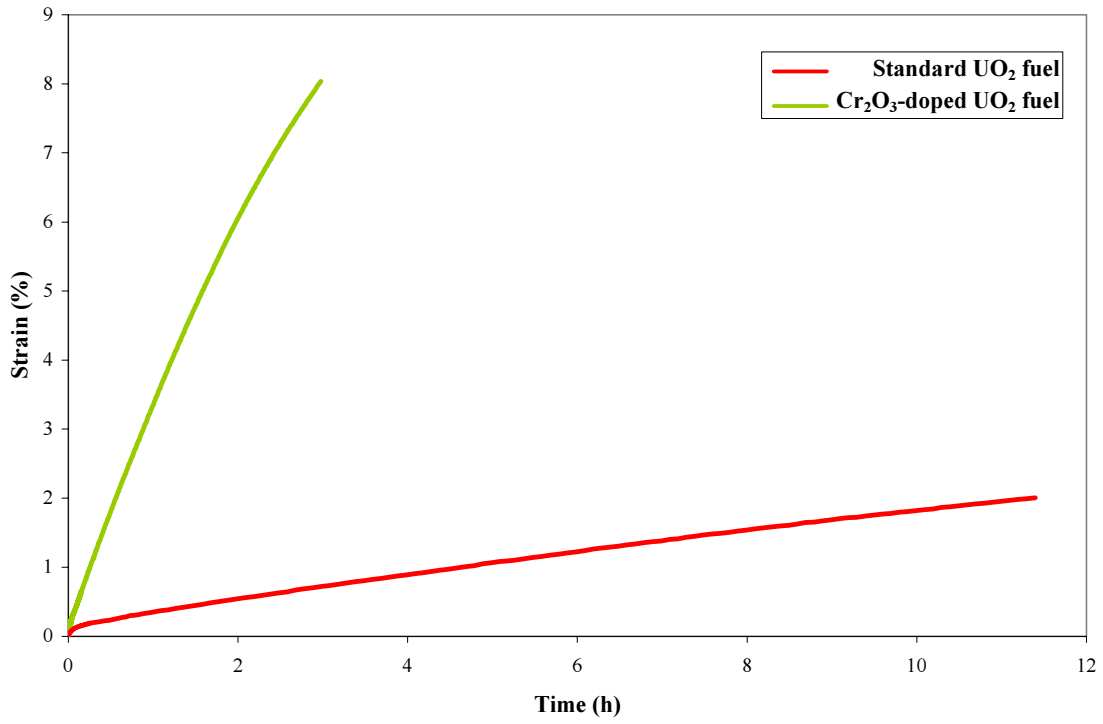


FIG. 2. Effect of Cr₂O₃ addition on fuel creep behaviour at 1500°C and 45 Mpa.

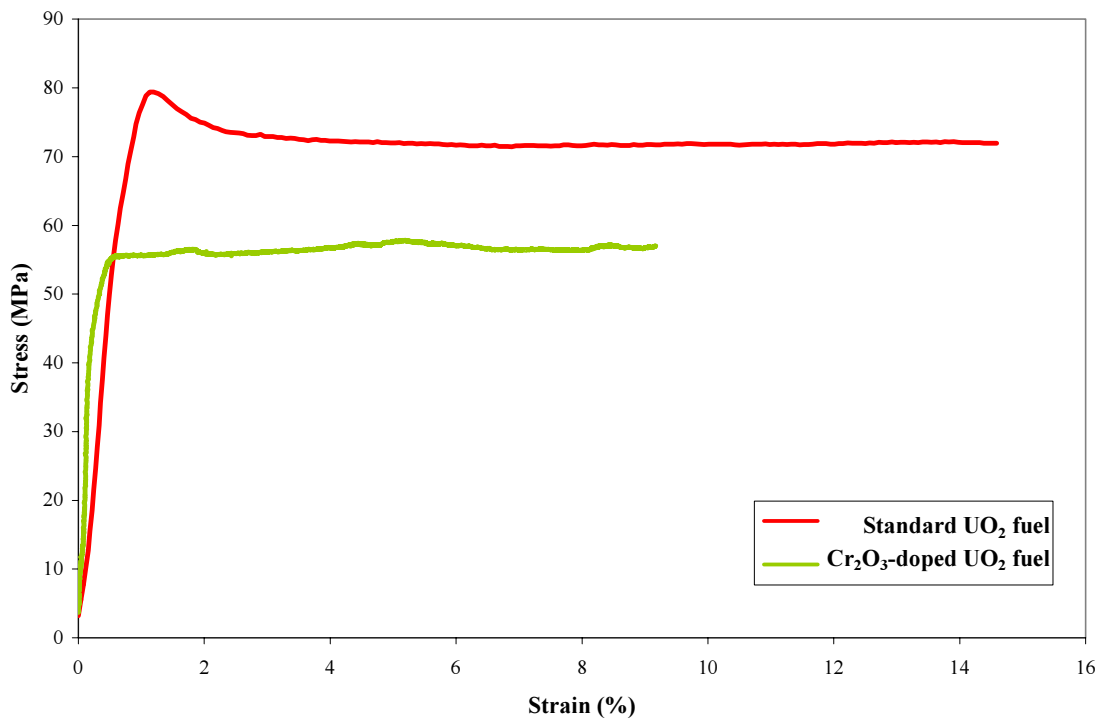


FIG. 3. Tests with constant applied strain rate ($\dot{\epsilon} = 9\%/h$) at 1500°C.

2.2. Irradiation experience acquired with Cr₂O₃-doped fuel

The CONCERTO program was launched in 1997 to verify the behaviour of the Cr₂O₃-doped fuel under PWR conditions up to a rod burn up around 60 GWd/tU. For this campaign, four 17×17 AFA2G assemblies were loaded with 36 lead rods, either full length or segmented rod types, all equipped with low-tin Zircaloy 4 cladding. The undoped and Cr₂O₃-doped pellets involved in the CONCERTO program were manufactured by FBFC using a dry route UO₂ powder. The two pellet batches were characterised by a sintered density of 95 % T.D and no detected open porosity. The fast grain growth that occurred during sintering in doped fuels (see § 2.1.) led to the sweeping of very fine porosity and then to a reduction in the density change after a 1700 °C-24 hours resintering test. As a result, the densification value for Cr₂O₃-doped UO₂ fuel was 0.11% T.D, while for standard UO₂ fuel the densification value was 0.86 % T.D.

After two irradiation cycles, discharged fuel rods were subjected to non-destructive examinations in the CEA hot cell laboratories before power ramp testing.

The visual inspection, as well as the Eddy Current tests, did not reveal any cladding defects. The global fuel rod elongation was equal to 0.30 % with no significant difference between rods with undoped or doped pellets. Diametral measurements showed primary ridges with an average height consistent with values for UO₂-Zy4 fuel rods after two annual irradiation cycles. The average cladding deformation of the doped rods was however slightly greater than the reference undoped UO₂ rods. It can be inferred that the doped fuel exhibits a lower in-reactor densification in agreement with the densification measurements made during manufacturing.

2.3. Ramp testing of Cr₂O₃-doped UO₂ fuel segments

The rod segments (rodlets) loaded with Cr₂O₃-doped UO₂ fuel were ramped in 2001 in the ISABELLE 1 loop of the OSIRIS experimental reactor reproducing PWR temperature and pressure conditions. The power level in the test is controlled by the positioning of the irradiation loop relative to the core. Ramping is performed by driving the loop rapidly nearby the core and any fuel rod failures are detected through the monitoring of the primary coolant activity. The ramp test scheme included a conditioning step around 200 W/cm in agreement with the average power undergone by the segments during their second irradiation cycle. A typical power ramp rate of 100 W/cm/min was then applied in order to simulate a PWR Class 2 transient. The terminal power levels were defined with respect to the current UO₂ – Zy-4 PCI threshold [10]. At the end of this test no failures were detected. Figures 4 and 5 clearly show that the advanced Cr₂O₃ doped fuel rods bring very significant gains compared to the current PCI threshold.

After the ramp tests, detailed PIEs on the two rodlets were performed in the CEA hot cell laboratories. Eddy Current testing did not reveal any defects on the cladding tubes. The diametral profilometries showed a clad diameter deformation consistent with the hold time at high power. One of the main findings is that existing primary ridges did not grow as a result of the ramp test, and even shrank, in the central part of the rod, according to secondary ridges growth. The comparison between neutron radiographs of the two segments before and after the ramps revealed that the pellet dishes are completely filled along the main part of the fissile column where the local power was above 430 W/cm.

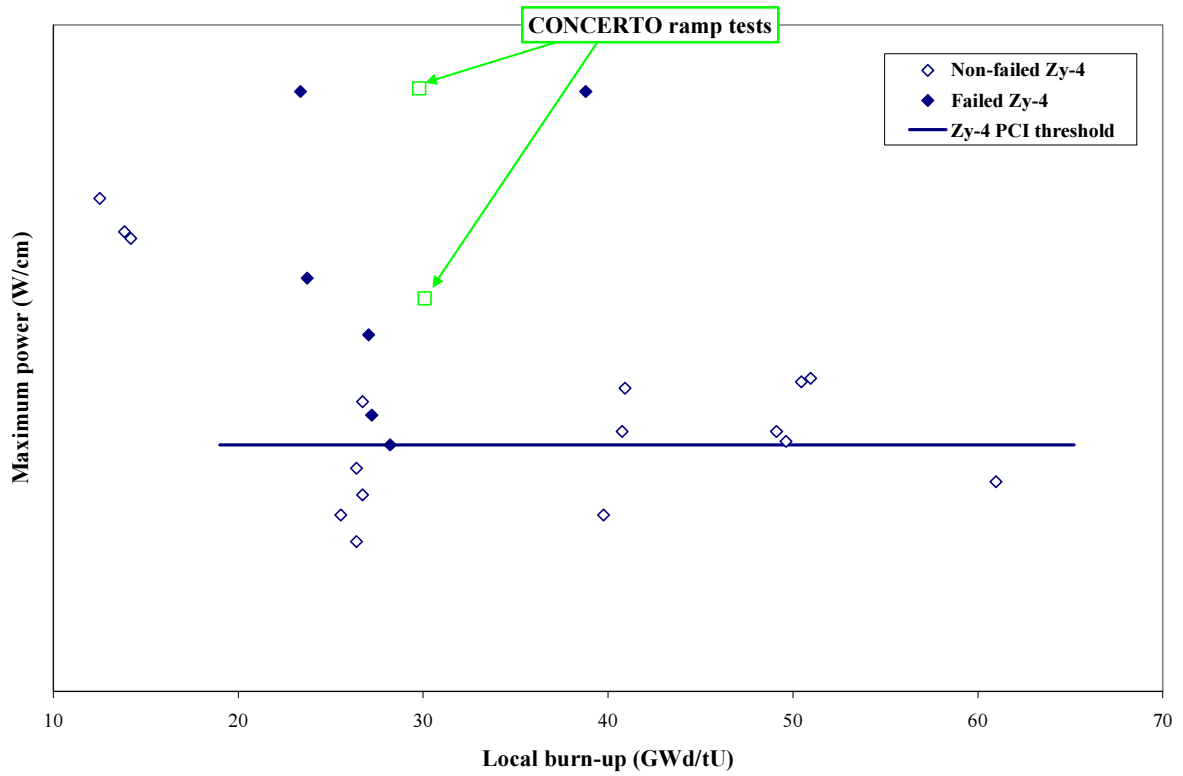


FIG. 4. UO_2 -Zy4 PCI threshold – Maximum power versus local burn-up.

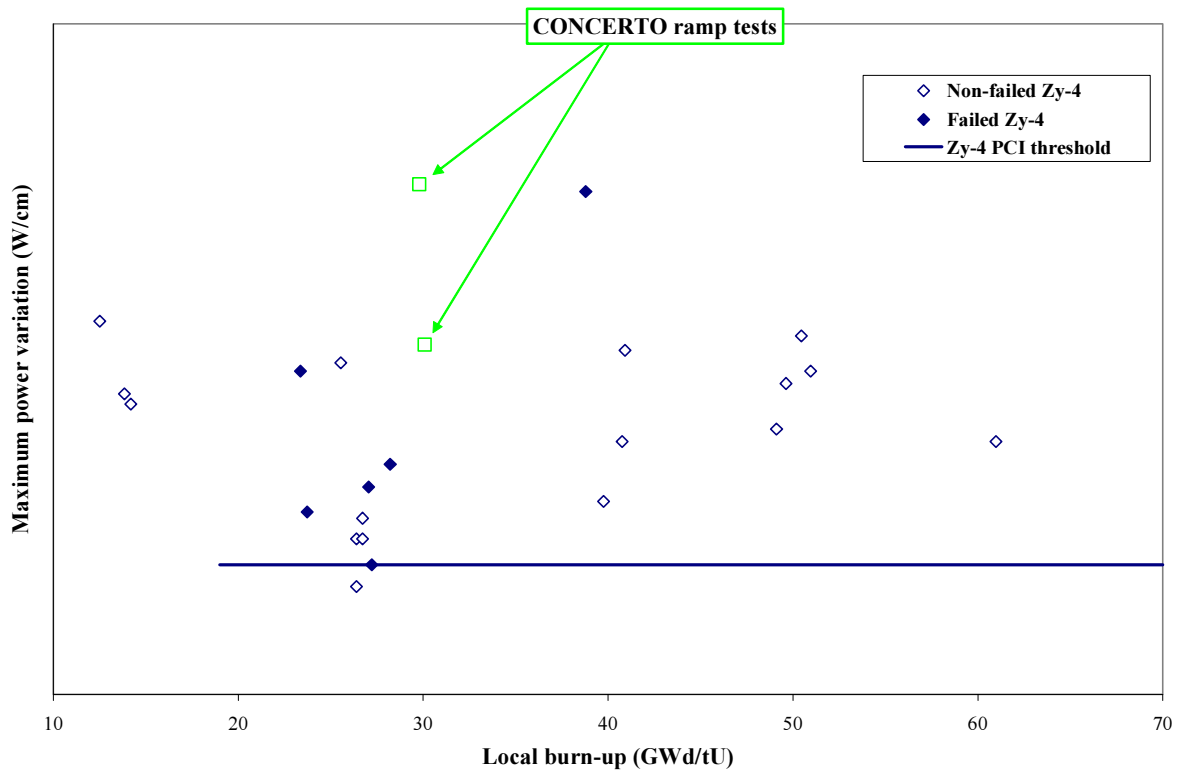


FIG. 5. UO_2 -Zy4 PCI threshold – Maximum power variation versus local burn-up.

Optical macrographs of the ramped fuel showed interesting features. Figure 6 presents radial and longitudinal sections in the high power region. On the transverse cross section, numerous radial fine cracks are observed at the pellet periphery, which stop at a thick circumferential crack. This latter crack, probably generated during cooling, seems magnified by the important decohesion of the large-grain UO_2 microstructure. In the central part of the fuel, only four or five main fragments, nearly stuck together, are visible. In the longitudinal cross section, a network of four main transverse cracks is observed. However, the pellet centre appears restructured probably due to crack healing by intensive creep at high temperature. This phenomenon is particularly marked at inter-pellet planes where the flow of material has led to complete filling of the pellet dishes. The voids remaining at the circumferential interfaces are due to the lower temperature at the periphery where the creep rate is lower. This global flow of fuel to the centre of the pellet leads to the applied load on the cladding being reduced, in particular at inter-pellet planes, where failures, when occurring, are generally initiated during power ramp testing.

According to these observations performed after 12 hours holding time, it can be presumed that the better behaviour of the Cr_2O_3 doped fuel results from different and interacting phenomena occurring during the transient or during the first minutes of the maximum power level namely an enhanced creep rate combined with an increase of the cracking at the pellet periphery. Both effects have a favourable influence on the stress distribution in the fuel with a more homogenous loading of the cladding during transient conditions at the moment of maximum risk of failure.

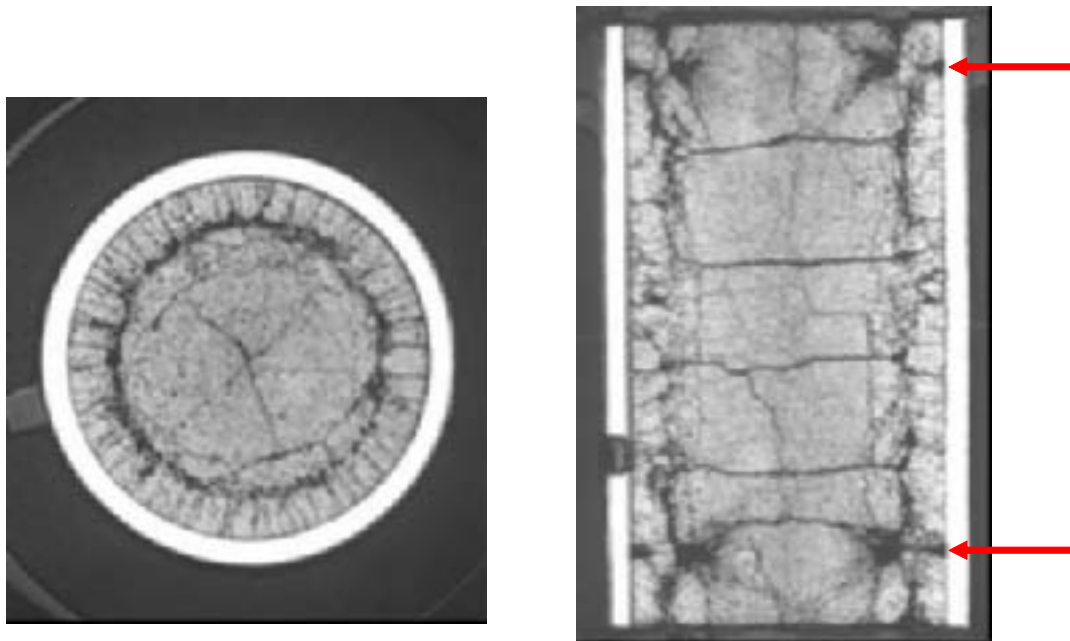


FIG. 6. Transverse and longitudinal sections from Cr_2O_3 -doped fuel after ramp testing (the red arrows indicate inter-pellet planes).

The large secondary ridges observed on the CONCERTO segments are considered to be due to the very high powers and the 12 hour holding times that have induced a significant gaseous swelling at the pellet mid-plane. Nevertheless, the analysis of the cladding deformation in the low power zones of the CONCERTO segments shows that the secondary ridge development

is similar while the global increase of cladding diameter is greater than that of standard UO_2 fuel at an equivalent power.

However, the rod puncturing tests made after the two CONCERTO transients indicated that fission gas release of these fuel rods was low in spite of the bubble swelling due to high power levels. This may indicate that the Cr_2O_3 doped UO_2 fuel improves the fission gas retention capability. PIE shows that the large grain microstructure of the Cr_2O_3 doped fuel reduces the amount of fission gases accumulated in the grain boundaries. This trend has been also observed with the TANOX analytical experiment [11]. The TANOX device located in the SILOE reactor was designed to rapidly achieve significant burn-ups in fuels at relatively low temperatures so as to avoid fission gas release.

During the irradiation up to 9 GWd/t, the instrumented fuel rods allowed the measurement on-line of the central temperatures and no degradation of the thermal conductivity was observed for Cr_2O_3 doped fuel in comparison with the reference UO_2 fuel. The thermal annealing tests performed after irradiation at 1700 °C up to 5 hours showed a reduction by a factor of 3 on fission gas release for Cr_2O_3 doped fuel compared to standard UO_2 fuel. The improved better fission gas retention capability of the doped fuel was directly attributed to the enlargement of the grain size. Also, the destructive examinations revealed a better intragranular fission gas bubbles linkage on micrometer or nanometer scale inclusions formed by some Cr_2O_3 that remained undissolved after sintering and precipitated during cooling.

This set of positive results was followed by verification at higher burn-up (65 GWd/tU) with the TANOXOS experiment. This irradiation campaign performed in the OSIRIS reactor in a similar manner to the TANOX program, has confirmed that the Cr_2O_3 addition in the UO_2 matrix does not result in any additional fuel thermal conductivity degradation. Thermal annealing tests and microstructural examinations after the TANOXOS irradiation campaign are underway. First results confirm the fission gas retention capability of the Cr_2O_3 doped fuel at high burn-up.

Finally, post-ramp gamma-scans highlighted a significant migration of caesium and iodine to inter-pellet planes due to the high temperature during ramps. Nevertheless, these corrosive fission products did not induce the failure of the cladding tubes thanks to the favourable mechanical conditions.

3. MOX FUEL DEVELOPMENT PROGRAM

The operational performance of the MOX fuel rods and assemblies has been assessed by many number of inspection and measurement campaigns performed in reactor spent fuel pools, in hot cell laboratories and but also in analytical programs [2]. The highlights of the important MOX European experience feedback are:

- Any technical problems resulting from the MOX fuel have been encountered;
- The reliability of MOX assemblies is as good as UO_2 fuel.

Since the use of MOX fuel in French PWRs has now reached its industrial maturity, the main challenge remains to achieve the same standards as UO_2 fuel performance in terms of discharge burn-up and fuel management. Initially, the objective is to achieve parity between UO_2 and MOX fuels at 52 GWd/tM in 2004 by means of a management strategy of $\frac{1}{4}$ core refuelling for the annual cycles of both fuel types in EDF 900 MWe units. The next step should be the development of a MOX fuel capable of a discharge burn-up of ~ 60 GWd/tM or

more. In support of this high burn-up target, it is desirable to improve the current fuel product technology.

In addition to the design improvements of the fuel rod and assembly structure, R&D activities are similar to those developed for UO_2 , with particular emphasis on the minimization of fission gas release that today appears to be the main limitation to achieving very high burn-ups. At the same time, checks must be carried out to ensure that the other MOX fuel properties (mechanical creep properties, etc) are not unfavourably changed with regard to overall behaviour, and are satisfactory for high burn-up applications (pellet-clad interaction, physical-chemical and thermal properties). The R&D is focussed as a matter of priority, on the current MOX-MIMAS product, but in the longer term perspective, also aims at developing fuels with improved microstructures. The existence of a thermal threshold beyond which FGR is accelerated, is confirmed for MOX fuel as it has been for UO_2 but with a higher level of release. Studies are now under way to examine thoroughly the links between the heterogeneity of the MOX microstructure (size and Pu content of $(\text{U,Pu})\text{O}_2$ particles, microstructure of the UO_2 matrix) and the mechanisms and kinetics of FGR in normal and transient conditions.

To this end, two types of improvements are being studied:

- A reduction in the size of the PuO_2 rich-particles. Today, it is thought that this parameter may influence the retention and/or the release of fission gases, although this effect has not yet been precisely quantified.

For this phase, the current MIMAS process, used in particular in the COGEMA MELOX factory at Marcoule, has not been significantly modified. The desired objective was reached by means of an optimisation of the sieving operation of the primary blend. As illustrated in Figure 7, in the current MOX MIMAS fuel, about 25% of the total plutonium content of the pellet is contained in the Pu-rich particles above $30\ \mu\text{m}$ size. However, it was reduced to less than 10 % in the optimised microstructure. Lead fuel rods, using M5™ cladding, are currently being irradiated in an EDF reactor. The improvement in fission gas retention will be evaluated by PIE in 2005.

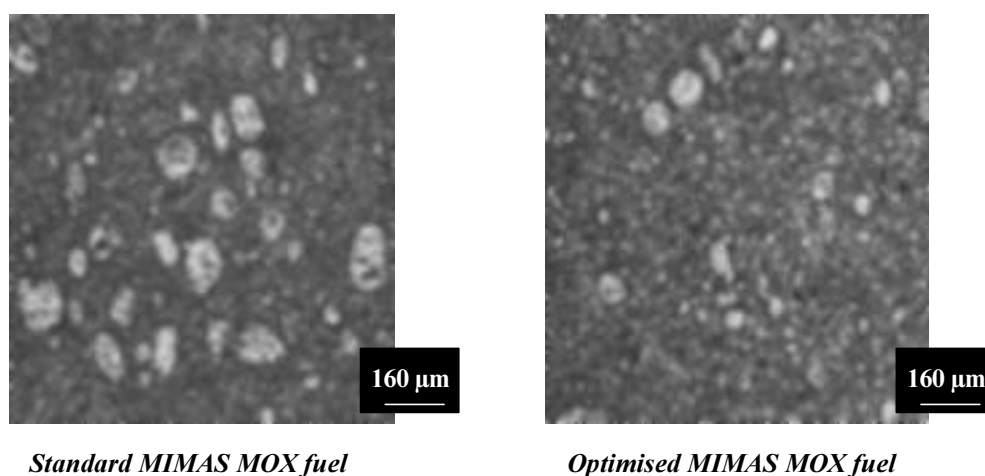


FIG. 7. Optimization of the MIMAS MOX fuel microstructure.

- An increase in the fuel matrix grain size, while keeping a smaller agglomerate size. Instrumented fuel rodlets are being irradiated in experimental reactors with different potential solutions in order to investigate:
 - The role played by the microstructure in the behaviour of fission gases with the objective of determining whether the agglomerate size and its Pu content is a more or less important parameter in comparison to microstructures with homogeneous and heterogeneous plutonium distribution;
 - The use of additives in the form of different oxides, added in small quantities (in the range of 500 – 2000 ppm) to oxide (U,Pu)O₂. In the case of UO₂, it has been proved that such additions, and in particular chromium oxide, can reduce the release of fission gases, both by enlarging the grain and by causing the gases to diffuse more slowly.

Improved microstructures have already been obtained at a laboratory scale. Transposition of the technology and tests to an industrial line is now contemplated as well as the launching of experimental irradiations.

4. CONCLUSION

The need for enhanced in-reactor performance has led to the development of advanced UO₂ and MOX fuels aiming to eliminate the pellet cladding interaction problem and to reduce the fission gas release at high burn-up. As observed with MOX fuel, reduction of PCI consequences can be achieved by an enhancement of the fuel viscoplastic deformation under power transient situations. For fission gas release, the fuel microstructure characterised by its grain size and level of homogeneity has a direct influence on the phenomenon.

The CONCERTO program, which is the outcome of a development process initiated between the CEA research laboratories and the French industrial operators, has led to the development of an advanced microstructure for UO₂ fuel. This fuel is characterised by the addition of chromium oxide which gives rise to a large grain microstructure with better viscoplastic properties. After two annual irradiation cycles in a PWR reactor, the large grain microstructure shows significant improvement with respect to PCI performance. The extensive creep of the doped fuel into the pellet dishes and the cracking at the pellet periphery are assumed to be mechanisms responsible for the enhanced PCI resistance observed in power ramp testing. Moreover, rod punctures after ramps indicated a higher fission gas retention capability of the Cr₂O₃ doped fuel. This trend has to be confirmed at high burn-up with post-irradiation examinations of CONCERTO fuel rods after four and five irradiation cycles. The program achieved fuel rod burn-ups of ~60 GWd/tU in 2003. In the meantime, the completion of the destructive examinations after the ramp tests will help to identify all the mechanisms involved in improved PCI behaviour.

The very promising results of the CONCERTO program led Framatome-ANP, in cooperation with EDF and the CEA, to launch in mid-2001 the irradiation of lead fuel rods with Cr₂O₃ doped UO₂ pellets loaded in M5™ cladding tubes. This irradiation campaign, performed in an EDF 1300 MWe reactor, aims to acquire all the data required to demonstrate the ability of this fuel to be a high burn-up PCI remedy in order to satisfy future customer needs for improved fuel management and greater power plant operating flexibility.

With an increasing experience feedback, the use of MOX fuel in the European LWRs has now reached industrial maturity. In addition to the constant accumulation of data from surveillance programs, an extensive R&D program is continuing to better understand, model and validate

high burn-up fuel behaviour under nominal and transients conditions. In France, beyond the objective of achieving parity between UO_2 and MOX at burn-up of 52 GWd/tM, programs are performed with the aim to further improve the performance of the MOX fuel product. The development is essentially focused on the reduction of fission gas release, which constitutes the major obstacle in reaching very high burn-ups. To this end, optimisation of the current MIMAS microstructure has been already achieved. For the next ten years, the development of advanced microstructures is viewed for a MOX fuel capable of reaching assembly burn-ups of at least 60 GWd/tM.

ACKNOWLEDGEMENTS

The French R&D work is carried out with the cooperation of Electricité de France (EdF). The authors wish to acknowledge the support and the aid of the many persons who are participating in these programs.

REFERENCES

- [1] WEST, J.P. et al., “Challenges for the nuclear fuel. A utility perspective”, Light Water Reactor Fuel Performance, (Proc. ANS Int. Top. Mtg. Park City, 2000), American Nuclear Society, La Grange Park, IL (2000) 4-14.
- [2] BLANPAIN, P. et al., “MOX Fuel: A common experience”. Annual Mtg. Nuclear Technology, 2002, May 14–16, Stuttgart, Germany, GNS, (2002) 154.
- [3] GUERIN, Y. et al. “Microstructure evolution and in-reactor behaviour of MOX fuel”. Light Water Reactor Fuel Performance, (Proc. ANS Int. Top. Mtg. Park City, 2000), American Nuclear Society, La Grange Park, IL (2000) 706–719.
- [4] NONON, Ch. et al. “Impact of fuel microstructure on PCI behaviour”. Improved Pellet Materials and Designs, (Proc. IAEA Tech. Comm. Mtg. Brussels, 2003), IAEA, Vienna (in press).
- [5] DEHAUDT, Ph, CHOTARD, A., “Développement de combustibles avancés pour les REP” (Development of advanced fuels for PWRs), *Revue Générale Nucléaire*, **3**, (1997), 43.
- [6] DEHAUDT, Ph. et al., “New UO_2 fuel studies”. Advances in Pellet Technology for Improved Performance at High Burn up, (Proc. IAEA Tech. Comm. Mtg. Tokyo, 1996), IAEA-TECDOC-1036, Vienna (1998), 27–38.
- [7] DHERBEY, F. et al., “Elevated temperature creep of polycrystalline uranium dioxide: from microscopic mechanisms to macroscopic behaviour”, *Acta Materiala*, **50**, (2002), 1495–1505.
- [8] GUERIN, Y., “Etude par compression à hautes températures de la déformation plastique du bioxyde et du monocarbure d’uranium”, (Study of plastic deformation of uranium dioxide and monocarbide by compression) PhD Thesis, Université Claude Bernard, Lyon, France, (1973).
- [9] DUGUAY, C. et al., “High temperature mechanical tests performed on doped fuel”, Advances in Pellet Technology for Improved Performance at High Burn up, (Proc. IAEA Tech. Comm. Mtg. Tokyo, 1996), IAEA TECDOC-1036, Vienna (1998), 409–419.
- [10] BLANPAIN, P. MERMAZ, F., “PCI criteria and methodology in PWRs”, Annual Mtg. Nuclear Technology, 2000, February 29–March 01, Karlsruhe, Germany, (2000), GNS, CD-ROM.
- [11] VALIN, S. et al., “Synthesis of the advanced UO_2 microstructures program in the TANOX device”. Improved Pellet Materials and Designs, (Proc. IAEA Tech. Comm. Mtg. Brussels, 2003), IAEA, Vienna (in press).

SYNTHESIS OF THE RESULTS OBTAINED ON THE ADVANCED UO₂ MICROSTRUCTURES IRRADIATED IN THE TANOX DEVICE

S. VALIN¹, L. CAILLOT¹, Ph. DEHAUDT², Y. GUERIN¹,
A. MOCELLIN¹, C. DELAFOY³, A. CHOTARD³

¹ Commissariat à l'Energie Atomique, Cadarache

² Commissariat à l'Energie Atomique, Saclay

³ Framatome ANP, Lyon

France

Abstract

In order to achieve higher burn-ups in PWR, new fuels are required with improved gas retention capacities. In this context, the Advanced UO₂ Microstructures program, first presented in Tokyo (TCM 1996), aimed at fabricating, irradiating and testing new UO₂ fuels intended for high-burnup and for PCMI effect reduction. A large number of UO₂ fuels were fabricated, which allowed to evaluate the influence of numerous parameters: grain size, stoichiometry, additives with various concentration and chemical form. Small fuel rods were irradiated in the TANOX device, in the Siloé reactor, to a burn-up of about 10 GWd/t_U. The temperature at the centre of the annular pellets was controlled and maintained under 700°C in order to avoid activation of thermal gas release. After irradiation, the rod was punctured; the clad was cut to take the pellets out. The fission gas retention capacities of the different kinds of fuels were assessed by post-irradiation annealing tests. The anneals were performed in a high frequency furnace at 1700°C; ⁸⁵Kr released from the fuel was measured by gamma spectrometry. Micrographic examinations were performed on each kind of pellets before and after annealing tests. The results show that the fuels with best fission gas retention are characterized by both a large grain size (over 50 µm) and intragranular precipitates or defects, which are favourable to bubble nucleation and pinning. This type of microstructure can be achieved by adding Cr₂O₃ at a percentage over the solubility limit. Cr₂O₃ then stimulates grain growth and also forms oxide precipitates. Gas retention can be even larger with an improved intergranular retention capacity, which is obtained by adding SiO₂ to Cr₂O₃. Hyperstoichiometric (UO_{2,01} or UO_{2,02}) large grain fuel also showed an improved fission gas retention capacity. On the basis of these results, several microstructures were selected for a further study of gas retention at high burn-up (65 GWd/t_U). A new irradiation program of doped UO₂ fuels started in the TANOXOS device, in the Osiris reactor.

1. INTRODUCTION

As fission gas release in PWR fuel rods increases with burn-up, new kinds of fuels are required with improved fission gas retention capacities. The program on advanced UO₂ microstructures has been launched by the Commissariat à l'Energie Atomique (CEA) with the objective of finding new microstructures, which can withstand high burn-ups (70–80 GWd/t_U) with better fission gas retention. The PCMI effect is also taken into account by selecting the microstructures with the best viscoplastic properties.

The advanced UO₂ microstructures program allowed first to define new microstructures which can achieve improved gas retention and viscoplastic properties, then to fabricate the fuels, to irradiate them in a special analytical irradiation device (TANOX) and to test the fission gas retention capacity by means of post-irradiation annealing tests.

The TANOX irradiation device was described in a paper [1] presented at the previous Technical Committee Meeting held in Tokyo in 1996. First results were then also given about UO₂, UO_{2,01} and UO_{2,02} fission gas retention during high temperature anneals. The present

paper gives a synthesis of the results obtained with various kinds of microstructures characterized by different grain size, stoichiometry, dopants...

2. DESCRIPTION OF THE ADVANCED UO₂ MICROSTRUCTURES

2.1. Characteristics of the improved UO₂ microstructures

The required characteristics for improved UO₂ fuel microstructures are:

- **a large grain size:** in order to increase path length for fission gas diffusion from grain interiors to boundaries,
- **precipitates:** which are favourable to gas bubble nucleation and pinning,
- **a glassy intergranular phase:** in order to improve grain boundary sliding under stress deformation.

Fabrication studies [2,3,4,5] were performed in order to define the UO₂ microstructures, which achieve these characteristics. They showed that the use of a corundum type oxide (Al₂O₃, Ti₂O₃, V₂O₃, Cr₂O₃) as a dopant and grain growth activator is efficient to obtain a large grain size. By adding chromium oxide (Cr₂O₃) at a percentage over its solubility limit in UO₂, a microstructure with both a large grain size and chromium oxide precipitates was obtained. Precipitates could also be formed by adding magnesium oxide (MgO) to UO₂. A glassy intergranular phase was obtained by adding silica (SiO₂) to a corundum type oxide.

Furthermore, compression tests performed on large grain sized (doped or undoped) fuels showed that their creep behaviour was improved at high stresses in comparison to standard UO₂ fuel [6,7].

2.2. Description of the UO₂ fuels

On the basis on these results, many types of advanced doped UO₂ fuels were fabricated. Some others were also fabricated in order to study the effect of one single or two parameters (such as grain size or stoichiometry) on the fuel release behaviour. Micrographic examinations of the fuels were performed after fabrication.

The references and characteristics of the fuels are given in Table I.

For the fabrication of the T1-4b, T1-5a, T1-5b, T1-6a and T1-6b fuels, Cr₂O₃ was used to enhance grain growth. With 0.07 % Cr₂O₃, a grain size of about 20-25 μm is reached; Cr₂O₃ forms a substitutional solid solution with UO₂ and promotes grain growth. When exceeding the solubility limit of chromium oxide in uranium dioxide (about 0.07 %, under these sintering conditions), a larger grain size is obtained: about 60 to 65 μm for T1-5b and T1-6b. The grain growth is then believed to be linked to a second mechanism, i.e. the formation of an eutectic between Cr and Cr₂O₃ with a composition close to CrO, and the dissolution and diffusion of uranium in the liquid phase [2,3]. Excess of insoluble Cr₂O₃ forms second phase precipitates.

A reducing anneal was performed on T1-6a and T1-6b fuels after sintering to reduce the chromium oxide of the precipitates into metallic chromium (Table I). This metal may be useful to fix the oxygen, which is liberated by fission, and so to control the oxygen potential of the fuel.

In the T1-7a to T1-9b fuels (Table I), other additives than Cr₂O₃ were used: MgO and ZrO₂ with the objective of forming precipitates, SiO₂ and Al₂O₃ in order to create a glassy intergranular phase, which could be observed on the micrographs. The T1-7a and T1-7b fuels have a rather low density, with large pores in the ZrO₂ doped fuel.

Silica is thought to impede grain growth in Cr₂O₃ doped UO₂ if a too large percentage is added. This could be why the grain size of the T1-8a to T1-9b fuels, which contain 0.1 % to 0.2 % SiO₂, have a smaller grain size than the other fuels doped with 0.2 % Cr₂O₃.

Table I. Characteristics of the fuels

Fuel reference	Fuel type ^a	Grain size (centre of the pellets)	Density	Sintering gas and temperature	Post-sintering anneal ^b
T1-1a	Standard UO ₂	13 μm	10.47	H ₂ – 1800°C	/
T1-1b	Large-grained UO ₂	50 μm	10.61	H ₂ – 1800°C	A
T1-2a	UO _{2.01}	14 μm	10.55	H ₂ – 1800°C	B
T1-2b	Large-grained UO _{2.01}	50 μm	10.60	H ₂ – 1800°C	A + B
T1-3a	UO _{2.02}	13 μm	10.56	H ₂ – 1800°C	B
T1-3b	Large-grained UO _{2.02}	50 μm	10.61	H ₂ – 1800°C	A + B
T1-4a	Same T1-1a and T1-1b				
T1-4b	UO ₂ + 0.2 % Cr ₂ O ₃ + 0.05 % SiO ₂	57 μm	10.60	H ₂ + 1,7 % H ₂ O – 1700°C	/
T1-5a	UO ₂ + 0.07 % Cr ₂ O ₃	25 μm	10.61	H ₂ + 1,7 % H ₂ O – 1700°C	/
T1-5b	UO ₂ + 0.2 % Cr ₂ O ₃	62 μm	10.60	H ₂ + 1,7 % H ₂ O – 1700°C	/
T1-6a	UO ₂ + 0.07 % Cr ₂ O ₃ (reduced)	19 μm	10.65	H ₂ + 1,7 % H ₂ O – 1700°C	C
T1-6b	UO ₂ + 0.2 % Cr ₂ O ₃ (reduced)	63 μm	10.60	H ₂ + 1,7 % H ₂ O – 1700°C	C
T1-7a	UO ₂ + 1 % MgO	6 μm	10.02	CO ₂ – 1250°C	D
T1-7b	UO ₂ + 0.8 % ZrO ₂	30 μm	9.96	CO ₂ – 1250°C	D
T1-8a	UO ₂ + 0.2 % Cr ₂ O ₃ (reduced) + 0.15 % SiO ₂ + 0.8 % ZrO ₂	34 μm	10.60	H ₂ + 1,7 % H ₂ O – 1700°C	C
T1-8b	UO ₂ + 0.2 % Cr ₂ O ₃ (reduced) + 0.15 % SiO ₂	38 μm	10.55	H ₂ + 1,7 % H ₂ O – 1610°C	C
T1-9a	UO ₂ + 0.2 % Cr ₂ O ₃ (reduced) + 0.2 % SiO ₂ + 0.01 % Al ₂ O ₃	34 μm	10.52	H ₂ + 1,7 % H ₂ O – 1610°C	C
T1-9b	UO ₂ + 0.2 % Cr ₂ O ₃ (reduced) + 0.1 % SiO ₂ + 0.01 % Al ₂ O ₃	31 μm	10.48	H ₂ + 1,7 % H ₂ O – 1610°C	C

^a All the compositions are given for pre-sintered fuels.

^bA: 100 h at 1800°C under H₂ + 1,7 % H₂O to increase the grain size.

B: oxidizing anneal at 700°C under He + 100 ppm O₂ to reach hyperstoichiometry.

C: anneal performed to reduce the chromium oxide precipitates into metallic chromium: 5 h at 1400°C under H₂.

D: reducing anneal to bring the fuel back to stoichiometry after the oxidizing sintering under CO₂: 4 h at 1100°C under H₂.

3. IRRADIATION IN THE TANOX DEVICE

3.1. The fuel rods

9 fuel rods were fabricated (T1-x, x from 1 to 9). Each of them contained 20 pellets, 10 of them made from the “T1-xa” fuel (Table I) and placed at the bottom of the fuel stack, and the 10 others from the “T1-xb” fuel and placed at the top. The height of the pellets is about 5 mm and the diameter is 4.9 mm. The 10 pellets in the top half of the stack have a central hole (diameter: 1.3 mm) allowing the introduction of a centre-line thermocouple. The cladding is made of stainless steel, with sometimes a platinum internal coating intended to maintain the hyperstoichiometry of the fuel (rods T1-2 and T1-3). Each fuel rod is placed in an overcladding made of aluminium alloy, which isolates it from the primary coolant of the reactor. The pellet – cladding and cladding – overcladding gaps are filled with helium; their widths are reduced (about 15 μm and 10 μm respectively) to improve heat transfers. Such a design allows high fission densities to be reached in the fuel while keeping the fuel temperature at a rather low level.

3.2. The TANOX device

The TANOX device is located in the pool, at the periphery of the Siloé reactor core (Grenoble). It can be used to irradiate 6 rods simultaneously (Fig. 1). The rods in their overcladdings are placed in a barrel which allows their overall rotation or permutation to homogenize the burn-ups of the rods. They can also be loaded and unloaded independently.

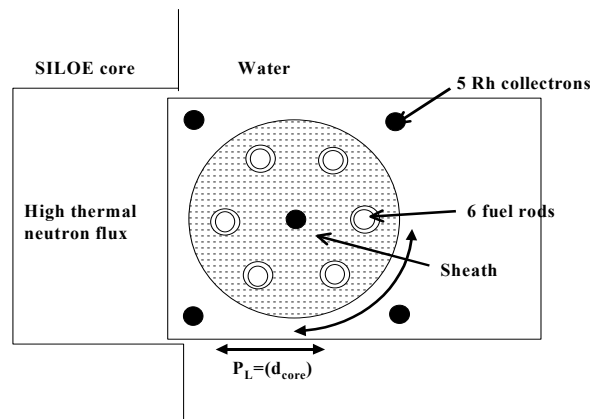


FIG. 1. Schematic view of the TANOX device (above view).

The device is fixed to a displacement system; so its distance to the reactor core can be modified to adjust the irradiation linear power. Neutron flux is measured by collectrons.

3.3. Irradiation conditions

The irradiation is controlled by the temperature measurements at the centre of the annular pellets of each rod which does not exceed 700°C. The burn-up of the fuels at the end of the irradiation is about 10 GWd/t_U (PWR equivalent value, i.e. given for an energy per fission of 200 MeV). A quantitative gamma spectrometry analysis was performed on each rod to confirm the fuel burn-up; the results are given in Table II.

These irradiation conditions (low burn-up and temperature) have been chosen to accumulate fission products in the fuel without activating thermal diffusion mechanisms (in view of the post-irradiation annealing experiments).

After irradiation, six of the fuel rods were punctured and their gas was analysed. The ^{85}Kr quantification showed that very little gas was released during irradiation as expected (maximum of 0.12 % for T1-7: Table II).

Table II. Fuel rods burn-ups confirmed by gamma spectrometry and fission gas release during irradiation

	T1-1	T1-2	T1-3	T1-4	T1-5	T1-6	T1-7	T1-8	T1-9
Burn-up (PWR equivalent value, MWd/t_U)	9091	9091	8757	8910	9226	9078	8736	9755	9092
^{85}Kr release during irradiation	0.07 %	0.08%	0.09%	/	/	/	0.12 %	0.06 %	0.1 %

3.4. Thermal analysis

The thermal behaviour of the fuels was studied by analysing the evolution of the central temperature of the pellets, measured by the thermocouple, as a function of the fissile power. This study is described in a previous paper [1]. It shows that the hyper-stoichiometric $\text{UO}_{2.02}$ fuel has a lower thermal conductivity compared to UO_2 as expected. The behaviour of the $\text{UO}_{2.01}$ fuel and of the doped UO_2 fuels is rather similar to that of standard UO_2 .

4. POST-IRRADIATION ANNEALING TESTS AND MICROGRAPHIC EXAMINATIONS

After puncturing, each fuel rod cladding was cut and the pellets were removed in order to perform the annealing tests and examinations.

Almost no micro-structural evolution can be observed on the micrographs of the fuel pellets after irradiation. The only change is the disappearance of the U_4O_9 needles, which had been observed on the polished and etched samples of the as-fabricated $\text{UO}_{2.01}$ and $\text{UO}_{2.02}$ fuels.

4.1. Annealing experiments device

The device used for the annealing experiments is shown in Fig. 2. Its main components are: the high frequency furnace placed in a hot cell, and the gloves box for gas collection (Toeppler pump) and trapping.

The sample is placed into a crucible, which is coupled to the high frequency (100 kHz) coil placed around the quartz tube constituting the furnace, and heated up by induction. Before starting the thermal treatment, vacuum is made in the furnace by using a primary and a turbo pump. During the annealing experiment, the sample temperature is measured by a thermocouple and by a pyrometer.

Fission gas release is determined after each experiment by analysing the gas which has been trapped in the gloves box. Gamma spectrometry is used to quantify the ^{85}Kr release.

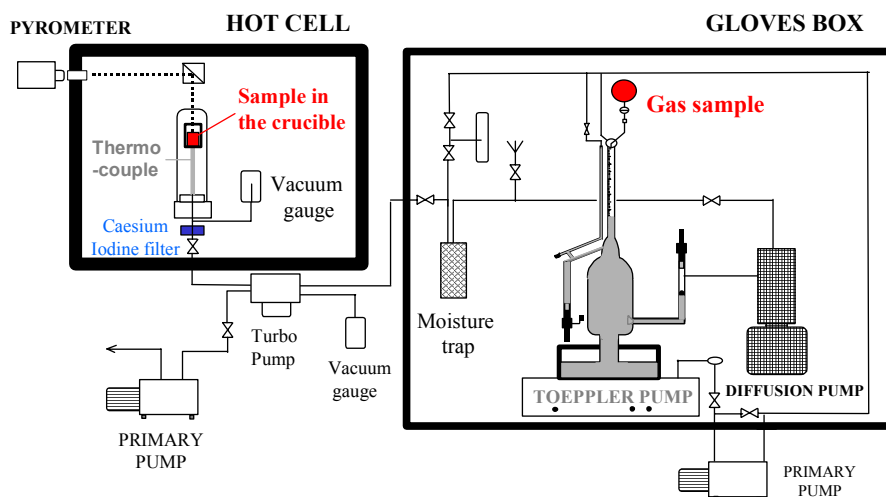


FIG. 2. Annealing experiments device

4.2. Fission gas release results

The annealing tests were performed at 1700°C and lasted 30 minutes or 5 hours, with an intermediate gas sampling after 30 minutes too.

The mean values measured for each type of fuel are given in Table III (the ^{85}Kr release fractions are calculated by dividing the number of ^{85}Kr released atoms by the number of ^{85}Kr atoms created in the fuel, which is obtained by calculation).

The same annealing tests were performed several times on some fuel batches. The results are rather reproducible, with gas release values comprised in $\pm 30\%$ of the mean value at most (more often in $\pm 13\%$), for all the tested fuels. The only exception is UO_2 standard fuel (T1-1a), which gives very variable results from one test to another (from 13% to 46.9% after 5 hours at 1700°C). The reason for this discrepancy has not yet been understood.

Large-grained UO_2 fuel without additive (T1-1b) is therefore chosen as the reference for the comparison of gas release results.

The gas release during the first 30 minutes of the test is at least equal to one third of the release during 5 hours.

The UO_{2+x} small-grained fuel (T1-2a, T1-3a) does not release less gas than large-grained UO_2 fuel, although large-grained UO_{2+x} fuels (T1-2b, T1-3b) unexpectedly show a good fission gas retention during the anneals.

The fuels containing only Cr_2O_3 as a dopant show an improved gas retention, especially those containing 0.2% Cr_2O_3 (T1-5b, T1-6b). This improvement is not only due to grain size enlargement but also to the presence of dopant in the fuel. T1-5a grain size is smaller than T1-1b one, however its gas release is lower.

The influence of silica is positive for T1-4b fuel (0.05%) although it is not in the other fuels for which the quantity is higher and which have been submitted to a reduction anneal (T1-8a to T1-9b).

Table III. Mean values of ^{85}Kr release during the annealing tests

Fuel reference	Fuel type	Grain size	^{85}Kr release after 30 min at 1700°C	^{85}Kr release after 5 h at 1700°C
T1-1b / T1-4a	Large-grained UO_2	50 μm	13.4 %	28.9 %
T1-2a	$\text{UO}_{2.01}$	14 μm	13.1 %	38.8 %
T1-2b	Large-grained $\text{UO}_{2.01}$	50 μm	2.0 %	2.8 %
T1-3a	$\text{UO}_{2.02}$	13 μm	9.5 %	24.0 %
T1-3b	Large-grained $\text{UO}_{2.02}$	50 μm	7.0 %	7.6 %
T1-4b	$\text{UO}_2 + 0.2 \% \text{Cr}_2\text{O}_3 + 0.05 \% \text{SiO}_2$	57 μm	2.8 %	5.1 %
T1-5a	$\text{UO}_2 + 0.07 \% \text{Cr}_2\text{O}_3$	25 μm	10.1 %	14.6 %
T1-5b	$\text{UO}_2 + 0.2 \% \text{Cr}_2\text{O}_3$	62 μm	5.6 %	9.7 %
T1-6a	$\text{UO}_2 + 0.07 \% \text{Cr}_2\text{O}_3$ (reduced)	19 μm	14.6%	31.5%
T1-6b	$\text{UO}_2 + 0.2 \% \text{Cr}_2\text{O}_3$ (reduced)	63 μm	6.8 %	14.2%
T1-7a	$\text{UO}_2 + 1 \% \text{MgO}$	6 μm	9.9 %	/
T1-7b	$\text{UO}_2 + 0.8 \% \text{ZrO}_2$	30 μm	17.5 %	48.9 %
T1-8a	$\text{UO}_2 + 0.2 \% \text{Cr}_2\text{O}_3$ (reduced) + 0.15 % SiO_2 + 0.8 % ZrO_2	34 μm	13.3 %	41.6 %
T1-8b	$\text{UO}_2 + 0.2 \% \text{Cr}_2\text{O}_3$ (reduced) + 0.15 % SiO_2	38 μm	12.2 %	34.1 %
T1-9a	$\text{UO}_2 + 0.2 \% \text{Cr}_2\text{O}_3$ (reduced) + 0.2 % SiO_2 + 0.01 % Al_2O_3	34 μm	10.7 %	27.9 %
T1-9b	$\text{UO}_2 + 0.2 \% \text{Cr}_2\text{O}_3$ (reduced) + 0.1 % SiO_2 + 0.01 % Al_2O_3	31 μm	23.1 %	46.4 %

The addition of MgO , ZrO_2 or Al_2O_3 does not lead to a better gas retention compared to UO_2 large-grained fuel.

4.3. Micrographic examinations

Cross-sections of the annealed pellets were examined by optical micrography before and after etching.

After 5 hours at 1700°C, the microstructure of the UO_{2+x} fuels with normal grain size is quite similar to that of a stoichiometric UO_2 sample with about 30 % release, with well-formed intragranular and intergranular bubbles (Fig. 3a). As for the large-grain size fuels, $\text{UO}_{2.01}$ and $\text{UO}_{2.02}$ fuels show more intragranular bubbles than UO_2 (Fig. 3b and 3c).

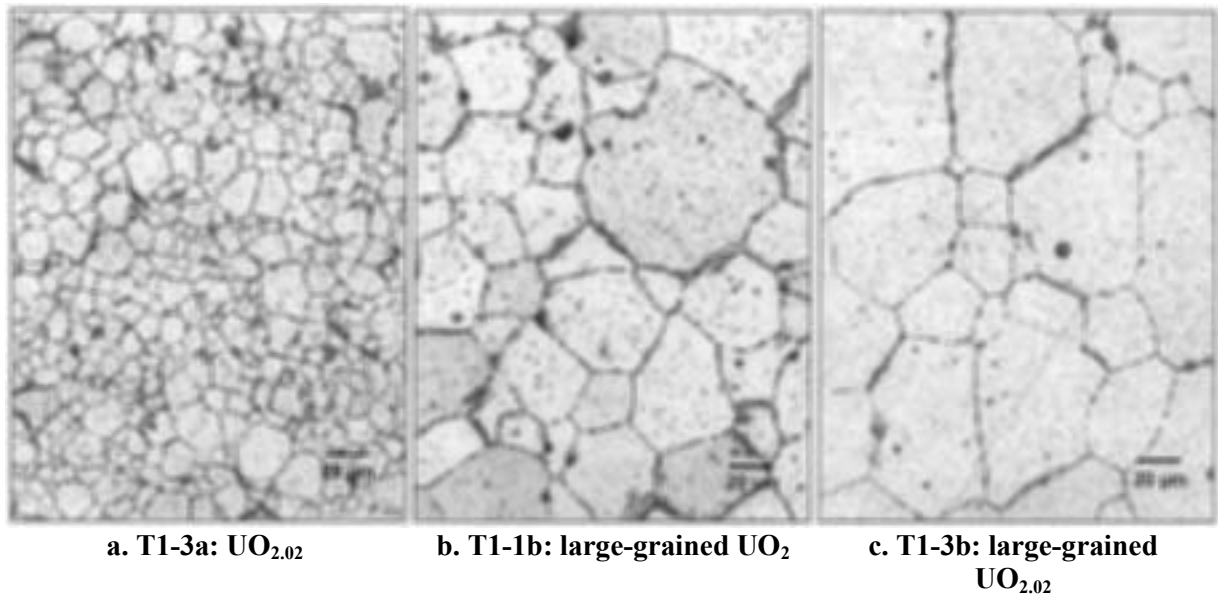


FIG. 3. Micrographs of the T1-3a, T1-1b and T1-3b samples annealed at 1700°C for 5 hours – as etched

A comparison between the micrographs of the T1-4b to T1-6b fuels shows fewer intragranular bubbles in the fuels, which have been reduced after annealing (T1-6a and T1-6b). The T1-4b fuel, with its glassy phase on grain boundaries, exhibits rounded intergranular bubbles (Fig. 4).

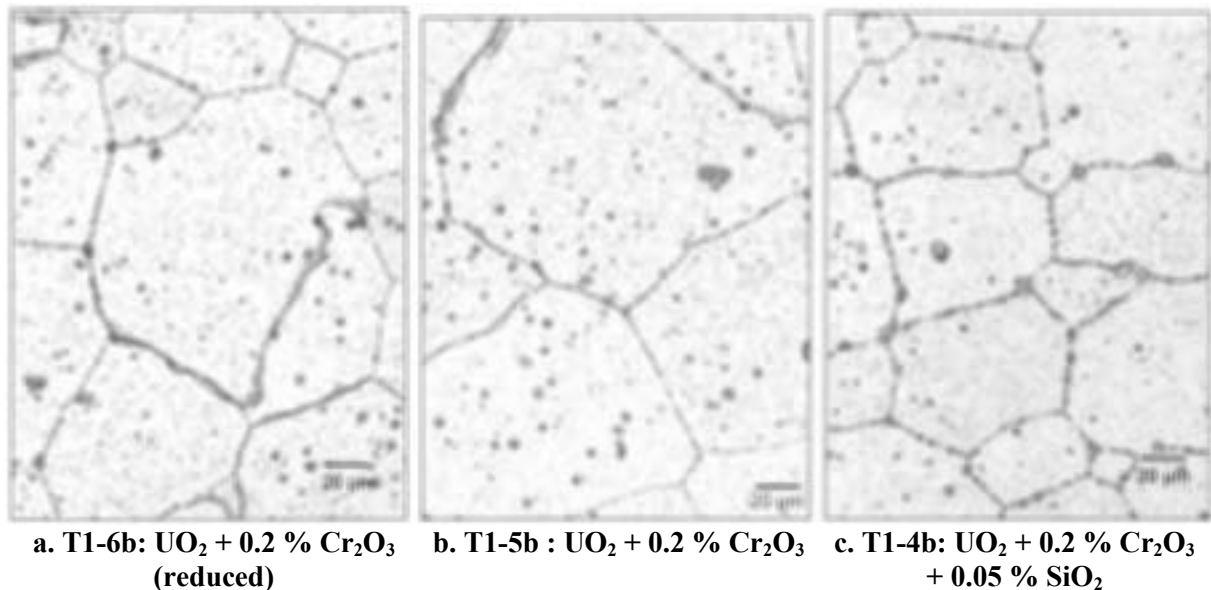
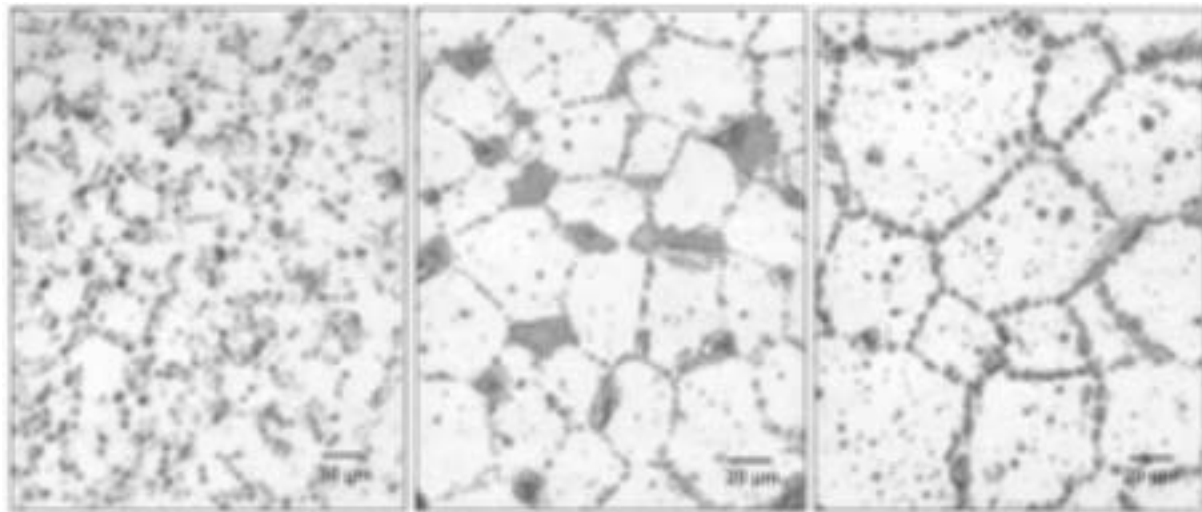


FIG. 4. Micrographs of the T1-6b, T1-5b and T1-4b samples annealed at 1700°C for 5 hours – as etched

The T1-7a fuel, doped with MgO, has very large and numerous bubbles on grain boundaries (Fig. 5a). The T1-7b fuel, doped with ZrO_2 , still shows large pores on grain boundaries, as well as bubbles (Fig. 5b). The three fuels T1-8b, T1-9a and T1-9b, doped with silica, chromium oxide, and aluminium oxide for the two latter, exhibit intragranular bubbles and very large intergranular bubbles (Fig. 5c) which may be linked to the glassy phase clearly visible in the samples after irradiation.



a. T1-7a: $\text{UO}_2 + 1\% \text{MgO}$ b. T1-7b: $\text{UO}_2 + 0.8\% \text{ZrO}_2$ c. T1-8b: $\text{UO}_2 + 0.2\% \text{Cr}_2\text{O}_3$ (reduced) + $0.15\% \text{SiO}_2$

FIG. 5. Micrographs of the T1-7a, T1-7b and T1-8b samples annealed at 1700°C for 5 hours – no etching

4.4. Discussion

Several studies have been performed to test the performance of large-grained fuels containing different types of additives. Large-grained fuels usually show an improved fission gas retention capacity: large-grained UO_2 doped with MgO (which forms precipitates)[8], with aluminosilicate [9], with titanium oxide [9], or with niobium oxide [10]. However, some additives can apparently also increase fission gas diffusion coefficient: Cr_2O_3 [11,12], Nb_2O_5 [13], TiO_2 [13]. In some cases, this diffusion acceleration even counteracts the favourable effect of grain size [9,10].

Few studies were performed to test the global retention capacity of Cr_2O_3 doped UO_2 fuel. In Killeen's study [11], the percentage of Cr_2O_3 (0.5 %) in UO_2 was very high, and Cr_2O_3 seemed not to be well distributed within the fuel after sintering. So Cr_2O_3 diffusion took place during irradiation, inducing grain growth, which probably affected fission gas release results. The study performed by Kashibe and Une [12] gave results about gas diffusion coefficient in UO_2 fuel containing dissolved Cr_2O_3 . The effects of large grain size and of chromium oxide precipitates were not investigated, and they are believed to play the major role in fission gas retention in the present study.

As for hyperstoichiometric fuel, $\text{UO}_{2.05}$ fuel with a grain size of 24 μm was shown to release less fission gas than standard UO_2 fuel during ramp tests [14]; however, fuel swelling was greater, which is in agreement with our observations concerning a large number of intragranular bubbles in large-grained hyperstoichiometric fuels.

Another specific study [15,16] concerning undoped UO_2 and UO_{2+x} large-grained fuels (T1-1b, T1-2b, T1-3b) was performed. Calculations showed that the release measured during the post-irradiation anneals could be interpreted as gas diffusion with an eventual temporary trapping in intergranular bubbles. The release measured at the beginning of the anneals is due to fission gas situated nearby grain boundaries, which diffuses readily towards them as soon as temperature is increased. During the steady state part of the test, the release rate decreases because the gas close to grain boundaries has been released, and because gas diffusion is

slowed down by gas trapping into intragranular bubbles. The activation energy for gas diffusion was shown to be close to uranium self diffusion in UO_2 or UO_{2+x} (550 and 350 kJ/mol respectively).

Fig. 6 shows the 5 hours release results for each fuel as a function of the grain size.

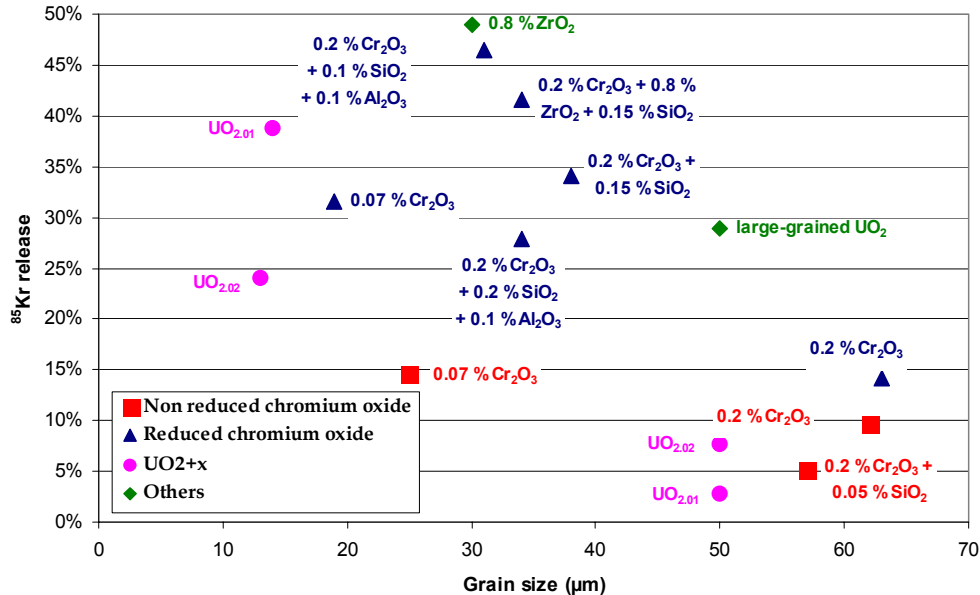


FIG. 6. ⁸⁵Kr release results after annealing tests of 5 hours at 1700°C.

The best gas retention results are obtained with fuels having the larger grain sizes (over 50 µm). However, this characteristic is not sufficient as the large-grained UO_2 fuel release reaches 30%. The other essential characteristic for an improved fission gas retention is the presence of intragranular sites favourable to bubble nucleation and pinning. These sites are structural defects due to the hyperstoichiometry in UO_{2+x} and second phase precipitates in fuels doped with 0.2% Cr_2O_3 . The intragranular bubbles formed on these sites can be observed on the micrographs. It seems that the reducing anneal performed on some fuel batches induced a disappearance of some of these precipitates (higher release and fewer bubbles).

Using ZrO_2 as a dopant was not efficient to create precipitates. The glassy intergranular phase in T1-4b fuel decreased fission gas release by improving fission gas retention on grain boundaries; in the other fuels doped with SiO_2 , this could not be achieved as introducing too much silica impedes grain growth induced by Cr_2O_3 .

5. CONCLUSION AND OUTLOOK

Different kinds of undoped and doped UO_2 fuels were fabricated and irradiated in the TANOX device, in the Siloé reactor. The temperature at the centre of the annular pellets was maintained under 700°C until the end of the irradiation so as to avoid activation of thermal gas diffusion and release. The pellets, which had reached a burn-up of about 10 GWd/t_U, were then submitted to post-irradiation annealing tests at 1700°C intended to stimulate fission gas release and to test their retention capacity. The ⁸⁵Kr release was measured by gamma spectrometry after 30 minutes and 5 hours at 1700°C, and the samples were examined by optical micrography.

The results show that the fuels with best fission gas retention are characterized by both a large grain size (over 50 μm) and intragranular sites which are favourable to gas bubble nucleation and pinning. These characteristics are achieved in (i) large grained $\text{UO}_{2.01}$ and $\text{UO}_{2.02}$ fuels in which structural defects due to the hyperstoichiometry are favourable to bubble nucleation, (ii) UO_2 doped with 0.2% Cr_2O_3 which acts as a grain growth activator and also forms second phase precipitates. Gas release can even be lower if intergranular gas retention is improved by the addition of a small quantity of silica.

On the basis of these results, several microstructures were selected for a further study of gas retention at high burn-up: UO_2 doped with 0.2% Cr_2O_3 , submitted or not to a post-sintering reducing anneal, UO_2 doped with 0.2% Cr_2O_3 and 0.02 % SiO_2 and $\text{UO}_{2.02}$ doped with 0.2 % Cr_2O_3 . These fuels were irradiated in the TANOXOS device located in the Osiris reactor, to a burn-up of 65 GWd/t_U . After irradiation, fuel samples were submitted to annealing tests; the first recent results show that doped stoichiometric fuels have a better gas retention capacity than undoped fuel and prove their interest for high burn-up conditions.

Besides these analytical studies, an irradiation of doped UO_2 fuels was launched in order to test their behaviour in a PWR (CONCERTO program, directed by FRAMATOME-ANP in cooperation with EDF and the CEA). The fuels were doped with Cr_2O_3 , SiO_2 , and/or Al_2O_3 and they were manufactured by FBFC.

Some power ramp tests were performed on chromium oxide doped UO_2 segments, which had been discharged after two PWR irradiation cycles [17]. These ramps aimed at testing the behaviour of the fuel in conditions of pellet-cladding mechanical interaction. The segments could withstand very high ramp power levels without failure. Moreover, rod punctures performed after ramp tests showed a lower fission gas release compared to standard UO_2 , which confirms the improved fission gas retention capacity of the doped fuel.

These very promising results concerning the PCMI performance and the improved fission gas retention capacity of chromia doped fuel led FRAMATOME-ANP to launch in 2001 the irradiation of lead fuel rods containing chromium oxide fuel pellets loaded in M5^{TM} cladding tubes. This irradiation aims at obtaining all the data required to demonstrate the ability of this advanced fuel to become a high burn-up and PCMI remedy.

ACKNOWLEDGEMENTS

The authors would like to acknowledge all the persons involved in the fabrication, irradiation, and examinations of the advanced UO_2 fuels. We especially wish to thank S. Ravel for the annealing tests and G. Eminet for the micrographic examinations.

REFERENCES

- [1] Ph. DEHAUDT, L. CAILLOT, G. DELETTE, G. EMINET, A. MOCELLIN, "Irradiation of UO_{2+x} fuels in the TANOX device", Advances in Pellet Technology for Improved Performance at High Burnup, Proc. IAEA Tech. Com. Mtg Tokyo, Japan, 28 Oct–1 Nov. 1996), IAEA-TECDOC-1036, Vienna (1998) 277.
- [2] L. BOURGEOIS, Contribution à l'étude du rôle des dopants dans la densification et la croissance cristalline du dioxyde d'uranium (Contribution to the Investigation of Densification of Crystalline Uranium Dioxide by Dopants), Thesis, Institut National Polytechnique de Grenoble, 1992.

- [3] L. BOURGEOIS, PH. DEHAUDT, C. LEMAIGNAN, A. HAMMOU, Factors governing microstructure development of Cr₂O₃-doped UO₂ during sintering, *Journal of Nuclear Materials*, 297 (2001) 313–326.
- [4] V. PERES, Contribution à l'étude de la dispersion de particules de phases secondaires dans le dioxyde d'uranium polycristallin (Contribution to the Investigation of 2nd Phase Particles in Polycrystalline Uranium Dioxide), Thesis, Institut National Polytechnique de Grenoble, 1994.
- [5] V. PERES, L. BOURGEOIS, PH. DEHAUDT, Grain growth and Ostwald ripening in chromia-doped uranium dioxide, *Journal de Physique IV*, colloque C7, vol. 3 (nov. 1993).
- [6] C. DUGUAY, A. MOCELLIN, PH. DEHAUDT, M. SLADKOFF, High temperature mechanical tests performed on doped fuels, Proc. IAEA Tech.1 Com. Mtg Tokyo, Japan, 28 Oct–1 Nov. 1996), IAEA-TECDOC-1036, Vienna (1998) 409.
- [7] C. VIVANT-DUGUAY, Contribution à l'étude du fluage du dioxyde d'uranium. Rôle des activateurs de croissance cristalline, (Contribution to the Investigation of Creep of Uranium Dioxide, Role of Activators)Thesis, Institut National des Sciences Appliquées de Lyon, 1998.
- [8] P.T. SAWBRIDGE, C. BAKER, R.M. CORNELL, K.W. JONES, D. REED, J.B. AINSCOUGH, The irradiation performance of magnesia-doped UO₂ fuel, *Journal of Nuclear Materials*, 95 (1980) 119–128.
- [9] R. YUDA, H. HARADA, M. HIRAI, T. HOSOKAWA, K. UNE, S. KASHIBE, S. SHIMIZU, T. KUBO, Effects of pellet microstructure on irradiation behavior of UO₂ fuel, *Journal of Nuclear Materials*, 248 (1997) 262–267.
- [10] K. UNE, S. KASHIBE, K. ITO, Fission gas behavior during postirradiation annealing of large grained UO₂ fuels irradiated to 23 GWd/t, *Journal of Nuclear Science and Technology*, 30 [3] (1993) 221–231.
- [11] J.C. KILLEEN, Fission gas release and swelling in UO₂ doped with Cr₂O₃, *Journal of Nuclear Materials*, 88 (1980) 177–184.
- [12] S. KASHIBE, K. UNE, Effect of additives (Cr₂O₃, Al₂O₃, SiO₂, MgO) on diffusional release of ¹³³Xe from UO₂ fuels, *Journal of Nuclear Materials*, 254 (1998) 234–242.
- [13] K. UNE, I. TANABE, M. OGUMA, Effects of additives and the oxygen potential on the fission gas diffusion in UO₂ fuel, *Journal of Nuclear Materials*, 150 (1987) 93–99.
- [14] J.H. DAVIES, E.V. HOSHI, D.L. ZIMMERMAN, Ramp test behavior of high O/U fuel, *Journal of Nuclear Materials*, 270 (1999) 87–95.
- [15] S. VALIN, Etude des mécanismes microstructuraux liés au relâchement des gaz de fission du dioxyde d'uranium irradié, (Investigation of Mechanism of FGR from Irradiated Uranium Dioxide) Thesis, Institut National Polytechnique de Grenoble, 1999.
- [16] S. VALIN, A. MOCELLIN, G. EMINET, S. RAVEL, J.C. JOUBERT, Modelling the behaviour of intergranular fission gas during out-of-pile annealing, *Fission Gas Behaviour in Water Reactor Fuels* (Proc. OECD/NEA-IAEA Seminar Cadarache, France, 26–29 Sept. 2000), OECD/NEA, Paris (2001).
- [17] Ch. DELAFOY, P. BLANPAIN, C. MAURY, PH. DEHAUDT, CH. NONON, S. VALIN, Advanced UO₂ fuel with improved PCI resistance and fission gas retention capability, TOPFUEL 2003, (Proc. Int. Conf. Würzburg, Germany, 16-19 March 2003), Inforum GmbH, Germany, CD-ROM.

FISSION GAS RELEASE FROM HIGH BURN-UP UO₂ FUELS UNDER SIMULATED OUT-OF-PILE LOCA CONDITIONS

Y. PONTILLON, D. PARRAT, M.P. FERROUD PLATTET
S. RAVEL¹, G. DUCROS, C. STRUZIK
CEA Lez Cadarache,
Saint Paul Durance

A. HARRER
EDF/SEPTEN/TE
Villeurbanne Cedex,
France

Abstract

A specific emphasis has been put recently in France on mechanisms, which promote Fission Gas Release (FGR) in Loss Of Coolant Accident (LOCA) thermal conditions. One of the most useful information for understanding the FGR mechanisms is to achieve reliable tests to measure the absolute level and the time dependence of the released gases and the corresponding fuel micro-structural changes during representative thermal transients. In order to obtain these data, the so-called "GASPARD" programme has started at the beginning of 2000 at the CEA, in collaboration with EDF. The first step of this programme deals with short sections of UO₂ fuel rods irradiated in power reactors during 4 and 6 cycles. The experimental process consists in annealing the fuel samples in out-of-pile conditions, from 300°C up to a temperature ranged between 900°C and 1600°C, with a wide range of temperature increase rates (from 0.2°C/s up to 20°C/s). The upper temperature is maintained during several minutes or is immediately decreased. The release rate of ⁸⁵Kr is measured by on-line gamma spectrometry and delayed gamma spectrometry on a gas sample. Stable isotopes are measured by gas chromatography coupled to a mass spectrometry. Specific post-test observation devices are then used (e.g. metallographic inspection, Scanning Electron Microscopy). The present communication focuses firstly on the description of the GASPARD experimental process, then on experimental facility implemented at the CEA/DEN for fast transient and LOCA reproductions. After that, the results regarding 4 cycles UO₂ fuel are presented and discussed, and a good agreement with the CEA code METEOR calculations is pointed out.

1. INTRODUCTION

1.1. R and D requirements on fuels for current reactors

The current generation of LWRs have operated very successfully for over 30 years, and with plant lifetime extension programmes (PLEX), individual reactors are expected to reach a lifetime approaching 60 years, i.e., up to the year 2030. Regarding the fuel properties and the fuel behaviour under neutron flux, much of the start-up R&D has been completed, although safety issues appropriate to high burn-up are still being addressed.

However, on the short and medium-term, the liberalisation of the electricity market lead operators and fuel vendors to consider a variety of means to enhance plant performance and reduce costs. This trend has taken place in the last several years and is likely to continue in the long term. In the fuel area it is supported by a few basis orientations, such as burn-up extension of standard fuels, new types of fuel, more efficient fuel management schemes, new cladding materials and new fuel assembly designs.

¹ Laue Langevin Institute (ILL) –Reactor Division - 6 rue J. Horowitz – BP 156 - F-38042 Grenoble Cedex 9.

As a consequence of this evolution, there is a permanent need to reassess the reactor safety studies, in order to ensure that these progresses take place without detriment to safety. This includes improving the knowledge and upgrading the calculation tools used for safety assessment. Utilities will need to continuously review and to update eventually the technical basis and the assumptions used for the design analysis of the fuel core. This will require not only that the database for transient analyses is extended to broader conditions and materials, but also that the uncertainties associated with such database and its use for specific applications is adequately quantified. A successful strategy to reach these objectives is to gain reliable experimental data from separate effects experiments carried out in Material Test Reactors (MTRs) or in hot cell laboratories.

1.2. Importance of studies on Fission Gas Release

1.2.1. High burn-up UO₂ fuel behaviour

The fuel enrichment limit in force today is equivalent to less than 5 wt% ²³⁵U. This limits fuel assembly discharge burn-up to around 60 to 65 GWd.t_U⁻¹. Most commercial reactors have a lower burn-up limit, and support work is in hand to improve effectiveness of the standard fuel and to approach the limit set by the enrichment. Several evolved products are in testing in Material Test Reactors (MTRs) and in power reactors:

- (i) improved UO₂, with large grain size including or not additives in the matrix or at the grain boundaries,
- (ii) integrated Burnable Absorber Fuels, such as uranium-gadolinium fuels.

There are two principal concerns: rod over-pressure due to the high inventory of fission gases at high burn-up and the potential behaviour of the High Burn-up Structure (HBS). The latter is first observed in the pellet rim at pellet averaged burn-up levels ~ 50 GWd.t_U⁻¹ and extends radially inwards at higher burn-up. The concern for normal operation is that it may increase slightly fuel temperatures and also fission gas release by acting as a thermal barrier due to the poor thermal conductivity of the HBS.

1.2.2. Introduction of MOX

A prerequisite for the loading of MOX fuel in current reactors is that MOX safety requirements should not be different from those required for UO₂. Studies to date have shown that there is little difference in the behaviour of the two types of fuel. However, whereas MOX is more compliant, resulting in reduced PCMI, it has a higher remnant reactivity at high burn-up, hence powers, fuel temperatures and fission gas release (FGR) are likely to be greater than for UO₂ fuel in the event of a transient.

1.2.3. The FGR GASPARD programme at CEA

Fission gas release is an important input data of the fuel licensing process, either in normal operation or as the radioactive “source term”, relatively to the consequences of a nuclear incident and/or accident on the surrounding populations as well as on the environment. For this purpose, several R&D programs have been recently initiated in France through joint actions between the Commissariat à l’Energie Atomique (CEA) and Electricité de France (EDF), including occasionally a support from Framatome-ANP or the Nuclear Radioprotection and Safety Institute (IRSN).

Within this framework, a specific emphasis has been put recently on mechanisms, which promote the Fission Gas Release (FGR) in Loss Of Coolant Accident (LOCA) thermal conditions, mainly thanks to the so-called “GASPARD” programme. One of the most useful information for understanding the FGR mechanisms is to achieve reliable tests to measure the absolute level and the time dependence of the released gases and the corresponding fuel micro-structural changes during representative thermal transients. This database is used:

- to define the fission product (FP) “source term” out of the damaged rods during a given type of accidental sequence,
- to verify if existing safety criteria are well adapted to new fuels,
- to enhance models predicting behaviour of various fuels during an accidental sequence, thanks to the understanding and quantifying of the basis mechanisms.

2. DESCRIPTION OF THE GASPARD EXPERIMENTAL PROCESS

2.1. Experimental sample

In the GASPARD programme, each experimental sample is constituted by one fuel pellet with its clad. This sample has been cut in a fuel rod stack. Manufacturing data of the sample and its power history in a power reactor are known as precisely as possible, to be able to calculate the “reference status” at the beginning of the thermal transient. To improve the analytical status of the process, a tenth of samples are generally prepared just before the thermal transient campaign, by cutting a unique fuel rod section.

The corresponding experimental process consists in three steps: i) re-irradiation of the rod section in a research reactor, ii) transfer in hot cell laboratory and test performance with on-line measurements, and iii) post-test examinations.

i) Re-irradiation in a Material Test Reactor

This first step is optional, if only long half-life and stable isotopes have to be measured. Re-irradiation lasted a few days at low linear heat generation rate: between 10 and 20 W.cm⁻¹. This permits to create short and intermediate half-life FP. Due to the low power and the short re-irradiation time, these FP are mainly located inside the fissile grains, in intra-granular position. Long half-life fission product distribution, representative of the in power reactor end-of-life, is normally not affected by this re-irradiation period.

ii) Transfer in hot cell laboratory and test performance with on-line measurements

Decay and transportation times of the re-irradiated section from the MTR to the hot cell laboratory are short in order to measure intermediate half-lives FP, which are interesting for the goals of the programme. It has been possible to receive the stack 2 or 3 days after the end of the re-irradiation.

After reception, a longitudinal gamma scanning is carried out, in order to adjust the fissile power of the re-irradiation and to calculate the precise inventory of the FP, especially for noble gases, following a general procedure, which was already described in details [1]. The thermal transient is then carried out on each sample. This campaign occurs one or two weeks after the end of the re-irradiation.

For this purpose, sample is put in a devoted furnace. Accidental sequence consists in the reproduction of the temperature history expected in a power reactor for such an accident, with

a controlled atmosphere. In this case, experimental parameters are precisely fixed and monitored during the sequence. Sample is continuously swept by a gas flow, and FP are measured in this gas by on-line gamma spectrometry and, after, by other means. More details are presented in § 4.1 below.

iii) Post-test examinations

After sequence, some samples can be examined by non destructive and destructive PIE: longitudinal or radial metallographic inspection, fractography, SIMS,... Main goals of these examinations are:

- to appreciate the evolution of the FP distribution, especially for noble gases, thanks to similar examinations carried out on a reference sample (re-irradiated or not, but without accidental sequence),
- to detect microstructure changes of the matrix, especially in terms of cracks distribution and pellet embrittlement.

However, this step has not been implemented in the first GASPARD campaign concerning 4 cycles UO₂ fuel, which is the scope of the present paper.

2.2. Interest of the GASPARD analytical experiments

Through this kind of experimental protocol, reproduction of a LOCA sequence, as expected in a power reactor, is only partial. Some steps of the accidental sequence can not be reproduced, such as:

- (i) the initial step (roughly a dozen of seconds) during which the radial temperature gradient in the pellet is important,
- (ii) the final step, corresponding to the reflooding of the rod.

Quantitative effect of the first step on FP release is deduced from calculations.

The standard measurement concerns radioactive and stable noble gases. Measurement of volatile and non-volatile FP (iodine and caesium isotopes...) is more complex . For this purpose, the accidental sequence is performed in a specific device, as for the HEVA-VERCORS programme [2–8].

However, such analytical tests are rather easy to prepare and to set up. When several samples can be re-irradiated at the same time and are available, it is possible to test, during a same campaign, the influence of the following parameters on the FP release:

- time history of the sample temperature (elevation rate, maximum value, plateau duration,...),
- type and microstructure of the fuel,
- burn-up value.

Moreover, detection and quantification of short or intermediate half-life FP permit to determine the contribution of intra-granular FP to the global release.

This large database enables to identify parameters, which promote the FP release and specially the FGR. This leads to release mechanisms identification and quantification [9], and

permits to set up physical laws which will be introduced in codes, in order to enhance or optimise existing models [10, 11].

3. THERMAL ANALYSES FACILITY FOR LOCA-TYPE THERMAL TRANSIENT SIMULATIONS

This facility has been used for several years at CEA Grenoble, in the hot cell Laboratory LAMA, in order to fulfil several analytical programmes on FGR, such as the ADAGIO programme. It has been already presented [12] and the first results obtained with the ADAGIO programme discussed [13, 14]. So the following presentation will be relatively brief.

3.1. Main components used in the GASPARD programme

The word ADAGIO is a French acronym for “Discriminating Analysis of Accumulation of Intergranular and Occluded Gas”. The device has been adapted from Canadian experiment using the CEA expertise in radioactive gas measurement. Figure 1 shows a schematic view of the facility. This view describes all the equipment of the heat analysis device with on-line and cumulative gas measurements.

It could be divided in three main parts:

- the shielded hot cell, containing the furnace,
- the monitoring system of the sweeping gas by gamma spectrometry,
- the gloves box, containing the cold traps or vacuum capacities.

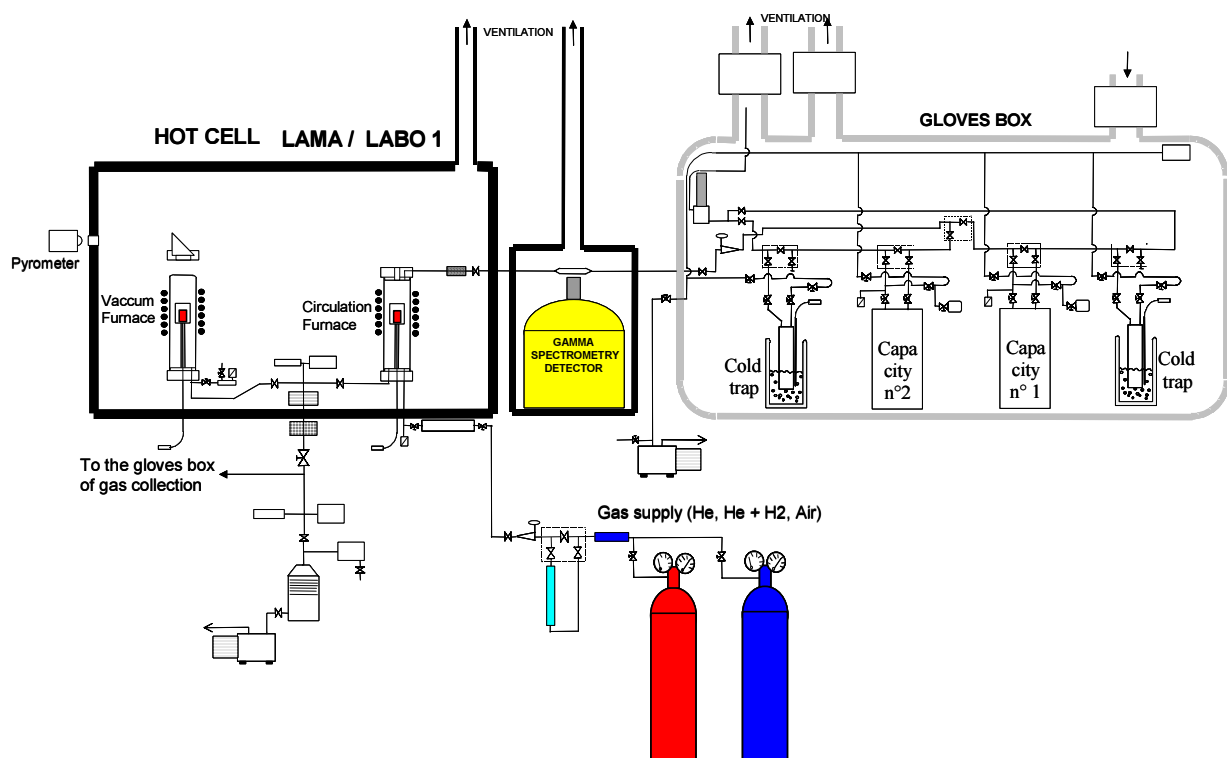


FIG. 1. Experimental device used in the GASPARD programme.

3.1.1. Furnace and associated temperature measurement means

The furnace used for the GASPARD programme is based on the high frequency (H.F.) heating principle. It is constituted by water cooled copper turns where 100 KHz electric current is circulating. An inducing current takes place in the metallic crucible and warms it. A quartz tube avoids any gas leakage out of the furnace. It is the most often used and is called “circulation furnace”. The sample is swept by gas (see more details in § 4-1-2 and 4-1-3). A schematic view of this furnace is presented on figure 2.

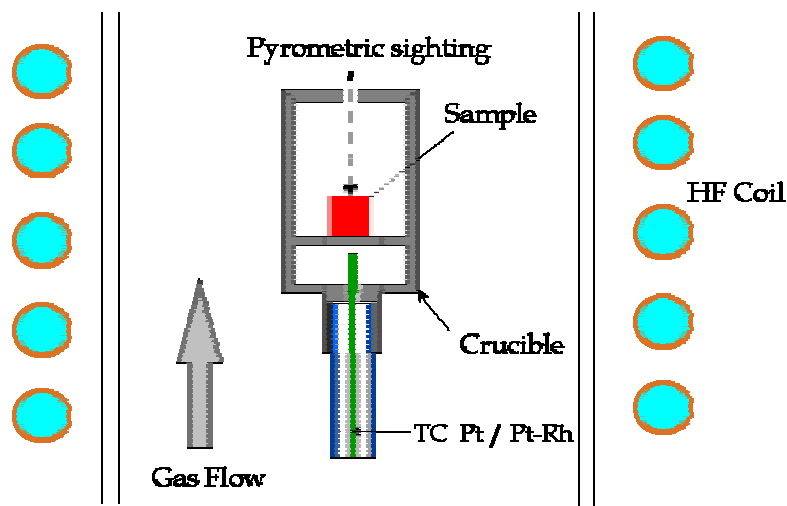


FIG. 2. Diagram of the circulation furnace used for GASPARD.

The pellet temperature is measured by two ways (see figure 2):

- (i) a thermocouple is placed in a small chamber at the bottom part of the crucible (Pt / Pt-Rh, or W / W-Re, depending on the atmosphere and the final temperature). This chamber is supposed to be at the same temperature as the sample chamber,
- (ii) a two wavelengths pyrometer, which only works above 1270°K (1000°C), gives another measurement by direct sighting into the sample chamber.

3.1.2. Filtration and monitoring of the sweeping gas

A dry gas flow provided by cylinders is regulated at the entrance of the hot cell. The sample is placed into the crucible, and during the whole annealing, the specimen is swept by flow of helium. Temperature, pressure and flow rate are recorded. After the furnace, sweeping gas loaded with radioactive tracers is routed through filters. These filters, constituted by metallic porous plates, stop emitted aerosols carrying in particular iodine and caesium isotopes.

After filters, radioactive noble gases pass in a delay chamber, in front of a gamma detector, where the radioactive gases concentration is monitored. The very sensitive gamma detector is calibrated to give a quantitative value of the FGR.

3.1.3. Storage of the FP in the gloves box

Downstream of the delay chamber, the gas is coming into the gloves box, where only xenon and krypton are stored in two liquid cold traps sets. During the experiment, one set of traps is working and the second one is prepared in case of emergency. The purified gas is controlled at the exit of the gloves box by means of an ionisation chamber.

Another possibility is to store all the sweeping gas used during a test in pre-voided capacities of big volume (roughly 12 litres). Two capacities are presently used, but if capacities become filled in case of long tests, cold traps are required.

3.2. Performances of the experimental device used for GASPARD

3.2.1. Temperature measurement means and performances of the circulation furnace

The maximum temperature achievable with the H.F. circulation furnace is 2020°K (1750°C), with a maximum rising speed about 20°K/s. Uncertainty on the temperature value is estimated at +/- 30°K. When the temperature elevation rate is 20°K/s, an axial (bottom-up) temperature gradient inside the pellet of roughly 20°K is estimated by calculation. A programming unit allows to set up fast thermal transients without overshoots and with a very good reproducibility.

With this furnace, thermocouple measurement is considered as the reference. It is confirmed, in the temperature range up to 1520°K (1250°C), by a very good agreement between thermocouple and pyrometric measurements. Above 1600°K (1330°C), an obscuration of the optic fibre occurs and forbids the comparison.

The circulation furnace permits to control the atmosphere in contact with the fuel, which is an important parameter for FGR measurement. The GASPARD programme used purified He, with less than 0.4 vpm water vapour and less than 0.1 vpm O₂.

3.2.2. Performances of the FGR measurement system

An important advantage of the device is to be able to quantify the FGR thanks to three independent measurement means:

- (a) The delay chamber and the associated on-line gamma spectrometer are located in a shielded chamber. The crystal is of Ge HP, P type, with a 60 % efficiency (see figure 3). These components are designed to detect a FGR minimum cumulated value of 1% for ⁸⁵Kr and 0.1% for ¹³³Xe, after a test duration of 1 hour carried out on a 200 mg fuel sample at a burn-up of 50 GWd.t_{hm}⁻¹. Calibration of this system is ensured thanks to ¹³³Xe – ⁸⁵Kr standard gas sources.

When tests are performed after a short decay time since the end of re-irradiation, other isotopes, such as ^{133m}Xe (2.2 days of half-life) and ^{131m}Xe (11.9 days) are also detectable.

- (b) A gamma spectrometry of the capacities ensures a second measurement of the total radioactive FGR. Calibration of this system is ensured thanks to a ¹⁵²Eu – ¹³³Ba standard liquid source, with auto-absorption calculations. Efficiency curve is completed with points coming from a second calibration with a ¹³³Xe – ⁸⁵Kr standard gas source.

A comparison with the on-line gamma spectrometry analysis results permits to confirm the correct calibration of the both devices.

- (c) A gas chromatography coupled to a quadru-polar mass spectrometer (GC-MS) permits to measure stable FGR and isotopic composition of stable noble gases. Minimum concentrations of Krypton and Xenon in the carrier gas are 0.15 and 0.07 vpm respectively. Main interest of this method is to be able to measure the fractional release of each stable isotope, whereas gamma spectrometry quantifies FGR only for ⁸⁵Kr and ¹³³Xe.

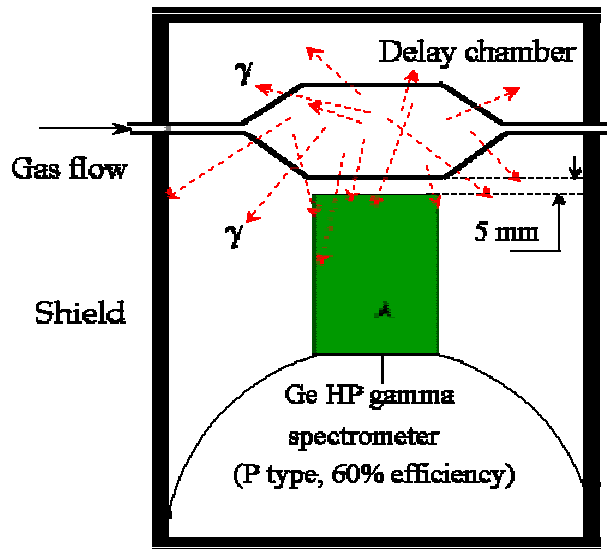


FIG. 3. Diagram of the on-line quantitative gamma spectrometry.

4. FISSION GAS RELEASE FROM 4 CYCLES UO₂ FUELS UNDER SIMULATED OUT-OF-PILE LOCA CONDITIONS

4.1. Type of thermal time history

In the GASPARD programme, a LOCA type sequence is constituted by following steps (see figure 4):

- a slow temperature increase is firstly applied to the rod section from room temperature up to a thermalization value,
- a thermalization plateau is maintained during roughly 30 mn, in order to approach (and to be slightly under) the thermal condition of the peripheral zone of a pellet at the beginning of a LOCA,
- a quick increase of the temperature is applied, from this thermalization value up to a fixed maximum value T_{max} , ranging from 1170°K (900°C) up to 1870°K (1600°C),
- a plateau is maintained at this maximum value, from a few minutes up to 15 mn. In some tests, there is no plateau,
- heating regulation is then stopped and temperature decreases down to room temperature thanks to natural convection.

Temperature (T)

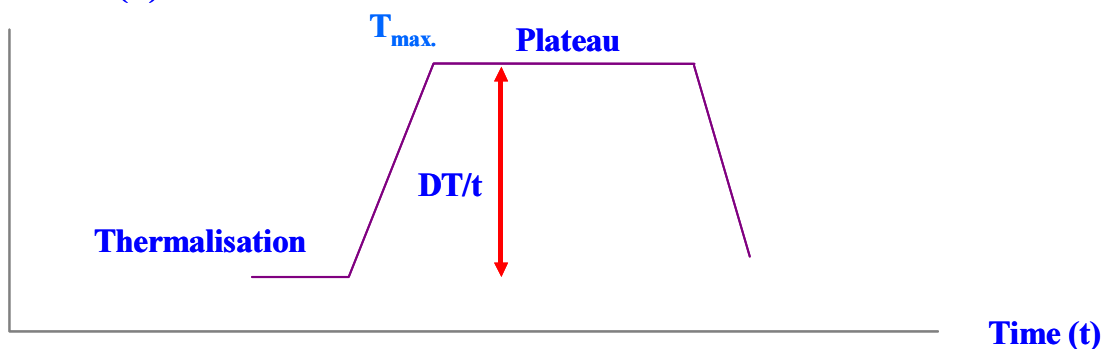


FIG. 4. Temperature time history during a LOCA type sequence performed on a fuel sample.

4.2. Results of the thermal analysis campaign performed on standard 4 cycles UO₂

4.2.1. Base irradiation of the GASPARD samples

Annealing tests of this campaign were performed on two different standard PWR UO₂ fuels in order to increase knowledge about fission gas release mechanisms. The UO₂ fuel pellets were manufactured by the standard industrial process. The ²³⁵U initial enrichments were 3.1 % and 4,5 % respectively for the so-called “rod A” and “rod B” batch of experiments. The “rod A” batch of experiments was performed on samples irradiated locally up to a burn-up of 48.0 GWd.t_U⁻¹, i.e. four irradiation cycles in Fessenheim reactor, followed by a long storage time (roughly 15 years). The other one was performed on recent UO₂ irradiated locally up to 48.5 GWd.t_U⁻¹ (four irradiation cycles in Gravelines reactor).

FGR results after base irradiation have been measured by puncturing and are summarized on table 3.

4.2.2. Thermal analyses performance and results

According to the general procedure explained above, the experimental sequences effectively applied during this campaign are displayed in Table 1 below, together with the corresponding ⁸⁵Kr FGR.

Table 1. “Rod A” and “rod B” experimental sequences applied during the 4 cycles UO₂ campaign together with the corresponding ⁸⁵Kr FGR.

Rod A	T increase rate	T Max.	Upper plateau duration	⁸⁵ Kr FGR (% of the initial inventory)
Test A5-0	0.2 °C/s	1200°C	15 mn	2.8
Test A5-5 (1)	20 °C/s	1400°C	2 mn	5.0
Test A5-5 (2)	20 °C/s	1600°C	0 mn	7.1

Rod B	T increase rate	T Max.	Upper plateau duration	⁸⁵ Kr FGR (% of the initial inventory)
Test A5-0	0.2 °C/s	1200°C	15 mn	8.8
Test A5-1	10 °C/s	1200°C	10 mn	5.4
Test A5-2	20 °C/s	1200°C	10 mn	5.2
Test A5-2bis	20 °C/s	1200°C	0 mn	3.3
Test A5-3	20 °C/s	1000°C	10 mn	3.2

⁸⁵Kr release kinetics for rod A and rod B during the A5-0 tests, measured by on-line gamma spectrometry, are shown in Figure 5 and 6 respectively. “85Kr” corresponds to the raw values, and “85Kr deconv” corresponds to the values corrected from the hydraulic transfer function of the system (transit time and homogenisation in the furnace volume).

Besides, post-test analysis (GC-MS) were performed on stable isotopes after A5-0 (rod B) and A5-2bis (rod B) tests. Table 2 shows the corresponding results (i.e. Kr and Xe isotopic distributions) together with a comparison to the values obtained by gamma spectrometry for ⁸⁵Kr.

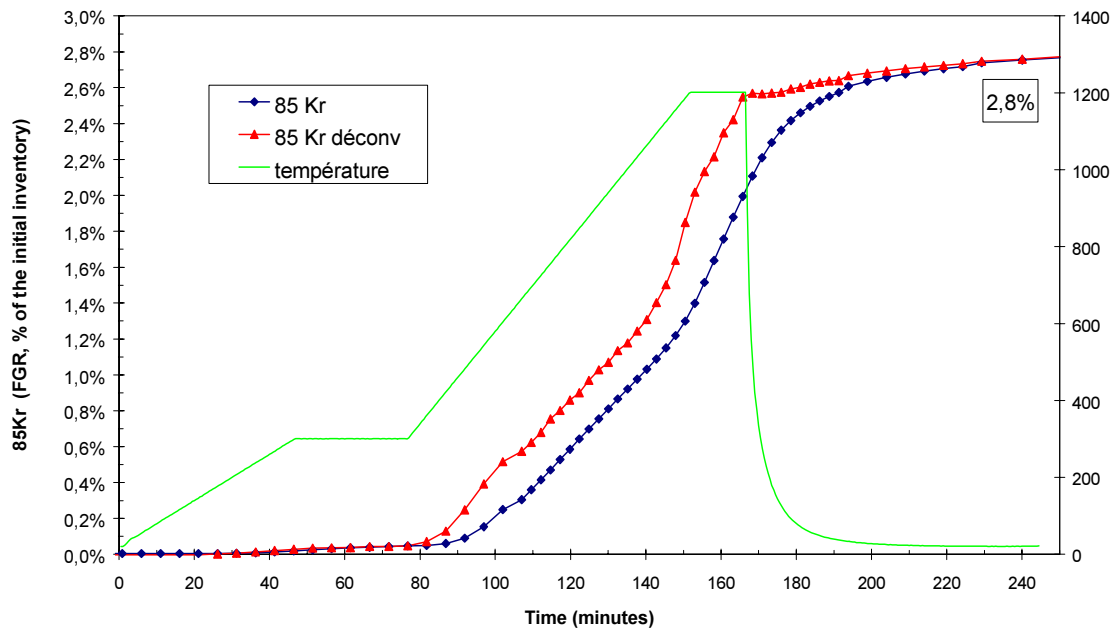


FIG. 5: ^{85}Kr release kinetics (rod A - test A5-0).

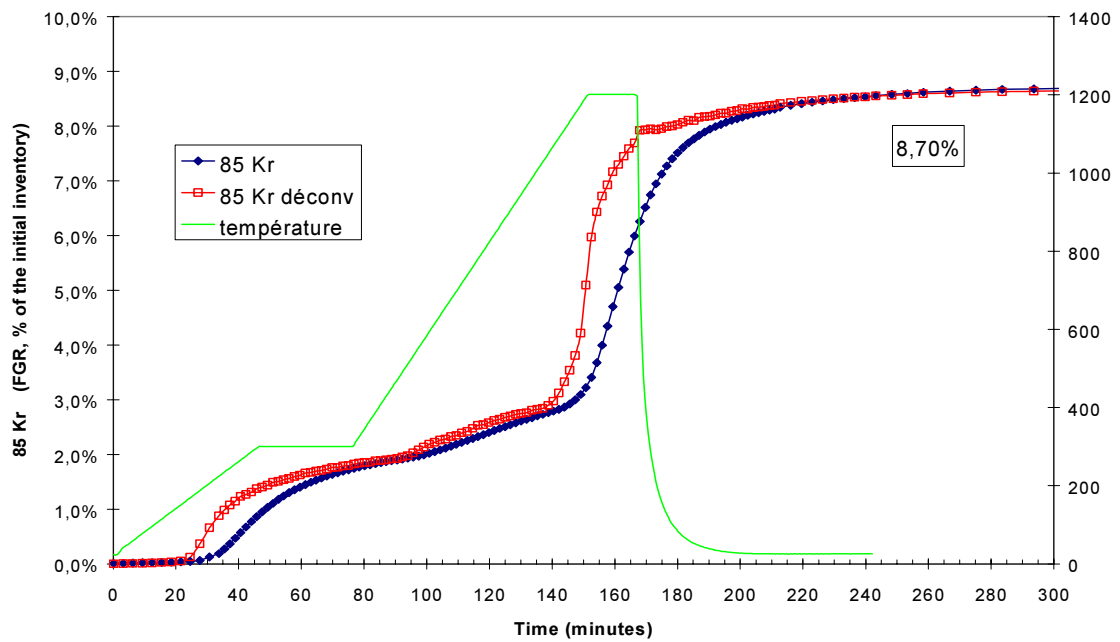


FIG. 6: ^{85}Kr release kinetics (rod B - test A5-0).

Table 2. Rod B: FGR obtained by GC-MS for noble gases (Kr and Xe) after A5-0 and A5-2bis tests.

Rod B	A5-0 (% of the initial inventory)	A5-2bis (% of the initial inventory)
⁸³ Kr	7.1	3.1
⁸⁴ Kr	9.9	3.9
⁸⁵ Kr (GC-MS / Sp. γ)	8.2 / 8.8	3.7 / 3.3
⁸⁶ Kr	7.8	3.0
Kr	8.4	3.3
¹³¹ Xe	8.7	3.8
¹³² Xe	9.4	4.0
¹³⁴ Xe	9.4	3.9
¹³⁶ Xe	8.6	3.7
Xe	9.0	3.8

4.2.3. Result assessment

First of all, it is important to note that whatever the technique employed in order to determine the FGR, the results are very similar. In fact, the differences observed between these results - for a same experimental sequence- are inferior at 0.6 %.

A striking difference between the two batches of tests concerns mainly the total release of ⁸⁵Kr for a same thermal history, as shown in Table 1. The fractional release for “rod B” was larger during a considered test than that for “rod A”, despite a similar burn-up : 8.8 % and 2.8 % for “rod B” and “rod A” respectively (test A5-0).

Moreover, as far as the release rate is concerned, another difference is observed (figures 1 and 2): the release begin to be measurable at $T < 200^{\circ}\text{C}$ for “rod B” and reaches ~2% at the end of the thermalization plateau (300°C). In the “rod A” case, no significant release is measured before the increase of temperature from the thermalization plateau to the upper plateau. One can note that the same general behaviour is obtained with all the tests regarding “rod B” batch of experiments (i.e. FGR ranging from 1.4 % up to 2 % for temperature ranging from room temperature up to 300°C).

The last important points, which need to be highlighted, regarding ⁸⁵Kr behaviour, are related to the parameters, which seem to affect its total release. From a general point of view, one can observe that two main parameters influence the final FGR value:

- (i) the duration of the test: the total gas release fraction is higher for the A5-0 test (rod B) than for all the other “rod B” tests;
- (ii) a critical temperature (estimated on-line around 1100°C): the total gas release fraction increases if this temperature is reached or exceeded and maintained during a few minutes: 8.8%, 5.4 % and 5.2% respectively for A5-0, A5-1 and A5-2 to be compared to 3.3% (A5-2bis) and 3.2% (A5-3).

Finally, for the test which is the most representative of a thermal LOCA sequence (A5-2, rod B, from 300°C), it has been determined that the total FGR value is roughly equally distributed between the increase of temperature and the upper temperature plateau.

4.3. Comparison of the 4 cycles UO₂ campaign results with the CEA fuel performance code METEOR

The aims assigned to the calculation of the GASPARD experiments is:

- (i) to help to the understanding of the phenomena involved in fission gas behaviour during thermal analyses,
- (ii) to assess this behaviour in order to be able to extrapolate to LOCA conditions in reactor.

4.3.1. Adaptation of the METEOR code to thermal transient modelling

Base irradiation and thermal upgraded version of the CEA fuel behaviour code METEOR. This code is notably used to determine the thermal-mechanical behaviour of the fuel rod, the fission gases distribution and release and the fuel microstructure evolution under neutron flux (HBS and MOX plutonium cluster behaviour. Several papers have already described this code (e.g. [15] and [16]).

Several improvements have been implemented in the upgraded version of METEOR to allow the GASPARD test analysis and interpretation:

- a) during base irradiation, a better description of the specific surface of the grain boundary before inter-connection, and a rim model increasing the fission gas bubbles retention capability thanks to an overpressure hypothesis,
- b) during thermal transient, the introduction of a grain boundary rupture threshold due to the inter-granular gas bubbles overpressure is added to the interconnection bubbles modelling. A description of the intra-granular gas thermal diffusion in atomic form has also been taken into account, which was not described before as the matter of fact for normal cooling conditions, diffusion of bubbles under thermal gradient is considered as preponderant in transient conditions.

4.3.2. Calculation unfolding and parameters reproduced

Base irradiation of the long fuel-rod has been calculated. For each GASPARD sample, the end-of-life inter-granular / intra-granular fission gas distribution is calculated. At power conditions however the current version of the code doesn't allow to calculate the bubbles spectrum (number and size). Calculated FGR in the free volumes has been compared to the experimental results obtained by rod puncturing.

GASPARD thermal transient has been reproduced from external clad temperature and pressure time history. The code is well fit also to describe as precisely as possible the stress conditions in the fuel which are specific due to the loss of the cladding constraint, axially because of the experimental procedure and radially due to the loss of clad mechanical properties with the micro structural transition phase around 1120°K (850 °C).

4.3.3. Comparison METEOR code calculations – experimental results for 4 cycles UO₂ samples

- (a) Gases distribution at the end of the base irradiation

FGR distribution and release at the end of the irradiation in power reactor are summarized on table 3 below (FGR are given in % of the inventory built up during base irradiation):

Table 3. Fission gas distribution at the end of the base irradiation for two 4 cycles UO₂ fuels

UO ₂ 4 cycles Rod A	Burn-up (GWd.t-1)	Measured FGR (%)	Calculated FGR (%)	Calculated quantity of gas in inter- granular position (%)	Calculated quantity of gas in intra- granular position (%)
Mean value (father rod)	43.1	0.43	0.32	9.5	90.2
Mean value (GASPARD samples)	48.0	/	0.37	10.4	89.2
UO ₂ 4 cycles Rod B	Burn-up (GWd.t-1)	Measured FGR (%)	Calculated FGR (%)	Calculated quantity of gas in inter- granular position (%)	Calculated quantity of gas in intra- granular position (%)
Mean value (GASPARD samples)	48.5	/	2.2	7.9	89.9

As shown on table 3, there is a good agreement between calculated and measured FGR for father-rod A. For rod B (which was a segmented father-rod), measurement of the FGR has not been performed on the GASPARD segment, but it is worthwhile to notice that a FGR equal to 2% has been measured on a neighbouring segment of the same father-rod. This value is in good agreement with the FGR calculation for rod B.

(b) FGR during the GASPARD thermal analyses and evolution of the gases distribution during the transient

Table 4 below shows:

- the quantity of ⁸⁵Kr released during the test and measured by on-line gamma spectrometry,
- the corresponding calculated value,
- the calculated proportion of intra-granular gases which had time to migrate until inter-granular position during the test,
- the calculated proportion of gases which still remains in inter-granular position at the end of the thermal analysis.

All the values are given in percentage of the inventory born during the base irradiation (the 4 cycles UO₂ samples have not been re-irradiated).

(c) ⁸⁵Kr release kinetics during the heat analysis

The METEOR code has been used for calculation of the stable isotope release kinetic during a heat analysis. An example of the calculation result, compared to the experimental kinetic, is given on figures 7 (cumulated FGR versus time) and 8 (instantaneous release) for the rod B – test A5-0. The experimental kinetic has been corrected from the hydraulical transfer function of the device. There is a quite good agreement between calculated and experimental kinetics, indicating that release mechanisms are correctly described in the METEOR code.

Table 4. 4 cycles UO₂ FGR during the GASPARD thermal analyses and evolution of the gases distribution during the transient

Test number T increase rate / Tmax / upper plateau duration Rod A	Measured ⁸⁵ Kr FGR (%)	Calculated ⁸⁵ Kr FGR (%)	Inter-granular remaining inventory (%)	Intra-granular inventory decrease (%)
Test A5-0 0.2°C/s / 1200°C / 15 mn	2.8	9.4	0.75	< 0.4
Test A5-5(1) 20°C/s / 1400°C / 2 mn	5.0	7.3	2.6	< 0.4
Test A5-5(2) 20°C/s / 1600°C / 0 mn	7.1	7.1	2.8	< 0.4
Rod B				
A5-0 0.2°C/s / 1200°C / 15 mn	8.8	8.1	0.68	0.2
A5-1 10°C/s / 1200°C / 10 mn	5.4	5.9	2.2	0.2
A5-2 20°C/s / 1200°C / 10 mn	5.2	5.3	2.8	0.2
A5-2bis 20°C/s / 1200°C / 0 mn	3.3	3.8	3.7	0.09
A5-3 20°C/s / 1000°C / 10 mn	3.2	4.8	2.7	

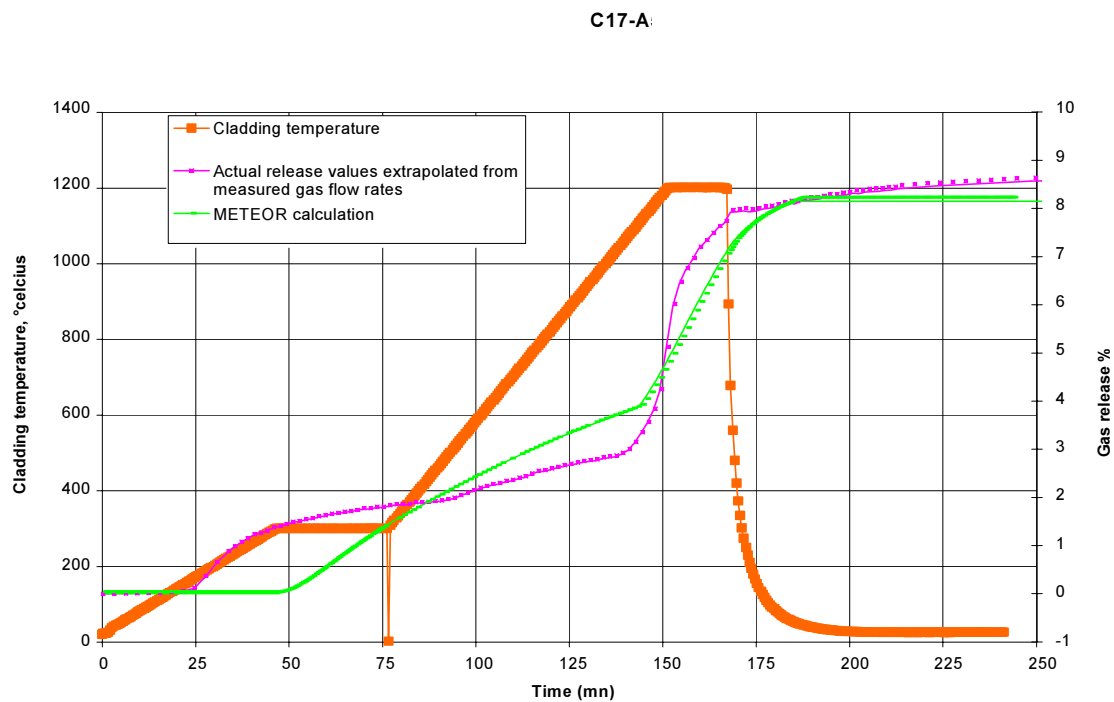


FIG. 7. Comparison calculation – measurement for the cumulated FGR kinetic (Rod B – test A5-0).

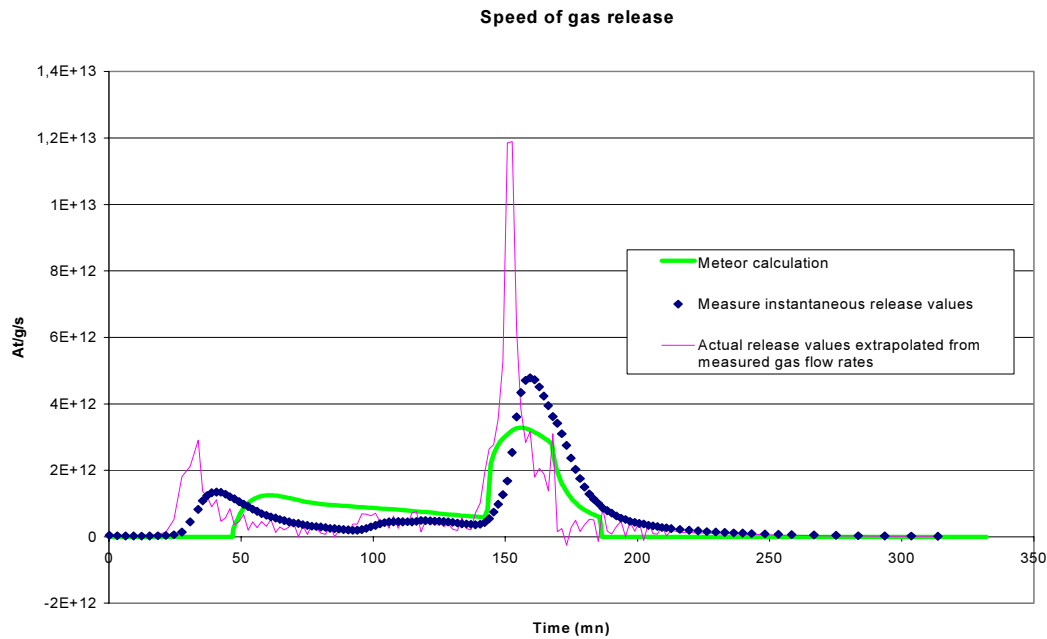


FIG. 8. Comparison calculation – measurement for the instantaneous gas release. (Rod B – test A5-0)

4.3.4. Analysis of the comparison calculations – experimental results for 4 cycles UO_2 samples

There is a good agreement between measured and calculated FGR during the thermal analyses, even for a large range of maximum temperature. This shows that the basis mechanisms promoting release of noble gases during this type of thermal transient are correctly identified and that the dependence of their efficiency versus temperature is at the right level.

These released quantities are fully compatible with the gas inventory in inter-granular position calculated by METEOR. However, at the end of the test, the calculated inter-granular quantity is very low. On another hand, the filling of grain boundaries with gases coming from inside the grains is quite low, mainly due to the short time at high temperature (above roughly $1100^{\circ}C$), which is not sufficient to activate diffusion flow in a significant way. This remark is based only on the calculation results, because samples have not been re-irradiated, so detection of a middle half-life radionuclide coming from an intra-granular inventory (such as ^{133}Xe) was not possible (see § 3.2).

All these observations mean physically that, for a 4 cycles UO_2 fuel, which undergoes a thermal transient representative of a LOCA-type sequence:

(i) the fission gas release out of the fuel is partly due to the bubbles interconnection (diffusion of atoms and vacancies at high temperature), partly to increase of their radius, and partly to the release of gases present in over-pressurized bubbles at the fractured grain boundaries.

(ii) for the same burn-up, the global FGR ranges from 3% to 9%, depending on the manufacturing microstructure, the irradiation history of the fuel and the temperature profile of the thermal transient.

(iii) a contribution to global FGR from gases placed in intra-granular position may exist, but experimental protocol didn't allow to measure it. However calculations show it is probably very low (fractional release less than 1%).

(iv) a large majority of the inter-granular gas inventory has been released even for short tests. The mechanisms proposed in i) seem to be very efficient to empty this gas into cracks or open porosity. The remaining gas inventory in inter-granular position after test is low, roughly from 1 to 3%.

(v) these conclusions show that the METEOR fuel performance code reproduces correctly the distribution of fission gases in the UO_2 fuel matrix at the beginning of the thermal analyses. Moreover, the mechanisms promoting the FGR are now correctly identified and quantified. This is notably confirmed by the good FGR kinetic reproduction.

5. CONCLUSIONS

Through an example of an out-of-pile experimental programme performed on standard 4 cycles UO_2 fuel under LOCA-type tests, this paper has shown the importance of separate effect experiments on small fuel samples to identify and quantify basic mechanisms promoting FGR out of the fuel matrix. The main objective is to provide code developers with reliable tests measuring the absolute level and the time dependence of the released fission gases and the corresponding fuel micro-structural changes during representative thermal transients.

This database is used to improve the fuel behaviour prediction capability, thanks to a better understanding. A noticeable application is to forecast the fission product "source term" out of a damaged rod during a given type of accidental sequence, with the aim to verify if existing safety criteria are well adapted to high burn-ups and to new types of fuels.

The first step of the GASPARD programme detailed in this paper shows all the benefits of a coupled approach "experimental database" and "test interpretation by models", in terms of fuel microstructure behaviour understanding.

It is clear that this experimental strategy is worthwhile to be applied to new fuels during their qualification process. For this purpose, and in order to replace as soon as possible the ADAGIO facility shutdown at the end of 2002, the CEA is assembling a new thermal analyses facility in the hot cell laboratory LECA at the CEA Cadarache, called "Pre-Mesange".

This facility will allow the same functions as the ADAGIO facility and will be operational at the end of 2003. A first campaign is scheduled on 6 cycles UO_2 to compare results obtained with the both facilities.

REFERENCES

- [1] Y. PONTILLON, C. ROURE, B. LACROIX, T. MARTELLA, S. RAVEL, B. GLEIZES, G. DUCROS : « Spectrométrie gamma : Un outil essentiel à l'étude du combustible irradié et du relâchement des produits de fission », («Gamma-spectrometry : Essential tool to study FGR from irradiated fuel » Journées de spectrométrie gamma et X 2002, Septembre 2002, Saclay (France) 43.

- [2] G. DUCROS, P.P. MALGOUYRES, M. KISSANE, D. BOULAUD, M. DURIN, A. MAILLIAT: "Fission product release and fuel behaviour under severe-accidental conditions: synthesis of the VERCORS 1 to 6 experimental program", LWR Fuel Performance (Proc. Int. Topical Meeting Park City, Utah-USA, April, 10–13, 2000), ANS, La Grange Park, Ill, 2000), CD-ROM.
- [3] B. ANDRÉ, G. DUCROS, J.P. LEVEQUE, D. MARO, M.F. OSBORNE, R.A. LORENZ, Nucl. Technol. 114, (1996), 23.
- [4] Y. PONTILLON, P. P. MALGOUYRES, F. CECCALDI, M. KISSANE, D. BOULAUD, M. DURIN: "Fission-product release and fuel behaviour in severe accident conditions: results of the first VERCORS RT experiments concerning MOX (UO₂/PuO₂) fuel", CSARP Annual Review Meeting, May, 7–9, 2001, Washington D.C.
- [5] Y. PONTILLON, F. CECCALDI, G. DUCROS, P.P. MALGOUYRES, M. KISSANE, D. BOULAUD,, J.M. EVRARD, "Fission product release and fuel behaviour in severe accident conditions : results of the first VERCORS RT experiments concerning UO₂ and UO₂-ZrO₂ debris-bed", Cooperative Severe Accident Research Program meeting, May, 2002, Albuquerque, New Mexico, U.S.A.
- [6] G. DUCROS, M.P. FERROUD-PLATTET, P.P. MALGOUYRES, M. TOURASSE, D. BOULAUD: "The VERCORS HT program: parametric study of fission product release up to molten core conditions", CSARP Annual Review Meeting, May, 5–8, 1997, Bethesda
- [7] Y. PONTILLON, G. DUCROS, P.P. MALGOUYRES, C. FICHE, M. KISSANE, D. BOULAUS, J.M. EVRARD, "Fission product release and transport in severe-accident conditions: comparison between VERCORS HT1/HT2/HT3 experiments concerning UO₂ fuel in reducing and oxidizing conditions with and without control rod components", Cooperative Severe Accident Research Program meeting, May 2003, Bethesda, Maryland, U.S.A.
- [8] Y. PONTILLON, G. DUCROS, P. P. MALGOUYRES : "Effect of high burn up and MOX fuels on fission product release from VERCORS tests", 5th PHEBUS FP Seminar, June 2003, Aix-en-Provence, France
- [9] S. VALIN, A. MOCELLIN, G. EMINET, J.C. JOUBERT: "Modelling the behaviour of intergranular fission gas during out of pile annealing", Fission Gas Behaviour in Water Reactors Fuels (Proc. Int. Seminar Cadarache, France, September, 26–29, 2000), OECD/NEA, Paris, France (2001) 357.
- [10] L. NOIROT, C. STRUZIK, P. GARCIA, J. NOIROT : « A mechanistic fission gas behaviour model for UO₂ and MOX fuels", Fission Gas Behaviour in Water Reactors Fuels (Proc. Int. Seminar Cadarache, France, September, 26–29, 2000), OECD/NEA, Paris, France (2001) 131.
- [11] E. MULLER, F. LEMOINE, R. SAUREL : « A dynamic model for the fission gas induced swelling in high BU fuel under fast power transient », Fission Gas Behaviour in Water Reactors Fuels (Proc. Int. Seminar Cadarache, France, September, 26–29, 2000), OECD/NEA, Paris, France (2001) 211.
- [12] S. RAVEL, G. DUCROS, T. PETIT, L. CAILLOT, G. EMINET: "Partition of grain boundary and matrix gas inventories in nuclear fuel : the ADAGIO facility", European Working Group "Hot Laboratories and Remote Handling" Meeting, September, 21–23, 1998, Windscale (UK).
- [13] Y. PONTILLON, S. RAVEL, D. PARRAT, M.P. FERROUD-PLATTET, Y. GUÉRIN: "Fission gaz release under fast and transient conditions : Analytical devices implemented at Commissariat à l’Energie Atomique", Fuel Behaviour under Transient and LOCA Conditions (Proc. IAEA Tech. Com. Mtg Halden, Norway, 10/14, September, 2001), IAEA-TECDOC-1320, Vienna (2002) 241.

- [14] S. RAVEL, E. MULLER, G. EMINET, L. CAILLOT : « Partition of grain boundary and matrix gas inventories : results obtained with the ADAGIO facility », Fission Gas Behaviour in Water Reactors Fuels (Proc. Int. Seminar Cadarache, France, September, 26–29, 2000), OECD/NEA, Paris, France (2001) 347.
- [15] C. STRUZIK, P. GARCIA, L. NOIROT : « A comparative study on fission gas behaviour in UO₂ and MOX fuels using the METEOR fuel performance code », Fission Gas Behaviour in Water Reactors Fuels (Proc. Int. Seminar Cadarache, France, September, 26-29, 2000), OECD/NEA, Paris, France (2001) 511.
- [16] C. STRUZIK, M. MOYNE, J.P. PIRON: “High burn-up modelling of UO₂ and MOX fuel with METEOR/TRANSURANUS Version V 1.5”, LWR Fuel Performance, (Proc. Int. Topical Meeting, Portland, Oregon-USA, March, 2–6, 1997), ANS, La Grange Park, Ill, USA (1998) 126.

EVOLUTION OF FUEL PELLET STRUCTURE AND
THERMAL PROPERTIES AT HIGH BURNUP

(Session 4)

Chairpersons

V. NOVIKOV
Russian Federation

D. PARRAT
France

THE MICROMOX PROJECT: A STUDY ABOUT THE IMPACT OF ALTERNATIVE MOX FUEL MICROSTRUCTURES ON FGR

M. LIPPENS⁽¹⁾, P. COOK⁽²⁾, PH. RAISON⁽³⁾
R.J.M. KONINGS⁽⁴⁾, K. BAKKER⁽⁵⁾, C. HELLWIG⁽⁶⁾

⁽¹⁾ Belgonucleaire S.A,
Belgium

⁽²⁾ British Nuclear Fuel Limited,
United Kingdom

⁽³⁾ JRC - Institute for Energy,
Netherlands

⁽⁴⁾ JRC - Institute for Transuranium Elements,
Germany

⁽⁵⁾ Nuclear Research and Consultancy Group,
The Netherlands

⁽⁶⁾ Paul Scherrer Institut,
Switzerland

Abstract

MICROMOX project inscribes in a research program for reducing the MOX fuel burnup limitation due to its excessive fission gas release, which leads to large consumption of margins relatively to design criteria. In order to reduce the amount of gas release and the associated inner pressure, fuels with increased gas retention capability is envisioned to be used. In this framework MOX fuels presenting potentially different degrees of gas retention will be fabricated, irradiated and tested under transient conditions. Four different fuels are considered in the present studies: homogeneous MOX fuel with large grain size that is expected to have a better gas retention capability, MOX fuel showing a constant Pu distribution at microscopic level, MOX fuel showing at micron size level an irregular Pu distribution that probably has a lower gas retention, and an UO₂ fuel with standard grain size to be used as reference material. These fuels are loaded in instrumented rodlets and irradiated at moderate rating in the High Flux Reactor (HFR) to achieve a burnup of 60 GWd/tM in 2 years. All along the irradiation, the central temperature and inner pressure evolution are recorded. The end of the irradiation consists in a temperature transient in which the fission gas release is followed as a function of fuel temperature. Post-irradiation examinations of fuels will be made, focusing on fission gas release and fuel microstructure. The behaviour of the irradiated fuel will be simulated by different codes dedicated to the in-reactor fuel thermal – mechanical performance. MICROMOX project is a cost shared action developed in the 5th EC FP, which started on October 1, 2000.

1. INTRODUCTION

High burnup is technically less easy to achieve with (U,Pu)O₂ (MOX) fuel than with standard UO₂ fuels because of the larger rod inner pressure build-up resulting from an increased fission gas release (FGR) [1], due to the intrinsic nature of the MOX fuel (neutronic properties, physical properties, fuel microstructure).

Reduction of gas release and rod inner pressure are however possible by combining or using one of the following methods: increase of rod inner free volume, reduction of fuel central temperature, use of fuel with increased capability of gas retention.

The objectives of the MICROMOX project are to fabricate, irradiate to burnup close to 60 GWd/tM and test in transient conditions MOX fuels potentially representing different degrees of gas retention.

Better gas retention in MOX fuel by increase of its grain size is contemplated, based on a similar successful experiment performed on UO₂ [2]. One of the major objectives of MICROMOX project is to demonstrate and to quantify the obtained advantages to use MOX fuel with larger grain size.

MOX fuels prepared by mechanical blending of UO₂ and PuO₂ powders show at microscopic level a fine dispersion of the Pu in the UO₂ matrix with micron size zones of relatively high Pu content. These zones are considered by some authors as contributing to the high FGR observed in MOX fuel [1]. To quantify the gas release which could be attributed to the presence of Pu-rich zones, the MICROMOX project has for objective to fabricate, test and model MOX fuel showing an uniform distribution of the Pu at the microscopic scale and to compare its performance to the one of a MOX fuel showing a Pu distribution under the form of micron size Pu-rich zones.

The fuel test matrix of the MICROMOX Project is composed of:

- MOX fuel showing an uniform Pu distribution and a large grain size,
- MOX fuel showing an uniform Pu distribution and a standard grain size,
- MOX fuel showing an inhomogeneous Pu distribution and a standard grain size,
- UO₂ fuel of standard characteristics, used as reference.

This paper presents the organization of the project, highlights its main technical aspects, and summarizes its present status.

2. PROJECT DESCRIPTION

2.1. Partnership

To achieve the MICROMOX objectives, a consortium has been constituted, grouping partners involved in fuel development, fuel fabrication, and/or fuel design: BELGONUCLEAIRE (BN), British Nuclear Fuel Limited (BNFL), Institute for Transuranium (ITU), Institute for Energy (IE), Nuclear Research and consultancy Group (NRG) and Paul Scherrer Institut (PSI).

These partners contribute all to the good performance of the project with specific leadership:

- fuel rodlet design: BN;
- fuel sample-holder design and construction : IE and NRG;
- fuel and rodlets fabrication: ITU;
- irradiation: NRG and IE;
- post-irradiation examination: NRG and PSI;
- modelling: BN, BNFL, ITU, and PSI .

2.2. Technical description

2.2.1. Fuel rodlets

The fuel pellets are fabricated according to standard specifications for LWR, for their specific chemical and micro-structural properties.

The enrichments for MOX and UO₂ that would allow to obtain the high specific power and to rapidly accumulate the burnup is about 9.5% Pu/(U+Pu) and 13.2% U235 respectively.

Homogeneous fuels MOX and UO₂ are fabricated according to the SOL-GEL technique while the heterogeneous MOX fuel is produced by direct mechanical blending of pure UO₂ and PuO₂ powders.

Large grain size in homogeneous MOX fuel is achieved by sintering in moistened atmosphere.

Figures 1 to 3 highlight the obtained fuel microstructures. Figure 1 illustrates for the homogeneous MOX fuels the difference in grain size (10µm for the small grain and 21 µm for the large). Alpha-radiographies point out the Pu-rich particle presence for the heterogeneous MOX fuel (Figure 2). Ceramography on this fuel (Figure 3) shows grain size difference in the UO₂ matrix (4 µm) and in the Pu-rich particles (14µm).

The fuel rodlets are composed of a short fuel stack (about 7 cm length) loaded in stainless steel cladding (6.55 x 5.65 mm). For each fuel type, two rodlets are fabricated. For each pair, one rodlet is instrumented with central thermocouple and pressure transducer; the other one is not instrumented. Both rodlets types are filled with 6 bar He to prevent any thermal feedback during irradiation. The mounting of the instrumented rodlets was performed at NRG/IE while the uninstrumented rodlets were mounted at ITU.

2.2.2. The sample-holder

The eight rodlets will be irradiated in the HFR by means of a dedicated sample-holder loaded in a TRIO irradiation rig [3]. The sample-holder consists of a stagnant sodium bath (200 cc) contained in a stainless steel cylinder 65 cm long (Figure 4). It is loaded in one of the three channels of the TRIO rig, which occupies one HFR core periphery position.

The heat transfer from the rodlet is carried out by thermal conduction through the sodium bath, steel containments and a gas gap in between. The adjustment of the gas in the gas gap allows to modify the rodlet temperature.

The sample holder is instrumented with 28 thermocouples, 9 gamma scan wires and 4 neutron fluence monitors.

2.2.3. Irradiation conditions

The general technical purpose of the experiment is the measurement of FGR during a temperature transient for different fuel types irradiated at a burnup close to 60 GWd/tM. To match that objective, the base irradiation up to about 60 GWd/tM will be carried out at linear power as high as possible, but low enough to prevent massive fuel restructuring and fission gas release. For a MOX segment, the initial linear power will be around 260 W/cm and will decrease down to 150 W/cm by the end of the two years of irradiation. The base irradiation will be terminated by rapid fuel temperature excursion simulating the one that occurs during commercial reactor operations. The transient will be followed by a hold of a few days at the transient terminal power.

During irradiation, the experiment is monitored by on-line instrumentation that consists of pressure transducers and thermocouples, positioned around the fuel rodlets and in the fuel rodlets. This will allow to continuously follow and detect the influence of the base irradiation and the transient on the fuel performance.

2.2.4. Post-Irradiation Examinations (P.I.E)

After discharge of the sample holder from the core, neutron radiography will be performed and the gamma-scan wires and neutron fluence monitors will be recovered for measurements.

The fuel rodlets will be submitted to non-destructive and destructive examinations to confirm neutronic calculations and burnup, to correlate in-reactor pressure measurement and rodlets fission gas release, and to study fuel microstructure and extent of fission product redistribution. Most of these works will be done at NRG with contribution of PSI for the burnup radiochemical determination.

2.2.5. Fuel modelling

Despite excellent calibration of codes and reliability of fuels design calculations, fuel modelling still remains a delicate work, especially regarding the description of fission gas release in complex structures. For that reason, it has been proposed to have in the MICROMOX project, a comparison of the performance of thermal-mechanical codes simulating the fuel in-reactor performance, and to run the codes for the MICROMOX fuels.

The codes COMETHE, ENIGMA-X, TRANSURANUS and TRANSURANUS/PSI, developed by BN, BNFL, ITU and PSI respectively, will be used for this comparison. The PSI code is based on TRANSURANUS, extended with the latest, mechanical fission gas release model developed at PSI.

First a benchmarking of the codes was performed against test data. After irradiation, the codes will simulate the behaviour of the eight fuel rodlets for the complete irradiation history.

The main outputs (central temperature and inner pressure evolution) will be compared to the experimental data, leading to better understanding of the different model approaches.

3. MAIN ACHIEVEMENTS

The MICROMOX project officially started in October 2000. Today, the fuel rodlet design and fabrication, and sample holder design, fabrication and mounting are completed. The start of irradiation is scheduled for October 2003. The end of the project is foreseen for mid 2006.

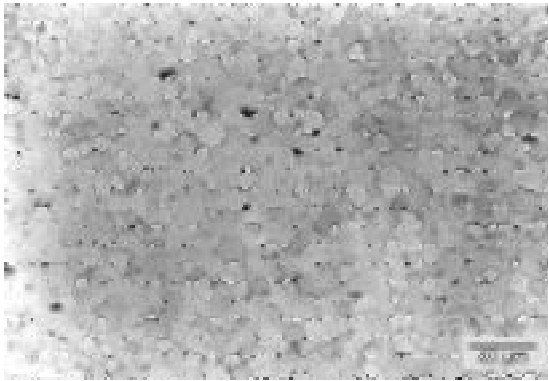
4. CONCLUSIONS

High burnup achievement with MOX fuels is presently limited due to excessive fission gas release (FGR). MOX fuels presenting potential for increased gas retention are tested in the MICROMOX project launched with the support of the EU 5th framework programme in collaboration between BN, BNFL, JRC-IE, JRC-ITU, NRG and PSI.

Today, the rodlet and sampleholder design is completed as well as the fuel pellet fabrication and the rodlets and sample holder mountings. The irradiation starts in October 2003.

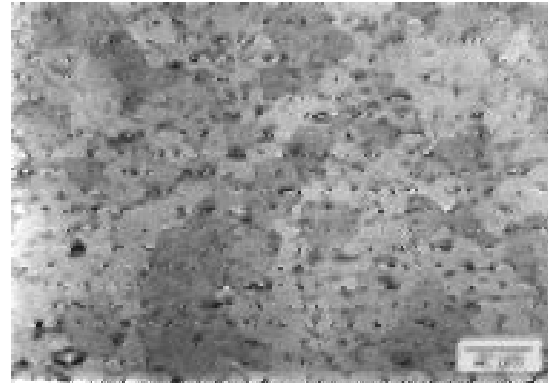
Experimental results on FGR will be obtained in 2003 up to 2005 during base irradiation and mid 2005 in transient conditions.

Small grain MOX fuel



G = 10 μ m

Large grain MOX fuel



G = 21 μ m

Figure 1. Grain size in homogeneous MOX fuel.s

Homogeneous MOX fuel



Heterogeneous MOX fuel

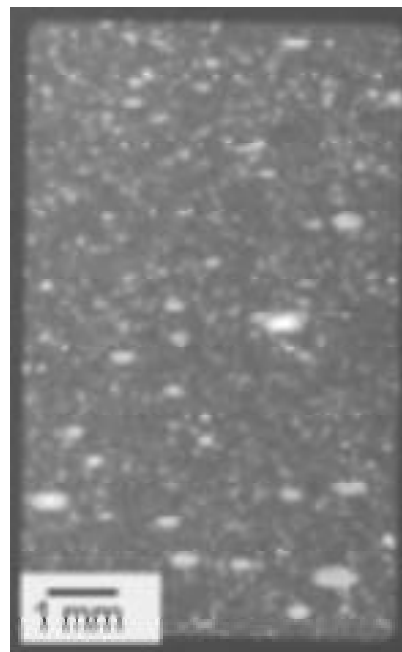


Figure 2. Pu distribution through alpha-radiography.

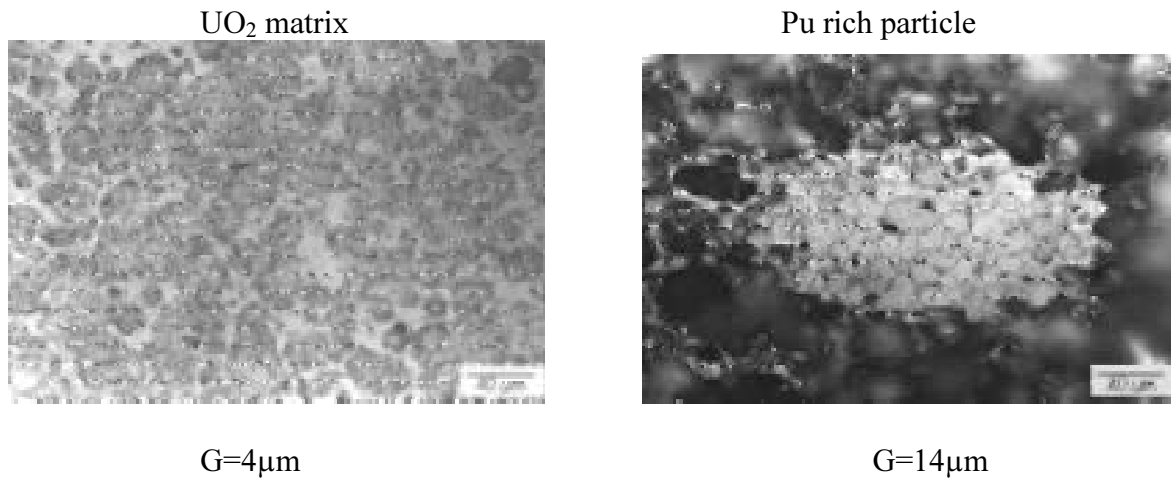


Figure 3. Grain size in heterogeneous MOX fuel.

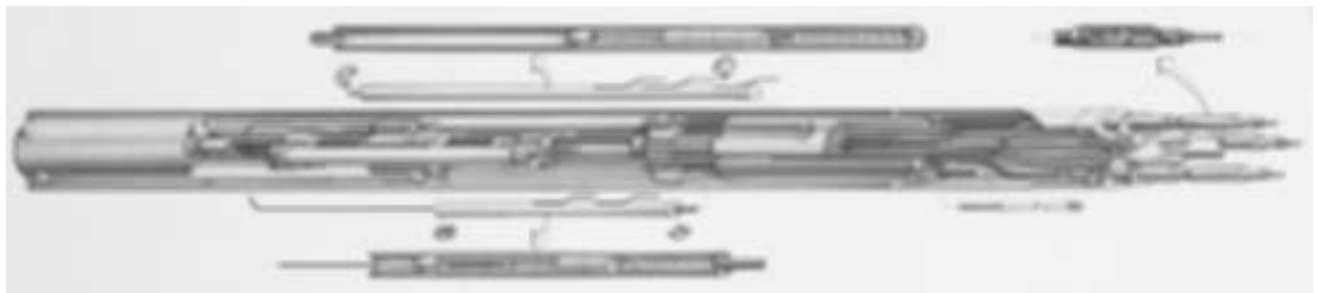


Figure 4. Sample holder.

REFERENCES

- [1] P. BLANPAIN et Al., “MOX Fuel Experience in French Power Plants”, LWR Fuel Performance (Proc. Int. Top. Meeting West Palm Beach, Florida, April 1994), ANS, La Grange Park, Ill (1994) 718.
- [2] M. HIRAI et Al. “Performance of improved UO₂ Pellets at High temperature”, LWR Fuel Performance (Proc. ANS Topical Meeting Portland, Oregon, USA, March 1997), ANS, La Grange Park, Ill (1997) 490.
- [3] EUROPEAN UNION, J. AHLF, A. ZURITA, eds, “High Flux Reactor (HFR) Petten - Characteristics of the installation and the Irradiation facilities”, EUR 15151 EN, 1993.

OXIDE FUEL — MICROSTRUCTURE AND COMPOSITION VARIATION (OMICO)¹

M. VERWERFT¹, M. WÉBER¹, S. LEMEHOV¹, V. SOBOLEV¹, TH. Aoust¹,
V. KUZMINOV¹,
J. SOMERS², G. TOURY², J. MCGINLEY², C. SELFSLAGS², A. SCHUBERT², D. HAAS²,
PH. VESCO³ AND P. BLANPAIN³

¹ SCK•CEN
Mol, Belgium

² JRC-ITU
Karlsruhe, Germany

³ Framatome ANP
Lyon, France

Abstract

The mixed (U,Pu)O₂ (MOX) fuel currently used in Light Water Reactors (LWR's) is similar to UO₂ fuel in many aspects, but it differs by its heterogeneous microstructure with enriched islands in a depleted matrix. Even though well-validated codes for MOX fuel exist, there is still discussion on the role of the MOX microstructure, especially regarding fission gas release. The EC co-sponsored 5th Framework Project “Oxide Fuel – Microstructure and Composition Variation” (OMICO) studies and models the influence of microstructure and matrix composition on nuclear fuel behaviour in Pressurised Water Reactor conditions. This presentation will give an overview of the objectives and status of the OMICO project. A matrix of six instrumented and six non-instrumented fuel rod segments will be irradiated under representative pressurised water conditions. There are three fuel compositions (UO₂, (U,Pu)O₂ and (Th,Pu)O₂), each with two microstructures (homogeneous and fine dispersed ceramic-in-ceramic). The homogeneous fuels are prepared using the sol-gel method and the heterogeneous fuels are prepared by powder metallurgical routes: the MICronised MASTer blend or MIMAS process for the UO₂, (U,Pu)O₂ fuels and a similar method for the (Th,Pu)O₂ fuel. Theoretical work will be performed to incorporate the different fuel types in fuel performance codes and the experimental results of the in-pile and out-of-pile data will serve as the basis for code benchmarking and model development. The OMICO project started in October 2001 and is now approaching its in-reactor phase. During the first two years of the program execution, the detailed design and fuel production were completed and pin assembly is nearly completed. The start of the irradiation is foreseen in March 2004 and last for two years. On the theoretical side, the first benchmarking exercise between three fuel performance codes (TRANSURANUS, COPERNIC and FEMAXI) was performed using the design parameters and expected irradiation history. Advances were made in the assessment of the power density profiles for the (Th,Pu)O₂ fuels, for which little data are currently available.

1. INTRODUCTION

The proposed test matrix compares in a systematic way the behavior of three different fuel compositions (UO₂, (U,Pu)O₂ and (Th,Pu)O₂), and for each composition, two different microstructures are inter-compared (homogeneous and fine dispersed ceramic-in-ceramic).

¹ Work co-financed by the European Commission under the 5th Framework Program of the Euratom (Research and Training in the field of Nuclear Energy).

This results in six different fuel types, which will be assembled in a small experimental assembly and irradiated under representative Pressurized Water Reactor conditions (i.e. at 155 bar, 300°C, with controlled water chemistry: 400 ppm B, $6.9 < \text{pH}_{300} < 7.4$ and 25 cc/kg $<[\text{H}_2] < 35$ cc/kg). The primary objective is to provide insight in the separate effects of fuel chemistry (matrix composition) and the degree of dispersion of the fissile material (microstructure).

Two sets of six fuel rods will be irradiated, one set instrumented for pressure and temperature measurement, and a second set that can be unloaded at different intervals for non-destructive analyses. The on-line measurement of two essential parameters (gas pressure and central temperature), complemented by intermittent out-of-pile non-destructive tests provides a set of data with which the calculated predictions of fuel behaviour are to be compared. The flexibility of irradiation conditions offered by a materials testing reactor allows imposing specific irradiation conditions, the results of which are available on-line, to test various hypotheses on the response of the fuel.

2. WORK PROGRAM

The project is divided in six work packages:

1. Detailed design of the experiment, including: the detailed design of the fuel and fuel rod, an elementary design of the irradiation rig and the definition of an irradiation history;
2. Fuel fabrication, fuel rod assembly and instrumentation and transport. Standard fabrication controls on the as-fabricated fuel and fuel rods is also part of this work package;
3. As the proposed experiment makes use of experimental fuel, a more detailed characterization, with emphasis on the microstructure, O/M ratio and thermal properties is essential for the correct modeling of its properties;
4. Irradiation experiment:
 - a. Development of the irradiation rig, preparation of the on-line measurements and the detailed calculation of the irradiation history;
 - b. Actual irradiation, including the on-line measurement of the temperature and internal pressure of the instrumented fuel pins;
5. Intermittent out-of-pile non-destructive post-irradiation tests which are complementary to the on-line measurements;
6. Benchmarking of fuel performance codes as well as the development of an improved model for fission gas release based on the experimental results.

3. MAIN ACHIEVEMENTS

Until now, activities focused mainly on design (WP1, completed), fuel fabrication and rod assembly (WP2, almost completed), preparation for the irradiation (WP4a, almost completed) and modeling (WP6). The achievements obtained in these work packages are detailed in the following paragraphs.

3.1. Design calculations

The initial irradiation history was determined on the basis of the OMICO targets: in order to study the thermal threshold for fission gas release, it was decided to aim at a few percent FGR during the second year of irradiation in the pressurized water loop CALLISTO of the BR-2

reactor at Mol. Further constraints were imposed on the irradiation history: the threshold of fuel restructuring should not be reached, sufficient burnup should be obtained within the given time frame (210 effective full power days) and the fissile isotope distribution should be representative etc. These constraints have led to a search for an optimal compromise between fuel pin diameter, fissile isotope content, irradiation conditions etc. The essential results of the design optimization process are presented in table I.

The energy distribution in the fuel rods is determined with 3-D neutron transport code calculations. In order to account for the complex geometry of the BR2 Materials Test Reactor with a variety of irradiation programs, two recently introduced, independent and detailed MCNP models of BR2 were used. They include the nearly exact geometrical representation not only of the driver fuel elements with their axial burn-up distribution, but also of partially inserted control and regulating rods, of experimental devices and of radioisotope production rigs. This approach allows taking into account all perturbing effects. Several benchmark exercises were performed using the results of in-pile and out-of pile measurements of a running experiment in the same CALLISTO loop [1, 2]. These exercises reduced the uncertainty margins of predictive calculations with the recently introduced 3D models.

Table I. Pellet design parameters

		A	B	C	G	H	I
Fuel type		UO ₂	(Th,Pu)O ₂	UO ₂	(U,Pu)O ₂	(Th,Pu)O ₂	(U,Pu)O ₂
Technology		sol-gel	sol-gel	MIMAS	sol-gel	SOLMAS	MIMAS
Enrichment*	%	9.0	8.0	9.0	9.1	12.8	9.0
Density	%	95	96	95	96	95	95
Grain size	µm	12	5	5	12	5	5
Densification	%	0.1	0	0.4	0.1	0	0.4
Height	mm	7.14	7.14	7.14	7.14	7.14	7.14
Diameter	mm	5.9	5.9	5.9	5.9	5.9	5.9

Fuel performance calculations were made with different codes (FEMAXI-V, TRANSURANUS and COPERNIC). The code calculations show good correspondence between all three codes regarding the UO₂ fuel rods, but more important discrepancies for both mixed oxide fuels (U,Pu)O₂ and (Th,Pu)O₂. At that stage, in-depth investigations and code detailed cross-comparisons are necessary to understand the discrepancies and to assess a common base for further modeling work. It was originally foreseen to cover these aspects in work package 6.

The fuel performance calculations predict a systematic higher temperature for:

- (U,Pu)O₂ fuels as compared to UO₂ (despite of lower linear heat rates for MOX)
- MIMAS-type fuels as compared to sol-gel type fuels.

The same systematic differences can be seen in the calculated fission gas release. As soon as the empirical threshold for onset of fission gas release is exceeded, the predicted effect of the fuel composition (MOX vs. UO₂) is larger than that of the fuel production route (MIMAS vs. sol-gel).

3.2. Fuel production and pin assembly

For the OMICO irradiation test three homogeneous and three heterogeneous fuels have been fabricated. The homogeneous UO_2 , $(\text{Th,Pu})\text{O}_2$ and $(\text{U,Pu})\text{O}_2$ have been manufactured using the ITU sol gel method. The MIMAS process, used to produce the heterogeneous UO_2 and $(\text{U,Pu})\text{O}_2$ fuels, is based on powder metallurgy, in which a primary blend is formed by milling of the constituents and is then diluted to give the final secondary blend. The SOLMAS process, used to produce the heterogeneous $(\text{Th,Pu})\text{O}_2$ fuel, differs from the MIMAS process in that the primary blend is prepared by the sol gel process. The enrichment of the fissile component (Pu or ^{235}U) in the primary blends was 30%. The density of the product pellets is given in Table 2.

Table II. As-fabricated pellet dimension and density

	Fuel		Diameter (mm)	Height (mm)	Density		
					%TD	STD	Spec.($\pm 1\%$)
A	UO_2	homo	5.907	7.755	96.0	0.1	95
B	$(\text{Th,Pu})\text{O}_2$	homo	5.905	7.416	98.0	0.3	96
C	UO_2	hetero	5.901	7.894	95.2	0.2	95
G	$(\text{U,Pu})\text{O}_2$	homo	5.904	7.393	96.1	0.3	96
H	$(\text{Th,Pu})\text{O}_2$	hetero	5.903	7.052	96.6	0.6	95
I	$(\text{U,Pu})\text{O}_2$	hetero	5.903	7.698	95.7	0.3	95

The microstructure of the $(\text{Th,Pu})\text{O}_2$ fuel is shown in Figure 1. Porosity outlines the original sol gel beads. The autoradiograph indicates that interdiffusion between the ThO_2 matrix and the $(\text{Th,Pu})\text{O}_2$ primary blend occurs within the pellet, but to a much lesser extent within *ca.* 300 μm of the periphery. Though not so clear in the ceramograph shown here, less porosity is observed in this external region.

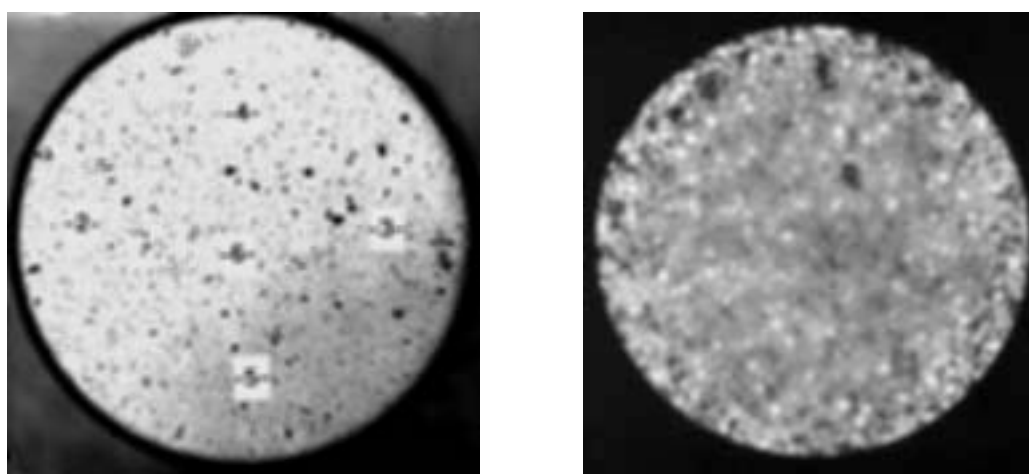


FIG. 1 Ceramograph (left) and alpha autoradiograph (right) of the heterogeneous $(\text{Th,Pu})\text{O}_2$ fuel (diameter= 5.9 mm).

3.3. In-pile experimental part: rig modifications and experiment control

The CALLISTO experimental facility in which the OMICO fuel rods will be irradiated needed several adaptations to comply with the program requirements. A new zircaloy-4 fuel basket is made of two parts that can be disconnected:

- a. the upper basket (figure 2) containing the instrumented fuel rods, the electrical cables of which are fixed to the existing CALLISTO components and
- b. the lower basket designed to allow non-instrumented rods to be loaded and unloaded during reactor shut-downs.

The OMICO irradiation experiment requires extensive instrumentation, not only of the fuel rods themselves (pressure and temperature), but also neutron measurement (to allow on-line assessment of the irradiation conditions) and coolant temperature measurements (for general operating of CALLISTO as well as for thermal balance: bundle power registration).

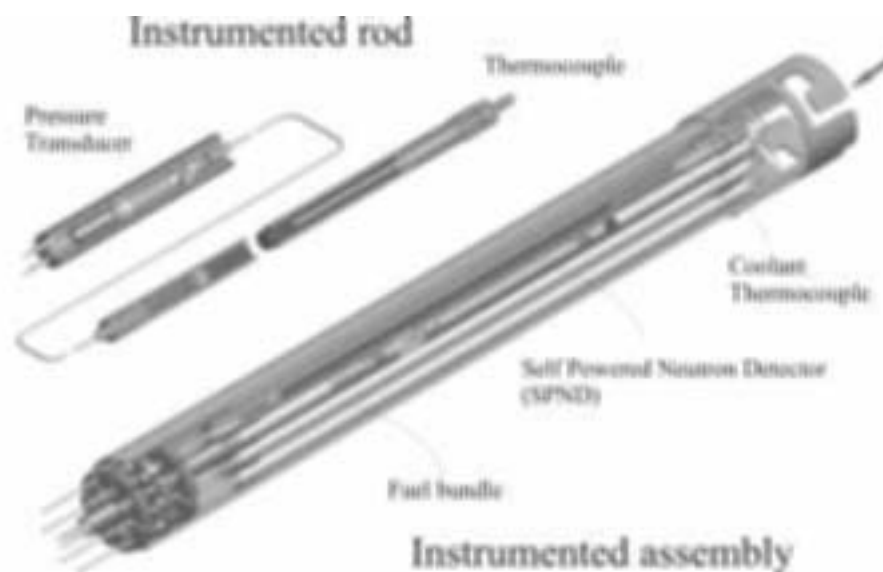


FIG. 2. Three-dimensional view of a fuel rod instrumented with central thermocouple and pressure transducer (top left) and the bundle of instrumented fuel rods in its assembly (bottom right). The length of the fuel bundle is approximately 35 cm (the bottom is at the right, the top at the left side and the water flow is indicated by the arrow).

The CALLISTO In-Pile Section upper flange was extensively modified to allow the feed through of approximately 40 instrument read-out cables. It is now qualified according to the ASME III Class 1 construction code. Because of the non-standard rods and because of the basket splitting, the CALLISTO standard procedure [3] used to measure the on-line linear power of each individual rod needed to be updated. The new on-line power measurement method relies on the existing one, on calibration processes (for which a mock-up was specially constructed) and on data from the MCNP predictive calculations. This method will be validated with data gained from previous CALLISTO programmes and by comparison with the interim Non Destructive Testing results (gamma-spectrometry) and with Self Powered Neutron Detector measurements.

The fabrication and the reception of most new rig parts are completed; completion of the components assembly is waiting for the rod delivery. Modifications of the rod on-line measurements are running and fuel rod detectors are ready for assembly.

3.4. Theoretical developments

Fuel modeling in general follows two main directions: development of models for individual fuel properties (such as thermal conductivity, heat generation profile, radial burnup distributions, isotope in-pile depletion/burning and build-up, etc.) and development of integral tools, i.e. fuel performance codes, capable of predicting in-reactor behavior of fuel rods. At SCK•CEN, two new modules for the mechanistic fuel performance code MACROS have been developed and verified against existing data sets: a new version of the Depletion Model and a material module FISMAT – Fissile Materials Tabulator, which comprises the individual models for predicting thermal properties of uranium or thorium based mixed-oxide fuels containing plutonium and/or minor actinides.

The depletion module is developed such that the calculations are made with respect to the actual structure of the fuel, which can be heterogeneous or homogeneous. A routine for thermal conductivity evolution is developed based on the Ziman-Callaway theory of transport phenomena in solids and the Landau theory of sound waves propagation and attenuation in crystalline media [4]. The approach is such that reasonable predictions can be made for the thermal conductivity of materials even when only limited experimental data exist. Indeed a part of the OMICO program will provide such data for the fresh homogeneous U and Th MOX fuels.

4. DISSEMINATION AND EXPLOITATION OF THE RESULTS

A major part of the project's results are shared with third parties through the project's website (<http://www.sckcen.be/omico>). Currently, several institutes and universities have access to the latest results to perform independent fuel performance calculations using these data. Fuel behavior data are not yet available, but will of course serve for benchmarking purposes. The technical modifications to the high-temperature, high pressure loop were implemented after a complete pre-test qualification procedure, and once qualified for the OMICO project, have been duplicated to other test sections and are now being implemented in other research projects (LIRES, FIKS-CT-2000-00012).

5. CONCLUSIONS

The OMICO project has an ambitious goal of providing experimental data that directly address the complex interplay between fission gas behavior, chemical environment and physical dispersion of fissile isotopes. These data are yet to be obtained since the in-pile part of the project did not yet start. But already in its preparation, the project shows several valuable intermediate results: reduction of uncertainties in predictive power calculations, successful fuel fabrication using the sol-gel, MIMAS and SOLMAS fuel fabrication processes on laboratory scale, technical improvements of the in-pile equipment. Theoretical modeling efforts are also in their preparation state where several underlying modules are being tested and validated separately against pre-existing data.

REFERENCES

- [1] KUZMINOV, V., KOONONEN, E., “Power distribution in MOX fuel rods. Benchmark irradiation”, Report BLG-951 (2003) SCK-CEN.
- [2] AOUST, T., VERBOOMEN, B., MALAMBU, E., “BACCHANAL benchmark: Comparison of MCNP and DORT with g-Spectrometry and Thermal Balance”, Report BLG-921 (2003) SCK-CEN.
- [3] MALAMBU, E., DE RAEDT, C., WEBER, W., “Assessment of the linear power level in fuel rods irradiated in the CALLISTO loop in the high flux material testing reactor BR2”, Research Reactor Fuel Management (Proc. 3rd Int. Topical Meeting Bruges, 1999) ENS (1999).
- [4] LEMEKHOV, S.E., SOBOLEV, V., VAN UFFELEN, P., “Modelling thermal conductivity and self-irradiation effects in mixed oxide fuels”, Journal Nucl. Mat., **320** (2003) 66–76.

ON THE CHARACTERIZATION OF PLUTONIUM DISTRIBUTION IN MIMAS MOX BY IMAGE ANALYSIS

G. OUDINET, I. MUNOZ-VIALLARD, M.-J. GOTTA
Commissariat à l'Énergie Atomique CEA,
Saint-Paul-Lez-Durance

J.M. BECKER
CPE (Chimie Physique Électronique),
Villeurbanne Cedex

G. CHIARELLI, R. CASTELLI
COGEMA,
Bagnols sur Cèze Cedex, France

Abstract

A better understanding of MOX fuel in-pile behaviour requires a very detailed characterization of the Pu distribution in the matrix before and after irradiation. Electron Microprobe Analysis (EPMA) can be used to determine chemical elements distributions with a 1 μm spatial resolution. Quantitative EPMA investigations are generally performed along a straight line (linescan). This paper describes the development of X-ray microanalysis techniques to produce semi-quantitative “maps” of plutonium concentrations in order to characterize, in a short time, and with reasonable accuracy, large areas of fuel microstructure (1 mm^2). A new segmentation technique is then proposed, based on statistics, so as to finely describe the MIMAS MOX fuel microstructure. To demonstrate the reliability of this new method, three materials are finely characterized. In each case, the results demonstrate the good and reliable accuracy of this new characterization methodology. The analysis method used is currently able to identify 3 so-called phases (the Pu-rich agglomerates, a reticulated phase and the uranium-enriched agglomerates) and to quantify the ratio, the plutonium distribution and the plutonium content of these three phases. On the microscopic scale, different quantities are evidenced between these three types of MOX fuels. The impact of the fabrication process on the microstructure is seen in the surface distribution variations of the plutonium and in the local plutonium content variations. The analysis tool developed within this study was validated on a 2 cycles irradiated MOX fuel and should help to improve the correlation between the impact of the fresh MOX fuel microstructure and its in pile behaviour.

1. INTRODUCTION

MOX fuel has been used in French PWRs since 1987. About 2000 MOX fuel assemblies have been loaded or will be loaded in 20 EDF 900 MWe reactors. Several of these have reached a depletion rate close to 50 GWD/T on average. It has been demonstrated that their present design allows them to reach 52 GWD/T under EDF reactor operating conditions. One of the industrial goals is to demonstrate that MOX fuel can achieve even greater performances. This demonstration is based on the irradiated fuel surveillance programs conducted since the beginning of plutonium recycling in French PWRs. These programs include the characterization of fuels at different stages of their irradiation.

This paper explains the methods developed to finely characterize fresh and irradiated MOX fuel microstructures and especially the plutonium distribution within the fuel, using microprobe images. First, the automated method of semi-quantification of X mappings associated to the plutonium element is described. Then, the method of automatic segmentation into several

phases (typical of MOX fuel), based on the counting statistic associated to this image acquisition technique, is shown. All these methods are then applied to three different industrial fuels:— A is representative of a standard EDF MOX MIMAS; it is a high plutonium content pellet (7.2% Pu/(U+Pu)) taken randomly from a MELOX batch;— B is an experimental MOX MIMAS fuel with a high plutonium content (7.1% Pu/(U+Pu)) elaborated so that the plutonium agglomerates are smaller than the standard ones;— C is a MOX MIMAS fuel with a very high plutonium content (11.1%) made in a standard way.

2. PRESENTATION OF THE ANALYZED MATERIAL

The MIMAS (MIcronized MASTer blend) process is today the most widely used industrial process to fabricate MOX fuel. It consists of two distinct steps. A mixture composed of plutonium dioxide, uranium dioxide and scrap, so that the resulting plutonium content is less than 30%, is finely ground. The obtained powder, called “master blend”, is then sifted and diluted in uranium dioxide until it reaches the aimed plutonium content. This secondary mixture is then pressed into pellets, which are then sintered and straightened to the specified diameter. This perfectly controlled process results in a material made of agglomerates with a plutonium content at most equal to that of the master blend, and of U-rich agglomerates without plutonium separated by a coating phase whose plutonium content is average.

On the microscopic scale, the X mappings acquired with the microprobe allow the fine analysis of the coating phase in which UO_2 and PuO_2 form a continuous solid solution (FIG. 1, where pixels are all the more white that plutonium concentration is high).

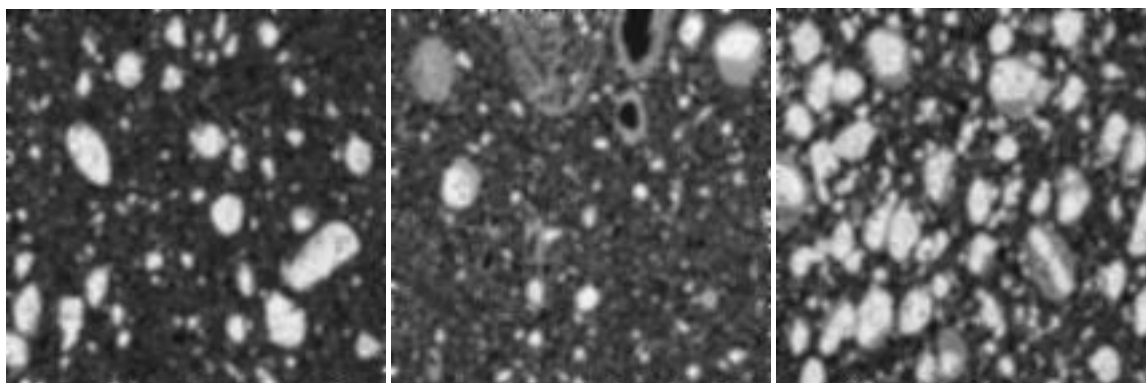


FIG. 1. X ray images of Pu in non-irradiated standard MOX (materials A, B and C).

A universal characterization method is required for this step to objectively compare the different batches and to quantify the evolution of their microstructure during irradiation. Image analysis is an efficient tool, which has enabled the development of automated methods of semi-quantification and of segmentation of microprobe mappings [1]. These methods are described below.

3. EXPERIMENTAL METHODS

3.1. Problem of microprobe mapping quantification

The electronic microprobe uses a beam of accelerated electrons with a controlled intensity to scan the surface to analyze. The interaction of electrons with the material produces energy under the form of X

photons, which are characteristic of the element to be analyzed. The spatial resolution associated with this technique is of about one micrometer, considering our acquisition conditions.

A localized measurement acquired with the microprobe accurately determines the plutonium concentration within the material. But making a map of a millimetre square with such an accuracy (25 seconds per point) would require ten months of continuous acquisition. However, the analysis of microprobe mappings to reach global parameters (e.g. uranium or plutonium contents of agglomerates) requires accuracy only for the average values. A lesser accuracy on punctual values can then be compensated by statistics on many measurements. The choice was therefore made to use mappings, which had been quickly acquired (17 ms per point) and to combine them with the help of an equation giving plutonium concentrations as a function of the counting levels (grey levels on the image). The determination of this equation is further described.

3.2. Semi-quantification method for microprobe mappings

The response of a material to the solicitation of an electronic beam, expressed in number of shots per nanoampere per second, and such as described in detail by Ancey *et al.* [2], can be simplified in the case of heavy elements such as plutonium. It was verified that this response was quasi-linear as a function of the Pu concentration (the correlation coefficient in FIG. 2 being higher than 0.999).

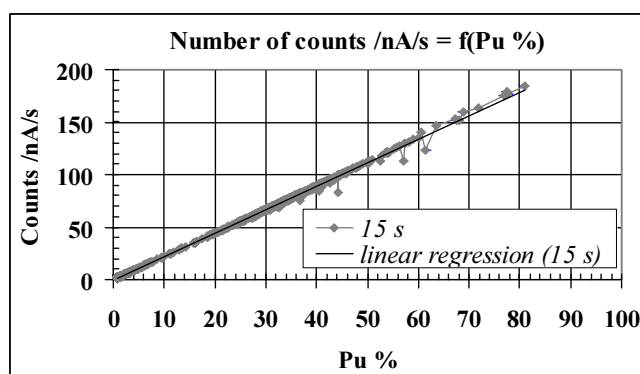


FIG. 2. Number of counts per nanoampere per second versus Pu concentration, and linear regression.

Thus, a linear equation giving plutonium concentration as a function of the level of activity measured by the microprobe, taking into account ray interferences and background noise, is proposed. This equation is the result of using the accurate quantitative profile acquisition, localized on an horizontal or vertical segment included in the image to be quantified. To do so, a pure PuO₂ standard is used. The intensities measured on the standard and on the sample on the M β ray of plutonium are corrected by the integration of the background noise and the potential interference of the M γ ray of uranium. The relative intensity between the analyzed sample and the standard, called k-ratio, is then corrected of its atomic number, absorption and fluorescence effects (ZAF type correction factors) to obtain the precise plutonium concentration, thanks to the knowledge of its concentration in the standard sample (88.2 % Pu). The profile obtained in this way only requires three hours of acquisition.

However, its precise positioning on the image to be quantified depends on the displacement precision of the sample-carrier stage, and on slight variations in acquisition conditions. Thus, a correlation algorithm is used to accurately reposition the profile on the image (FIG. 3). The most commonly recorded correlation coefficients exceed 0.95, leading to the establishment, by means of linear regression with a least square method, of the coefficients of the line modelling the material linear response.

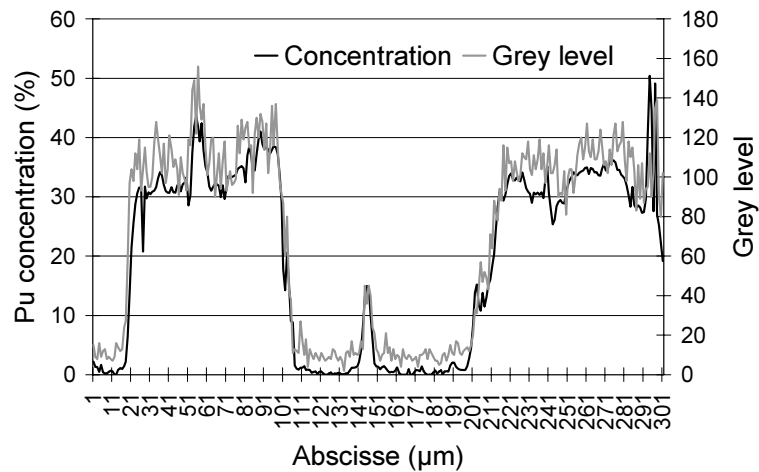


FIG. 3. Agreement between quantitative profile and grey levels of image (laboratory sample).

The uncertainty calculated globally on the average plutonium content of a whole field (by taking into account the fact that the response in each image pixel follows a Poisson distribution [2] and the fact that the uncertainty is classically calculated on the line coefficients by linear regression) is much lower than the variability between the fields. It is therefore the latter which will be used as an order of magnitude in measurement uncertainty, given the fact that our characterizations systematically involve at least six fields.

Our quantification method was validated by comparing the results obtained during precise quantitative measurements using a microprobe on a 2500 points grid to those obtained in the same place using the microprobe image and our transition equation from grey levels to concentrations. The validations thus carried out on part of a U-rich agglomerate and part of a Pu-rich agglomerate are shown in Table 1. FIG. 4 shows the plutonium quantification results of part of a microprobe image of a MOX fuel.

Table 1. Validation of the quantification method (laboratory sample)

Pu %	Pu-rich agglomerate	U-rich agglomerate
Microprobe quantification	36.09±0.01	0.19±0.01
Calculated	36.2±0.2	0.00±0.12

NB: this validation, shown in FIG. 4 and Table 1, is based on samples different from A, B and C materials. Especially, the Pu content of the master blend in this sample is of 40%.

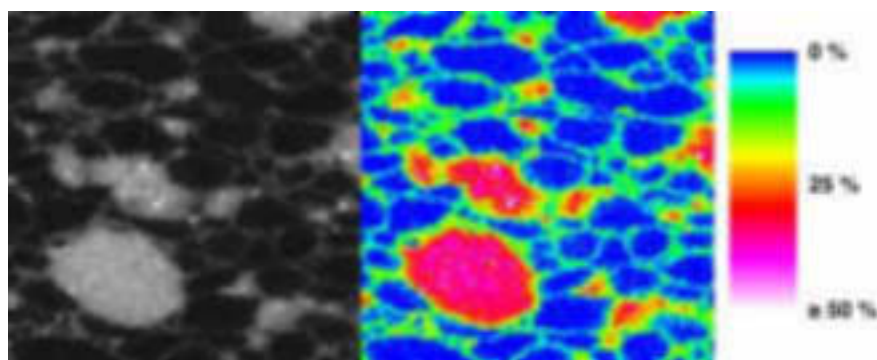


FIG. 4. Quantification of an X ray image of Pu in a non-irradiated advanced MOX (laboratory sample).

3.3. Segmentation method

The study of the behaviour under irradiation of MOX fuel is mainly focused on the study of fissile areas, namely those with high plutonium contents. Each microprobe image must therefore be divided into three phases: uranium phase, plutonium phase and coating phase. The common methods of histogram thresholding (maximization of interclass variance [3, 4], thresholding by maximization of entropy [5, 6], histogram discrete derivatives [7], etc.) reveal themselves not to be robust enough faced with the local over-concentrations and too sensitive to image noise. They also provide results whose quality greatly depends on the microstructure, and which sometimes end up segmenting only the plutonium phase in an inaccurate manner. Below, an adapted thresholding method is proposed, which is more robust and therefore more universal, taking into account both the grey levels and the pixel vicinity. The counting of activity associated to any punctual measurement made with a microprobe can be modelled using a Poisson distribution [8, 9]. It is thus possible to associate a confidence interval to both the master blend and to a nil content. Thus, we can immediately define on the semi-quantified image the areas statistically compatible with the master blend (which will be the “cores” of the Pu-rich agglomerates) and those compatible with a nil content (which will be the “cores” of the U-rich agglomerates). The remaining areas are submitted to a more complex analysis. The plutonium they contain may come from its diffusion from the Pu-rich agglomerates during the sintering phase. We marked each point in these zones with the distance to the closest Pu-rich agglomerate. However, the U-rich agglomerates initially being diffusional environments different from those of the coating zone, potential modifications induced by the latter on the diffusion of plutonium were taken into account. We thus used a geodesic distance from the closest Pu-rich agglomerate instead of a classical Euclidean distance.

The concentration of each pixel in the remaining zones can thus be correlated with the distance to the closest Pu-rich agglomerate, allowing the plotting on a graph of the average plutonium concentration as a function of distance. FIG. 5 is a graph of this kind. It shows that the plutonium concentration drastically drops over a small distance near the Pu-rich agglomerates, then stabilizes at a value which can be assimilated to the average concentration of the coating phase. The graph can thus be modelled by two line segments. The maximum concentration represented on the graph is used as the threshold level: the pixels of the upper concentration or that equal to this threshold and located in the direct vicinity of a Pu-rich agglomerate “core” are thus joined to these “cores”. The other pixels are attributed to the coating phase.

The uranium agglomerates cannot undergo the same treatment since the grey levels representing them contain too much noise. They are thus simply assimilated to their “cores”.

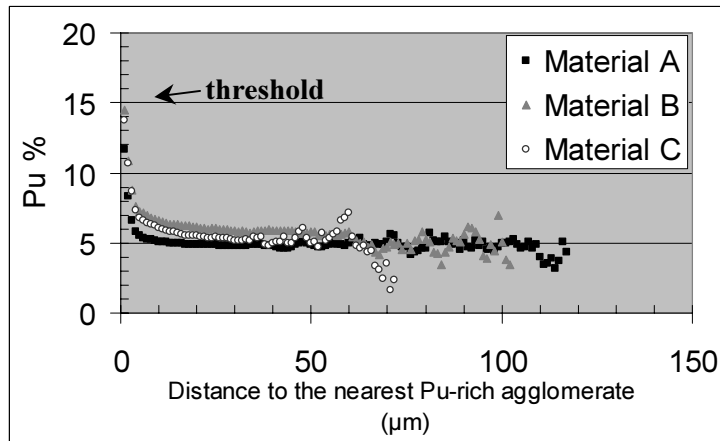


FIG. 5. Mean Pu concentration versus the nearest Pu-rich agglomerate distance.

FIG. 6 illustrates the segmentation of the sample A in FIG. 1 using our algorithm. The visual correspondence is satisfactory since the three phases are clearly shown and are in agreement with the morphology of the uranium agglomerates (black zones) and Pu-rich agglomerates (white zones). The coating phase (grey zone) appears connected, which is consistent from a physics point of view.

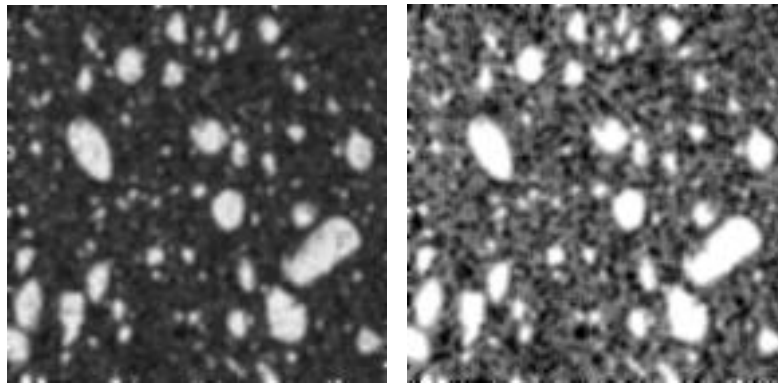


FIG. 6. Segmentation result (material A)

This method is much less sensitive to microstructure variations than the histogram thresholding methods as it is independent from the shape of the histogram in the grey levels of the images. Moreover, it simultaneously conducts an analysis of contents and of vicinity, which seems more pertinent than to separate these two analyzes, using the viewpoint of the notion of domain with homogeneous properties, well defined by Jeulin [10].

4. EXPERIMENTAL RESULTS ON FRESH FUEL

4.1. Detection of phases

The result of the phase segmentation using the method described in Paragraph 3.3 differentiates three phases within the MOX MIMAS fuel and determines the surface of each of them. The surface fraction of the phases is shown in Table 2 for the analyzed materials. The uncertainties associated to the calculated values correspond to the dispersion among the six analyzed fields per batch (confidence interval at $2\cdot\sigma$). These are comparable from one batch to

another. The dilution factor is identical for batches A and B. The volume percentage of the master blend, which is experimentally introduced during the fabrication phase is close to 26% for batches A and B and to 39% for batch C. The proportionality factor between the amount of master blend introduced during fabrication and the surface fraction of agglomerates measured by image analysis is noted F_p . This factor is systematically greater than 1 since part of the plutonium is transferred in the coating phase during the different fabrication steps. It is close to 2 in the case of batch A and greater than 3 in the case of batch B (Table 2). The plutonium and uranium phases are less extensive in batch B, the coating phase being predominant. This is illustrated in the microprobe image shown in FIG. 2, sample B.

Table 2. Phases distribution and proportionality factor F_p .

	Material A	Material B	Material C
Pu-rich agglomerate (S%)	14 ± 2	7 ± 1	30 ± 2
“Coating phase” (S%)	51 ± 1	61 ± 1	48 ± 2
U-rich agglomerate (S%)	36 ± 1	31 ± 1	23 ± 2
F_p	1.9	3.5	1.4

4.2. Size spectrum of Pu-rich agglomerates

Within the framework of the program on the development of MOX fuels, the aim of the COGEMA was to reduce the size of the plutonium enriched agglomerates [11]. This parameter may influence the retention and/or release of fission gases, although this effect has not yet been quantified [12, 13]. The use of a technique involving both the grinding and sifting actions, and replacing the forced sifting method allowed us to reach this objective. It was used for the elaboration of batch B. Indeed, the comparison between batches A and B shows that with a similar final Pu content, the size spectrum of the Pu-rich agglomerates has changed towards smaller sizes (FIG. 7). The population of small agglomerates ($<20 \mu\text{m}$) occupies a surface fraction, which is twice as large: about 29% of the total agglomerate surface, to be compared to 12% in the case of batch A. One can also notice on the cumulated graph that in batch B, more plutonium is contained into small size agglomerates. As less plutonium is globally contained into agglomerates than in batch A, small size agglomerates contain relatively more plutonium than large size ones, which is the expected goal.

4.3. Size spectrum of U-rich agglomerates

The same type of spectrum can be obtained for the uranium phase FIG. 8. The granulometric distribution of the initial UO_2 rough powder batches is today centred around $30 \mu\text{m}$ [14]. The thermal retraction (about 15% of the volume), the small U/Pu global interdiffusion (about $5 \mu\text{m}$ for 4 hours of sintering at 1700°C and $\Delta G_{\text{O}_2} = -370 \text{ kJ/mole}$), as well as a potential abrasion of the agglomerates during the dilution phase in the fabrication process tend to move this spectrum towards slightly smaller sizes. FIG. 8 shows distributions centred around $20 \mu\text{m}$. The average calculated sizes for the U-rich agglomerates are respectively $27 \mu\text{m}$, $20 \mu\text{m}$ and $22 \mu\text{m}$.

4.4. Global plutonium content

The calibration equation of the grey levels of Pu content is calculated according to the method described in Paragraph 3.2. The semi-quantification of the microprobe images using this technique allows access to the average plutonium content of the analyzed fields and to the average plutonium content of each phase. Table 3 illustrates the differences observed between the calculated values and the experimental values measured by chemical dissolution of (U,Pu)O₂ pellets. Good agreement is obtained between the calculated values using the semi-quantification method and those expected. This reinforces the coherence in the choice of the calibration line.

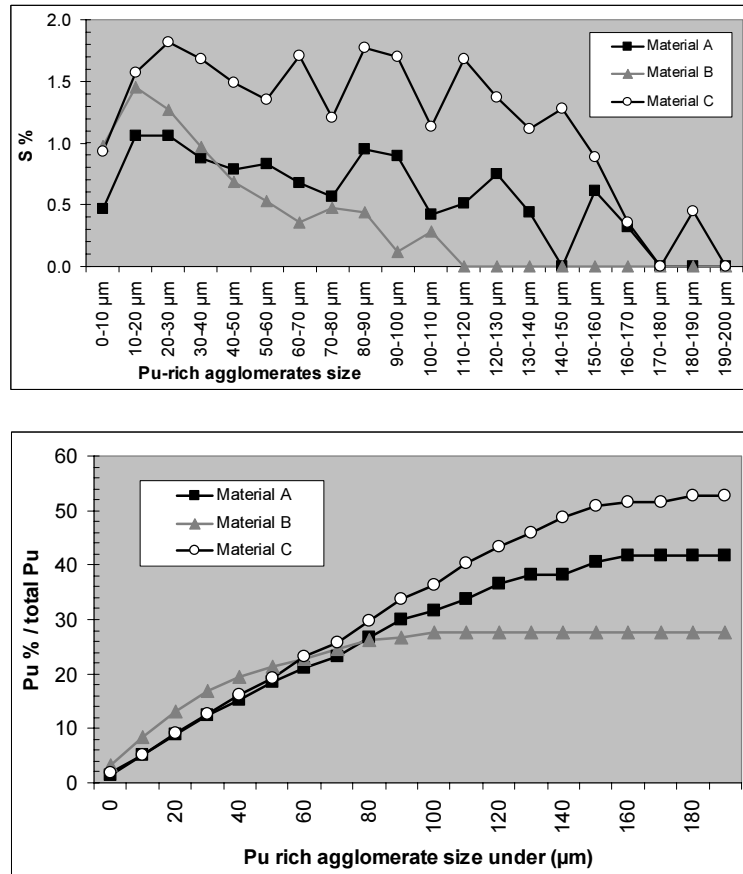


FIG. 7. Pu-rich agglomerate size spectra, and cumulated plutonium percentage relative to the total plutonium content.

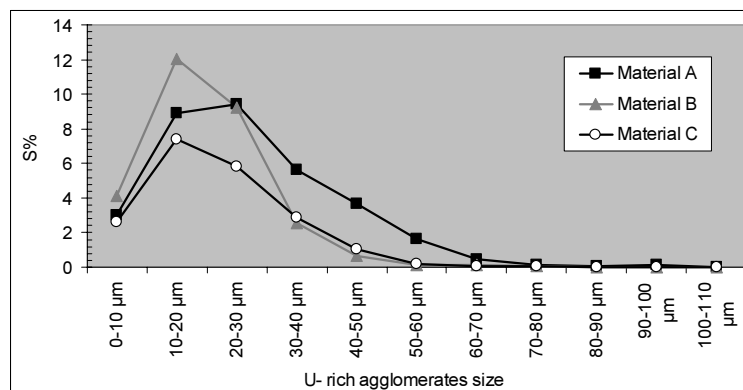


FIG.8. U-rich agglomerate size spectra.

Table 3. Global Pu content.

Pu/(U+Pu) content (wt %)	Material A	Material B	Material C
Calculated	7.2 ± 0.4	7.4 ± 0.3	11.9 ± 0.5
Experimental	7.2	7.1	11.1

4.5. Analysis of different phases : quantification of their distribution and plutonium concentration

The surface distribution is analyzed as a function of the three present phases: plutonium enriched agglomerates, coating phase and uranium enriched agglomerates. An element of comparison was defined by the Fp factor which represents the proportionality factor between the quantity of master blend introduced during fabrication and the surface fraction of the agglomerates measured by image analysis. This factor takes different values for batches A and C and indicates that for the same fabrication process, the final content in the Pu-rich agglomerates is not directly proportional to the introduced volume percentage of master blend. Moreover, for batches A and B, the difference of a factor 2 noticed on the Fp factor shows the influence of the grinding-sifting process. The granulometric distribution of the master blend thus obtained has two effects. The percentage of Pu-rich agglomerates is reduced. However, the fine particles are spread in the coating phase, which then becomes predominant. The quantity of agglomerates coming from the master blend and their morphological characteristics (cohesion degree, granulometry, density...) have a direct impact on the plutonium distribution in the final sintered pellet.

The plutonium contained in each of the phases has been quantified (Table 4). The three batches have master blend agglomerates with an equivalent plutonium content (about 24% Pu/(U+Pu)). However, the coating phase of batches B and C contains more plutonium (about 7% Pu/(U+Pu), to be compared to 5.7%).

Table 4. Phases Pu content.

Pu content (wt %)	Material A	Material B	Material C
Pu-rich agglomerate	24.0 ± 0.2	23.9 ± 0.2	23.7 ± 0.1
“Coating phase”	5.7 ± 0.1	7.1 ± 0.2	7.2 ± 0.1
U-rich agglomerate	0.5 ± 0.1	0.5 ± 0.1	0.5 ± 0.1

It is worth noting that (Table 5) for batch B, much more than half of the plutonium is contained in the coating phase (67% total Pu). In a standard MOX fuel the plutonium is equally divided between the two phases: agglomerates and coating. The microprobe coupled to the image analysis treatment allowed a better understanding of the microstructure of MOX fuels, on the microscopic scale.

Table 5. Plutonium ratio of phases versus material

Pu % / total Pu	Material A	Material B	Material C
Pu-rich agglomerates	51 ± 4	30 ± 2	66 ± 2
“Coating phase”	46 ± 3	67 ± 2	33 ± 2
U-rich agglomerates	3 ± 1	3 ± 1	1 ± 1

5. VALIDATION OF THE SEGMENTATION METHOD ON A 2 CYCLES IRRADIATED FUEL

5.1. Segmentation

The fuel irradiation in a reactor has two main consequences:

- the plutonium is burned by fission reactions which locally reduce its concentration;
- the neutronic fertilization of uranium 238 increases the plutonium content in the uranium zones.

Within a fuel pellet, the progressive uniformization of the plutonium concentration during irradiation makes the identification of plutonium areas more difficult. It is however of major importance to be able to analyze in the same way the fresh fuel and the fuel after one or two irradiation cycles, so as to characterize its evolution as best as possible.

The segmentation method presented above being based more on the notion of homogeneous domain than on Pu-rich agglomerate, we tested it on fuel irradiated for two cycles so as to validate its use on non-fresh material.

5.2. Experimental results

The analyzed material is a MOX MIMAS 2 cycles irradiated fuel. The average content of the pellet (4.86% Pu/(U+Pu)) was determined by microprobe analysis (quantitative points). A quantitative profile of 126 points (1 μ m a point) as well as a qualitative mapping (zone of 1024x1024 pixels with 1 μ m² a pixel and grey levels ranging from 1 to 199) were made. The semi-quantification of the image of the material led to a positioning of the profile on the map with a correlation coefficient of 0.93 (FIG. 9). The average calculated value of the field is then 4.60% Pu/(U+Pu), a value compatible with the interfield variations by a few tenths of percent.

Our segmentation method is based on the knowledge of the plutonium content in the “core” of the agglomerates, as well as a nil content in plutonium in the “core” of uranium agglomerates. These assumptions are not verified in the case of irradiated fuel. That is why the plutonium content in the “cores” of the different agglomerates was evaluated using recordings found on the semi-quantified map.

Following the semi-quantification and segmentation phase, the agglomerates and the coating phase are visually contoured correctly and in a similar way to what is obtained on fresh fuel FIG. 10. Moreover, the statistical compatibility test identified large pores and helped in eliminating their pixels from the final results, which brings the average calculated content to 4.62 % instead of 4.60 %. This method is relatively indifferent to the local absence of matter.

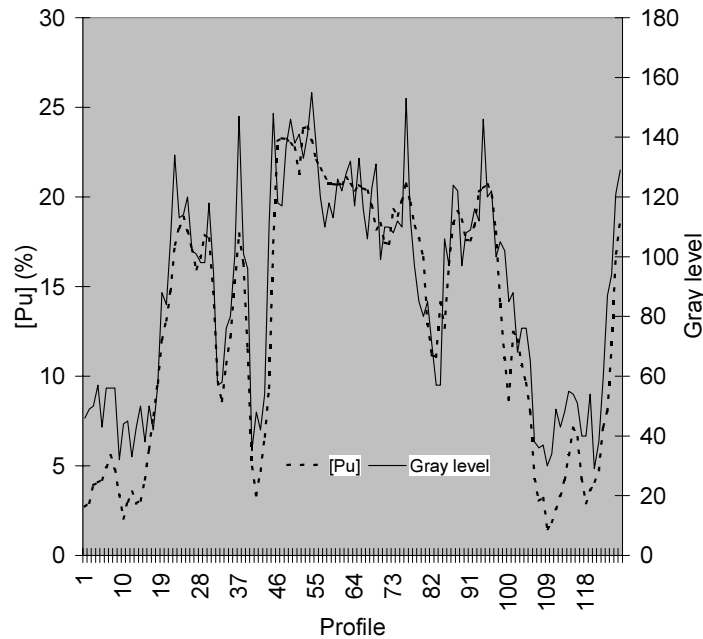


FIG. 9. Agreement between the Pu concentration and the gray levels on an image of a 2 cycles irradiated fuel

5.3. Conclusion and perspectives

The segmentation method would require more validation tests on irradiated fuel. However, its operating principle as well as first results indicate that the characterization of fuels irradiated two times is of equivalent quality to that obtained on fresh fuel. The absence of matter (pores, cracks) which appear during irradiation are easily identifiable, which is of considerable interest in finding a reliable characterization of irradiated fuels.

6. CONCLUSION AND OUTLOOK

The industrial aim to increase in the long term the depletion rate of MOX fuels in France beyond 52 GWd/T is today justified and requires further analysis and understanding of its behaviour under irradiation. It is thus necessary to have tools of fine characterization of microstructures available. The development and validation on fresh or depleted fuel of a method of automatic thresholding of the images acquired with a Castaing electronic microprobe would allow the quantification of the different phases (UO_2 , master blend agglomerates and coating phase) and the improved comparison between the different types of MOX microstructures, during their lifetime. Quantified elements are given for the distribution and plutonium content of the three phases. They show a noticeable impact of the fabrication process (dilution and sifting steps). The goal to obtain Pu-rich agglomerates of reduced size has been reached with a better distribution of the plutonium in the pellet.

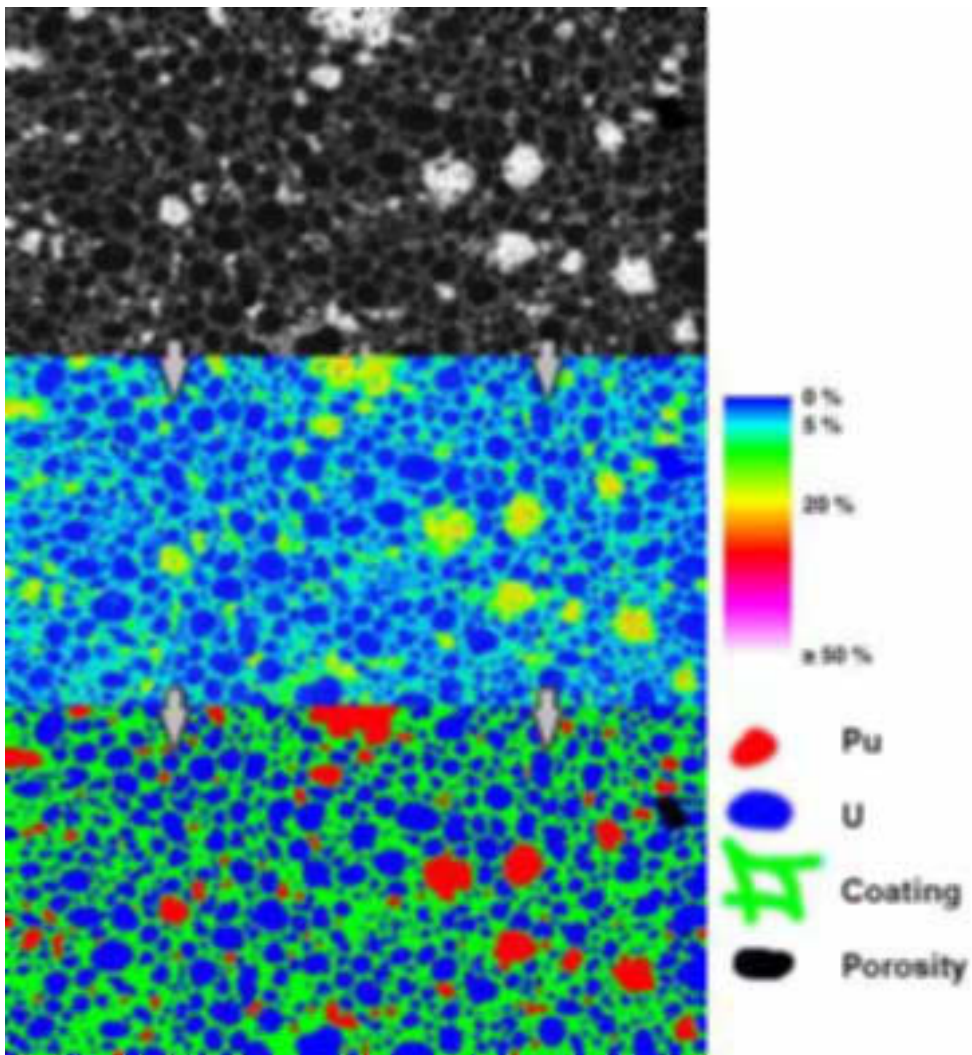


FIG. 10. Application of the segmentation method to an image of a 2 cycles irradiated fuel.

REFERENCES

- [1] G. OUDINET, "Analyse d'images et modélisation 2D/3D de la microstructure du combustible MOX" (Image analysis and 2D/3D structure modelling of MOX fuel), Thèse de l'Université Jean Monnet, Saint-Étienne, March 2003.
- [2] F. MAURICE, L. MENY, R. TIXIER, "Microanalyse et microscopie électronique à balayage" (Microanalysis and transmission electron microscopy) -Ecole d'Eté de S^t Martin d'Hères, 11–16 septembre 1978, les Editions de Physique, 1991.
- [3] M. COSTER, J.L. CHERMANT "Précis d'analyse d'images" (Precise image analysis), Presse du CNRS, March 1989.
- [4] F. CHAROLLAIS, "Analyse d'images : un outil pour caractériser et modéliser la microstructure du combustible MOX" (Image analysis : tool for characterization and modelling structure of MOX fuel), Thèse de l'université de Caen, October 1997.

- [5] J. N. KAPUR, P.K. SAHOO, A.K.C. WONG, "A new method of gray level picture thresholding using the entropy of the histogram", *Computer vision, graphics and image processing*, vol. 29, pp 273–285, 1985.
- [6] R. ZEBOUJ, "Filtrage, seuillage automatique, contraste et contours : du prétraitement à l'analyse d'images" (Filtering, contrast and contours : pre-treatment for image analysis) Thèse de l'université de Saint-Etienne, April 1988.
- [7] A. BOULORE " Etude et modélisation de la densification en pile des oxydes nucléaires UO₂ et MOX ", (Study and modelling in-pile densification of UO₂ et MOX fuels) thèse à l'Institut National Polytechnique de Grenoble et de l'Ecole Nationale Supérieure de Mines de Saint Etienne, March 2001.
- [8] M. ANCEY, F. BASTENAIRE, R. TIXIER, *J. Phys. D* 10, pp 817–830, 1977.
- [9] F. MAURICE, J. RUSTE, "Ensemble de comptage en spectrométrie de rayons X à dispersion de longueur d'onde et à sélection d'énergie: principe, contrôle, réglage" (Counting treatment in X-ray spectrometry regarding wave length, and energy selection : principle, control and adjustment), private communication, 1978.
- [10] D. JEULIN, "Recent developments of image analysis in material sciences", *Mem. ETUD. Sci. Rev. Metall.*, vol. 85, n° 3, pp 135-149, March 1988.
- [11] P. BLANPAIN, C. CALLENS, W. GOLL, G. CHIARELLI, J.L. GUILLET "MOX Fuel Performance and development" TOP FUEL 2001, Stockholm, May 2001, ENS (2001), CD-ROM.
- [12] Y. GUERIN, J. NOIROT, D. LESPIAUX, C. STRUZIK, P. GARCIA, P. BLANPAIN, G. CHAIGNE, "Microstructure evolution and in reactor behavior of MOX Fuel", *Light Water Reactor Fuel Performance (Proc. Int. Topical Meeting Park City, USA, April 2000)*, ANS, La Grange Park, Ill (2000) CD-ROM.
- [13] S.B. FISCHER, R. J. WHITE, P.M.A. COOK, S. BREMIER, R.C. CORCORAN, R. STRATTON, C.T. WALKER, P.K. IVISON AND I.D. PALMER, "Microstructure of irradiated SBR MOX fuel and its relationship to fission gas release", *J. Nucl. Mat.*, 306, (Dec. 2002), 153–172.
- [14] J. FOURCADE, "Etude de la mise en forme par pressage uni-axial des poudres de combustible nucléaire" (Study of the preparation of powder for pressing nuclear fuel), Thèse de l'université de Montpellier, December 2002.

MODELLING NON-STANDARD MIXED OXIDE FUELS WITH THE MECHANISTIC CODE MACROS: NEUTRONIC AND HETEROGENEITY EFFECTS¹

S.E. LEMEHOV, K. GOVERS, M. VERWERFT
SCK•CEN,
Mol, Belgium

Abstract

MACROS is a computer code for the neutronic, thermal and mechanical analysis of fuel rods in nuclear reactors, which is developed at SCK•CEN. In the paper the recent developments made to cope with non-standard fuels are summarized with emphasis on neutronic effects and its outcomes. First results are presented of verification calculations made for reference fuel rods from the international DOMO project where differences between UO₂ and homogeneous and heterogeneous MOX fuels have been extensively studied.

1. INTRODUCTION

With continuously increasing computing power, there is a parallel development of increasingly sophisticated computing models that are capable of representing the details of the complex interactions in nuclear fuel. Yet, the ultimate dream of fuel modelling, namely being able to calculate the fuel rod evolution from first principles and not to depend on correlations, is far from realistic today. In this paper, the recent developments for the MACROS code, which is essentially based on a multiscale, mechanistic approach, are presented. Using such an approach, it becomes possible to assess in detail the physical characteristics of nuclear fuels and to compare the local evolution of materials features (such as grain and pore evolution, local fission product clustering, mobility and release fractions) with detailed experiments.

The primary functional objective of the MACROS code, which initiated its development, is to assess in-pile behaviour of non-standard fuels, such as thorium-based fuels and fuels containing elevated concentrations of minor actinides. In this paper, we present part of the verification calculations that were recently performed with the MACROS code using data from UO₂, quasi-homogeneous and fine-dispersed MOX fuels, irradiated in BWR conditions. Special emphasis is put on the fission gas release phenomenon.

A code that is based on physical models rather than on correlations generally has a broader applicability range and is expected to provide reliable results even when experimental data are scarce. It is especially suited to assess results obtained in off-standard, experimental irradiation conditions and/or from novel fuel types. In this paper, we will present the comparison of calculated and experimental results obtained from the DOMO international program for uranium dioxide and two different MOX fuels, each with a different microstructure. The assessment includes the power density profile and its evolution with increasing burn-up; an assessment of the microstructure evolution and a discussion of mesoscopic aspects of fission gas release mechanisms in fuels with varying degree of heterogeneity.

¹ Work co-financed by the European Commission under the 5th Framework Program of the Euratom (Research and Training in Nuclear Energy).EVOL cluster, OMICO project, FIKS-CT-2001-00141.

The DOMO program provides a set of 60 fuel segments comprising UO_2 (20 segments) and two different MOX fuel types (40 segments). The main differences between the two MOX types are related to the dispersion of the fissile material and a difference in U^{235} content. The fuel rod segments were irradiated in the DODEWAARD Boiling Water Reactor and reached burnup values up to 58GWd/tM (peak pellet). Segments were unloaded at different intervals (at burnup values 27GWd/tM, 49GWd/tM and 58GWd/tM) and subjected to transient tests in the BR-2 Materials test reactor. Extensive non-destructive and destructive post-irradiation examinations were performed on base irradiated and on transient tested segments providing excellent database for verification both neutronic and mechanistic models.

It is commonly observed that LWR MOX fuel operated at comparable conditions shows higher fission gas release than standard UO_2 fuel. Fission gas release is essentially temperature dependent process. It was stated in some research works that the differences can be explained in terms of different in-pile temperatures. In view of general importance of this problem comparative analysis of several test fuel rods from DOMO project containing UO_2 fuel, homogeneous MOX and inhomogeneous (MIMAS) MOX have been analysed with the MACROS code to assess necessity of further model modifications.

2. SUMMARY OF THE MACROS CODE

MACROS (Mechanistic Analysis Code for Reactor Oxide Systems) is programmed in FORTRAN 90/95 as a code to analyze neutronic, thermal and mechanical behaviour of fuel rods under steady-state LWR, FR and ADS irradiation conditions and to address some aspects of long term storage of spent fuel. The MACROS code uses the one-cell approach where a cell consists of the fuel rod itself and an equivalent amount of coolant/moderator. It is developed to simulate fuel rod behaviour when the power and other boundary conditions change sufficiently slowly, i.e. close to steady-state conditions. The main objective of the code is to address issues of high burnup fuels as realistically as possible by means of coupling neutronic models, hydraulic considerations and conventional fuel performance models. Emphasis is placed on applicability to model in-pile behaviour of homogeneous and heterogeneous mixed oxides with high contents of plutonium and/or minor actinides.

The MACROS code was conceived by coupling the steady-state fuel performance code ASFAD [2] with the one-cell depletion code PLUTON [3, 4], which originally was developed as a code to generate radial burnup and power profiles needed for the JAERI fuel behaviour code FEMAXI-V.

The MACROS code calculates temperature, internal pressure, and deformation of a fuel rod as function of the fuel rod power history and coolant/moderator boundary conditions. Light water, heavy water and Pb-Bi coolants/moderators are included in the code. The main phenomena and properties modelled by the code include:

- 1) material properties (C_p , C_v , α_v , λ , etc.),
- 2) radial heat conduction through the fuel and cladding,
- 3) cladding elastic, creep and plastic deformations,
- 4) fuel-cladding mechanical interaction,
- 5) fission product build-up, including He (approximately 100 nuclides in total),
- 6) solid, pseudo-solid, and gas swelling,

- 7) fission gas release,
- 8) fuel rod internal pressure,
- 9) heat transfer between fuel and cladding,
- 10) clad oxidation on the fuel side and on the coolant side (only for water at present),
- 11) radial distribution of volumetric heat generation rate,
- 12) Depletion problem (evolution of initial vector of fissile and fertile isotopes).

The code contains or models necessary fuel and clad properties, coolant/moderator properties, and heat transfer correlations. The code itself and some thermal-mechanical models are still under development; integral predictions of mechanical behaviour have not yet been sufficiently verified against qualified databases. On the other hand, neutronic aspects (depletion module) of the code and models to predict material properties have been properly validated for UO₂, MOX and to a lesser extent for MA-mixed oxides considered for burning in LWR (thermal spectrum), FR and ADS (fast spectrum).

The close coupling of the thermal/mechanical and neutronic modelling is needed when dealing with heterogeneous configurations of fuel arrangement, i.e. separation of moderator-coolant and absorber-fuel. Neutronic effects determine non-uniform power generation and burnup distributions both in radial and axial directions. With burnup increase the as-fabricated fuel properties change considerably following time-power irradiation history and actual hydraulic conditions. Fuels irradiated in thermal neutron spectra are much more sensitive to these changes in comparison with targets irradiated in a fast neutron spectrum. However, some scenarios of burning minor actinides consider both spectra. Therefore, the MACROS code was designed with sufficient flexibility to account for either fast or thermal spectra.

One of the principal tools of nuclear reaction rate analysis is multigroup diffusion theory. For the basic assumption of multigroup theory to be valid in the presence of absorbers (in fact, all MA-fuels, MOX, thoria-based and UO₂-based fuels) it would be necessary to deal with a large number of energy groups. Even for a completely homogeneous medium in which diffusion theory is legitimate (e.g. a medium in which the fuel is ideally dissolved in moderator-coolant), the determination of few-group parameters needed for solving the depletion/build-up problem can be relatively difficult. For the common case of fuel assemblies composed of fuel rod lattices, which is a truly heterogeneous case, the situation is considerably worse. However, for fuel performance modelling true multigroup approach is not practically feasible and the problem is to formulate and apply few-group neutronic models to handle the depletion problem adequately up to high burnup and to provide the inputs for thermal-mechanical modelling of fuel rod behaviour (i.e. radial power distribution, radial burnup profile, and matrix inventory with fission products). This has been solved with an introduction of a new burnup model (PLUTON2 depletion module) in replacement of the original PLUTON burnup model.

3. COUPLING NEUTRONIC AND THERMAL BEHAVIOUR EFFECTS

3.1. Methodology and general approach

The temperature distribution under steady-state conditions is described by the Fick thermal heat flow law, which can be presented in the form as follows:

$$2\pi\lambda(T)\frac{dT}{dr} = - \int_{R_{CL}}^r q_V(r')2\pi r' dr' \quad (1)$$

where λ is the fuel thermal conductivity (W/m-K), T = local temperature at radial position r across the fuel cross-section; R_{CL} internal fuel pellet radius, and $q_V(r)$ is the volumetric heat generation density (W/m³).

Both left hand and right hand sides of the Fick equation (Eq.1) are time-dependent. The fuel depletion analysis in the MACROS code is coupled with solutions of the static multigroup equations for spatial (radial) distributions of the neutron flux in fuel and moderator. This also includes coupling of thermal-hydraulic and thermal-mechanical calculations to account for self-shielding and effects of temperature and fuel density changes. At the end of each time step interval, the depleted atomic densities of nuclides are used to calculate new group constants, flux shape in all principal energy groups, local macroscopic cross-sections, radial fission rate density and burnup profile. The group microscopic cross-sections will change with time as the fuel depletes and its density evolves, since the neutron spectrum in the fuel cell will experience changes as well as self-shielding. The MACROS code depletion module subdivides each time step of fuel thermal and mechanical behaviour in a number of shorter depletion steps in such a way that the two basic approximations – constant flux and constant power – become similar.

The left side of equation (1) depends on the structural and thermo-physical characteristics of the fuel such as porosity, accumulated fission products, lattice constants, melting temperature, etc., while the right hand side is mostly determined by the neutronic properties of fuel and local assembly environment in the core (via the neutron flux boundary conditions).

The MACROS model for thermal conductivity, $\lambda(T)$, has been developed and verified to cope with phonon-phonon resistive and non-resistive scattering processes, point defect scattering; one, two and three dimensional lattice defect scattering processes. In this way, the model accounts for burnup-induced degradation effects including self-irradiation effects (induced by build-up/presence of plutonium and minor actinides) and can predict thermal conductivity of Debye-like solids. Full description of this model with verification exercises and applications can be found in references [5, 6].

The calculation of the power density $q_V(r)$ is sensitive to the fission and capture cross sections of the fuel in the specific neutron spectrum. The fission and capture cross sections for plutonium and uranium isotopes have different characteristics which induce different neutronic behaviour between MOX and UO₂ fuel rods. This is essentially due to rapid conversion of ²³⁹Pu to ²⁴⁰Pu, which is in thermal spectra a very strong absorber, and further conversion of ²⁴⁰Pu to ²⁴¹Pu which is fissile and has the highest fission and capture thermal cross sections among 238 to 243 plutonium isotopes. As a consequence, MOX fuel to show a higher radial flux depression, more gradual radial variation of fission rate density and much slow the reactivity decreases with burnup. This means that for high burnup, MOX fuel will operate at a higher power than UO₂ fuel at comparable power conditions.

Modeling radial fission rate density needed to calculate fuel temperature as for the MACROS code is based on general multigroup formula:

$$q_V(r) = \bar{q}_V \frac{\sum_j \sum_{k=1}^{K_{Group}} \chi_j^{(f)} \Sigma_{jk}^{(f)}(r) \Phi_k(r)}{\left\langle \sum_j \sum_{k=1}^{K_{Group}} \chi_j^{(f)} \Sigma_{jk}^{(f)}(r) \Phi_k(r) \right\rangle} \quad (2)$$

where \bar{q}_V is the section average volumetric heat rate determined by the linear heat generation rate (LHGR) assumed to be known; j represents all fissile and fertile isotopes, $\chi_j^{(f)}$ is the energy release per fission (200 MeV/fission by default for all isotopes, unless given differently in inputs), K_{Group} is the number of energy groups, $\Sigma_{jk}^{(f)}(r)$ and $\Phi_k(r)$ are local group macroscopic cross-sections and group neutron flux, respectively. Averaging in the denominator is made in the fuel cross-section.

For inhomogeneous fuel compositions, the products $\chi_j^{(f)} \Sigma_{jk}^{(f)}(r) \Phi_k(r)$ are calculated separately for the matrix and the agglomerates of inhomogeneity, i.e., fissile enriched islands (Pu-spots in case of MOX fuel). An average value is then calculated with the corresponding weight fractions of the homogeneous matrix and the agglomerates.

For UO₂ fuelled thermal reactor systems, the neutron energies may be reasonably divided into three principal groups, according to the traditional approach adopted in neutronic calculations. For MOX thermal reactor systems it is necessary to consider at least one more group, which should include 1-eV giant resonance in ²⁴⁰Pu. The presence of a large and sharp resonance at 1 eV in ²⁴⁰Pu results in increasing conversion of fertile ²⁴⁰Pu into fissile isotope ²⁴¹Pu. The narrowness of this resonance causes the absorption of epithermal neutrons in ²⁴⁰Pu to be strongly self-shielded and, consequently, the effective (one-group collapsed) cross-section of ²⁴⁰Pu will be a function of cell neutron spectrum and concentration (atomic density) of this isotope at any given time. The significance of this effect can be appreciated by noting that the effective (one-group) cross-section of this isotope in MOX is more than two times the effective thermal (Maxwellian average) cross-section and depends on actual concentration of this isotope up to very high burnup. In view of this importance 1-eV giant resonance in ²⁴⁰Pu was provided with its own group with lethargy width $\Delta u = 1.5$.

Since a couple of years, the helium release of MOX receives quite some interest, especially with respect to the future development of MOX technology, when the fuels are expected to contain higher contents of the heavier Pu isotopes, or in relation to the loading of MOX fuels with elevated Am contents (long pre-loading storage). Helium generation and release is furthermore the primary concern of fuels that are currently envisaged for plutonium and minor actinide (MA) burning purposes. Already in standard MOX fuel, helium is produced in non-negligible quantities: roughly equal to that of fission generated krypton. On the lattice scale helium induces an additional phonon resistivity and contributes to the thermal conductivity degradation. Accounting for helium required additional modifications to the original neutronic subroutines: re-grouping of the few group constants, extension of the nuclide vector and some fundamental modifications in the calculation approach were implemented.

In its original approach (PLUTON code), the set of equations for build-up/burning fissile and fertile isotopes were solved and implemented in an analytical form with inevitable simplifications. These simplifications were related to the analytical form of the solution of the depletion equations wherein some important cross-contributions were ignored. A second simplification related to the use of the basic (and standard) assumption known as “constant power approximation”. Instead of constant power, one can alternatively assume that the

neutron flux can be treated as constant over the time interval of interest, which is also widely used and is in fact the “standard” assumption in depletion analysis. The isotopic depletion resulting from the assumption of constant flux or constant power is quite different quantitatively (constant power approximation tends to under predict the depletion rate, while constant flux approximation tends to over predict the depletion rate), unless the chosen time step is sufficiently short.

A new solver was then developed with specific purpose to cover any number of simultaneous differential equations describing build-up and burning of fissile and fertile isotopes; to overcome limitations of the analytical solution and to reconcile the two basic approximations for power and flux. It becomes possible by representing depletion rate equations for fissile and fertile isotopes in an operator form as follows:

$$\frac{d\vec{u}}{dbu} = A \cdot \hat{S} \cdot \vec{u} \text{ or } \frac{d\vec{u}}{dz} = \hat{S} \cdot \vec{u} \quad (3)$$

with given initial concentration vector $\vec{u}_0 = \vec{u}|_{bu=bu_0}$ of fissile and fertile nuclides. Here “bu” is the burnup; “A” is a quasi-constant numerical coefficient (depending on section average macroscopic fission cross-section, fuel density and fraction of heavy metals in the oxide); $dz = A \cdot dbu$ is the dimensionless burnup increment, and \hat{S} is the cross-section matrix constructed with microscopic absorption and capture cross-sections (spectra weighed) and decay constants. The general solution of the buildup/burning operator equation (3) can be written as a series expansion:

$$\vec{u}(\Delta z) = \vec{u}_0 + \sum_{n=1}^{\infty} \frac{(\Delta z)^n}{n!} \vec{u}_n \quad (4)$$

where $\vec{u}_n \equiv \hat{S}^n \vec{u}_{n-1}$, $n \geq 1$. With appropriately short burnup steps only the first 4 or 6 terms may be taken into account, which would correspond to 4th or 6th order standard Runge-Kutta procedure.

The operator form of solution of simultaneous differential equations is very effective, easy to program, fast and convenient for modifications if new fissile or fertile isotopes should be taken into consideration for some specific fuel targets. It includes automatically any conversion cross-contributions for particular isotopes.

The current version of the MACROS code employs optionally a user defined multigrouping or a few-group approach (by default) with grouping microscopic cross-sections in accordance with the neutron energy ranges as shown in Table 1.

Table 1. A few-group structure

Energy range	LWR & HBWR cores	FR/ADS/MYRRHA
0.0001 to 0.53158 eV	Maxwellian spectrum	Maxwellian spectrum
0.53158 to 2.3824 eV	1-eV Giant Resonance	1-eV Giant Resonance
2.3824 eV to 20 keV (resonance range)	1/E “Fermi spectrum”	Slowing-down spectrum
20 keV to 1 MeV Non-resonance range	1/E “Low fast Fermi spectrum”	1/E “Low fast Fermi spectrum”
1 to 20 MeV	Fission spectrum	Fission spectrum

In thermal spectra typical for commercial LWR cores the relative weight of non-resonance low fast energy group is only about 5 %, which is still roughly two times higher than that of fast energy group. In fast core spectra (MYRRHA) with relative weight ≈ 70 % and lethargy width $\Delta u_g \approx 4$ this group is manifesting a major neutron group for capture (i.e. for the breeding & depletion problem) and to a lesser extent also a supplementary group for fission. The significance of this neutron group can be appreciated by noting that roughly half of americium-241 is converted to higher isotopes due to this group.

Modifications of the burnup model do not lead to major corrections in predictions of depletion rate for standard UO_2 fuel irradiated in LWR or HBWR conditions. One may expect, however, non-negligible improvements in MOX fuel calculation and important improvements for fuels containing elevated concentrations of MA or irradiated in a fast flux where microconstants are characterized by quite small and comparable absolute values, and consequently cross contributions in rate equations of minor actinide nuclides become very important.

3.2. Verification calculations: comparison with local isotopic composition profiles

Design and fabrication parameters of reference three fuel rods selected for comparative code calculations are shown in Table 2.

Figures 1 and 2 illustrate the importance of accounting for the low energy resonances for LWR MOX. Figure 1 shows calculation results made with the original version of the PLUTON burnup model for a quasi-homogeneous MOX sample (DOMO-J04) irradiated in the Dodewaard BWR reactor. In general, the agreement is quite satisfactory except for ^{240}Pu . Introduction an additional group, which covers the 1-eV giant resonance in ^{240}Pu , improves the agreement between experimental and calculation results as illustrated in Fig. 2. The relative $\text{Pu}/(\text{U}+\text{Pu})$ ratio distributions as measured with SIMS and calculated with the MACROS code are shown in Fig. 3. Both measurements and calculations show that the breeding rate of ^{239}Pu and conversion of ^{240}Pu are very high in the first 300 μm (see Fig. 3 and 4), however this fact does not come out so drastically in the isotopic composition plot (Fig. 2). Apart from that the ^{241}Pu and ^{242}Pu distributions are rather flat (see Fig. 5) indicating thus the dualism of breeding/conversion and fission in the outer half of MOX fuel, which is not a case for standard UO_2 fuel where all plutonium distributions follow accordingly radial burnup distribution as EPMA reveals.

Irradiation histories of the reference fuel rods are given in Fig. 6 and 7. Summary of calculated radial power and temperature profiles for different burn-ups are shown in Fig. 8 to 10. Irradiation of MOX fuel had started with rather gradual power profile and with burnup increase one can see the effect of flattering power profile in the internal part of fuel and steepening in the outer part of fuel characterized by width ≈ 300 μm . Such burnup dependent behaviour of power profile in the MOX fuel effectively influences temperature distribution. The steeper power profile, the lower centreline temperature. Thus steepening power profile in the MOX fuel leads to compensate (to some limited degree) effect of temperature increase due to degradation of thermal conductivity. At the same time gradual increase with burnup in fission rate density towards fuel centre “works” on an increase of centreline temperature. In UO_2 fuel irradiated in thermal spectra only steepening effect is observed.

Table 2. Reference DOMO Fuel Rod Fabrication and Design Characteristics

Parameters	Rod U09	Rod J04	Rod X43
Fuel type	Homogeneous	Homogeneous	Heterogeneous
Fuel enriched length, mm		280.9	
Fuel weight, g		247.64	
Initial Density, %TD	95.459	95.52	94.3434
Initial Enrichment (U-235/U)	4.941	0.73	0.239
Initial weight content of UO ₂ (%)	100	94.50	92.67
Initial weight content of PuO ₂ (%)		5.50	7.33
Plutonium vector (weight fractions):			
Pu-238	n/a	0.77	1.405
Pu-239	n/a	67.67	61.844
Pu-240	n/a	21.14	23.38
Pu-241	n/a	7.85	8.826
Pu-242	n/a	2.57	4.546
Fractional weight of Pu-rich particles (%)	n/a	n/a	10 (assumed)
Fraction of U in Pu-rich particles (%)	n/a	n/a	75 ()
Pu-rich particle size (μm)	n/a	n/a	215
Fuel content (w/o)			
U235	4.941	0.73	0.239
Pu-total	n/a	5.44	6.431
Pu-fissile	n/a	4.1	4.545
Average Grain Size (μm)	9.25	7.1	9.87
X = O/M – 2	0.000	-0.01	-0.001
Initial Clad Outer Diameter (mm)	12.291	12.291	12.288
Initial Clad Inner Diameter (mm)	10.556	10.556	10.550
Initial Fuel Outer Diameter (mm)	10.357	10.354	10.352
Initial Fuel Inner Diameter (mm)	0.0	0.0	0.0
Fill Gas/Pressure (MPa)	He/	He/0.53	He/0.53
Fuel rod free volume (cm ³)		6.23	6.23
Fuel rod upper plenum volume (cm ³)		5.11	5.11
Rod average burnup, GWd/t(IHM)	53.51	55.55	55.55
Rod maximum burnup, GWd/t(IHM)	55.08	57.49	57.49

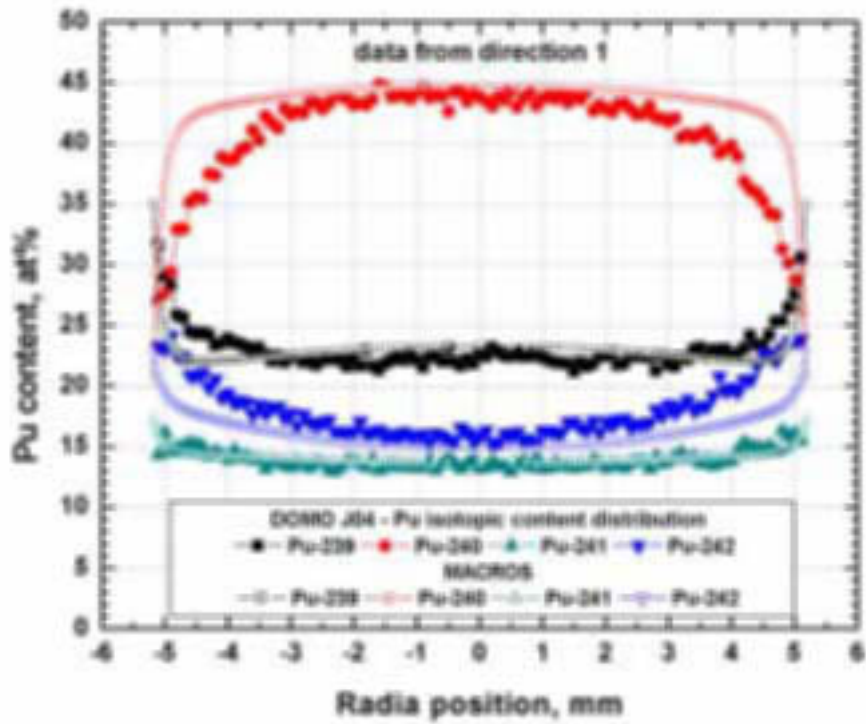


FIG. 1. Sample J04, measured local isotopic Pu compositions (at %) along directions 1 to 3 and calculation results obtained with the original three-group version of PLUTON code.

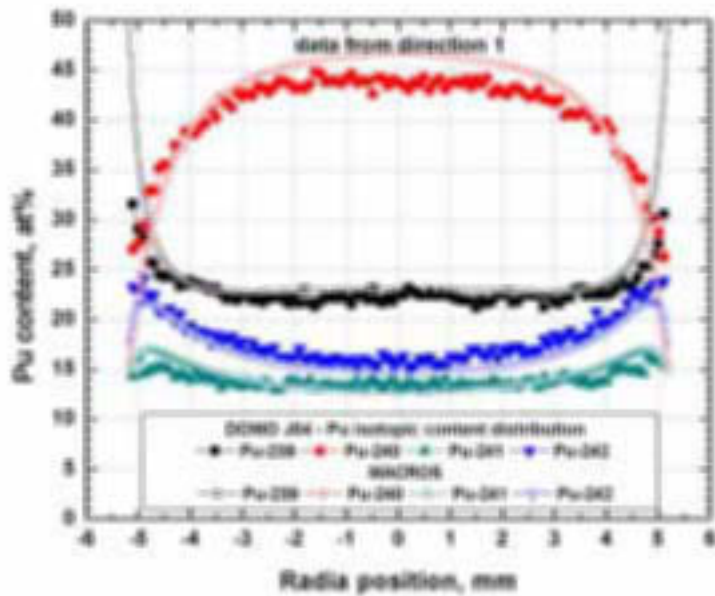


FIG. 2. Sample J04, measured local isotopic Pu compositions (at %) along directions 1 to 3 and calculation results obtained with the MACROS code (PLUTON2 burnup model).

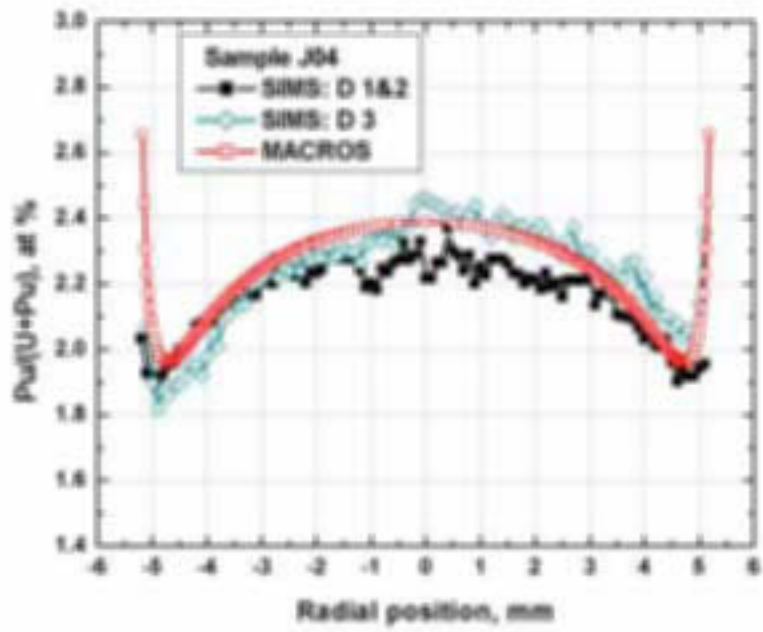


FIG. 3. Sample J04, $Pu/(U+Pu)$ ratio distributions as measured with SIMS and calculated with the MACROS code (PLUTON2 burnup model). Experimental points show measurements along directions 1 to 3.

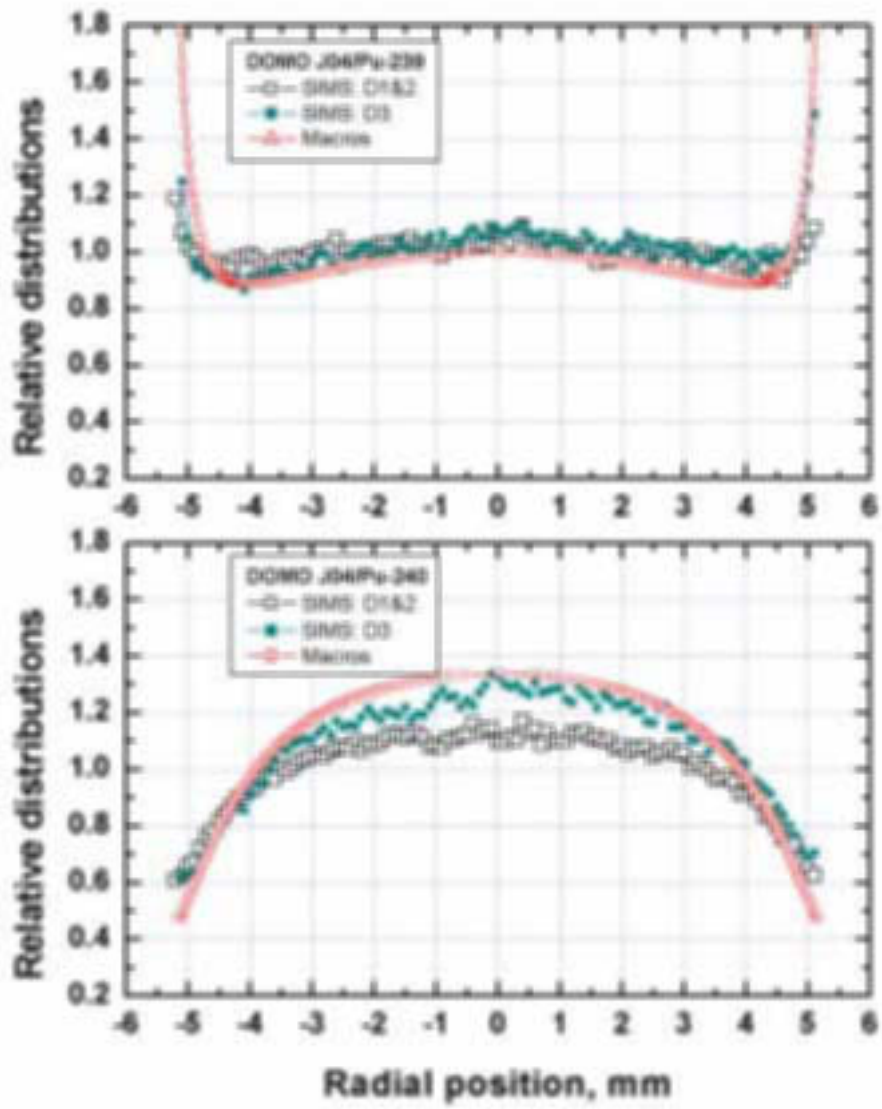


FIG. 4. Sample J04, experimental ^{239}Pu and ^{240}Pu distributions (relative to average concentration 1.0) along direction 1 to 3 and as-calculated with the MACROS code.

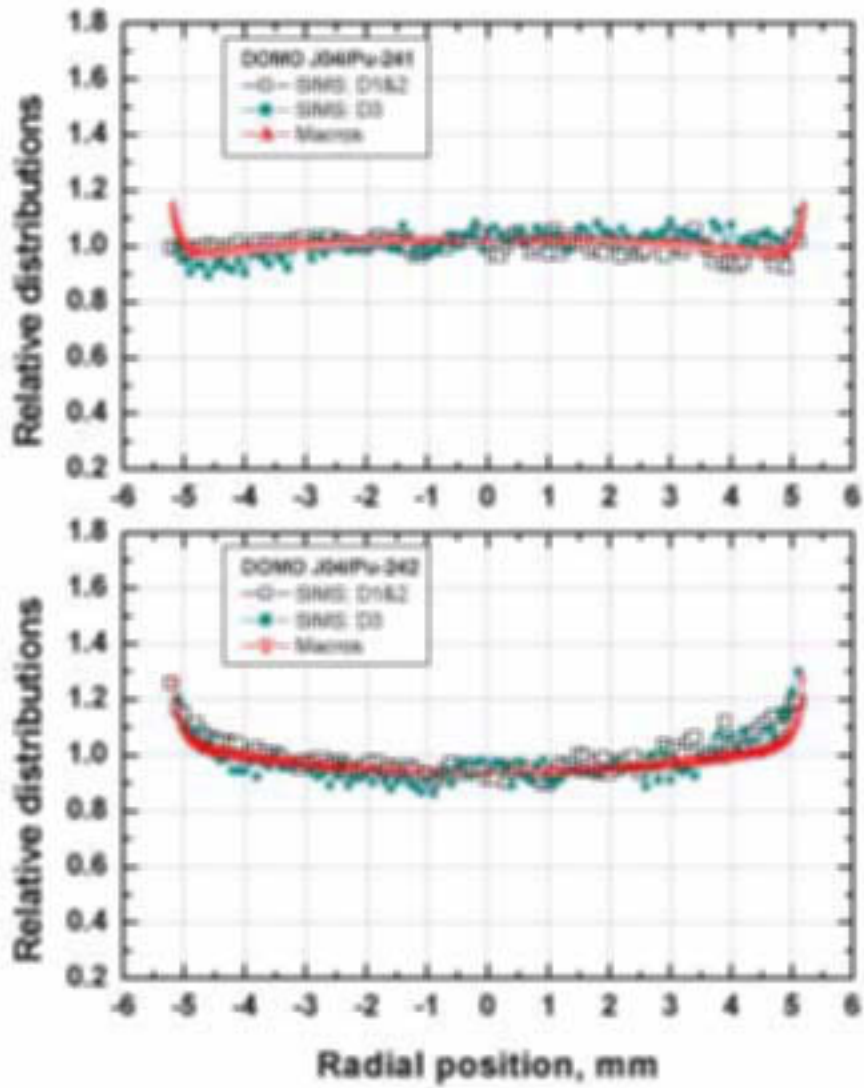


FIG. 5. Sample J04, experimental ^{241}Pu and ^{242}Pu distributions (relative to average concentration 1.0) along direction 1 to 3 and as-calculated with the MACROS code.

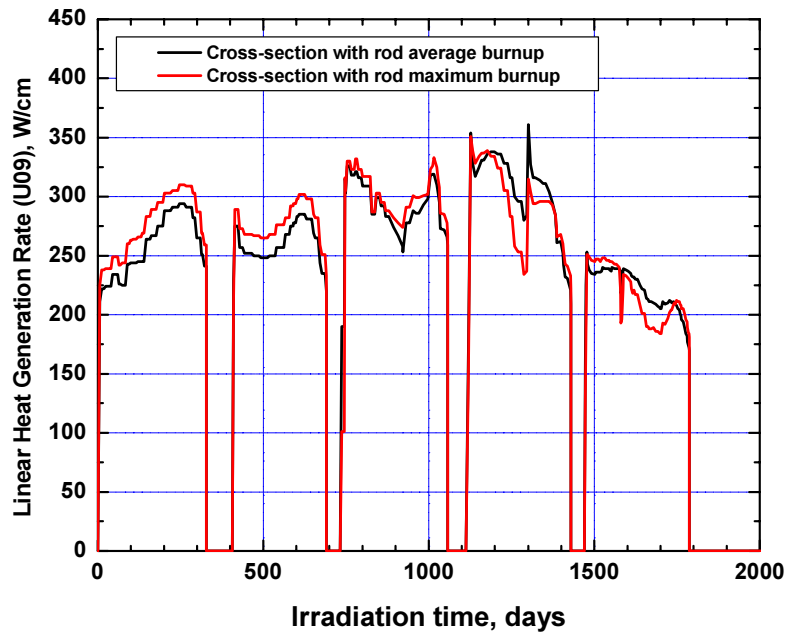


FIG. 6. Irradiation History for DOMO UO_2 Rod U09.

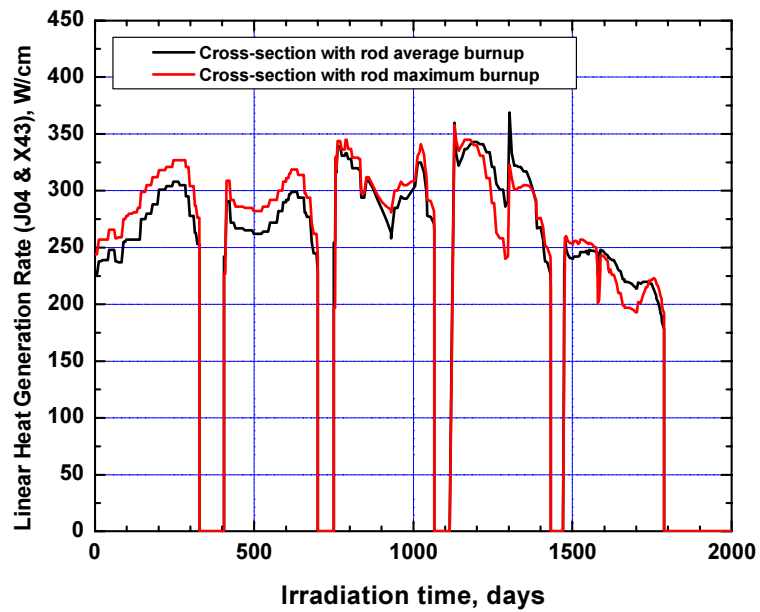


FIG. 7. Irradiation History for DOMO MOX Fuel Rods X43 and J04.

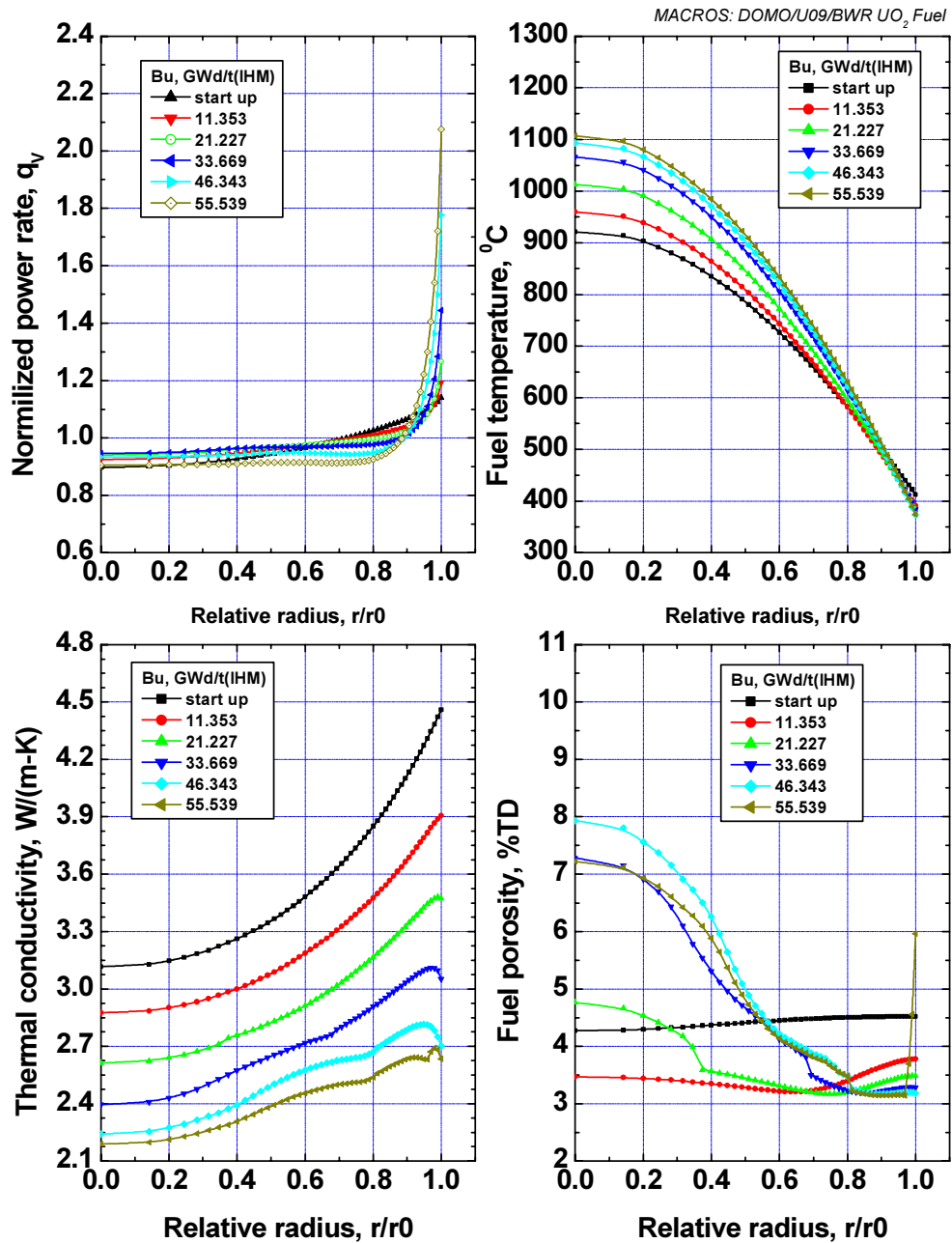


FIG. 8. Calculated results as a function of radial position and burnup for the DOMO UO₂ fuel rod U09.

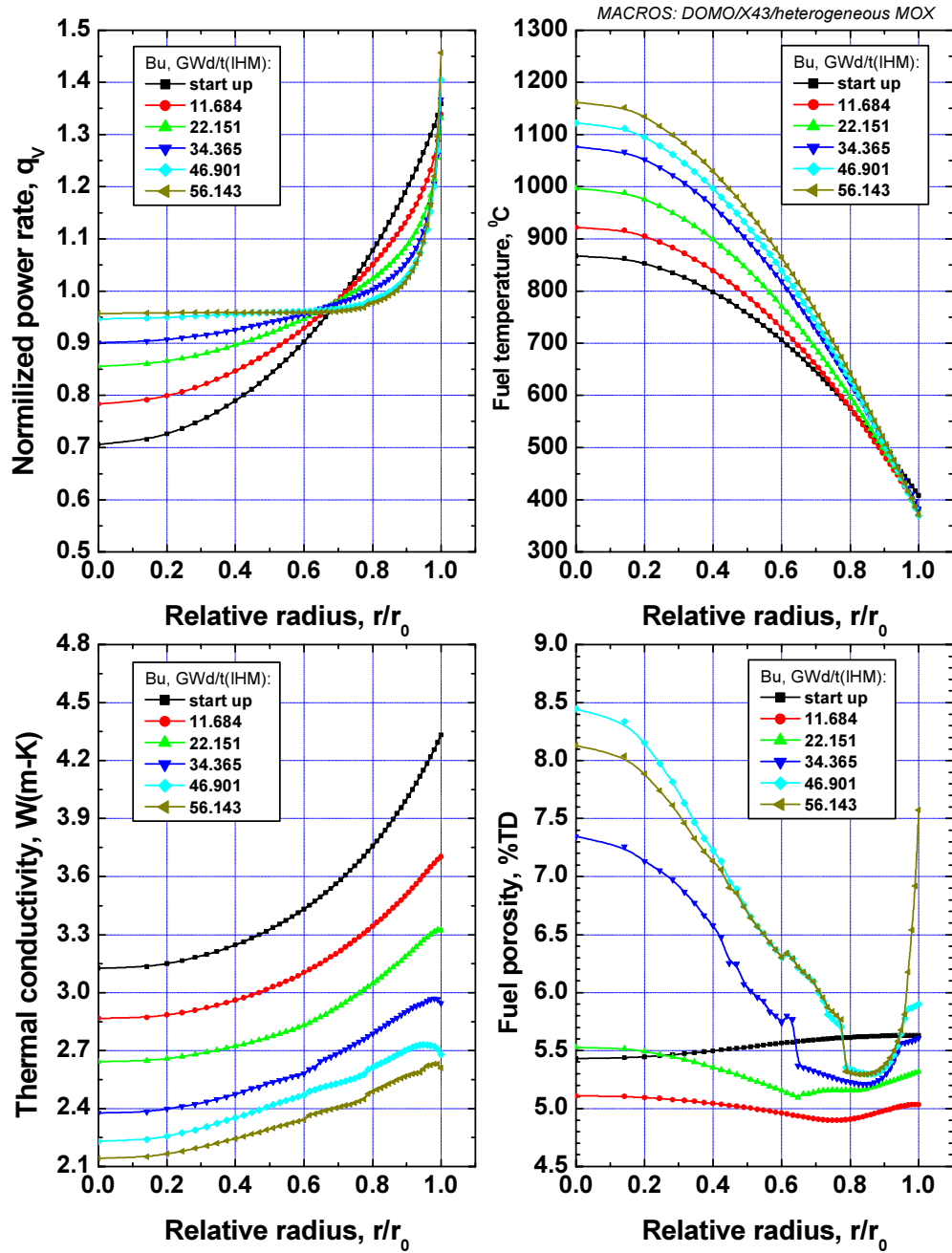


FIG. 9. Calculated results as a function of radial position and burnup for the DOMO heterogeneous MOX fuel rod X43.

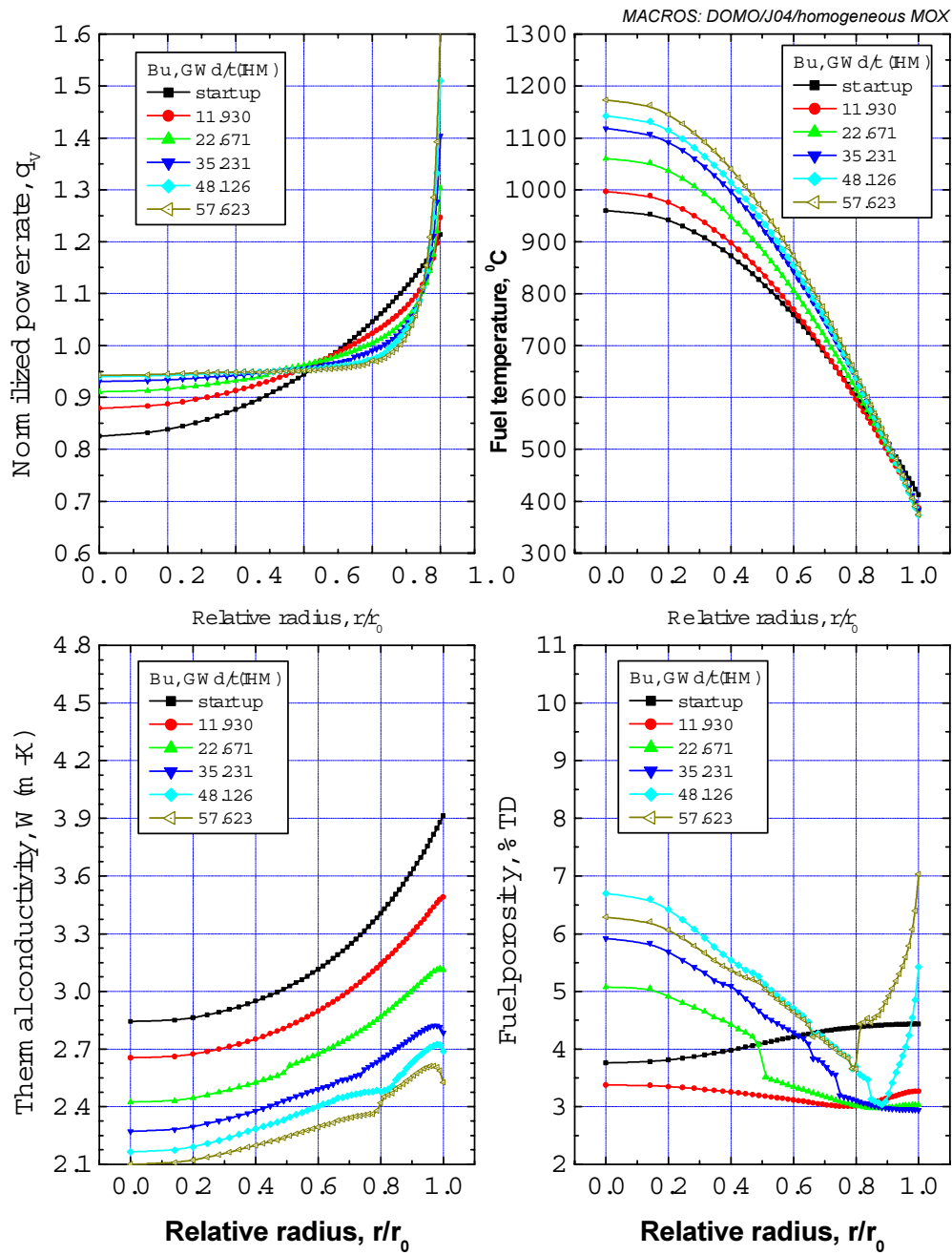


FIG. 10. Calculated results as a function of radial position and burnup for the DOMO homogeneous MOX fuel rod J04.

4. MODELLING FISSION GAS RELEASE

With verified neutronic outputs, a comparative analysis of fission gas release and end-of-life radial gas balance distributions in three fuel rods segments from the DOMO program has been performed.

Most theoretical fission gas release (FGR) models are based on the assumption that FGR is a two step process: (1) fission gas atoms diffuse inside grain or/and precipitate into intra-granular bubbles and inter-granular porosity and (2) after reaching the certain saturation conditions can be released to pin free volume. As a consequence, fission gas is released after ending an incubation time interim depending on temperature and porosity. At high accumulated burn-ups the matrix becomes unstable and is subdivided in small crystals (high burnup structure formation). This process is often referred to as “rim structure formation”, referring to the specific case of homogeneous fuels, where the higher peripheral burnup results in the onset of this specific restructuring of the peripheral regions inwards. In inhomogeneous fuels (MIMAS-based MOX fuels) HBS formation occurs in the Pu rich islands and is not restricted to the rim regions only. The restructuring and subdivision of the crystal structure results in an a-thermal, non-diffusionl release of the accumulated Xe, which generally becomes occluded in large pores that are the most typical aspect of the HBS formation process.

A detailed description of the diffusional mechanisms of FGR has been given by White and Tucker [7]. The FGR model of the MACROS code essentially uses their principal model assumptions with modifications for calculating in-pile diffusion and self-diffusion coefficients as well as porosity formation and development.

The HBS formation and Xe depletion is modelled in the MACROS code based on a concept of internal energy threshold and expressed in terms of lattice pressure. It is assumed that when the internal lattice pressure exceeds the shear modulus dislocations may be formed and the irreversible degradation of the crystal structure begins. It is generally accepted that the largest contribution to solid swelling comes from fission gas contributions, but that other fission products also contribute. The concept of solid swelling is used as starting point for the estimation of lattice pressure. Fission gasses are the main contributor to lattice pressure since they need the largest volume (85 \AA^3) in lattice to occupy and make the largest contribution to solid swelling and lattice pressure. From neutronic outputs, the FGR subroutine receives concentrations of main solid swelling contributors and heavy metals. The distortion of lattice in terms of lattice pressure is expressed in terms of the atomic fraction of defects with different ionic or atomic radius from the host atoms. In MOX matrix an additional contribution comes from the local plutonium content. The higher local plutonium content the higher its partial contribution to the lattice pressure and the lower critical concentration of lattice fission gases that starts HBS formation.

Calculations for a homogeneous MOX with 5.5 wt% of initial PuO_2 content have shown that the lattice pressure threshold is exceeded at local BU value of 50 GWd/t(IHM) at the pellet edge, corresponding to a critical concentration of lattice gas of 1.25 atom % (the ratio of the lattice fission gas number to the total number of heavy metal sites). For UO_2 fuels, the critical concentration of lattice gas as calculated was found to be 1.65 at % and was exceeded at the pellet edge at local burnup of 61 GWd/t(IHM).

In the physical background the MACROS FGR model uses results of investigation of dislocation cell-structure formation in highly irradiated fuels made by J.Spino et al [8, 9] and Xe-depletion equation introduced by K. Lassman et al [10].

For DOMO calculations to be close to basic realistic observations, the high burnup structure pore density was modelled with semi-empirical correlation as follows:

$$N_{\text{pore}}(r) = N_{\text{pore}}^{(\text{max})} r_{\text{res}}(r) + N_{\text{pore}}^{(\text{min})} f_{\text{fast}}(r) \quad (5)$$

where $N_{\text{pore}}(r)$ = HBS pore density (pores per cc); $N_{\text{pore}}^{(\text{max})} = 10^{11}$ pores/cc and $N_{\text{pore}}^{(\text{min})} = 10^8$ pores/cc are correspondingly the maximum and the minimum HBS pore densities observed by J.Spino et al [8] in highly irradiated UO_2 fuels; $r_{\text{res}}(r)$ = normalized function describing radial attenuation of epithermal neutrons in fuel, and $f_{\text{fast}}(r)$ = is the normalized function of fast neutron flux distribution in the fuel.

There were two reasons behind the use of $r_{\text{res}}(r)$ and $f_{\text{fast}}(r)$ functions. The first reason is evident: attenuation of resonance neutrons and advancing the flux of fast neutrons from fuel periphery to center mainly determine the radial shape function of burnup profile. A linear or quasi-linear relationship between the local HBS porosity and local burnup is observed in UO_2 high burnup fuels [8]. Secondly, the dislocation network responsible for the polygonisation of the original grain structure needs a continuous source of interstitials and vacancies that can be provided at low temperatures only by fission fragments or by neutrons with high energy via recoil interactions with lattice nuclei.

Thus, current version of the MACROS FGR model for the HBS formation calculates from microscopic and macroscopic solid state considerations the onset of polygonisation and concurrent Xe depletion and uses semi-empirical approach to model porosity increase in HBS fuel regions. It uses solid state considerations again to calculate gas balance in the fuel and growth of pores. The results of model calculations for the DOMO reference fuel rods are discussed below.

Figure 11 shows an integral fission gas release in three fuel rods as functions of irradiation time. The normalized to LHGR = 250 W/cm and water temperature 300 C centerline fuel temperatures are shown on Fig. 12 indicating the scale of resulting temperature increase due to degradation processes. It is interesting to note that normalized temperature for X43 fuel rod was calculated roughly 50 C lower than that for UO_2 fuel rod, what is to be attributed according to code calculations to differences between behaviour in radial fission rate density.

As can be also seen from this figure UO_2 fuel rod (U09) was operated at lower temperatures than MOX fuel rods with a consequently lower integral fission gas release.

End-of-life gas balance across the fuel radius for UO_2 fuel (U09) and homogeneous MOX fuel (J04) in comparison with EPMA measurements is shown in Fig. 13 and 14. The intermediate conclusion from this verification exercise is evident: both MOX and UO_2 fuel show quite similar radial gas balance distributions and observed differences in integral FGR can be explained in term of different thermal conditions during the in-reactor irradiation. There is no indication of necessity to consider any specific mechanisms of FGR in MOX. The reasonable agreement in terms of integral FGR and local gas balance can be archived with conventional two step diffusional mechanism of FGR and Xe-depletion due to HBS formation. Further research is needed to better understand the kinetic of HBS formation in connection with grain structure polygonization.

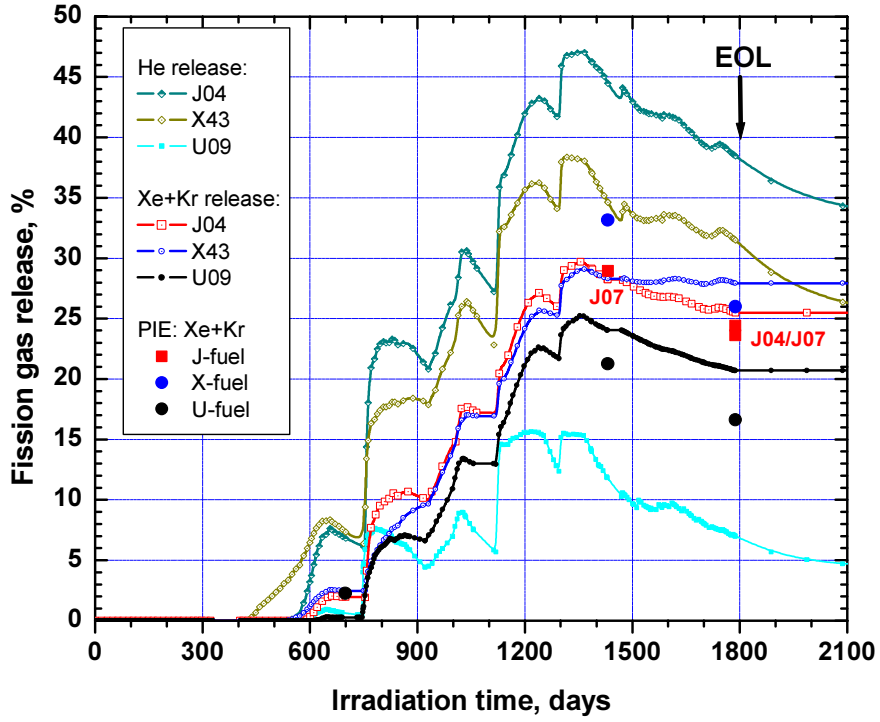


FIG. 11. MACROS Verification Calculations: Integral FGR in reference DOMO fuel rods.

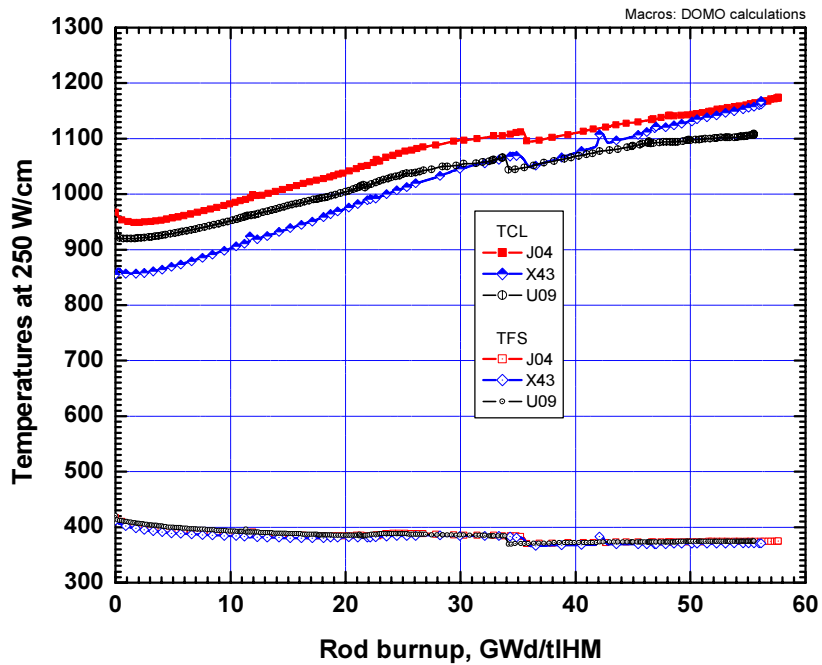


FIG. 12. MACROS Verification Calculations: Centerline Fuel temperatures normalized to ALHR = 250 W/cm.

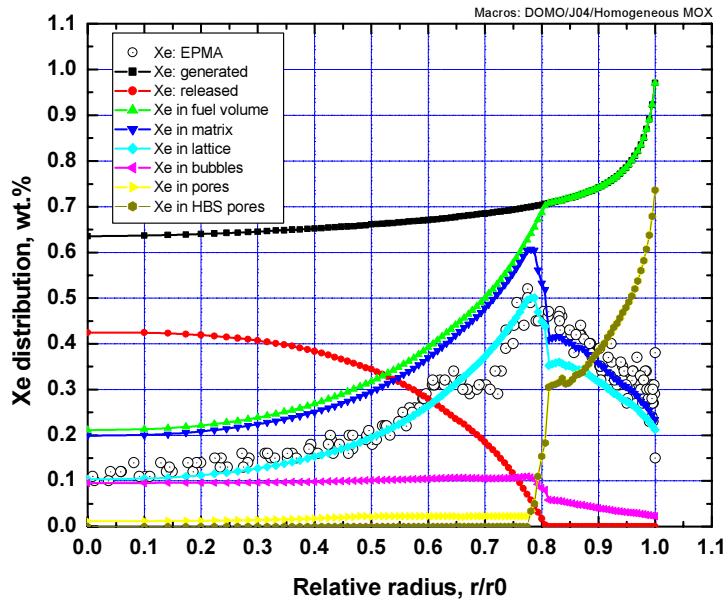


FIG. 13. MACROS Verification calculations for radial gasbalance distributions: J04-sample; homogeneous MOX.

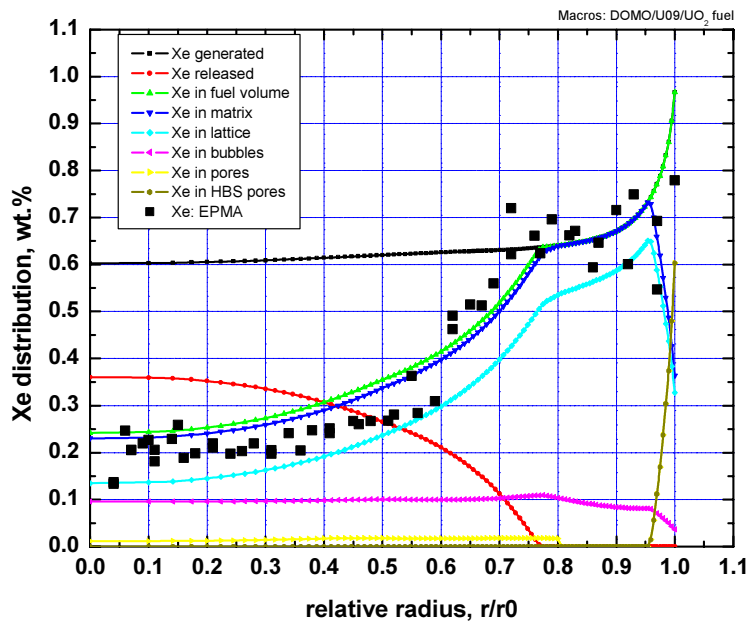


FIG. 14. MACROS Verification calculations for radial gas balance distributions: U09-sample; standard UO₂ fuel.

5. CONCLUSION

The present paper has shown that it is possible to assess the in-pile behaviour of nuclear fuels on the basis of general solid state and neutron physical considerations. Throughout the development of the MACROS code, it became apparent that more detailed approaches to describe the solid state evolutions will add a deeper insight to the different phenomena, but that the most fundamental part of a fuel behaviour code is the neutronic subroutine. If power density and defect creation is well accounted for, quite predictions can be made without further fine tuning of fuel-specific engineering parameters. It is not claimed that the accuracy will be higher than codes that rely on vast databases, but that this approach can add to the general insight in the physical phenomena and can make advancements in novel areas, where little experimental data is available, such as the role of He in degraded MOX, minor actinide fuels, fuel behaviour in off-standard spectral conditions etc.

REFERENCES

- [1] L. MERTENS, DOMO: Post-irradiation testing and Irradiation Programme of BWR MOX Fuel Rods, Final Report, SCK-CEN DOM 99/61, February 1997.
- [2] S.E. LEMEHOV, "Computer Code ASFAD: Status, Recent Developments and Applications", LWR Fuel Performance (Proc. Int. Topical Mtg West Palm Beach, FL, USA, 1994), ANS, La Grange Park, Ill, USA (1994) 162.
- [3] S.E. LEMEHOV and M. SUZUKI, *PLUTON*: A three-group model for the radial distribution of plutonium, burnup and power profiles in highly irradiated LWR fuel rods, Nucl. Technol., **3** (2001), 153-168.
- [4] S.E. LEMEHOV and M. SUZUKI, "PLUTON: Three-Group Neutronic Code for Burnup Analysis of Isotope Generation and Depletion in Highly Irradiated LWR Fuel Rods" JAERI Research Report, JAERI-DATA/Code 2001-025. (Available on request: OECD NEA Data Bank: <http://www.nea.fr> or RIST-Japan: <http://www.rist.or.jp/ehome.htm>) (2001) JAERI.
- [5] S.E. LEMEHOV, P. VAN UFFELEN, and V. SOBOLEV, Modelling Thermal Conductivity of Mixed Oxide Fuels, in EHPG Meeting, Report HPR-359, vol. 2, (HRP, Norway) September 2002.
- [6] S.E. LEMEHOV, V. SOBOLEV, and P. VAN UFFELEN, Modelling Thermal Conductivity and Self-irradiation Effects in Mixed Oxide Fuels. – J. Nuclear Materials, **320** (2003), 66-76.
- [7] R.J. WHITE, M.O. TUCKER, J. Nuclear Materials, **118** (1983) 1.
- [8] J. SPINO, K. VENNIX, M. COQUERELLE, "Detailed characterisation of the rim microstructure in PWR fuels in the burn-up range 40-67 GWd/tM," J. Nuclear Materials, **231** (1996) 179-190.
- [9] J. SPINO AND D. PAPAIOANNOU, "Lattice parameter changes associated with the rim structure formation in high burn-up UO₂ fuels by micro X-ray diffraction," J. Nuclear Materials, **281** (2000) 146-162.
- [10] K. LASSMANN, C.T. WALKER, J. VAN DE LAAR, F. LINDSTRÖM, "Modelling the high burnup UO₂ structure in LWR fuel," J. Nuclear Materials, **226** (1995) 1.

PELLET CLADDING INTERACTION (PCI)

(Session 5)

Chairpersons

J.G. CHUNG
Republic of Korea

M. LLORET
Spain

IMPACT OF FUEL MICROSTRUCTURE ON PCI BEHAVIOUR

C. NONON¹, S. LANSIART¹, C. STRUZIK¹, D. PLANCQ¹,
S. MARTIN², G.M. DECROIX², O. RABOUILLE²
S. BEGUIN³, B. JULIEN⁴

¹. Commissariat à l'Energie Atomique, Cadarache, France

². Commissariat à l'Energie Atomique, Saclay, France

³. EDF/SEPTEN, Villeurbanne, France

⁴. Framatome ANP, Lyon, France

Abstract

Besides testing the performances of present and future PWR fuel rods designs, CEA, EDF & FRAMATOME-ANP conduct jointly experimental programs devoted to understanding and modelling of PCI rod behaviour. They aim both at identifying the actual origin of beneficial fuel effects, as regard to the risk of cladding failure, and getting information on the kinetics of some important phenomena, such as fragmentation, creep and gaseous swelling of the pellet as well as crack initiation in the cladding. Since SCC failure generally occurs in the very first minutes of holding time at high power, the mechanical state of the rod at the end of power increase may be considered as crucial. So zero holding time similar ramps have been performed on rods with Zy-4 cladding and three different types of fuel: two-cycle uranium dioxide, two-cycle MOX fuel and four-cycle uranium dioxide. Thanks to identical irradiation conditions, experimental results are directly comparable. They give relevant data concerning the kinetics of cladding deformation and ridges evolution, of dimple filling and pellet fragmentation... For instance, enhanced fuel creep of MOX fuel is proved to occur in the time delay of the transient whereas, in the same time, its radial crack pattern evolution reveals weak and quite similar to that of standard UO₂. For high burn-up UO₂ fuel, considered too as beneficial from PCI point of view, the pellet radial peripheral cracks appear clearly more numerous while the cladding deformation looks different from that of MOX rod, especially with primary ridges exacerbated by the ramp. Post-calculations of these experiments have been performed, using 1D and 3D finite element modelling. The preliminary analysis allows ranking of the different phenomena responsible for the observed deformations of the pellet and the cladding, highlights the effect of a slight pellet height reduction and suggests improvements of some fuel laws.

1. INTRODUCTION

In the 1970's cladding failures due to severe power increase conditions occurred both in BWR's and PWR's. The root cause of these failures was quickly identified as stress corrosion cracking, induced by the combination of pellet clad mechanical interaction and aggressive fission products (iodine) release [1]. To insure cladding integrity under normal operating and incidental situations, rod design remedies were developed (e.g. Zr liner at the inner surface of the BWR rod cladding) and operating restrictive rules were established [2] (e.g. limitation of the maximum power level and of the power increase rate in PWR's). These solutions revealed quite efficient in the past. But today manoeuvrability increase has become an important economical challenge, especially in France where 75-80% of the electricity production comes from nuclear plants. On the other hand utilities introduce throughout the world more demanding operational strategies, resulting in higher burnups and higher possible neutron

solicitation at the end of the rod life. So new PCI remedies, consistent with burn-up extension, are being developed by different fuel manufacturers (e.g. large grain size fuel, obtained with niobia [3] or chromia [4] dopants).

In the framework of the coordinate CEA-EDF-FRAMATOME ANP research program, beside testing the performances of present and future designs [4], we investigate basic properties of fuel and cladding [5, 6] and conduct tests under irradiation particularly dedicated to understanding and modelling of PCI rod behaviour [7].

The purpose of this paper consists in showing some features of the differential behaviour of three types of fuel microstructure and relating them to the well-known differences in PCI resistance of the corresponding rods. For this, we compare the results of three very similar experiments, with simplified power histories, performed respectively on two-cycle uranium dioxide, on two-cycle MOX fuel and on four-cycle uranium dioxide. There is no doubt that different MOX fuels are able to undergo high power variations without any apparent damage [8]; the same trend is often reported concerning burn-up effect on UO₂ fuel [9], even though we must point out that no quantitative determination of the benefit has been provided yet. Since the most critical moment for cladding damage initiation can be situated at the end of the power increase phase of conventional ramp tests, when pellet expansion and expansion rate are both important while cladding viscous flow is still weak, power ramp tests were performed up to the same terminal level and then immediately interrupted: this results in “freezing” the thermo mechanical state of the components and considerably reducing the risk of screening major PCI features by various time dependent parasitic effects.

2. EXPERIMENTAL

2.1. Fuel rods design and base irradiation

The three fuel rods tested were all of PWR 17x17 type design, manufactured by FRAMATOME-ANP and loaded in EDF power reactors.

The first rod, named J12, contained standard UO₂ pellets and was irradiated up to 24 GWd/t_U. It is a segmented rod, composed with independent short fuel rodlets screwed end-to-end, which allows direct re-irradiation in experimental reactor. Three segments were extracted from this mother rod for ramp tests at different holding time [10]. Only the experiment performed on the second span J12/2 is described in this paper.

The design of the two other rods, H06 and G04, is the standard FRAMATOME one, with a 3650 mm long fuel stack. The H06 rod contained standard UO₂ pellets and was irradiated up to 48 GWd/t_U whereas G04 fuel is an heterogeneous MOX resulting from the MIMAS manufacturing process with 5,8% of Pu. It is characterized by the presence of Pu-rich clusters and achieved 25 GWd/t_U. The rodlets named H06/5 and G04/2 were re-fabricated by extracting respectively the fifth and the second span of their mother rod, adding lower and upper plugs and re-pressurizing to the same pressure as the one measured at the end of the base-irradiation, thus following the qualified process named “FABRICE” [11].

The fabrication and irradiation data of each rod are described in Table I.

Before re-fabrication, each mother rod was subjected to detailed non-destructive and destructive examinations in the CEA hot cell laboratories: visual inspection, eddy current, profilometry, gamma scanning, optical microscopy... These examinations allowed in

particular checking the soundness of the rods and determining the exact position of the fuel stack before cutting. Following re-fabrication, the rodlets were subjected to further pre-ramp exams such as profilometry, neutron radiography or gamma scanning, which will be used to be compared with the post-ramp examinations.

Table I: Fuel rod fabrication and base-irradiation data

Rod	J12/2	H06/5	G04/2
Fuel assembly design		17x17 PWR	
Fuel type	UO ₂	UO ₂	MOX MIMAS TU2
Re-fabricated rodlet characteristics			
Average burn-up (GWd/t _U)	26	51	28
Active length (mm)	436	359	350
He pressure (MPa)	- ^a	3,1	3
Pellet parameters			
Length / Diameter ratio	1,7	1,7	1,4
Chamfering	Yes	No	Yes
Double dishing	Yes	Yes	Yes
Cladding characteristics	Zircaloy-4	Zircaloy-4	Zircaloy-4
Metallurgical state	stress relieved	stress relieved	stress relieved

^a : No re-pressurizing – pressure equal to end of life in base-irradiation

2.2. Irradiation data

2.2.1. Ramp test device

The rodlets J12/2, H06/5 and G04/2 were all ramped in the ISABELLE 1 loop of the experimental reactor OSIRIS at CEA Saclay [12]. This device allows simulating PWR thermo-hydraulic and chemical conditions. The movement of the irradiation loop towards the core controls the power level in the rod. The rate of power increase was approximately 10 kW/m/min. During the test, the power is controlled by two independent methods. The first one is the heat balance based on a thermo-hydraulic analysis of inlet and outlet temperatures. The second one is based on a neutron analysis from current measurements taken by self-powered neutron detectors, with two time scales response time and a neutron modelling of the ISABELLE 1 loop. To calculate the accurate level of maximal power in the rod, it is necessary to establish the axial power profile along the rodlet, which is determined by gamma scanning, performed after the test. Rod failure is detected during the test thanks to delayed neutron and gamma ray measurements in the coolant and time of failure is determined by the analyse of the elongation sensor signal.

2.2.2. Power histories

The test scheme selected for these three ramps is similar: conditioning power level followed by a transient of about 10 kW/m/min, and zero holding time at terminal level. The pre-heating holding time is operated at an appropriate power level to re-establish the thermo-mechanical and chemical state of the rod achieved at the end of the base-irradiation. The aim of this experimental program is to provide new data for understanding the main mechanisms involved during the transient and to observe the rod thermo-mechanical state at the end of the power increase phase. The first experiment, conducted on the 2-cycle UO₂, was carried out in two steps to observe the phenomenon after two progressive power increases. Then, in order to make comparison between the 3 rods behaviour easier, the final power at the end of the two

next transients has been specified to the same value as the second phase of the first one: about 45 kW/m which is slightly greater than the power level for which rod failures have been already observed.

The whole ramp test schedule is described in Table II.

Table II: Ramp tests power levels

	J12/2 – 1 st phase	J12/2 – 2 nd phase	H06/5	G04/2
Fuel type	UO ₂	UO ₂	UO ₂	MOX MIMAS TU2
Rodlet average burn-up GWd/t _U	26	26	51	28
Conditioning power W/cm	200	240	200	190
Range of final power W/cm	415-420	445-450	455-460	445-450
	No failure	No failure	No failure	No failure

One of the main findings of this ramp test program is that no failure was detected in any rodlet even in the 2-cycle uranium dioxide for which the terminal power level was higher than the PCI power threshold. The large examination campaigns performed on the three rods after the tests confirms the absence of damage of the cladding and gives a lot of information of the differences in pellet evolution.

2.3. Post-ramp examinations

Non-destructive as well as destructive examinations were performed on the rodlets J12/2, H06/5 and G04/2 following the ramp tests. Profilometry, neutron radiography, eddy current tests and gamma scanning were carried out in the same facilities as before ramp. Next, rodlets were punctured to evaluate fission gas release fractions and several samples were cut around the maximum power level for cladding SEM analysis and fuel optical microscopy.

2.3.1. Cladding evolution

Cladding damage:

Eddy current tests did not reveal any defect on the cladding after each of the three experiments. However, stress corrosion damage signs have been researched through SEM analysis of the cladding fracture surfaces. PCI crack initiation generally occurs at the inner surface of the cladding at the pellet-pellet interface. The typical feature is the occurrence of a small intergranular corrosion zone surrounding the crack initiation site, followed by a large brittle fracture zone, mainly of transgranular type with typical fluting associated. The final rupture of the remaining ligament is due to plastic instability and appears ductile [13].

On each rod, only possible traces of the first step have been observed, on a thin thickness of 10 µm, both in front of the pellets interface and at the mid-plane. Actually this damaged thickness corresponds roughly to the penetration depth of the recoil fission products during base irradiation [14]. So it can be concluded that no iodine-induced stress corrosion cracking could be identified on the rods. This means that crack initiation is not developed during the transient but during hold time, since 2-cycle Zy-4/UO₂ rod is known to fail at a lower power level when maintained several minutes.

In addition, these examinations show that high burn-up does not increase the sensitivity to I-SCC in the conditions of the ramp tests. Indeed, the thickness of the very superficial damaged zone was equal on the two-cycle and on the four-cycle rods.

Cladding strain:

Profilometries, performed on the rods before and after the ramp tests, are compared in order to quantify the differences between the three rods cladding diameter increase and ridges evolution. Figures 1 to 3 plot the diametral profiles and power distribution deduced from gamma scanning, versus axial position for each rod. Diametral variations induced by the power transient in the maximum power area of the rod are gathered in Table III.

Table III: cladding diameter and ridges height diametral evolution measured on the three rods out-of-pile in the maximum power area.

Type of fuel rodlet	UO ₂ – 2 cycles J12/2 (end of phase2)	MOX – 2 cycles G04/2	UO ₂ – 4 cycles H06/5
Maximum power	445-450 W/cm	445-450 W/cm	455-460 W/cm
Cladding outer diameter increase on mid-pellet	≈ 10 μm	≈ 15 μm	≈ 30 μm
Primary ridges height increase	< 5 μm	< 1 μm	< 5 μm
Secondary ridges height increase	< 5 μm	< 2 μm	< 10 μm

The cladding deformation at the mid-pellet position is plotted versus the local power at the ramp terminal level on Figure 4. This figure shows that the three rodlets can be classified according to their permanent deformation. The J12/2 rodlet begins to have a permanent deformation since a local power of 35 kW/m. At the maximum power of about 45 kW/m, its permanent deformation achieves around 10 μm, whereas that of G04/2 rodlet is 1,5 times higher and H06/5, 3 times higher.

Fig.1 – J12/2 cladding diameter changes – UO₂ - 26 GWd/t_U

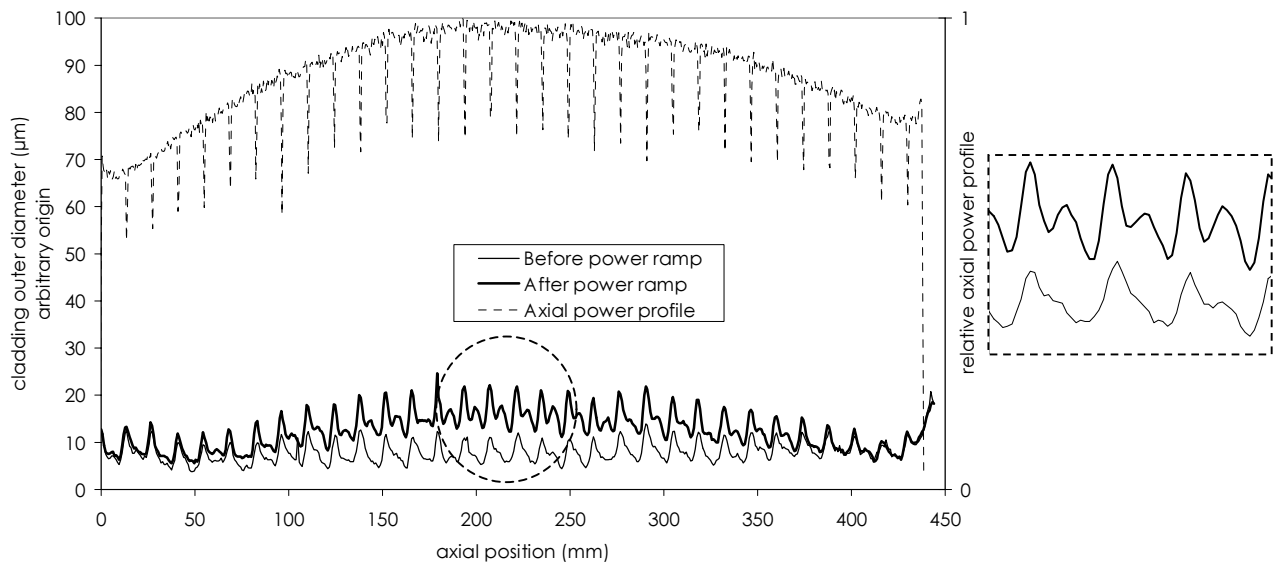


Fig.2 – G04/2 cladding diameter changes – MOX - 28 GWd/t_U

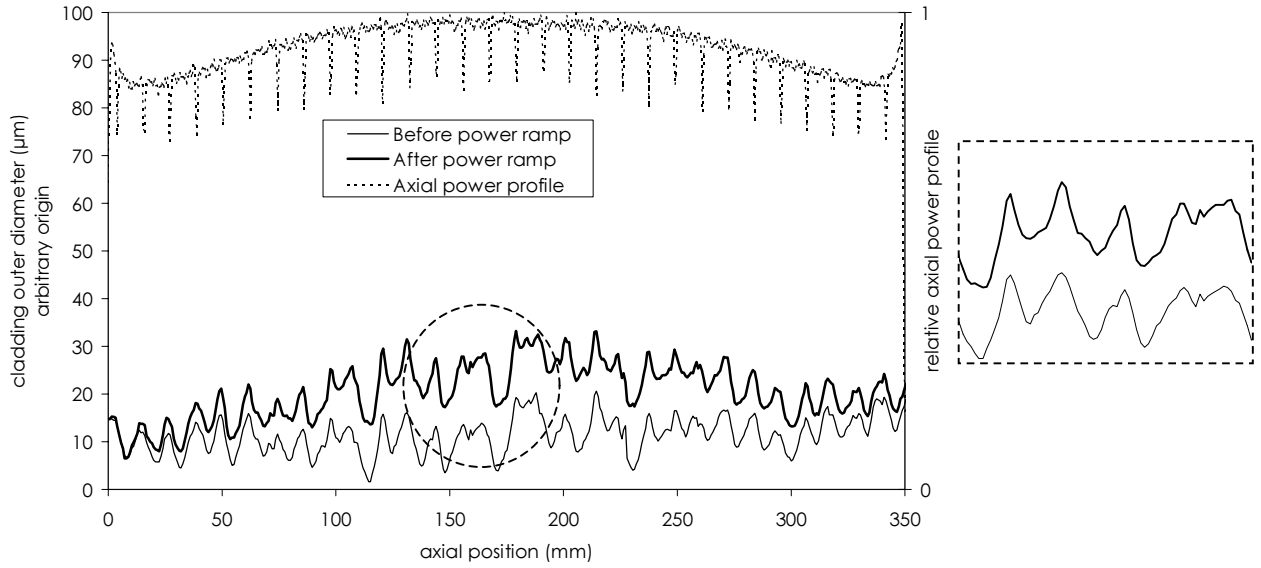


Fig.3 – H06/5 cladding diameter changes – UO₂ - 51 GWd/t_U

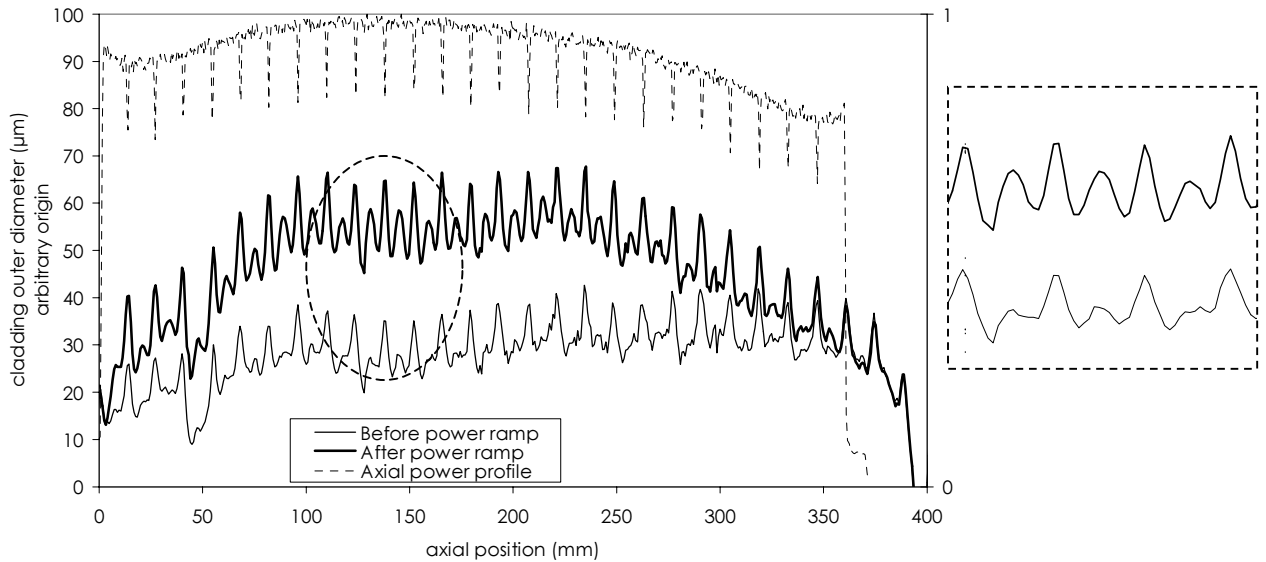


Fig.4 – Cladding deformation at mid-pellet evolution versus local power

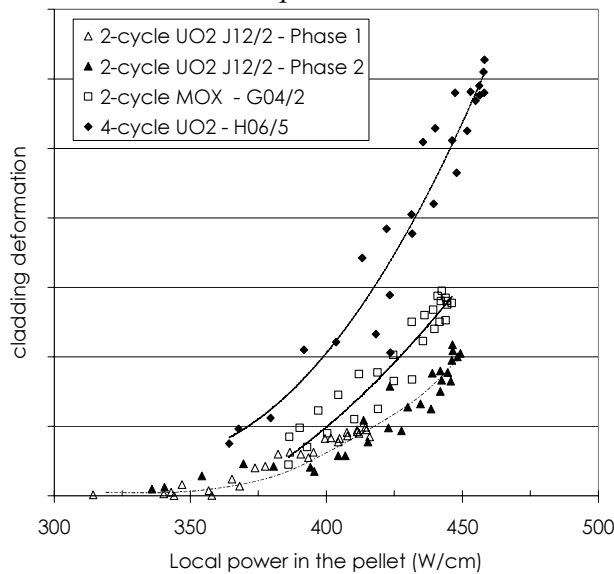
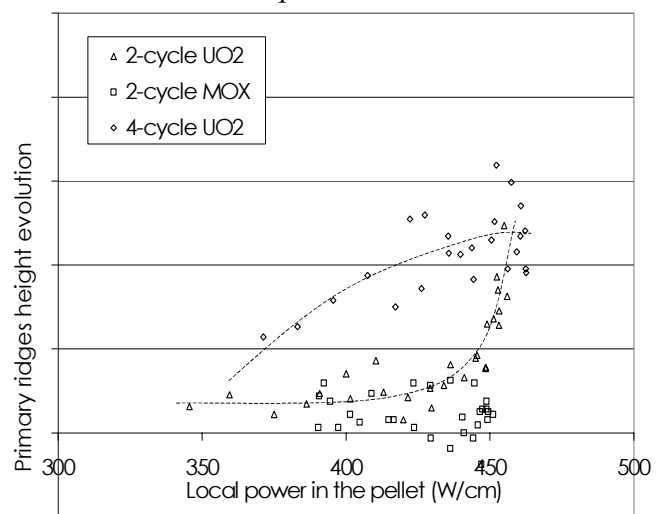


Fig.5 – Primary ridges height evolution versus local power



In addition, profilometries analysis emphases that ridges evolution is quite different according to the type of rod. During the transient, the 2-cycle UO₂ primary and secondary ridges grow so that secondary ridges raise half the primary ridges height in the central part of the rod. Power dependence of primary ridges increase is more accentuated than for 4-cycle UO₂ (see Figure 5) for which secondary ridges evolution is favoured. The MOX fuel rod is standing apart among the others by presenting no ridges evolution.

2.3.2. Pellet evolution

Transverse and longitudinal sections were cut from the high rating region of each rod for optical microscopy examinations.

Pellet cracking pattern

Table IV gathers transverse sections of the three rods ramped with Zero Holding Time (ZHT) at terminal level and shows the comparison with those obtained on the same type of rods before the ramp test and after a 12 hours holding time ramp at roughly 43 kW/m.

Four features appear clearly:

- **The effect of the transient:** this short phase induces the apparition of peripheral radial cracks, which are typical of a ramped fuel pellet. The crack pattern in the centre of the pellet is weakly changed;
- **The effect of holding time,** which contributes to increase the number of peripheral radial cracks. If holding time and power are sufficient, the main cracks in the centre of the pellet are healed and a circumferential crack, whose radius depends on these parameters, is created during cooling;
- **The effect of the pellet type:** the additional fractures created by the ZHT ramp are quietly similar for 2-cycle UO₂ and 2-cycle MOX (about ten). But the number of peripheral radial cracks that can be counted after a 12 hours holding time ramp is more numerous for MOX fuel (≈ 50) than for UO₂ (≈ 30). This suggests some interaction between the cracks formation process and the time dependent phenomena which affect fuel during holding time, differently for UO₂ and MOX, such as viscous flow, gaseous swelling...;
- **The effect of burn-up:** the impact of the transient phase on the third rod, H06/5, is stronger than for the other rods. The radial crack network observed at the periphery of the pellet is more developed than in the case of 2-cycle fuels (UO₂ and MOX), especially in the inter-pellet plan. Crack healing seems to begin at the very end of the power increase, on a limited area centred on the axis, in likely close connection with the degradation of thermal conductivity of fuel at high burn-up. After a long holding time, the number of radial cracks increases on a wider scale.

Longitudinal sections (see Table V) complete these observations and reveal a greater number of fractures in the higher burn-up UO₂ pellet and a much less crack volume in the MOX pellet, compared to 2-cycle UO₂ where large fractures and fragments movement can be observed.

Dimples filling

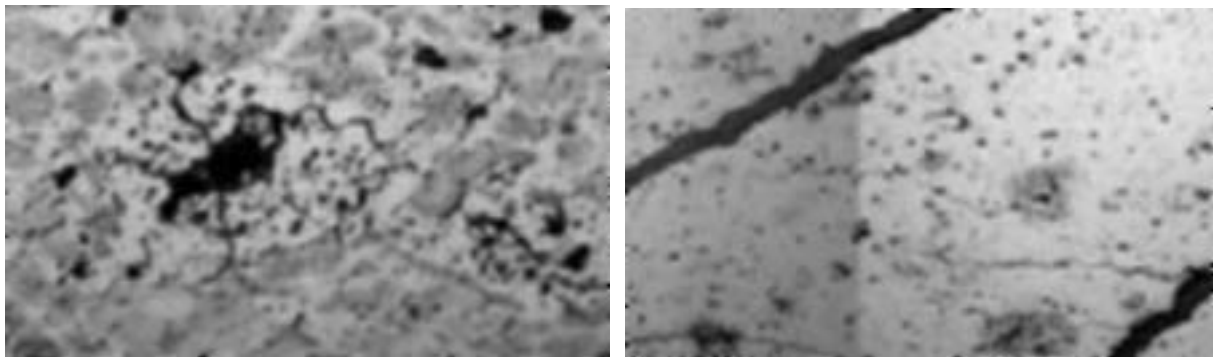
Dish dimensions were measured on axial micrographic examinations in the maximum power area (see Table V). Partial filling of dishes for 2-cycle MOX and 4-cycle UO₂ was found and reached respectively 25 and 20 % whereas no evolution was observed on the 2-cycle UO₂. This observation is the sign of an enhanced creep rate for MOX and high burn-up UO₂, which is consistent with profilometry analysis concerning ridges evolution, developed in section 2.3.1. Closer examinations in the vicinity of the partially filled dishings revealed oriented intergranular fractures, whose directions are parallel to dishing surface. Intergranular decohesion may be compared to microstructural damages observation of pellets submitted to compression experiments, for which oriented crack opening are created at stress level of 50 MPa and temperature about 1450°C [15]. They can also be favoured by preferential intergranular swelling in the direction perpendicular to the free surface.

2.3.3. Fission gas release and microstructure evolution

The rods J12/2 and G04/2 were punctured to evaluate fission gas release fractions. Measures confirm the higher level of release for MOX fuel (< 3%) compared to UO₂ (<1 %) [16], which means that the single transient phase contributes partly to overall release analysed after long holding time ramp tests

Microstructure analysis revealed in the central part of the MOX pellet ($r/R < 0,25$) burst Pu-rich clusters than can take part in gas release (Figure n°6).

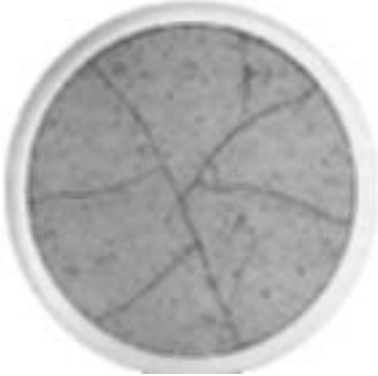
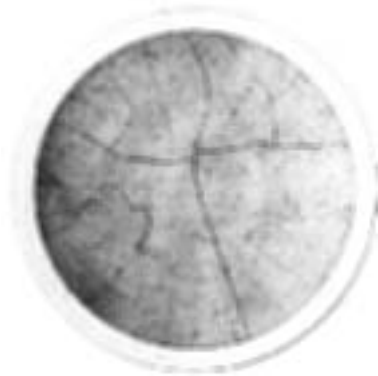
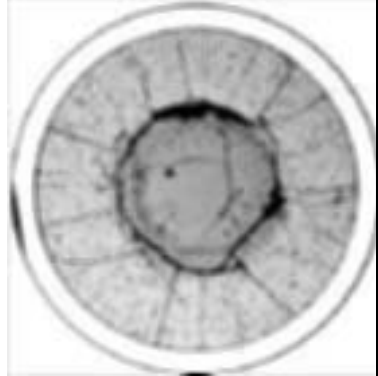
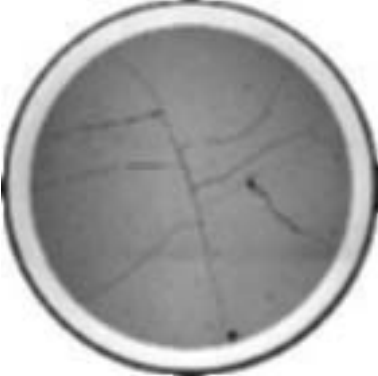
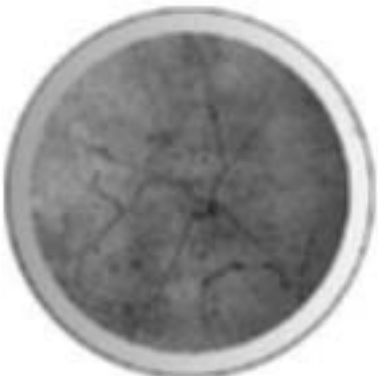
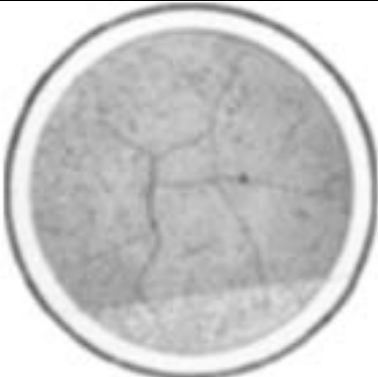
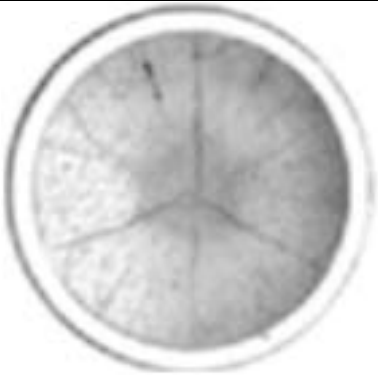
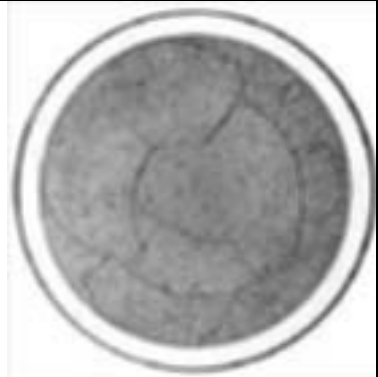
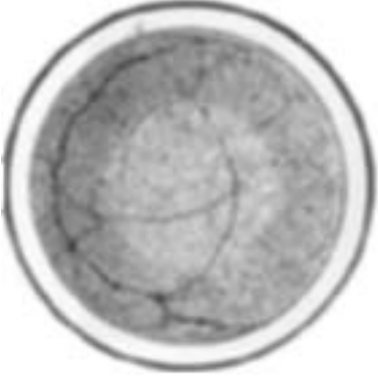
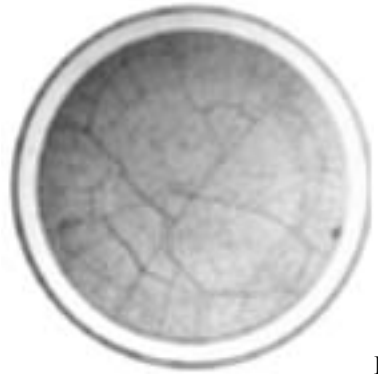
*Fig. 6 – fractured Pu-clusters in the central part of the MOX pellet after ZHT ramp test
Left: in the vicinity of the interpellet – Right: in the mid-pellet plane*



Intragranular bubbles precipitation limit of H06/5 fuel ($r/R \approx 0,51$) is higher than that of 2-cycle UO₂ J12/2 ($r/R \approx 0,46$) and is smaller than that obtained for 4-cycle UO₂ after 12 hours holding time ($r/R \approx 0,7$). Gas fission bubbles can grow during the time scale of the transient in the high burn-up fuel and progress more quickly during holding time if maintained. Furthermore, grain boundaries in the central part of the high burn-up fuel are strongly open at the mid-plane, in the direction perpendicular to axis and in the vicinity of large cracks (Figure n°7). This may be provided by the compressive stress accumulated during heating and restored during cooling

RIM structure was revealed in the periphery of the pellet, consistent with burn-up level (51 GWd/t_U). Figure 8 shows radial fuel cracks dying in the zirconia layer and the remaining contact between pellet and cladding.

Table IV. Cross-sections from UO₂ 26 GWd/t_U – MOX 28 GWd/t_U and UO₂ 51 GWd/t_U fuel rodlets after base-irradiation, after a zero holding time ramp and after a 12 hours holding time ramp.

	Before ramp test	After zero holding time ramp test - P ≈ 450 W/cm	After 12 hours holding time ramp test - P ≈ 430 W/cm
UO ₂ – 2 cycles	 MP	 MP	 MP
MOX – 2 cycles	 MP	 MP	 MP
UO ₂ – 4 cycles		 MP	 MP
	 IP	 IP	

MP: Mid-Pellet - IP: Inter-Pellet

Table V. Longitudinal sections from UO_2 26 GWd/t_U – MOX 28 GWd/t_U and UO_2 51 GWd/t_U fuel rodlets after zero holding time ramp test

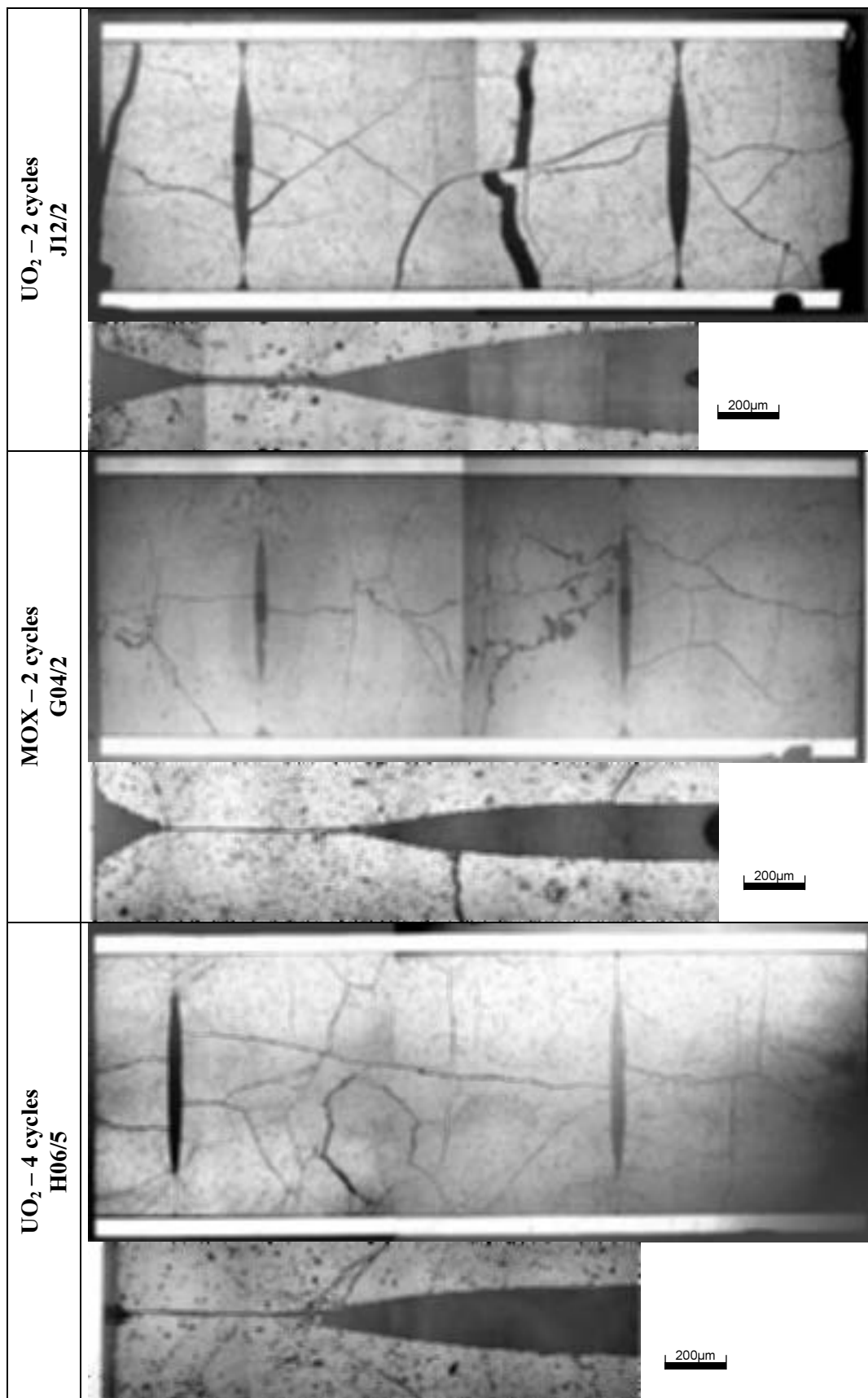


Fig.7 – open grain boundaries near axial fracture in the central area of H06/5 pellet after ZHT ramp test

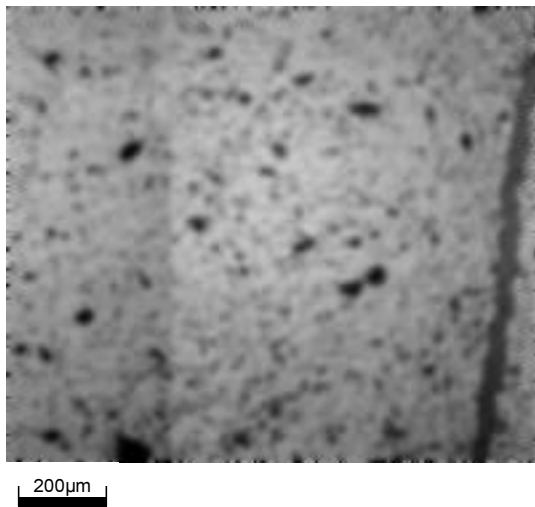
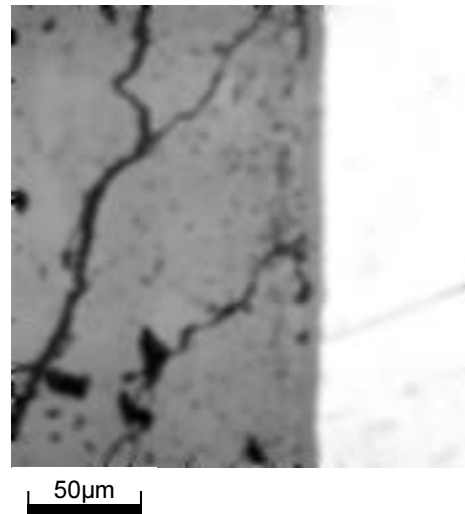


Fig.8 – pellet to cladding interface: RIM structure and internal zirconia in the H06/5 pellet after ZHT ramp test



3. DISCUSSION

The observations which have been shown in that work, concerning strains of stress relieved Zy-4 cladding, ridges evolution, pellet cracking, dimples filling... give evidence of differences in the rods behaviour during transients that are related to the differences of fuel microstructure in the three experiments.

The good PCI performances of MOX fuel and the beneficial burn-up effect on PCI behaviour of UO₂ fuel have been reported previously. However experimental results show that the cladding strain for these two types of rods is higher than for 2-cycle UO₂. It means that the strain imposed by fuel pellet expansion is higher for MOX and high burn-up UO₂ but that this larger deformation is over compensated by beneficial effects on some phenomena such as fuel viscous flow, pellet stiffness, clad punching by the pellet fragments... First of all, sensitivity calculations have been conducted with 1D1/2 computation to identify the origin of the differences in cladding strains at mid-pellet and to assess the thermal loading of the three rods. Then, local effects have been considered with multi-dimensional modelling, in particular to improve ridges building understanding. Since no ridges evolution appears in the 2-cycle MOX case, in comparison with the 2-cycle UO₂, these two ramp tests have been simulated with TOUTATIS 3D.

3.1. Modelling support – 1D1/2 analysis

The computer code METEOR [17] has been used in support to the analysis of the experiments.

This is a mono-dimensional code, which calculates the thermo-mechanical and physico-chemical behaviour of PWR fuel rods. This code integrates the best models and laws to compute fuel behaviour under nominal and incidental conditions and is designed to be as

physical as possible. However, fuel, cladding and coolant are processed by 1D1/2 model, which does not take into consideration local mechanical effects.

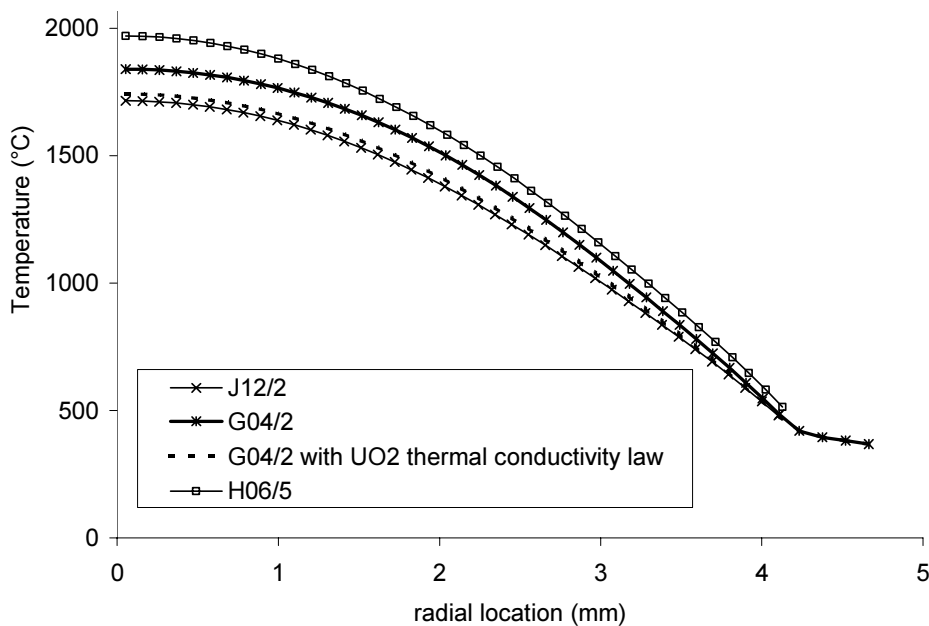
Post-calculations of the ramp tests require the preliminary computation of the base irradiation in PWR to obtain a good representation of the re-fabricated rod at the beginning of the power transient. Only the second step relative to power ramp calculation is described here. It consists in representing the rod in several axial slices for which clad external temperature and local linear power are imposed.

Sensitivity of cladding strain calculation to models relative to fuel swelling or thermal properties was studied. The axial power profile is particularly useful to assess the relevance of model description.

The temperature distribution in the fuel pellet for the three rods is compared on Figure 9.

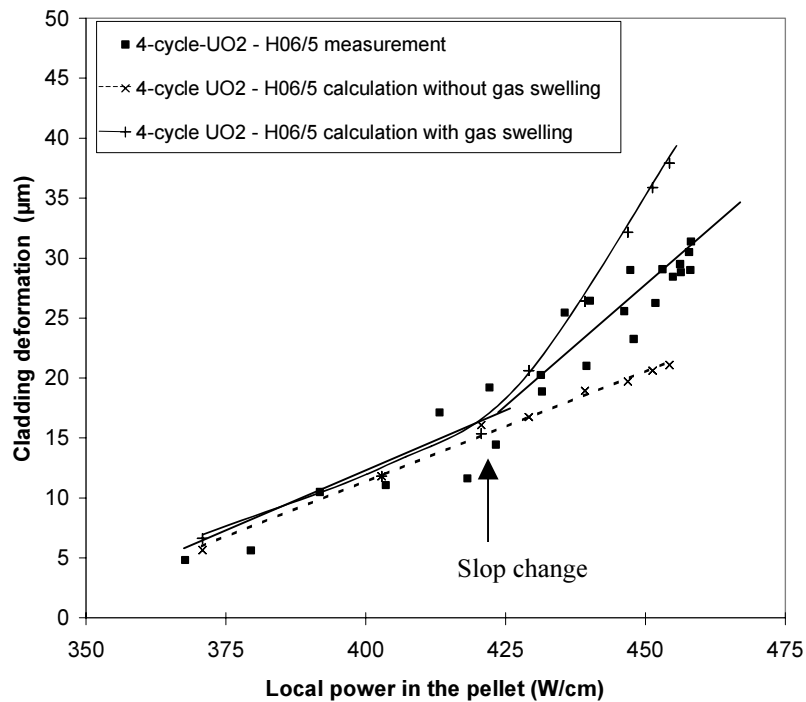
The impact of fuel thermal conductivity property is noteworthy for MOX fuel. Temperature in the central part of the pellet achieves 1840°C whereas the use of UO₂ conductivity law induces a maximal temperature of 1740°C (close to J12/2 result). Thermal loading directly influences the cladding diameter change due to the transient: 10 µm for UO₂ law instead of 16 µm for MOX law.

Fig.9 – Temperature distribution in the pellet at maximum power level.



The same inference can be reported to the 4-cycle UO₂ case. Temperature in the centre of the pellet was evaluated to be 150°C superior to those obtained in the 2-cycle rodlet because of thermal conductivity degradation due to burn-up. But whereas fission gas swelling is not significant during the phase of power increase for the 2-cycle UO₂ and MOX, calculation without gaseous swelling under transient conditions underestimates diameter changes in the 4-cycle UO₂ case (≈ -10 µm), as shown on Figure 10.

Fig.10 – Cladding deformation of H06/5 rod against local ramp terminal power.



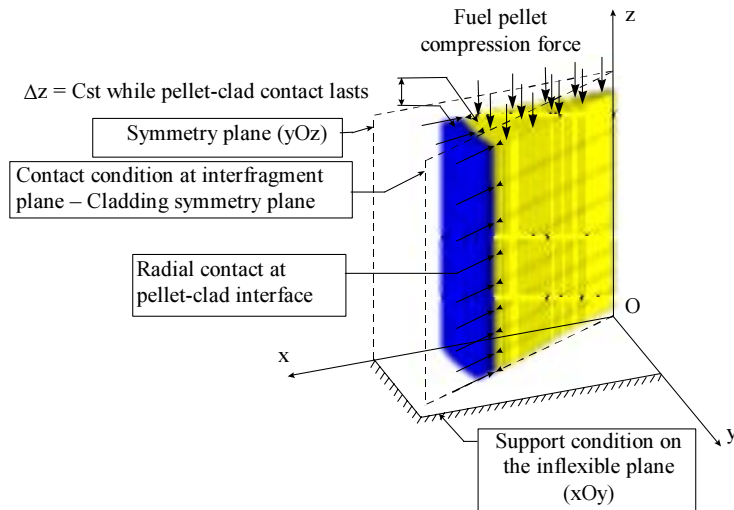
The use of the gaseous swelling model well reproduces the increase of deformation slop observed since 42 kW/m. The power dependence of this increase suggests an intragranular bubble swelling mechanism. Sensitivity calculations revealed that the higher slope is sensitive to the initial bubble population description, which thus strongly influences the mechanism kinetics. This result confirms the occurrence of gaseous swelling during a short transient in the case of high burn-up UO_2 , firstly pointed out following the microscopy examinations. Compared to 2-cycle fuels one, the stronger central temperature can also contribute to accelerate intragranular bubble swelling.

3.2 Modelling support – 3D analysis

The main objective of the TOUTATIS code [18] is to simulate the pellet cladding mechanical interaction and the resulting possible local damage of the cladding, taking into account materials and geometrical non linearities such as fuel or cladding viscoplasticity and contacts between surfaces warped by the thermal gradient (lateral surfaces or bases of a pellet fragment). To model all these non linearities, FE discretization and non-linear resolution algorithms are required. The general FE code CAST3M developments have been chosen to elaborate the computing scheme, using 2D or 3D discretizations of the fuel rod at the pellet scale. With relevant boundary conditions, the discretization is limited to one quarter of a pellet fragment and the associated cladding portion (Fig. 11). By symmetries, this volume can be considered as representative of the whole part of the rod submitted to given irradiation conditions. Concerning the mechanical conditions at pellet-cladding interface, the imposed relations for the calculations reported here are:

- contact without friction in the circumferential direction,
- no axial relative movement between pellets and cladding at mid-pellet when contact is established.

Fig. 11. TOUTATIS 3D discretization of 1/4 fragment - symmetry and boundary conditions.



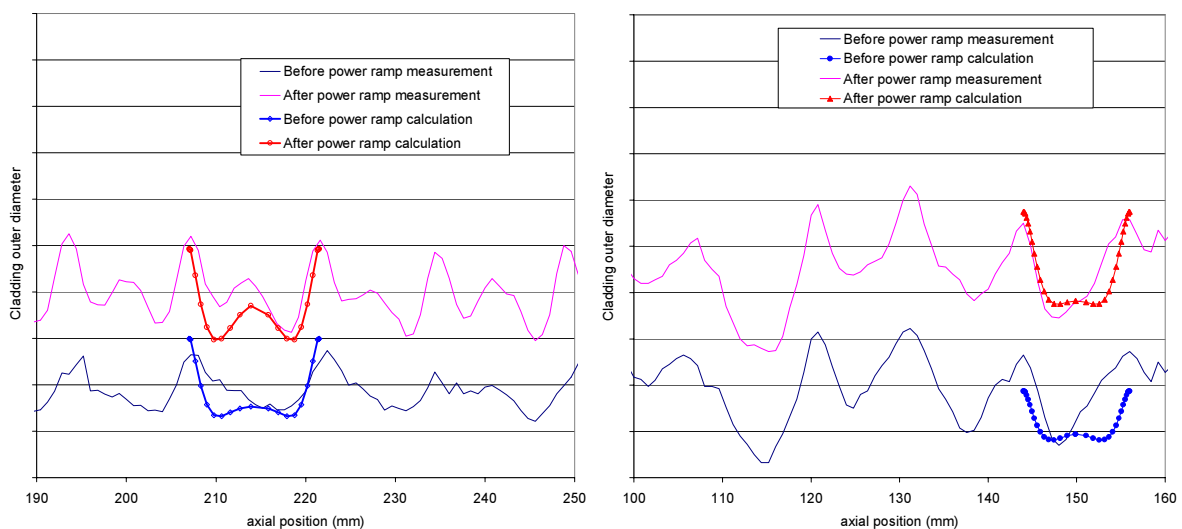
The behaviour of fission gases in transient conditions is not yet modelled in the 3D scheme; therefore the 1D results derived from METEOR/TU are commonly introduced in the TOUTATIS calculation, as additional displacements. Nevertheless, this calculation schedule was not necessary in the present study since fission gas swelling did not reveal significant in the two ramp tests simulated.

The power ramps were calculated after an adjusted computation of the PWR pre-irradiation.

For 2-cycle MOX fuel base-irradiation, the use of the UO_2 creep law gives surprisingly good estimation of cladding diameter and interface ridges height. This results suggests that irradiation creep kinetics is similar for MOX and for UO_2 .

The use of UO_2 creep law was maintained for the ramp test computation. Despite this, we can see on Figure 12 that the ridges calculation at the end of the transient differs between J12/2 and G04/2 experiments.

Fig. 12. Cladding deformation and ridges height evolution simulation with TOUTATIS 3D – Left: J12/2 ramp test – Right: G04/2 ramp test



Both computations are in good agreement with experimental results in terms of cladding overall deformation and secondary ridges heights. We can particularly notice that the absence of secondary ridges in the MOX experiment is well represented.

Secondary ridges are known to appear for sufficiently slim pellets and sufficiently large overall fuel displacement. They take place at mid-pellets because of plane of symmetry condition and distance to inter-pellet, which reduces the possibility of creep in axial direction towards the dishings [19].

The large ramp test database and specially the J12 serial [10] have revealed that secondary ridges progress with power level and holding time. Kinetics of growth is accelerated by fuel burn-up. Nevertheless, secondary ridges can also appear in fresh fuel during ramp test [20], which proves that gas swelling is not necessary to create a greater strain at the mid-plane. In that case, secondary ridges building is due to fuel creep in the vicinities of pellet-interface and pellet fragments movement both leading to shrink the pellet diameter in the off-ridges area. Computational results thus reveal that ridges building difference is related to the weak reduction in fuel pellet length to diameter ratio in the MOX case ($L/D \approx 1,4$), compared to the UO_2 case ($L/D \approx 1,7$), which confirms previous work [21].

However, the numerical simulation points up a growing of primary ridges in the MOX case, due to the power increase, which is not observed experimentally.

Primary ridges evolution is due to dual mechanisms: thermal expansion increasing during power transient, leading to "hourglass" shape amplification and fuel creep towards the dishing, with the opposite effect. The overestimation of the primary ridges increase, with the use of the UO_2 thermal creep law, leads to the conclusion that the fuel creep rate during the transient is higher for MOX than for UO_2 in addition of temperature effect. This result is in good qualitative agreement with the comparative observations of dimples filling. Moreover, this interpretation is supported by the results of the second part of the analytical experiment DEFORMOX [20,22], carried out on pre-irradiated MOX fuel. The favourable behaviour of MOX has been partly attributed to its heterogeneous microstructure with presence of Pu-rich zones, where burn-up is locally higher. Computations are still in progress in order to quantify the thermal creep enhancement of MOX fuel in the ZHT experiment.

The 4-cycle UO_2 was not simulated with TOUTATIS 3D but the same conclusion can be reported : in spite of a superior overall cladding strain and thermal loading compared to 2-cycle UO_2 , its primary ridges have a limited growing. This is an emphasis of fuel creep enhancement due to microstructure evolution with burn-up and temperature effects. Secondary ridges size is related to fuel swelling contribution.

3.3. Fuel cracking and local effects

Fuel cracking has to be considered in fuel rod thermo-mechanical analysis for many reasons:

- Pellet fracturing is known to have a non negligible influence on the thermal behaviour of a rod [23];
- Cracks take part to stress distribution in the fuel pellet. Thus fractures creation is strongly coupled with stress dependent phenomena such as fuel creep or fission gas swelling [17];
- I-SCC PCI failure is due to localised mechanical loading in the region of the main radial cracks mouth. The degree of strain intensification is related to the number of radial cracks and the cladding-fuel frictional coefficient [18,24].

The number of radial cracks at the periphery of the pellet and crack configuration evolution are thus indicators of rods performance in transients condition. Experimental results acquired with ZHT power ramp test show on each rod peripheral cracks development at the end of power increase, due to fuel pellet thermal dilatation expansion and stress distribution. For the high burn-up rodlet, the more numerous radial peripheral cracks both in the mid-plane and at the pellet interface, at the end of the transient, is undeniable. In the MOX case, radial cracks building enhancement occurs later in the power history, during the holding time. Indeed, the analysis of irradiation parameters (final power, holding time) reveals that peripheral cracks evolution can be linked to fuel swelling and creep kinetics. As the viscous central area of the pellet expands, tensile hoop stress tends to increase in the fuel periphery. Radial cracks in the brittle periphery are so more numerous and shorter. This is the reason why crack pattern evolution is more accentuated in the MOX case, in comparison with UO_2 at the same burn-up. In other respects, the smaller crack volume in the MOX pellet and fragments cohesion, observed after the ZHT ramp test, appears to be the signs of fuel creep initiation into the space available.

The distinctive feature of the H06/5 rod is its high burn-up, which provides a RIM structure in the periphery of the pellet. The chemical continuity between the fuel and the cladding provides a strong contact and may modify sliding movement of cracks mouth. Moreover the RIM material is porous, which provides a loss of rigidity to the periphery of the pellet in contact with the clad [9]. RIM material higher toughness would be able to dissipate applied mechanical energy [25]. All these effects lead to decrease the local stress concentration factor in the cladding.

In that sense, cracks formation may be a contribution to benefit regarding the risk of failure associated to burn-up effect, whereas viscous phenomena are supposed to be the origin of MOX better behaviour.

4. CONCLUSION

The three ZHT ramp tests were conducted on three different type of fuel rods with a zero holding time and a similar final power in order to distinguish their thermo-mechanical behaviour during the single transient phase and to relate them to the well known differences in PCI resistance.

Experimental results revealed significant differences between kinetics of the phenomena involved in each type of fuel rod, during the few minutes of power increase:

- No iodine-induced stress corrosion cracking on any cladding, which suggests that crack initiation is not developed during the transient but during hold time,
- Larger diameter changes measured on the 2-cycle MOX and 4-cycle UO_2 , in comparison with the 2-cycle UO_2 ,
- Fuel creep enhancement for MOX and high burn-up fuel, observed through dimples filling, crack pattern and ridges height evolution,
- Important radial cracks building in the periphery of the 4-cycle UO_2 pellet and especially in the interpellet plan,
- Crack healing initiation and intragranular swelling in the centre of the high burn-up UO_2 .

Post-calculations of the three experiments were carried out to support analysis.

Mono-dimensional modelling allowed comparing thermal loading and relating them to cladding strain differences. Since no gaseous swelling occurred during the transient, both for UO₂ and MOX fuel after 2-cycle base irradiation, the gaseous swelling model was tested only on the 4-cycle UO₂ experiment. It appears that the model needs to be refined in the short time scale of the transient.

Multi-dimensional modelling revealed the impact of pellet geometry on ridges building during the power increase. Sensitivity calculations to fuel creep laws lead to conclude that irradiation creep is similar for MOX and UO₂ during base-irradiation while thermal creep is enhanced for MOX, even compared to UO₂ at the same temperature.

Added to the similar crack pattern of 2-cycle MOX and UO₂, at the end of power increase, this allows to attribute the higher PCI performance of MOX to fuel thermal creep enhancement. In the 4-cycle UO₂ case, this effect is added to pellet fracturation impact, for which cracking pattern is clearly changed during the transient.

It is important to notice that the large ramp tests database analysis revealed a strong interaction between the cracks formation process and the time dependent phenomena, which affect fuel during power variations and holding time.

To improve a predictive understanding capacity as regards to the risk of failure of the cladding, it seems now necessary to develop a multi-dimensional evolutive crack model, based on the pertinent mechanical characterization of the pellet.

From an experimental point of view, the success of the Zero Holding Time ramp program leads us to continue with this type of experiment to complete understanding of new fuel microstructure behaviour such as large-grain doped fuel.

REFERENCES

- [1] J.H DAVIES, H. S ROSENBAUM, T.C ROWLAND, J.S ARMIJO, "Fuel pellet cladding interaction in light water reactors", ASEE Annual Conference Proceedings (1984) 45.
- [2] P. PERMEZEL, P. PUPIER, N. WAECKEL, "PCMI limits on French PWR", LWR Fuel Performance (Proc.Int. Topical Meeting Palm Beach, Fl, USA, 1994), ANS, La Grange Park, Ill (1994) 687.
- [3] D.A HOWL, I.D PALMER, I.R TOPLISS, "Niobia-doped fuel as a PCI remedy", LWR Fuel Performance (Proc.Int. Topical Meeting Palm Beach, Fl, USA, 1994), ANS, La Grange Park, Ill (1994) 694.
- [4] CH. DELAFOY, P. BLANPAIN, C. MAURY, PH. DEHAUDT, C. NONON, S. VALIN, "Advanced UO₂ fuel with improved PCI resistance and fission gas retention capability", Topfuel 2003 (Proc. Int Mtg Würzburg, Germany, 2003) Inforum GmbH (2003), CD-ROM.
- [5] D. GILBON, A. SONIAK, S. DORIOT, J. P. MARDON – "Irradiation creep and growth behavior and microstructural evolution of advanced Zr-based alloys", Zirconium in the Nuclear Industry, (Proc. 12th Int.Symposium Toronto, June 15-18, 1998) ASTM, 100 Barr Harbor Drive, West Conshohocken, PA (2000) 51.
- [6] A. SONIAK, N. L'HULLIER, J.P. MARDON, V. REBEYROLLE, P. BOUFFIOUX, C. BERNAUDAT – "Irradiation creep behavior of Zr-base alloys", Zirconium in the Nuclear Industry, (Proc. 13th Int. Symposium Annecy, France, June 11-14, 2001) ASTM, 100 Barr Harbor Drive, West Conshohocken, PA (2002) 837.

- [7] S. BOURREAU, S. LANSIART, P. COUFFIN, C. VERDEAU et al. – “Influence of the hold period on the fuel rod behaviour during a power ramp” - Proceedings of the IAEA Technical Committee Meeting, Nyköping, Sweden (1998)
- [8] P. BLANPAIN, X. THIBAUT, J.P Pages, “Recent results from in-reactor MOX fuel - Performance in France and improvement program”, LWR Fuel Performance, (Proc. Int. Topical Meeting Portland, Oregon, USA, 1997) ANS, La Grange Park, Ill (1997) 39.
- [9] A.P CLARKE, PA TEMPEST, JH SHEA, “A PWR PCI failure criterion to burnups of 60 GWd/t_U using the ENIGMA code”, Proceedings of the IAEA Technical Committee Meeting, Nyköping, Sweden (1998)
- [10] S. BOURREAU et al, “Ramp testing of PWR Fuel and multi-dimensional finite element modelling of PCMI”, LWR Fuel Performance (Proc. Int. Topical Meeting Park City, Utah, 2000) ANS, La Grange Park, Ill (2000) CD-ROM.
- [11] J. JOSEPH, J. ROYER, M. GROSGEORGE – “Transient behaviour of Fragema fuel rods previously irradiated under commercial conditions”, LWR fuel performance, (Proc. Int. Topical Meeting Williamsburg, 1988), ANS, La Grange Park, Ill (1989) 225.
- [12] A. ALBERMAN et al., “Technique for power ramp tests in the ISABELLE 1 loop of the OSIRIS reactor”, Nuclear Engineering and Design 168 (1997) p 293-303
- [13] O. FANDEUR, L. ROUILLON, P. PILVIN, P. JACQUES, V. REBEYROLLE – “Modelling of stress corrosion cracking in zirconium alloys”, Nuclear Fuel Behaviour Modelling at High Burnup and its Experimental Support (Proc. IAEA Technical Committee Meeting, Windermere, UK, 2000) IAEA-TECDOC-1233, Vienna (2001) 153.
- [14] M.FREGONESEA, F.LEFEBVRE, C.LEMAIGNAN, T.MAGNIN – “Influence of recoil-implanted and thermally released iodine on I-SCC of Zircaloy-4 in PCI-conditions : chemical aspects” – Journal of Nuclear Materials 265 (1999) 245-254.
- [15] F. DHERBEY, F. LOUCHET, A. MOCELLIN, S. LECLERCQ, “Elevated temperature creep of polycrystalline uranium dioxide : from microscopic mechanisms to macroscopic behaviour”, Acta Materialia 50 (2002).
- [16] P. BLANPAIN, L. BRUNEL, X. THIBAUT, M. TROTABAS, “MOX fuel performance in the french PWRs - status and developments”, LWR Fuel Performance (Proc. Int. Topical Meeting Park City, Utah, 2000) ANS, La Grange Park, Ill (2000) CD-ROM.
- [17] PH. GARCIA, C. STRUZIK, M. AGARD, V. LOUCHE, “Mono-dimensional mechanical modelling of fuel rods under normal and off-normal operating conditions”, Nuclear Engineering and Design 216 (2002) p 183-201.
- [18] J. BROCHARD, F. BENTEJAC, N. HOURDEQUIN, “Modelling of Pellet Cladding Interaction in PWR fuel”, SMIRT (Proc. Int. Conf, 2001) ASME (2001) CD-ROM.
- [19] K. YANAGISAWA, H. SAITO, “A study on bamboo ridge deformation induced by pellet-cladding interaction, Nuclear Engineering and Design 97” (1986) p 339-346.
- [20] L. CAILLOT, A. CHOTARD, J.P BERTON; “Analytical studies of the behaviour of MOX fuel”, LWR Fuel Performance, (Proc. Int. Topical Meeting Portland, Oregon, USA, 1997) ANS, La Grange Park, Ill (1997) 62.
- [21] F. BENTEJAC et al., “Fuel rod modelling during transients : the TOUTATIS code”, Nuclear Fuel Behaviour Modelling at High Burnup and its Experimental Support (Proc. IAEA Technical Committee Meeting, Windermere, UK, 2000) IAEA-TECDOC-1233, Vienna (2001) 175.
- [22] L. CAILLOT, “Analytical experiment DEFORMOX 2 synthesis” – Personal communication - CEA
- [23] C. BERNAUDAT, “Mechanical behaviour modelling of fractured nuclear fuel pellets”, Nuclear Engineering and Design 156 (1995) p 373-381

- [24] A. YU, SP. WALKER, RT.FENNER, “Pellet-clad bonding during PCMI” - Nuclear Engineering and Design 121 (1990) p 53-58
- [25] D. BARON, J. SPINO, “Does RIM microstructure formation degrade the fuel rod performance?”, Technical and Economic Limits to Fuel Burnup Extension (Proc. Technical Committee Meeting, San Carlos de Bariloche, Argentina, 1999), IAEA-TECDOC-1299, Vienna (2002) 41.

A PROCEDURE FOR ANALYZING THE MECHANICAL BEHAVIOR OF LWR FUEL ROD

Y.M. KIM, Y.S. YANG, C.B. LEE, Y.H. JUNG,
LWR Fuel Development Division,
Korea Atomic Energy Research Institute,
Daejeon, Republic of Korea

Abstract

The study set up a procedure for analyzing the mechanical behavior of a fuel rod under the operational conditions, which can be used in high burnup UO₂ fuel performance analysis code, INFRA. A contact analysis model was developed by Lagrange multiplier method and inserted into a finite element program for thermal and mechanical analysis. Displacement, strains, stresses and contact pressure of pellet and cladding were calculated at linear heat generation rates between 130 and 600 W/cm and at frictional coefficients between 0 and 1 by using finite element analysis module and ABAQUS. Results of both programs showed very good agreement. Cladding elongation calculated by finite element analysis module was compared with in-pile test results for UO₂ PWR rod. Rearrangement of pellet was suggested to describe cladding relaxation. Estimated and experimental results were well in agreement at frictional coefficients between 0.50 and 0.55. But results were very sensitive to the difference between predicted and measured fuel rod temperature. Accurate estimation of fuel rod temperature are required. Finite element analysis module can be successfully used to analyze the thermal and mechanical behavior of a fuel rod in any LWR UO₂ fuel performance analysis code.

1. INTRODUCTION

High burnup UO₂ fuel rod performance analysis code INFRA (INtegrated Fuel Rod Analysis) was developed in Korea Atomic Energy Research Institute[1]. It analyzes the effects of rim microstructure, conductivity degradation, fuel swelling, cladding corrosion and creep, creep-out behavior due to fission gas release, and the mechanical behavior of pellet and cladding by finite element method. INFRA code is expected to analyze UO₂ fuel rod behavior up to 100 MWD/kgU-rod avg. burnup and 10 w/o U²³⁵ enrichment.

Mechanical behaviors of pellet and cladding are stress and strain distribution in the fuel rod, pellet-cladding mechanical interaction (PCMI), and pellet cracking by thermal stress due to temperature gradient. FEA(Finite Element Analysis) program without PCMI analysis tools can be easily obtained in many literatures. Presently, crack initiation is analyzed by assuming three-dimensional crack path [2]. Three-dimensional crack analysis are being tried by using strain energy density [3]. However, general method for crack analysis is not yet clearly defined. Since PCMI affects greatly the failure behavior, including crack, of high burnup fuel rod, it is important to set up a correct and effective PCMI analysis method.

In this study, contact analysis method for estimating PCMI was set up and inserted into a FEA program for calculating stress and strain distribution of a structure. The integrated FEA module was connected to the main routine of INFRA. The module was validated with commercial structural analysis software, and cladding elongation from FEA module and re-irradiation test of fuel rod was compared.

2. FINITE ELEMENT ANALYSIS MODULE

2.1. Finite element analysis module in INFRA

PCMI analysis program written in FORTRAN was integrated to previously developed FEA program for structural analysis[4], and then the combined program was inserted in INFRA code. Figure 1 shows the calculation procedure by FEA module in INFRA. FEA module calculates the mechanical behaviors of a-quarter pellet and adjacent cladding with load incremental method by using basic data from INFRA, and does not change any function of the other routine in INFRA. Data being transferred from INFRA to FEA module are geometric dimension, temperature, mechanical loads, and some physical quantities such as density, flux, fluence, etc. Mechanical analysis results from FEA module are displacement, stress, strain and strain energy density of pellet and cladding, and contact state and pressure between pellet and cladding.



FIG. 1. Calculation flow by finite element analysis module in INFRA.

2.2. Finite element modeling of pellet and cladding

Figure 2 shows loading and boundary conditions for a quarter of pellet and the adjacent cladding set up by radial and axial symmetry assumptions. Gas pressure between pellet and cladding is applied on the outer surface of pellet and the inner surface of the cladding. Coolant pressure is applied on the outer surface of cladding. Axial force from coolant and gas pressure is applied on the top part of cladding. Two-dimensional axi-symmetric finite element model, shown in Figure 3, was set up for pellet and cladding. A quarter-pellet was divided into five radial and three axial elements. Adjacent cladding was divided into three axial elements. Eight-node serendipity finite element was employed. Pellet was assumed to move freely in axial direction. By symmetry conditions, it is assumed that the radial center of pellet and the axial center of pellet and cladding are not displaced.

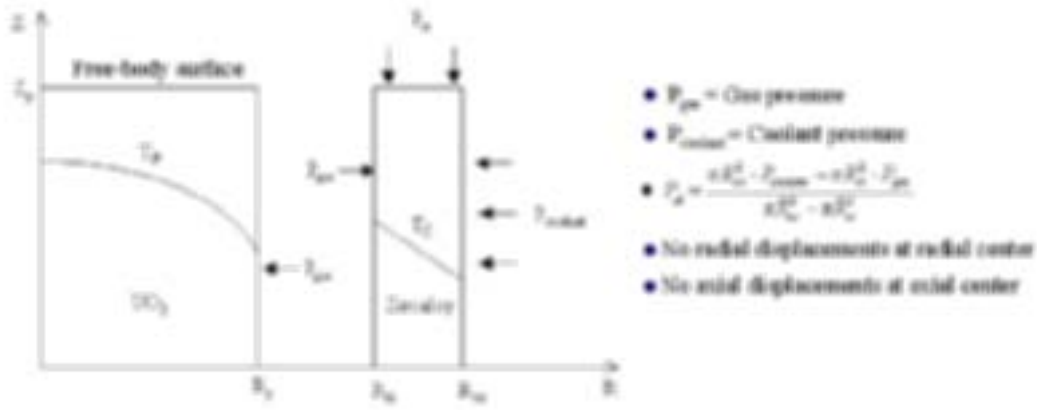


FIG. 2. Loading and boundary conditions for pellet and cladding.

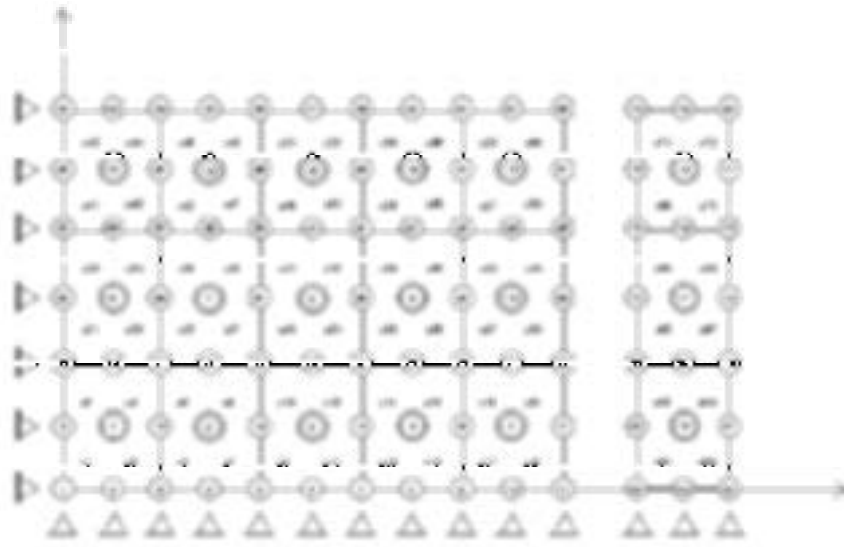


FIG. 3. Geometric finite element modeling for pellet and cladding.

Stress-strain and strain-displacement incremental relations were set up to represent the thermal, elastic, plastic, creep and rearrangement behaviors of a fuel rod, which are given by

$$\{\varepsilon\} = [B]\{x\} \quad (1)$$

$$\{\sigma\} = [D](\{\varepsilon\} - \{\varepsilon^{pl}\} - \{\varepsilon^{th}\} - \{\varepsilon^{cr}\} - \{\varepsilon^{ra}\}) \quad (2)$$

where $\{\varepsilon\}$ is total strain vector, $[B]$ is strain-displacement matrix, $\{x\} = \{u \ w\}^T$ is displacement vector, u is radial displacement, w is axial displacement, $\{\sigma\}$ is stress vector, $[D]$ is elasticity matrix, $\{\varepsilon^{pl}\}$ is plastic strain vector, $\{\varepsilon^{th}\}$ is thermal strain vector, $\{\varepsilon^{cr}\}$ is creep strain vector, $\{\varepsilon^{ra}\}$ is rearrangement strain vector which is calculated from rearrangement strain rate in section 4. Equations (1) and (2) will be inserted to total potential energy in section 2.3 in order to obtain finite element equilibrium equation.

2.3. Contact analysis model

Contact states and pressures at the surface of pellet and cladding in the gap should be calculated in order to correctly describe the deformation and failure behavior of fuel rod. Two problems frequently arising in contact analysis are chattering and penetration. Chattering means a continuing repetition of open and closed state during numerical iteration. Penetration is overlap of contact surfaces. Numerical methods used to traditionally estimate PCMI are penalty method [5,6] or Lagrange multiplier technique [7,8]. Penalty method is easy to be implemented in finite element equation. It maintains the symmetry of stiffness matrix in finite element equation. However, the value of penalty constant must be determined by user. If the value of penalty constant is too large, penetration occurs. If the value of penalty constant is too small, contact does not occur. In Lagrange multiplier technique, constraints are added to finite element equation, so stiffness matrix is not symmetric any more. Then calculation becomes very slow. However, Lagrange multiplier technique gives correct solution. In case of finite element model of Figure 3, it is judged through some screening calculations that penalty method could not prevent chattering and penetration, and Lagrange multiplier technique did not greatly increase calculation time since the number of elements was small. Lagrange multiplier technique was selected as a contact method for PCMI analysis for those reasons.

Figure 4 presents three modes of contact behaviors, i.e., open, stick and slip states. In open state, pellet approaches to cladding due to thermal expansion and swelling, but pellet and cladding are not yet contacted. In the first stage of stick state, soft contact between pellet and cladding occurs. Contact forces of the same magnitude act on the interface of pellet and cladding in the opposite direction. Strong contact between pellet and cladding occurs with further expansion of pellet. If contact force becomes equal to frictional force on the contact surface, pellet and cladding slip each other.

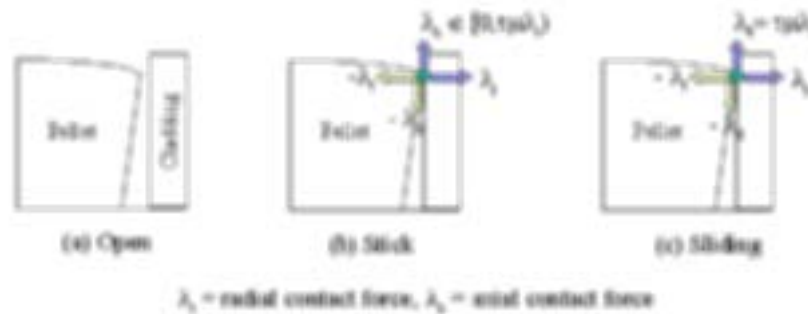


FIG. 4. Contact modes of pellet and cladding.

There are no constraints in the open state of Figure 4 (a). The total potential energy for open system is

$$\Pi_{OP} = \frac{1}{2} \int_{\Omega} \{\varepsilon\}^T \{\sigma\} d\Omega - \{x\}^T \{r\} \quad (3)$$

where Π_{OP} is total potential energy for open system, $\{r\}$ is load vector, Ω is volume considered, superscript T means transposed vector or matrix.

In stick node, gap thickness is zero and axial displacement of pellet node is equal to that of cladding node. Thus constraints for stick node are written by

$$g_r = g_r^0 - u_p + u_c = 0 \quad (4)$$

$$g_z = -w_p + w_c = 0 \quad (5)$$

where g_r is radial gap thickness, g_r^0 is initial radial gap thickness, g_z is difference of axial displacement between pellet and cladding, u_p is radial displacement of pellet node, u_c is radial displacement of cladding node, w_p is axial displacement of pellet node, w_c is axial displacement of cladding node. Constraints of stick node are applied to total potential energy as follows.

$$\Pi_{ST} = \frac{1}{2} \int_{\Omega} \{\varepsilon\}^T \{\sigma\} d\Omega - \{x\}^T \{r\} + \{g\}^T \{\lambda\} \quad (6)$$

where Π_{ST} is total potential energy for stick system, $\{g\}^T = \{g_r \ g_z\}$, $\{\lambda\} = \{\lambda_r \ \lambda_z\}^T$ is vector of Lagrange multipliers. Lagrange multipliers, λ_r and λ_z , mean physically radial and axial contact forces on pellet surface, respectively, and their values are always less than or equal to zero. Thus the value of $\{g\}^T \{\lambda\}$ is always zero.

In slip state, axial displacement of pellet node is not equal to that of cladding node any more. The constraint for slip node is Equation (4) only. Axial force becomes equal to frictional force. According to Coulomb's law of friction, frictional force is defined as follows.

$$\lambda_z = \tau \mu \lambda_r \quad (7)$$

where μ is frictional coefficient, τ is dimensionless variable which represents the direction of frictional force, defined by

$$\tau = \begin{cases} +1 & \text{for } w_p - w_c > 0 \\ 0 & \text{for } w_p - w_c = 0 \\ -1 & \text{for } w_p - w_c < 0 \end{cases} \quad (8)$$

The total potential energy for system including slip state is

$$\Pi_{SL} = \frac{1}{2} \int_{\Omega} \{\varepsilon\}^T \{\sigma\} d\Omega - \{x\}^T (\{r\} + \tau \mu \lambda_r \{e\}) + g_r \lambda_r \quad (9)$$

where Π_{SL} is total potential energy for slip system and the vector $\{e\}^T$ equals to $\{0 \dots 0 -1 \ 0 \ 0 \dots 0 \ 1 \ 0 \ 0 \dots 0\}$. In vector $\{e\}$, -1 and 1 appear at the location of pellet and cladding node in finite element equation, respectively. Frictional forces at pellet and cladding node are explicitly applied to load term in total potential energy.

Minimum potential energy principle indicates that the body being subject to loads is in stable equilibrium condition at minimum potential energy [9]. Finite element equation can be obtained after equations (1), (2), (4) and (5) are inserted to total potential energy equations (3), (6) and (9) and then total potential energy equations are minimized. Table 1 summarizes finite element equation, gap thickness, and contact force according to contact states. Figure 5 is flow chart for performing contact analysis for all nodal pairs of pellet and cladding in the gap. The scheme consists of solution (A→B) and contact judgment (B→A) steps. In solution step, new contact variables are calculated according to old contact state. In contact judgment step, new contact states are determined by using criteria consisting of variables from solution step. With contact analysis scheme of Figure 5, convergence occurred after two or three iterations without forcibly assuming contact state. This means that the developed contact analysis method is successful in preventing chattering.

Table 1. Finite element equations according to contact states

Contact states	Finite element equation	Gap thickness	Contact force increment
OPEN	$[K]^{(m-1)a} \{dx\}^{(m)b} = \{dr\}^{(m)}$	> 0	$d\lambda_{r,k}^{(m)} = 0$ $d\lambda_{z,k}^{(m)} = 0$
STICK	$\begin{bmatrix} [K]^{(m-1)} & \{e_{r,k}\}^d & \{e_{z,k}\}^e \\ \{e_{r,k}\}^T & 0 & 0 \\ \{e_{z,k}\}^T & 0 & 0 \end{bmatrix} \begin{Bmatrix} \{dx\}^{(m)} \\ d\lambda_{r,k}^{(m)} \\ d\lambda_{z,k}^{(m)} \end{Bmatrix} = \begin{Bmatrix} \{dr\}^{(m)} \\ -g_{r,k}^{(m-1)} \\ -g_{z,k}^{(m-1)} \end{Bmatrix}$	0	$d\lambda_{r,k}^{(m)} \leq 0$ $d\lambda_{z,k}^{(m)} \leq 0$
SLIP	$\begin{bmatrix} [K]^{(m-1)} & \{e'_{r,k}\}^f \\ \{e_{r,k}\}^T & 0 \end{bmatrix} \begin{Bmatrix} \{dx\}^{(m)} \\ d\lambda_{r,k}^{(m)} \end{Bmatrix} = \begin{Bmatrix} \{dr\}^{(m)} \\ -g_{r,k}^{(m-1)} \end{Bmatrix}$	0	$d\lambda_{r,k}^{(m)} \leq 0$ $d\lambda_{z,k}^{(m)} = \tau\mu d\lambda_{r,k}^{(m)}$

- ^a $[K]$ = stiffness matrix
- ^b (m) = load step number
- ^c k = contact nodal pair number
- ^d $\{e_{r,k}\} = \{0 \dots 0 -1 0 0 0 \dots 0 1 0 0 0 \dots 0\}^T$
- ^e $\{e_{z,k}\} = \{0 \dots 0 0 -1 0 \dots 0 0 1 0 0 \dots 0\}^T$
- ^f $\{e'_{r,k}\} = \{0 \dots 0 -1 -\tau\mu 0 \dots 0 1 \tau\mu 0 0 \dots 0\}^T$

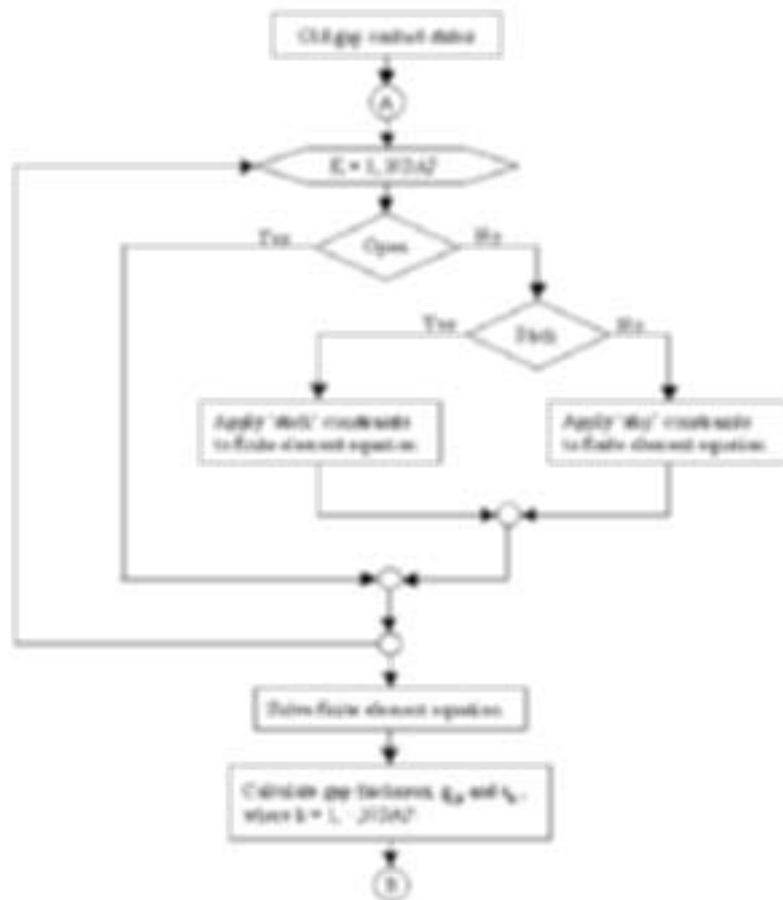


FIG. 5. Contact analysis flow for all nodal pairs in gap.

Table 2. Geometric, material and loading data for test calculation.

Data	Value
Pellet material	Uranium dioxide
Pellet outside diameter (mm)	10.86
Pellet length (mm)	12.70
Dish depth (mm)	0.0343
Spherical radius of dish (mm)	25.3
Dish shoulder (mm)	1.28
Fractional density of UO ₂	0.99
Gap thickness (mm)	0.02
Cladding material	Zircaloy
Cladding outside diameter (mm)	12.79
Cladding inside diameter (mm)	10.91
Gas pressure (MPa)	0.230 ~ 0.233
Coolant pressure (MPa)	3.447
Axial pressure on cladding (MPa)	12.034 ~ 12.044

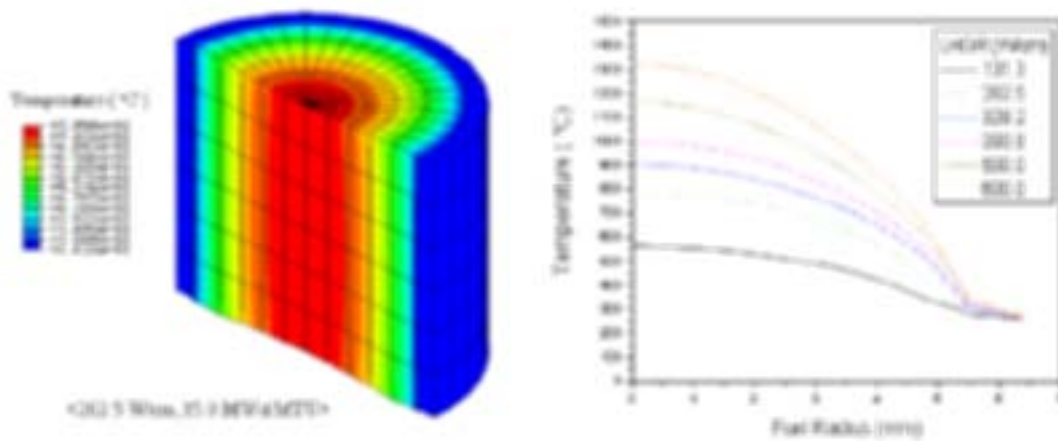


FIG. 6. Temperature distribution in fuel rod for test.

Table 3. Thermal and mechanical data for test calculation

Material	UO ₂	Zircaloy
Young's modulus, E (Pa)	$2.26 \times 10^{11}(1-1.131 \times 10^{-4}T^3)[1-2.62(1-D^b)]$	$9.8067 \times 10^4(9.900 \times 10^5-566.9T)$
Poisson's ratio, ν	0.316	$0.3303+8.376 \times 10^{-5}T$
Virgin yield stress, Y ₀ (Pa)	<ul style="list-style-type: none"> • $1176.1-1.688T+8.179 \times 10^{-4}T^2-1.293 \times 10^{-7}T^3$ • T = 1800 °C if T > 1800 °C 	<ul style="list-style-type: none"> • $9.8067 \times 10^6(58.93-0.1491T)$, T ≤ 220 °C • $9.8067 \times 10^6(31.32-0.0213T)$, 220 < T ≤ 450 °C • $9.8067 \times 10^6 \times 21.735T$, T > 450 °C
Strain hardening parameter, H _T (Pa)	0	0
Thermal expansion coefficients, α (°C ⁻¹)	<ul style="list-style-type: none"> • $\alpha = 7.107 \times 10^{-6}+5.162 \times 10^{-9}T+3.420 \times 10^{-13}T^2$ • $\alpha_r^c = \alpha_z^d = \alpha_\theta^e = \alpha, \alpha_{rz}^f = 0$ 	<ul style="list-style-type: none"> • $\alpha_r = 6.721 \times 10^{-6} = \alpha_\theta$, • $\alpha_z = 4.441 \times 10^{-6}, \alpha_{rz} = 0$

^a T = temperature (°C⁻¹)

^b D = fractional density of UO₂ (-)

^c α_r = radial thermal expansion coefficients (°C⁻¹)

^d α_z = axial thermal expansion coefficients (°C⁻¹)

^e α_θ = circumferential thermal expansion coefficients (°C⁻¹)

^f α_{rz} = shear thermal expansion coefficients (°C⁻¹)

Figure 7 shows circumferential strain in the top Gauss points of pellet and cladding at various LHGR. Figure 8 shows circumferential stress in the top and axial center Gauss points of pellet and cladding at various LHGR. Circumferential strain and stress from both program are in good agreement. Figure 9 shows radial and axial contact pressure on the inner surface of cladding at various LHGR. Radial and axial contact pressure increase with LHGR. Contact pressure from both program are in a little disagreement. This is due to the different contact analysis scheme of both program. ABAQUS uses surface-to-node contact scheme rigorously. FEA module uses simple node-to-node contact scheme. However, it is judged that such a little disagreement between contact pressure from ABAQUS and FEA module is acceptable. Figure 10 shows circumferential strain in the top Gauss points at various frictional coefficients. Figure 11 shows circumferential stress in the axial center Gauss points at various frictional coefficients. Circumferential strain and stress from both program are in good agreement.

Figure 12 shows effect of frictional coefficients on axial stress and strain at 500 W/cm. Axial strain and stress increase with frictional coefficients near the radial center, vice versa near the pellet surface. Frictional resistance for pellet expansion near pellet surface increases with frictional coefficients. And that accelerates pellet material near the radial center to expand more easily because top part of pellet is not constraint. Figure 13 shows effect of frictional coefficients on contact pressure. Axial contact pressure near pellet cusp clearly increases with frictional coefficients and vice versa in case of radial contact pressure. Both contact pressure are higher near pellet cusp than in the other region. This means that ridging reduces and cladding elongation increases with frictional coefficients. Figure 14 shows deformed shape of pellet and cladding like an hourglass. Pellet is more axially displaced than cladding because all contact nodal pairs are in slip state.

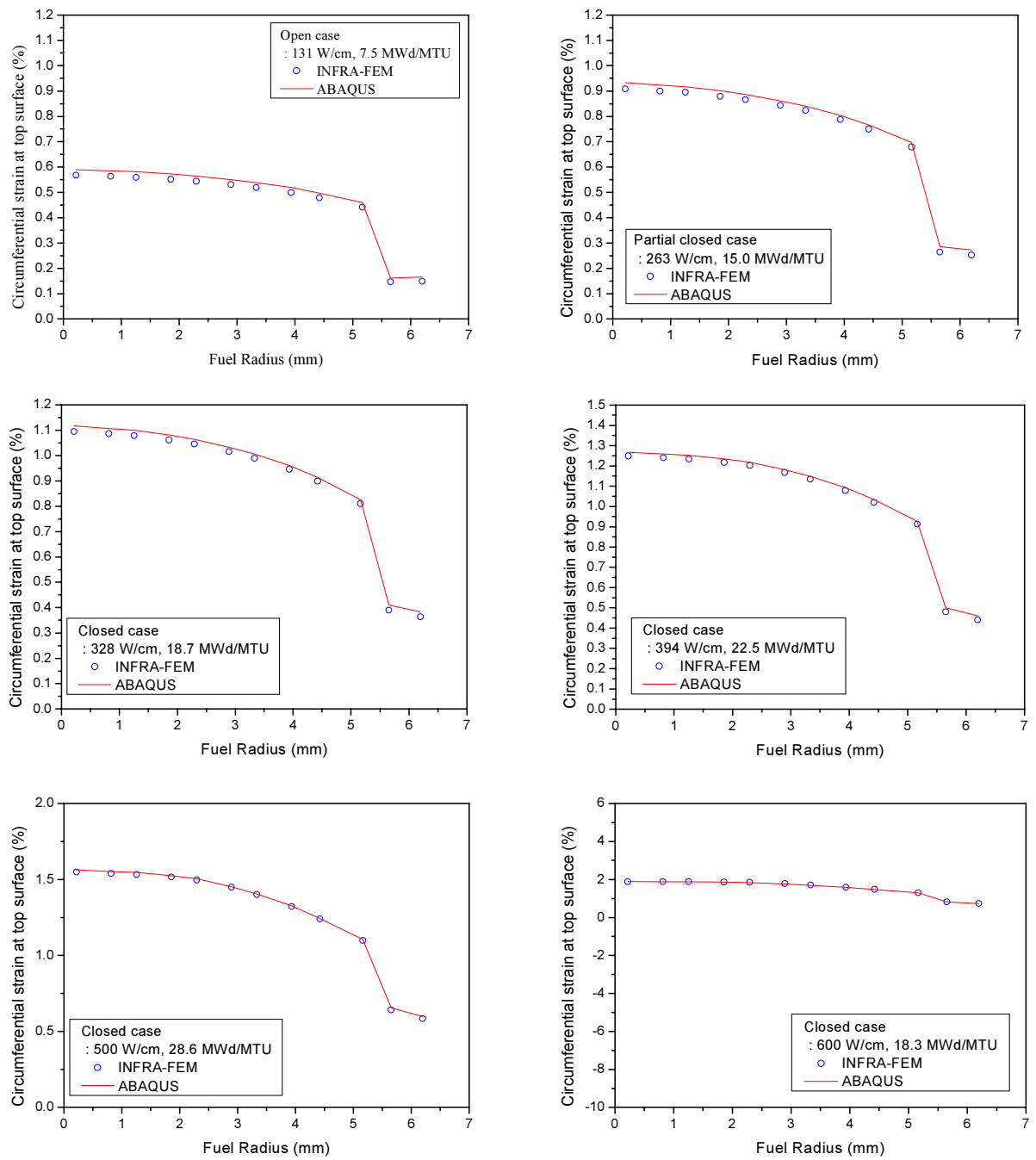


FIG. 7. Circumferential strain at the top points of a quarter-pellet and cladding ($\mu=0.3$).

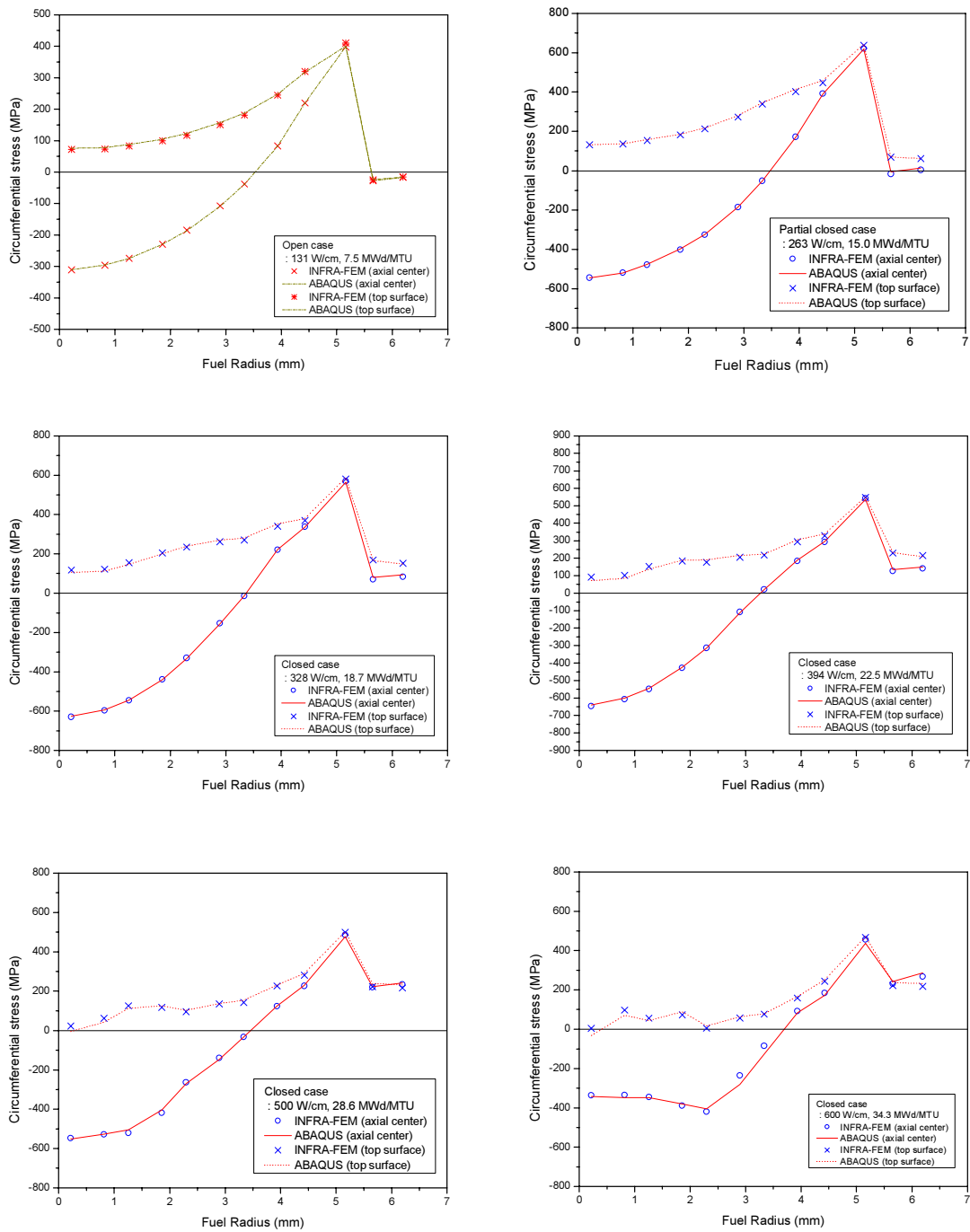


FIG. 8. Circumferential stress at the top points of a quarter-pellet and cladding ($\mu=0.3$).

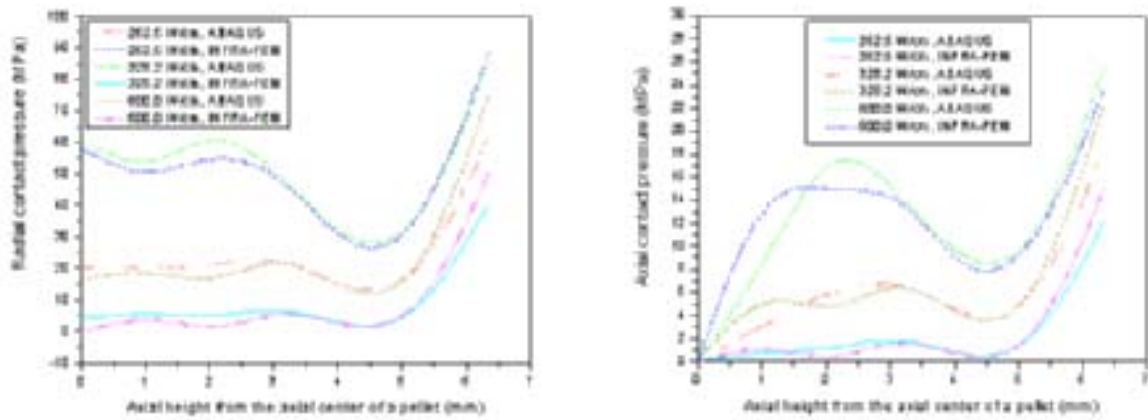


FIG. 9. Contact pressure at various linear heat generation rate.

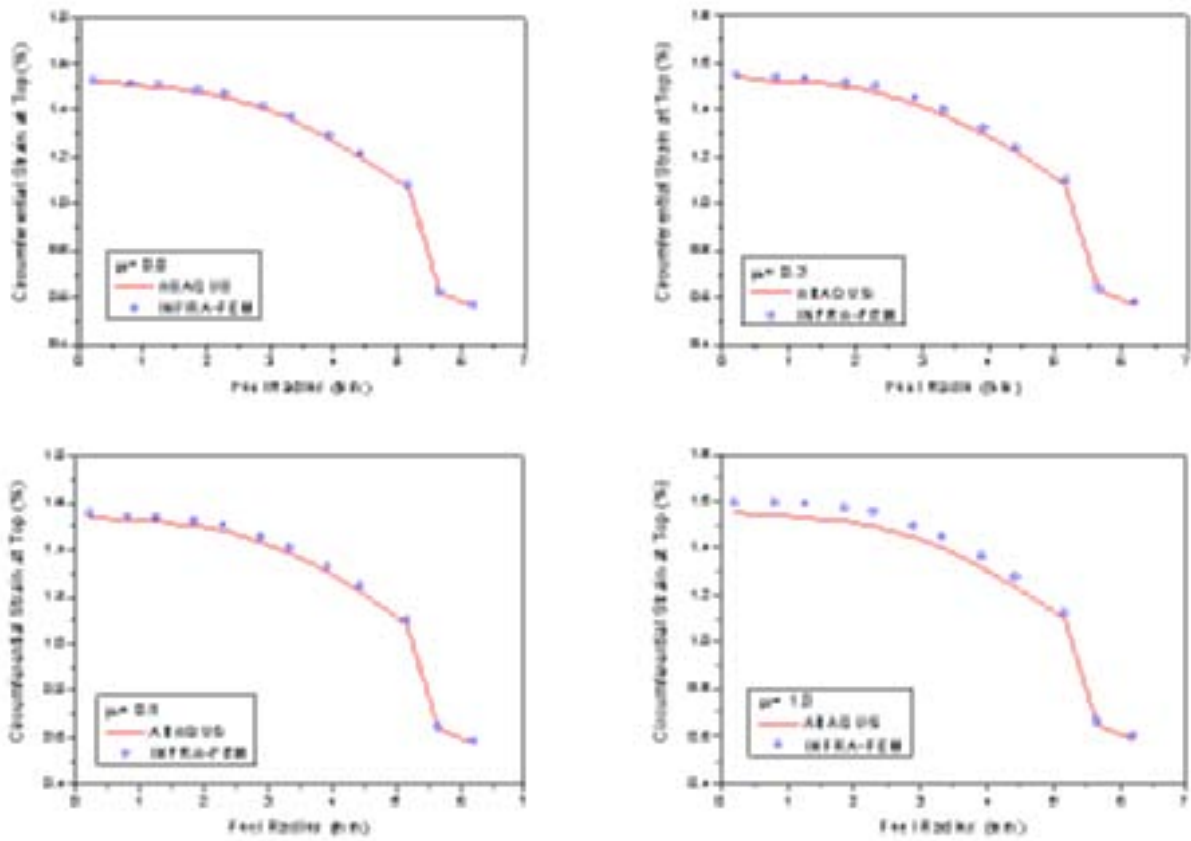


FIG. 10. Circumferential strain at various frictional coefficients.

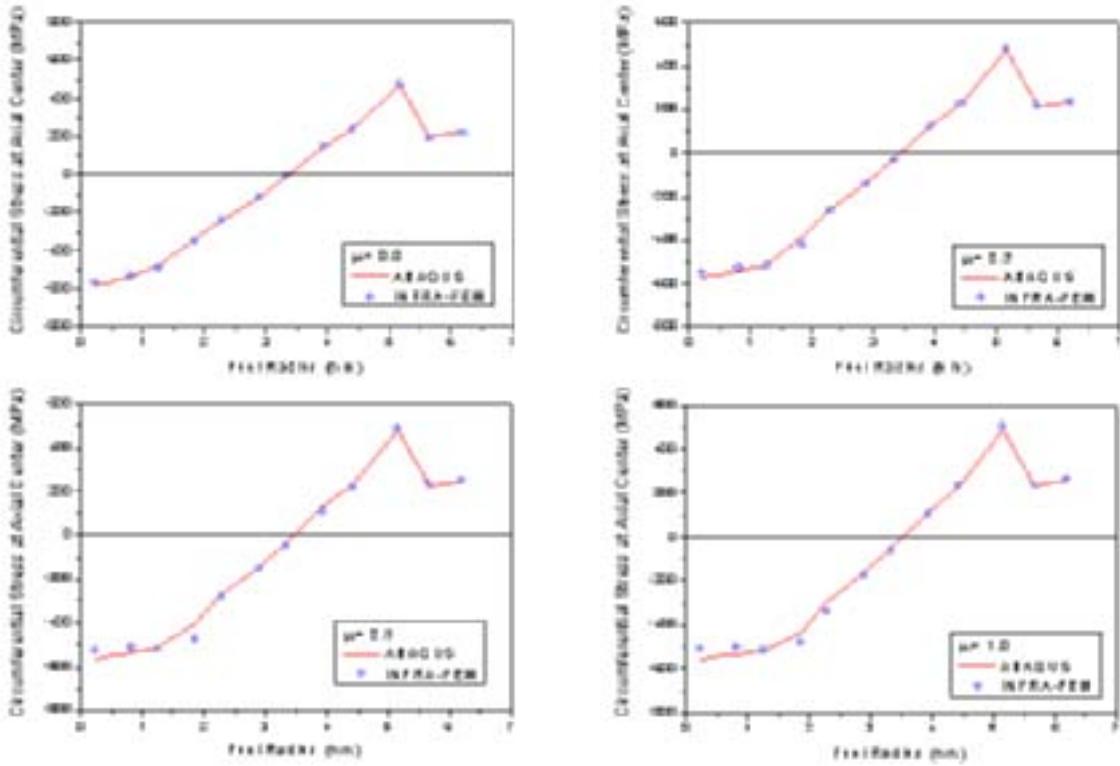


FIG. 11. Circumferential stress at various frictional coefficients.

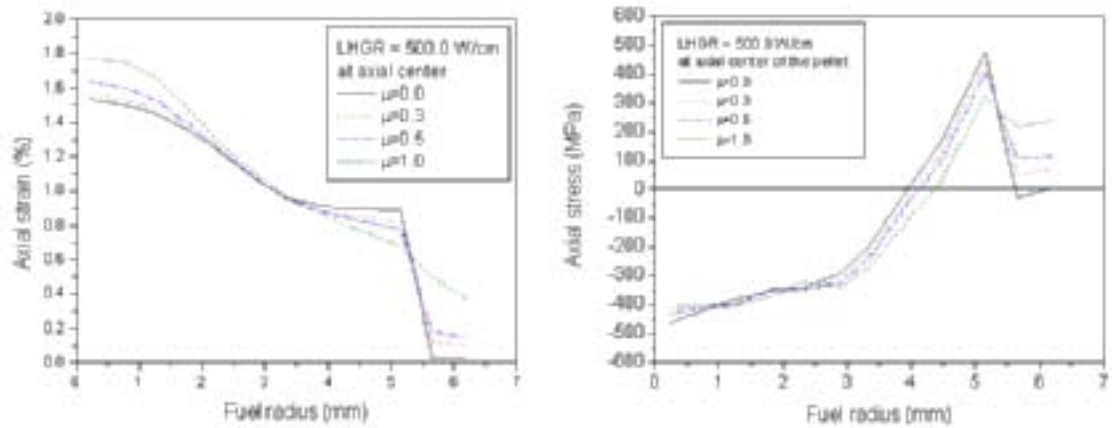


FIG. 12. Effect of frictional coefficient on axial stress and strain.

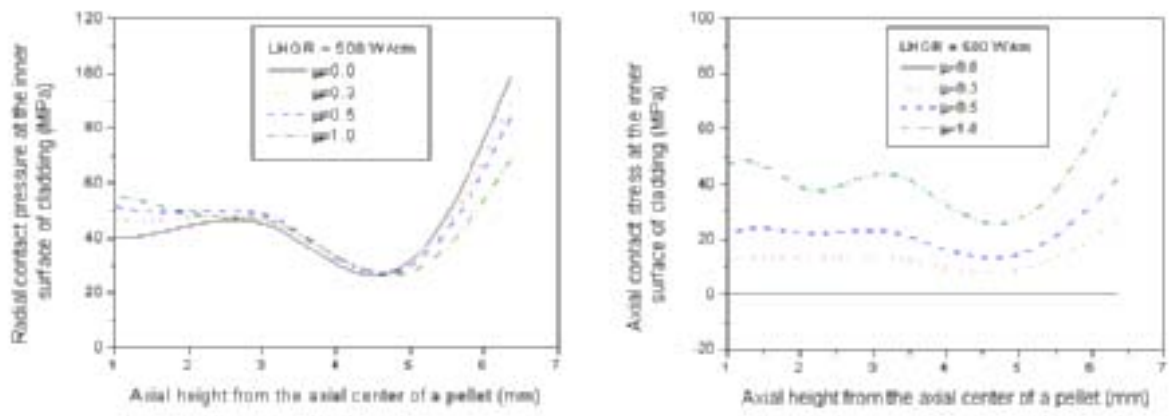


FIG. 13. Effect of frictional coefficient on contact pressure.



FIG. 14. Deformed shape of pellet and cladding.

4. CALCULATION OF CLADDING RELAXATION

In-pile tests showed that strain relaxation of cladding occurred during high power level was held. Cladding decreases axially under constant high power. It was suggested that cladding relaxation was caused by dimensional changes in the pellet [12]. Pellet thermally expands like an hourglass and peripheral cusp of pellet pushes out cladding, causing the elongation and ridging of cladding. Change in pellet volume reduces the size of pellet cusp and its force pushing out cladding. Then cladding relaxation occurs.

Cladding elongation calculated by the finite element program was compared with re-irradiation results of rod 3 used in IFA 629.2, which is a UO₂ PWR rod operated up to 50 MWd/kgUO₂ at Ringhals [13]. Material rearrangement within pellet appeared in Figures 15 was considered as one of major factors reducing the size of pellet cusp in order to describe the cladding relaxation. It is assumed in this model that pellet material is cracked or fractured and then rearranged during operation. Irradiation creep strain rate in Reference [13] was simply assumed as a mathematical model for rearrangement, but the related constant was newly determined.

$$\dot{\varepsilon}_e^{ra} = 5.25 \times 10^{-27} \dot{F} \sigma_e \quad (8)$$

where $\dot{\varepsilon}_e^{ra}$ is effective strain rate for rearrangement (s⁻¹), \dot{F} is fission rate (fissions/(m³·s)), σ_e is effective stress at the rearranged region of pellet (MPa). Effect of pellet creep on cladding elongation was also estimated by using pellet creep model in MATPRO[11].

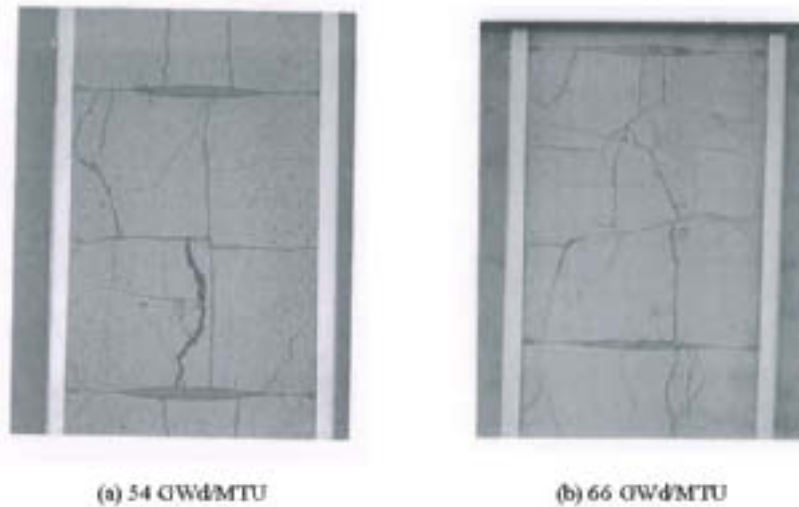


FIG. 15. Rearranged pellets (K23 fuel rod from Ulchin-2, Korea).

History of LHGR and temperature at fuel center of IFA 629.2 rod 3 is shown in Figure 16. INFRA underestimated temperature by 50 °C in some time interval. Figure 17 shows cladding elongation history at various frictional coefficients when rearrangement is applied. Cladding elongation increases with frictional coefficients. According to Coulomb's law of friction, axial contact force on cladding surface is proportional to frictional coefficient. Two results show best agreement at frictional coefficient between 0.5 and 0.55. Figure 18 shows cladding elongation history at frictional coefficient 0.5 with rearrangement, frictional coefficient 0.55 with rearrangement, and frictional coefficient 0.55 without rearrangement. Before 4.5 day, cladding

elongation history at frictional coefficient 0.5 with rearrangement is very well agreed. After 4.5 day, cladding elongation history at frictional coefficient 0.55 with rearrangement is very well agreed. Figure 19 shows cladding elongation between 4 and 5 days according to LHGR. Relaxation of cladding elongation occurred at 140 W/cm.

Disagreement occurring below 140 W/cm is due to difference of temperature between INFRA prediction and measurement. Table 3 presents creep and rearrangement strain of pellet cusp at 5.3 day when LHGR is highest. Rearrangement strain is 10^4 to 10^5 times larger than creep strain. This means that the effect of pellet creep upon the cladding relaxation is insignificant.

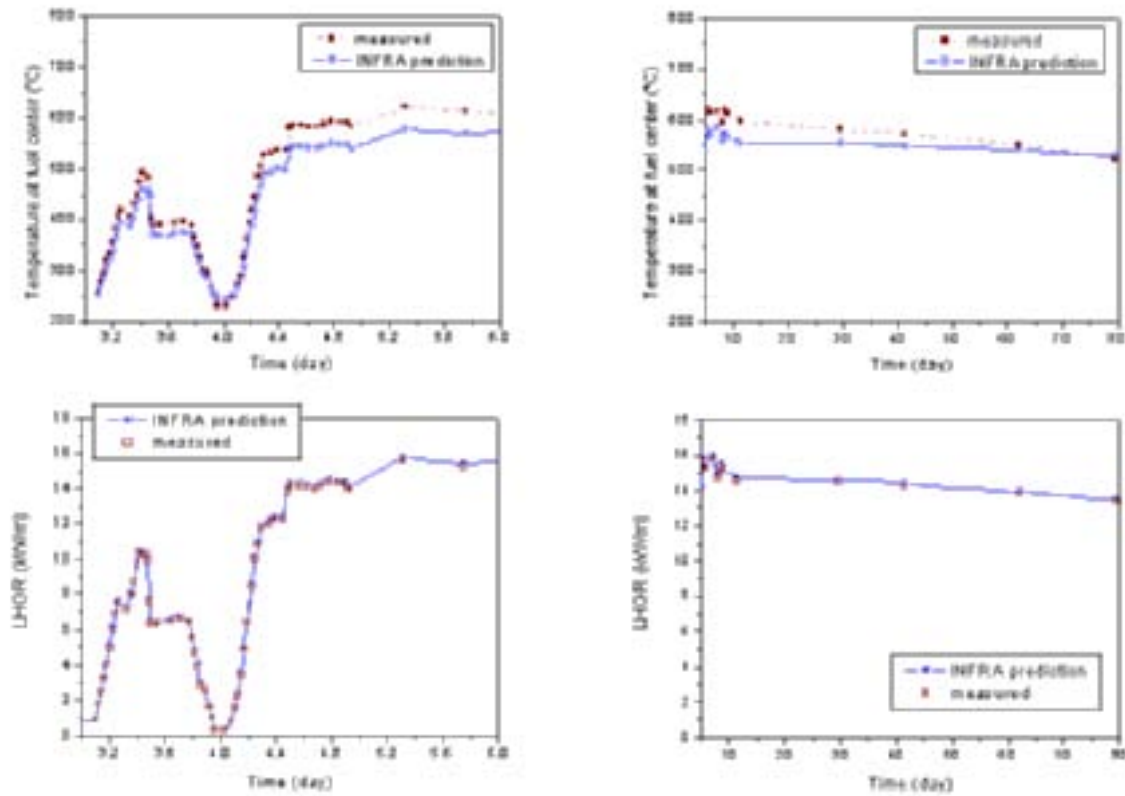


FIG. 16. Temperature and LHGR history.

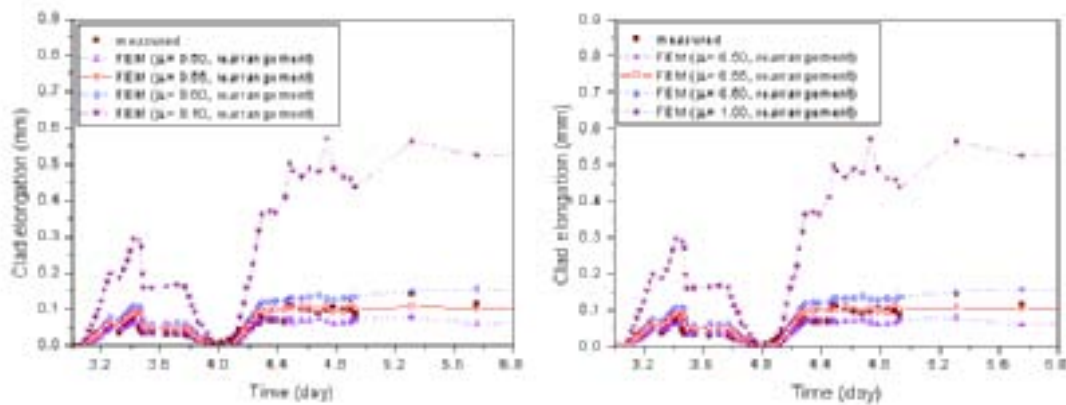


FIG. 17. Cladding elongation history at various frictional coefficients.

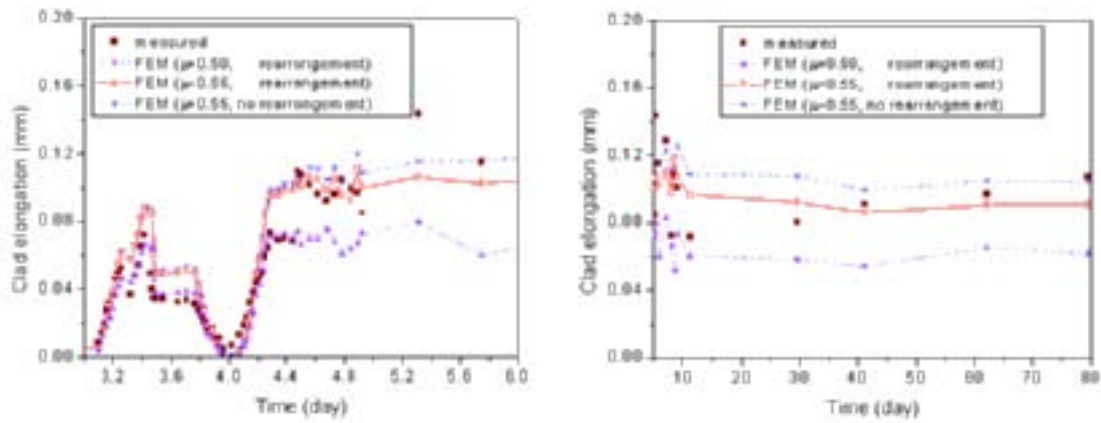


FIG. 17. Cladding elongation history with and without rearrangement.

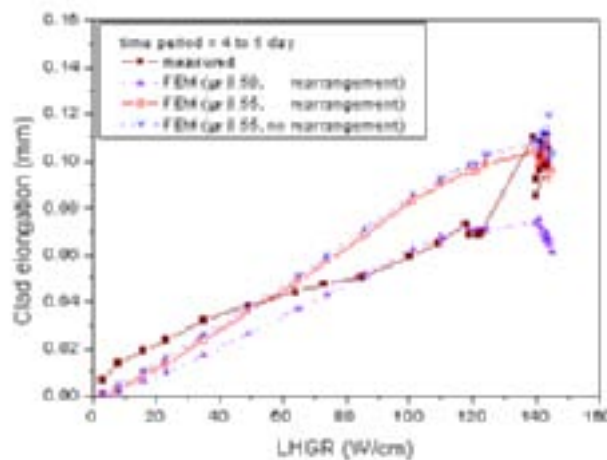


FIG. 19. Cladding elongation vs. power level.

Table 3. Creep and rearrangement strain of pellet cusp at 5.3 day

Strain(%) \ Deformation model	Creep	Rearrangement
Radial strain	0.2537×10^{-6}	-0.1855×10^{-2}
Axial strain	-0.2815×10^{-6}	-0.1446×10^{-2}
Circumferential strain	0.4581×10^{-7}	0.3301×10^{-2}

5. CONCLUSION

A model to analyze pellet and cladding contact was developed by Lagrange multiplier method and was successfully applied to PCMI estimation. Solution is normally converged after two or three iterations without chattering and penetration.

FEA module for mechanical behavior analysis at fuel rod was developed and validated by comparison with the commercial FEA code predictions. Stress, strain and PCMI results for fuel rod were calculated at LHGR between 130 and 600 W/cm and at frictional coefficients between 0 and 1 by using FEA module and ABAQUS. Both results showed very good agreement.

From the in-pile PCMI measured data for 50 MWD/kgU fuel, best-fitted values of frictional coefficient in PCMI was derived as 0.5 ~ 0.55. Rearrangement of the pellet is the main cause of the cladding relaxation during fuel rod power transient, while the effect of pellet creep upon the cladding relaxation is insignificant.

FEA module can be successfully used to analyze the thermal and mechanical characteristics of fuel rod in any LWR UO₂ fuel performance analysis code.

ACKNOWLEDGEMENT

This work has been carried out under the Nuclear R&D Program supported by Ministry of Science and Technology in Korea.

REFERENCES

- [1] LEE, C.B., BANG, J.G., KIM, D.H., KIM, Y.M., YANG, Y.S., AND JUNG, Y.H., "Development of UO₂ Fuel Rod Performance Code, INFRA", KNS Topical Meeting, (Autumn 2001).
- [2] BROCHARD, J., F. BENTEJAC, N. HOURDEQUIN, S. SEROR, C. VERDEAU, O. FANDEUR, S. LANSIART, P. VERPEAUX, "Modelling of Pellet Cladding Interaction in PWR fuel," SMiRT 16, Washington DC, (2001).
- [3] BOUCHARD, P.O., F. BAY AND Y. CHASTEL, "Numerical modelling of crack propagation: automatic remeshing and comparison of different criteria," *Comput. Method Appl. Mech. Engrg.*, **192**, pp. 3887-3908 (2003).
- [4] KWON, Y.D. AND SHIN, S.H., Finite Element Analysis of Fuel Rod, KAERI/CM-399/99 (2000).
- [5] MASSIH, A.R., T. RAJALA AND L.O. JERNKVIST, "Analyses of Pellet-Clad Mechanical Interaction Behaviour of Different ABB Atom Fuel Rod Designs," SMiRT-12 (1993).
- [6] LEVY, S. AND J.P.D. WILKINSON, "A Three-dimensional Study of Nuclear Fuel Rod Behavior during Startup," *Nuclear Engineering and Design*, **29**, pp. 157-166 (1974).
- [7] SUZUKI, M., Light Water Reactor Fuel Analysis Code FEMAXI-V (VER.1), JAERI-Data/Code 2000-030 (2000).
- [8] MASSIH, A.R., T. RAJALA AND L.O. JERNKVIST, "Analyses of Pellet-Clad Mechanical Interaction Behaviour of Different ABB Atom Fuel Rod Designs," *Nuclear Engineering and Design*, **156**, pp. 383-391 (1995).
- [9] UNDERHILL, W.R.C., M.A. DOKAINISH, G.E. ORAVAS, "A method for contact problems using virtual elements," *Comput. Methods Appl. Mech. Engrg.*, **143**, pp. 229-247 (1997).
- [10] ABAQUS/Standard, User's Manual, ver. 5.8, Hibbitt, Karlsson & Sorensen, Inc., U.S.A. (1998).
- [11] HAGRMAN, D.T., editor, SCDAP/RELAP5/MOD3.1 Code Manual Volume IV: MATPRO -- A Library of Materials Properties for Light-Water-Reactor Accident Analysis, NUREG/CR-6150 (1993).
- [12] WHITE, R.J., Measurement of Pellet and Clad Dimensional Changes in the Halden, HWR-678 (2001).
- [13] BROHAN, P., The Re-irradiation of High Burn-up Ex PWR UO₂ Fuel in IFA 629.2, HWR-635 (2000).

DEVELOPMENT OF LOW-STRAIN RESISTANT FUEL FOR POWER REACTOR FUEL RODS

Yu.K. Bibilashvili¹, F.G. Reshetnikov¹, V.V. Novikov¹
A.V. Medvedev¹, O.V. Milovanov¹, A.V. Kuleshov¹
E.N. Mikheev¹, V.I. Kuznetsov¹, V.B. Malygin², K.V. Naboichenko²
A.N. Sokolov², V.I. Tokarev³, Yu.V. Pimenov⁴

¹ A.A. Bochvar VNIINM

² MEPhI

³ Institute of Reactor Materials

⁴ TSC TVEL

Abstract

The paper presents the results of laboratory-scale study of impact of different additives, including Al-Si-Nb oxides, on structure and creep and swelling rates of UO₂ pellets. Data are provided for both out-of-pile and in-pile tests. It has been proposed that doping UO₂ pellets with addition of Al-Si-Nb oxides decreases pellet-cladding interaction. Some conclusions on mechanism of additive's impact on structure and properties of UO₂ pellets were also proposed.

1. INTRODUCTION

In our country the idea of developing low-strain resistant fuel was first formulated in mid 70-ies of the last century [1]. However, the developments and implementation of the intensive investigations into the performance of such fuel were embarked upon at the very beginning of 90-ies.

Under laboratory conditions at different temperatures the influence was studied that is produced by various additives, namely, iron oxides, niobium, silicon, aluminum and their combinations, on creep. The subsequent comparative analysis proved that the most promising approach to the resolution of the problem relevant to lowering down the strain resistance is to alloy uranium dioxide with mullite (3Al₂O₃2SiO₂) which forms intergranular precipitates of low shear resistance strength phases and niobium oxide as a solid solution [2, 3].

The phase and elemental analysis have revealed that niobium oxide is available as a solid solution while alumosilicate is located along the grain boundaries.

It is not feasible to design and validate the use of a novel type of fuel without studying its properties both under laboratory conditions and irradiation. The most important characteristics that govern the stress-strained condition of claddings, the life-time parameters and state of a fuel rod in emergency are its properties determined in in-pile experiments: irradiation induced creep, swelling, densification.

The paper discusses the data of the experimental studies that were acquired at the end of 2002.

2. CHARACTERIZATION OF INVESTIGATED SPECIMENS

Specimens of pilot and semi-commercial batches of fuel pellets including those manufactured at the Electrostal Machinery Plant were used in the experiments.

Except for the additives that were introduced the pellets were manufactured by the standard production process. The characterization of the specimens is given in table 1.

Table 1 - Characterization of Specimens Studied

Composition	Density, g/cm ³	Grain size, μm	O/Me ratio
UO ₂	10.4	11	2.0015
UO ₂ +Mullite 0.25% mass (2SiO ₂ 3Al ₂ O ₃)+Nb ₂ O ₅ 0.1% mass	10.4	16	2.0032

The phase and elemental analysis have shown that niobium oxide is available as a solid solution; aluminosilicate is located along grain boundaries. The introduced additives increase the grain sizes (by approximately a factor 1.5-2).

3. OUT-OF-PILE INVESTIGATIONS (THERMAL CREEP OF STANDARD AND MODIFIED URANIUM DIOXIDE)

The basic results of investigation:

- The creep rate of modified uranium dioxide (containing additives) at 1200–1500 C is 15-20 times higher than that of uranium dioxide without additives produced at the same temperature of sintering (fig. 1);
- The yield strength of alloyed uranium dioxide at the strain rates within (10^{-3} - 2×10^{-2}) 1/hour at 1200–1500 C is 1.5-8 times lower than that of standard uranium dioxide; this will substantially reduce the force interaction between a fuel column and a cladding in transients (fig. 2, 3);
- The temperature of the brittle-to-ductile transition of modified uranium dioxide is on the average 180° lower than that of the fuel produced by the standard process (fig. 4).

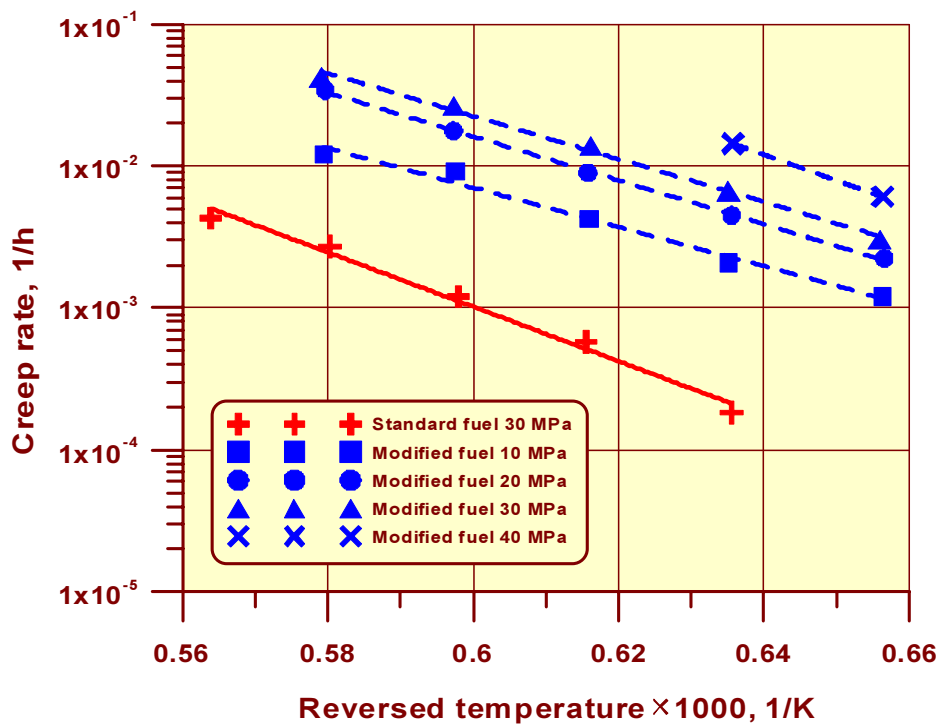


FIG. 1. Creep rate of standard and modified UO₂ vs reversed temperature.

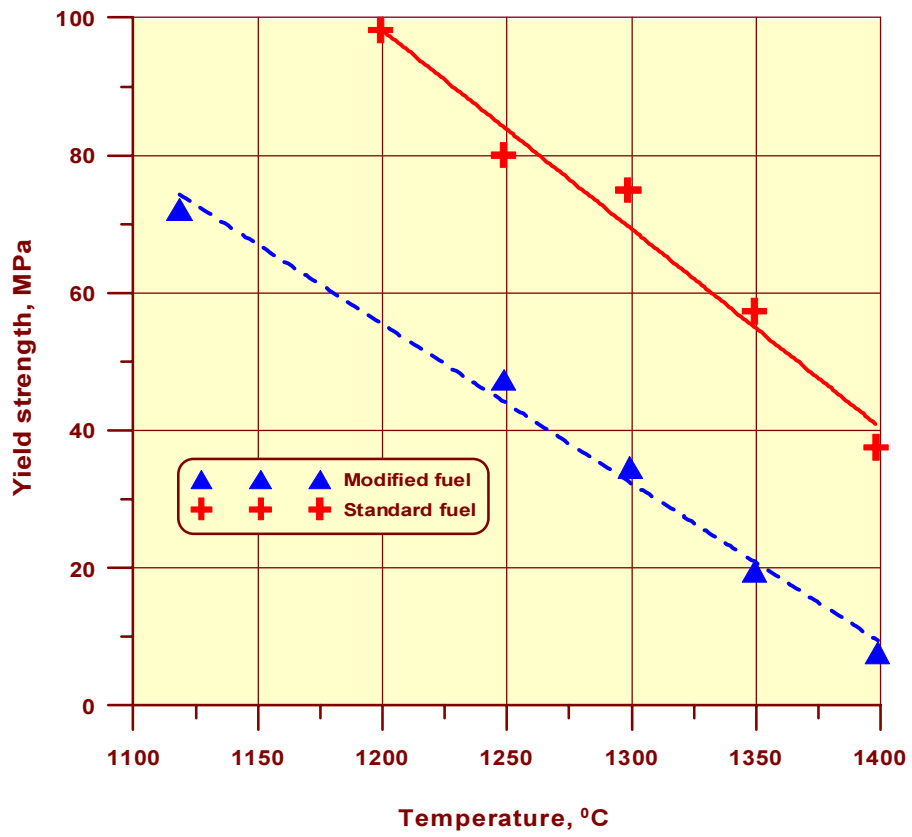


FIG. 2. Temperature dependence of yield strength (strain rate $(8-9) \cdot 10^{-3}$ 1/h).

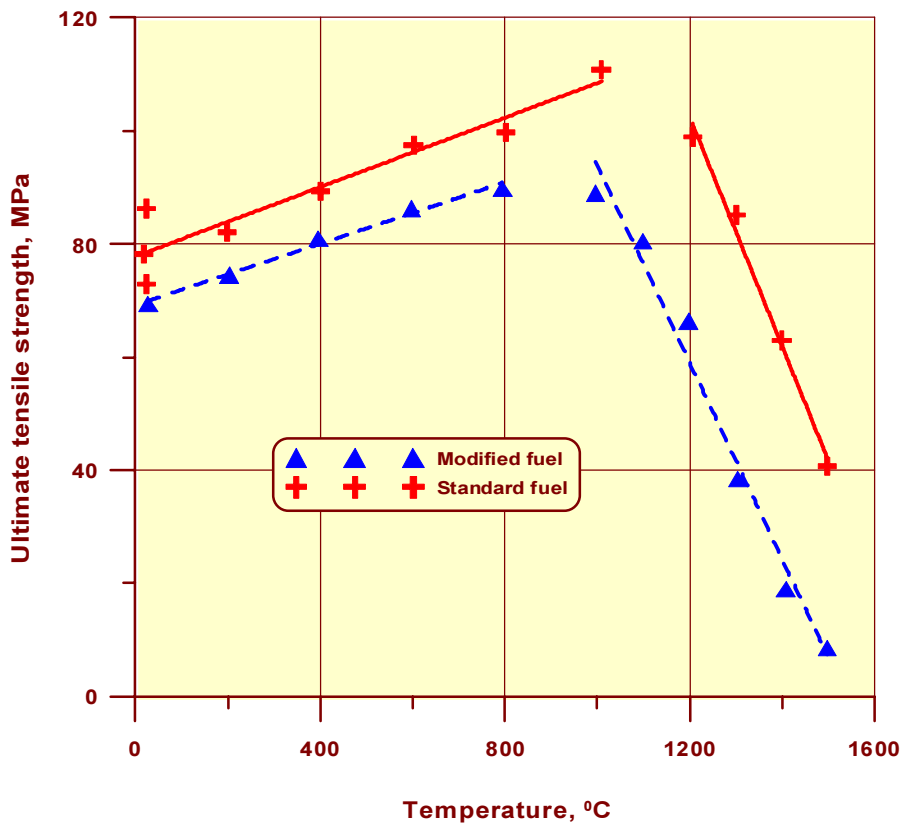


FIG. 3. Temperature dependence of ultimate tensile strength (strain rate $1 \cdot 10^{-2}$ 1/h).

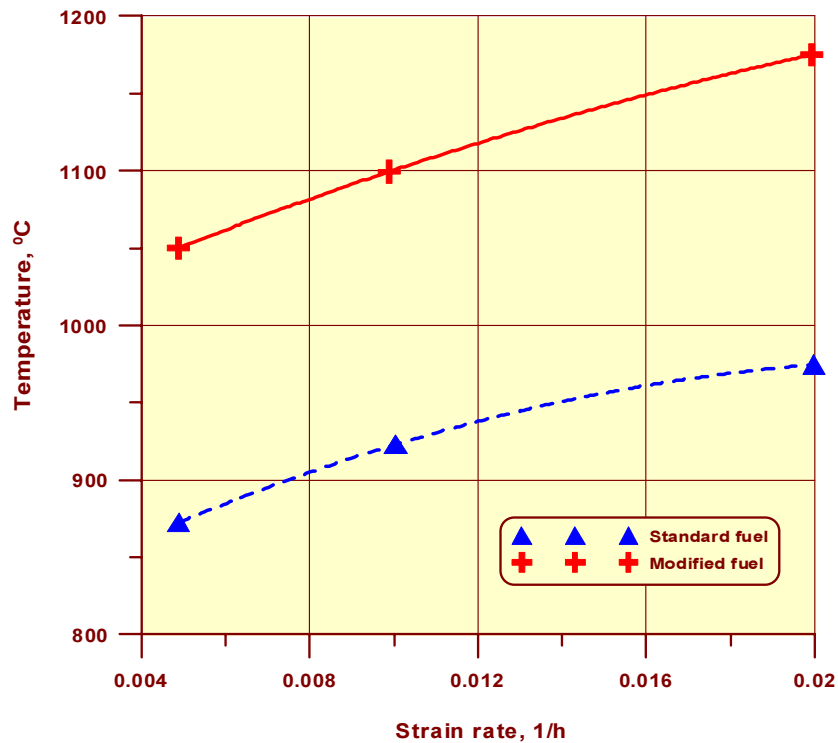


FIG. 4. Brittle-to-ductile transition temperature vs strain rate.

The investigations have demonstrated that the strain resistance of modified uranium dioxide is much lower compared that of the fuel having the standard composition. Along with the lower temperature of the brittle-to-ductile transition this allows the prediction of a substantial reduction in the fuel-cladding interaction in the process of operation in the base and transient modes. The larger grain sizes attained via adding niobium oxide have to promote the retention of volatile and fission gases within the fuel core.

4. INVESTIGATION OF MODIFIED URANIUM DIOXIDE PERFORMANCE UNDER IRRADIATION

The creation of novel types of fuel and validation of its use are not feasible without investigating its properties in the process of irradiation. Among its most important characteristics there are irradiation effected creep, swelling and densification.

To resolve the issued challenges the investigation procedures were worked up in detail as applied to the IVV-2 reactor irradiation conditions.

The VVER-1000 fuel power density is 400-800 W/cm³. Pellets of standard dimensions fracture because of thermal stress arising due to radial temperature gradients at the bulk power density above 200 W/cm³. At the first stage of designing the procedures the work was carried out to validate the shape and dimensions of the specimen. With this aim in view distributions of temperatures and thermal stress in variously shaped specimens were calculated. The calculations evidenced that at the standard power densities thermal stresses do not exceed the ultimate tensile strength of the specimens shaped as hollow cylinders having the walls 1.2-1.6 mm thick.

The technical characteristics of the designed experimental devices are presented in table 2.

Table 2 - Basic Technical Characteristics of Experimental Devices

Characteristics	Purpose	Experimental device	
		<i>Creep-URAL</i>	<i>Swelling-URAL</i>
		Irradiation creep studies	Swelling and irradiation densification studies
Test temperature, °C		200 - 1200	200 - 900
Error of temperature measurement *, %		2 - 3	2 - 3
Maximal compressive force on specimen, N		120	3-5
Error of force determination, %		1.5	not measured
Range of travels, µm		± 2500 ± 500	± 2500 ± 500
Error of travel measurement, %		0.5 - 1, 0	0.5 - 1, 0
Specimen sizes, mm:			
length		10 - 11	10 - 11
outer diameter/inner diameter		7.2/4, 0	7.2/4, 0
outer diameter/inner diameter		7.5/4,5	7.5/4,5
Power density of specimen, W/cm ³		600	600
Quantity of specimens		2	8 - 15
Overall sizes of facility, mm:			
diameter		58	48
length		6500	6500

* Relative reduced errors are given.

Dimensional changes under irradiation are the important characteristic of nuclear fuel that governs the closure of fuel column-cladding gaps, fuel rod temperature conditions and behaviour in emergency as well as the stress-strained condition of a cladding. Dimensional changes of fuel, particularly, of uranium dioxide are controlled by the processes of irradiation effected densification and swelling.

The work studied dimensional changes of modified low strain resistant UO₂ pellets under irradiation. The results are compared to the previously acquired data on the dimensional changes of the standard UO₂ pellets /3/.

Variations in the length of the modified UO₂ pellet column VS time at the irradiation temperature of 640-670 °C are illustrated in fig. 5.

Under irradiation the reduction in the fuel column length is observable effected by the irradiation induced densification. The maximal reduction in the fuel column length equals 0.11%, which corresponds to the volume change by 0.33%. The densification process terminates at the burn-up of ~ (7-8)·10¹⁹ fiss./cm³. The resultant value is substantially lower than the permissible volume reduction that is limited by the VVER-1000 fuel rod design to 1.2%.

The irradiation induced creep of the modified low strain resistant fuel was investigated in the IRT and IVV-2 reactors in temperature range from 280 to 1210 °C, stress – from 10 to 32 MPa, fission density – from 9·10¹² to 1.3·10¹³ fiss/cm³s. Irradiation induced creep rate VS stress of modified UO₂ show in fig. 6.

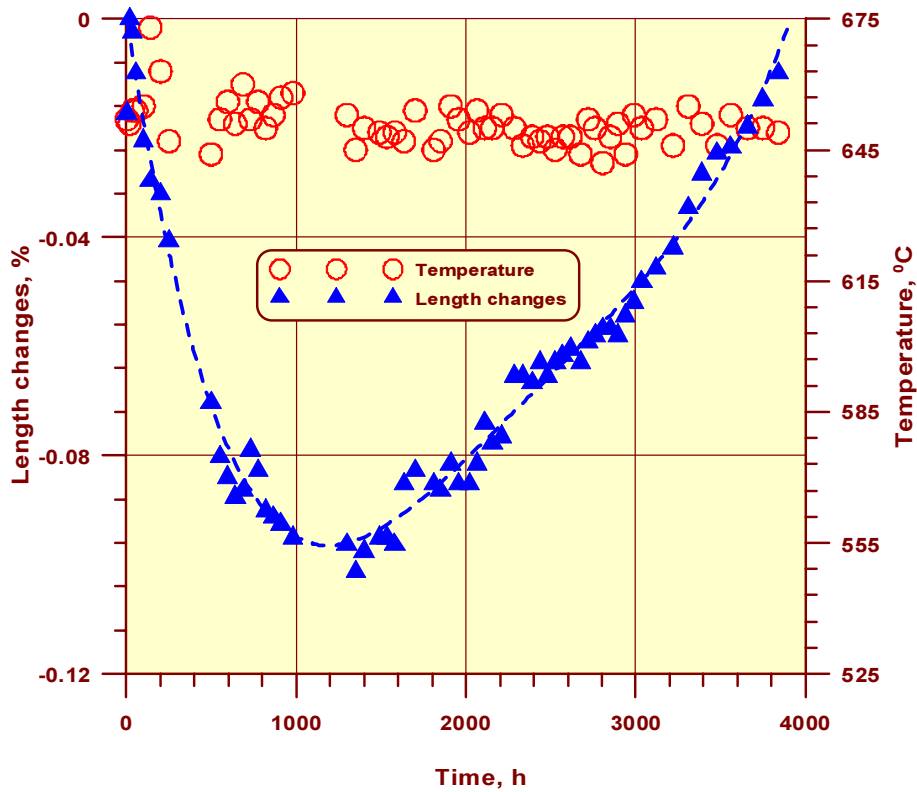


FIG. 5. Length variations in low strain resistant UO_2 pellet column VS irradiation time (Fission density of $1.7 \cdot 10^{13}$ fiss/cm³s).

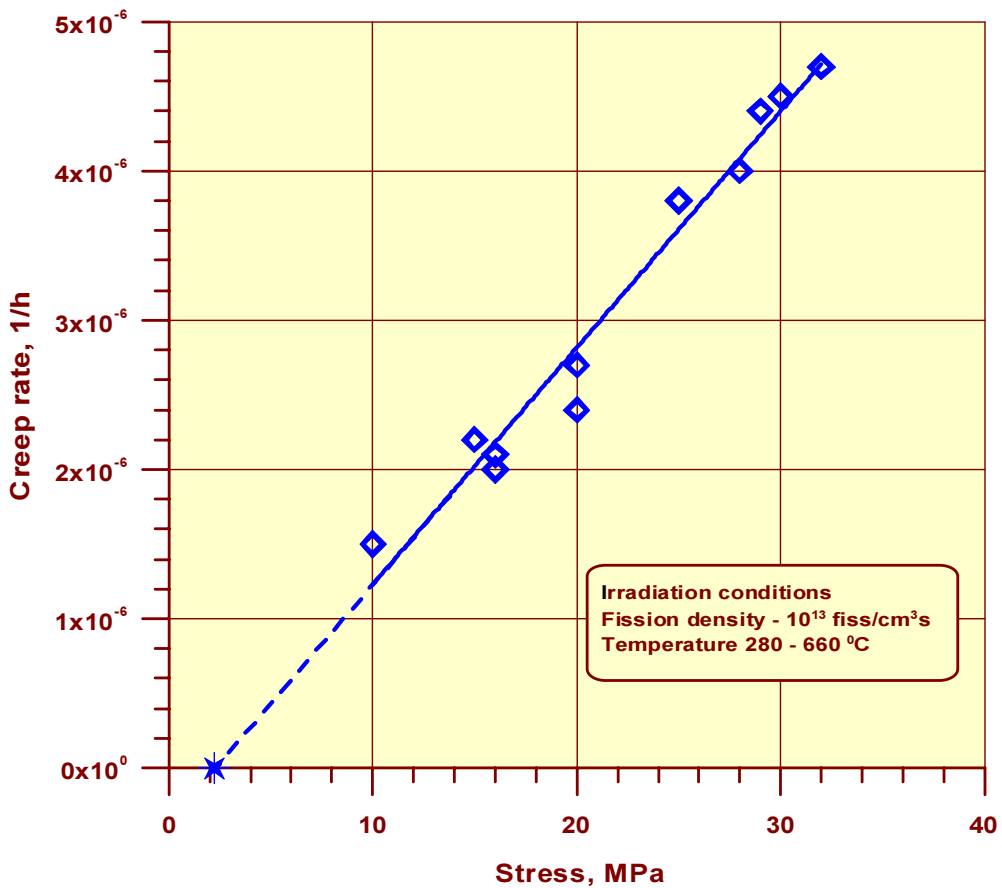


FIG. 6. Irradiation creep rate of modified UO_2 vs stress (Fission density 10^{13} fiss/cm³s, temperature 280 – 660 C.)

It is evident from the presented results that the creep rate vs stress dependence might be described with the linear equation of the following type $\xi = A \cdot (\sigma - \sigma_{th})$ where the coefficient A is a linear function of fission density. The threshold stresses σ_{th} might be interpreted to be stresses at which the creep rate equals the swelling rate of fuel. This parameter determines the level of the force interaction between the cladding and the swelling fuel under the steady-state conditions of the fuel operation.

For the conventional UO_2 fuel the extent of the threshold stresses is within 8-15 MPa (depending on the temperature). The authors' data on the threshold stresses for modified UO_2 are equal to ~ 1.5 -3.0 MPa (are likely to be also temperature dependent).

The results of reactor creep rate investigations (in temperature range from 280 to 1210 C) reduced to the fission density of $10^{13} 1/cm^3$ and the stress of 30 MPa are demonstrated in fig. 7.

The comparison indicates modified UO_2 that in a low temperature range the rate of the irradiation induced creep of modified UO_2 is a factor of 2.5-5.0 higher than that of the fuel produced by the standard process.

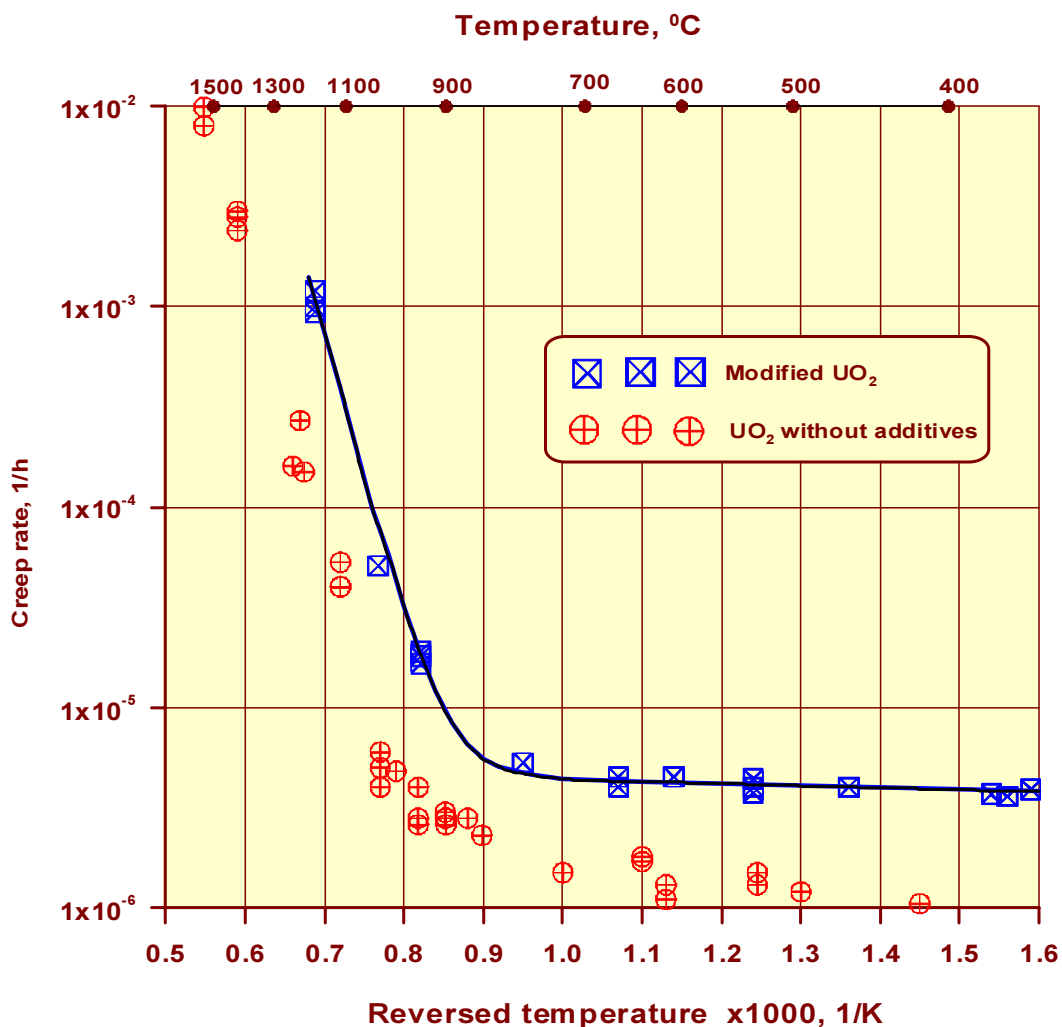


FIG. 7. Reactor creep vs temperature (The results are reduced to the fission density of $10^{13} 1/cm^3$ and the stress of 30 MPa).

Proceeding from the acquired data it might be expected that the use of modified uranium dioxide shall substantially decrease the fuel-cladding mechanical interaction parameters and correspondingly, improve the reliability of fuel rod. Under steady-state conditions at a high burn-up the decreased fuel-cladding interaction is due to a higher irradiation creep rate and lower threshold stresses suppressing, in transients and load-follow-to lower yield strength and a lower temperature of a brittle-to-ductile transition.

As an example in fig. 8 the calculations results of fuel rod clad hoop stresses during of power rise following short-time operation at 50% N_{nom} VVER-1000 are represented both modified and standard UO_2 .

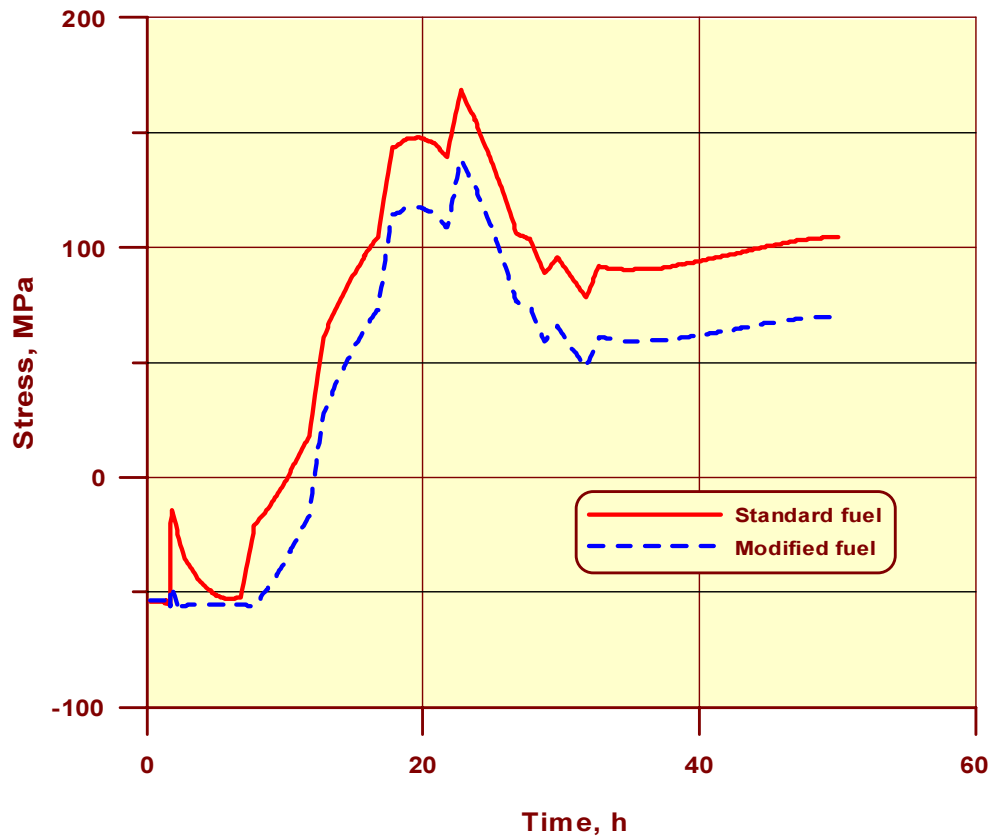


FIG. 8. Fuel rod clad hoop stresses during of power rise following short-time operation at 50% N_{nom} .

5. CONCLUSION

- Specimens of modified UO_2 containing additives were investigated. The mass contents of alloying elements are as follows: Al-(0.1-0.13)%, Si-(0.06-0.075)%, Nb-(0.06-0.1)%.
- In IVV-2 reactor the investigations of low strain resistant fuel were carried out to determine its irradiation induced creep, densification, swelling and stresses suppressing swelling. The investigations were carried out at the fission density $\sim(1.5-1.7) \cdot 10^{13}$ fissions/cm³s.
- Based on the acquired data it might be expected that the use of modified uranium dioxide shall decrease the fuel-cladding mechanical interaction.

REFERENCES

- [1] RESHETNIKOV F.G., "Problems in Designing Nuclear Power Reactor Fuel", Reactor Materials Science (Proc. Int. Conf, Alushta, SU, 1978), TSNIATOMINFORM, Moscow. v. 4 (1978) 23.
- [2] KULESHOV A.V., MALYGIN D.B., MILOVANOV O.V., MIKHEEV E.N., Influence of Alloying in Uranium Dioxide Creep Characteristics. Scientific Session on MphEI-99. Collect. of Sci. Papers, M; MphEI, v.5, p. 64.
- [3] BIBILASHVILI YU.K., MALYGIN V.B., MEDVEDEV A.V., et al., "Experimental of Developing Low Strain Resistant Oxide Fuel for Power Reactor Fuels", Characterization and Control in Nuclear Fuel Fabrication (Proc. Int. Conf, Hyderabad, India, , 6-12 December, 2002) (in press).

OBSERVATION OF A PELLETT-CLADDING BONDING LAYER IN HIGH POWER FUEL

S. VAN DEN BERGHE, A. LEENAERS
B. VOS, L. SANNEN, M. VERWERFT
Belgian Nuclear Research Centre SCK•CEN,
Reactor Materials Research Dept.,
Mol, Belgium

Abstract

This paper reports on a detailed Electron Probe Microanalysis investigation of duplex bonding layers observed at the fuel-cladding interface of PWR fuel rods that were subjected to high linear powers (220-320 W/cm). The various phases encountered, from the cladding inward, were identified as Zr, ZrO₂, Zr-Cs-O, U-Cs-O and UO₂. Cesium concentrations as high as 6-7 at% were observed in the Zr-Cs-O layer and concentrations of about 3 at% are found in the U-Cs-O layer. High concentrations of Cs were also found on the grain boundaries of the UO₂ fuel, up to several hundred microns into the fuel. The good bonding between cladding and fuel has as a result that the cold gap runs through the fuel, with the bonding layer and a thin fuel layer sticking firmly on the cladding. In an effort to reproduce the formation of these bonding layers in laboratory conditions, sealed zircaloy tubes, containing cesium molybdate (Cs₂MoO₄), were heated in a tubular furnace to temperatures of 600-800°C. It appears that the oxygen potential plays an important role in the formation of such bonding layers. Formation of Cs-Zr-O interaction layers could be observed at sufficiently low oxygen potentials.

1. INTRODUCTION

Fuel-cladding interaction and the formation of fuel-cladding bonding layers with specific chemical, physical and mechanical properties is of importance regarding the evolution of thermal conductivity as well as in the context of PCMI. It is also important in the framework of long term storage of spent fuel where the phases formed at the fuel cladding boundary are considered to be the first to be leached in case of cladding failure.

Inner surface cladding oxidation and subsequent mechanical bonding between the fuel pellet and the cladding are well-known phenomena of high burnup and high duty fuels but the chemical composition and formation conditions of the complex bonding layers are much less documented. In this study, we report on the detailed observation of cesium-rich phases in pellet-cladding bonding layers of zircaloy-clad high duty LWR fuels. Some straightforward laboratory experiments complement the fuel observations and allow confirming that the formation mechanisms proposed on the basis of thermodynamic considerations apply even though the fuel-clad interface system is never at equilibrium.

2. EXPERIMENTAL

2.1. Fuel samples

The observation of fuel clad bonding and the formation of multilayer bonding layers are typical for high duty fuels. The case study presented here is taken from old fuel samples that

were re-investigated in the framework of long term intermediate storage of nuclear fuel. Samples were taken from UO₂ fuel rods (enrichment of 2.5%) that have been irradiated in the Dodewaard Boiling Water Reactor (BWR) between 1971 and 1974. The fuel rods have undergone peak powers between 220 and 320 W/cm and have end-of-life burnups of around 23 GWd/t_M. After unloading, the fuel rods were cut and the segments were stored in air in sealed canisters. In 2001, the canisters were unloaded and samples were cut from the segments in the framework of a post-irradiation examination campaign focusing on the long-term interim storage of fuel [1, 2]. Because of the irradiation characteristics of these rods, the cladding-fuel interface was also examined closely, resulting in the observations reported below.

2.2. Sample preparation and examination

The samples have been embedded in epoxy resin and polished with diamond grinding discs of successively finer grain size, finishing on cloth with diamond paste of 3 µm and 1 µm. Before mounting the sample in the electron microscopes, the samples were coated with carbon to prevent charging.

Optical microscopy was performed on a Reichert Telatom 3 shielded optical microscope, equipped with a digital image acquisition system.

Scanning electron microscopy is performed on a shielded Jeol JSM6310 microscope, equipped with a secondary electron and backscattered electron detector.

The electron probe micro-analysis (EPMA) is performed on a shielded CAMEBAX-R microbeam, upgraded with digital image and X-ray acquisition programs (SAMx Suite).

3. RESULTS

3.1. Optical and Scanning Electron Microscopy

The optical micrographs of the sample, taken close to the pellet-cladding interface (FIG. 1a), show a duplex bonding layer. From the cladding inward, one can first observe the pure zircalloy cladding, then the grey ZrO₂ oxidation layer, followed by the darker grey bonding layer. A piece of fuel material is adhering to this bonding layer, followed by the fuel-cladding gap.

A similar image is generated with scanning electron microscopy (FIG. 1b and c), where the use of backscattered electron imaging provides a clear view of the interaction layer on top of the ZrO₂ (FIG. 1c). The backscattered electron image shows that the Cs-Zr-O layer has all the aspects of a liquid or at least viscous mixture of a U-rich phase and a Zr-rich phase.

The interaction layer is not visible at all locations on the cladding, but it covers roughly 50% of the fuel-cladding interface. The aspect of the layers is always identical and the bonding between the layer and the fuel is very strong as witnessed by the fact that always part of the fuel is found to adhere to the bonding layer, with the fuel-cladding gap inside the fuel.

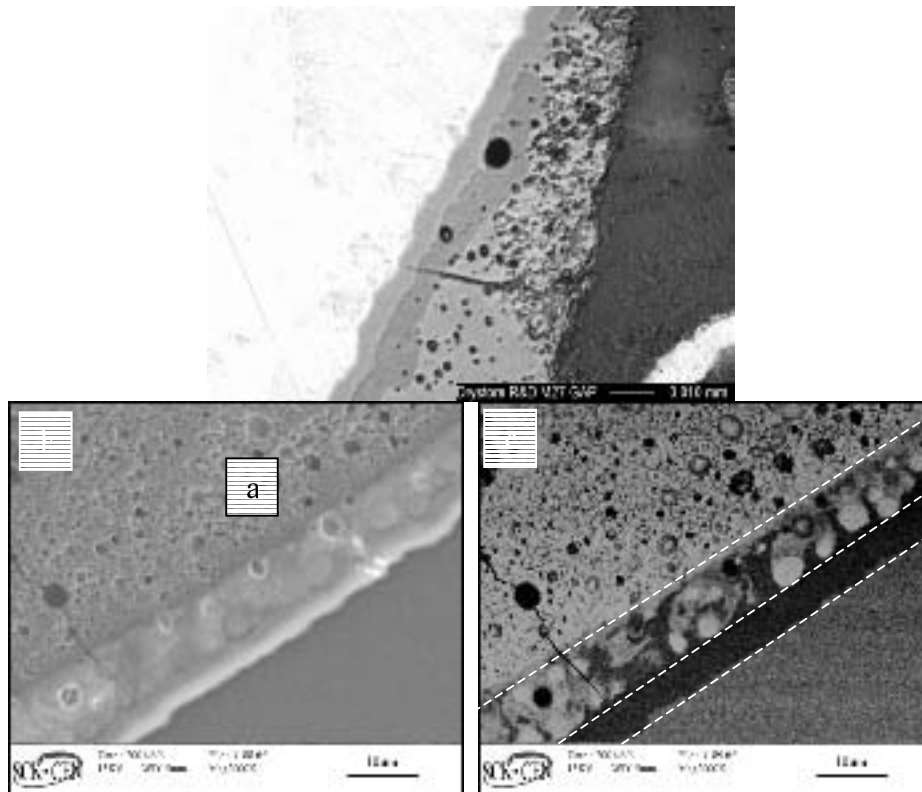


FIG. 1 : Optical micrograph (a) and scanning electron images (b and c) of the pellet-cladding interface. (b) Secondary electron image and (c) backscattered electron image. The backscattered electron image shows composition variation (Z-contrast imaging). Image c is taken with backscattered electrons and shows the density distribution. The dotted lines show the boundaries of the different layers.

3.2. Electron Probe Microanalysis

The X-ray mappings taken with the microprobe show the repartition of the elements involved in this bonding layer, namely Zr, Cs, U and O. It is evident from the mappings in FIG. 2 that the bonding layer consists of three consecutive phases. On the cladding, we first find a thin ZrO_2 layer. On this oxide layer, a Cs-Zr-O interaction layer has formed. This layer is not completely homogeneous. Inside it, we observe inclusions of a Cs-enriched U-O phase, similar to the material found in the first zone of the fuel. Beside the inclusions, the layer also shows some intermixing with the uranium from the fuel. The last layer in the sequence is a Cs-rich uranium oxide layer, which forms the first zone of the fuel adhering to the bonding layer.

Semi-quantitative line scan data taken across the bonding layer (FIG. 3) show the element concentrations in each layer. The line scan is taken across an inclusion of Cs-enriched U-O phase adhering to the cladding. We can distinguish the different phases present: A is the pure zircalloy cladding, B is the ZrO_2 oxidation layer, C is the Cs-U-O interaction phase and D is the Cs-Zr-O phase. It is observed that the Cs concentration does not exceed 10 at%.

Elevated Cs concentrations on the fuel grain boundaries are observed up to several hundreds of microns into the fuel (Figure 2f).

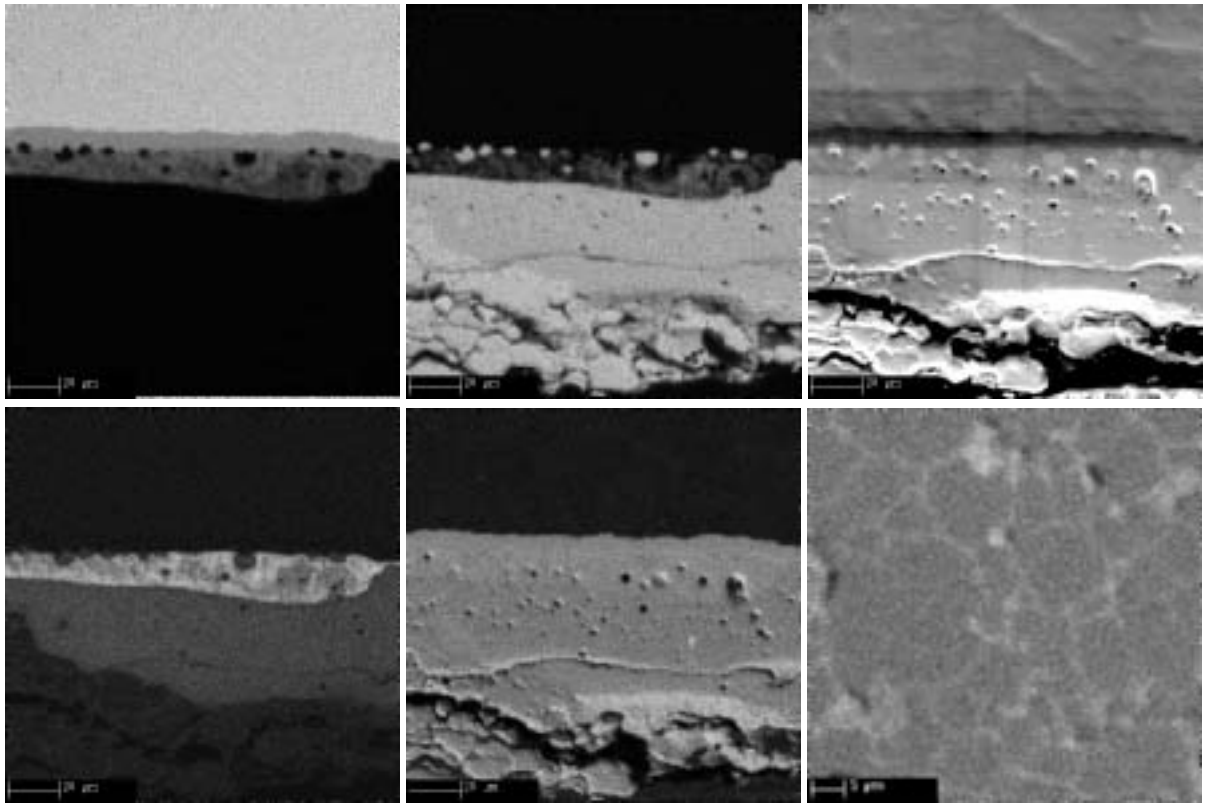


FIG. 2 : X-ray mappings of the pellet-cladding interaction layer, showing the repartition of (a) Zr, (b) U, (d) Cs and (e) O, as well as an SEM image (c) . The three consecutive layers ZrO_2 , Cs-Zr-O and Cs-U-O ase discussed in the text can be clearly discerned. In (f) a detailed view of the Cs-enriched grain boundaries as observed in the fuel, is given.

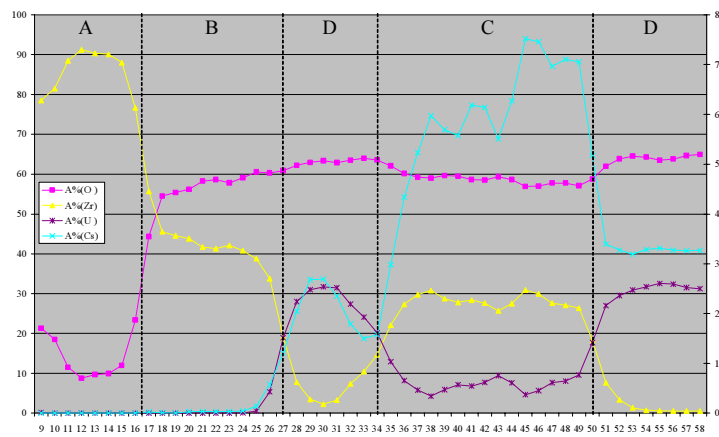
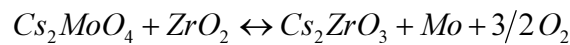


FIG. 3 : Line scan data taken at the location of the X-ray mappings in FIG. 2. Phase A represents the zircalloy cladding and phase B is the ZrO_2 layer. The line is drawn across a piece of Cs-U-O phase (phase D) adhering to the ZrO_2 layer (phase B). Phase C corresponds to the Cs-Zr-O phase.

3.3. Separate Effects Tests (SET)

In order to reproduce the interaction between cesium and the zircalloy, separate effect tests were performed by heating a closed zircalloy capsule containing cesium molybdate. The molybdate Cs_2MoO_4 was chosen because it is easier to handle compared to metallic cesium or

the cesium oxides and because it is reported to be less stable than the zirconates [3]. Zircalloy capsules were used with and without pre-oxidation treatment to evaluate the influence of a pre-existing ZrO_2 layer. It is assumed that the oxygen potential inside the capsules will be lowered by the presence of the metallic Zr, after which the molybdates will decompose and the zirconates will form if a ZrO_2 layer is present on the cladding surface.



The ZrO_2 layer is required, since none of the cesium zirconates are in equilibrium with metallic Zr, as seen in the ternary diagram of FIG. 1 [4].

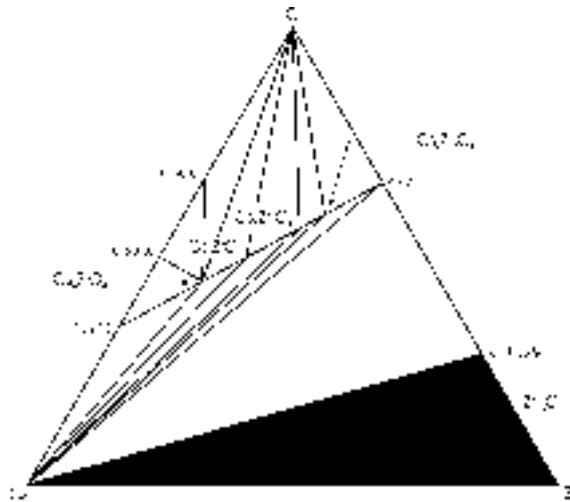


FIG. 4 : Ternary diagram of the Cs-Zr-O system. It is clear that no tie lines exist between the zirconate phases and the metallic Zr. (After S. Dash)

After thermal treatments at 600°C for 300h for the unoxidised zircalloy tubes and 800°C for 75h for the pre-oxidised tubes, metallic Mo is found, witnessing the reduction of the molybdates. An interaction layer is formed by a phase containing cesium and zirconium. It is found that a pre-existing ZrO_2 layer is not required and can even inhibit the formation of the zirconates because the oxide layer is normally protective and prevents the lowering of the oxygen potential inside the tube. At 800°C, the oxide layer will no longer sufficiently protect the zircalloy surface and the formation of the interaction phase will proceed.

4. DISCUSSION

From the observations, we can deduce that a bonding layer, involving cesium, has formed between the zircalloy cladding and the irradiated fuel. On top of the ZrO_2 layer, which is commonly found in all irradiated fuels, we find a Cs-Zr-O phase, followed by a Cs-rich U-O layer.

Observations similar to these have been made by the authors on different high duty fuels, all presenting the same layers in the exact same order. In the open literature, a few accounts of a similar interaction layer have been found, one observation made on a UO_2 rod irradiated at the Obrigheim Nuclear Power Station at a LHGR of 400 W/cm [5] up to a burnup of about 40 GWd/t_M and a recent report on the behavior of UO_2 irradiated at the BR3 reactor at power levels of 170-350 W/cm up to $\sim 45 GWd/t_M$ [6]. A similar bonding layer observation has also

been made, although less detailed, on a transient tested UO_2 fuel rod from the Third Risø Fission Gas Project. The fuel is reported to be irradiated at a high rating [7].

Thermodynamically, the interaction between zirconium oxide ZrO_2 and cesium (oxide) can lead to formation of cesium zirconates in the temperature-oxygen potential conditions present in these fuel elements close to the cladding [3]. None of the various cesium zirconate phases are in equilibrium with metallic Zr [4], which is in accordance with the observations, as the zircalloy and the Cs-Zr-O interaction phase are always separated by a ZrO_2 layer. The zirconates are reported as the most stable cesium compounds, compared to uranates or molybdates.

From the results of the SETs, we can conclude that the oxygen potential is a very important parameter in the formation of the zirconates. Although the temperatures of the SETs were higher than those occurring at the actual fuel cladding during irradiation, even at high power, it is believed that this mainly influences the kinetics of the interaction and not so much the thermodynamics. The SETs prove that the lowering of the oxygen potential by the Zr/ZrO_2 couple is an absolute requirement for the formation of the zirconate interaction phase. The SETs furthermore demonstrate by the length of the thermal treatments required, that the kinetics of formation of these compounds is exceedingly slow.

There are two possible explanations for the elevated Cs concentrations found on the pellet periphery. Because of the high linear powers generated by these fuels during their time in the reactor, the center line temperatures have become very elevated ($>1500^\circ\text{C}$). As such, the temperature regime becomes more comparable to Liquid-Metal Fast Breeder Reactor (LMFBR) fuel pins. For these, axial migration of Cs has been observed on numerous occasions [8] as well as for transient tested UO_2 fuel [7]. It is possible that cesium has migrated axially out of the fuel pellet and has condensed on the pellet-pellet interface and as such has reached the fuel-cladding gap. From there, it can re-penetrate the fuel and form cesium zirconate with the ZrO_2 .

In contrast to axial migration, radial migration of cesium down the temperature gradient from the pellet center to the periphery with formation of cesium zirconate at the pellet-cladding interface is another possibility. At high temperatures, the behavior of cesium is similar to that of xenon [7], but at the temperatures that occur close to the cladding, cesium is found as a liquid, which is in agreement with the viscous nature the bonding layer presents. The radial migration can also explain the high cesium concentrations on the grain boundaries, found rather deep into the fuel pellet.

5. CONCLUSIONS

The observation of a duplex bonding layer in high-duty fuels has been studied in detail in this article. Although previous reports of such interaction layers exist, the experimental findings in this work have allowed to demonstrate that the most important parameters in the formation of these layers are the oxygen potential and the temperature.

High enough temperatures are required for the mobility of the cesium in the fuel. Either through axial or radial transport, the cesium migrates to the pellet-cladding interface. The local conditions close to the cladding, namely the presence of the metallic zirconium/zirconium oxide couple, generate a very low oxygen potential. The ZrO_2 layer formed on the inner surface of the zircalloy tubing reacts with the cesium with formation of cesium zirconate.

The formation of these compounds has very slow kinetics and as such, these layers are not always formed when cesium is transported out of the fuel pellets. For ramp tested UO₂, which is only subjected to high power during a short transient, insufficient time is available for formation of these compounds. Therefore, high-duty fuels are the most likely candidates for the observation of these bonding layers. Because these fuels are irradiated at high temperature during their entire stay in the reactor, cesium accumulates in the pellet-cladding gap during the entire irradiation and as such, the formation of the zirconates can take place.

REFERENCES

- [1] LEENAERS, et al., Microstructure of Spent MOX Fuel Stored under Dry Air for 25 Years, Environmental Management, (Proc. 8th International Conference September 30 - October 4 2001) CD-ROM.
- [2] LEENAERS, L. SANNEN, S. VAN DEN BERGHE and M. VERWERFT, "Oxidation of spent UO₂ fuel stored in moist environment", Journal of Nuclear Materials **317**(2-3), (2003), 226-233.
- [3] R. KOHLI, *Thermochimica Acta* **65**(2-3), (1983), 285-293.
- [4] S. DASH, D. D. SOOD and R. PRASAD, "Phase diagram and thermodynamic calculations of alkali and alkaline earth metal zirconates" Journal of Nuclear Materials **228**(1), (1996), 83-116.
- [5] H. KLEYKAMP, "The chemical state of LWR high-power rods under irradiation", Journal of Nuclear Materials **84**(1-2), (1979), 109-117.
- [6] S. K. YAGNIK, A. J. MACHIELS and R. L. YANG, "Characterization of UO₂ irradiated in the BR-3 reactor", Journal of Nuclear Materials **270**(1-2), (1999), 65-73.
- [7] T. WALKER, C. BAGGER and M. MOGENSEN, "Observations on the release of cesium from UO₂ fuel Journal of Nuclear Materials **240**(1), (1996), 32-42.
- [8] H. FURUYA, et al., "Axial distribution of cesium in heterogeneous FBR fuel pins", Journal of Nuclear Materials **201**, (1993), 46-53.

LIST OF PARTICIPANTS

Asakura, K	Japan Nuclear Cycle Development Institute (JNC), Naka-gun, Ibaraki, Japan
Bairiot, H.	FEX, Mol, Belgium
Basak, U.	Bhabha Atomic Research Centre, Mumbai, India
Basselier, J.	BELGONUCLEAIRE, Brussels, Belgium
Bibilashvili, Y. K.	A.A. Bochvar All-Russian Research Institute of Inorganic Materials (VNIINM), Moscow, Russian Federation
Blancher, J.	COGEMA-BUR, Bagnols sur Ceze, France
Blanpain, P.	Framatome ANP, Lyon, France
Bosso, S.	Tractebel, Brussels, Belgium
Castelli, R.	COGEMA-BUR, Bagnols sur Ceze, France
Charlier, A.	Tractebel, Brussels, Belgium
Chung, J.G.	Kepeco, Yuseong-Gu, Daejeon, Rep. of Korea
Couture, J.-M.	Canadian Nuclear Safety Commission, Ottawa, Canada
Dalleur, J.-P.	Tractebel, Brussels, Belgium
Declercq, C.	Tractebel, Brussels, Belgium
Dehautd, Ph.	CEA/SARCLAY, Gif sur Yvette, France

Dekeyser, J.	SCK-CEN, Mol, Belgium
Delafoy, C.T.	Framatome ANP, Lyon, France
Delette, G.	Commissariat à l'Energie Atomique, Grenoble, France
Deng, H.	Yibin Nuclear Fuel Elements Plant, Sichuan, China
Dörr, W.	Framatome ANP GmbH, Erlangen, Germany
Druenne, H.	Tractebel, Brussels, Belgium
Frans, C.	Tractebel, Brussels, Belgium
Goethals, S.	Tractebel, Brussels, Belgium
Govers, K.	SCK-CEN, Mol, Belgium
Jadot, J.-J.	Tractebel, Brussels, Belgium
Jayaraj, R.N.	Nuclear Fuel Complex, Hyderabad, India
Kim, Y.M.	Korea Atomic Energy Research Institute, Yuseong, Daejeon, Rep. of Korea
Koulechov, A. V.	A.A. Bochvar All-Russian Research Institute of Inorganic Materials (VNIINM), Moscow, Russian Federation
Kuznetsov, V.I.	A.A. Bochvar All-Russian Research Institute of Inorganic Materials (VNIINM), Moscow, Russian Federation
Kuznetsova, N.V.	ULBA Metallurgical Plant, Ust-Kamenogorsk, Kazakstan
Lemehov, S.E.	SCK-CEN, Mol, Belgium

Lindbäck, J.-E.	Westinghouse Atom AB, Vasteras, Sweden
Lippens, M.	BELGONUCLEAIRE, Brussels, Belgium
Lloret, M.	Enusa Industrias Avanzadas SA, Madrid, Spain
Maeder, C.P.	Swiss Federal Nuclear Safety Inspectorate (HSK), Villigen, Switzerland
Malygin, V.B.	Moscow Engineering Physics Institute, Moscow, Russian Federation
Manych, A	ULBA Metallurgical Plant, Ust-Kamenogorsk, Kazakstan
Menghini, J.	Comision Nacional de Energia Atomica, Buenos Aires, Argentina
Nonon, C.N.	CEA-CE Cadarache, Saint Paul Lez Durance, France
Novikov, V.	A.A. Bochvar All-Russian Research Institute of Inorganic Materials (VNIINM), Moscow, Russian Federation
Ohai, D.	Institute for Nuclear Research, Pitesti-Mioveni, Romania
Ohira, K.	Nuclear Fuel Industries, Ltd, Tokai Works, Naka-gun, Ibaraki, Japan
Ohtani, T.	Japan Nuclear Cycle Development Institute (JNC), Tokai-mura, Naka-gun, Ibaraki, Japan,
Oudinet, G.	CEA-CE Cadarache, Saint Paul Lez Durance, France
Pagano, L.	CTMSP, Ipero, Brazil
Parrat, D.	CEA-CE Cadarache, Saint Paul Lez Durance, France
Pimenov, Y.	JSC TVEL, Moscow, Russian Federation

Pontillon, Y.	CEA-CE Cadarache, Saint Paul Lez Durance, France
Rudling, P.S.	ANT International, Uppsala, Sweden
Schneidesch, C.	Tractebel, Brussels, Belgium
Serna, J.	Enusa Industrias Avanzadas SA, Madrid, Spain
Song, K.W.	Korea Atomic Energy Research Institute, Yuseong, Daejeon, Rep. of Korea
Stockmann, Y.	VROM Kernfysische Dienst, Den Haag, Netherlands
Svoboda, R.	CEZ A. S. JE Temelin, Czech Republic
Valin, S.	CEA-CE Cadarache, Saint Paul Lez Durance, France
Van Den Berghe, S.W.N.	SCK-CEN, Mol, Belgium
Van Vyve, J.	Tractebel, Brussels, Belgium
Verwerft, M.	SCK-CEN, Mol, Belgium
Wright, J.	OECD Halden Reactor Project, Halden, Norway
Yoo, H.	Kepeco, Yuseong-Gu, Daejeon, Rep. of Korea

